THE HYROCARBON SOURCE POTENTIAL OF THE PALAEOZOIC ROCKS OF THE GHADAMES BASIN, NW LIBYA

BY

MOHAMED HROUDA

A thesis submitted to the University of Newcastle upon Tyne

In partial fulfillment of the requirements for the degree of

Doctor of Philosophy

In the Faculty of Science

School of Civil Engineering and Geosciences

University of Newcastle upon Tyne, U.K.

November 2004

DECLARATION

I hereby certify that the content of this thesis is the original work of the author, except where otherwise acknowledged, and has not been submitted previously for a degree at this, or any other, university.

Mohamed Hrouda

Acknowledgments

I would like to thank my supervisor, Dr. Richard Tyson, for his help and guidance throughout this project, his constructive criticism and correction of my manuscript. I would like to thank my co-supervisor, Dr. Paul Farrimond for his help and guidance for the molecular geochemistry part of this project.

I would like to thank Petroleum Research center (PRC) for their financial support of this project. I wish to express my thanks to the general manager of the PRC Dr. Burima A. Belgasuem, exploration manager Dr. Mahmmud El-Bakai, administration manager Mr. Mahmmud El-Souri, Mr. Muhammed El-Teari, Mr. Ali El-Fetouri from NOC and Mr. Abuelsaoud Addaloush from AGCO for their support, advice and encouragement.

I would like to acknowledge the technical assistance provided by several people at NRG, namely Paul Donohoe, Ian Harrison, Rob Hunter, Trevor Whitfield, Dr. Mick Frank.

A special thanks to my wife, for her encouragements, support and patience during my study, my daughter Haneen, Ragad and Maryam to whom I owe a lot. My parents and family also deserve special thanks for their support and encouragements.

Abstract

Lower Silurian and Upper Devonian organic-rich "hot shales" are the source of almost all Palaeozoic oils in North Africa and the Middle East. They are also developed in the Ghadames Basin, and a better understanding of their organic facies character, maturity and their correlation to Palaeozoic oils of the basin is considered crucial for the future oil exploration strategy. Core and ditch cuttings samples from the alternating transgressive and regressive marine sandstone and shales of the Tanezzuft, Acacus, Tadrart, Ouan Kasa, Aouinet Ouenine, and Tahara formations are investigated using a combination of organic geochemistry, palynofacies and organic petrology.

The bulk geochemical results demonstrate the presence of various organic-rich horizons within the Silurian and Devonian formations. The total organic carbon (TOC) values are generally between 0.5 and 25.0%. The highest TOC values are measured within the dark-coloured non-bioturbated graptolitic "hot shales" of the Silurian lower Tanezzuft Formation (average 7%), and the Devonian Aouinet Ouenine Formation (average 2%); other formations such as Tahara Sandstone Formation contain some thin black shales interbeds that have an average TOC of 4.5%. Hydrogen indices (HI) are mostly below 450, 150-435 in the lower Tanezzuft Formation, and reaching 50-300 in the Aouinet Ouenine Formation. Palynofacies analysis permits the recognition of different organic facies: a terrestrially-dominated oxic facies in the Upper Devonian, oxic nearshore shallow marine to proximal shelf facies enriched in thin-walled prasinophyte algal phycomata (leiospheres) with low AOM and phytoclasts in alternating sandstone and shale of the Upper and Lower Silurian, and dysoxic-anoxic hemipelagic facies dominated by well preserved AOM (genetically oil-prone Type II kerogen) in the Lower Silurian lower Tanezzuft Formation 'hot-shale'. Results from 25 boreholes distributed throughout the basin indicate a significant spatial variation in the Silurian hot shales, including significant variation in gamma ray values, hot shale thickness and organic facies quality.

Maturity evaluation based on Tmax, SCI, ACI, $\%VR_E$, biomarker and aromatic hydrocarbon distributions for Lower Silurian lower Tanezzuft "hot-shale" source rock facies revealed a trend of increasing maturity from middle mature (oil expulsion zone)

in the north and south east to very mature (gas generation zone) towards the central and southwestern parts of the Ghadames Basin. The Upper Devonian samples are immature in the northern and south eastern parts of the basin and mature in the southwestern and central parts of the basin.

Oil-source correlations revealed that all the analysed Palaeozoic oils of the Ghadames Basin display similar facies features to the Lower Silurian Tanezzuft Formation source rock facies. Therefore there is a high probability that these oils were generated from the Lower Silurian 'hot-shale' source rocks. Maturity evaluation of the oil samples based on the biomarker and aromatic hydrocarbon ratios revealed that the oil samples collected from the oil fields located in the south and southwestern parts of the basin are more mature than the oil samples collected from the northern parts of the basin. This is consistent with the maturity trends of the source rocks of the Ghadames Basin.

Most of the Upper Devonian source rock samples have unusual proportions of the 20S isomers (relative to 20R isomers) of the C_{29} $\alpha\alpha\alpha$ steranes, with values of more than 55% 20S. Such high values could be due to factors other than maturity.

CONTENTS

CHAPTER 1.0

INTRODUCTION

1.0 INTRODUCTION

1.1 Background and objectives

Exploration for oil in the Palaeozoic of Libya started in 1957, with Exxon's small Devonian Atshan discovery located on the southwest extension of the Gargaf Arch. In the following few years several additional small discoveries were made, including Bir Tlacsin and Tigi to the north, Gazeil and Z1-66 in the central area, and the El Hamada field complex in the south. Because these oil and gas discoveries were small and uneconomic, attention shifted towards the Cretaceous and early Tertiary plays in the Sirt Basin. Subsequently, following successful Palaeozoic exploration by Lasmo, Repsol and Agip in northwest and southwest Libya, the region has again become a centre of exploration activity (Boote *et al.*, 1998). The sweet oil and gas of the later oil fields are most likely sourced from the Lower Silurian "hot" shales with perhaps a minor contribution from the largely immature Upper Devonian shales. Previous geochemical results (e.g. Hamyouni *et al.*, 1984; Rahoma *et al.*, 1994) indicate that the Silurian "hot shales" are important in Libya, as indeed are equivalent Silurian source rocks deposited on the Gondwana shelf in Algeria (Legrand, 1985b; Malla *et al.*, 1997), Saudi Arabia (Husseini, 1991; McGillivray *et al.*, 1992), southeast Turkey and northeast Syria (Ala *et al.*, 1979; Beydoun, 1988), Iran (Ala *et al.*, 1980) and Oman (Grantham *et al.*, 1988).

The Palaeozoic strata in western Libya have been a subject of intensive sedimentological and stratigraphical investigation (Klitzsch, 1969, 1970; Bellini & Massa, 1980; Belhaj, 1996). To date the geochemical and palynological data relating to hydrocarbon source potential remain rather few and scattered, with just a limited number of publications and internal reports. The geochemical data is insufficient and their resolution is poor (largely TOC, pyrolysis, and transmitted light microscopy on a small number of isolated samples). Further study using a combination of organic geochemistry and organic petrology analyses is therefore necessary for a more complete assessment of the potential of the basin.

The principal objectives of this thesis are to:

i. Evaluate the depositional controls on the accumulation and preservation of its organic matter
ii. Geochemically characterize the source rock facies in the basin
iii. Assess the vertical and lateral variations in organic matter assemblages with reference to depositional environment and proximal-distal variation.
iv. Determine the maturity gradients in the basin.
v. Identify the main source of the various oils in the basin.

1.2 Regional setting of Ghadames Basin.

The Ghadames Basin covers a large portion of northwest Libya (Fig.1.1), and extends across Libya's western international border into Algeria and Tunisia. On its south west flank is the Qarqaf Arch. The basin is bounded by the Gharyan-Nafusa Uplift in the north. Towards the east, most of the Ghadames Basin sedimentary section is completely covered by Mesozoic strata extending westward from the Sirt Basin. The Ghadames Basin generally is considered an intra-cratonic sag basin. It contains an estimated 4000 metres of predominantly Palaeozoic siliciclastic sediments. Subsequently, the basin was truncated by Mesozoic and younger sections.

The present day margins of the Ghadames and Murzuk basins are represented by structures uplifted during the Hercynian and Alpine orogenies (Klitzsch, 1970; Selley, 1997b). These structures do not define the extent of Palaeozoic depocentres, which were open toward the north (Fig. 1.2) and formed part of a regionally extensive Gondwana continental shelf (Klitzsch, 1981: Selley, 1997b; Boote *et al.*, 1998). The Palaeozoic depocentres parallel older Precambrian structural trends.

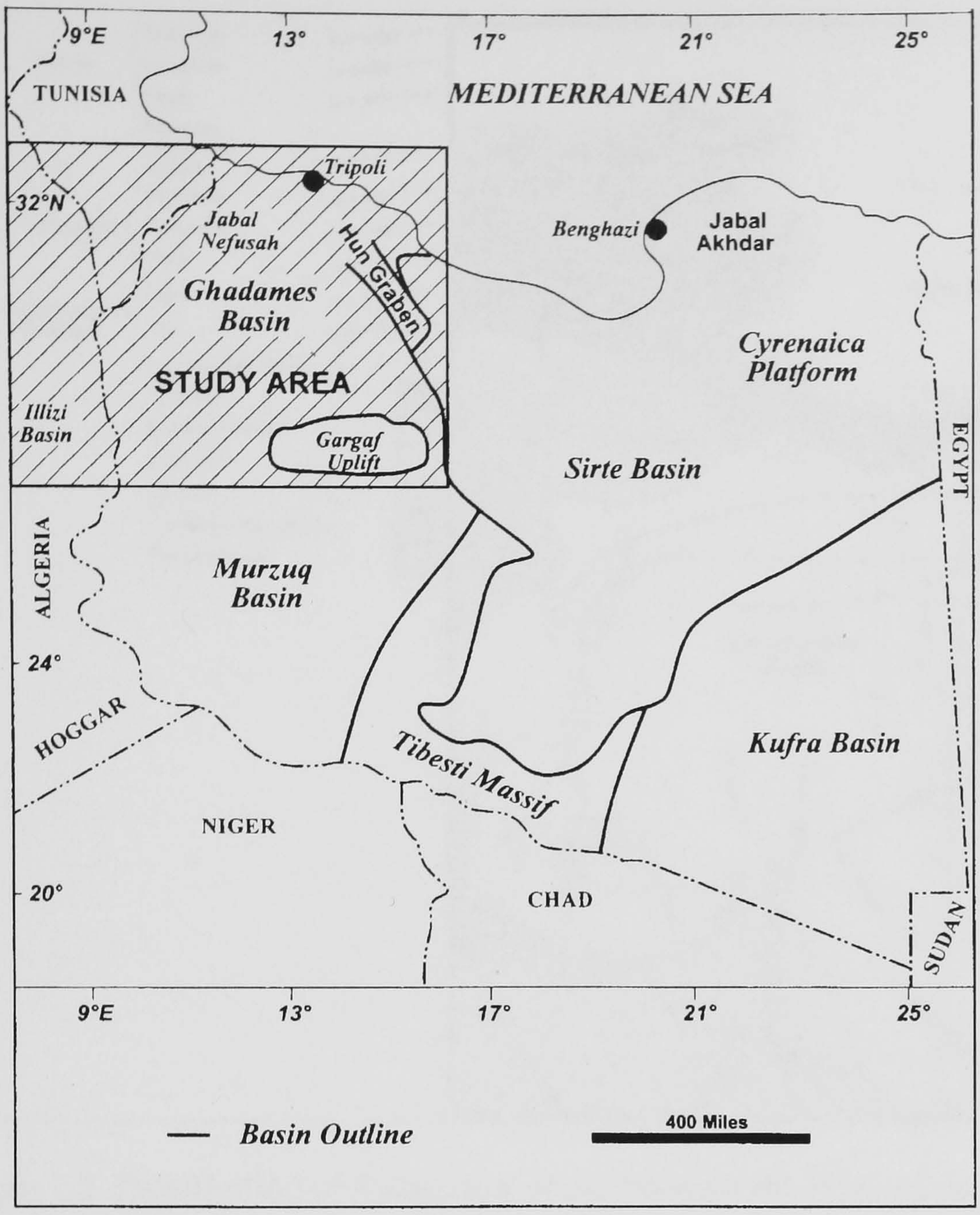

Figure 1.1. Location map of the Ghadames Basin (from Belhaj, 2000).

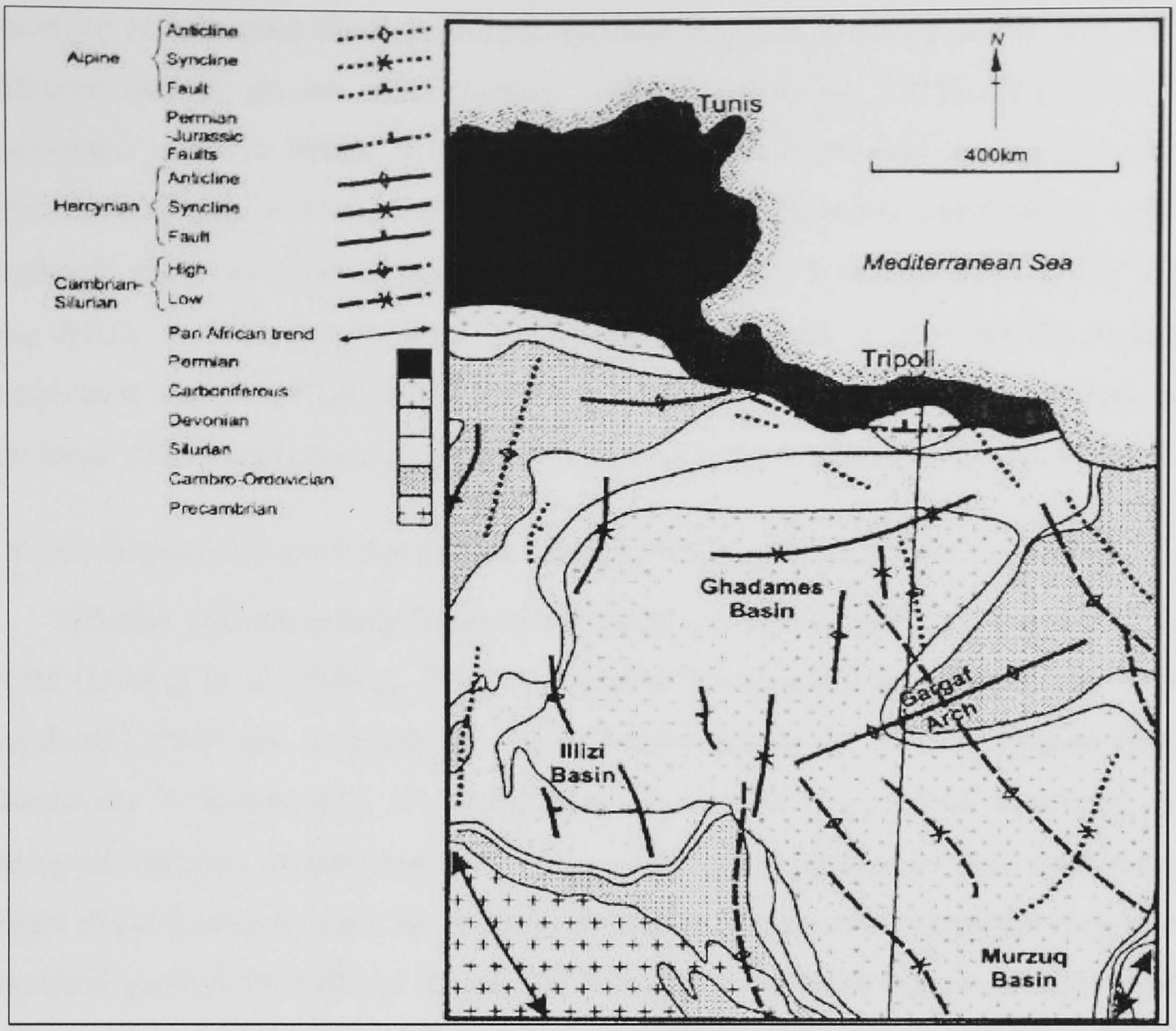

Figure 1.2. Distribution of Palaeozoic rocks beneath the Hercynian unconformity (from Sutcliffe *et al.*, 2000).

1.3 Silurian-Devonian Stratigraphic and Sedimentological Models

In North Africa the Lower Silurian is represented by a widespread hemipelagic shale unit, deposited during a major transgression (Fig. 1.3) following the melting of the late Ordovician ice cap (Husseini, 1990; Lüning *et al.*, 2000a; Fig. 1.4). Many continental shelves were flooded and dysoxic-anoxic conditions developed immediately after (Dabard & Paris, 1986). During the Silurian, Gondwana was moving northward to mid-palaeolatitudes and intense oceanic upwelling and palaeo-organic productivity occurred at its northern margin (Paris & Robardet, 1990; Moore *et al.*, 1993). Furthermore, the absence of ice allowed thermal stratification of the water column to be maintained (Moore *et al.*, 1993). The initial early Silurian transgression was replaced by deposition of prograding sand-rich deltas during the late early and late Silurian (Bellini & Massa, 1980). Late Silurian-Early Devonian

tectonism re-organised the depositional systems to create localised palaeo-highs and sediment sources on the shelf (Belhaj, 1996; Boote *et al.* 1998). The Devonian continental shelf in North Africa had a low gradient and low subsidence rates, typically resulting in limited accommodation space. Therefore, even during small-amplitude sea-level changes, palaeoshorelines were capable of migrating rapidly over long distances. This also implies that organic facies ought to be relatively uniform everywhere that stratification occurred (i.e. where the water was deep enough) but that rapid widespread changes could occur as a result of temporal watermass changes.

1.3.1 Geological Evidence for Dysoxic-Anoxic Palaeoenvironments

Silurian dysoxic-anoxic black shale facies are known from many parts of the world (Lüning *et al.*, 2000a). The most intense Silurian anoxic event on the North Gondwana shelf was restricted to a short period during the earliest Silurian (early Llandovery = Ruddanian). The mechanism by which organic-rich sediments are deposited remains controversial; however, petroleum geologists will continue to regard dysoxic-anoxic black shale facies as their major source rock prospect because empirical geological evidence shows that these facies have the highest content of oil-prone organic matter and produce the greatest yields of hydrocarbons (Tyson, 1995, p. 122). A brief summary of the some criteria being used to support the interpretations for the dysoxic-anoxic depositional conditions of the Lower Silurian 'hot-shale' is given in Table 1.1.

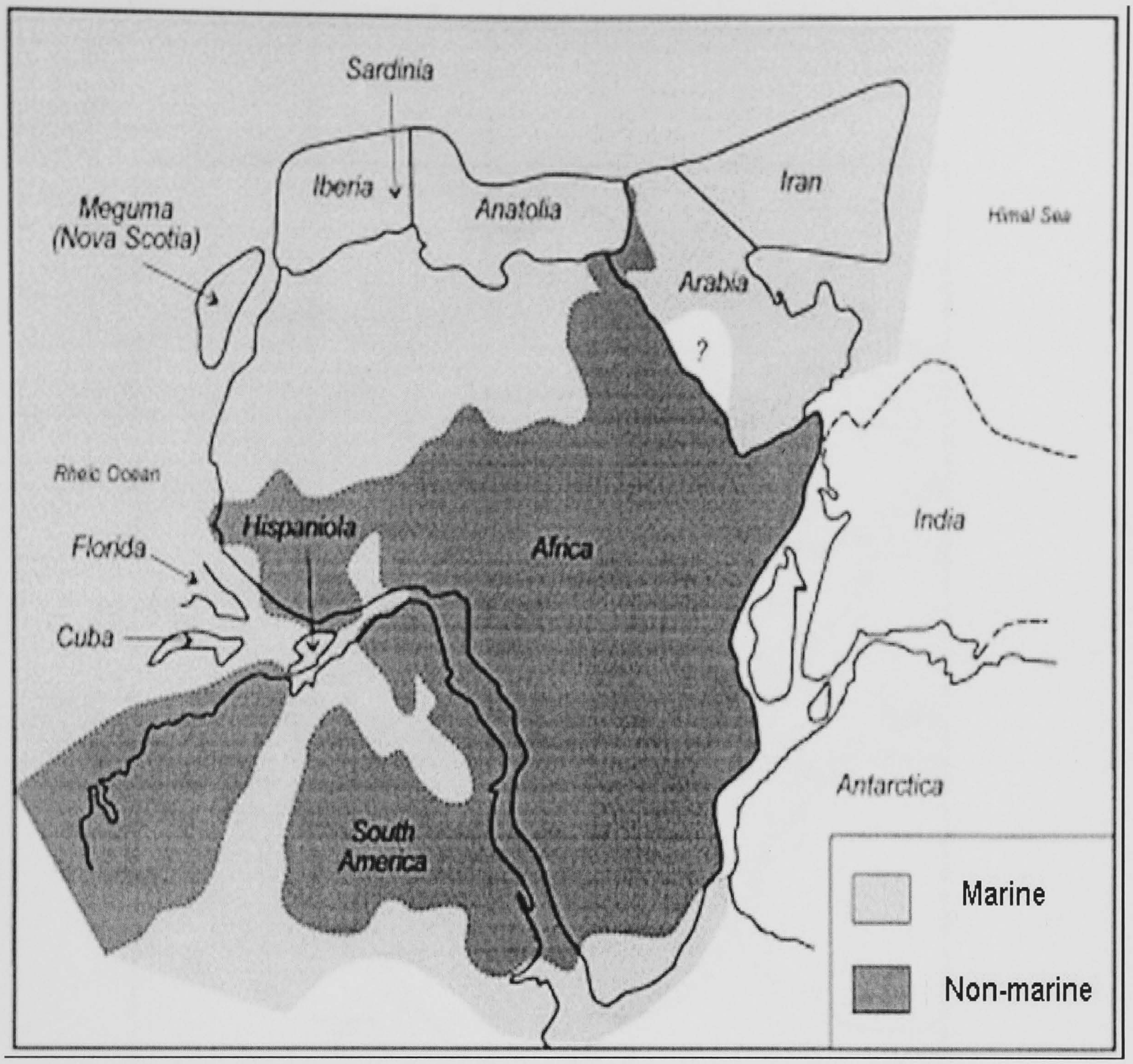

Figure 1.3. Early Silurian palaeogeographic map of Gondwana (from Lüning *et al.*, 2000).

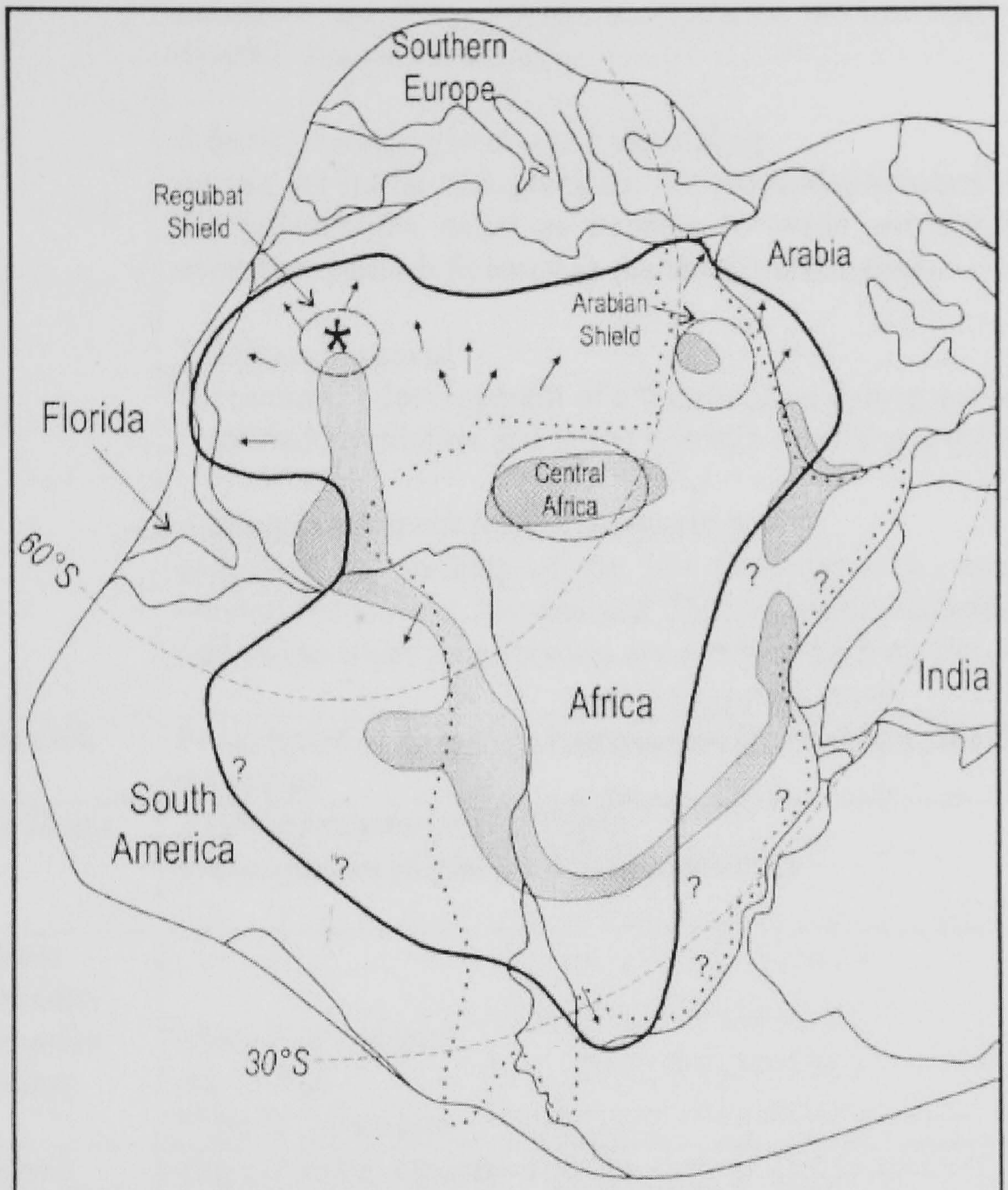

Figure 1.4. Late Ordovician palaegeographic reconstruction of West Gondwana (from Sutcliffe *et al.*, 2000b).

Sedimentology	Graptolitic Black shale Finally laminated
Palaeoecology	*1-North Gondwanan upwelling* resultant high flux of organic matter to the sea floor may have created dysoxic-anoxic conditions. *2-Initial transgression and basin silling* during the initial transgression, the palaeodepressions were flooded while the palaeohighs acted as barriers to water circulation, enhancing the overall oxygen-deficiency in the shelf watermasses. 3-*Seasonal anoxia* the recurrent development of a thermocline during the summer caused restricted circulation and led to dysoxia-anoxia and enhanced preservation *4-Postglacial fresh water stratification* following the melting of the late Ordovician ice cap much freshwater entered the earliest Silurian sea. Due to density differences between fresh and saline water stratification occurred, enhancing the oxygen deficiency.
Ichnofossils	Progressive reduction in bioturbation (ichnofossil abundance, size and diversity)
Organic facies	AOM-dominated assemblages prasinophytes of plankton often dominant
Organic geochemistry (of immature sediment)	TOC:3–6% range HI : ≥ 500 Type II–I kerogen
Inorganic geochemistry	High uranium content Increase formation of smaller pyrite framboids that are less variable in size

Table 1.1. Geological criteria being used to support the interpretations for dysoxic-anoxic palaeoenvironment of the Lower Silurian shale (Based on Lüning *et al.*, 2000a).

1.3.2 Silurian succession

Silurian rocks are widespread in Libya. In the Ghadames Basin they are formally grouped into a lower clay-rich unit and an upper, sand-rich deltaic unit, the Tanezzuft and Acacus formations, respectively. The Silurian sediments are generally conformable on the Ordovician Memouniat Formation (Fig. 1.5).

Tanezzuft Formation

The Tanezzuft Formation (up to 700m thick) represents a deep marine shale, defined at its base by graptolitic claystones and shales that are intercalated with hummocky cross stratified or current-rippled siltstones to fine-grained sandstones (Bellini & Massa, 1980; Klitizsch, 1981). Desio (1963) was the first to describe these shales from a locality 100 km north of Wadi Ayadhar in the Murzuq Basin, but it was Klitzsch (1969) who first proposed the type section of Tanezzuft Formation near Wadi Ayadhar. He included the whole sequence of shales that overlie the Memouniat sands of Late Ordovician age and underlie the Akakus Formation of Middle-Late Silurian age. The lowermost rocks of this formation onlap a palaeotopography (Klitzsch, 1968) and tend to be organic-rich shales, probably deposited under a stratified water column with anoxic to dysoxic bottom-waters. Core samples from Silurian strata in western Libya have previously yielded excellent assemblages of graptolites and miospores. Massa and Collomb (1960) and Collomb (1962) reported graptolites from Tanezzuft Formation assignable to zones 18–22 of the British Llandoverian. Hoffmeister (1959) reported *Ambitisporites* as the then oldest known trilete spores from Tanezzuft Formation in the Murzuq Basin. Berry (in Gray & Boucot, 1971) assigned these spores to the Llandoverian on the basis of graptolites. Richardson and Ioannides (1973) reported a diverse assemblage of miospores, acritarchs and chitinozoans associated with graptolites from the Silurian of NW Libya. They concluded that their assemblages were of latest Wenlockian-Ludlovian age. The above information suggests that the Tanezzuft Formation ranges in age from Llandoverian in the Murzuq Basin and southern portion of the Ghadames Basin, to Wenlockian or Early Ludlovian in the Ghadames Basin, which reflects a northward regression during the Silurian.

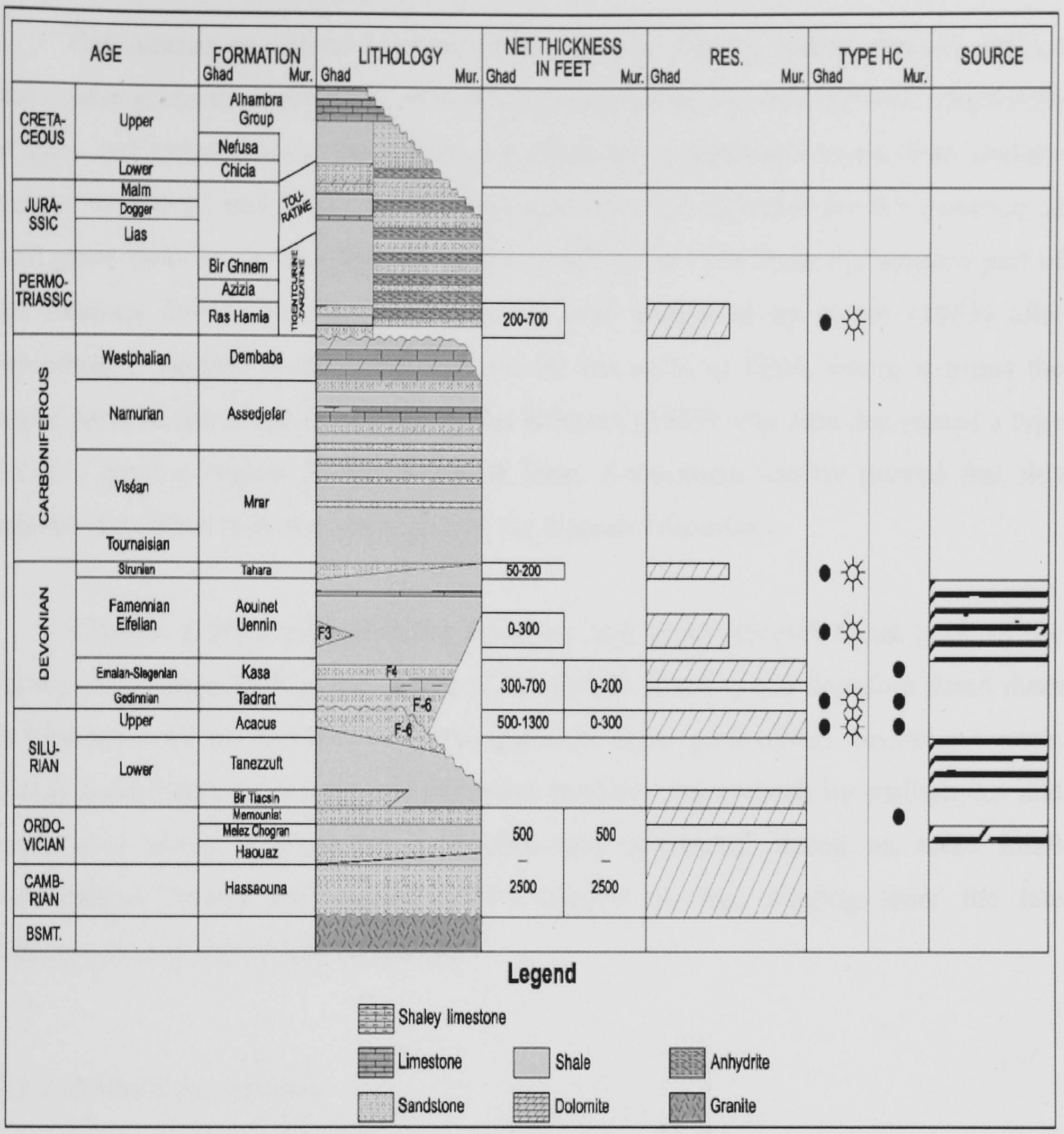

Figure 1.5. General stratigraphic section of the Ghadames Basin northwestern, Libya.

Acacus Formation

The Acacus sandstone consists of ferruginous, fine to coarse grained, rippled and coarse grained, rippled and cross-bedded sandstone, intercalated with minor beds of grey and green shales. The lithofacies document a regressive trend from shallow marine to littoral and finally continental environments indicated by the presence of land plant remains. It was first described by Kilian in 1928 from the western part of the Murzuq Basin, but the name Acacus was suggested by Desio (1963) after describing a section in the Jabal Acacus, 50 km north of Ghat, where it forms the upper parts of the range. However, it was Klitzsch (1969) who first designated a type section, from a region 50 km south of Ghat. Subsequent studies proved that this section represents only the lower part of the Acacus Formation.

Klitzsch (1969) compared the *Harlania* and graptolite-rich basal parts of the Acacus Formation with zones 19–20 0f the British Silurian and therefore dated them as Llandoverian. In the eastern Murzuq Basin the upper parts of this formation contain a rich assemblage of lower vascular plant remains, represented by psilophytes and lycophytes along with marine graptolites and acritarchs. Based on these fossil assemblages Massa and Jaeger (1970) suggest an age ranging from the late Llandoverian to the earliest Siegenian.

1.3.3 Devonian succession

Devonian rocks are exposed along the margins of the Ghadames Basin. In the central part of the basin a nearly complete sequence of Devonian rocks can be found. Lower, Middle and Upper Devonian strata are recorded (Fig.1.5). The lower boundary of this sequence is a major regional unconformity, the "Ardennian unconformity" which is present in most Palaeozoic basins in North Africa (Belhaj, 1996).

Tadrart Formation:

The Lower Devonian strata of the Tadrart Sandstone are variable in thickness (approximately 400m) and include both continental and marine silciclastics. Colomb (1962) introduced the term "Gres de Tadrart" after the Tadrart Hills in the western parts of the Murzuq Basin. Later workers adopted the name Tadrart Formation. It is composed of massive and cross-bedded sandstone interbedded with minor ferruginous

claystones. The upper part is characterized by thin laminations of fine-grained sandstone and siltstone, which is rich in fossil wood debris (Mamgain, 1990). In the Ghadames basin subsurface, the Tadrart Formation has been reported to contain well-preserved miospores and plant debris. On the basis of stratigraphic position and palynological analysis, the age of this sequence is considered to range from Siegenian to early Emsian (Massa & Moreau-Benoit, 1976).

Ouan Kasa Formation

The Ouan Kasa Formation (10–120m thick) is characterised by a succession of intercalated siltstones, claystones and fine-grained sandstones that rest conformably on the Tadrart Formation. The Ouan Kasa Formation was deposited during a modest transgression of the early Devonian seas in the Murzuq and Ghadames basins. The presence of ferruginous oolites and ripples at different level of the sequence suggest a constant turbulence movement of water. A full-marine fauna is preserved, along with many oolitic horizons. Bioturbation is common. The Ouan Kasa Formation is Emsian in age (Mergl & Massa, 1992).

Aouinet Ouenine Formation

The Upper Devonian section is divided into five cycles of alternating shale, siltstone and sandstone. It is contains both radioactive shale and limestone. The Aouinet Ouenine Formation includes the lower four cycles. The fifth and upper cycle is the Tahara Formation. The term Aouinet Ouenine was first introduced by Lelubre (1946) based on a borehole in the western part of Jabal Gargaf in Fazzan (southern Libya). The Aouinet Ouenine Formation (up to 300m thick) has an unconformable to disconformable base. It is characterised by stacked coarsening-upward cycles 20–50m in thickness comprising intercalated, bioturbated siltstones and shales that grade upward into medium-grained cross-bedded sandstones. These cycles preserve a marine fauna and ichnofauna. The age of Aouinet Ouenine Formation ranges from Eifelian to Famennian (Massa *et al.*, 1976; Banerjee, 1980; Belhaj, 1996).

Tahara Formation

In the subsurface of the Ghadames Basin, the uppermost Devonian is represented by sandy and shaley facies with frequent lateral variation in lithology. The type section is in the Wadi Tahara. The unit was first described by Massa and

Moreau-Benoit (1976) as a 50–70m thick succession of fine-grained sandstone with frequent ferruginous levels, interbedded with shales. Seidl and Rohlich (1984) pointed out that this formation should be included in the Aouinet Ouenine Group, because it originally was a part of that unit. According to Bellini and Massa (1980) the deposition of this unit took place in a deltaic environment, under substantial continental influence as indicated by the presence of lycophytic debris. El-Rwemi (1991) reported the presence of minor amounts of pyrite and glauconite as indicators of very slow sedimentation.

Palynological analysis of core samples from the Ghadames basin carried out by Massa and Moreau-Benoit (1976) attribute this formation to Palynozone II, which corresponds to the uppermost Famennian.

1.4 Previous Geochemical work on North Africa and the Middle East

The Lower Silurian siliciclastic sediments form a progradational sequence that was deposited on a broad continental shelf of Gondwana during deglaciation of the Gondwanan polar ice cap (Fig. 1.6; Ziegler *et al.*, 1977; Bellini & Massa, 1980; Spjeldaes, 1981; Husseini, 1990, 1991, Mahmoud *et al.*, 1992). In the Middle East and North Africa, "hot" shales typically occur at the base of the Silurian shale unit and form an important regional source rock (Mahmoud *et al.*, 1992; Aoudeh & Al-Hajri, 1995). These "hot" shales are interpreted to have formed synchronously during the initial transgression in palaeodepressions (e.g. Aoudeh & Al-Hajiri, 1995), such as incised valleys of the preceding lowstand, or within intrashelf basins. Areal distribution of this organic-rich unit, therefore, is laterally highly variable. The Silurian shale is traceable over large area of North Africa and Arabia and is bound by unconformities of interregional scale (Wolfart, 1981; Destombes *et al.*, 1988, Mahmud *et al.*, 1992; Fig. 1.7).

The radioactive shale zones in North Africa show a great continuity of facies over a very wide area. These illite-dominated shales have a high uranium content, with abundant organic matter and pyrite. The marine microfossils that are present are very abundant but show little diversity. They are mainly the prasinophyte algae,

acritarchs, chitinozoans. The conditions of deposition of these sediments seem to be controlled by the circulation of oceanic waters and the emplacement, in shallow water, of dysoxic-anoxic water between the ventilated surface layer and the oxygenated deeper water originating from the melting of polar ice (Combaz, 1986).

In Libya, the entire Lower Silurian shale unit reaches a maximum thickness of 700m in the north west Libyan Ghadames Basin (Klitzsch, 1995) and 500m in the south west Libya Murzuk Basin (El-Arnauti *et. al.*, 1988). In the Ghadames Basin several radioactive shale units in the lower Tanezzuft Formation have been identified; these shales were deposited in an open marine outer neritic environment, indicated by presence of abundant of acritarchs and chitinozoans, and are biostratigraphically assigned to the Llandoverian (Belhaj, 1998). Many wells in the Murzuk and Ghadames basins contain hot shales with thicknesses of up to 25m at the base of the lower Silurian shale unit. The alternating shale and siltstone of the upper Tanezzuft Formation shows little stratigraphic variance in contained organic matter, and typically consists of a poor to fairly gas-prone shale, with a mean TOC of 0.66 wt.% (Hamyouni *et al.*, 1984; Rahoma *et al.*, 1994).

Based on a regional geochemical study of more than 800 cutting samples from Ordovician-Carboniferous successions from 11 wells located in the eastern part of the Ghadames Basin, eastern Tunisia and north west Libya, Hangari *et al* (2000) reports that the Tanezzuft Formation in wells AMC-1, EBP-1, and C1-NC100 display fair to good source rock potential. The average total organic carbon (TOC) and hydrogen index (HI) values range from 2.0 to 8.2 wt%, and 237 to 403 respectively. Microscope examination of samples from the organic-rich zone indicates that they contain predominantly amorphous organic matter (AOM); and spore colour index (SCI) and Tmax values that correspond to the main oil generation zone.

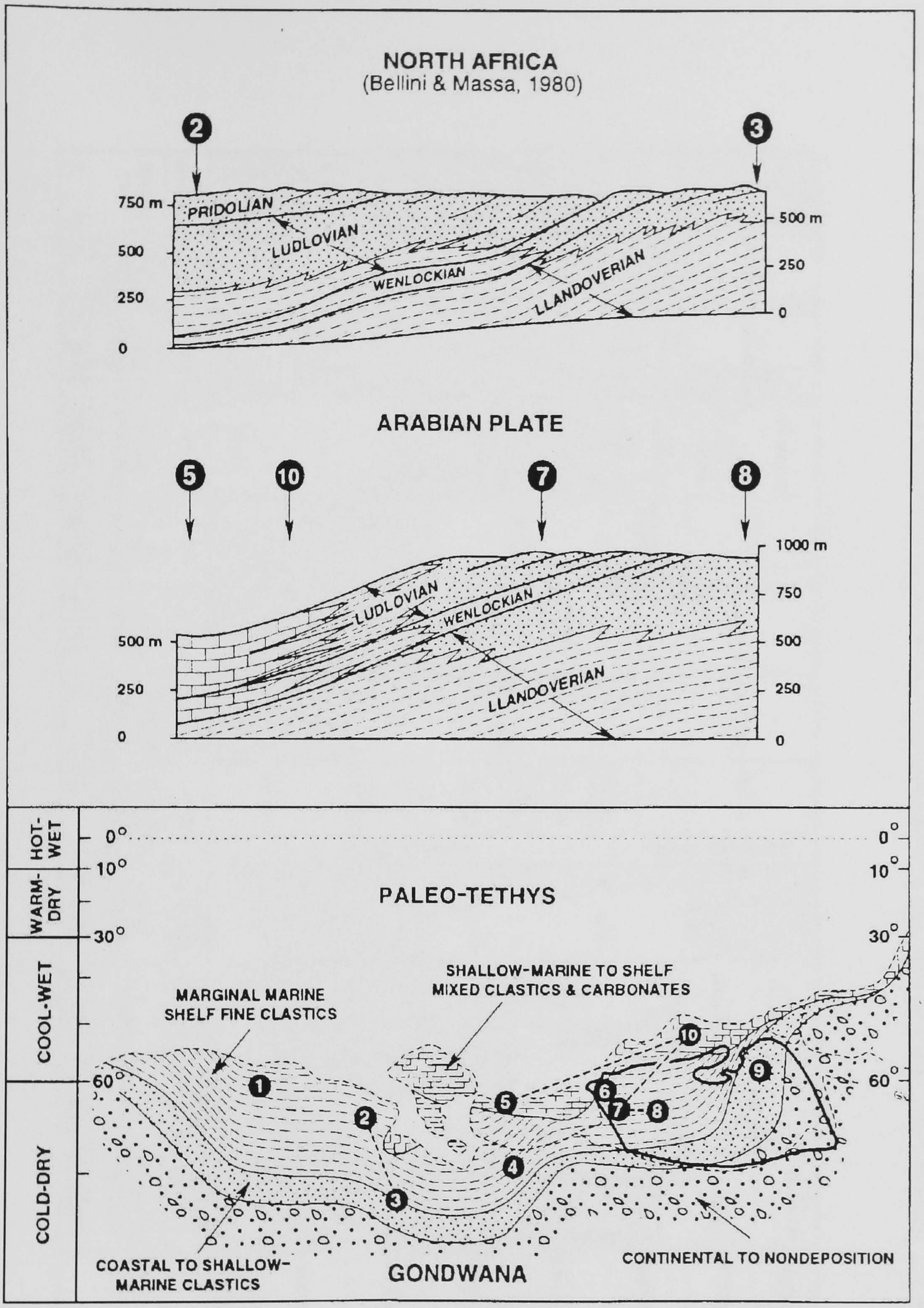

Figure 1.6. Early Silurian palaeogeography, climate, and associated environments of deposition (from Mahmoud *et al.*, 1992).

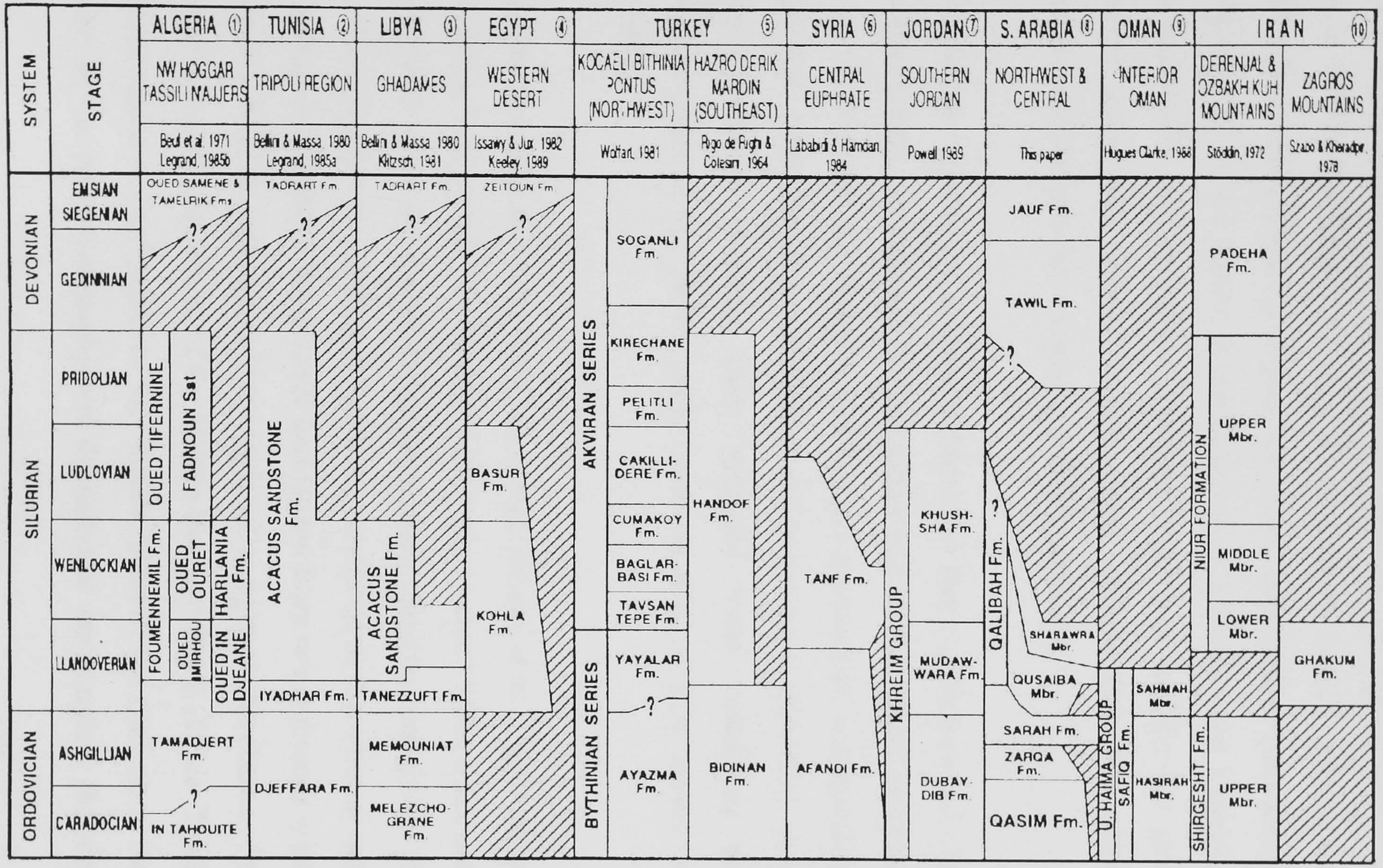

Figure 1.7. Stratigraphic correlation of the Lower Palaeozoic rocks of the Gondwana margin (from Mahmoud *et al.*, 1992).

Malla *et al.* (1997) report that the equivalent Silurian hot shales from south-eastern part of Algeria are organic-rich and have excellent oil-generating potential, (TOC values between 2% and 16%). The richest zone is located on the northern flank of the Ghadames Basin where the TOC values increases progressively from 8% in Bir Berkin, to 12% in Bir Rbaa, 14% in El Borma and 16% north of El Borma. Malla *et al.* (1997) also reported that the richest zone of Lower Silurian hot shales in the Illizi Basin is situated in the south, in the direction of Tinfouye and Irlalene, where the TOC exceeds 8%. Microscopic examination indicates that the hot shale kerogen consists of amorphous organic matter, algae, chitinozoans and graptolites; the *Tasmanites*-rich horizons have higher petroleum potential.

In eastern Algeria, the Barkine (Ghadames) Basin includes basal Llandoverian-Wenlockian (25m) and Frasnian (120m) source rocks. The richest samples have TOC values up to 10% and HI values up to 550 that correlate well with gamma ray values of >100 API. This facies is interpreted as having been deposited under oxygen-deficient conditions resulting from restricted water circulation and density stratification (Yahi *et al.*, 2001), partly based on plots of TOC versus total sulphur (Yahi, 1999).

Subsurface data from Central Arabia (McGillivary *et al.*, 1992) indicate that the Silurian shale, here termed the Qalibah Formation, is about 950m thick and deposited disconformably over the Upper Ordovician-Lower Silurian periglacial Zarqa-Sarah siliciclastics. The Lower Silurian sequence is described in the outcrop near the town of Al Qalibah in the North West Saudi Arabia, and from two reference wells in central Saudi Arabia. Silurian graptolites faunas indicate a regional correlation of the Qalibah to the equivalent Silurian facies of the Middle East and North Africa. Thickness maps indicate the regional distribution of the various facies of the Qalibah in Saudi Arabia in relation to the palaeogeography and depositional environment (Mahmoud *et al.*, 1992).

A high-resolution chitinozoan-based biostratigraphic study of the Lower Silurian in Saudi Arabia was carried out by Aoudeh and Al-Hajri (1995) who also integrated biostratigraphic graptolite data. On basis of 27 datasets from wells and outcrops, Aoudah and Al-Hajri (1995) were able to show the diachronous nature of

the basal Silurian shales and demonstrated the close links that exist with trends in organic richness and the onset of early Silurian shale deposition. The main hot shale unit in Saudi Arabia occurs at the base of the Silurian shales succession and is dated as early Rhuddanian (*S. fragilis* and early *B. postrobusta* chitinozoans zones, *acuminatus* and lower *atavus* graptolite zones) which represents the earliest Llandovery (Fig. 1.8).

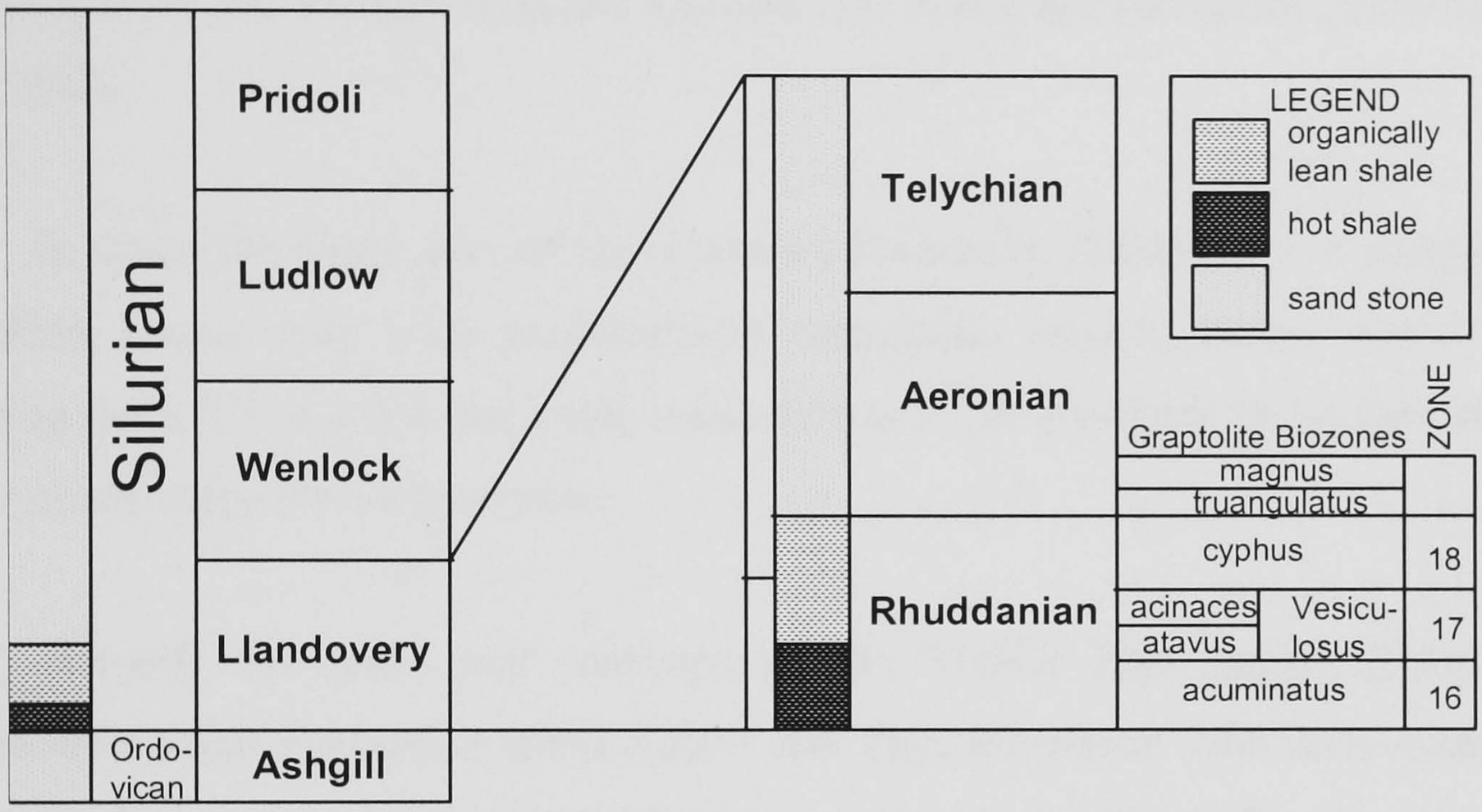

Figure 1.8. The Lower Silurian stratigraphy and graptolite biozones with the stratigraphic position of potential hot-shale units in North Africa and Saudi Arabia (after Lüning *et al.*, 2000a).

The Qusaiba Member of the Qalibah which is about 600m thick, consists of two distinct units. The lowermost is radioactive hot shale deposited during the maximum flooding event. These shales are dark grey to black, organic-rich with a maximum TOC content of 6.2%. Overlying the hot shale unit is a thick sequence of non-radioactive, light to medium grey shale that is poorly to moderately organic-rich. The hot shale unit attains a thickness of only 20–70m but is developed regionally (Mahmoud *et al.*, 1992). It is possible to trace this source rock horizon on well logs throughout the Middle East using a cut-off value of 150 API gamma-ray units to distinguish it from non-source shale (Cole *et al.*, 1994; Jones *et al.*, 1999). Cole (1994) reports that the basal Qusaiba "hot" shales of the Lower Silurian, from wells located across the central and northern part of Saudi Arabia contained good to excellent organic richness (average TOC of 4.1%, n = 352), with a maximum TOC of

20.1%. Monnier (1990) cites TOC values of 2.0 to 6.2% for a number of black shale samples at the base of Qusaiba Member in the Hawtah-1 well of central Arabia.

The gas chromatography-mass spectrometry selected-ion monitoring techniques for detecting sterane, terpane and monoaromatic and triaromatic steroids show that all biomarkers occur at very low concentrations in Palaeozoic Arabian super-light crude (Mahmoud *et al.*, 1992). But that the C_{27}–C_{29} steranes and diasteranes of the Palaeozoic oil and extracts from the Qusaiba Hot shales are correlated (Mahmoud *et al.*, 1992).

In Qatar the lower part of the Sharawra Formation (Silurian) is a marginal to excellent source rock with predominantly sapropelic organic matter and a TOC ranging from 0.5 to 7.0%; the shale currently has a low pyrolysis yield, indicating a post mature stage for oil generation.

Towards the north and northeast of the Middle East region (Syria) the Palaeozoic Swab Formation (Ordovician) and Tanf Formation (Silurian) consist of graptolitic shales interbedded with siltstone and sandstone. The shales reaches up to 1200m within a depression in central Syria with intervals of organic-rich shales a few metres thick scattered throughout the section and somewhat richer in the Tanf than in the Swab formations. The low hydrogen indices and high Tmax values indicate that the organic matter is mature, especially in the Swab Formation (Best *et al.*, 1993; Alsharhan *et al.*, 1997).

Beydoun (1988) states that the Silurian graptolitic hot shales of the Jordanian Mudawrra Formation are believed to be the best potential source rock for Risha gas, having a TOC ranging from 0.8–1.3%. Based on subsurface correlations of the Silurian rocks of eastern Jordan, Al-Haba *et al.* (1994) concluded that the Silurian rocks may be up to 2,000 m thick in the Rutbah-Ga'ara Uplift area of the Western Desert of Iraq. In the Akkas-1 well the Lower Silurian marine "hot" shale, is up to 65m thick, and is believed to be the main Palaeozoic source rock in the Western and southwestern Deserts (Aqrawi, 1998).

In the Zagros Basin of southwest Iran a highly mature Silurian hot shale with 3% TOC has been recognized at the base of Gahkum Formation (Alsharhan *et al.*, 1997).

In the southeastern part of Turkey the Dadas Formation of upper Silurian-Lower Devonian age is divided into members I to III (Alsharhan *et al.*, 1997). Member I has a thickness ranging from 49 to 101m of shale with argillaceous limestone bands; it has TOC values of 1.7 to 5.0% and a mixture of Type II and III kerogen. The presence of C_{25} alkanes and abundance of C_{29} steranes relative to C_{27} steranes are characteristic of terrestrial organic matter. Member II has a thickness ranging from 5.5 to 317m of shale, with limestone and sandstone intercalations and a few significant potential source intervals with Type II kerogen. The lower member III consists of shale and sandstone intercalations, with thin dolomite, limestone and marl interbeds ranging in thickness from 22 to 113m; it has excellent source potential with a TOC range of 1.7 to 5.0% and Type II kerogen with some Type III terrestrial organic matter (Alsharhan *et al.*, 1997).

This review shows the Arabian plate during Silurian time occupied a paleogeographic position similar in depositional strike to southwestern Libya along Gondwana's northern shelf. The depositional model of the Lower Silurian Tanezzuft Formation can be extrapolated through Middle East region into Algeria and Tunisia

CHAPTER 2.0

METHODS

2.0 METHODS

2.1 Sampling

2.1.1 Sampling Strategy

The sampling strategy for this project was based on that described in Tyson (1995). Wells were selected according to the shale contents of the cored interval, and their stratigraphic and geographical location chosen in order to give adequate coverage of the Silurian Devonian succession and provide information on north-south and east-west variation. The samples were taken from cores and cuttings from twelve oil-producing wells (Fig. 2.1 & Table 2.1). For palynofacies and biomarker analyses only core samples were selected. The lithology of the samples is mainly fine-grained but varies from shales to silty shale and siltstone (Appendix I). In addition, seven oil samples from different oil fields throughout the basin were collected for molecular geochemistry.

2.1.2 Sampling Method and Sample Description

The core and cutting samples were washed with water to remove drilling mud and other contamination and placed in an oven (at 30°C) and left overnight to dry. The core samples were described in hand specimen and the parameters listed below (after Tucker, 1982) were recorded. Shale samples from ditch cuttings were manually picked for bulk geochemical analysis; about 5–10g from all samples were powdered using an Electronic Mortar Grinder and then transferred to labelled vials.

A) Colour (using the GSA Rock Color Chart)
B) Presence or absence of sedimentary structure (e.g. lamination)
C) Any conspicuous minerals (e.g. mica flakes, pyrite)
D) Fossils (type, abundance)
E) Presence or absence of bioturbation
F) Presence or absence of graptolites

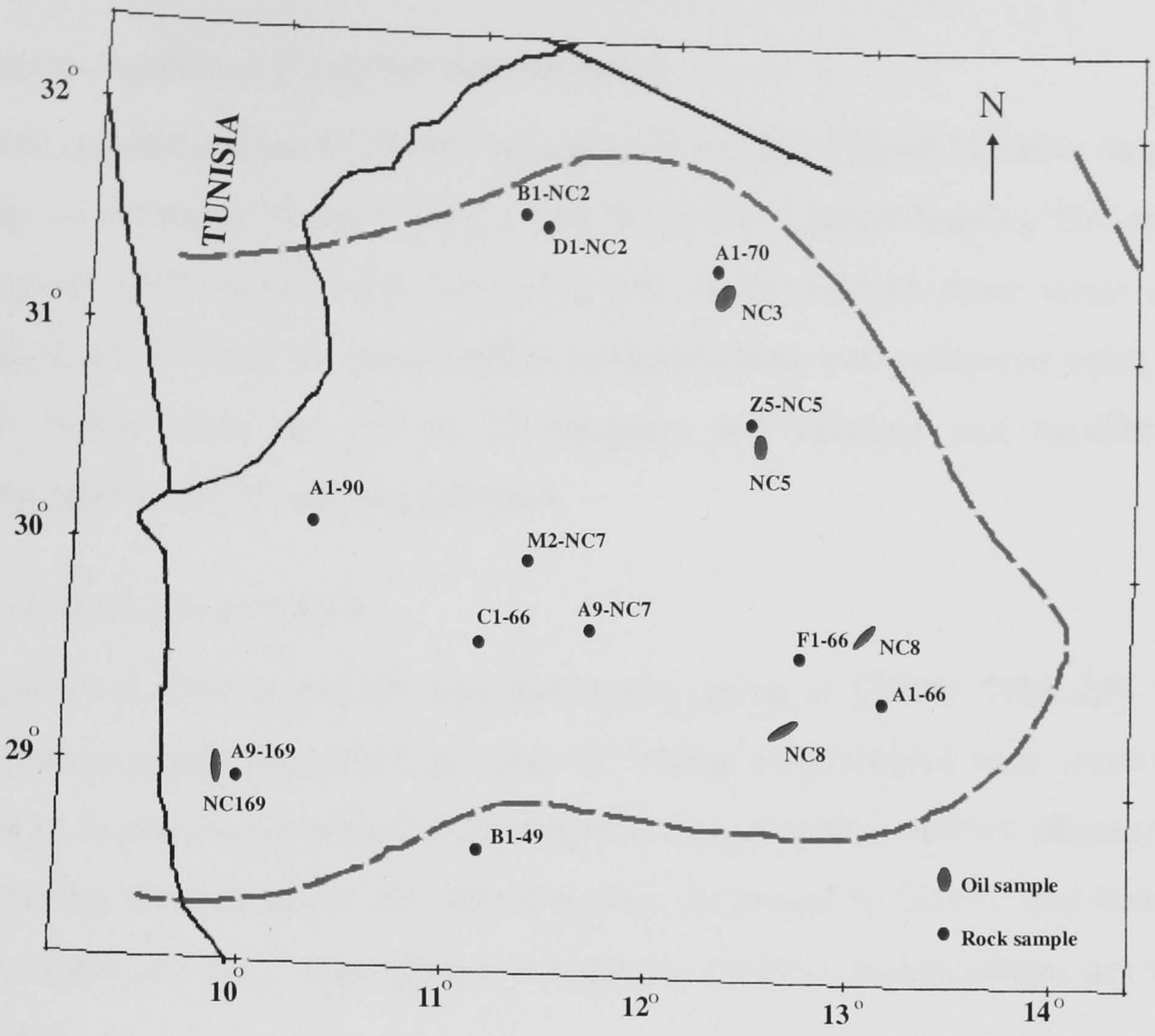

Figure 2.1. Location map for the wells studied.

Formation	Wells										
	F1-66	A1-66	B1-49	C1-26	M2-NC7	A9-NC7	A1-90	Z5-NC5	A1-70	D1-NC2	B2-NC2
lower Tanezzuft hot-shale	***11***	***1***									
	5		11		9		3	4	11	14	
upper Tanezzuft cool-shale	***3***	***8***	***2***				***4***	***7***	***12***		***6***
	6		12		10		11	8	8		
Acacus							***2***	***1***	***4***		
Tadrart	***1***										
Ouen Kasa		***2***							***1***		
Aouinet ouenine (A)					***2***				***1***		
									11	10	
Aouinet ouenine (B)		***1***									
					6						
Aouinet ouenine (C)		***2***	***8***	***8***							
	7		14		13		16				
Tahara	***1***				***3***	***16***	***2***				
			3								

Table 2.1 Sample distribution and types. Key: ***core***, cuttings.

2.2 Bulk geochemical methods

2.2.1 Organic carbon and sulphur determination

Total organic carbon (TOC wt.%) and total sulphur (TS wt.%) were determined on 100mg of powdered sample using a LECO LS-244 Carbon Sulphur Determinator. The samples were treated with 37% HCl and water washed three times and left overnight at 60 °C. Prior to measurement the instrument was calibrated using 5 to 10 standards before each run (20 to 25 samples) and checked and recalibrated, if necessary, after every 7th sample analysed.

2.2.2 Rock-Eval type pyrolysis

Rock-Eval type pyrolysis was performed using a LECO THA-200 thermal hydrocarbon analyser. Duplicate portions of 100mg of powdered rock were run and subjected to the following temperature programme (consisting of three phases):

1. During the first phase the temperature is increased to 100 °C and held at this temperature for 1 min. During this phase, gaseous hydrocarbons are released (S0).
2. Temperature is then increased at 25°C/min to 300°C where it is held for 2 minutes while the semi-volatile liquid and gaseous free hydrocarbons are released (S1).
3. The temperature is finally increased further at 25°C/min to 550°C, where it is held for 1.5 min. During this third phase the non-volatile organic matter, consisting of kerogen, heavy resins and asphaltenes, is pyrolysed and hydrocarbons are produced (S2).

The following parameters are measured by the LECO instrument; note that this device does not measure the S3 (oxygenated compound) peak (cf. Peters, 1986; Bordenave *et al.*, 1993):

- S0 = The amount of free gaseous hydrocarbons (HC) trapped in the rock matrix and released at approximately 100°C (mgHC/g of sediment).
- S1 = The amount of free liquid hydrocarbons in the rock matrix, distilled and released at approximately 300°C (mg HC/g of sediment).
- S2 = Hydrocarbons expelled from the cracking of kerogen, heavy resins and asphaltenes at 300 to 550°C. The S2 peak corresponds to the residual genetic hydrocarbon potential of the rock (mg HC/g of sediment).

- Tmax = The temperature (°C) at which the S2 peak reaches its maximum, which reflects mainly the thermal maturity of the sample, but also the kerogen type. The more mature the sample, the higher the temperature (activation energy) required to crack the remaining kerogen and heavy compounds (Bordenave *et al.*, 1993).

The Hydrogen Index (HI) of a rock is calculated from the S2 and TOC:

$$HI = S2/TOC \times 100 \text{ (mg HC/g TOC)}$$

According to Peters (1986), problems may arise when interpreting Rock-Eval derived parameters on samples with less than 0.5% TOC. Bordenave *et al.* (1993) give a lower significant limit of 0.3% TOC. This is because the kerogen pyrolysate is often adsorbed by the mineral matrix, resulting in erroneously low S2 and HI parameters and an erroneously high Tmax parameter (Peters, 1986; Bordenave *et al.*, 1993). This is particularly the case because the organic matter in low TOC samples is often terrestrial or poorly preserved, and thus has a low S2 yield. Various corrections for this matrix effect have been proposed:

- Comparison with pyrolysis results made on kerogen isolates (Peters, 1986), but this is time consuming, and accurate estimation of the TOC of pure organic matter can be difficult.
- Plotting TOC vs. S2 to determine the mean HI from the slope of the regression (Langford & Blanc-Valleron, 1990), but this is also influenced by changes in kerogen type as TOC increases.

2.3 Transmitted and blue light fluorescence microscopy

2.3.1 Sample Preparation

All core samples were processed using standard palynological techniques. Five grams of shale were processed per sample. The samples were disaggregated with a pestle and mortar (to pieces about 5mm diameter) and then subjected to 20% hydrochloric acid treatment to dissolve any carbonates; the samples were then allowed to stand until any reaction had stopped. After three washes with distilled water the samples were treated with 40% hydrofluoric acid to remove any silicate material, and were allowed to stand for at least 24 hours (longer if inorganic material could still be

observed). The samples were then decanted three times and the residues treated with 20% hydrochloric acid to remove newly formed fluoride compounds. After decanting of the hydrochloric acid the residues were washed through a 20 micrometre (μm) nylon mesh sieve, and the residue transferred to labelled vials. The organic residues for each sample were stirred prior to pipetting of a portion on to glass cover slips and being left to dry; the cover slip was then mounted on to standard slides using Elvacite (2204) mounting medium, an acrylic resin with low fluorescence.

2.3.2 Analysis

Counting and Fluorescence Scale

Each slide was examined under incident blue light fluorescence using an Olympus BH2-RFCA microscope at x20 magnification (or x40 for more detailed examination of particular particles). This was primarily to determine the preservation state of any amorphous organic matter (AOM) and palynomorphs present, according to the fluorescence preservation scale of Tyson (1995), a 6 point scale designed for evaluation of immature kerogen in outcrop and core samples.

FS 1: Kerogen is completely non-fluorescent (except for rare fluorescing palynomorphs). Rare in immature sediments.

1a) AOM rare/absent.

1b) AOM present (common to abundant)

FS 2: Most palynomorphs fluoresce but matrix of autochthonous AOM remains predominantly non-fluorescent.

2a) Palynomorphs show dull orange-yellow fluorescence

2b) Palynomorphs show yellow-green fluorescence

FS 3: Most palynomorphs fluoresce; matrix of AOM shows dull fluorescence just visible above background.

FS 4: AOM matrix shows moderate and heterogeneous fluorescence (intensity is close to that of ordinary *in situ* palynomorphs).

FS 5: AOM matrix shows strong and heterogeneous fluorescence (intensity is close to that of ordinary *in situ* palynomorphs).

FS 6: Matrix of AOM shows rather homogeneous and very strong fluorescence, bright yellow, like telalginite (such as prasinophytes). Rare in marine sediments.

Kerogen Counts

Point counts of 300 particles were carried out at x20 magnification on all slides in the study, with additional counts being made where necessary to give a minimum total of 50 particles in the phytoclast category. The data were recorded on an electronic point counter, but the counts were made using manual traverses, taking between fifteen and thirty minutes to perform (average ca. twenty-five minutes per slide). The particles were classified into the kerogen categories shown in Table 2.2 (see section 2.4 for definitions). The data are relative numeric frequencies as they are not corrected for particle size or thickness.

Palynomorph Counts

Most slides were than also subjected to a detailed analysis of the palynomorph fraction based on a further count of 500 palynomorphs which took between twenty five and fifty minutes to perform (average thirty to thirty five minutes). Table 2.3 shows categories used for the palynomorph counts. The data was again recorded on an electronic point counter and traverses made manually.

Spore Colour Index (SCI)

Spores and acritarchs are originally pale yellow to colourless at the time of deposition. Increasing temperature changes their colour. Thermal maturity can be assessed by means of spore colour analysis, and supplemented by qualitative fluorescence of isolated kerogen in blue light. Spore colour data are presented in terms of the Robertson Spore Colour Index (SCI), which is determined by comparison of the colour of palynomorph in the samples with standard reference slides of single mounted palynomorphs. These palynomorphs are assigned values from 1–10 in order of increasing colour from transparent to pale yellow, orange and, finally black. In Lower Palaeozoic sequences, where vitrinite and land plant spores are absent, the acritarchs can be used instead of spores. Calibration studies have shown that the major colour change in acritarchs occurs in the late mature zone, i.e. later than for spores and pollen (Collins, 1990).

AOM (AOM)			
Phytoclasts (Tphy)	Black wood (Blk)		Equant (Equ)
			Lath (Lath)
	Brown wood (Bro)	Biostructured (Str)	Undegraded (Undg)
			Degraded (Deg)
		Non-biostructured (Ust)	Undegraded (Und)
			Corroded (Cor)
			Pseudoamorphous (Psu)
	Cuticle (Cu) Membranes (Mem)		
Palynomorphs (Tpaly)			Sporomorphs (Sporo)
			Marine plankton (Mp)
			Undifferentiated (Undiff)

Table 2.2. Kerogen count categories; rank of categories decreases from right to left.

Sporomorphs (Sporo)	Spores (Sp)	Thick-walled (Tks)
		Thin-walled (TnS)
Marine plankton (Mp)	Acritarchs (Acri)	Acanthomorphs (Acan)
		Polygonomorphs (Poly) Veryhachiids
		Netromorphs (Netro)
		Micrhystridium (Mic)
	Prasinophytes	*Tasmanites* type (Tas)
		Leiospheres (Lei)
	Zoomorphs	Chitinozoa (Chi)
		Scolecodonts (Sco)
	Zooclast	Graptolite (Grap)
Others	Undifferentiated (Undiff)	

Table 2.3. Palynomoph categories; rank of categories decreases from right to left. Graptolites are not palynomorphs (rather zooclasts) but were counted at the same time as the palynomorphs.

2.4 Definition of Kerogen and Palynomorph Categories

Kerogen and palynomorph categories used in this study are listed in Appendices II and III. The kerogen categories are distinguished primarily on the basis of shape, structure and colour. There are three main categories: phytoclasts, Amorphous Organic Matter and palynomorphs. Each category is further subdivided into classes as seen in Plate I. Both the categories and classes are described below. The classification is based on one formulated by Tyson (1995).

2.4.1 Kerogen Classification

Phytoclasts

Most phytoclasts are derived from the lignified mechanical support tissue of higher plants, i.e. wood (Tyson, 1995). The phytoclasts within the sediments are mainly represented by dispersed tracheid and other woody tissues. The phytoclasts vary in colour and shape as a result of origin, sorting, and preservation. Phytoclasts are subdivided into several varieties.

Black wood

This includes all phytoclasts which are black and do not show any brown colouration. The margins of the particles are clearly defined, no internal structure is usually noted, but bordered pits are sometimes present. Distinguished from pyrite by outline (framboidal pyrite is distinctive because of its nodular outline) and surface reflectance when light is completely obstructed from the field of view (Tyson, 1989; Tuweni & Tyson, 1994). Subdivided by shape into:

Equant (length:width ratio <3)

Lath (length:width ratio >3)

Brown wood

Biostructured (= botanically structured) brown wood. Translucent, generally brown in colour; lath to equant in shape; clearly visible internal structure showing cells, ribs, thickenings and or pits. Divided into:

Undegraded: Sharp outline, may be slightly irregular.

Degraded: More diffuse outline, irregular.

Non-biostuctured (lacking botanical structure), translucent, generally brown in colour; lath to equant in shape. Divided into:

Undegraded: Sharp outline, may be slightly irregular.

Corroded: More irregular edges.

Pseudoamorphous: Often light brown in colour; usually equant in form; starting to show some features of AOM, particularly at margins, but mostly homogeneous in appearance, no pyrite specks, or inclusions.

Cuticle

Phytoclasts consisting of thin, transparent sheets, with cell outlines that are visible as ridges on one (inner) surface. "The particles are thin because only one layer of cell is present and only the outer wall of these cells is preserved" (Tyson, 1995). "Cuticle is very important because it is the only common phytoclasts that is oil-prone" (Tyson, 1995. p. 157), but it is rarely abundant on a whole rock basis.

Membranes

Pale grey, thin, sheet-like, irregular and often folded particles. Often pyrite specked and may be weakly fluorescent. Possibly cuticle without visible cells or zooclasts.

Palynomorphs

Three major subgroups of palynomorphs are distinguished; spores, marine phytoplankton and zoomorphs (animal derived palynomorphs including chitinozoans, scolecodonts).

Sporomorphs

All palynomorphs produced by terrestrial macrophytes; fluorescence properties vary.

Marine plankton

This category includes acritarchs and prasinophytes. Fluorescence properties vary, but often more greenish colours than sporomorphs.

Zoomorphs

Includes chitinozoans and scolecodonts.

Zooclasts

Includes graptolite fragments.

Undifferentiated palynomorphs

Unidentifiable palynomorphs that may be either sporomorphs or plankton.

Amorphous Organic Matter (AOM)

Yellow, orange, brown or grey, irregular particles varying from rounded to angular and with gradational margins. They are typically heterogeneous, usually pyrite specked, and have varied common micro-inclusions; fluorescence properties vary.

2.4.2 Palynomorph Classification

Spores

Produced by pteridophyte plants, these palynomorphs usually exhibit a trilete mark. They often show variable orange-yellow fluorescence. They have been subdivided into thick-walled forms with markedly thickened outer walls (also often ornamented and large) and. thin-walled forms that are more typical and often smaller.

Acritarchs

The acritarchs are a polyphyletic group of palynomorphs whose name means 'of uncertain origin' (Tyson, 1995). Based on their mode of occurrence, it is almost universally accepted that the great majority of, if not all, acritarchs are marine phytoplankton. Acritarchs are most diverse during the Ordovician, Silurian, and Devonian. Acritarchs are characterised by varied ornament but are mostly acanthomorphs, polygonomorphs or netromorphs (Traverse, 1988); they typically show a strong (yellow-green) fluorescence when immature.

Leiospheres

Thin-walled spherical bodies lacking in sculpture and ornament and of probable prasinophyte origin (Traverse, 1988); typically brightly fluorescent.

Tasmanites

Large, thick, perforate walled palynomorphs produced by marine prasinophyte algae; typically brightly fluorescent and highly oil prone (Traverse, 1998; Tyson, 1993, 1995).

2.4.3 Discussion of Organic Matter Classification

This classification system, parts of which appear in Tyson (1984, 1989), is one of the more detailed that has been applied in palynofacies analysis (c.f. the proposed standard classification system in Traverse, 1994, p.3, and the comparison of various systems given in Tyson, 1993, p.156–157). It attempts to satisfy the criteria laid down in Tyson (1993, 1995) for detailed palynofacies work, taking into account the variables summarised below (see also section 2.5):

a) Any ecologically significant groupings that may be reflected by particle types (e.g. different types of marine plankton).
b) Any consistent or significant variation in size, morphology, or density likely to be reflected in the hydrodynamic behaviour of the particles (e.g. different types of phytoclasts and spores).
c) Any components with predictable differences in their geochemical character (e.g. AOM preservation, black vs. brown wood, telalginitic vs. ordinary palynomorphs).

2.5 Trends in the Distribution of the Different Particle Types

A full explanation of this topic can be found in Tyson (1993, 1995), and is only briefly reviewed below. Some of the generalized proximal-distal, redox and other trends shown by selected parameters are summarised in Table 2.4.

2.5.1 Kerogen

Percentage of phytoclasts

A high percentage of phytoclasts in the kerogen assemblage can reflect high supply, preferential preservation or preferential sedimentation depending on the nature of the assemblage (Tyson, 1993). Poorly sorted assemblages of mixed composition containing tissues that would not normally be preserved are characteristic of proximal settings close to the parent flora, where there is sufficient supply to dilute other

kerogen groups. This situation generally characterises inner shelf settings as most terrestrial organic matter in estuarine systems sediments out before salinities reach 3–10%, large amounts only reach the outer shelf when markedly high discharge occurs, or the shelf is particularly narrow (Muller, 1959; Wollast, 1983; Tyson, 1993). Dominantly refractory phytoclasts assemblages are characteristic of oxidising situations where only resistant (lignitic) woody material survives, such as fluvial and delta top settings where there is a strong chance of post-depositional oxidation. Similar assemblages dominate distal oxidising settings where only the resistant material has survived extended transport (Tyson, 1993). The hydraulic equivalence of phytoclasts material leads to high percentages occurring in sediments of predominantly coarse silt/fine sand grain size; in terrestrially dominated facies it is this relationship that largely controls TOC values (Tyson, 1993).

Parameter response	*Proximal>>>Distal trend*	*Increasing % sand*	*Distal anoxic facies*
% phytoclasts of kerogen	high>>>low	increases	decreases
% AOM of kerogen	low>>>high	decreases	increases
% palynomorphs of kerogen	low>>>high	decreases	decreases
AOM fluorescence	variable	decreases	increases
Opaque: translucent phytoclasts	Low>>> high	increases	increases
Black equant: lath wood	high>>>low	increases	
% cuticle (of phytoclasts)	high>>>low	may increase	negligible
% sporomorphs (of palynomorphs)	high>>>low>>>high	increases	increases
% spores (of sporomorphs)	high>>>low	increases	decreases
% thick-walled (of spores)	high>>>low	decreases	decreases
% marine plankton (of palynomorphs)	low>>>high>>>low	decreases	decreases
% acritarchs (of marine plankton) *	high>>>low	may increase	usually low
% prasinophytes of marine plankton *	low>>>high	no data	increases
long: short-spined acritarchs	low>>>high	decreases	may increase

Table 2.4. Palynofacies trends in marine sediments (from Tyson, 1993, 1995).

* Based on Mesozoic sediments; significance in Early Palaeozoic less certain

Percentage of AOM and its fluorescent intensity

Tyson (1993, p.162) states that high percentages of fluorescent AOM reflect enhanced preservation under reducing conditions and, to a lesser extent, sedimentation removed from active sources of terrestrial organic matter. Most of the marine organic matter in sediments is represented by AOM, but it is easily degraded when exposed to oxic conditions. However, due to the large reservoir of marine organic aggregates usually available for preservation, when conditions are sufficiently reducing it often swamps other kerogen components (Tyson, 1987, 1989, 1993).

The fluorescent intensity of the AOM is controlled by the redox conditions under which it was deposited; dysoxic-anoxic conditions preserve the labile hydrogen-rich components of the AOM. As the fluorescence as a whole is partly controlled by the planktonic source and inclusions within the particles, it is the fluorescence of the easily degraded matrix of heterogeneous amorphous particles that is the most sensitive indicator of redox conditions (Tyson, 1993).

Percentage of palynomorphs

The percentage of palynomorphs is primarily controlled by dilution by either AOM or phytoclasts; therefore, it is highest in settings where these two parameters are reduced (Tyson, 1993). In such cases the interpretation depends on the nature of the assemblage; for example, higher percentages of spores are found in proximal areas (see later), whilst prasinophyte algae are strongly correlated with the occurrence of marine organic-rich finely-laminated sediments deposited under dysoxic to anoxic conditions (Tyson, 1995).

Translucent:opaque phytoclast ratio

Opaque phytoclasts can be produced by either the oxidation of translucent particles (during prolonged transport or post-deposition), or as charcoal by wildfire (Tyson, 1993). They are commonly reported as being dominant in coarse grained, high energy, organic-poor facies such as distributary channel sands and point bars (Tyson, 1995). This relationship has lead to the development of the idea that opaque phytoclasts are hydraulically equivalent to sand grade material (Tyson, 1995). However, the association of opaque phytoclasts with coarse sediments is also partly a consequence of post-depositional oxidation of woody material within more porous

sediments (Tyson, 1995, p. 242), so the relationship is probably due to a combination of the two elements (Tyson, 1993). Tyson (1989) shows an increase offshore in fine grained opaque phytoclasts relative to translucent material. Tyson (1995) suggests that the transition from translucent to opaque phytoclasts is primarily a subaerial effect that happens before the particles enter the sea; the subsequent ratio reflects relative preservation (opaque greater than translucent) and size sorting (as opaque particles are generally smaller).

Equant:lath black wood ratio

The interpretation of the opaque:translucent phytoclast ratio depends greatly on the morphological form of the opaque (black) wood that is encountered. Lath-shaped black wood is supposedly 'extremely buoyant' (Whitaker *et al.*, 1992, p.173), and is selectively transported to more distal settings where it is commonly dominant. This relationship may also be partly due to the fact that lath material is the result of break down of larger particles (lath or equant in shape) and its extremely resistant nature (Whitaker *et al.*, 1992). Relative decreases in the equant:lath ratio can therefore be used to indicate a shift to more distal deposition (Tyson, 1995). However lath-shaped particles may increase in proximal, higher energy facies (Tyson, 1995, p. 245). It would appear that equant:lath sorting trends are also partly size dependant with lath-shaped particles increased in some high energy, proximal facies where they can be significantly larger than associated equant particles (Tyson, 1995; Frank & Tyson 1995).

Percentage of cuticle

Cuticle debris is derived primarily from leaves (Tyson, 1993). It was considered to be most buoyant type of terrestrially-derived organic matter, only deposited from the suspended load when energy conditions were particularly low (Tyson, 1995, p. 236). High percentages of cuticle have been found in deltaic distributary and prodeltaic facies by Parry *et al.* (1981) and Nagy *et al.* (1984); Tyson (1995) mentioned a strong correlation between cuticles in kerogen assemblage and macroscopic plant debris in the sample. In modern sediments cuticle debris shows a rapid decrease in abundance offshore (Tyson, 1995).

Phytoclast particle size

The particle size of tracheids, charcoal and cuticle have all been shown to decreases in an offshore direction, despite phytoclast particle size being potentially strongly affected by the granulometric composition of the sediment, proximity to source, and any fragmentation during maceration (Tyson, 1993). Tyson and Follows (2000) show that there is a good correlation between size, shape and preservation state of the microscopic plant debris assemblages and the actual distance of the sample site from coastal siliciclastic sediment source.

2.5.2 Palynomorphs

Percentage sporomorphs of total palynomorphs

This is dependant on the proximity of fluvio-deltaic sources and on the productivity of fossilising plankton (Tyson, 1993). Therefore, the highest percentages are found in proximal areas where lowered salinities or turbidity suppress any plankton production and sporomorph input is high (Tyson, 1993). High percentage are also found at sites near to the parent flora, characterised by an over representation of locally derived sporomorphs and high variability (Tyson, 1995).

Percentage marine plankton of total palynomorphs

High percentages occur in essentially the opposite situations to those of sporomorph maxima: areas that are removed from fluvio-deltaic sources, poorly vegetated or with high primary productivity (Tyson, 1993).

Percentage spores of sporomorphs

The presence of significant percentages of spores indicates substantial pteridophyte vegetation and humid conditions (Tyson, 1995). Spores generally tend to be abundant only in nearshore settings, but may be quite common in deep-sea sediments if the adjacent shelf is narrow and there is significant redeposition (Tyson, 1995).

Percentage thick-walled spores of total spores

Thick-walled spores decrease away from source due to hydraulic equivalence, the larger, denser spores being generally deposited first (e.g. Parry *et al.*, 1981; Habib, 1982). However, these spores can also be selectively concentrated in any coarser

sediment as there are few other palynomorphs of similar hydraulic equivalence (Tyson, 1993).

Percentage acritarchs of marine plankton

The factors responsible for the Palaeozoic acritarchs distribution are globally dependent upon inshore-offshore position and on latitudinal situation. They are very comparable to the factors that influence the distribution of other phytoplanktonic groups at other times, particularly the dinoflagellates and their cyst assemblages (Le Hérissé, 2002). From the distribution of the acritarchs it is apparent that those with simple and thin-walled sphaeromorphs (leiospheres) tend to be most abundant nearer to the shore. In more distal shelf facies the acritarchs assemblages show an increase of longer-spined michrystridid genera, simple veryhachid polygonomorphs and some (large) netromorph taxa. Farther out in deep water basinal facies diversity is reduced and assemblages become dominated by thick-walled smooth sphaeromorph taxa, most of which are presumably prasinophytes (Tyson, 1995, p.320).

Percentage prasinophytes of marine plankton

Prasinophyte algae dominate the marine palynomoph assemblage when the production of other groups is suppressed, especially in dysoxic-anoxic facies. Although modern fossilising representatives are 'almost exclusively marine' (Tyson 1993, p.170) the fossils phycomata (pelagic organic bodies) have often been regarded as having a brackish affinity, and have been found dominating lagoonal and shallow water carbonate facies. This could be attributed to the reason given above, or due to the holoplanktonic nature of the prasinophytes which allows them to be transported into these facies (Tyson, 1993); the apparent brackish affinity is often based more on earlier interpretations, including the probably erroneous post-glacial brackish interpretation of the North African Silurian by Combaz (1967) rather than direct evidence (Tyson, 1995).

2.6 Details of Data Analysis

All the raw counts data were entered into a spreadsheet (EXCEL) and the simple and recalculated percentages were computed, and entire spreadsheet imported into SPSS where statistical procedures and other forms of data manipulation were

carried out, including the calculation of means, standard deviations, etc. using the descriptive statistics options.

2.6.1 "Dummy" Variables

All the samples description parameters (colour, sedimentary structure, conspicuous minerals, fossils, bioturbation and graptolites) were classified into different groups based on a hand specimen description (Table 2.5). These variables were encoded in order to enter them into the SPSS so that they could be used to help with interpretation and production of diagrams.

Lithology	**Dominant lithology**	**Fossils**
1 = shale	1 = shale	0 = fossil absent
2 = argillaceous siltstone	2 = argillaceous siltstone	1 = fossil fragment present
3 = siltstone	3 = siltstone	2 = fossil fragment absent
4 = sandstone	4 = sandstone	3 = fossil present
Sedimentary structure	**Bioturbation**	4 = fossil absent
0 = absence of sedimentary structure	0 = non	**Graptolites**
1 = fine lamination	1 = present	0 = absence
2 = medium lamination	2 = strong	1 = present
3 = coarse lamination	**Pyrite**	2 = common
Colour	0 = absent	**Mica**
1 = black	1 = present	0 = rare
2 = brownish black	2 = abundance	1 = present
3 = greyish black		2 = abundance
4 = dark grey		
5 = medium grey		
6 = medium dark grey		
7 = medium light grey		
8 = light grey		
9 = very light grey		

Table 2.5. Key to encoded variables.

2.7 Reflected light Microscopy

2.7.1 Sample preparation

Crushed samples were mounted in small pill-boxes in five parts of resin mixed with a one part of hardener (epoxy) which then sets hard. Polishing these blocks involved grinding them on a diamond lap to remove surface irregularities. The blocks were then polished on machines called "laps" using 220 and 600 grade corundum paper, using isopropanol as a lubricant. A series of progressively finer alumina powers (5/20 grade followed by 3/50 and gamma), at about one minute per grade, were then used with a "Selvyt" cloth to provide the final polish.

2.7.2 Analysis

Petrological observation and vitrinite reflectance measurements were made on a Zeiss UMSP 50 microscope (linked to Coflex software for data acquisition) and using an x40/0.85 oil objective. The immersion oil used has a refractive index of 1.518 at 23°C in sodium light (589.3nm). The microscope stage must be perfectly horizontal to ensure the reflected light goes straight back up the microscope. The equipment was allowed to warm up for 30 to 60 minutes prior to measurements. The light source is a 12 volt, 100 watt tungsten filament lamp. Light from this source travels through a polarizer and a field iris diaphragm unit it reaches a glass plate reflector, which acts as the vertical illuminator. This reflects light on to the sample through the objective. It is then reflected back through the objective and passes through either the eye piece or to the photomultiplier. Light travelling to the photomultiplier passes through an aperture diaphragm and a "Schott" interference filter with a narrow ban pass peaking at 546 nm (green).

Blocks were plasticine mounted on glass slides using a special press to ensure that the surface of the block was parallel to the stage of microscope. Vitrinite reflectance is determined by comparing the intensity of light reflected back from the surface of the samples to that reflected back from a surface of known reflectance. The photomultiplier generates an electric signal whose strength is proportional to the light intensity entering it. The microscopy must be set up so that measuring aperture of the photomultiplier is centered on the same point as the crosswire seen down the

eyepieces. Stray light should be reduced as much as possible, and correction made for any dark current.

Vitrinite, graptolite and chitinozoan reflectance data were gathered by measuring the random reflectance of up to 50–100 individual particles of vitrinite or vitrinite-like macerals. The number may be reduced up to 10-30 in cases of low particle concentration. Whilst determining the reflectance of each sample, the stability of the microscope system was checked by re-measuring the reflectance of the certified standards (e.g. 0.436%, 0.59%, 0.917) made of glass or specific minerals (spinel, garnets, diamond, silicon carbide) at regular intervals, and after each sample or every 15 minutes. However, ideally 2 or 3 standards should be used to establish linearity of the measuring system. The same spot (0.16 μm) and diaphragm size were used for measuring both the standard and sample.

2.8 Molecular Geochemistry

2.8.1 Soxhlet extraction of source rock core samples

Cleaned and crushed core samples were extracted using a Soxtherm extraction apparatus. All cellulose extraction thimbles and cotton wool were pre-extracted in a Soxhlet for 24 hours using an azeotropic solvent mixture of DCM:MeOH (93:7). A weighed amount of the powdered shale samples (10 to 70 grams) were placed into pre-extracted cellulose thimbles. The cellulose thimbles, plugged with pre-extracted cotton wool, were then placed into the Soxtherm extraction apparatus. An azeotropic solvent mixture of 200 ml of DCM:MeOH (93:7) was used for the organic matter extraction. Activated copper turnings were added to the extraction flasks in order to remove any elemental sulphur from the extracts. The extraction was performed for 4 hours.

2.8.2 Thin layer chromatography (TLC)

A glass plate coated with activated silica gel (0.5mm thick) was prepared by adding 80 ml of distilled water to 40g of silica gel to form a slurry which was spread on the glass plates using a spreader. The plates were dried up in an oven (110 ^{o}C) overnight and then pre-developed in a developing tank with about 2 cm depth of ethyl acetate and filter paper inserts to provide a saturated atmosphere. Once the ethyl

acetate reached the top of the plate, the plate was removed and the top 1 cm was scraped off to remove any contamination. The plate was then reactivated in the oven for at least 2 hours before being used. Another developing tank was filled with nearly 2 cm depth of light petroleum ether, again with filter paper inserts. Approximately 15 to 20 mg of the extract was carefully spotted onto the plate in a horizontal line above the level of the solvent using a glass capillary. The plate was placed into the tank allowing the solvent to travel up the plates. Before being removed and left to dry for a few minutes. Once dry, the plate was sprayed with Rhodamine 6G dye and visualized under ultraviolet light; the aliphatic and aromatic hydrocarbon fraction bands were assigned and scraped off separately. The silica was then placed into separate short glass columns which has been plugged by a small piece of pre-extracted cotton wool with 1 cm of activated alumina on top, and washed through with 30 ml of DCM. The fractions were collected in clean round bottom flasks. The solvent was removed by rotary evaporator, and the fractions transferred to pre-weighed small vials and prepared for further analysis by Gas chromatography (GC), and gas Chromatography-Mass Spectrometry (GS-MS).

2.8.3 Gas chromatography (GC) of the aliphatic hydrocarbon fractions of the source rock.

The hydrocarbon fractions obtained from thin layer chromatography were analysed on a Fisons (Carlo Erba) Gas Chromatograph 8000 series equipped with automatic injection. Samples were analysed on a fused silica capillary column, HP-5 (5% polar methyl silicone stationary phase), film thickness 0.25 mm, 30m x 0.25 mm internal diameter. The gas chromatography oven was first held at 50°C for 2 minutes, then temperature programmed from 50 °C to 300 °C at 4 °C per minute, and then held at 300 °C for 20 minutes. The carrier gas was hydrogen with a flow rate of 1 ml/min at kpa column head pressure.

2.8.4 Gas Chromatography-Mass Spectrometry (GC-MS)

The GC-MS analyses of the aliphatic and aromatic hydrocarbon fractions obtained from oils and core samples were carried out using a Hewlett-Packard 6890 gas chromatograph fitted with a split/splitless injector (280°C) and interfaced to an HP 5973 Mass Selective Detector (electron voltage 70 eV, source temperature 230 °C, interface temperature 310 °C). Separation was performed on an HP-5 fused silica

capillary column (phenyl-methyl silicone stationary phase; 30m long, 0.25mm internal diameter, and 0.25 μm film thickness; pressure of 51.1 kpa). The mass spectrometer was operated in selective ion monitoring (SIM) mode for both fractions as well as full scan mode for a limited number of aliphatic and aromatic hydrocarbon fractions.

A fast heat temperature program was used to analyse the biomarkers (steranes and tricyclic terpanes and hopanes). The temperature used was 40 °C to 175 °C at 10 °C/min, then 175 °C to 225 °C at 6 °C/min, then 225 °C to 300 °C at 4 °C/min, and finally the temperature was held at 300 °C for 20 minutes. However a slow heating rate temperature program was used in the case of aromatic compounds. The oven temperature was first held at 40 °C for 5 minutes and then programmed from 40 °C to 300 °C with a 4 °C/min temperature ramp, the oven then held at 300 °C for 20 minutes.

Concentrations of individual steranes, tricyclic terpanes and hopanes were obtained by comparing the peak area of the appropriate compounds relative to 5 α (n)-androstane internal standard. The concentrations of biomarker compounds were calculated as follows:

$$X_{b(a)}\ (\mu g/\text{g oil, extract}) = \left(\frac{1000}{Wt.oil\ /\ extract}\right) x C_{IS}\ (\mu g)\ x \left(\frac{A_{b(a)}}{A_{IS}}\right)$$

Where, $X_{b(a)}$ = concentration (μg/g of oil or extract) of the compound to be quantified (biomarker);

Woil/extract = weight in mg of oil or rock extract taken for analysis;

C_{IS} = concentration in μg of surrogate standard added to the sample (5 α (n)-androstane for biomarker);

$A_{b(a)}$ = area of biomarker

A_{IS} = area of 5 α (n)- androstane.

CHAPTER 3.0

ORGANIC GEOCHEMISTRY

3.0 ORGANIC GEOCHEMISTRY

3.1 Introduction

3.1.1 Total organic carbon

The abundance of organic matter in sediments is usually expressed as the relative percentage of organic carbon on a dry weight basis; most organic-rich dysoxic-anoxic black shale facies generally show TOC values between 3% and 20%. The modal value for ancient shelf shales generally falls between 0.7 and 2.2% (Tyson, 1995). This technique provides a simple measure of the organic matter content of sediments, but there are problems with the interpretation of TOC data which need to be considered. The main problem is that of the dilution; because TOC is expressed as a relative percentage, it depends not only on the supply and preservation of organic matter but also on the supply and preservation of siliciclastic and biogenic material (Tyson, 1995). Also, geochemically significant changes in the organic matter may not be represented by a change in the TOC, particularly in phytoclasts-dominated settings where the metabolisable fraction represents only a minor constituent (Tyson, 1995). However, despite these problems TOC% is widely used as the analyses are simple and fast to carry out and give a good starting point for further organic geochemical methods, and can also provide an extra element of quantification to palynofacies studies when combined with percentage abundance data.

Relationship with Gamma Ray

Gamma ray logs measure the natural gamma ray radiation emitted from the formation and spectral logs the concentrations of potassium, uranium and thorium. It is known that the uranium is fixed at the sediment-water interface under reducing conditions and in the presence of a sorbant, which is usually organic matter or phosphate (Wignall & Meyers, 1988). Sediment enriched in uranium this tends to be deposited under anoxic conditions that allow both large amounts of organic matter to accumulate and uranium to be fixed (Wignall & Meyers, 1988). The correlation between high radioactivity (high gamma-ray) response and uranium in marine sediments have been shown previously (Rider, 1996; Jones & Stump, 1999). A relationship between organic carbon content and gamma ray logs for lower Silurian

shale in North Africa and the Middle East is well documented; shales are defined as "hot" if the gamma-ray values exceed 150 API units, which correlates approximately with a TOC of ≥3% (Lüning *et al.*, 2000 and references therein). The shale with TOC value >3% ('hot-shale') usually contains marine organic matter, and are thus oil-prone if immature (Demasion & Moore, 1980; Tyson 1995). The organic content of more mature black shales is reduced as a consequence of hydrocarbon generation and expulsion (by up to 66% for those with Type II kerogen) but the uranium content and gamma ray signature of the sediment is much less affected by this process (Lüning *et al.*, 2000). In general, uranium content/total organic carbon content ratio in a black shale is controlled by a number of factors which include the primary uranium content of the water body, the carbonate content and sedimentation rate, Palaeo-oceanoraphic condition, such as primary productivity and water-body stratification (Luning *et al.*, 2003).

TOC and Organic Matter Type

Correlation between TOC and grain size depends partly on the organic matter type and the hydraulic equivalence of the particles (Tyson, 1995). The TOC is positively correlated with silt content in Recent sediments of the upper part of Chesapeake Bay where terrestrial organic matter is dominant, TOC is correlated with clay content in the middle part of the bay where the organic matter is primarily phytoplankton-derived (Tyson, 1995, p. 89). A similar relationship is reported by Frank and Tyson (1995) who found that the positive relationship between silt and TOC content was presumably due to the hydrodynamic equivalence (and common fluvial source) of phytoclasts and silt particles.

In Mesozoic to Recent siliciclastic shelf settings, TOC values of less than 2–3% are usually associated with phytoclast-dominated kerogen assemblages, where the TOC content is largely determined by variations in absolute phytoclasts abundance (input + dilution). Sediments with more than 2–3% TOC are often dominated by phytoplankton-derived AOM, and the actual TOC determined by a combination of dilution, productivity and preservational factors (Tyson, 1995).

"PhytOC" and "AmOC" Values

This parameter, first described by Tyson (1989), is used to provide a better assessment of "absolute" abundance trends in phytoclasts. The "PhytOC" value is calculated as TOC x %Phytoclasts of (AOM + Phytoclasts)/100. Palynomorphs are excluded as they contribute only a minor fraction of the TOC compared with AOM and Phytoclasts. It should be noted that the parameter is not corrected for particle size or density, and that different kerogen types contain different percentage of carbon. Also the parameter is affected by dilution-dependent variations in TOC not just the supply of organic matter. The % PhyTOC value can be compared with the "AmOC" value (% TOC x %AOM of (Phytoclasts + AOM)/100, to distinguish the relative amounts of terrestrial and marine TOC.

3.1.2 Rock-Eval Pyrolysis

Rock-Eval pyrolysis is the one of the standard petroleum industry organic geochemical screening methods that when combined with TOC data allows the identification of potential source rocks and gives an idea of their quality. As is the case with TOC analysis, Rock-Eval pyrolysis is quick and easy to carry out, but there are also problems which must be addressed when interpreting the data. Peters (1986, p.321) states that 'Proper interpretation of Rock-Eval and TOC data requires information on lithologies, the relative abundance of OM and the mineral matrix, well conditions, the presence or lack of generated hydrocarbons. The main problem with Rock-Eval analyses performed on whole rock material is the 'mineral matrix effect', whereby kerogen-derived hydrocarbons are adsorbed onto the surface of clay minerals, reducing the S1 and S2 values (and consequently the Hydrogen Index) and increasing the Tmax (Orr, 1981; Katz, 1983; Peters, 1986; Tyson, 1995; cf. Bordenave *et al.*, p.244). This problem is greatest when the rock is organic lean (e.g. < 0.3% TOC) as the values of the parameters can approach the potential analytical errors, i.e. at 0.3% TOC the Tmax and S2 becomes unreliable (Bordenave *et al.*, 1993).

Kerogen Type

The number of variables involved in the determination of natural kerogen assemblages (e.g. variations in source, maturation, weathering) means that there is a gradational relationship between the four kerogen types that were first defined using

atypically pure end member compositions (Tyson, 1995; Table 6.2). In this study the kerogen type has been defined by cross-plots of S2 and TOC using the approach of Langford and Blanc-Valleron (1990). The kerogen type is empirically defined by plotting Type I/II and II/III lines on the graph assuming these correspond to HI values of 700 and 200 respectively (when immature), this allows a more certain assignation of kerogen type than with other methods where the natural mix of components results in uncertain Type I/II or II/III boundaries (Langford & Blanc-Valleron, 1990). However, this use of type indicates only the current nature of the kerogen, not its genetic type (source and preservation state) prior to any maturation effects. Rock matrix adsorption, and/or a 'dead carbon effect' (due to H-poor, TOC-rich inertinitic organic matter) is indicated by a positive intercept of the regression line on the *x*-axis, the larger the intercept value the greater the effect (Langford & Blanc-Valleron, 1990). The true average HI is given by the slope of the S2 v. TOC regression line multiplied by 100.

3.1.3 Organic Facies.

The organic facies approach defined by Jones (1987) is probably more realistic than kerogen Type in attempting to classify different kerogen assemblages as it takes into account the fact that the assemblages are controlled by preservational factors as well as their source, and that changes between assemblages are often gradational (Tyson, 1995; Table 3.1). An integrated approach combining bulk organic geochemistry (elemental analysis or Rock-Eval pyrolysis) and microscopy (transmitted and reflected light) is required for organic facies work. Tuweni and Tyson (1994) consider that TOC and pyrolysis combined with palynofacies analyses provides an excellent means of characterising organic facies.

The three main organic facies groups reflect anoxic-dysoxic (A, AB, B, BC), proximal fluvio-deltaic to prodeltaic-oxic shelf (C, CD), and distal slowly deposited, oxic facies (D) (Tyson, 1995).

ORGANIC FACIES	**A**	**AB**	**B**	**BC**	**C**	**CD**	**D**
% 'AOM' of kerogen	dominant			mod	usually low/absent		
'AOM' matrix fluorescence	highest		mod-weak		weak	usually absent	
% prasinophytes of plankton	highest	mod	rare	usually very rare			
% phytoclasts of kerogen	low (dilution)			mod	usually dominant		
Opaque:translucent phytoclasts	often high			usually low	increases		
Geochemical characteristics (for immature sediments)							
Hydrogen index	≥850	≥650	≥400	≥250	≥125	50-125	≥50
Kerogen type	I	I/II	II	II/III	III	III/IV	IV
TOC %	5-20+	3-10+		3-3+	<3	<0.5	
Environmental factors							
Proximal-distal trend	Distal			Proximal			Distal
Oxygen regime	Anoxic	Anoxic-dysoxic			Oxic		V.Oxic
Sediment accumulation rate	Low	Varies		High		Mod	Low
ORGANIC FACIES	**A**	**AB**	**B**	**BC**	**C**	**CD**	**D**

Table 3.1 Relationship between some selected palynofacies kerogen parameters and organic facies in idealized marine siliciclastics facies (general relative trends only) (from Tyson 1995; geochemical ranges from Jones, 1987).

3.2 Total Organic Carbon

In this study 108 core and 197 cutting samples from lower Palaeozoic succession were analyzed for total organic carbon content (TOC%), total sulphur (S%) and by Rock-Eval pyrolysis. Average results of (TOC, S, S1, S2, S3, HI, Tmax) by formation are presented in Tables 3.2 and 3.3.

The proportion of lithologies and dominant lithologies for the total number of samples which have been selected for total organic contents (TOC), are summarised in Tables 3.4 and 3.5. The sample set represents the finer grained sediments with shale, argillaceous siltstone and siltstone making up 100% of the rock types present. The four major formations are Tanezzuft, Acacus Sandstone, Aouinet Ouenine and Tahara Sandstone.

3.2.1 TOC Results

Total organic carbon contents of all 305 samples vary between 0.5 and 25%. The best TOC values were recorded within the lower Tanezzuft Formation hot-shale, where they range from 1.7 to 25% (average 7%), the Tahara Sandstone Formation ranging from 0.5 to 38.6% (average 4.9%) and the Aouinet Aouenine C Formation (1.4 to 5.1%, average 3%). Other units such as the upper Tanezzuft, Acacus, Aouinet Ouenine A & B and Ouen Kasa have low TOC contents (average 0.5%).

Box plots (quartile distributions) comparing the TOC values of cutting and core samples for each formation (Fig. 3.1) show that the highest median TOC values for each formation are found in the core samples, suggesting the TOC values of the cutting samples were diluted by caving effects.

Formation	Age	N	Value	TOC	S	C/S	S1	S2	HI	Tmax C°
Tahara	Devonian	22	Mean	4.9	0.5	25	1.1	9.4	127	436
			Stdev.	7.9	0.5	33	2	21.8	63	2.9
			Min	0.5	0	0.8	0.1	0.2	24	431
			Max	38.6	1.8	112.7	9.7	104	269	442
Aouint Ounine C		18	Mean	3	3	18.3	0.7	3.6	114	439
			Stdev.	0.9	0.9	35.2	0.4	1.9	48	3.9
			Min	1.4	0	0.7	0.1	0.4	17	429
			Max	5.1	3.4	153	1.5	6.9	179	445
Aouint Ounine A		5	Mean	0.3	0.6	1.12	0.3	0.3	102	433
			Stdev.	0.1	0.4	1.5	0.2	0	67	5
			Min	0.1	0.1	0.3	0.1	0.2	63	427
			Max	0.5	1.1	3.8	0.6	0.4	221	438
Acacus	Silurian	7	Mean	0.2	0.1	3.2	0.1	0.2	89	447
			Stdev.	0	0.1	2.4	0	0	34	31
			Min	0.1	0	0.4	0	0.1	24	433
			Max	0.2	0.3	8	0.3	0.2	123	512
upper Tanezzuft (cool-shale)		44	Mean	0.8	2.4	0.5	0.4	1.2	138	433
			Stdev.	0.5	1.6	0.6	0.3	1.3	65	16
			Min	0.2	0.09	0.1	0.1	0.2	17	364
			Max	2.3	5.6	2.5	1.2	5.8	257	447
lower Tanezzuft (hot-shale)		12	Mean	7.4	3.8	2.2	2.4	16.5	222	434
			Stdev.	5	3.1	1.2	1.4	11.5	57	3
			Min	1.7	1.2	0.9	1	3.1	152	427
			Max	20	11.7	5.1	5.7	40.6	383	440

Table 3.2 Summary of bulk geochemical analysis of the core samples by formation. Key: TOC: Total organic carbon content, wt%; S1: free hydrocarbons, mg HC/g rock; S2: potential hydrocarbons, mg HC/g rock; HI: Hydrogen index, mg HC/gTOC; N.: number of samples. Note did not edit out the obviously erroneous Tmax values, especially where TOC is low.

Formation	Age	N	Value	TOC	S	C/S	S1	S2	HI	Tmax C°
Tahara	Devonian	10	Mean	1.7	1.2	1.8	0.6	1.7	104	439
			Stdev.	0.5	1	1	0.2	1	51	2
			Min	1	0.3	0.6	0.3	0.8	32	434
			Max	2.5	3	4.3	1	4	198	442
Aouint Ounine C		51	Mean	1.7	1.6	1.2	0.5	1.9	107	438
			Stdev.	0.9	0.9	0.7	0.4	2.4	53	5
			Min	0.3	0.1	0.5	0.1	0.4	38	422
			Max	5.3	3.3	4.3	2.2	17	325	449
Aouint Ounine B		6	Mean	0.5	0.5	1	0.6	0.9	199	427
			Stdev.	0.3	0.4	0.4	0.2	0.3	65	35
			Min	0.2	0.1	0.5	0.3	0.4	120	354
			Max	0.9	1.3	1.5	0.8	1.3	298	442
Aouint Ounine A		21	Mean	0.2	0.3	1	0.3	0.3	120	424
			Stdev.	0.1	0.1	0.4	0.2	0.1	38	4
			Min	0.1	0.1	0.5	0.1	0.14	54	415
			Max	0.4	0.5	2	0.7	0.53	190	429
upper Tanezzuft (cool shale)	Silurian	61	Mean	0.6	2.3	0.3	0.4	0.7	103	430
			Stdev.	0.2	1.2	0.2	0.3	0.8	104	18
			Min	0.3	0.3	0.1	0.1	0	2	362
			Max	1	5.7	0.9	1.4	2.9	305	467
lower Tanezzuft (hot-shale)		48	Mean	6.2	3.4	1.9	2.5	17	167	444
			Stdev.	6.3	1.3	1.8	2.8	21	149	26
			Min	0.8	1.4	0.3	0.1	0.1	5	407
			Max	25.1	6.2	7.8	12.3	79	435	594

Table 3.3 Summary of bulk geochemical analysis of the cutting samples by formation
Key: TOC: Total organic carbon content, wt%; S1: free hydrocarbon, mg HC/g rock; S2: potential hydrocarbons, mg HC/g rock; HI: Hydrogen index, mg HC/gTOC; N.: number of samples. Note did not edit out the obviously erroneous Tmax values, especially where TOC is low.

Formation Name	%Shale	No. of cases	%Argillaceous siltstone	No. of cases	%Siltstone	No. of cases
Tahara	55	12	41	9	1	5
Aounit Ounine C	83	15	17	3	0	0
Aounit Ounine B	100	1	0	0	0	0
Aounit Ounine A	40	2	40	2	20	1
Ouan kasa	100	1	0	0	0	0
Tadrart	0	0	100	1	0	0
Acacus	71	5	0	0	29	2
Upper Tanezzuft	70	31	25	11	5	2
Lower Tanezzuft	92	11	8	1	0	0

Table 3.4. Lithology types and their proportions.

Formation Name	%Shale	No. of cases	%Sandstone	No. of cases
Tahara	5	1	95	21
Aounit Ounine C	0	0	100	18
Aounit Ounine B	100	1	0	0
Aounit Ounine A	100	5	0	0
Ouan kasa	100	1	0	0
Tadrart	0	0	100	1
Acacus	0	0	100	7
Upper Tanezzuft	93	41	7	3
Lower Tanezzuft	100	12	0	0

Table 3.5. Dominant lithologies and their proportions.

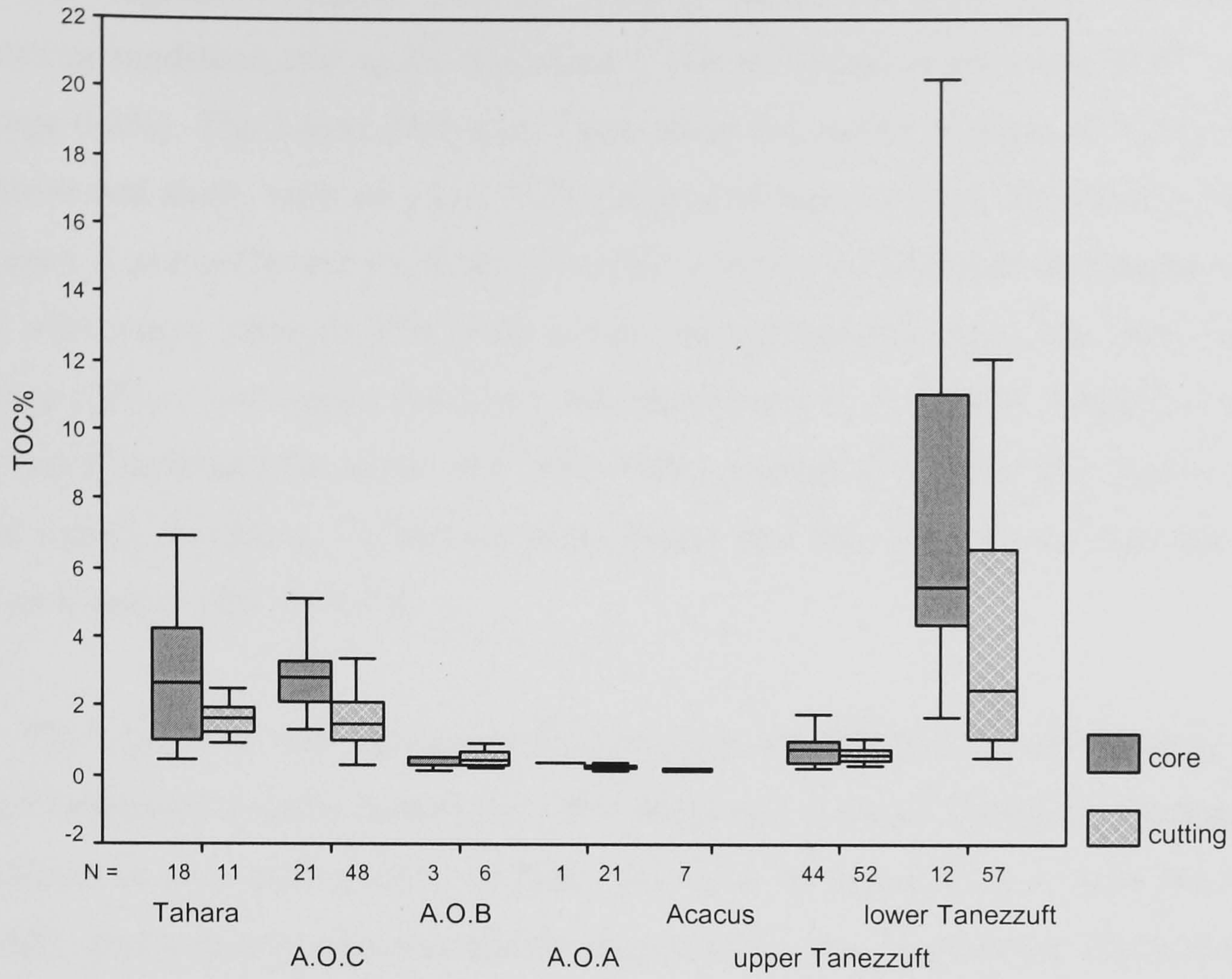

Figure 3.1. Box plot (quartile distributions) comparing the TOC values of cuttings and core samples for each formation (N = number of core and cuttings samples).

3.2.2 Relationships With Lithology

The overall stratigraphic trend in mean TOC (Fig. 3.2) reflects differences in lithology between the lithostratigraphic units, and thus the associated transgressive and regressive trends. The Lower Silurian Tanezzuft Formation consists almost entirely of marine shale and siltstone with minor sandstone, but can be subdivided into two distinct units based on gamma-ray response and lithology. The first unit is characterized by high radioactivity (API > 150) and consists of laminated dark grey to black shale that was deposited during basal Silurian the transgression. Deposition took place in a broad anoxic marine environment that extended over the greater part of Arabia and North Africa (see section 1.4). The maximum TOC value measured was 25% in (well A1-70, at 10170'), and the average 7%. The second unit, the upper Tanezzuft Formation consists of alternating shale and siltstone and exhibits a 'cool' gamma ray response, this unit typically has a TOC of < 1%.

The regressive Upper Silurian Acacus Sandstone Formation consists of alternating sandstone and shale, this shale is characterized by very low TOC values (average 0.2%). The Lower Devonian Ouan Kasa Formation consists of interbedded sandstone and shale, with very low TOC values (average < 0.2%). The Middle-Upper Devonian Aouient Ounine (A & B) Formation consists of interbedded sandstone and shale with minor siltstone, this shale is also characterized by very low TOC values (average 0.2%). The Upper Devonian Aouient Ounine C Formation consists of dark grey, black shale and limestone and TOC values average 3%. Other formations, such as the Tahara Sandstone Formation, also contain rare thin black shale interbeds that have an average TOC of 4.5%.

The regressive coarsening-upwards nature of the Silurian-Devonian succession (upper Tanezzuft, Acacus Sandstone, Ouan Kasa and Aouient Ounine A formations) is reflected in an overall decline in TOC. This is to be expected as organic matter is normally preferentially concentrated in shales rather than sandstones because most organic particles are "hydrodynamically equivalent to clay silt grads clasts" (Tyson 1987, p.48).

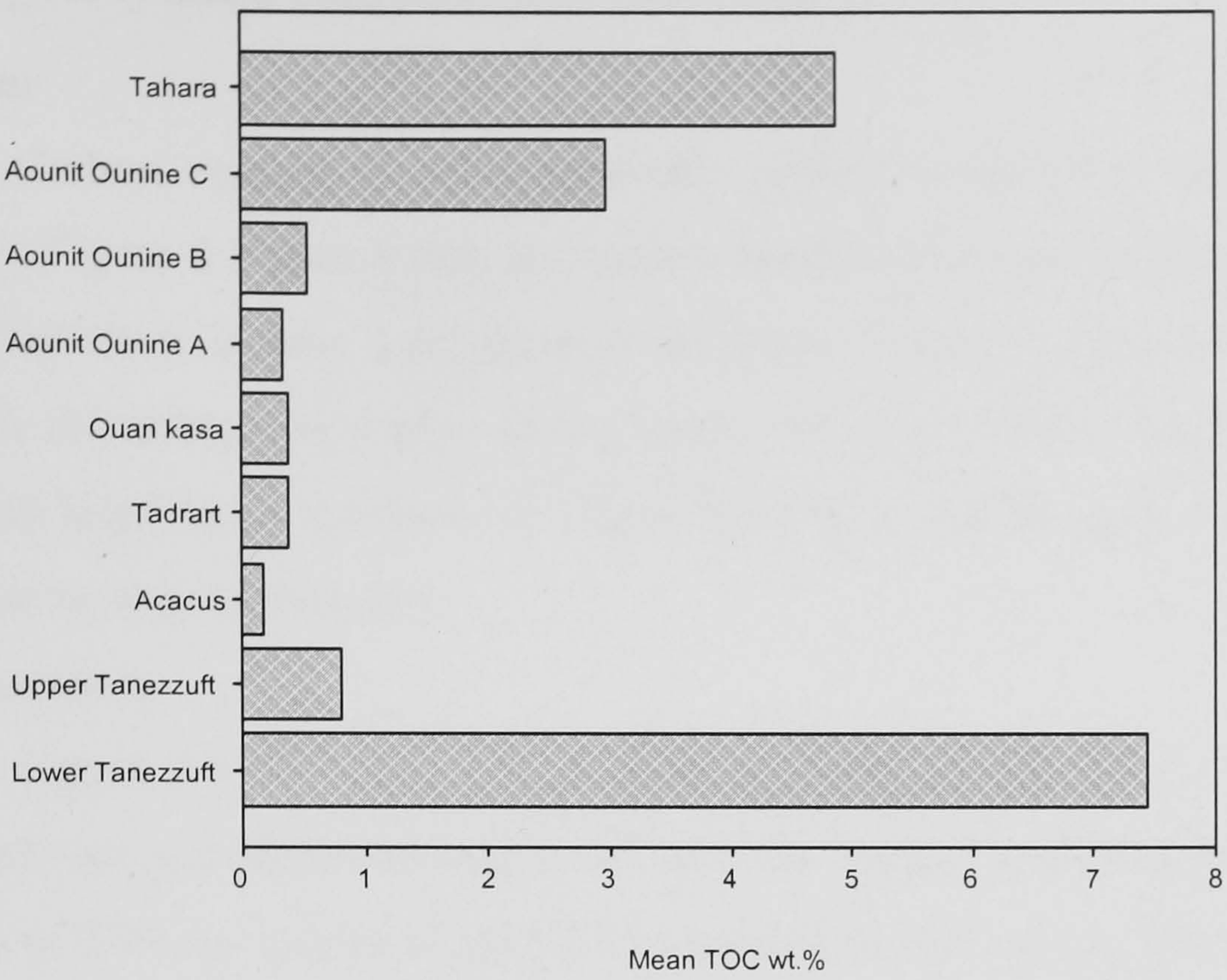

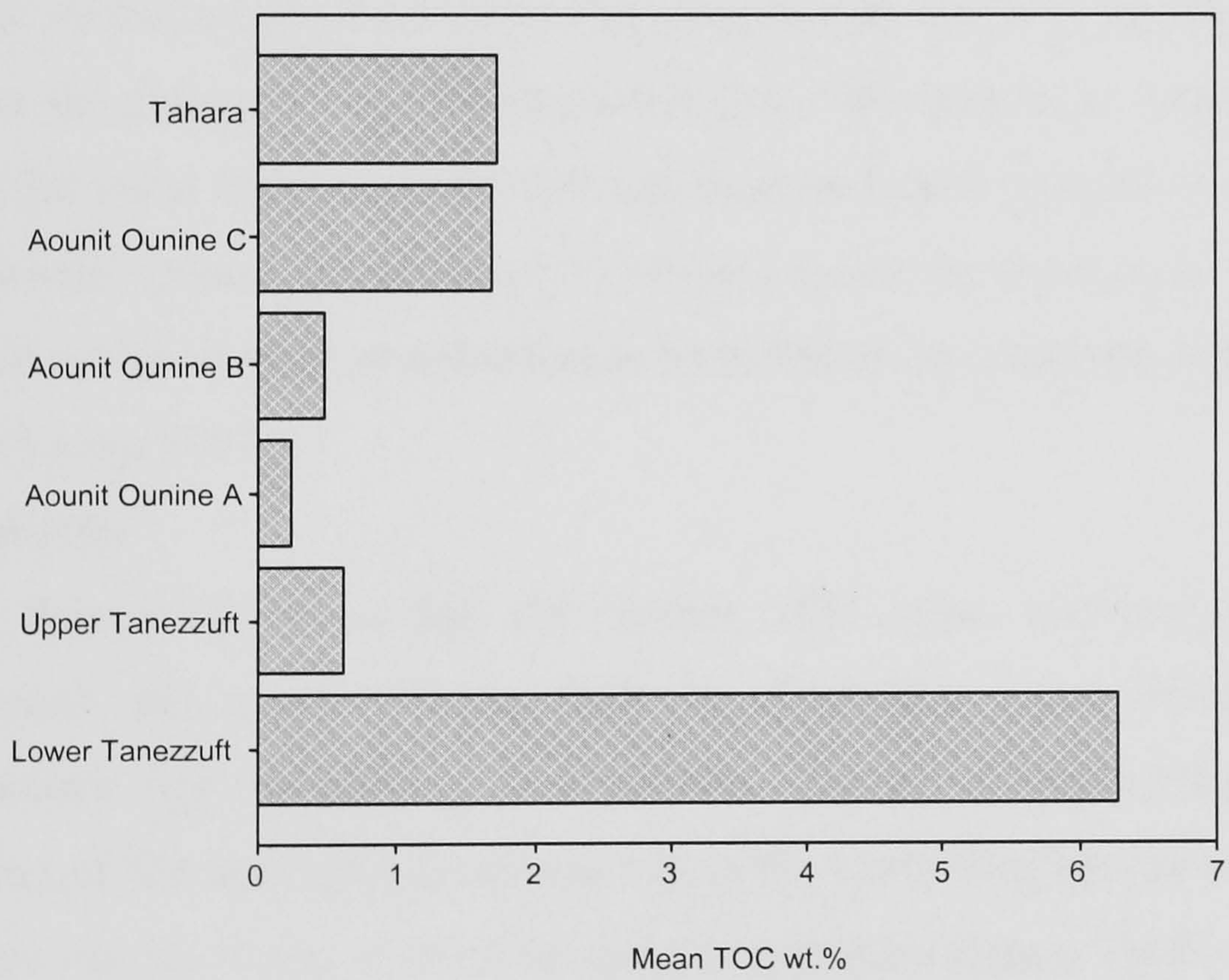

Figure 3.2 .Stratigraphic variation in total organic carbon contents (TOC%): (A) core samples, (B) cutting samples.

The Effect of Shale Characteristics (core samples only)

Colour

Carbon content is often generally related to sediment colours (Potter *et al.*, 1982). Figure 3.3 shows that the highest median TOC is found in the black category (10.7%); there is than a progressive decrease of 96% in relative terms to a value of 0.37% in medium light grey shale. Figure 3.4 shows that in the four formations that contain significant numbers of shales there is a similar decrease in TOC from the darkest to lightest samples.

Bioturbation

Figure 3.5 for whole dataset shows that the median TOC value decreases from non-bioturbated shales to heavily bioturbated shales by 93% in relative terms from a value of 2.9% to a value of 0.2%. The maximum TOC value shows a similar decrease from 38.6% in non-bioturbated shales to 0.3% in the heavily bioturbated category (4.3% for bioturbation present). The bioturbation levels in the Palaeozoic succession reflect the changing depositional conditions. The absence of bioturbation in samples from the basal Silurian Tanezzuft hot-shale indicates suboxic or anoxic depositional conditions. Greater preservation of organic matter in dysoxic-anoxic facies has often related to the absence or reduction in bioturbation as dissolved oxygen falls below 1-2 ml^{-1} (Tyson, 1995).

Graptolites

Figure 3.6 shows that the median TOC value increase from non-graptolitic Devonian and upper Silurian shales to graptolitic lower Silurian shales. Pelagic graptolites first appear in the Tremadoc. During a major transgression after the melting of the late Ordovician ice cap in the early Silurian the number of graptolite species rose to 70 (in the *Monograptus triangulates* Zone). There is then a decrease in number of species through the Wenlock, accompanied by a marine regression in many parts of the world, that saw a reduction of deep shelf platform muds and their replacement by carbonates in many regions (Leggett *et al.*, 1981). The graptolites subsequently became extinct during the Devonian.

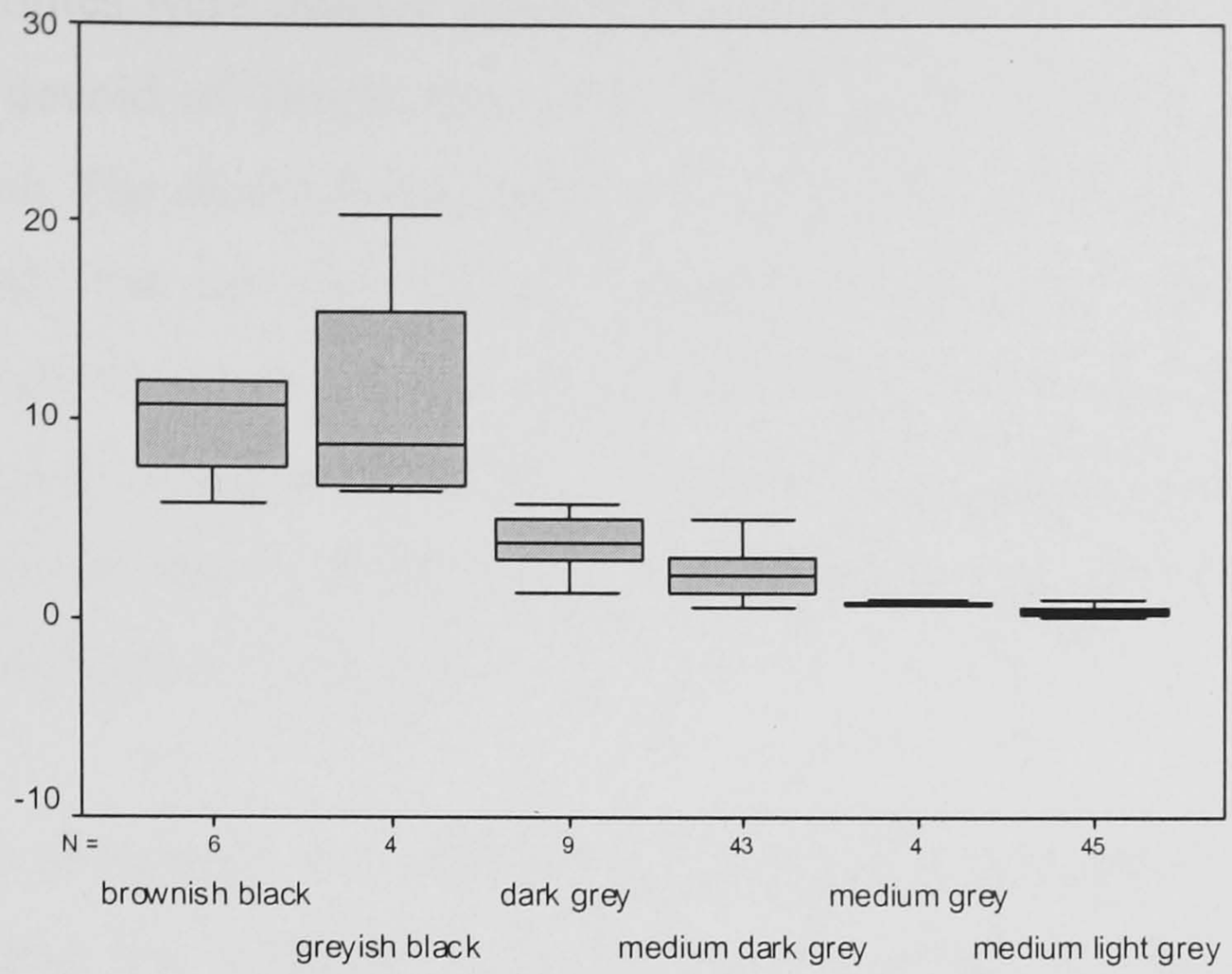

Figure 3.3. Box plot (quartile distributions) showing the relationship between shale colour and TOC values of the whole dataset (N = number of samples).

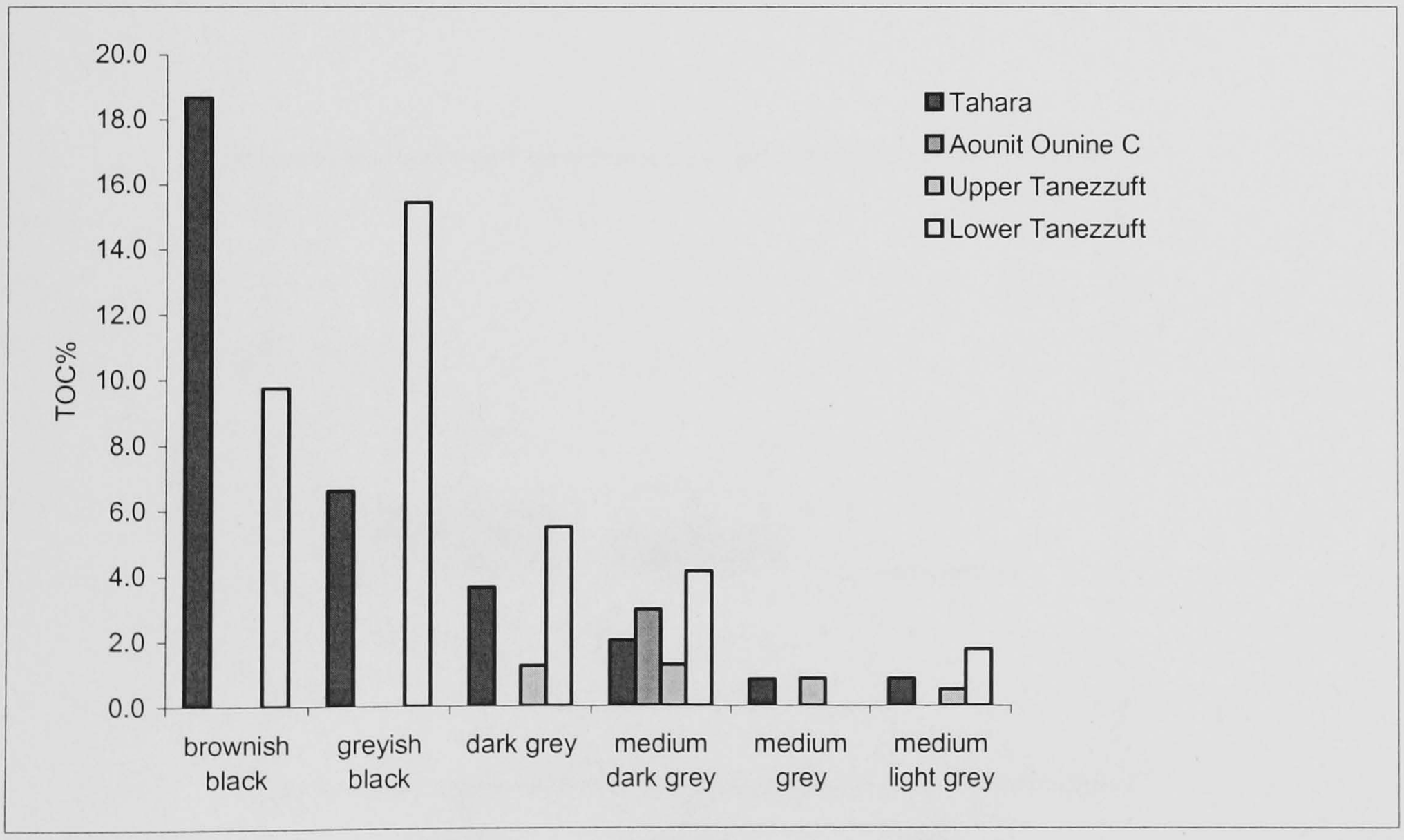

Figure 3.4. Mean TOC values in each shale colour category in the four formations examined.

The graptolites were pelagic and occur predominantly in dark mud-stone and shales that are "devoid of almost any other fossils" and commonly characterized by fine laminations. The absence of bioturbation, and locally abundant pyrite suggests that the living conditions and their site of fossilization were removed from vigorous wave action and from highly oxygenated bottom waters which would have supported active predators and scavengers (Bulman & Stormer 1971; Berry *et al.*, 1987). Berry *et al.* (1987) reported that the fauna developed adaptations for survival under conditions of low to no oxygen availability.

Graptolite abundance will reflect both the original abundance of the organisms and their dilution by sediment. High productivity could explain why there are more graptolites in the organic-rich shale, but so could low dilution due to low sedimentation rates during the early phase of transgression when the basin was starved of sediment. They may also be better preserved in the black shale facies.

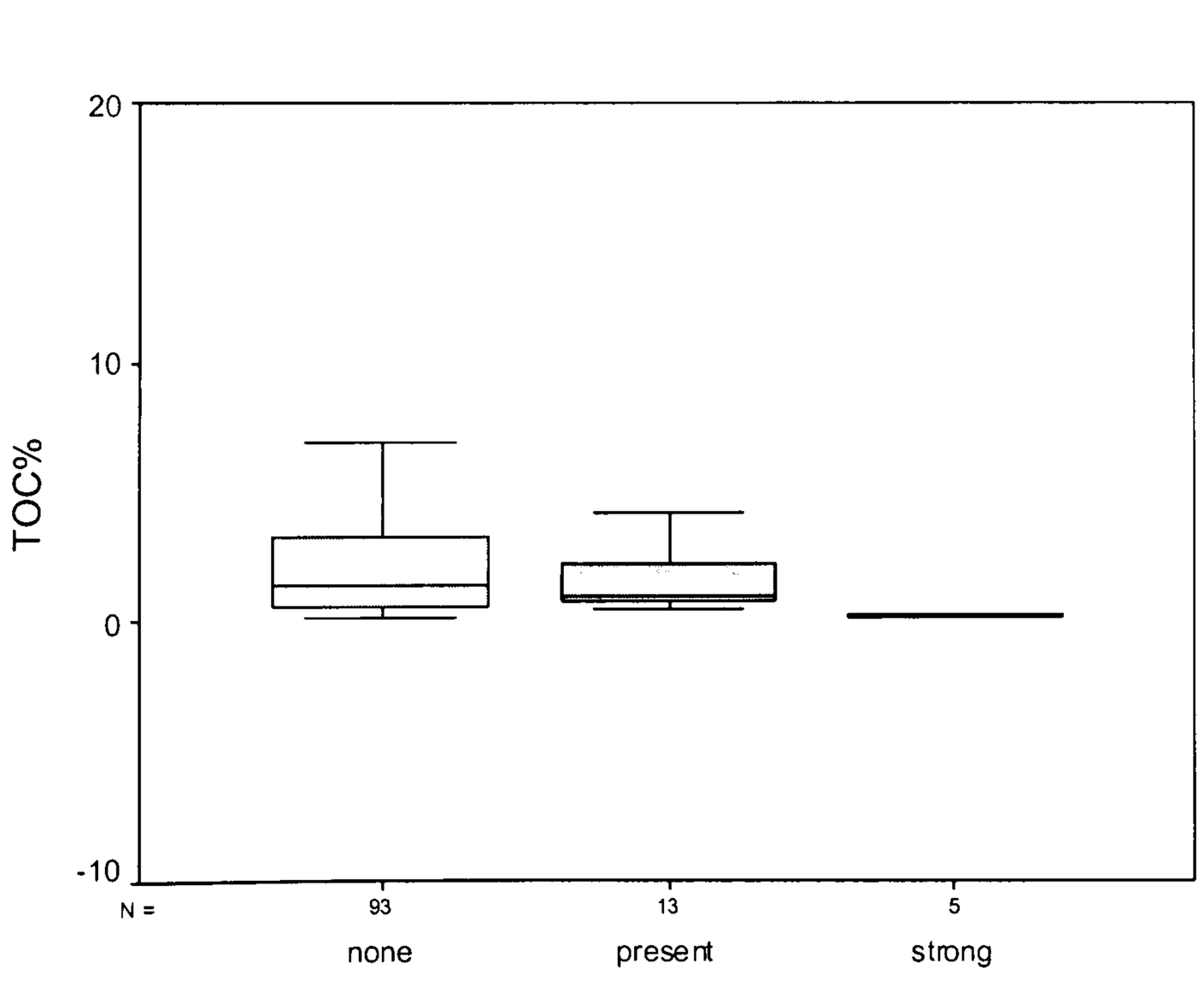

Figure 3.5. Box plot (quartile distributions) showing the relationship between bioturbation level and TOC values in the whole datase. (N = number of core samples).

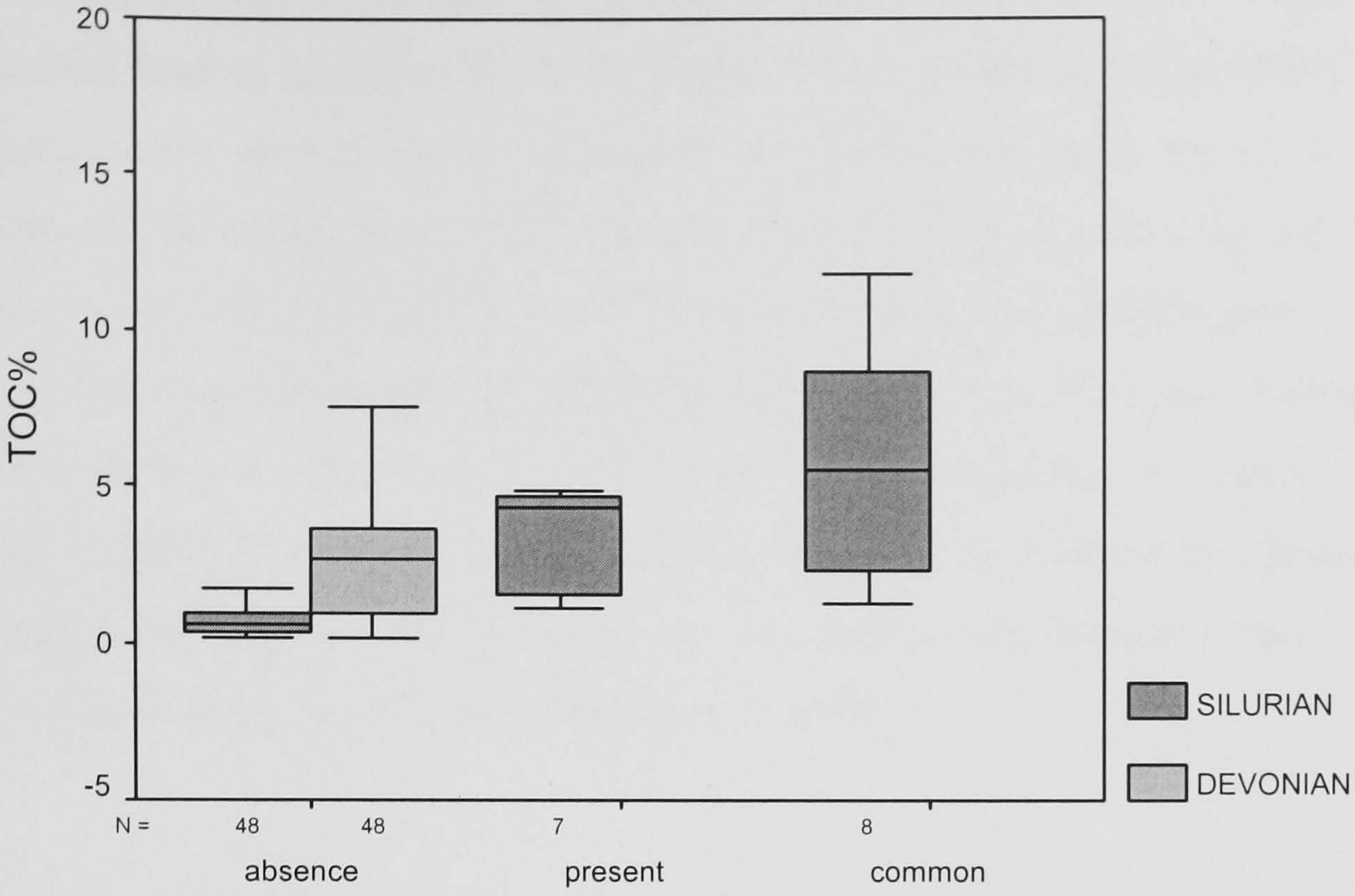

Fig. 3.6. Box plot (quartile distributions) showing the relationship between graptolite abundance and TOC values for the whole dataset, differentiated by period (N = number of core samples).

3.2.3 Relationship With Gamma Ray

Well log and TOC data were used to established a relationship between gamma-ray response level and organic richness. Figure 3.7 is a plot of gamma-ray response and organic richness (TOC) of the typical Tanezzuft hot-shale source facies in three different wells across the basin. The gamma-ray response is clearly positively correlated with TOC%. Wells A1-70 and F1-66 contain the basal Silurian hot-shale, identified by gamma-ray values > 150 API units. In well A1-90 the basal Silurian has a low TOC and low gamma-ray values (< 60 API units); this may be due to lower preservation under less anoxic conditions or greater dilution. In most basal Tanezzuft Formation penetrations in the study area a cutoff value of 150 API gamma-ray units can be used to distinguish potential source shales from non-source shales (cf. Lüning *et al.*, 2000). The isopach contour map of the 'hot-shale' (Fig. 3.8) was produced using around 25 digitized well logs and contoured using Surfer 6 for Windows). This map clearly indicates a significant spatial variation in hot shale thickness. Generally the thickest basal Tanezzuft hot shale lies in north and northeastern part of the basin,

pinching out toward the south and southwestern part where the entire Tanezzuft section becomes lean in organic carbon. The basal Silurian shale in the southern part of the basin can be considered as age-equivalent to the hot-shale occurs in the northern part of the basin, biostratigraphically assigned Early Llandovery (Belhaj, 1996; Luning *et al.*, 2000). The absence of the 'hot-shale' in this southern part of the basin may reflect deposition on a topographic palaeo-high with shallower and more oxygenated conditions. The progression from dysoxic-anoxic to more oxic environment would be accompanied by both a decrease in the preservation potential and increasing susceptibility of the sediment to erosion and dilution. This is in agreement with the interpretation of Luning *et al.*, (2000).

3.2.4 The Effect of Organic Matter Type

When only those samples dominated by AOM (>50%) are considered (Fig. 3.9) the highest median TOC values occur in the shale-dominated lithologies. When only the phytoclast-dominated samples are included (Fig. 3.9) the higher TOC values are found in sand-dominated categories. This is a common pattern (cf. Tyson, 1995).

Figure 3.10 show that the values of AmOC and PhytOC within the dominant lithology have almost identical trends as AOM (>50%) and phytoclasts. Thus, when, the percentage of AOM and phytoclasts in the shale and sand dominant lithology increases (Fig. 3.10) so does the TOC. The higher median TOC found in phytoclast-dominated sand may be partly due to autochthonous organic matter, as the potential for preserving this material is still relatively high in this category.

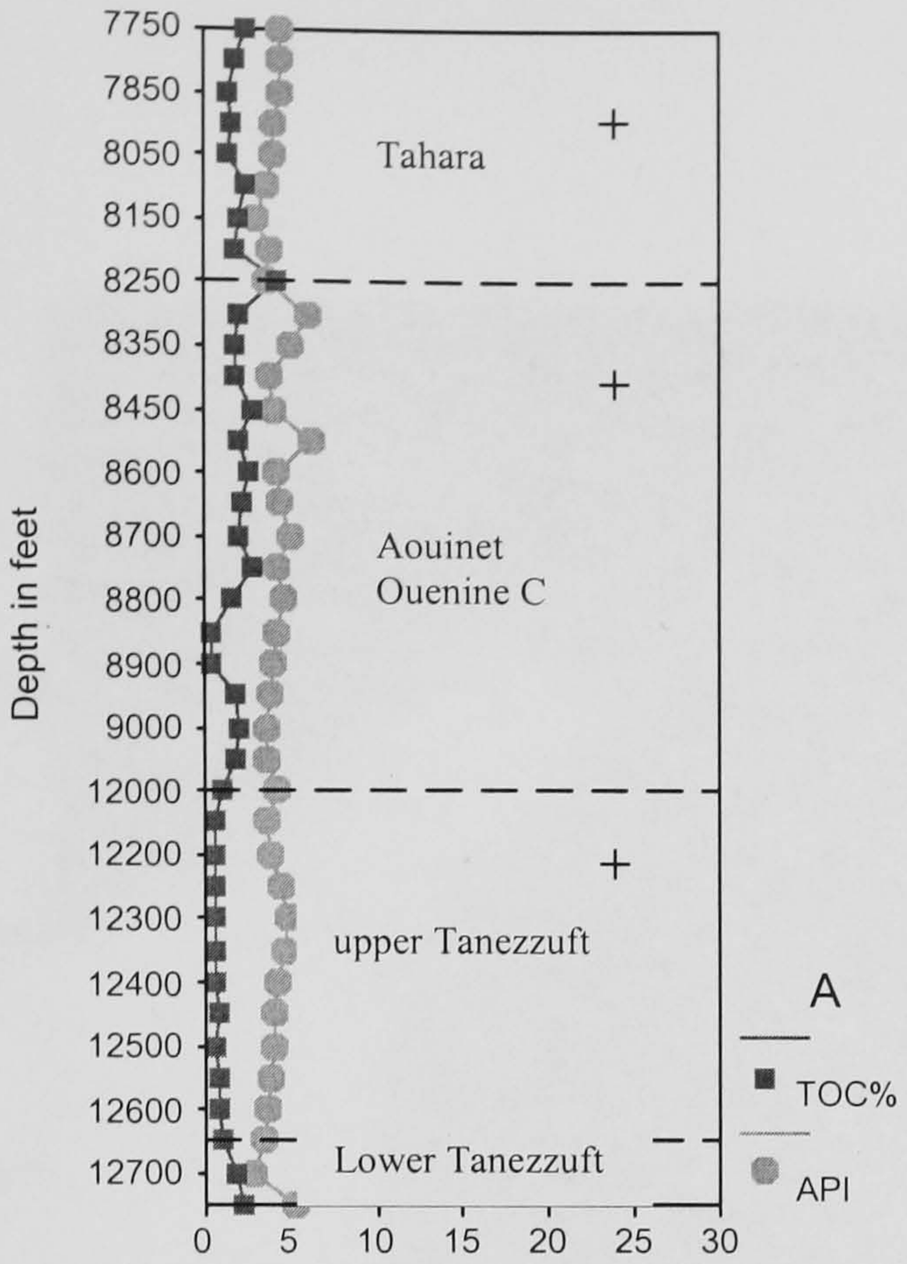

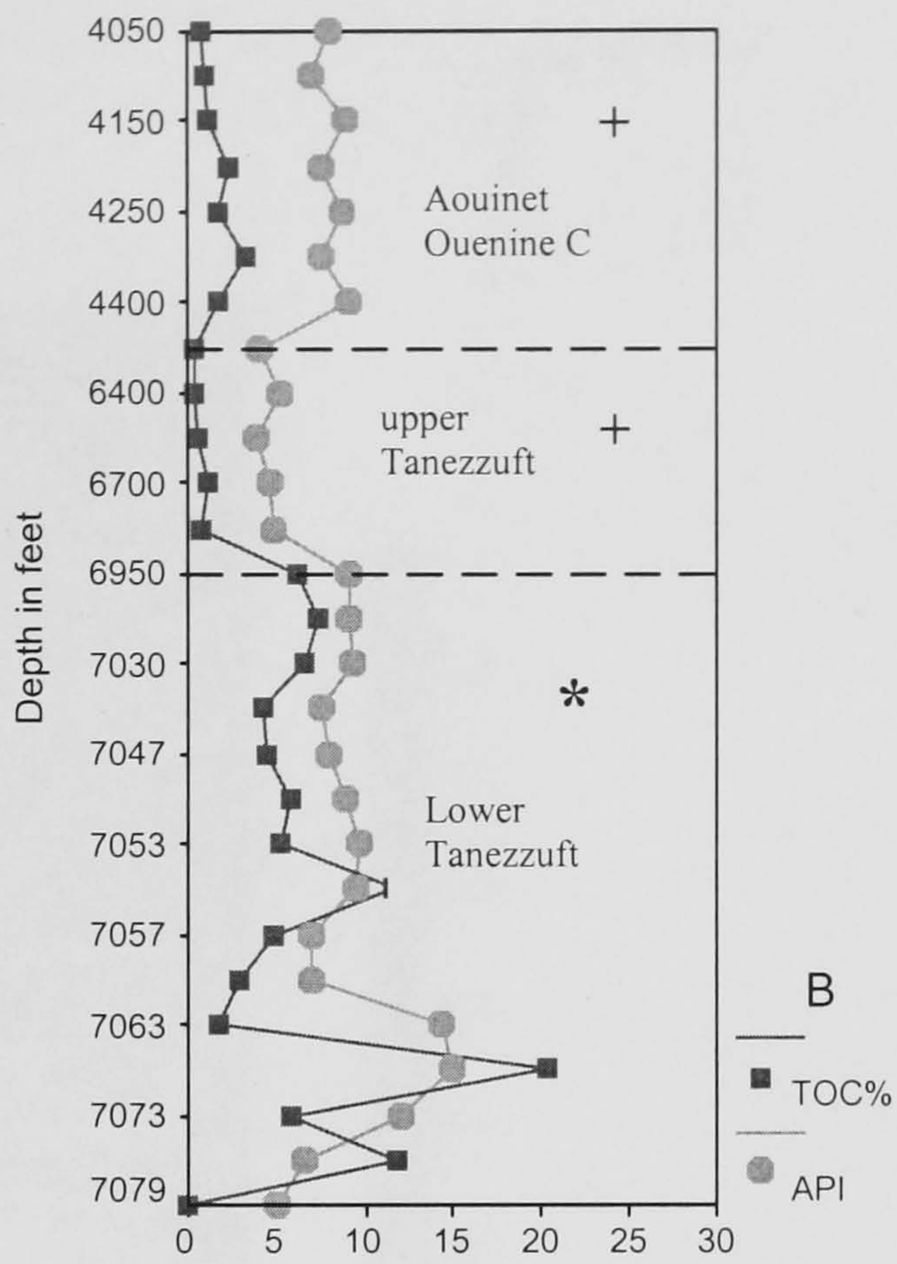

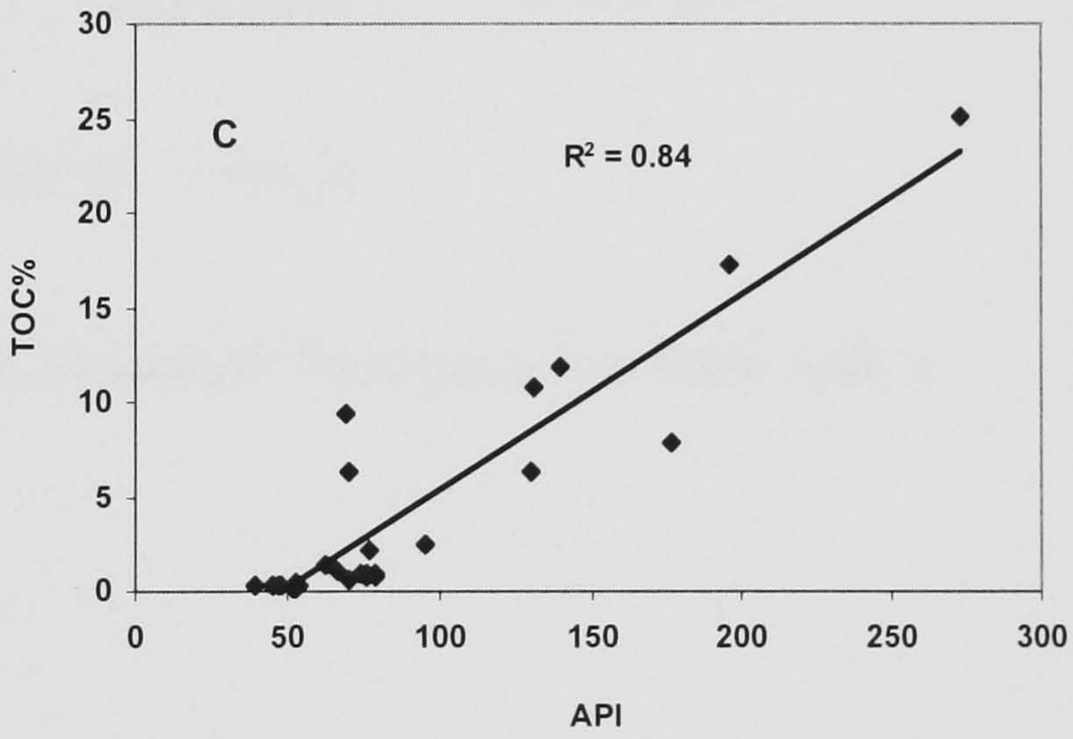

Figure 3.7. Gamma-ray log versus total organic carbon contents for: (A) well A1-90, (B) well F1-66, and (C) A1-70; each *x*-axis unit represents 10 API units. Cross plot of API and TOC content for Lower Silurian samples from well A1-70.

Key: * Core samples, + Cutting samples

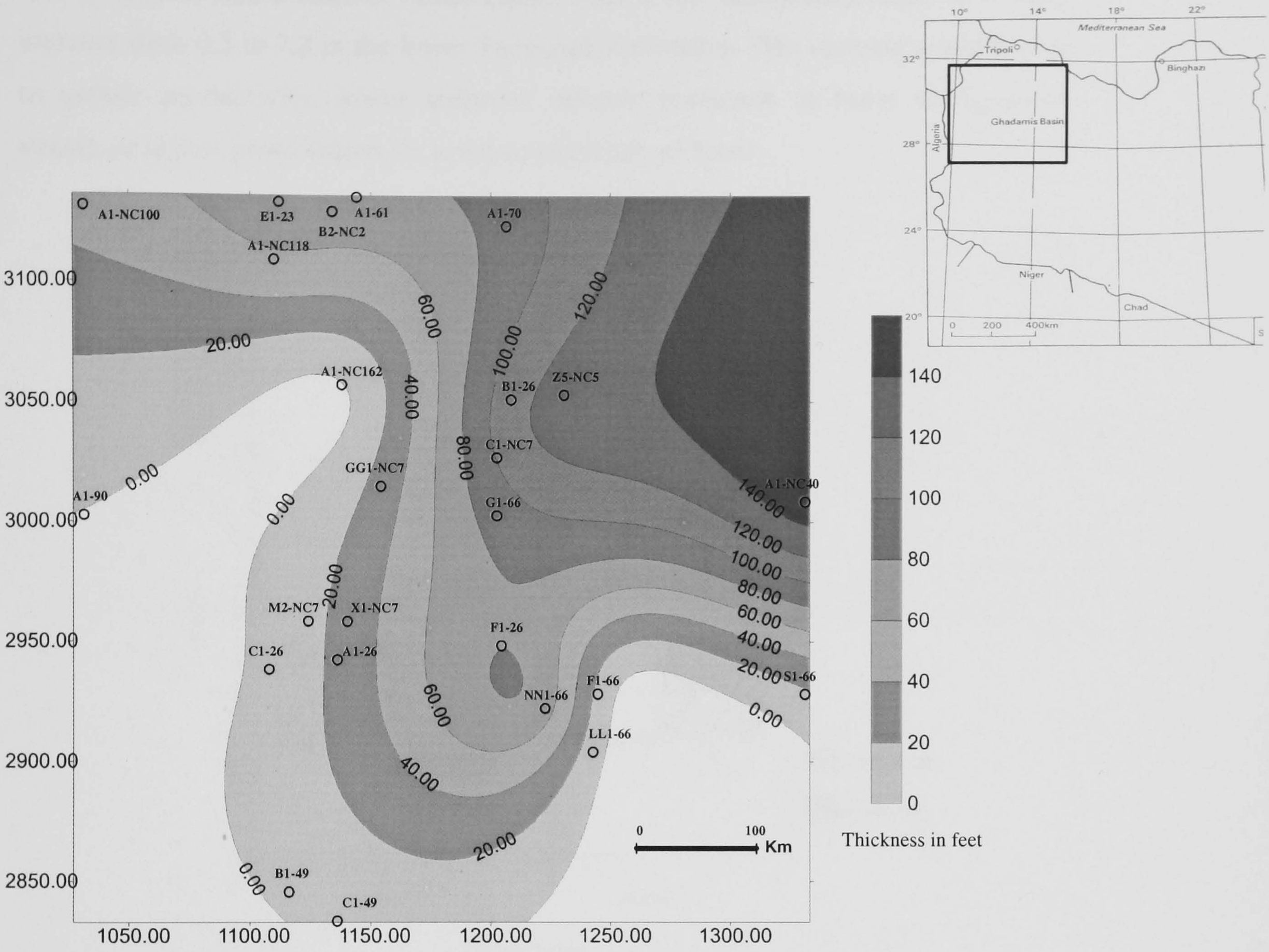

Figure 3.8. Isopach map for the basal Silurian Tanezzuft Formation hot shale with a gamma-ray response > 150 API units.

3.2.5 "PhytOC" and "AmOC" Values

The stratigraphic trends in mean values of PhytOC, and AmOC (Fig. 3.11) reflect differences in lithology and environments between the lithostratigraphic units. PhytOC values are "more" absolute than percentage phytoclasts values, although they are still affected by other variables such as sediment dilution (Tyson, 1989). The high PhyTOC values in the Upper Devonian Tahara Sandstone and upper Aouinet Ouenine C formations suggest that the quantity of phytoclasts increases in absolute terms (associated with greater fluviodeltaic input). The regressive marine coarse-grained Aouinet Ouenine A & B, Ouan Kasa, Tadrart and Acacus Sandstone formations

mostly exhibit stable AmOC values (apart from a few anomalies); there is a sharp increase from 0.3 to 7.8 in the lower Tanezzuft Formation. This increase could be due to greater productivity, lower sediment dilution (common in basal transgressive strata), or higher preservation, or some combination of these.

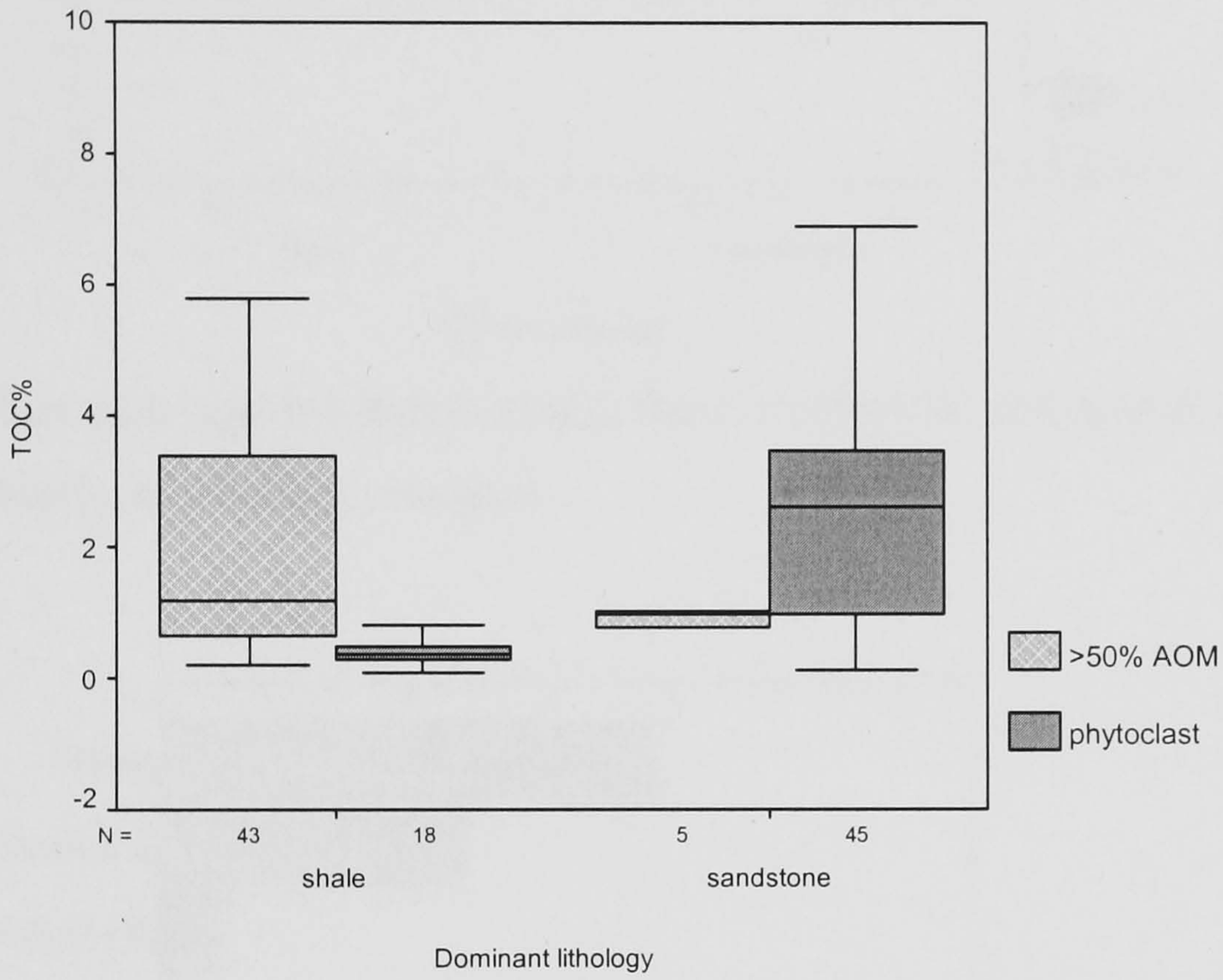

Figure 3.9. Box plot (quartile distributions) showing the TOC values within the dominant lithology category with respect to AOM and phytoclast dominance.

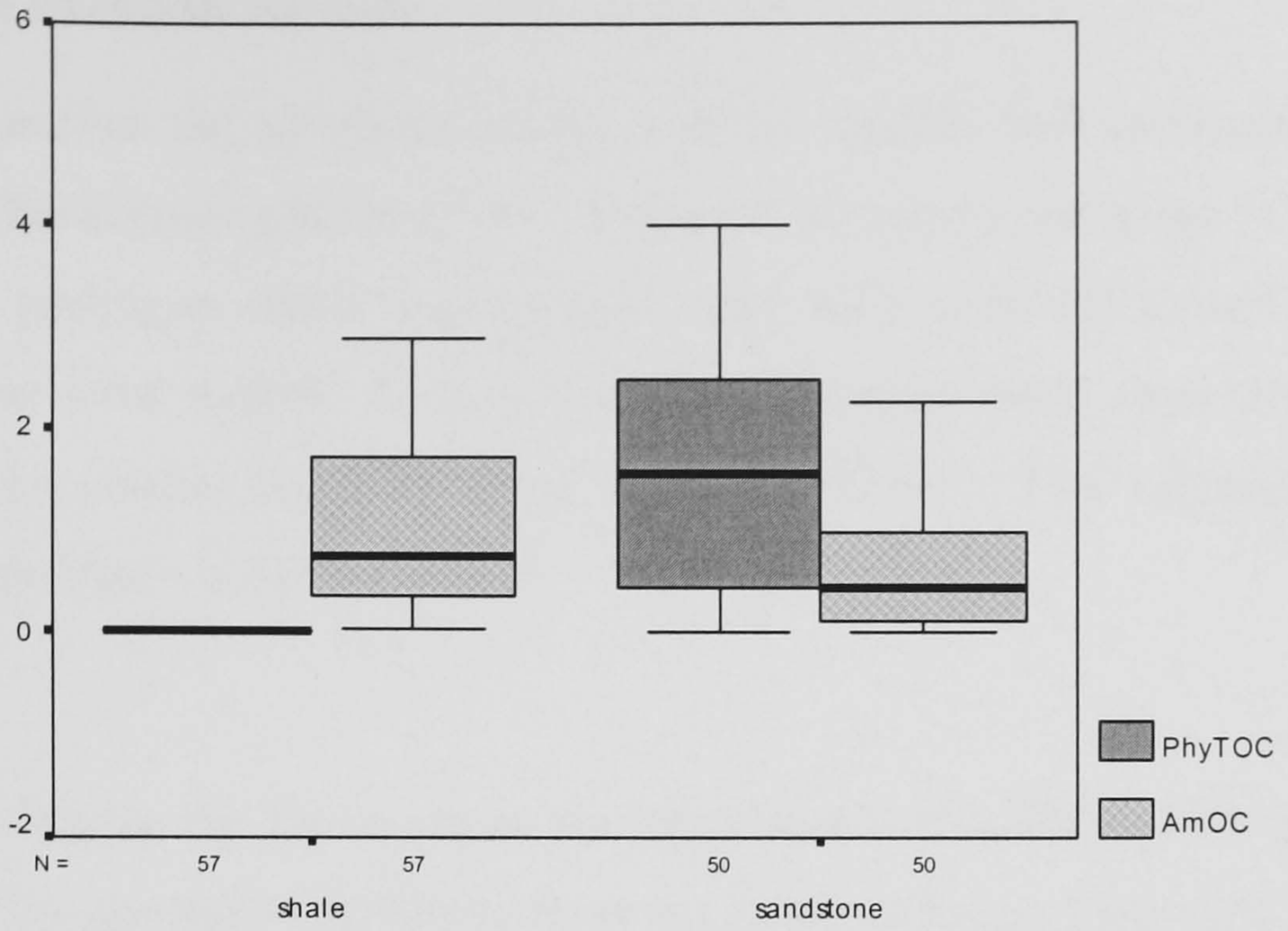

Figure 3.10. Box plot (quartile distributions) show the PhytOC and AmOC values within each dominant lithology category.

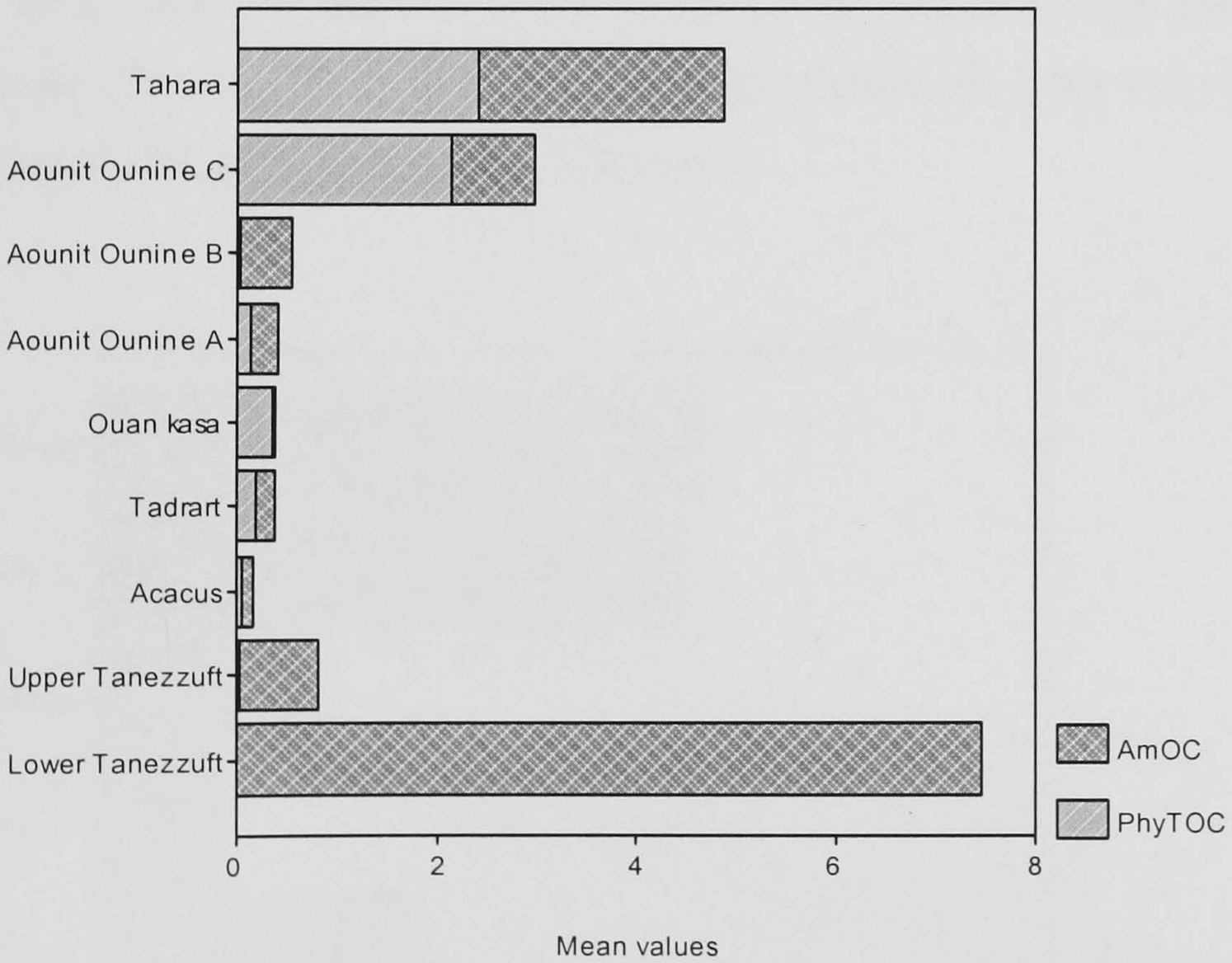

Figure 3.11. Stratigraphic trends in the mean values of PhytOC and AmOC.

3.3 Rock-Eval Pyrolysis Results

In this section the pyrolysis results will be studied and correlated with the optical data. The average pyrolysis results of each formation are given in Tables 3.2 and 3.3. The hydrogen index and kerogen type have been calculated using two approaches: the usual method of calculating the hydrogen index from the measured values sample by sample (S_2/TOC x 100), and using the S_2 v. TOC regression method of Langford and Blanc-Valleron (1990).

3.3.1 Tmax

For the whole dataset the Tmax values are between 415 and 467°C. The mean Tmax varies (Fig. 3.12) generally increasing from the Lower Silurian Tanezzuft Formation, to the Upper Devonian Tahara and Aouinet Ouenine C formations. The Tmax values are also influenced by kerogen type and TOC level. The samples from upper Tanezzuft and Aouinet Ouenine A & B formations have low TOC (average < 0.5%). For siliciclastic whole-rock samples, HI and Tmax are often respectively too low and too high where TOC contents are below 0.5%, owing to retention of hydrocarbons by clay minerals (Tyson, 1995). The Tmax maturity trends and their correlation with the optical maturity data are discussed in Chapter 5.

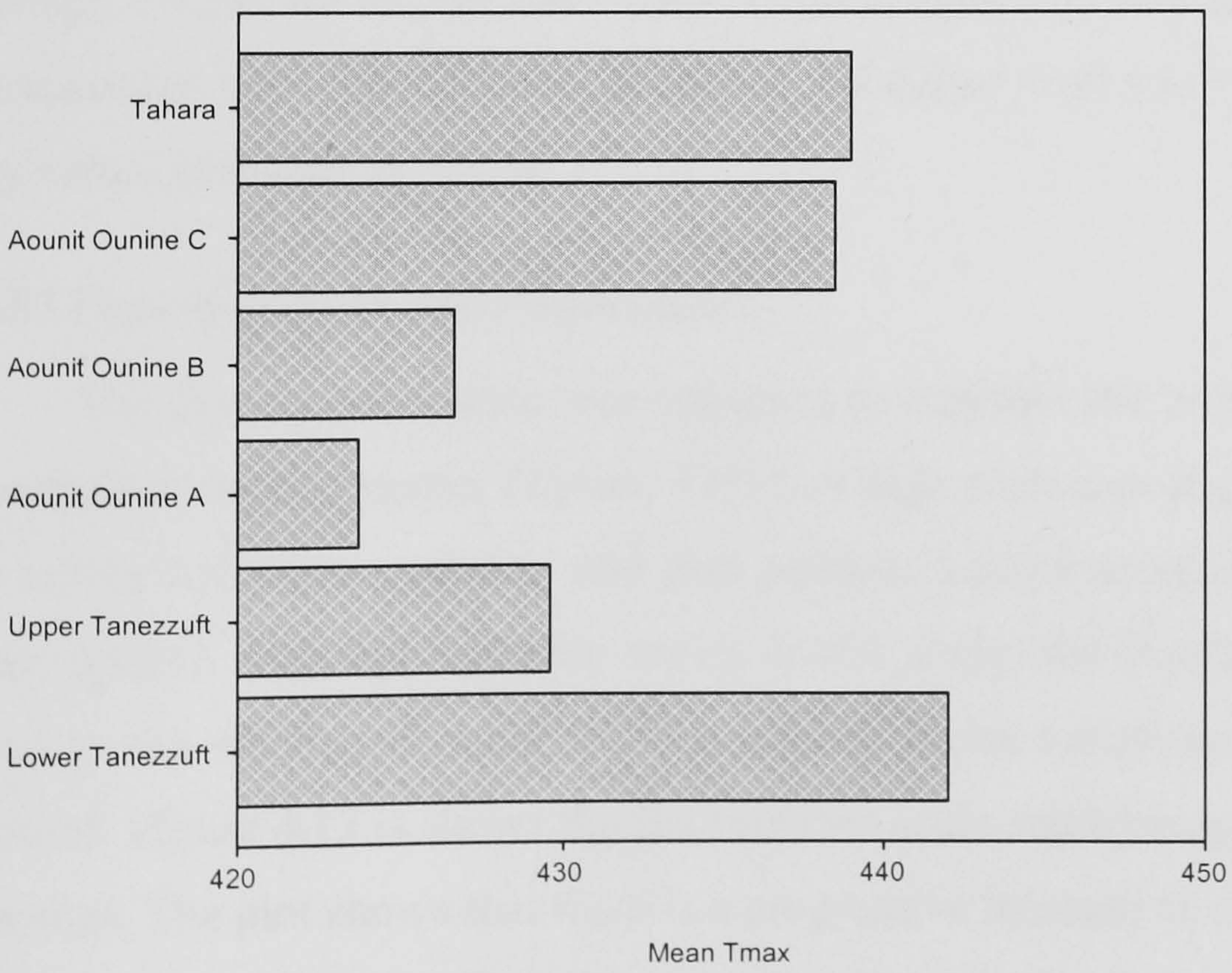

Figure 3.12. Stratigraphic trends in mean values of Tmax °C. The Tmax decreases in the older units clearly indicate the influence of facies.

3.3.2 Measured Hydrogen Index

The measured hydrogen indices (Table 3.2 & 3.3) are mostly below 450. Allowing for the affect of maturity the Lower Tanezzuft Formation almost certainly had a Type II genetic kerogen type. The Tahara Sandstone and Aouinet Ouenine C formations have HI values mostly corresponding to Type III kerogen. Other units, including the upper Tanezzuft, Acacus Sandstone and Aouinet Ouenine A & B formations correspond to intermediate Type III/II kerogen.

Most of the lower Tanezzuft "hot-shale" samples in wells located in the northern part of the basin (D1-NC2 and A1-70) are within the early mature zone: the Tmax ranges from 436 to 445 ^{o}C, and HI values correspond to Type II-III kerogen. Some samples have relatively high HI considering their maturity. The lower Tanezzuft "hot-shale" samples in well F1-66 (located in the south eastern part of the basin) are apparently within the late mature stage (Tmax ranges from 444 to 453 ^{o}C) but they have an HI of up to 250 (Type III kerogen). These rich samples correspond to intervals with gamma ray values of more than 150 API units. The samples from Lower Tanezzuft Formation are enriched in AOM content and genetically would almost certainly correspond to Type II kerogen. In the south western part of the basin, the HI of the lower Tanezzuft Formation is reduced to < 50 corresponding to IV kerogen (wells B1-49, M2-NC7 and A1-90); however, here this may reflect lower preservation under less anoxic conditions, associated with a low TOC and low gamma ray values (see section 3.2.3).

3.3.3 Hydrogen Index and Fluorescence

The fluorescence scale was designed to evaluate the preservation of immature amorphous organic matter (Tyson, 1995). A high scale means good preservation, and so higher hydrogen contents, and thus predicts a good potential rock (if maturity is appropriate). Although maturity varies in this study, the fluorescence scale was still used to see whether it could indicate organic facies variations within the sediments studied. Figure 4.13 is shows the fluorescence scale and hydrogen indices for the core samples. The plot shows that there is a progressive increase in the median HI of 470% in relative terms through fluorescence categories 1 to 4. A cross plot of the average HI versus average AOM fluorescence scale from 1 to 4 (Fig. 14) for the core samples shows a strong positive correlation of (r^2 = 0.93), but with only four values the

significance is limited. Interestingly some Silurian samples exhibit well preserved fluorescent AOM typical of Type II kerogen (fluorescence scale 5), but their HI values remain relatively low compared to what has been observed in Mesozoic studies (Tyson, pers.comm.).

3.3.4 TOC and Hydrogen Index

Katz (1983), and Tyson (1995) consider that the hydrogen indices have little meaning where TOC values are less than 0.3–0.5 %. However, hydrogen indices tend to be positively correlated with TOC values when the TOC is above 1%. Difference in the slopes of hydrogen indices versus TOC are partly

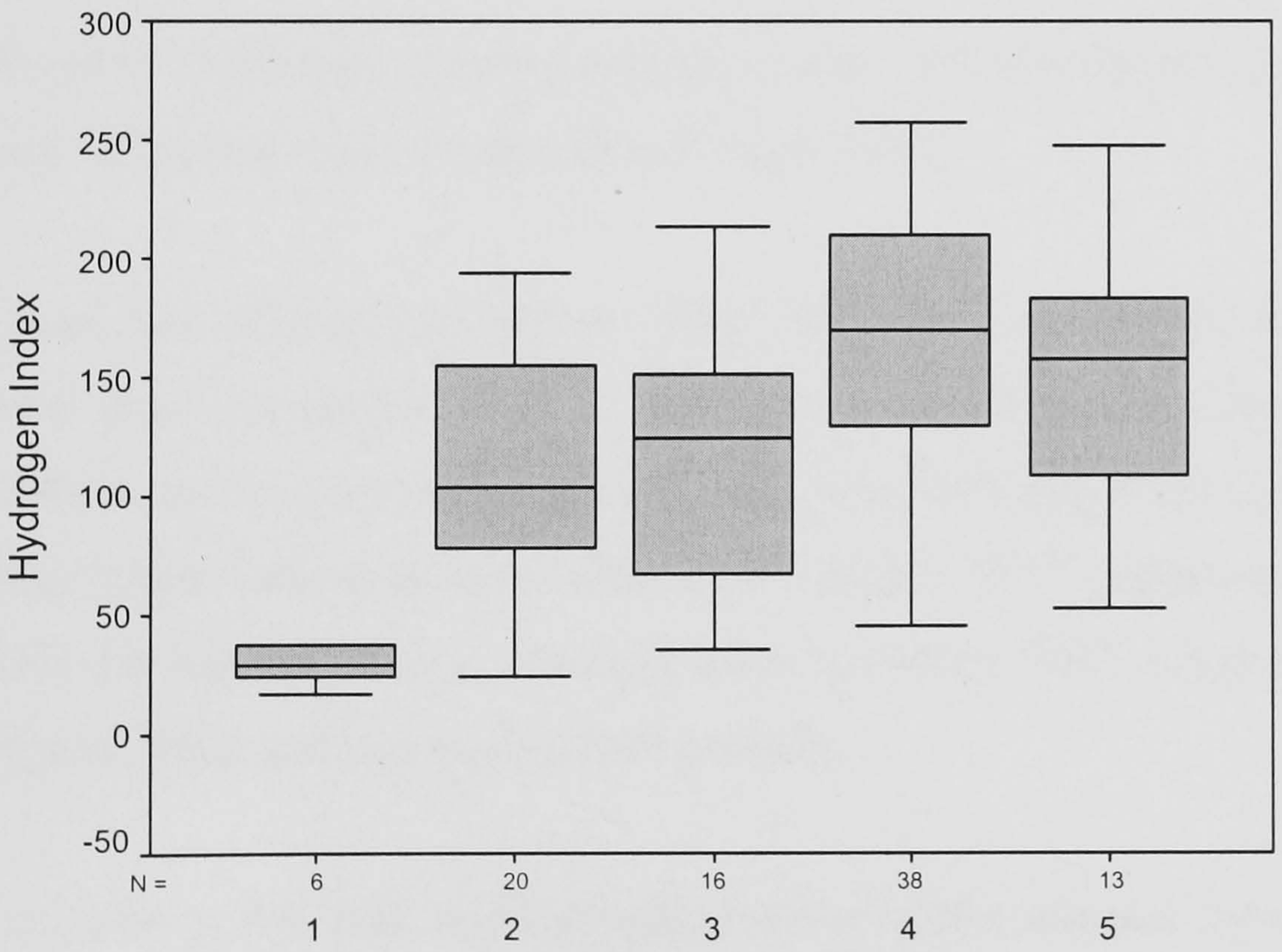

Figure 3.13. Box plots (quartile distributions) shows the relationship between fluorescence scale values and hydrogen indices.

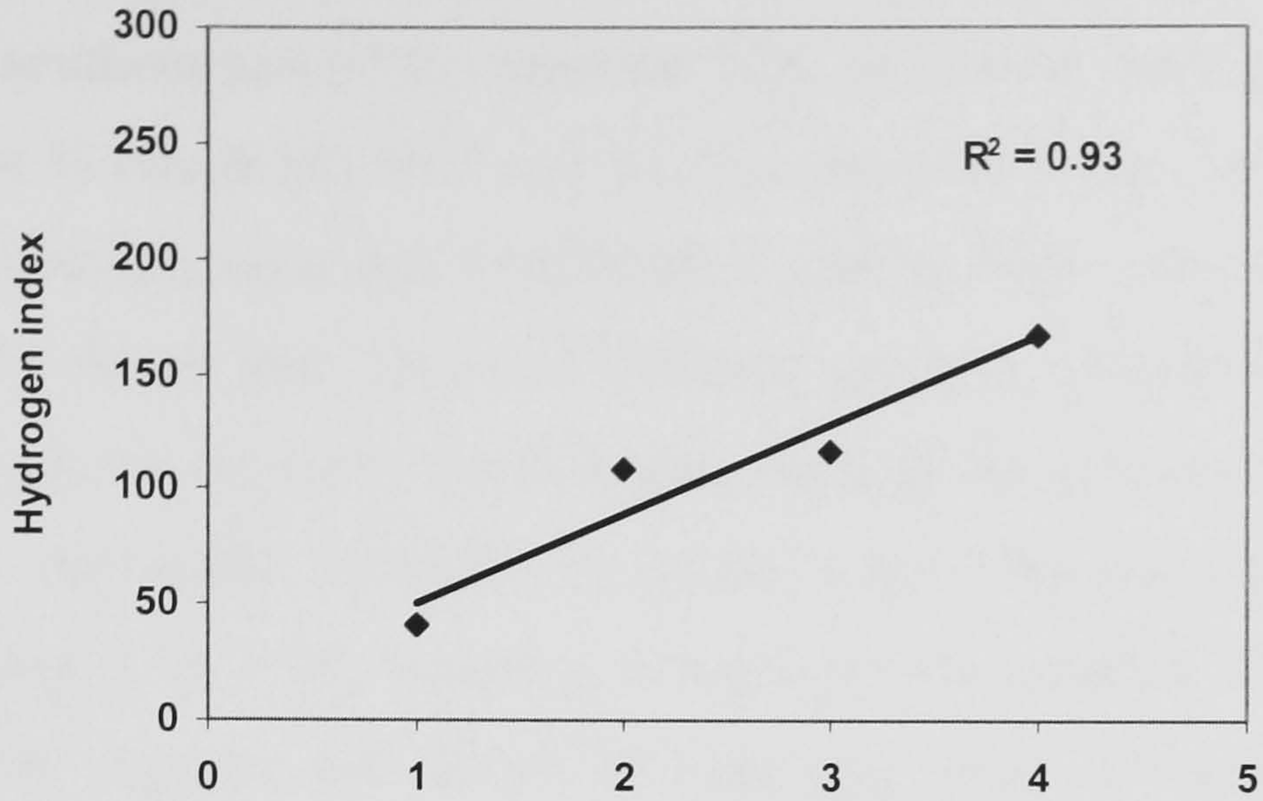

Figure 3.14. Cross plot of average hydrogen index of sample values for each fluorescence scale (core samples only).

due to differences in the type of initial organic matter, or in the degree of preservation as influenced by bottom water oxygenation (Tyson, 1995).

The cross plot of hydrogen indices versus TOC (Fig. 3.15) for the whole dataset shows a very poor correlation of ($r^2 < 0.2$), but within different formations from different wells a positive correlation can be found. The plots also show that the cutting samples from lower Tanezzuft Formation have a higher TOC compared to the core samples from the same formation. Cuttings often have less TOC; a higher TOC may be due to typical shale cuttings having been selected.

A cross plot of the TOC and hydrogen indices of the samples from Palaeozoic succession in wells F1-66 and A1-70 (Fig. 3.16), shows that there are two groups of samples. The first group represents the interbedded light to moderate dark shale with sandstone and siltstone (Tahara, Aouinet Ouenine A, Tadrart and the upper Tanezzuft formations), all of which are immature. The second group represents the laminated black shales of the lower Tanezzuft Formation 'hot-shale', which is considerably more mature in well F1-66 compared to well A1-70. The first group shows slightly higher hydrogen indices in the moderately dark shale samples. The non-linear curve of the second group show a wide range of TOC for little range in HI; thus TOC is not

mainly influenced by preservation here, but may reflect mostly variable dilution by sediment. In the southern part of the basin the TOC of Lower Tanezzuft Formation is reduced to < 6 wt % (wells M2-NC7 and B1-49); this may due to lower preservation under less anoxic conditions or due to dilution. A plot of TOC versus hydrogen index (Fig. 3.17 a & b) shows that there two different groups of samples with different trends. The first trend is shown by the dark grey shale of the Aouinet Ouenine and the upper Tanezzuft 'cool-shale' formation, a normal trend where hydrogen indices are positively correlated with TOC, occurring in early mature samples. The second trend is a flat to slightly negative and shown by light grey shale of the upper Tanezzuft Formation and black shale of lower Tanezzuft Formation; the low and constant hydrogen indices over a wide range of TOC values perhaps reflects variable dilution by sediment input. The slightly negative trend of the upper and lower Tanezzuft Formation may reflect higher maturity and thus greater reduction in hydrocarbon potential (S2).

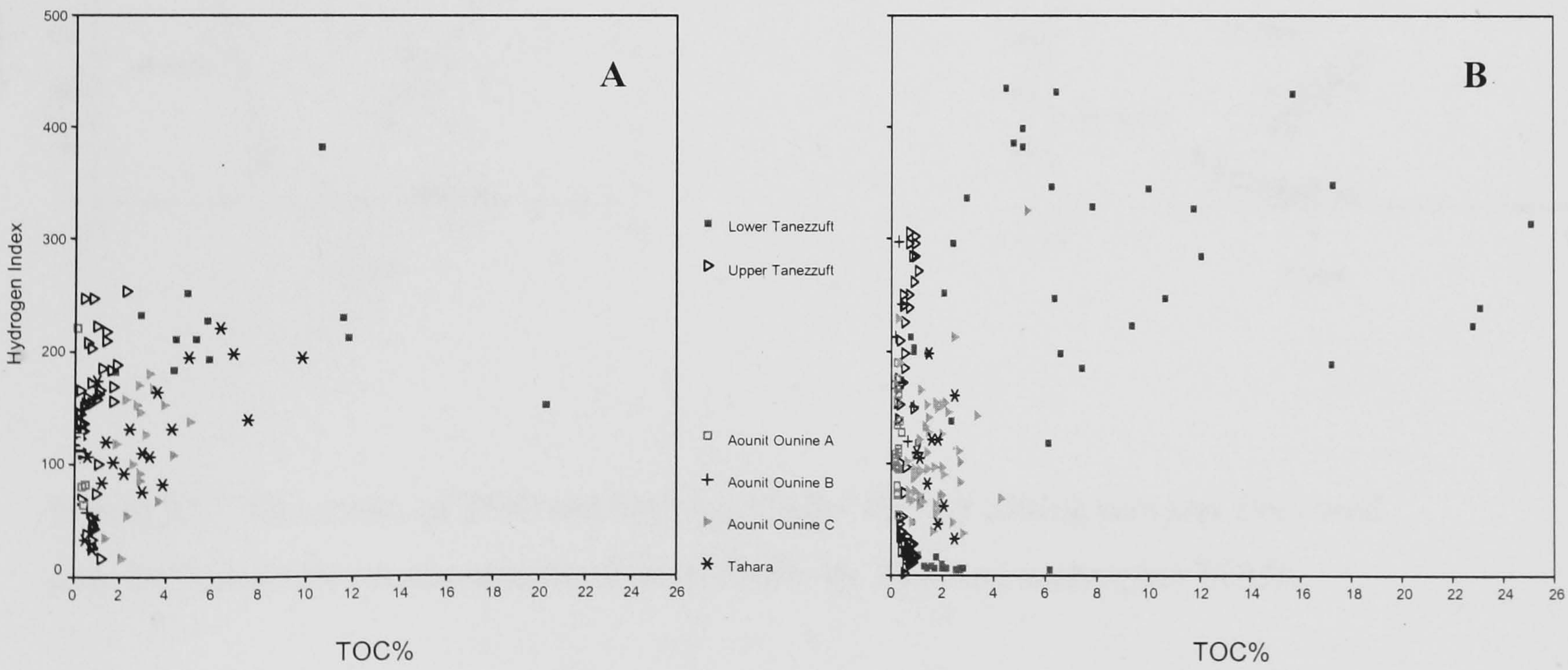

Figure 3.15. Cross plots of TOC and hydrogen index for (A) all core samples, and (B) all cutting samples.

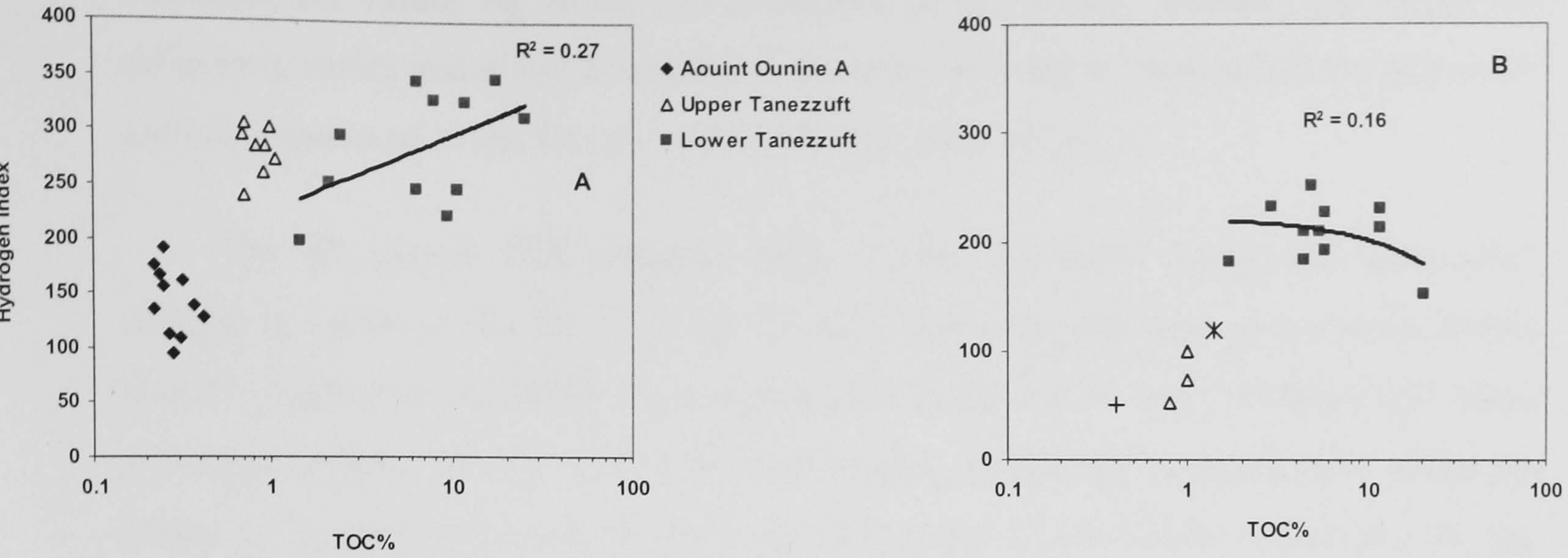

Figure 3.16. Cross plots of TOC and hydrogen index for (A) samples from well A1-70, and (B) samples from well F1-66. Note log scaling for TOC%.

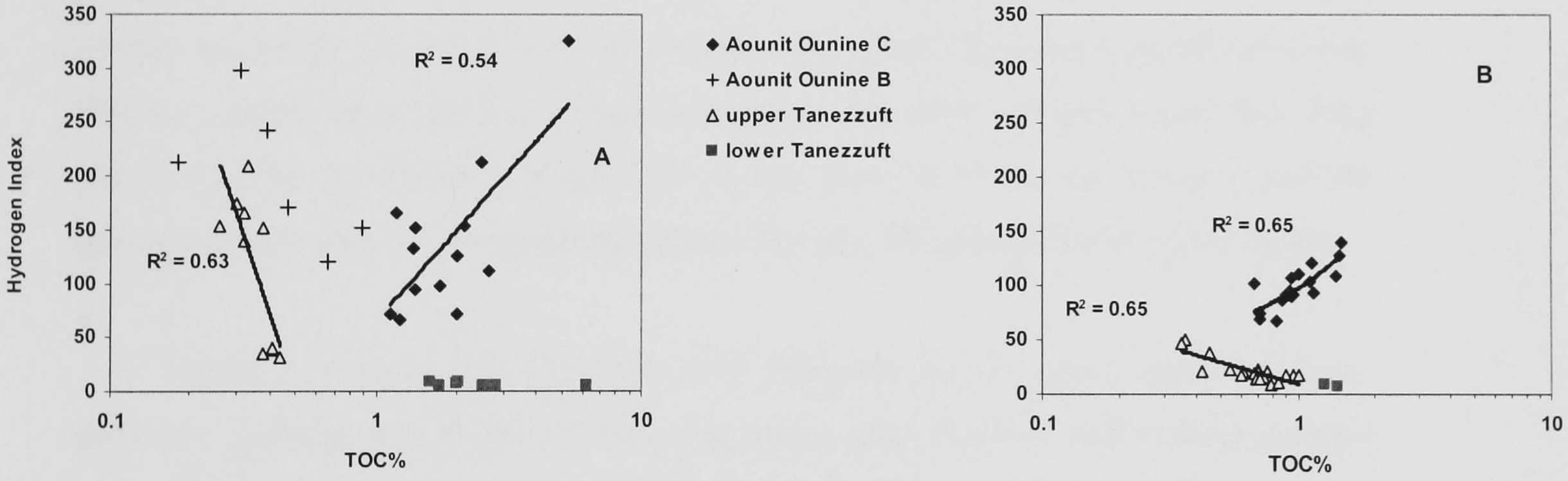

Figure 3.17. Cross plot of TOC and hydrogen index for (A) cutting samples from well M2- NC7, and (B) cutting samples from well B1-49. Note log scaling for TOC%.

3.3.5 Calculated Mean Hydrogen Index

The application of a linear regression on the S2 vs. TOC diagram is supposedly the best tool for calculating the average HI (Langford & Blanc-Valleron, 1990). The HI calculated from the slope of S2 vs. TOC is generally higher than the mean of

measured HI values by about 100 (Cornford *et al.*, 1998). Actually the degree of difference varies and is not linear and is cause by only the non-adsorbed and non-inert carbon being used in the HI calculation (Tyson, pers. comm.).

The S2 versus TOC diagram (Fig. 3.18A) for basal Tanezzuft "hot-shale" samples in wells A1-70, D1-NC2 and Z5-NC5 in the northern part of the basin, shows that the regression slopes for the samples from wells A1-70 and D1-NC2 yield mean hydrogen indices of 327 and 308 respectively, indicating a moderately oil-prone (Type II) kerogen. For well Z5-NC5, located about 75 km south of well A1-70, the calculated mean hydrogen index from the regression slope is only 236. The reduction in the hydrogen index is due to increasing maturity at this site. For the lower Tanezzuft "hot-shale" core samples in well F1-66 (located in the south eastern part of the basin, Fig. 3.18B), the regression slope indicates Type III kerogen with a mean hydrogen index of 160. This reflects the higher maturity and thus greater reduction in the hydrocarbon potential (S2). All these rich samples correspond to intervals with gamma ray values of more 150 API units. The samples from Lower Tanezzuft Formation are all enriched in AOM content and genetically (pre-maturation) would almost certainly have had good Type II kerogen. The other samples which fall along the *x*-axis (Fig. 3.18B) have a mean HI of less than 50, (Type IV kerogen) and are associated with very low gamma ray values. The low HI reflects lower preservation.

Figure 3.19 shows the S2 versus TOC diagram for the upper Tanezzuft cool-shale low gamma ray sample set. The regression slope for core and cutting samples indicates Type II-III kerogen, with a mean hydrogen indices of 226 and 334 respectively. On the basis of low TOC and pyrolytic yields, overall, the upper Tanezzuft shale may only contribute dry gas to the petroleum system at advanced maturity.

The S2 versus TOC diagram (Fig. 3.20) for the upper Devonian Tahara and Aouinet Ouenine C formations samples reveals the presence of gas-prone Type III kerogen, defined by the regression slope with a mean HI of 200. The Tahara and Aouinet Ouenine formations although enriched in phytoclasts still have a significant AOM content, and these Upper Devonian units may contribute to the oil in the Palaeozoic petroleum system.

Comparison of the *x*-intercepts (Table 3.6) shows that the matrix effect is most prevalent in the Tahara and Aouinet Ouenine C formations and has least effect in the upper and lower Tanezzuft formations respectively. Langford and Blanc-Valleron (1990, p.803) consider an intercept value of 0.6 to be 'fairly high'. The high *x*-intercept of the Upper Devonian units may also reflect the black wood (= 'dead carbon') content of the kerogen, as these units are enriched in phytoclasts.

Figure 3.19 shows the S2 versus TOC diagram for the upper Tanezzuft "cool-shale" low gamma ray sample set. The regression slope for the core and cutting samples indicates Type II-III kerogen, with a mean hydrogen indices of 226 and 334.

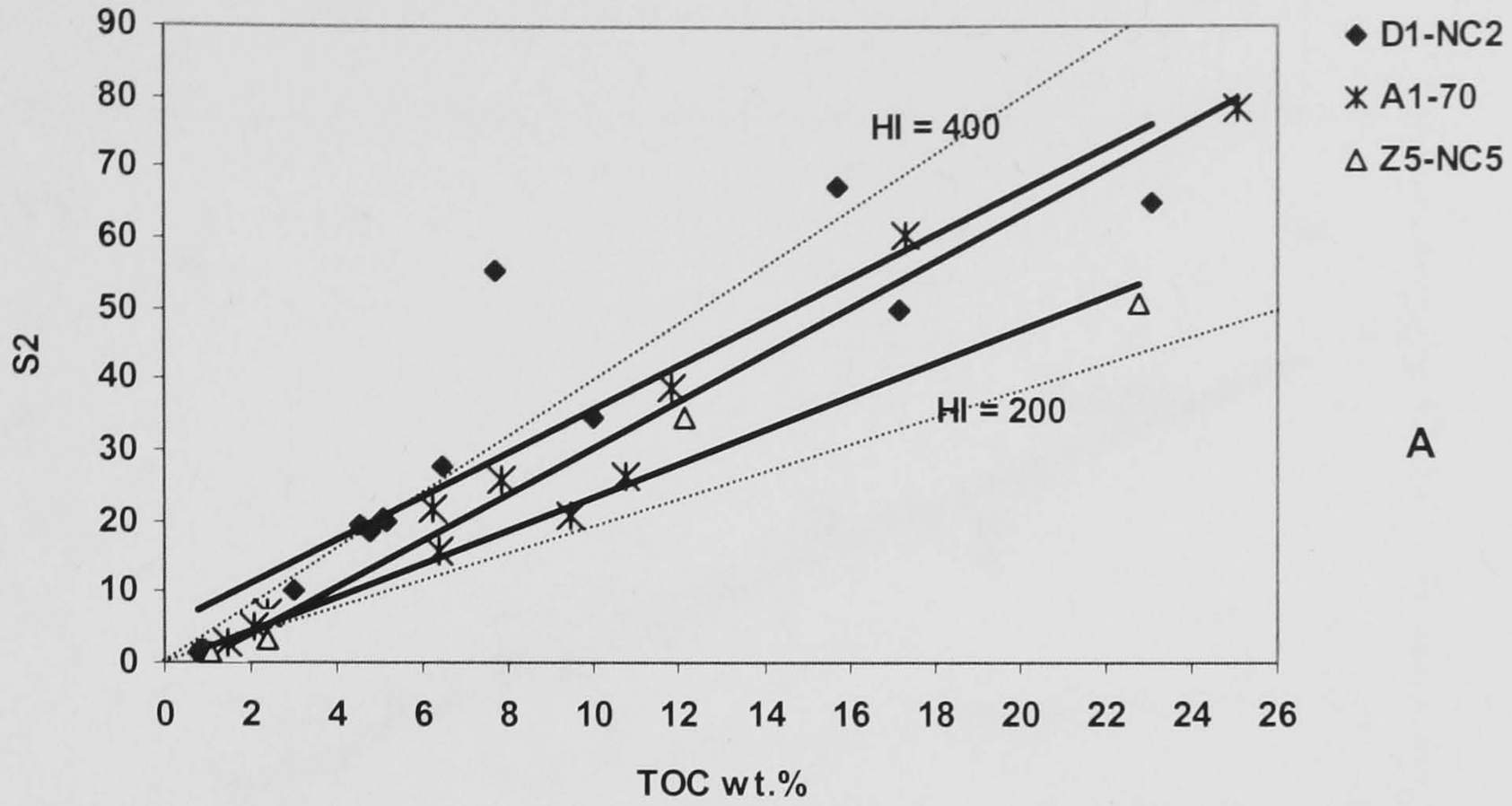

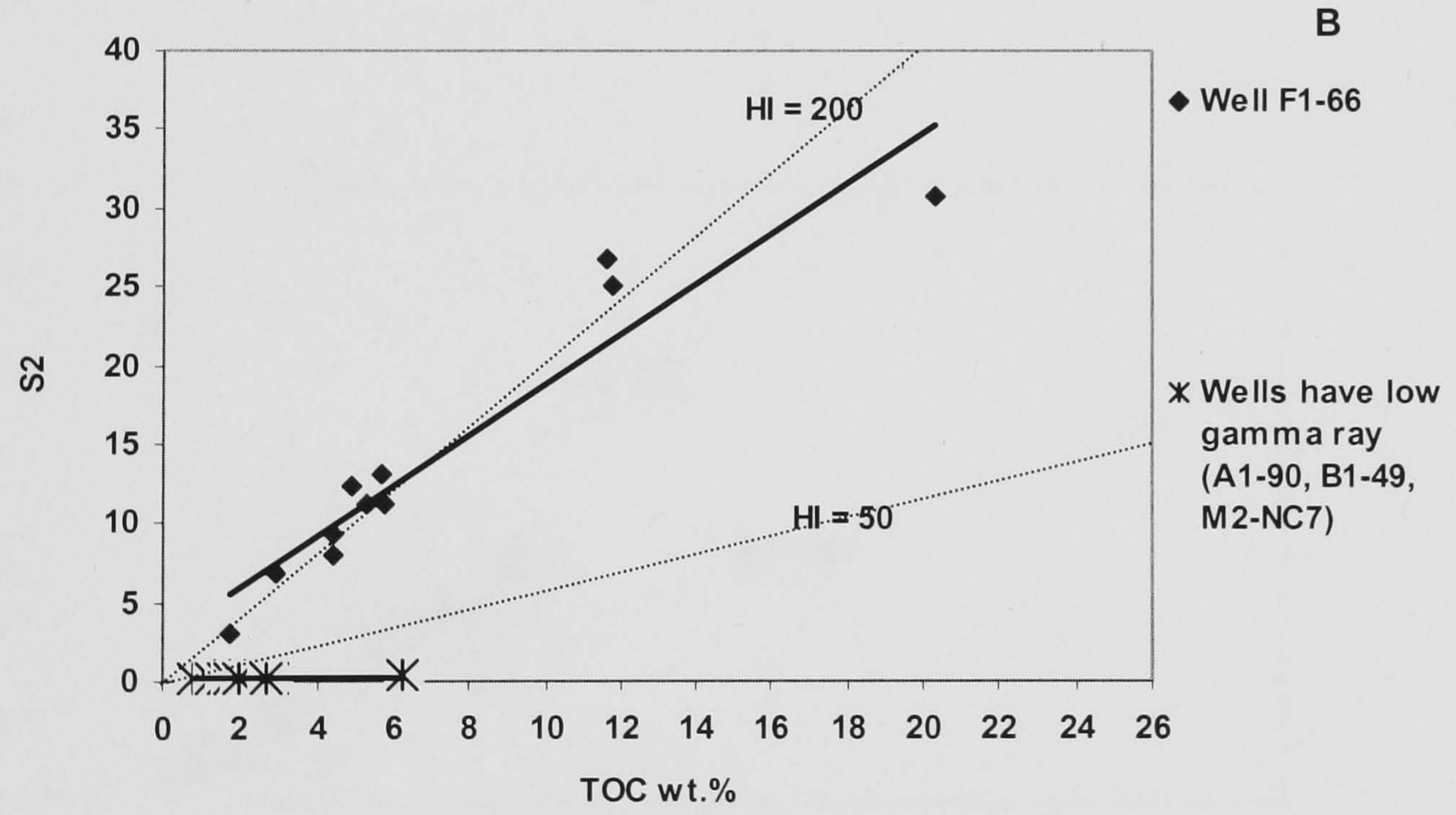

Figure 3.18. Cross plots of S2 versus Total Organic Carbon for the Lower Tanezzuft Formation "hot-shale": (A) cutting samples from wells A1-70, D1-NC2 and Z5-NC5, (B) core samples from well F1-66.

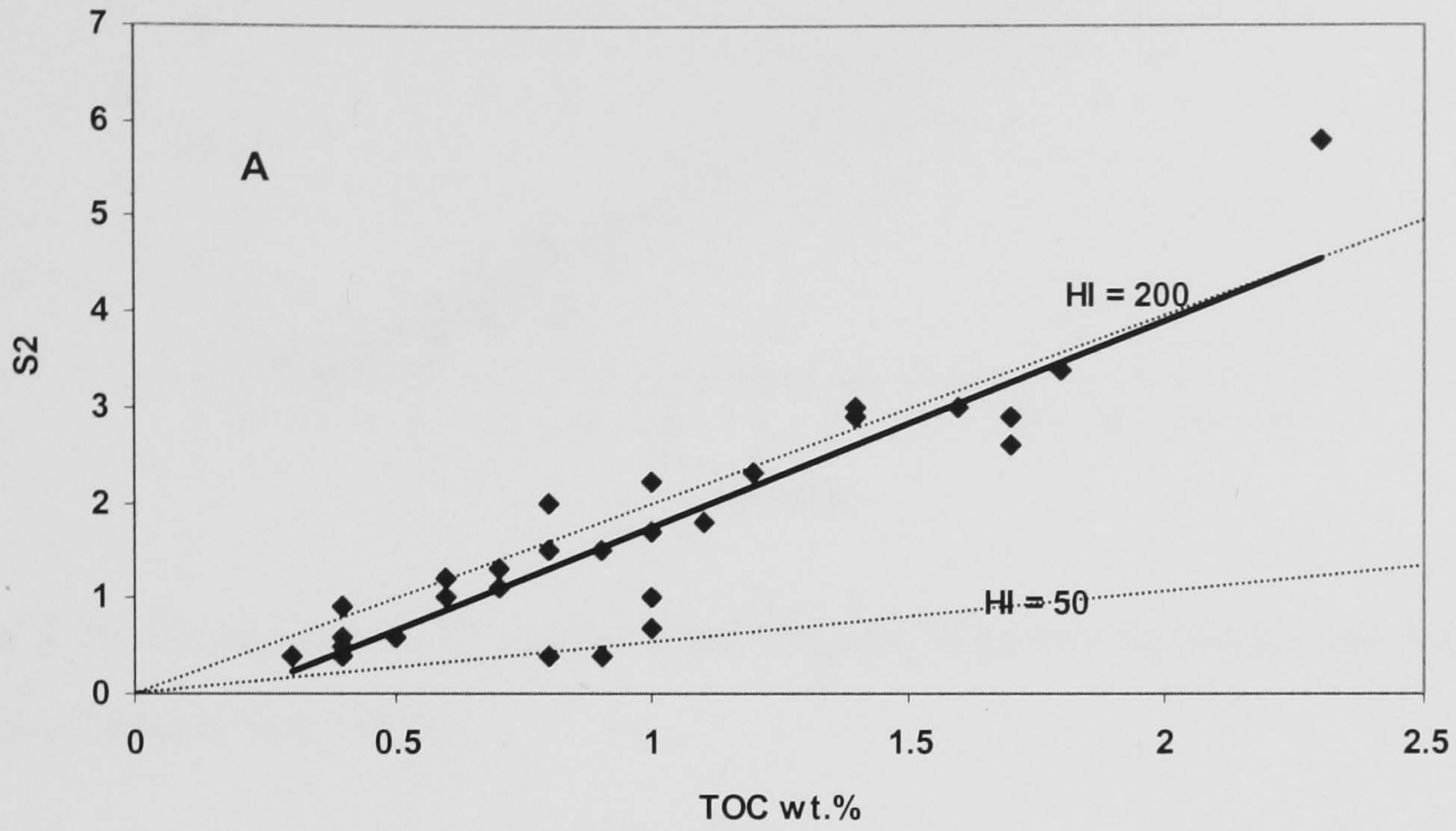

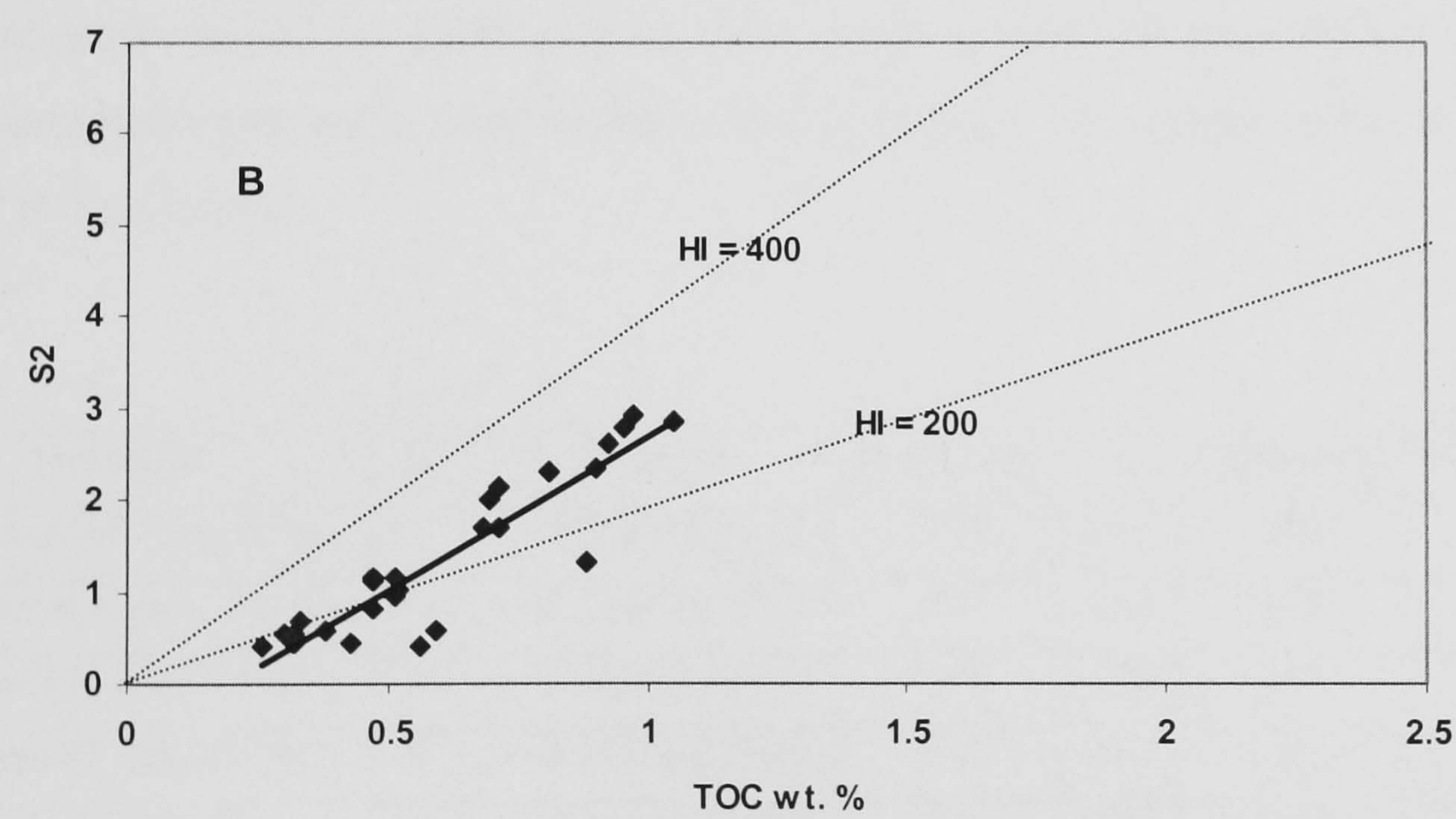

Figure 3.19. Cross plots of S2 versus Total Organic Carbon for the Upper Tanezzuft Formation "cool-Shale": (A) core samples, (B) cutting samples.

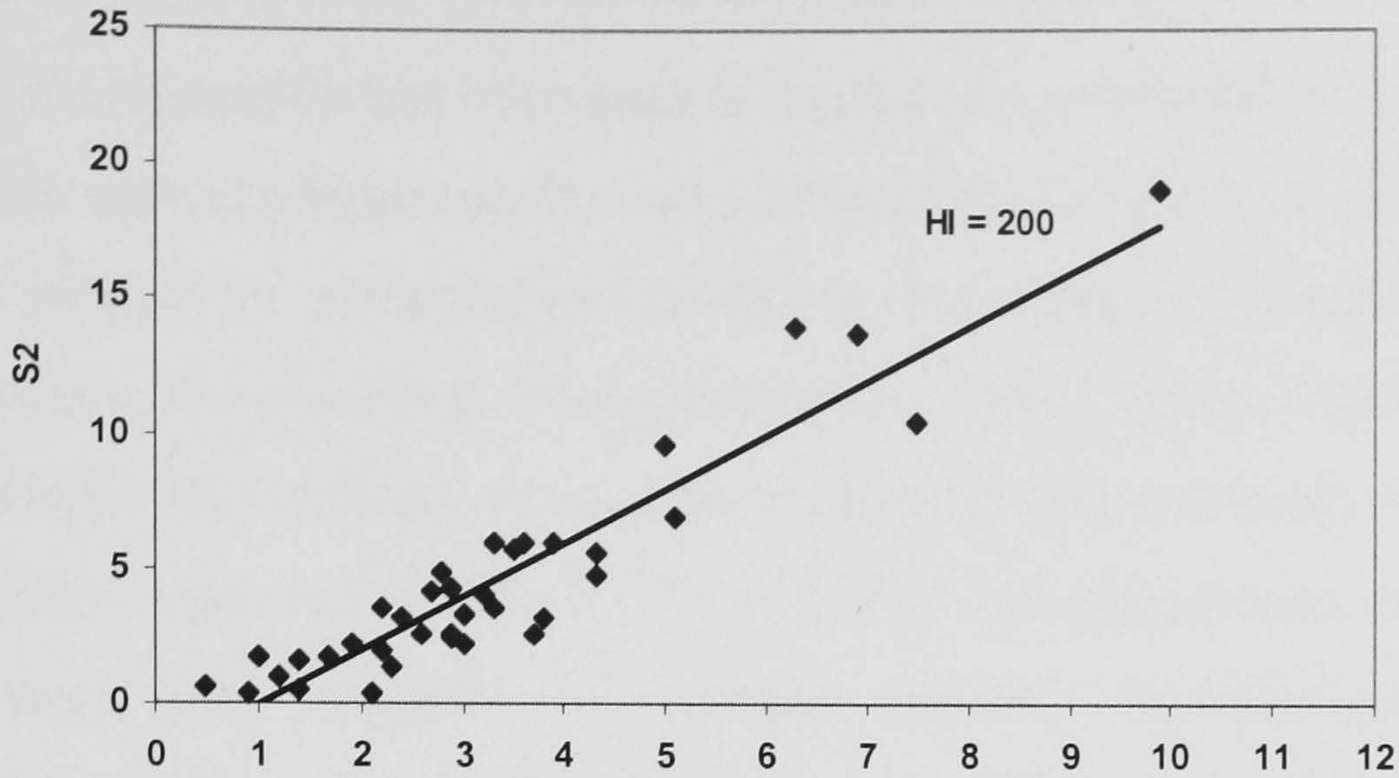

Figure 3.20. Cross plot of S2 versus Total Organic Carbon (wt %) for the Tahara and Aouinet Ouenine formations.

3.3.6 Comparison of Hydrogen Index Values

Table 3.6 shows the hydrogen index values for each major formation as measured and calculated by the S2 vs TOC methods. It can be seen that the hydrogen index values derived from the S2 vs TOC plot in some wells are significantly higher than the measured hydrogen index, even in phytoclast poor units. This suggests that the matrix effect is significant.

Formation	N	Equation	x-intercept	r^2	Sample HI	Slope HI
.L Tanezzuft, core, F1-66	11	y =1.599x+2.8457	-1.79	0.91	208	160
L.Tanezzuft, cutt., A1-70	11	y =3.2694x-2.3908	0.7	0.97	284	327
L.Tanezzuft, cutt, D1-NC2	14	y =3.0829x+4.9324	-1.6	0.82	361	308
L.Tanezzuft, cutt.,Z5-NC5	4	y =2.3631x-0.2364	0.1	0.97	191	236
U. Tanezzuft, core	35	y = 2.1683x-0.4366	0.2	0.84	196	217
U. Tanezzuft, cuttings	26	y = 3.3388x-0.652	0.2	0.83	220	334
Tahara, Aouinet Ouenine C core samples	38	y = 2.002x-2.0746	1.0	0.88	126	200

Table 3.6. S2 versus Total Organic Carbon equations for each major formation (with r^2 0.8 or higher) and the mean hydrogen index derived from different methods.

3.3.7 Multiple Regression of Optical and Hydrogen Index data

Multiple regression has been used to analyse the relationship between hydrogen index and the optical parameters that are considered most likely to influence it. These parameters include the percentage of AOM (or other liptinitic material), and its level of preservation (fluorescence) (Hartman-Stroup, 1987; Tyson, 1989, 1995 & refs. therein), plus the brown/black wood ratio (which can be particularly important at low hydrogen index value; cf. Frank & Tyson 1995). The parameters used as predictor variables were thus: %AOM of kerogen (AOM), %phytoclasts of kerogen, %membrane of phytoclasts, %cuticle of phytoclasts, brown:black wood ratio (Bro/blk), %*Tasmanites* of palynomorphs, and the Fluorescence Scale.

Whole Dataset

The adjusted r^2 and the standard error of the estimate (Table 3.7) shows a weak correlation between the independent variables and dependent variables (adjusted r^2 = 0.4) is low, suggesting that there is much variation about the mean HI that is not explained by the regression equation. This will reflect the combination of samples with different maturities and palynofacies.

Adjusted ^{r2}	0.4
Standard error of the estimate	48.4
Significant F	0.00
Number of samples	85

Table 3.7. Results of the multiple regression analysis for hydrogen index versus optical data, for the whole dataset.

By Formation

Multiple regression has also been carried out on a samples sets grouped based on similarity in maturity and palynofacies in order to reduce the scatter and permit a more meaningful estimate of HI.

Devonian Formations

A multiple regression was carried out for samples from the Tahara and Aouinet Ouenine C formations of wells A9-NC7 and B1-49. The adjusted r^2 and the standard error of the estimate values in both analyses show that there is a positive relationship between the independent and dependent variables (Table 3.8a), with adjusted r^2 values for the two wells of 0.75 and 0.82, respectively. The adjusted r^2 values show that more than 75% of the variation in HI can be explained by the optical data.

Examination of Table 3.8b shows that in the Tahara Sandstone Formation at well A9-NC7 the Brown/Black wood ratio is the only variable which does not have a significant effect on the HI; the most important three variables are the membrane, phytoclasts and AOM%. In the Aouinet Ouenine Formation at well B1-49 the beta and significance values suggest that the most important variable is %AOM, followed by the brown:black ratio and the %membrane of phytoclasts; the very low beta value for %phytoclasts suggests that this variable has little effect on the HI here.

Silurian Formations

Multiple regression was carried out for the Silurian formations (lower and upper Tanezzuft and Acacus Sandstone) from wells F1-66, A1-70, Z5-NC5, B1-NC2 and A1-66. The adjusted r^2 value in the upper Tanezzuft Formation at well A1-66 is greater than 0.91 showing a good explanatory power for the regression equation and good prediction of the HI (Table 3.9a). In the lower and upper Tanezzuft Formation at well F1-66 the lower r^2 value suggests that there is significant variation in the HI that is not explained by the regression equation.

Table 3.9b shows that in the upper Tanezzuft and Acacus Sandstone formations at well A1-70 and B1-NC2 prasinophytes (*Tasmanites*) followed by AOM are the only variables that have a significant effect on the HI; the very low beta value for Fluorescence Scale and cuticle suggests that these variables do not have any effect on the HI. For the upper Tanezzuft Formation of well A1-66, AOM is the only variable to have a significant effect on the HI. For the upper Tanezzuft Formation of well Z5-NC5 the beta and significance T values suggest that the most important variable is AOM.

a)

Unit	Tahara Sst. Fm. well A9-NC7	Aouinet Ouenine Fm. well B1-49
Adjusted r^2	0.750	0.820
Significant F	0.000	0.051
Number of samples	16	8
Mean of measured HI	124	116
Standard deviation of the measured HI	62	50

b)

	Tahara Sandstone Fm. well A9-NC7			Aouinet Ouenine Fm. well B1-49		
Variable	Beta	Sig. T	constant	Beta	Sig. T	constant
AOM%	0.316	0.021	1.036	-0.481	0.271	-4.689
Phytoclasts%	-0.416	0.061	-1.952	0.118	0.538	0.549
Membrane/ phytoclasts	0.808	0.000	16.739	-0.425	0.340	-10.984
Brown/black wood ratio	0.057	0.681	1.461	-0.477	0.200	-22.559

Table 3.8 Results. of the multiple regression analysis of hydrogen index versus optical data in Tahara Sandstone and Aouint Ounine formations from two different wells. Where Beta values are very low, this means that component will have very little impact on the predicted HI.

A)

Unit	**1**	**2**	**3**	**4**
Adjusted r^2	0.643	0.701	0.756	0.906
Significant F	0.003	0.106	0.035	0.002
Number of samples	16	8	8	9
Mean of the measured HI	137	141	170	200
Standard deviation of the measured HI	47	63	53	72

b)

	1			**2**			**3**			**4**		
Variable	Beta	Sig. T	constant	Beta	Sig. T	constant	Beta	Sig. T	constant	Beta	Sig. T	constant
AOM/ kerogen	0.20	0.48	0.45	0.72	0.21	2.15	0.03	0.88	0.17	1.07	0.00	7.442
Tasmanites/palynomorphs	0.68	0.02	4.639	0.68	0.17	8.311	0.93	0.02	7.925	-0.26	0.07	-36.24
Fluorescence Scale	0.09	0.62	5.364	2.19	0.19	194.327				-0.27	0.09	-12.335
Cuticle/ phytoclasts	0.08	0.65	4.639	2.38	0.18	108.637	0.00	0.99	0.838			

Table 3.9 Results of the multiple regression analysis of hydrogen index versus optical data in the Tanezzuft and Acacus formations. Units as follows: **1** Acacus and upper Tanezzuft well A1-70, **2** upper Tannezuft well Z5-NC5, **3** upper Tanezzuft well B1-NC2, **4** upper Tanezzuft well A1-66.

Predicted versus Measured Hydrogen Indices

The regression equations shown in Table 3.10 have been used to calculate a predicted HI value that could be compared with the measured HI. The cross plot of the predicted HI versus measured HI (Fig. 3.21) for the Upper Devonian samples from wells A9-NC7 and B1-49 shows a significant positive correlation of (r^2 = 0.87 and 0.92 respectively).

The cross plot of the predicted versus measured HI (Fig.3.22) for the Lower Silurian samples from wells A1-70, Z5-NC5, B1-NC2 and A1-66 show significant positive correlations (r^2 = 0.74, 0.87, 0.86 and 0.94 respectively).

Tahara Sandstone Formation at well A9-NC7 (r^2 = 0.75)

HI = 131.322+16.739(Mem) + 1.036(AOM) + 1.461(tblk/tbr) + -1.952(phy)

Aouint Ounine C Formation at well B1-49 (r^2 = 0.82)

HI = 187.687+ -10.99(Mem) + -4.683(AOM) + -22.559(tblk/tbr) + 0.549(phy)

Acacus and upper Tanezzuft formations at well A1-70 (r^2 = 0.64)

HI = 68.305 + 0.45(AOM) + 5.364(FS) + 4.639(Tas.) + 4.639(cut.)

Upper Tanezzuft Formation at well Z5-NC5 (r^2 = 0.70)

HI = -821.013 + 2.15(AOM) + 194.327(FS) + 8.311(Tas) + 108.637(cut.)

Upper Tanezzuft Formation at well B1-NC2 (r^2 = 0.76)

HI = 107.271 + 0.17(AOM) + 7.925(Tas.) + 0.838(cut.)

Upper Tanezzuft Formation at well A1-66 (r^2 = 0.91)

HI = -139.134 + 7.442(AOM) + -36.24(FS) + -12.335(Tas)

Table 3.10. Regression equations derived from multiple regression analysis.

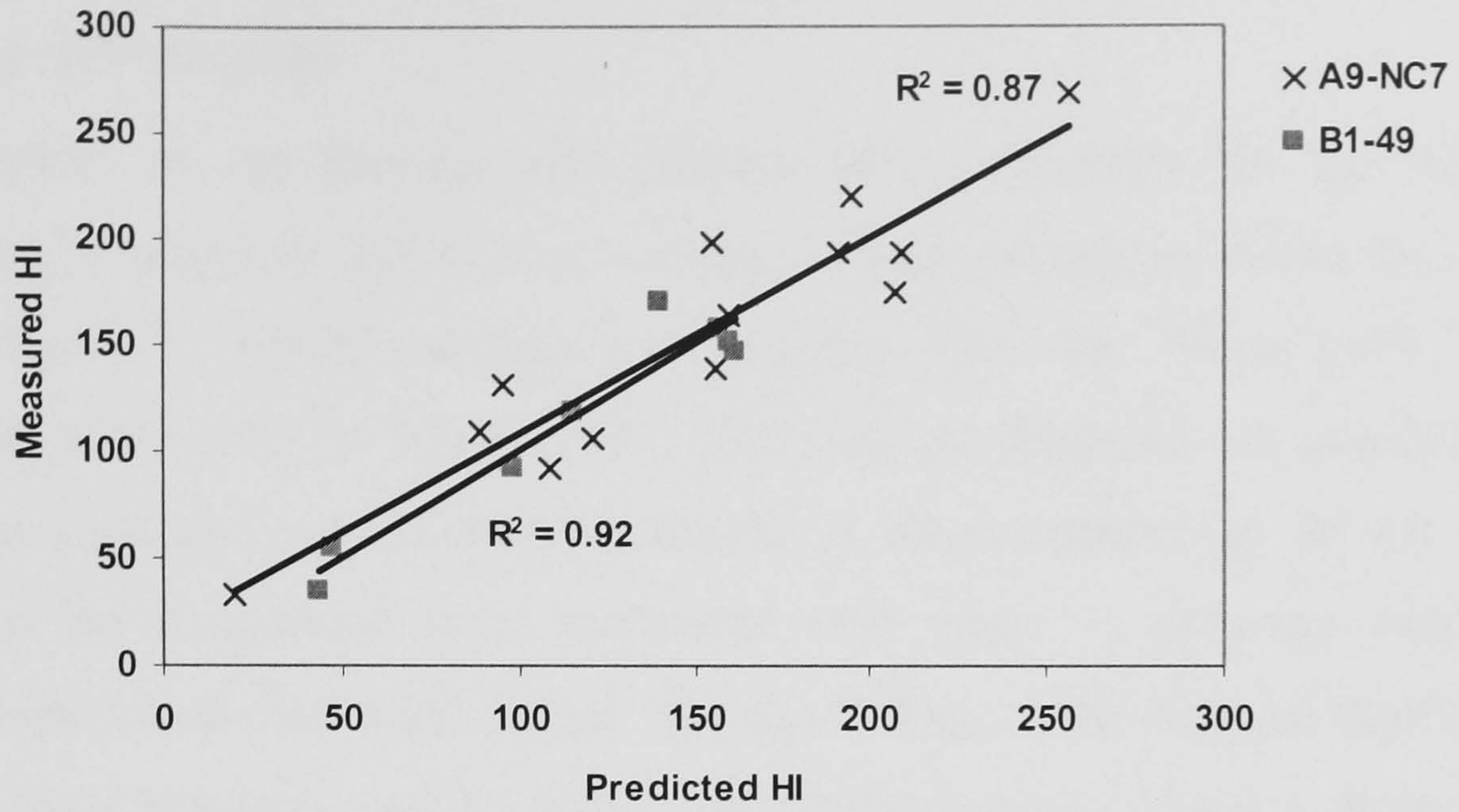

Figure 3.21. Cross plot of the measured and predicted hydrogen indices for theTahara Sandstone Formation of well A9-NC7, and Aouinet Ouenine Formation of well B1-49.

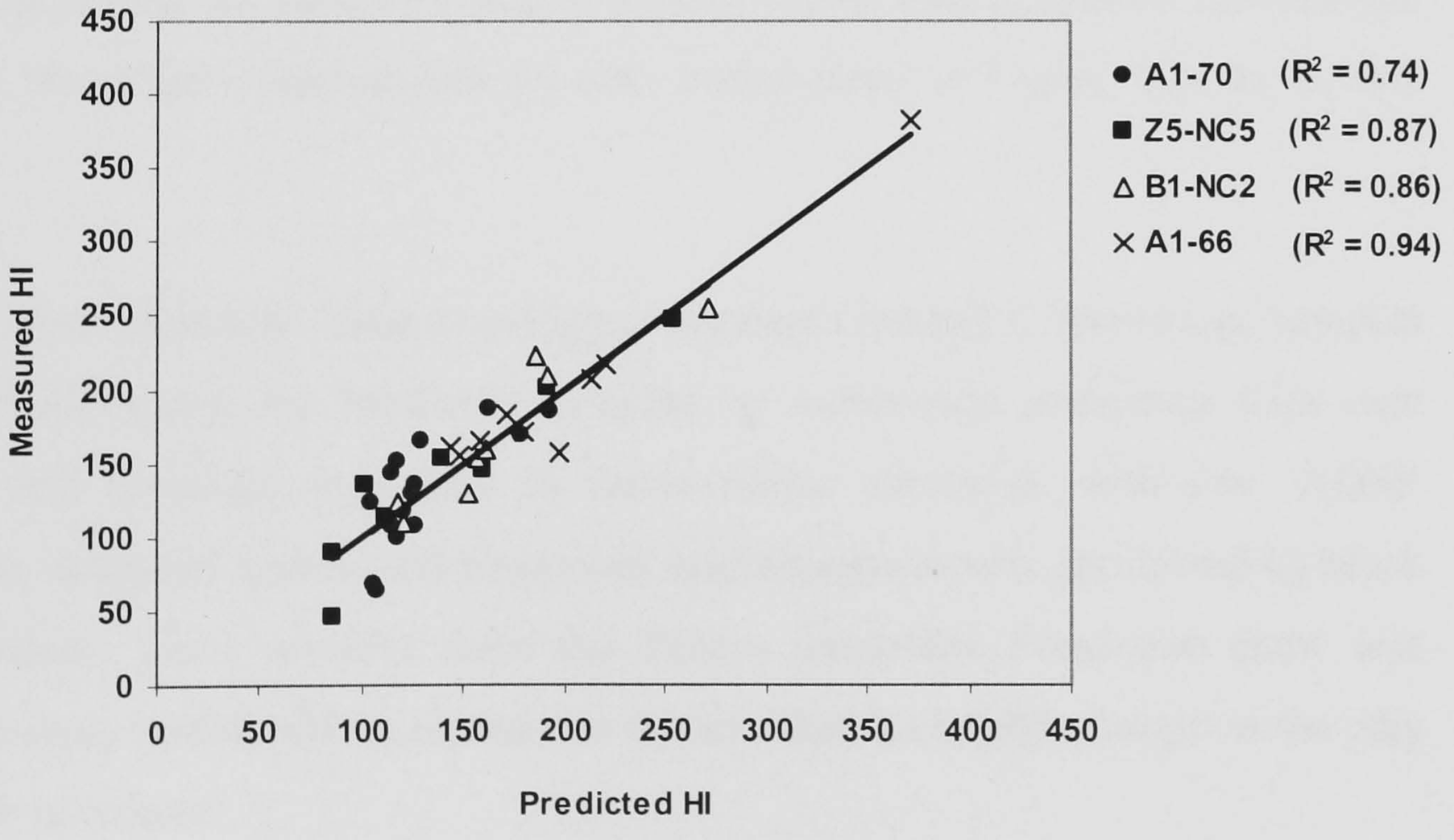

Figure 3.22. Cross plot of the measured and predicted hydrogen index for the Acacus and upper Tanezzuft formations of well A1-70, and the upper Tanezzuft of wells Z5-NC5, B1-NC2, A1-66.

3.4 Palynofacies

3.4.1 Ternary APP diagram

The values of the kerogen and palynomorph parameters for the different formations are presented in the form of a series of ternary diagrams where the sum of the three components plotted has been normalized to 100% (cf. Tyson, 1993, 1995). Following the convention of Tyson (1993, 1995), all the diagrams are oriented such that the most proximal constituent (Phytoclasts) is always plotted at the top of the diagram, and the component most associated with distal or reducing conditions (AOM) is plotted in the left hand corner. The top to base of the diagram represents a proximal to distal transition, and the left to right of the diagram reflects a change from reducing to oxidizing conditions (Tyson, 1995).

The nature of the kerogen assemblages is summarized in Figure 3.23 as ternary Amorphous Organic Matter-Phytoclast-Palynomorph (APP) diagrams (Tyson, 1995). The overall nature of phytoclast population (cuticle+membranes, brown wood, black wood), the major palynomorph groups (sporomorphs, marine plankton, undifferentiated) and the nature of marine organic-walled microplankton assemblages (acritarchs, leiospheres, tasmanites) are also summarized in Figure 4.24 as ternary diagrams.

The Upper Devonian Tahara and upper Aouinet Ouenine C formations samples plot in a field (which for Mesozoic samples is) commonly associated with oxic conditions and moderate proximity to fluvio-deltaic source(s), with low 'AOM' preservation, abundant spores, and phytoclast assemblages mostly dominated by black wood. However, some samples from the Tahara Sandstone Formation show less phytoclasts, more AOM, and an increase in the abundance of palynomorph as the clay size fraction increases.

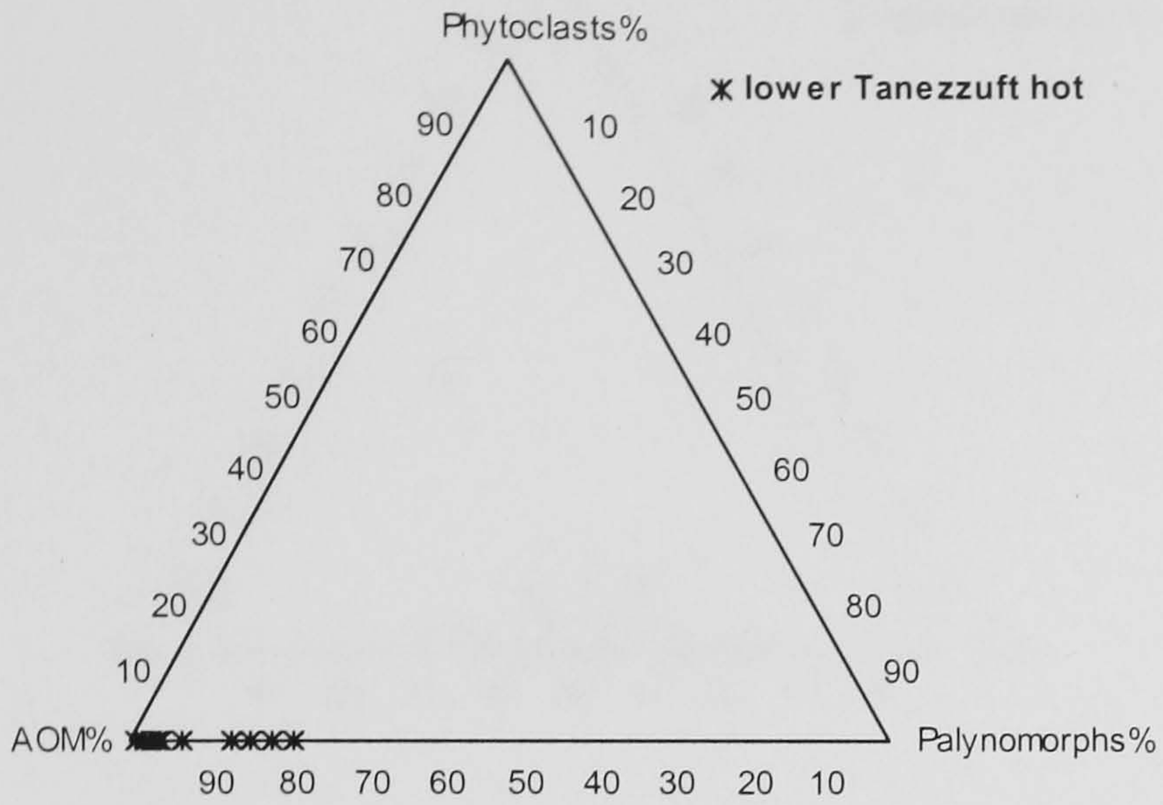

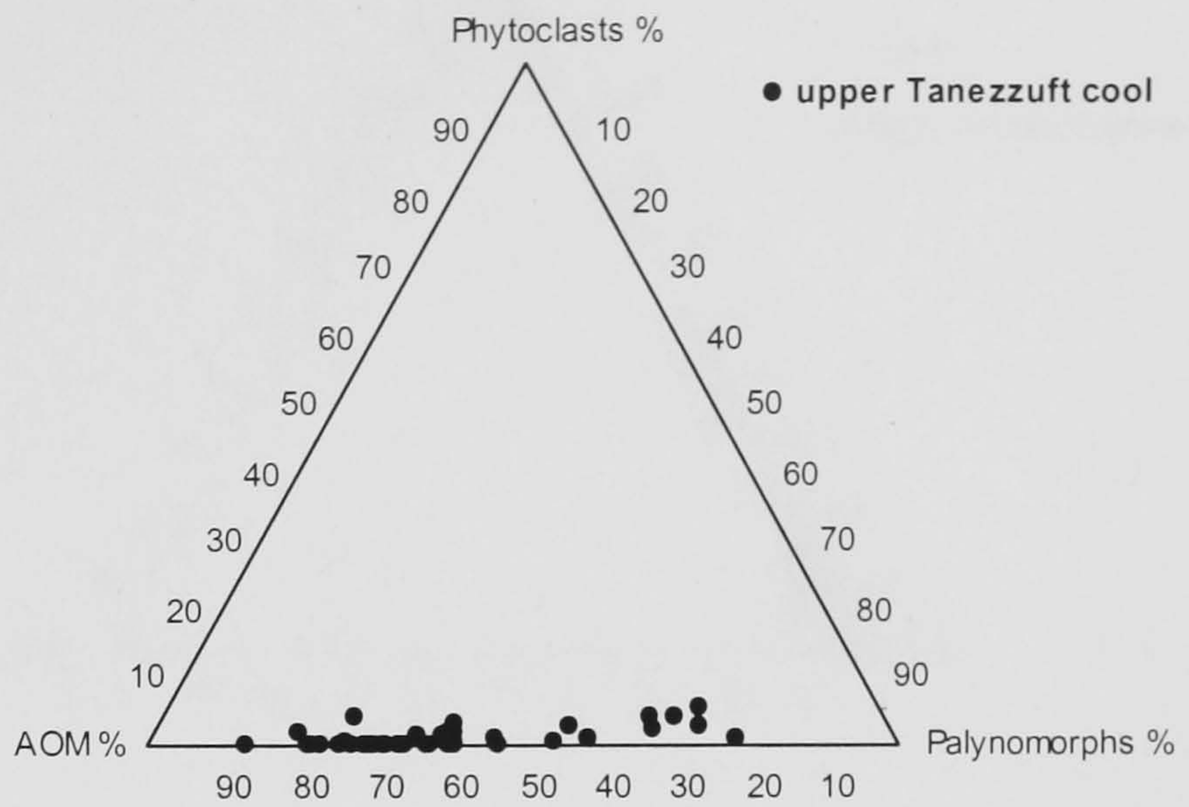

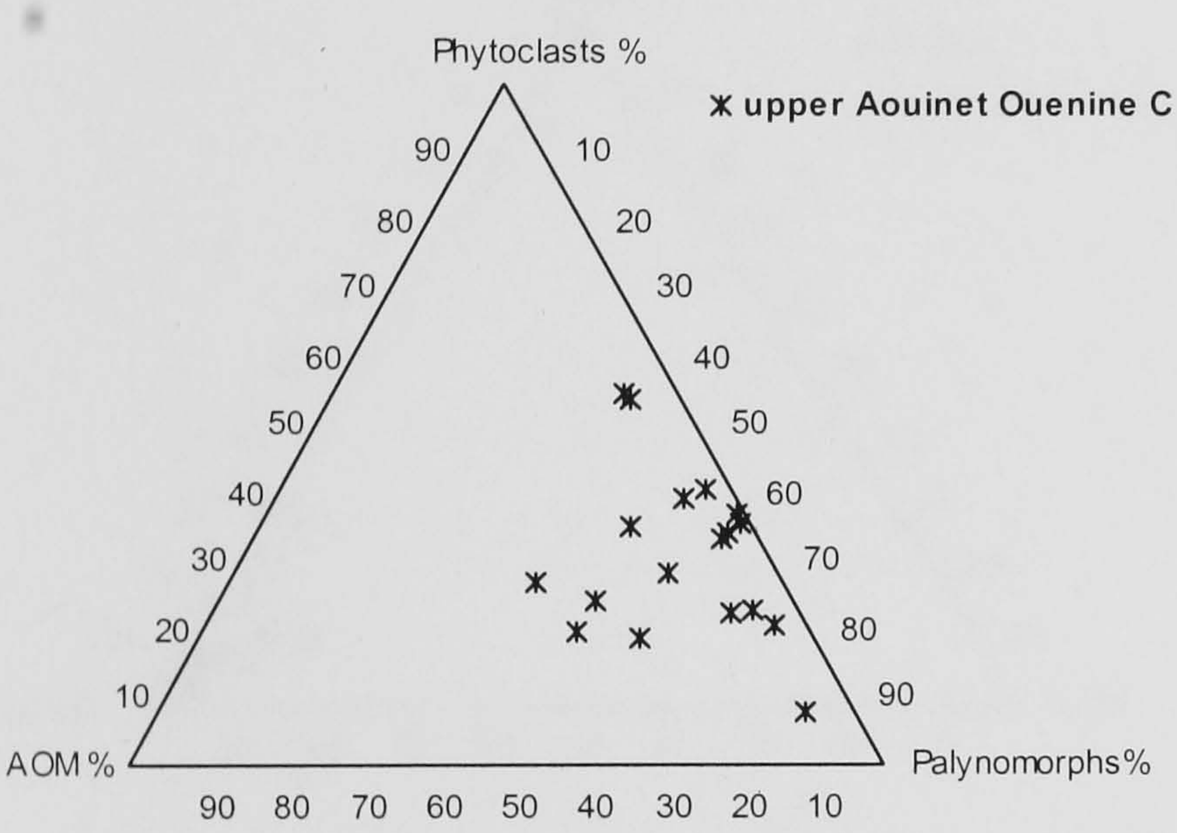

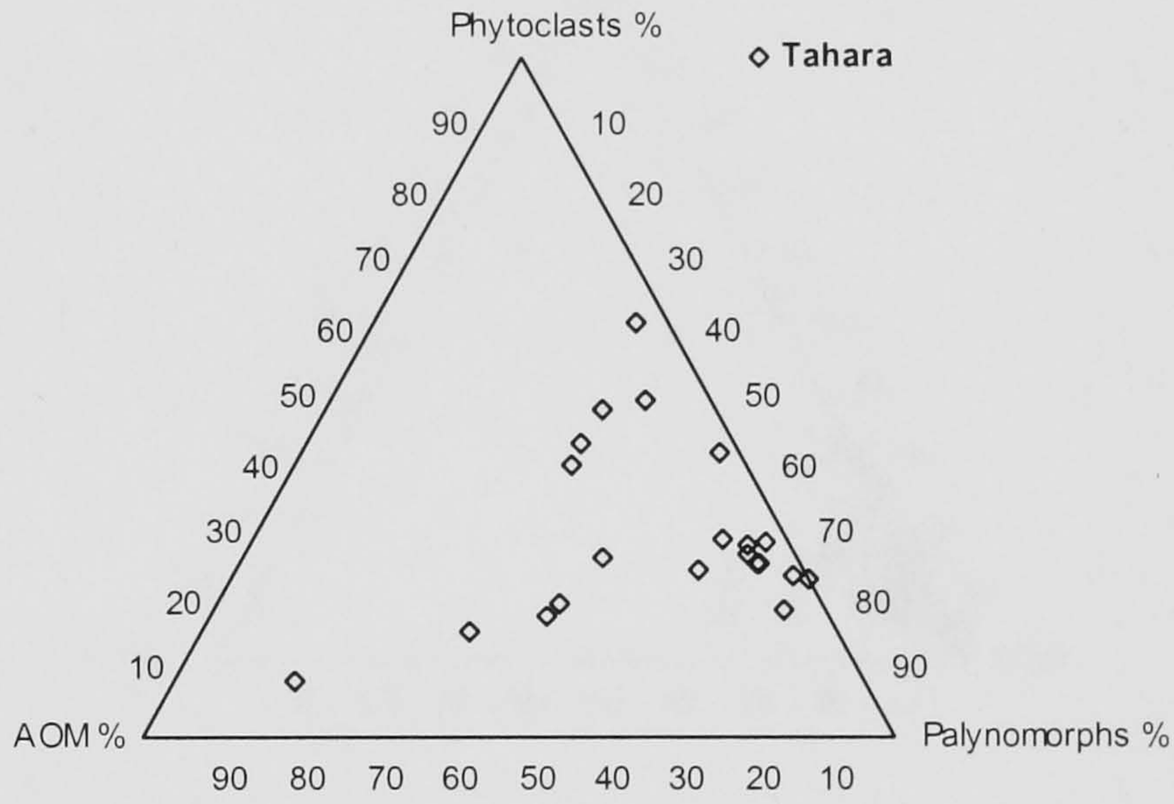

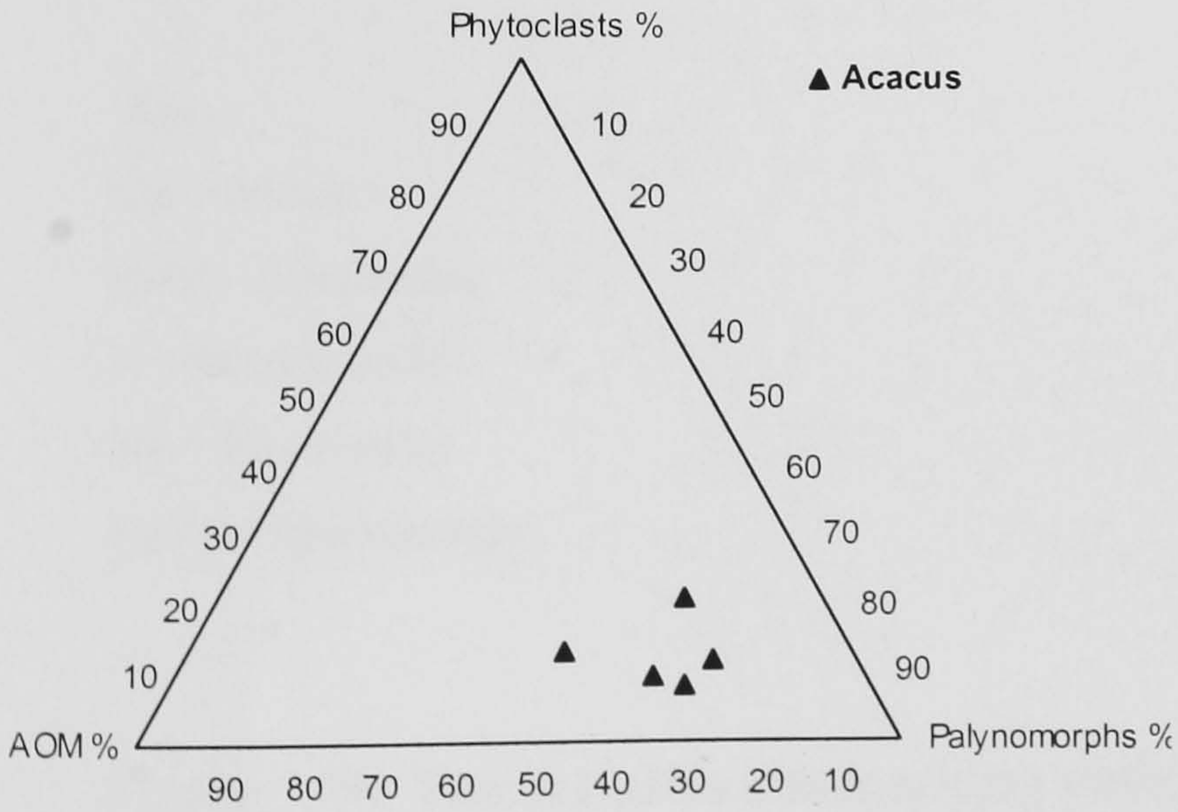

Figure 3.23. Ternary APP plots illustrating the varied palynofacies composition through the Lower Palaeozoic formations.

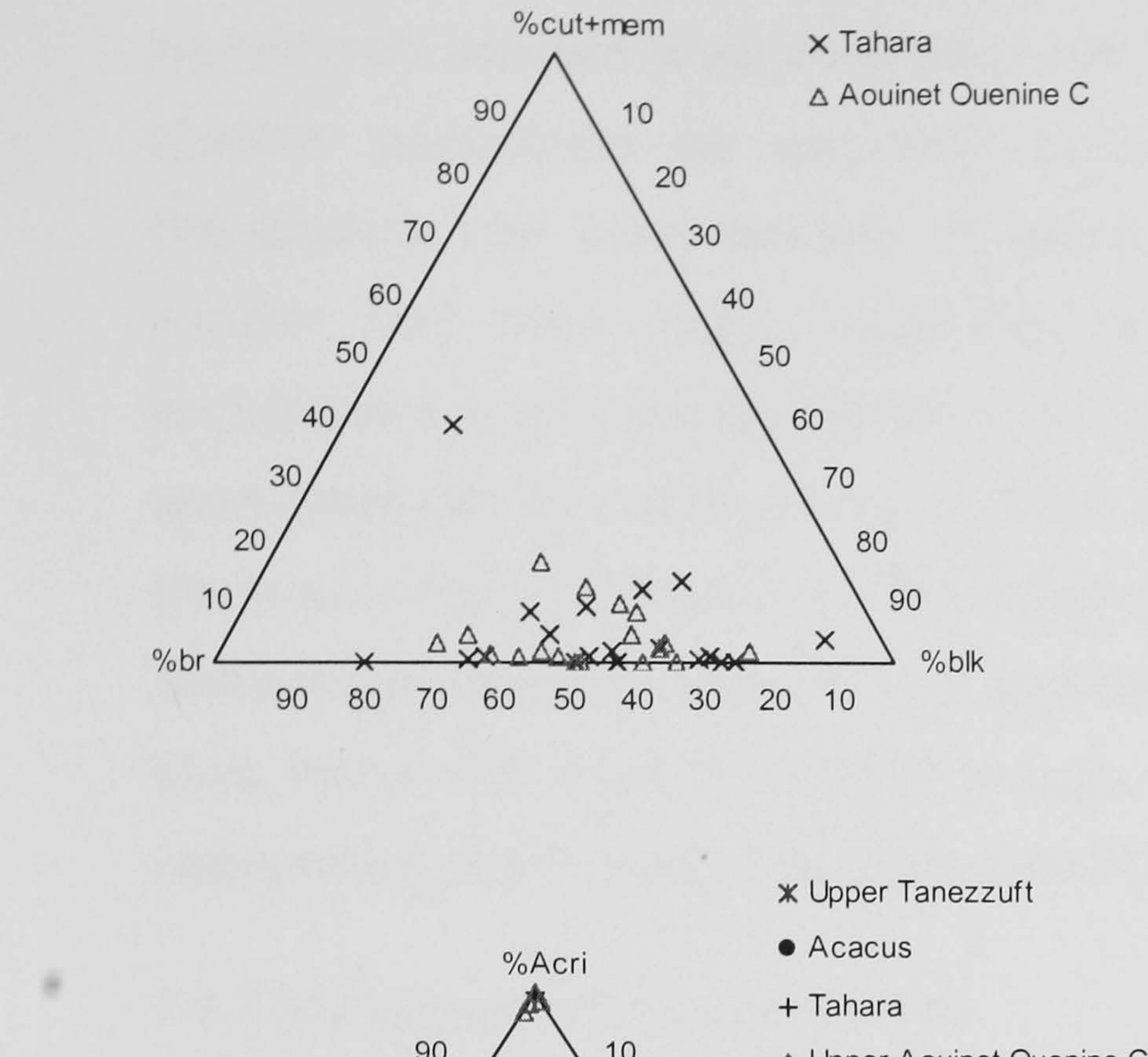

Key:

Cut = cuticle

mem = membranes

br = brown wood

blk = black wood

Sporo = sporomorphs

Undiff = undifferentiated

Mp = marine plankton

Acri =acritarchs

pras = prasinophytes

Chi = chitinozoans

lei = leiospheres

Tas = Tasmanites

Figure 3.24. Ternary plots summarising phytoclast and palynomorph assemblages.

The Upper Silurian Acacus Sandstone and upper Tanezzuft formation samples are relatively enriched in palynomorphs, with low AOM and phytoclasts. The marine plankton assemblages are dominated by simple and thin-walled prasinophytes (leiospheres), plus lesser amounts of spores and some tracheid-like fragments of possible land plant origin, suggesting more oxic nearshore shallow marine environments to proximal shelf facies with Type III kerogen. Some samples from the upper Tanezzuft Formation are rich in AOM, and exhibit an increase in thick-walled (*Tasmanites*-type prasinophytes). The samples from lower Tanezzuft Formation are dominated by probably originally well preserved AOM, which is typical of laminated black shales with Type II oil-prone kerogen deposited in distal stratified shelf sea basins with dysoxic-anoxic depositional conditions.

3.4.2 Stratigraphic plots of parameters

Ternary plots do not consider the stratigraphic position and the lateral variation of the data. Therefore, the mean values of selected parameters have been calculated for each unit and plotted to allow examination of the changes through time; the selected parameters have also been plotted against depth, to study the stratigraphic changes of the values for each formation.

Trends in parameters

Figure 3.25 shows that the mean AOM values decrease from the Lower Silurian basal Tanezzuft Formation to the Upper Silurian Acacus Sandstone Formation, reflecting the change from a more distal to proximal marine environment. The percentage of phytoclasts shows an overall increase from Lower Silurian Tanezzuft Formation to the Upper Devonian Tahara Sandstone and upper Aouinet Ouenine C formations, reflecting the change from shallow/deep marine to fluvio-deltaic facies. In the case of the palynomorphs, a gradual decrease is seen through the Silurian formations mainly due to AOM dilution apparently.

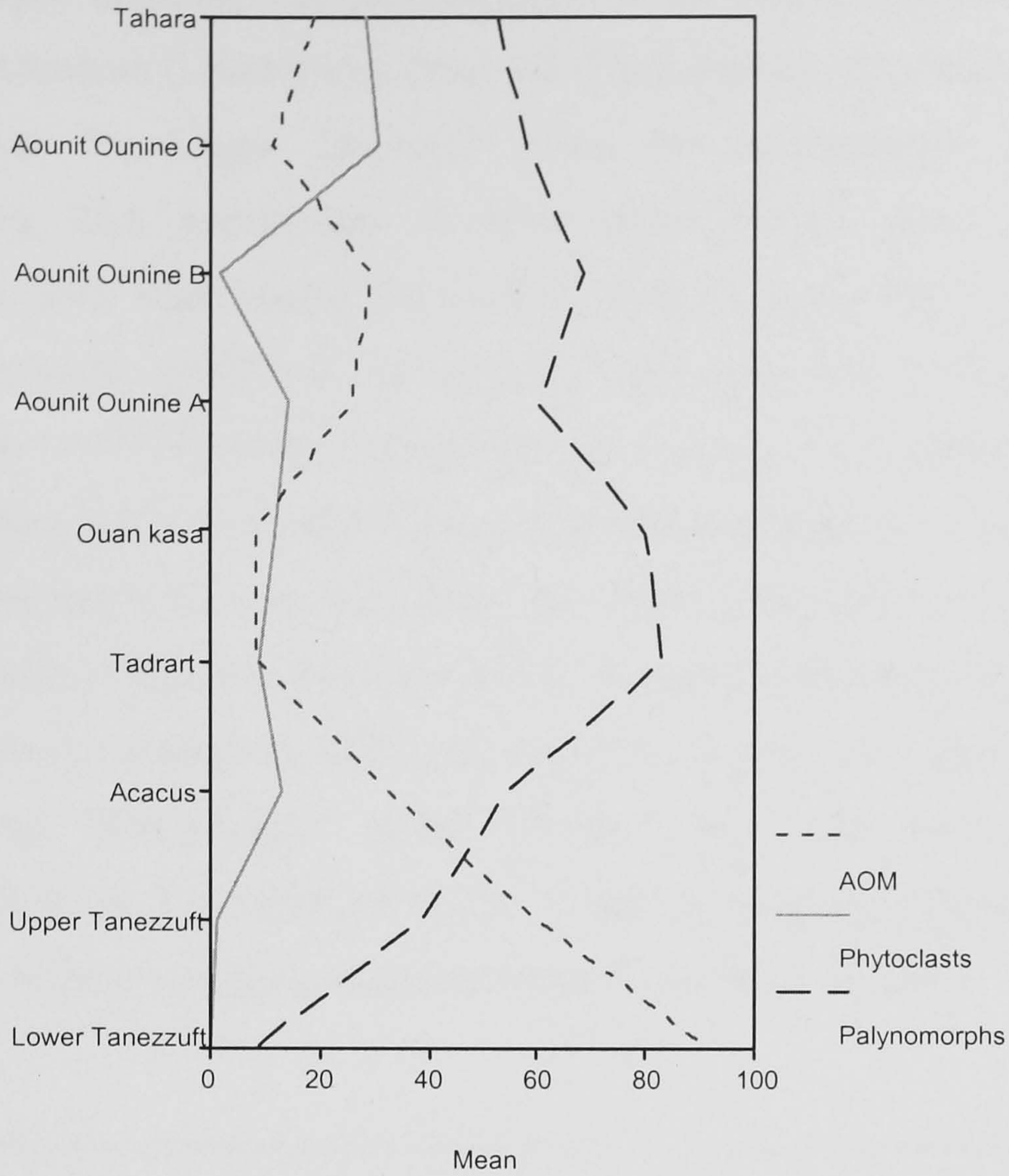

Figure 3.25. Mean values of the major kerogen groups for each stratigraphic unit in the Palaeozoic succession.

Within the phytoclast fraction (Fig. 3.26), the brown:black wood ratio generally increases from the Upper Devonian Tahara and upper Aouinet Ouenine C formations to the Lower Silurian Acacus and upper Tanezzuft formation, whereas the black equant:lath wood ratio shows the opposite trend. Suggesting that the depositional sitting changes from fluvio-deltaic to marine offshore facies. Opaque phytoclasts are probably enriched in sandstone because they are more refractory and survive degradation better (Tyson, 1995); lath-shaped black wood is selectively transported to more distal or low energy settings where it may dominate (Tyson, 1995). Generally the percentages of phytoclasts in the Silurian samples are low and dominated by fragments of sheet membranes or cuticle, or tubes with spiral thickening. Al-Ameri (1980) reports that the same fragments (classified into sheets and tubes) have no clear affinity; he suggested that they may belong to vascular plants, non-vascular land plants (e.g. bryophytes, algae) or some other group of organisms.

Sporomorphs dominate the palynomorphs in the Upper Devonian Tahara and upper Aouinet Ouenine C formations (Fig. 3.27), but decrease gradually in the Lower Silurian. Within the Upper Devonian units the sporomorphs are generally characterized by high percentages of thick-walled spores. Thick-walled spores decreases away from their source due to hydrodynamic equivalence, larger, denser spores being generally deposited first (Tyson, 1995). The ratio of thin:thick-walled spores shows an overall increase through the rest of the units examined, reflecting a distal shift in the depositional environment from fluvio-deltaic to offshore. The ratio of acritarchs:prasinophytes decreases from the Upper Devonian units to the Lower Silurian Tanezzuft Formation. The presence of prasinophytes is generally correlated with dysoxic-anoxic conditions, which are likely to be more abundant in any deeper water and more "hemipelagic" facies (Tyson, 1987). The association of the prasinophytes with the Tanezzuft Formation is thus in good agreement with its fine-grained, distal, relatively organic-rich, and "dysoxic-anoxic" character.

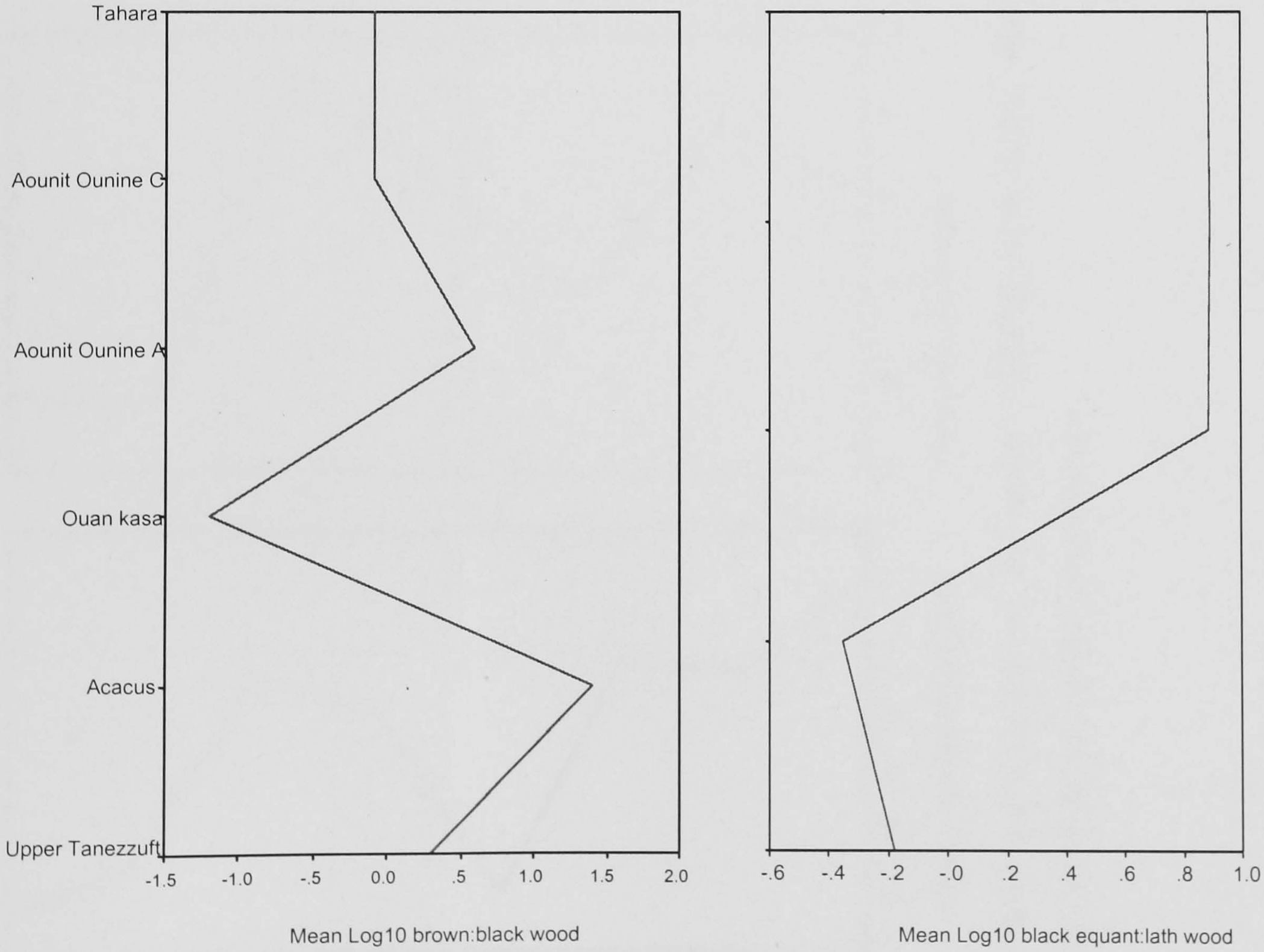

Figure 3.26. Mean log10 values of the brown:black wood and equant:lath black phytoclast ratios by stratigraphic unit through the Palaeozoic succession.

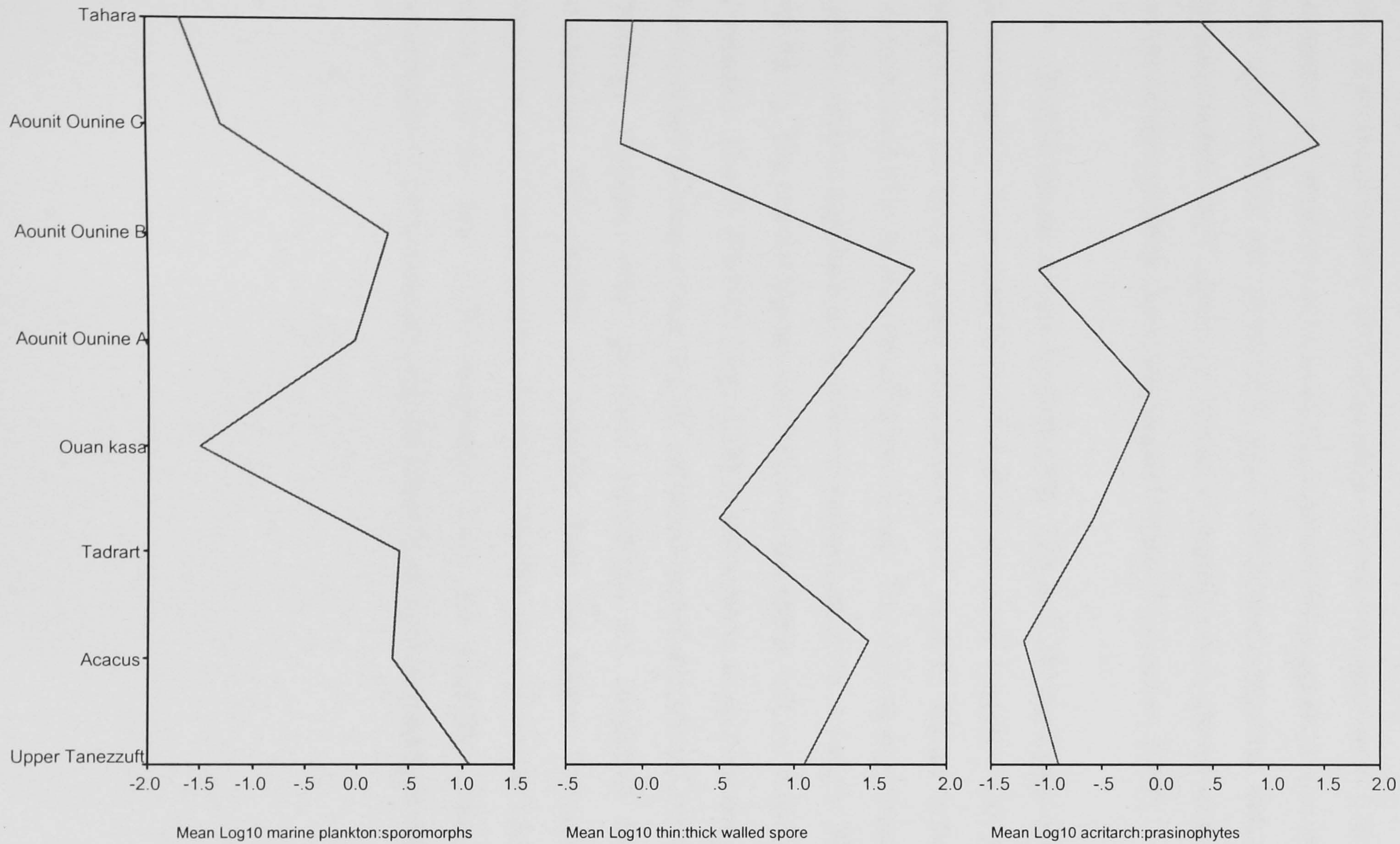

Figure 3.27. Mean log 10 values of the marine plankton:sporomorphs, thin:thick walled spore, and acritarch:prasinophyte ratios for each stratigraphic unit through the Palaeozoic succession.

Trends Through Each Well

The calculated optical kerogen parameters have been plotted against depth for each well in order to study the stratigraphical changes in the parameter values for each formation. In wells B1-49, A9-NC7 and C1-26 (located in the southern parts of the basin), the samples from upper Devonian Tahara Sandstone and upper Aouinet Ouenine C formations are characterised by the presence of high percentages of palynomorphs, which are dominated by thick-walled spores. The marine plankton are rare, and represented by acritarchs (three-spined *Veryhachium*). The high percentages of spores and presence of *Veryhachium* acritarchs suggests a nearshore environment. The *veryhachiids* are potentially good palaeoenvironmental indicators, with their general outline itself apparently related to ecology; four-spined species are considered to live farther offshore than three-spined forms (Le Herisse, 2002).

Within the phytoclast fraction (Fig. 3.28 & 3.29) the Upper Devonian sediment is consistently dominated by black and brown wood together with an increase in the proportion of black equant phytoclasts, and slightly higher percentages of non-biostructured over biostructured brown wood. The highest percentages of phytoclasts are recorded in argillaceous sandstones (maximum 61% in sample TH8 at 5721', well A9-NC7). The coarsening-upward nature of the upper section of the Tahara Sandstone Formation at well A9-NC7 (Fig. 3.28) is reflected in as upward decrease in TOC and the increase of phytoclasts and of corroded non-biostructured brown wood. As the lithology changes, more proximal conditions are suggested by the phytoclast assemblage. The number of samples from the Upper Devonian units Tahara Sandstone and Upper Aouinet Ouenine C for the rest of the wells (A1-70, A1-66, M2-NC2), are too few to be diagnostic. They are generally characterised by high percentages of palynomorphs (predominantly of thick-walled spores) and phytoclasts.

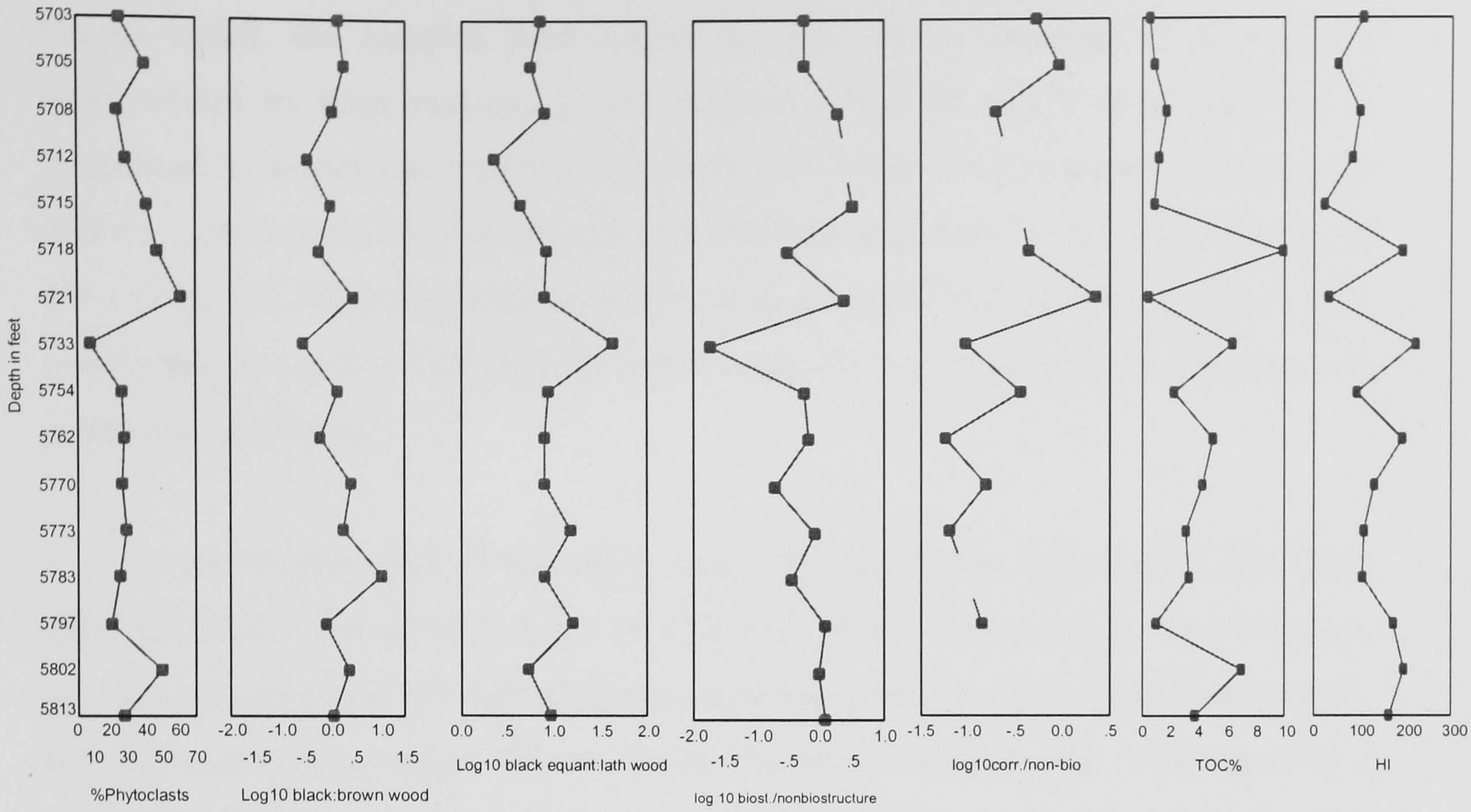

Figure 3.28 Selected phytoclast parameter variation through the Lower Palaeozoic succession in well A9-NC7, plus TOC and HI.

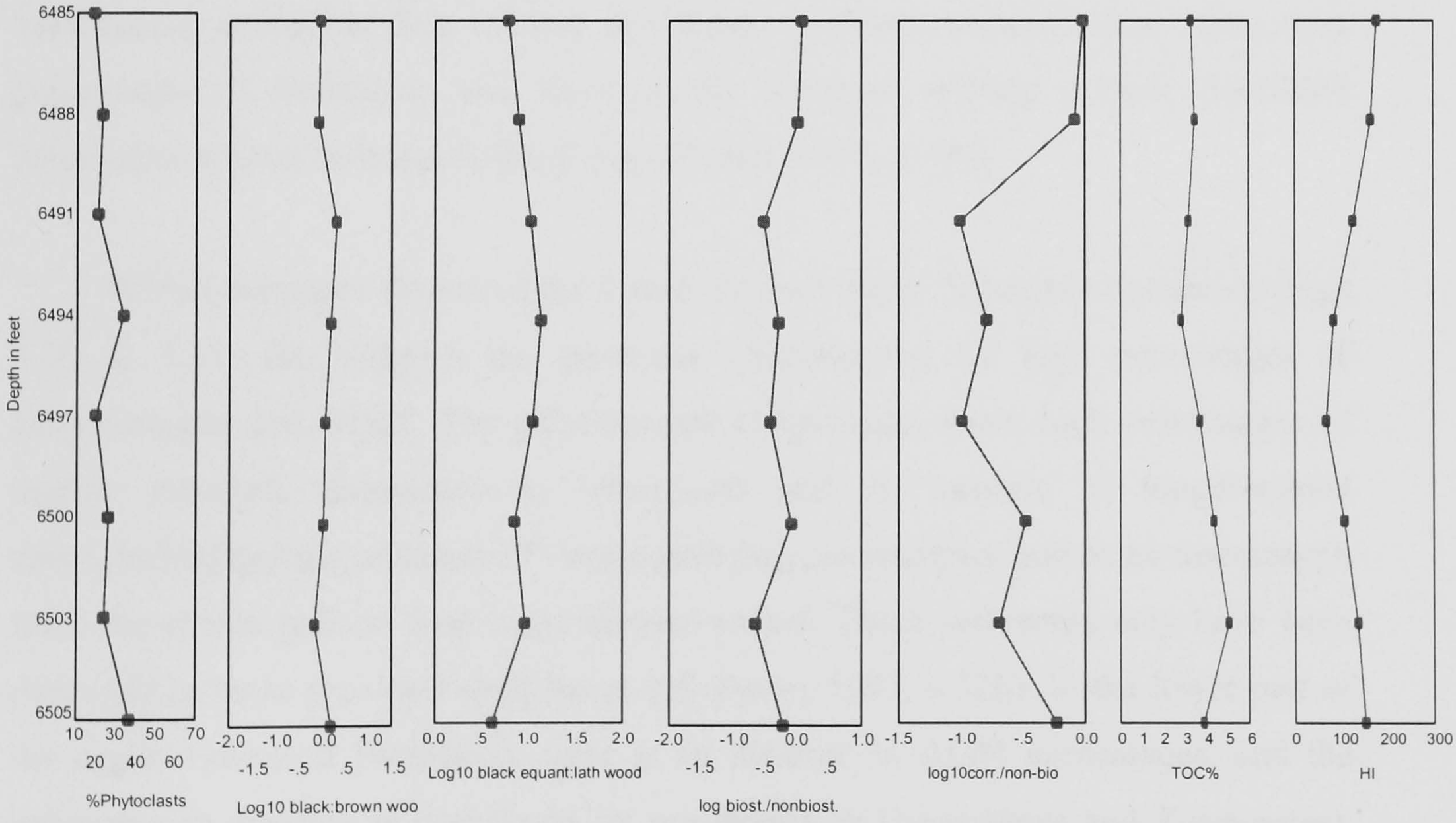

Figure 3.29. Variation in selected phytoclast parameters through the Lower Palaeozoic succession in well C1-26, plus TOC and HI.

In well B1-49, located in the southern part of the basin very near to the Al-Gargaf Uplift, the samples from Lower Silurian upper Tanezzuft Formation are characterised by high percentages of palynomorphs. The palynomorph fraction is dominated by spores and reworked acritarchs. Al-Ameri (1980) reported the presence of 64% of miospores and the presence of reworked acritarchs for the same section in the well B1-49, indicating that sediment was deposited in very nearshore facies. This section also has a low TOC content and low gamma ray values, due to dilution, and more oxic conditions.

In the northern part of the basin, three wells have been examined (A1-70, B1-NC2, Z5-NC5). The samples from the Upper Silurian Acacus Sandstone Formation are here characterised by high percentages of palynomorphs and AOM and slightly low phytoclast percentages. Within the palynomorph fraction (Fig. 3.30) there is a progressive increase in the percentages of marine plankton over sporomorphs. The marine assemblages are typically dominated by relatively simple and thin-walled prasinophytes (leiospheres), plus lesser amounts of acanthomorph and three-spined veryhachiid acritarchs. The relative abundance of these 'inshore' taxa, along with percentages of miospores and other woody material, reflects a more nearshore siliciclastic regime with sandy lithologies (Tyson, 1995, p.320).

Within the upper section of the Lower Silurian upper Tanezzuft Formation (Figs 3.30 & 3.31) the samples are generally characterized by high percentages of palynomorphs and AOM. The palynomorph assemblages show high percentages of marine plankton, dominated by leiospheres and an increase of longer-spined micrhystridid genera, presence of veryhachiid polygonomorphs, and some netromorph taxa; the spores present tend to be thinner-walled. These sediments may have been deposited in more proximal shelf facies (cf. Tyson, 1995, p.320). In the lower part of the upper Tanezzuft Formation, there is an increase in AOM percentages, and the palynomorph fraction is dominated by prasinophytes (leiospheres and *Tasmanites*). The highest content of thick-walled prasinophytes (*Tasmanites* type algae) occurs in lowermost part of the section within the distal wells (A1-70, B1-NC2). The increases of prasinophytes (leiospheres and *Tasmanites*) are especially typical in deep water dysoxic to anoxic basinal facies (Tyson, 1995).

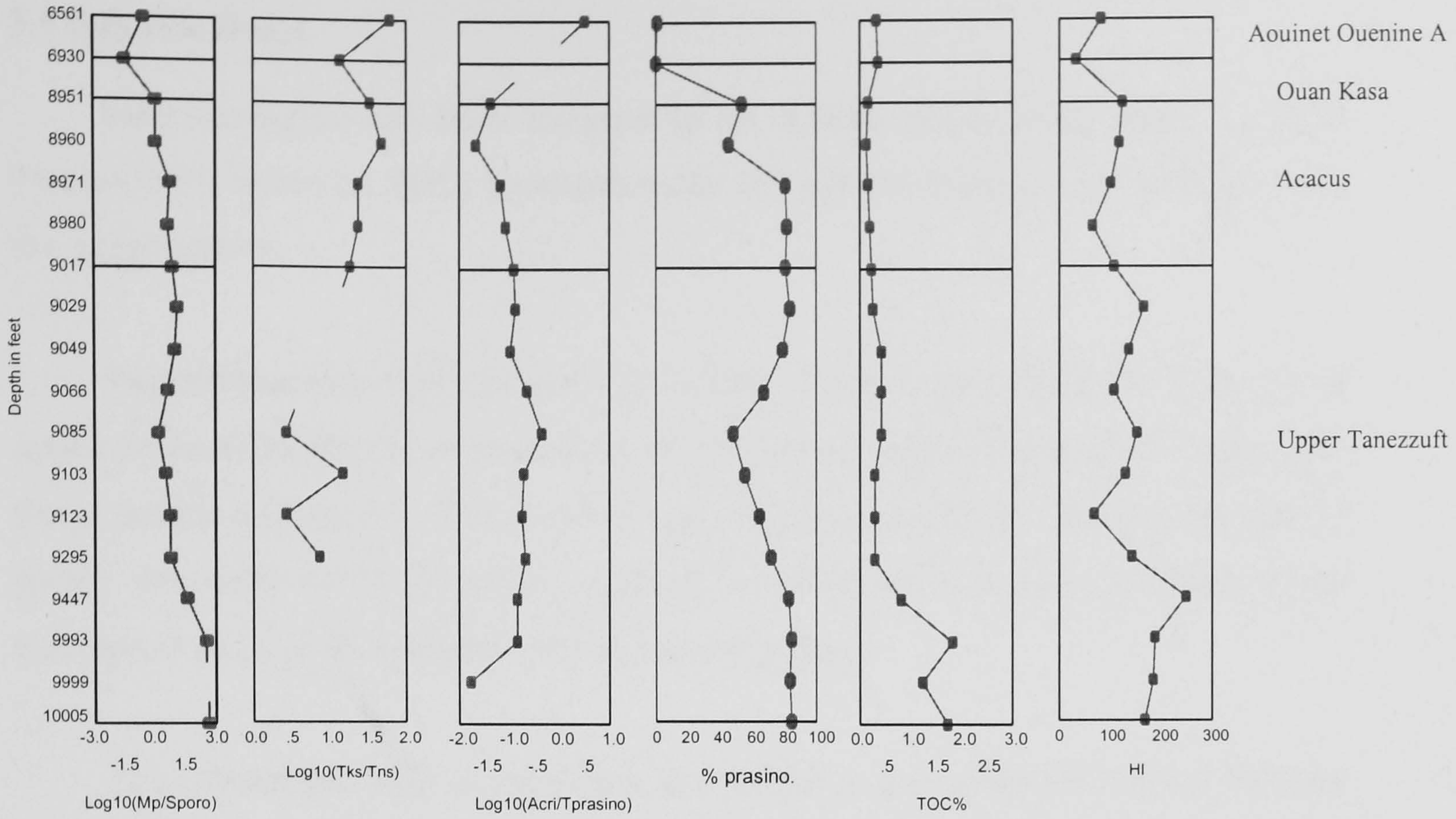

Log10(Mp/Sporo) = Log10 plankton:sporomorph ratio Log10(Tks/Tns) =Log10 thick-walled:thin-walled spore ratio

Log10(Acri/Tprasino) = Log10 ratio acritarchs:Total prasinophytes

% prasino = % prasinophytes of total marine plankton (leiospheres and *Tasmanites*)

Figure 4.30. Variation in selected palynomorph parameters through the Lower Palaeozoic succession in well A1-70, plus TOC and HI.

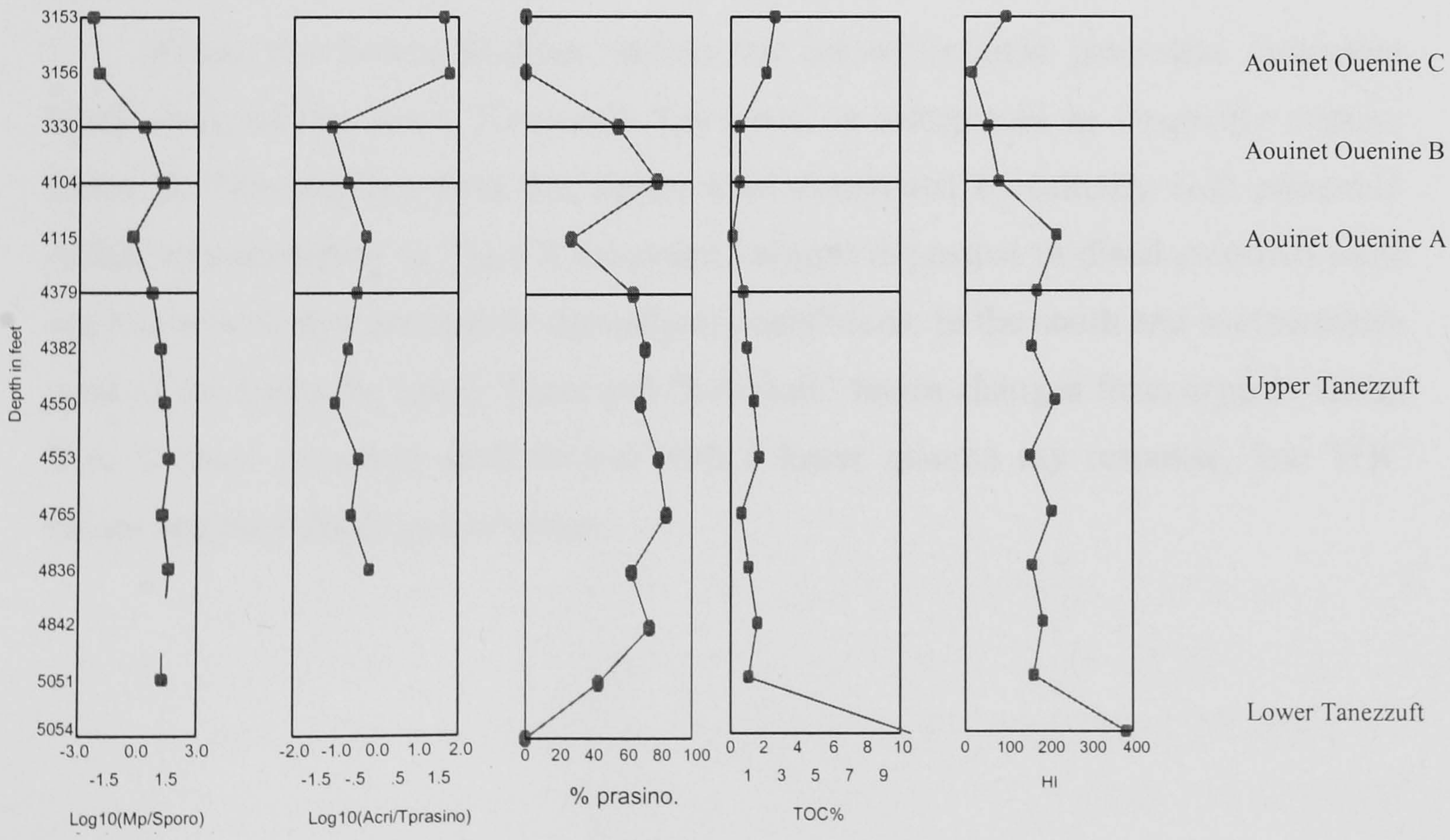

Figure 3.31. Variation in selected palynomorph parameters through the Lower Palaeozoic succession in well A1-66. Key as for Figure 4.30.

3.5 Organic facies

Each formation has been assigned to an organic facies using Table 3.1 after Tyson (1995) based on TOC, hydrogen index and genetic kerogen type inferred from the palynofacies.

The interbedded black and dark grey shales of the Upper Devonian Tahara and upper Aouinet Ouenine C formation are interpreted as organic facies C-CD (proximal fluvio-deltaic oxic facies). They have a high phytoclast input and low percentages of poorly preserved AOM (fluorescence scale 2, AOM non-fluorescent). These facies correspond to Type III kerogen with only gas potential.

The intercalated light and medium grey shales of the Upper and Lower Silurian Acacus and upper Tanezzuft formation are interpreted as organic facies C (oxic shallow marine to proximal shelf facies). This facies is relatively enriched in palynomorphs, with low AOM and phytoclasts. The marine plankton assemblages are dominated by simple and thin-walled prasinophyte (leiospheres), plus lesser amounts of spores and some tracheid-like fragment of possible land plant origin. Type III kerogen and gas potential are indicated.

Within the Lower Silurian section the non-bioturbated graptolitic laminated black shale of the lower Tanezzuft 'hot-shale' is interpreted as originally organic facies B. The samples from this facies were dominated by initially well preserved AOM, corresponding to Type II oil-prone kerogen deposited in distal stratified shelf sea basins with dysoxic-anoxic depositional conditions. In the south and southwestern parts of the basin the lower Tanezzuft 'hot-shale' facies changes from organic facies B to C (oxic proximal shelf facies) with a lower gamma ray response, low TOC values and poor AOM preservation.

3.6 Conclusions

The bulk geochemical results demonstrate the presence of various organic-rich horizons within lower Palaeozoic succession. The total organic carbon (TOC) values are generally between 0.5 and 25%. The best TOC values are measured within the dark-coloured non-bioturbated graptolitic "hot" shales of the lower Tanezzuft Formation (average 7%), and to a lesser extent the Aouinet Ouenine Formation (average 2%); other formations such as Tahara Sandstone Formation contain some thin black shales interbeds that have an average TOC 4.5%, but insufficient thickness for significant source potential. The current hydrogen indices (HI) are mostly below 450, 150–435 in the lower Tanezzuft Formation (maturity affected), and 50–300 in the Aouinet Ouenine Formation

The gamma ray values obtained from the digitized well logs data are positively correlated with the total organic carbon contents (TOC) of the Lower Silurian lower Tanezzuft 'hot-shale'. The isopach map of the 'hot-shale' (>150 API units) indicates a significant spatial variation in hot shale thickness. Generally the thickest basal Tanezzuft hot shale lies in north and northeastern part of the basin, pinching out toward the south and southwestern part of the basin. The absent of the 'hot-shale' in southwestern part of the basin may reflect deposition on a topographic palaeo-high, with shallower, more oxygenated marine conditions.

There is a good positive correlation between fluorescence level and hydrogen index for level 1-4 in the whole dataset, despite the influence of maturity. Interestingly, some Silurian samples exhibit well preserved fluorescent AOM typical of good Type II kerogen (i.e. fluorescence scale 5), but the HI values remain relatively low here.

Multiple regression suggests that the %AOM of kerogen, %phytoclasts of kerogen, %membrane of phytoclasts, brown:black wood ratio, and %*Tasmanites* of palynomorphs are the optical variables that have most direct or indirect influence on the hydrogen index; in the Lower Silurian formations the *Tasmanites* and AOM are the only variables that have a significant effect (because fluorescence is lost due to maturity), whilst in the Upper Devonian formations %AOM of kerogen, %phytoclasts

of kerogen, %membrane of phytoclasts, brown:black wood ratio are suggested as having the greatest influence on the hydrogen index. There is a good positive correlation between the measured and predicted hydrogen indices, but more samples are needed to confirm the statistical validity of the relationships.

The palynofacies data for the Lower Palaeozoic succession permit the recognition of different organic facies. The Upper Devonian Tahara and upper Aouinet Ouenine C formations samples are commonly associated with oxic conditions and moderate proximity to fluvio-deltaic source(s), with low 'AOM' preservation, abundant spores, and phytoclast assemblages, mostly dominated by black wood. The Upper Silurian Acacus Sandstone and upper Tanezzuft formation samples are relatively enriched in palynomorphs, with low AOM and phytoclasts. The marine plankton assemblages are dominated by simple and thin-walled prasinophyte (leiospheres), plus lesser amounts of spores and some tracheid-like fragments of probable land plant origin, suggesting more oxic nearshore shallow marine environments to proximal shelf facies. The samples from lower Tanezzuft Formation are dominated by probably originally well preserved AOM, which would be typical of laminated black shales with Type II oil-prone kerogen deposited in distal stratified shelf sea basins under dysoxic-anoxic depositional conditions.

CHAPTER 4.0

MOLECULAR GEOCHEMISTRY

4.0 MOLECULAR GEOCHEMISTRY

4.1 Introduction

The aim of this chapter is to present a regional molecular geochemistry outline of the study area which includes assessing the source facies and petroleum maturity variations of the potential Silurian and Devonian source rocks within the Ghadames Basin and of the reservoired petroleum throughout the Al-hamada field complex, (NC5, NC8), Al-Wafa field (NC169) and (NC3). The molecular geochemical studies have been carried out on core and oil samples from selected wells (Fig. 2.1).

In the Ghadames Basin the Tanezzuft, Acacus and Tadrart formations are the most important petroleum system, containing 59% of all the discovered oil (Hallet, 2002). Oil was generated primarily from the Tanezzuft hot shale (Hamyouni *et al.*, 1984; Rahoma *et al.*, 1994).

The present structural framework of the Ghadames Basin was produced by tectonic movements related to the Taconic, Caledonian, Hercynian and Austrian phases. This complex structural history has produced a wide variety of structural styles and trap types. Different reservoir levels are prospective within reservoir fairways covering differing parts of the basin. The Ordovician reservoirs have been penetrated by only a few wells, productive mainly in the areas where the reservoir characteristics have been improved by intensive fracturing. The most prolific zones are located mainly in the areas where the Caledonian and Hercynian movements were very active; these areas are close to the Gargaf Uplift. The Silurian formations include productive reservoirs, and in the north-western and southeastern part of the basin a number of oil fields were discovered that produce from the Upper Tanezzuft and Acacus sandstone formations., there are two discrete producing reservoirs within the Lower Devonian of the Ghadames Basin – the Tadrart and Ouan Kasa Formations; the Tadrart-F6 reservoir is a prolific producer over the southern part of the basin. The Middle-Upper Devonian sandstone reservoirs contain most of the oil and gas reserves in the Kebir Trend. Few oil fields were discovered in the area close to the Gargaf Uplift. The Lower Devonian play is water-bearing on the northern flank of the Ghadames Basin because of the erosional effect.

4.2 Bulk Geochemistry of Samples Selected For Molecular Study

In this study 23 core samples from the Lower Palaeozoic succession were selected for molecular geochemical analyses. These samples were previously analyzed for total organic carbon content and source rock potential by Rock-Eval pyrolysis (Table 4.1).

The Lower Silurian Tanezzuft Formation consists almost entirely of marine shale with minor siltstone and sandstone, but can be subdivided into distinct units based on gamma-ray response and lithology (Chapter 3.0). The first unit is characterized by high radioactivity and is composed of laminated dark grey to black shale; within this unit the maximum TOC value measured was 25 wt% and the average 7 wt%. The second unit, the upper Tanezzuft Formation consists of alternating shale and siltstone, and exhibits a 'cool' gamma ray response; this unit has a TOC of <1%. Seven samples from the Lower Silurian Tanezzuft Formation 'hot-shale' unit were selected with total organic carbon contents from 1.7 to 20.3 wt% (average 9.8 wt%). Five samples from the Lower Silurian Tanezzuft Formation 'cool-shale' unit were selected with total organic carbon contents of 0.4 to 1.2 wt% (average 0.8 wt%). The Upper Devonian core shale samples which have been selected have total organic carbon contents ranging from 2.4 to 38.6 wt% (average 7.3 wt%).

The Rock-Eval pyrolysis data agree well with the distribution of the total organic carbon contents (TOC) values. The selected Lower Silurian 'hot-shale' samples that are rich in organic carbon, revealed high residual petroleum potential ranging from 2.90 to 60.29 mg HC/g of rock (average 25.44 mg HC/g of rock). The Lower Silurian 'cool-shale' samples have low residual petroleum potential ranging from 0.20 to 1.0 mg HC/g of rock (average 0.5 mg HC/g of rock). The selected Upper Devonian shale samples revealed high residual petroleum potential range from 2.43 to 104 mg HC/g of rock (average 15.24 mg HC/g rock). The Tmax values for the 23 selected samples are between 422°C and 447°C, suggesting that not all the samples are effected by maturity; however, the Lower Silurian 'hot-shale' samples are generally more mature. The pyrolysis results and their correlation with the optical data for source rock facies and maturity were discussed in Chapters 3.0 and 5.0.

Well	Depth	Formation	Age	TOC (wt%)	S1 (mg HC/g rock)	S2 (mg HC/g rock)	HI (mg HC/g TOC)	PI (mg HC/g rock)	Tmax (°C)
B1-NC2	10108'	L.Tanezzuft (hot-shale)	L. Silurian	2.3	0.95	5.80	254	0.14	447
A1-70	10005'	L.Tanezzuft (hot-shale)	L. Silurian	1.7	0.60	2.90	169	0.17	445
A1-70	10155'	L.Tanezzuft (hot-shale)	L. Silurian	17.3	9.95	60.29	348	0.14	441
F1-66	7053'	L.Tanezzuft (hot-shale)	L. Silurian	5.3	1.93	11.08	210	0.15	435
F1-66	7054'	L.Tanezzuft (hot-shale)	L. Silurian	11.6	3.30	26.71	230	0.11	438
F1-66	7065'	L.Tanezzuft (hot-shale)	L. Silurian	20.3	3.99	30.78	152	0.11	427
A1-66	5054'	L.Tanezzuft (hot-shale)	L. Silurian	10.6	5.70	40.55	383	0.12	435
F1-66	6473'	U.Tanezzuft (cool-shale)	L. Silurian	1.0	0.46	1.02	100	0.31	434
A1-90	11921'	U.Tanezzuft (cool-shale)	L. Silurian	1.2	0.14	0.20	17	0.41	364
Z5-NC5	10124'	U.Tanezzuft (cool-shale)	L. Silurian	0.8	0.30	0.36	45	0.45	444
B1-49	2135m	U.Tanezzuft (cool-shale)	L. Silurian	0.9	0.47	0.36	42	0.57	428
A1-70	9049'	U.Tanezzuft (cool-shale)	L. Silurian	0.4	0.10	0.57	136	0.15	437
A9-NC7	5718'	Tahara	U.Devonian	9.9	2.04	19.14	194	0.10	441
A9-NC7	5733'	Tahara	U.Devonian	6.3	1.35	13.92	221	0.09	443
C1-26	6488'	Tahara	U.Devonian	3.5	0.86	5.74	166	0.13	440
C1-26	6494'	Tahara	U.Devonian	2.9	0.43	2.43	85	0.15	440
C1-26	6500'	Tahara	U.Devonian	4.3	0.86	4.67	108	0.16	440
M2-NC7	6227'	Tahara	U.Devonian	38.6	9.68	104	269	0.09	433
M2-NC7	6251'	Tahara	U.Devonian	3.8	0.40	3.12	81	0.11	437
A1-90	7569'	Tahara	U.Devonian	2.4	0.44	3.14	131	0.12	442
F1-66	4300'	Tahara	U.Devonian	3.4	0.24	4.78	142	0.05	422
B1-49	1434m	Tahara	U.Devonian	2.9	0.73	4.21	146	0.15	442
A1-66	3153'	Tahara	U.Devonian	2.6	0.38	2.58	99	0.13	430

Table 4.1. Bulk geochemical data showing the total organic carbon and pyrolysis data for the Silurian and Devonian rock samples selected for molecular geochemical analyses.

4.2 Molecular characterisation of the source rocks

4.2.1. Source Facies Characterisation

Normal Alkanes and Isoprenoid Alkanes

Representative gas chromatogram of the saturated hydrocarbon fraction showing the *n*-alkane and acyclic isoprenoid alkane distribution (*n*-C_{10}+) within typical Silurian and Devonian samples are displayed in Figures 4.1–4.3, and values for geochemical parameters based on *n*-alkanes and acyclic isoprenoid alkane distributions are given in Table 4.2. The Lower Silurian Tanezzuft Formation 'hot-shale' samples show an *n*-alkane distribution dominated generally by short-chain (*n*-C_{12} to *n*-C_{20}) over long-chain *n*-alkanes, and the *n*-C_{17}/*n*-C_{27} ratio ranges from 4.1 to 86.5; this is characteristic of marine organic matter and may suggest high algal input (Debyser *et al.*, 1977; Dastillung & Corbet, 1978). The samples from the Lower Silurian Tanezzuft Formation 'cool-shale' exhibit the same *n*-alkane distribution but slightly lower *n*-C_{17}/ *n*-C_{27} ratio ranges of 2.1 to 6.6. One sample collected from well A1-90 (11921') exhibited different features (Fig. 4.2): a significant presence of heavier *n*-alkanes at *n*-C_{22} to *n*-C_{30} and a very low *n*-C_{17}/*n*-C_{27} ratio, features that are usually associated with terrestrial higher plant waxes (Tissot & Welte, 1984). Within

the Devonian samples the distribution of *n*-alkanes is generally bimodal, being dominated by short-chain compounds with a relative dominance of odd carbon numbers.

The pristane/phytane (Pr/Ph) ratio for the Lower Silurian 'hot shale' samples varies between 1.0 to 1.7 suggesting facies differences between the samples. The Lower Silurian 'cool shale' has a slightly higher (Pr/Ph) ratio, suggesting changes in the organic facies and depositional condition.

The Devonian source rock samples show Pr/Ph ratios ranging from 1.0 to 2.5, suggesting a relatively more oxic depositional environment during the Upper Devonian compared to the Lower Silurian.

Sample	Location	depth (feet)	Pr/Ph	Pr/n-C_{17}	Ph/n-C_{18}	n-alkane index index n-C_{17}/n-C_{27}	Sum n-alkanes ($\mu\gamma$/g extract)
Silurian hot-shale							
	B1-NC2	10108	1.0	0.6	0.6	4.1	13600
	A1-70	10005	1.0	0.4	0.5	5.5	11211
	A1-70	10155	1.0	0.3	0.4	86.5	13127
	F1-66	7053	1.0	0.2	0.3	12.7	7124
	F1-66	7054	1.5	0.2	0.2	41	6266
	F1-66	7065	1.7	0.2	0.2	32	3221
	A1-66	5054	1.2	0.3	0.3	12.4	5583
Average			1.2	0.3	0.4	27.7	8590
Range			(1-1.7)	(0.2-0.6)	(0.2-0.6)	(4.1-86)	(3221-13600)
Silurian cool-shale							
	A1-70	9049	1.5	0.3	0.2	2.1	12657
	F1-66	6473	1.4	0.3	0.2	6.6	10504
	Z5-NC5	10124	1.2	0.5	0.4	2.7	9522
	A1-90	11921	1.0	0.3	0.3	0.3	24315
	B1-49	2135	1.7	0.1	0.1	2.9	3751
Average			1.4	0.3	0.2	2.9	12150
Range			(1-1.7)	(0.1-0.5)	(0.1-0.4)	(0.3-6.6.6)	(24315-3751)
Devonian							
	A9-NC7	5733	2.5	0.6	0.3	1.7	6096
	A9-NC7	5718	2.3	0.4	0.3	2.5	4291
	C1-26	6488	2.2	0.3	0.2	2.5	10315
	C1-26	6494	1.7	0.3	0.2	2.5	15517
	C1-26	6500	1.8	0.3	0.2	1.9	15670
	M2-NC7	6227	1.5	0.2	0.2	23.3	1842
	M2-NC7	6551	1.6	0.3	0.2	4.1	7523
	A1-90	7569	1.4	0.3	0.2	2.4	15480
	B1-49	1434	1	0.1	0.1	2.6	24420
	A1-66	3153	1.6	0.6	0.5	4.8	11862
	F1-66	4300	1.5	0.5	0.4	14	7061
Average			1.7	0.4	0.2	5.7	10916
Range			(1-2.5)	(0.1-0.6)	(0.1-0.5)	(1.7-23.3)	(1842-24420)

Table 4.2 Geochemical parameters obtained from the distributions of *n*-alkanes and isoprenoids for the Silurian and Devonian source rock samples.

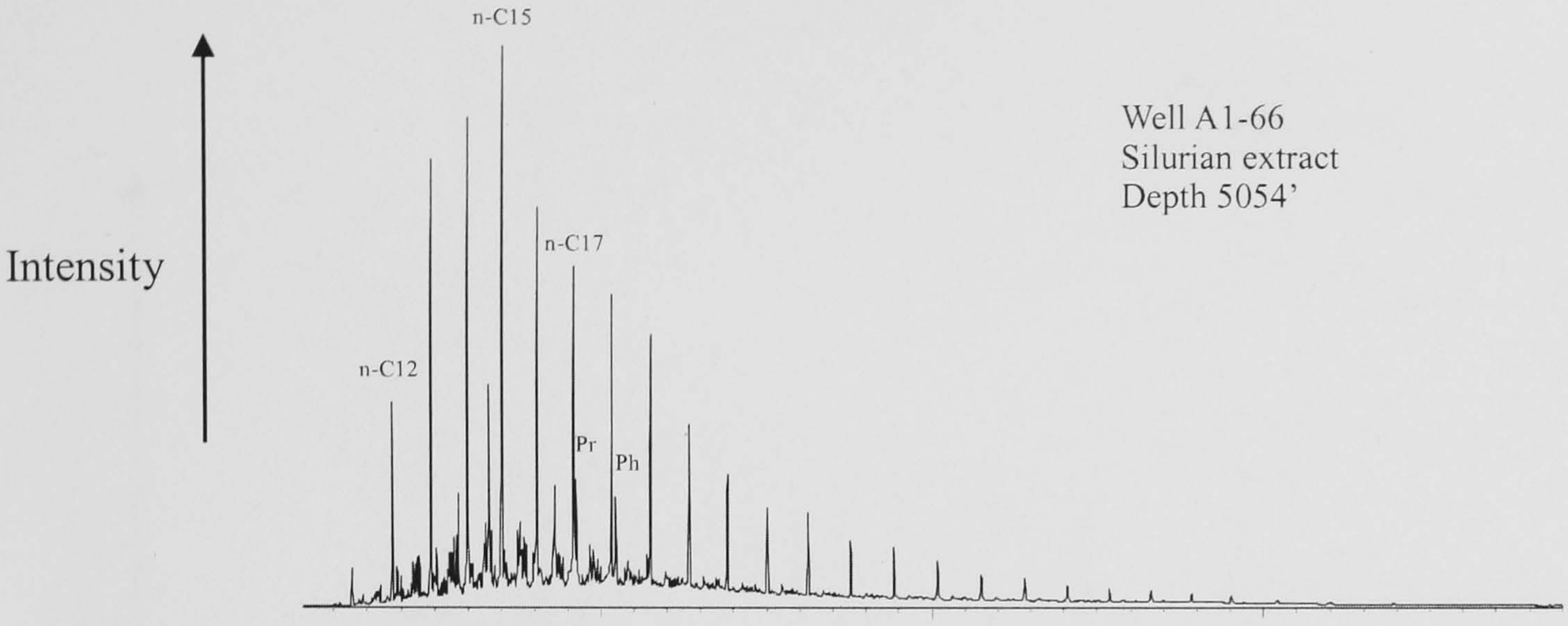

Figure 4.1. Gas chromatogram of the saturated hydrocarbon fraction extracted from a typical Silurian source rock 'hot shale'.

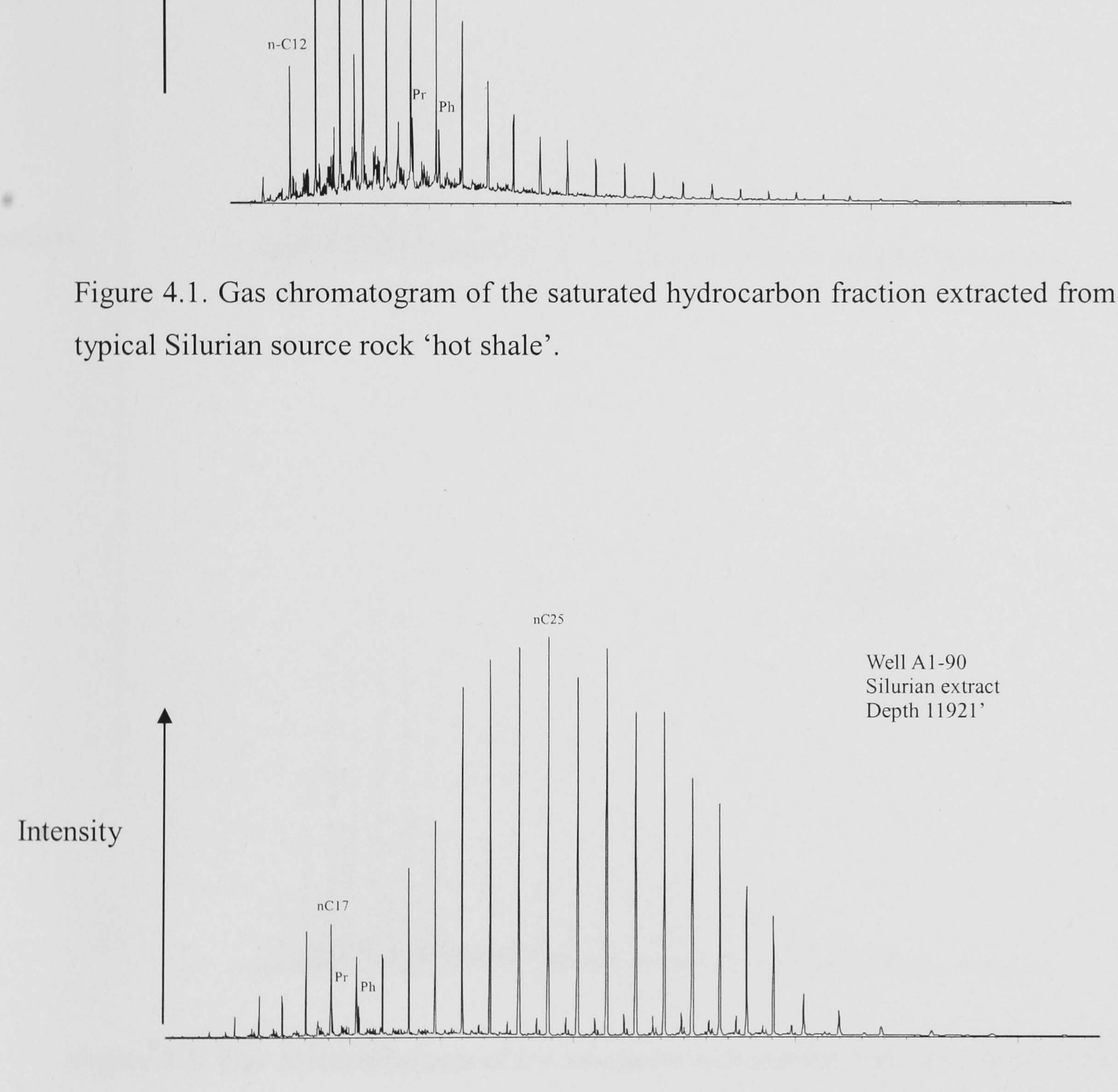

Figure 4.2. Gas chromatogram of the saturated hydrocarbon fraction extracted from a Silurian 'cool shale'.

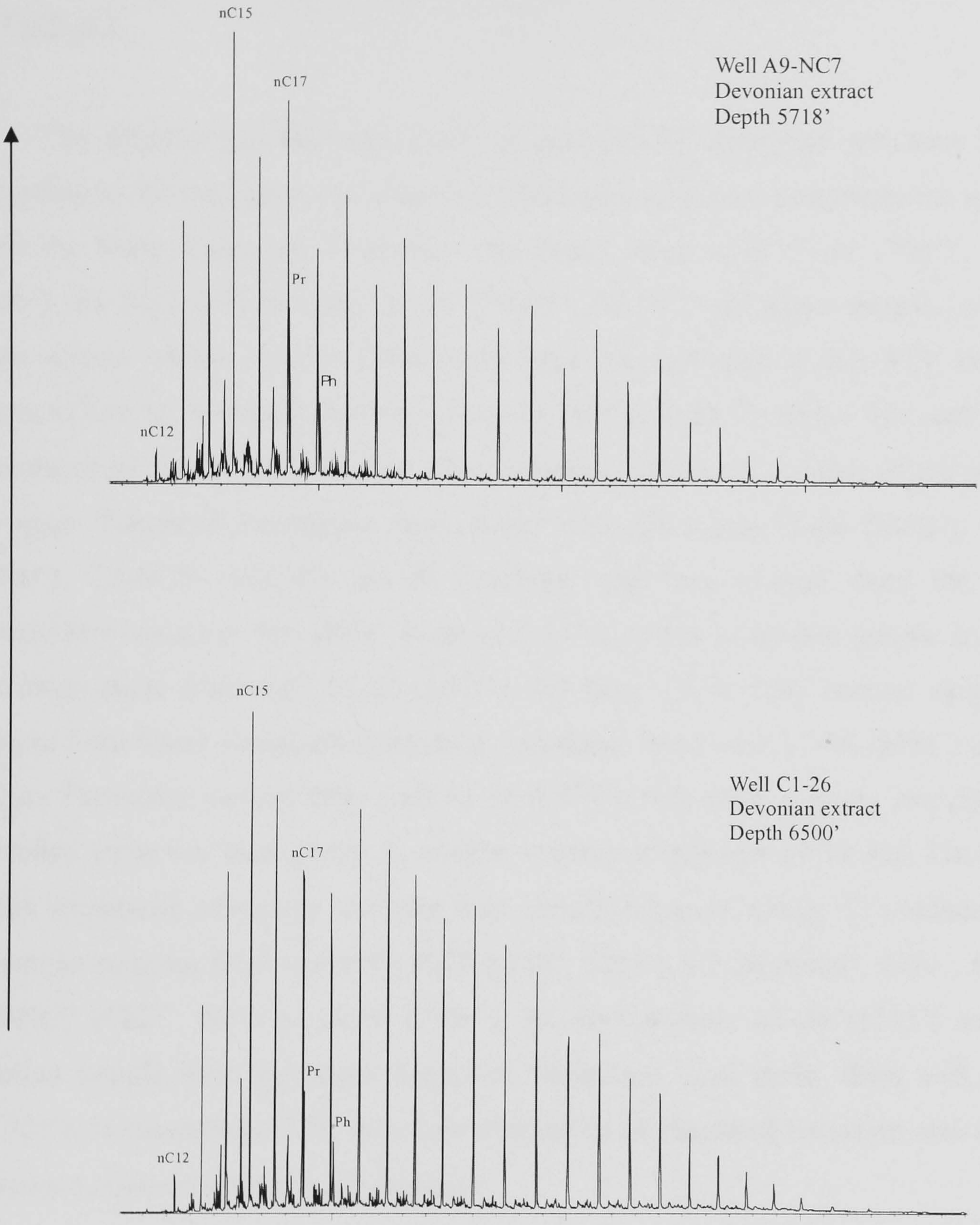

Figure 4.3. Gas chromatograms of the saturated hydrocarbon fraction extracted from Devonian samples.

Steranes and Triterpanes

Partial m/z 191 and 217 mass chromatograms showing typical distributions of the triterpanes and steranes in Silurian and Devonian rock samples are displayed in Figures 4.4 and 4.5; the geochemical ratios based on steranes and triterpanes are given in Table 4.3.

The Silurian and Devonian rock samples can be separated into three groups according to the triterpane and sterane distributions. Group A, comprises the samples from the lower Tanezzuft Formation 'hot shale' from wells F1-66 (7053', 7054', 7065'), B1-NC2 (10108') and A1-70 (10005', 10155'). All these samples revealed high organic carbon content (TOC) and petroleum potential (Table 4.1); they are characterised by abundant tricyclics from C_{20} to C_{26}, high Ts *versus* Tm, and higher abundance of regular steranes than 17α(H)-hopanes. Group B consists of the samples of upper Tanezzuft Formation 'cool shale' from the wells F1-66 (6473'), A1-70 (9049'), Z5-NC5 (10124'), B1-49 (2135m), with one sample from the lower Tanezzuft Formation 'hot-shale' from well A1-66 (5054') and one sample from the Devonian shale from well F1-66 (6473'). All have a low TOC content except the sample from lower Tanezzuft Formation 'hot shale' from well A1-66 (5054') and the Tahara Formation sample from well F1-66 (6473'); they show a lower abundance of extended tricyclics than group A, similar relative abundance of Ts and Tm, and a lower abundance of regular steranes than 17α(H)-hopanes. Group C, containing 10 Devonian samples from wells A9-NC7 (5718', 5733'), C1-26 (6488', 6494', 6500'), M2-NC7 (6227', 6251'), A1-90 (7569'), B1-49 (1434m), A1-66 (3153') and one Silurian sample from the upper Tanezzuft Formation 'cool shale' from well A1-90 (11921'), is characterised by very low abundance of extended tricyclics and regular steranes compared with 17α(H)-hopanes.

Well	Depth	Formation	Age	20S/ 20S+20R	ββ/αα+ββ	C_{29}Ts/(C_{29}Ts+C_{29}hop	C_{30}diahop/ (C_{30}hop+ C_{30}diahop)	C_{29}hop /C_{30} hop	Ts/Ts+Tm	C_{20}-C_{26}Tr/ C_{29}+C_{30} hop.	C_{29}ster./ C_{29}+C_{30}hop
B1-NC2	10108	L.Tanezzuft	L. Silurian	0.47	0.60	0.48	0.22	0.28	0.64	0.59	0.42
A1-70	10005	L.Tanezzuft	L. Silurian	0.52	0.62	0.44	0.20	0.29	0.46	0.59	0.48
A1-70	10155	L.Tanezzuft	L. Silurian	0.49	0.54	0.24	0.12	0.39	0.39	0.62	0.33
F1-66	7053	L.Tanezzuft	L. Silurian	0.50	0.60	0.32	0.18	0.40	0.73	0.75	0.42
F1-66	7054	L.Tanezzuft	L. Silurian	0.50	0.59	0.39	0.00	0.39	0.63	0.84	0.83
F1-66	7065	L.Tanezzuft	L. Silurian	0.54	0.59	0.33	0.00	0.46	0.58	0.88	0.82
A1-66	5054	L.Tanezzuft	L. Silurian	0.50	0.47	0.28	0.09	0.38	0.52	0.34	0.29
F1-66	6473	U.Tanezzuft	L. Silurian	0.47	0.46	0.31	0.11	0.38	0.51	0.36	0.38
A1-90	11921	U.Tanezzuft	L. Silurian	0.47	0.48	0.18	0.07	0.48	0.42	0.04	0.02
Z5-NC5	10124	U.Tanezzuft	L. Silurian	0.51	0.61	0.36	0.15	0.34	0.57	0.40	0.36
B1-49	2135	U.Tanezzuft	L. Silurian	0.46	0.47	0.18	0.07	0.49	0.45	0.37	0.14
A1-70	9049	U.Tanezzuft	L. Silurian	0.39	0.38	0.51	0.18	0.33	0.65	0.22	0.18
A9-NC7	5718	Tahara	U.Devonian	0.45	0.36	0.31	0.08	0.47	0.38	0.08	0.04
A9-NC7	5733	Tahara	U.Devonian	0.45	0.47	0.36	0.06	0.45	0.47	0.05	0.04
C1-26	6488	Tahara	U.Devonian	0.61	0.43	0.29	0.10	0.44	0.42	0.09	0.03
C1-26	6494	Tahara	U.Devonian	0.60	0.47	0.34	0.11	0.42	0.58	0.09	0.03
C1-26	6500	Tahara	U.Devonian	0.57	0.47	0.36	0.10	0.36	0.58	0.09	0.03
M2-NC7	6227	Tahara	U.Devonian	0.60	0.45	0.28	0.12	0.44	0.33	0.04	0.03
M2-NC7	6251	Tahara	U.Devonian	0.55	0.41	0.28	0.09	0.50	0.39	0.07	0.04
A1-90	7569	Tahara	U.Devonian	0.63	0.51	0.39	0.16	0.41	0.54	0.11	0.04
F1-66	4300	Tahara	U.Devonian	0.22	0.25	0.31	0.08	0.40	0.47	0.25	0.17
B1-49	1434	Tahara	U.Devonian	0.62	0.52	0.47	0.14	0.29	0.74	0.11	0.06
A1-66	3153	Tahara	U.Devonian	0.36	0.34	0.37	0.05	0.37	0.31	0.07	0.00

Table 4.3. Biomarker ratios for the Silurian and Devonian source rock samples.

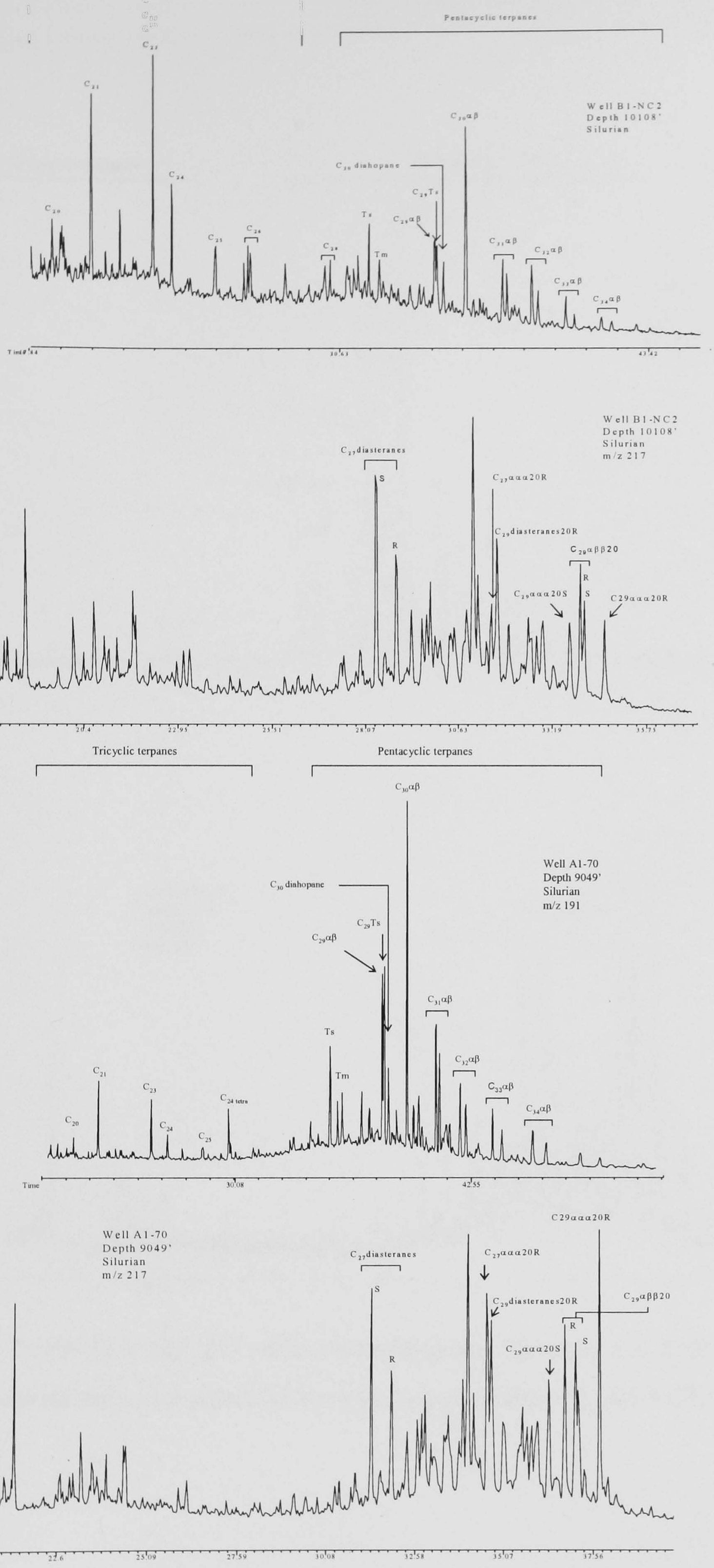

Figure 4.4. Partial m/z 191 and 217 mass chromatograms showing the distributions of triterpanes and steranes in two selected Silurian samples (Group A, B1-NC2, 10108'; Group B, A1-70, 9049').

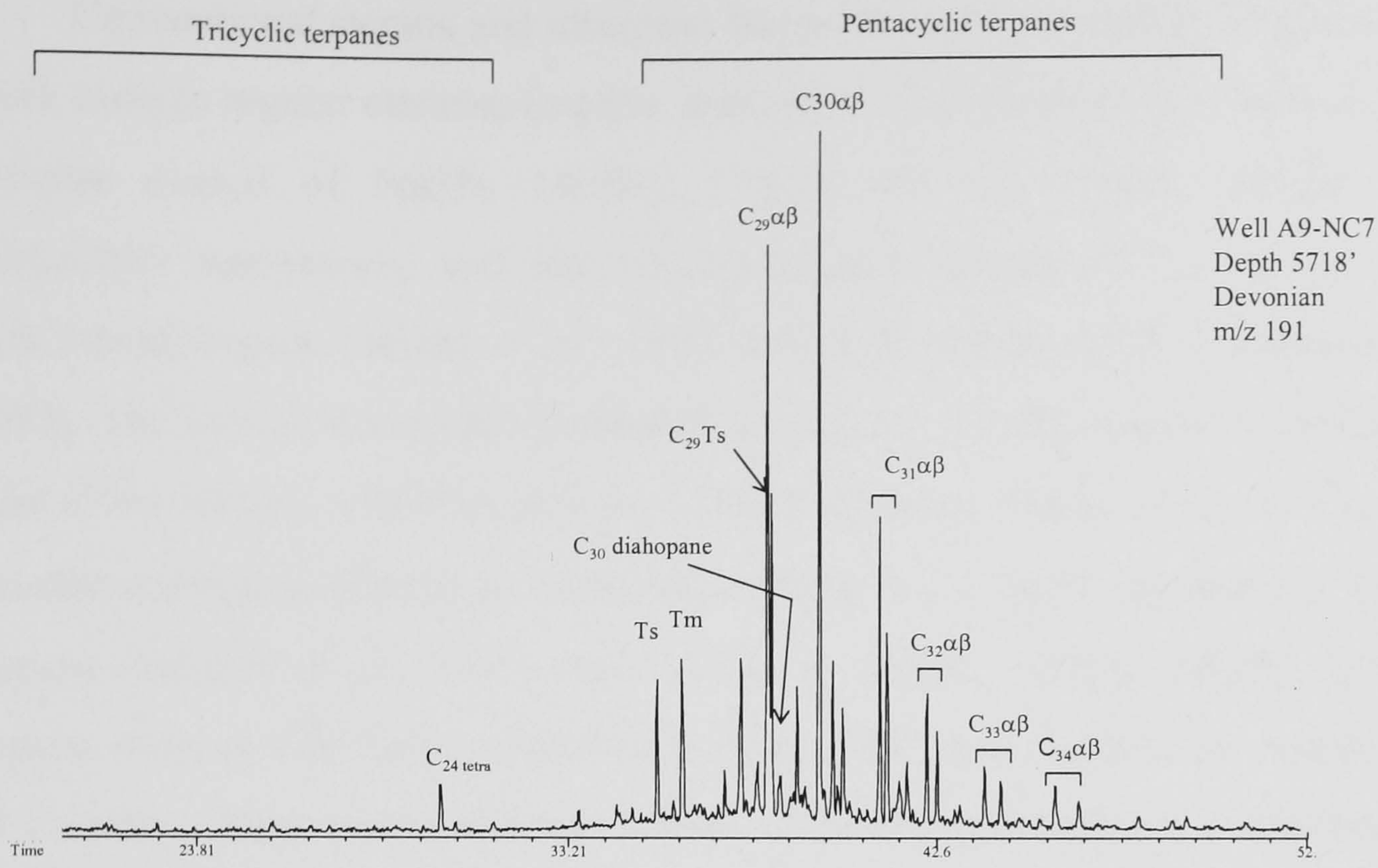

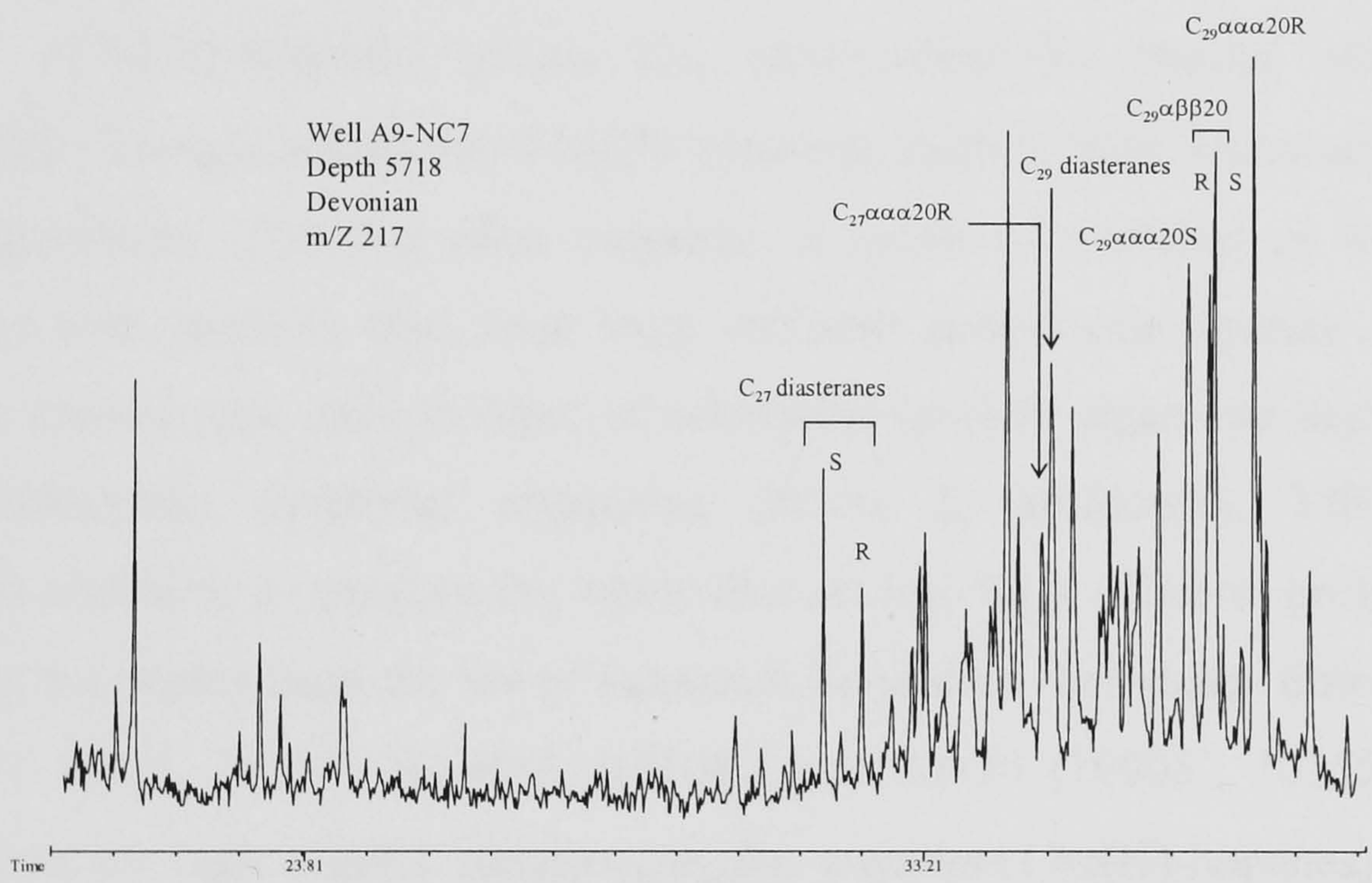

Figure 4.5. Partial m/z and 217 mass chromatograms showing the distributions of triterpanes and steranes in a selected Devonian sample (Group C, A9-NC7, 5718').

Conventional sterane and triterpane facies-sensitive parameters employed in this work include regular steranes/(regular steranes + 17α(H)hopanes), where the regular steranes consist of 5α(H), 14α(H), 17α(H) and C_{29} 5α(H), 14β(H), 17β(H) (20S+20R) compounds, and the 17α(H)-hopanes consist of C_{29} to C_{30} 17α(H) pseudohomologues (Seifert *et al.*, 1978; Tissot & Welte, 1984; Moldowan *et al.*, 1985). The extended tricyclics/(extended tricyclics + 17α(H)-hopanes) consist of the sum of the C_{20}-C_{26} tricyclics and the 17α(H) -hopanes consist of C_{29} to C_{30} 17α(H) pseudohomologues (Peters & Moldowan, 1993), C_{29} 17α(H) -hopane/C_{30} 17α(H) -hopane (Subroto *et al.*, 1991), the C_{27}-C_{28}-C_{29} 5α(H), 14β(H), 17β(H) (20S+20R) regular steranes distribution (Moldowan *et al.*, 1985) and the absolute concentrations of tricyclics, hopanes and steranes. Values of these parameters and concentrations of individual biomarker are provided in Appendix V.

Figure 4.6 is a crossplot of the extended C_{20}-C_{26} tricyclics/(extended C_{20}-C_{26} tricyclics +17α(H)-hopanes) versus C_{29} ααα+αββ(S+R) regular steranes/(C_{29} ααα+αββ(S+R) regular steranes+17α(H)-hopanes). Both of these ratios are primarily source parameters. The first ratio compares a group of bacterial or algal lipids (tricyclics) with markers that arise from different prokaryotic species (hopanes), whilst the second ratio reflects input of eukaryotic (mainly algae and higher plants) versus prokaryotic (bacteria) organisms (Peters & Moldowan, 1993). These parameters enable us to separate the whole data set into three different groups. Group A contains 6 samples from the lower Tanezzuft Formation 'hot-shale' from wells F1-66 (7053', 7054', 7065'), B1-NC2 (10108') and A1-70 (10005', 10155'), and is characterised by high regular steranes/(regular steranes+17α(H)-hopanes) and high extended tricyclics/(extended tricyclics+17α(H)-hopanes) ratios. The higher value of the regular steranes/(regular steranes+17α(H)-hopanes) seen in Group A suggests a better preservation of steroidal compounds in a less oxic depositional environment (Moldowan *et al.*, 1985; Connan *et al.*, 1986), whilst the higher value of the tricyclic/ 17α(H)-hopanes ratio suggests a higher input of a group of bacterial, algal lipids or *Tasmanites* (Volkman *et al.*, 1989; Aquino Neto *et al.*, 1989; Peters *et al.*, 1993).

Group B comprises 6 samples, including 4 samples from the upper Tanezzuft Formation 'cool shale' from the wells F1-66 (6473'), A1-70 (9049'), Z5-NC5

(10124'), B1-49 (2135m), with one sample from the lower Tanezzuft Formation 'hot shale' from well A1-66 (5054') and one sample of Devonian shale from well F1-66 (4300'). The biomarker distributions for these samples exhibit lower regular steranes/(regular steranes+17α(H)-hopanes). The differences in the biomarker distribution between groups A and B are probably due to differences in lithology and depositional conditions. Group B samples have lower TOC contents, except for the sample from well A1-66 (5054').

Figure 4.6 also shows another cluster of samples classified as Group C, which contains 9 Devonian shale samples: A9-NC7 (5718', 5733'), C1-26 (6488', 6494', 6500'), M2-NC7 (6227', 6251'), A1-90 (7569'), B1-49 (1434m) and one Silurian shale sample from the upper Tanezzuft Formation 'cool shale' from well A1-90 (11921'). All the samples from Group C are characterised by very low extended tricyclics and regular steranes, indicating that these samples were deposited under more oxic depositional conditions.

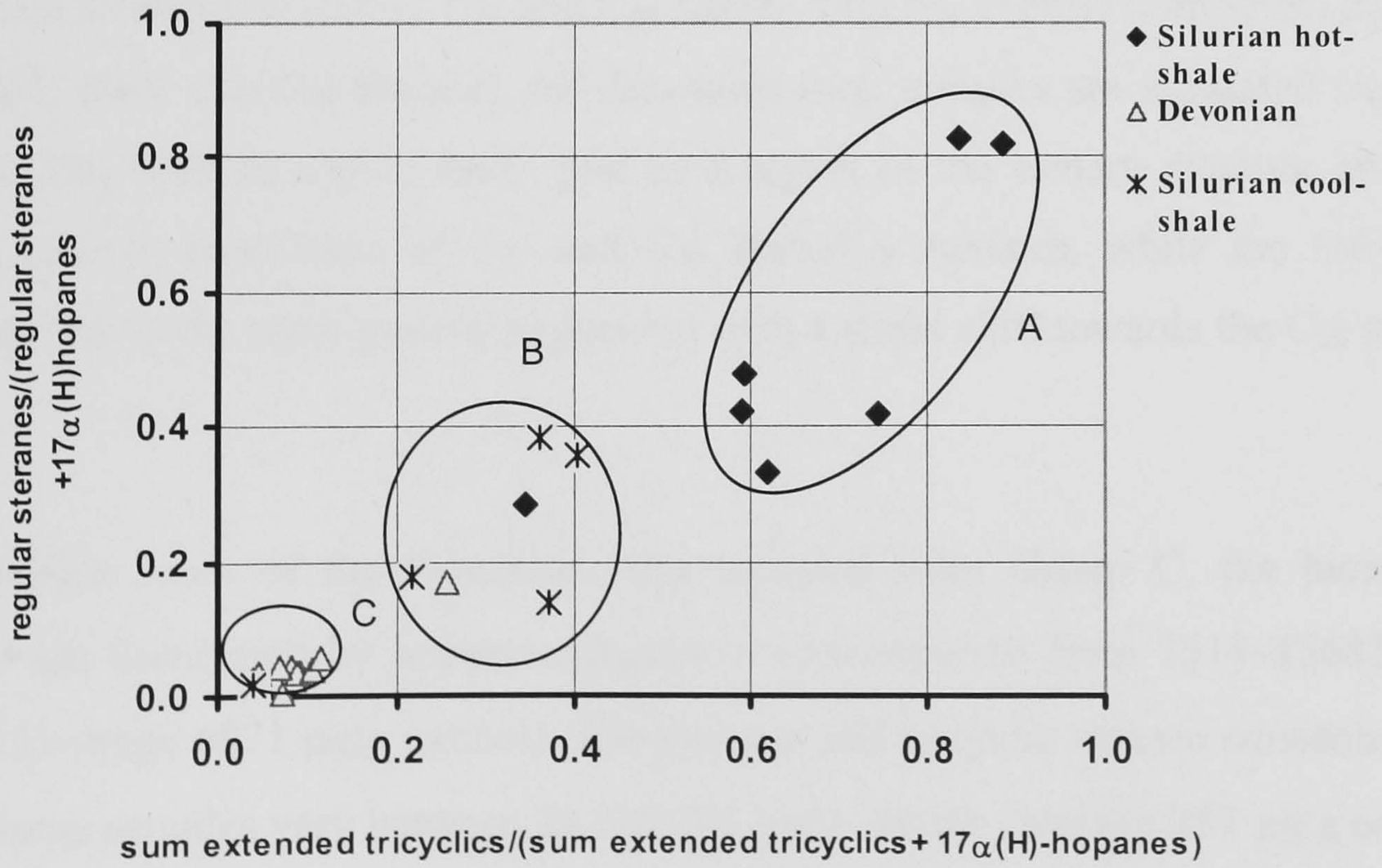

Figure 4.6. Cross plot of biomarker facies parameters for the Lower Silurian and Devonian source rocks, showing the three groups described in the text.

The relative abundances of C_{27}, C_{28} and C_{29} steranes in source rock and oils reflect the carbon number distribution of the sterols incorporated into sediments during their deposition, which is, in turn, indicative of the nature of the contributing organisms to the accumulated organic matter in the source rocks of oils (Mackenzie *et al.*, 1983; Moldowan *et al.*, 1985). For example, a high relative abundance of C_{29} steranes in oils may indicate a land-plant origin for the oils, in agreement with the high C_{29} sterol abundances in higher plants compared to the C_{27} sterol predominance in marine plankton (Huang & Meinschein, 1979). However, caution needs to be implemented when interpreting the distribution of the relative abundances of C_{27}, C_{28} and C_{29} steranes, as it has been reported that brown algae and many species of green algae contain predominantly C_{29} sterols (Moldowan *et al.*, 1985). Furthermore, 24-ethylcholest-5en-3β-ol (a C_{29} sterol) has been reported as a significant component in a mixed diatom culture (Volkman *et al.*, 1981). Nevertheless, sterane carbon number ternary diagrams are used extensively to show relationships between oils and/or source rock bitumens (Peters *et al.*, 1989, Peters & Moldowan, 1993). The principal use of the C_{27}-C_{28}-C_{29} sterane ternary diagrams is to distinguish groups of oils derived from different source rocks or different organic facies of the same source rock (Peters & Moldowan, 1993).

The distribution of C_{27}, C_{28} and C_{29} 5α(H), 14β(H), 17β(H) (20S+20R) steranes (Fig. 4.7) show that the Silurian and Devonian rock samples are separated into two groups. The Silurian source rocks plot in a region of the ternary diagram showing higher relative abundance of C_{27} and C_{29} than C_{28} steranes, while the Devonian samples plot in the same general region but with a slight shift towards the C_{28} sterane apex.

Within most of the Devonian rock samples from Group C, the biomarker alkanes are dominated by hopanes ranging in concentration from 3514–15682 μg/g extract (average 6871 μg/g extract). The steranes and tricyclic terpane concentrations in the same samples vary between 48 and 881 μg/g extract (average 487 μg/g extract) and 113 to 1876 μg/g extract (average 395 μg/g extract), respectively. Within the same group the Silurian 'cool shale' sample from well A1-90 (11921') is also dominated by hopanes (6090 μg/g extract) and has low sterane and tricyclic terpane

concentrations (198 and 139 μg/g extract respectively). The Silurian 'cool shale' of Group B has a lower concentration of hopanes than Group C, ranging from 95 to 2644 μg/g extract (average 961 μg/g); the steranes and tricyclic terpanes range from 32 to 978 μg/g extract (average 565 μg/g extract) and 32 to 335 μg/g extract (average 201 μg/g extract), respectively. By contrast, the Silurian lower Tanezzuft Formation 'hot shale' of Group A reveals a predominance of tricylics and steranes ranging from 60 to 302 μg/g extract (average 178 μg/g extract) and 141 to 648 μg/g extract (average 339 μg/g extract), respectively, with only low hopanes concentrations ranging from 20 to 394 μg/g extract (average 169 μg/g extract).

The combination of high concentrations of steranes and high regular steranes/17α (H)-hopanes ratios (Fig. 4.8) in most of the Silurian source rock samples of Group A indicates marine organic matter with major contributions from planktonic and/or benthic algae (e.g. Moldowan *et al.*, 1985; Peters & Moldowan, 1993). Low sterane concentrations and low regular sterane/17α (H)-hopane ratios in all the Devonian and the Silurian source rock samples of Group B are more indicative of microbially reworked organic matter (e.g. Tissot & Welte, 1984; Peters & Moldowan, 1993).

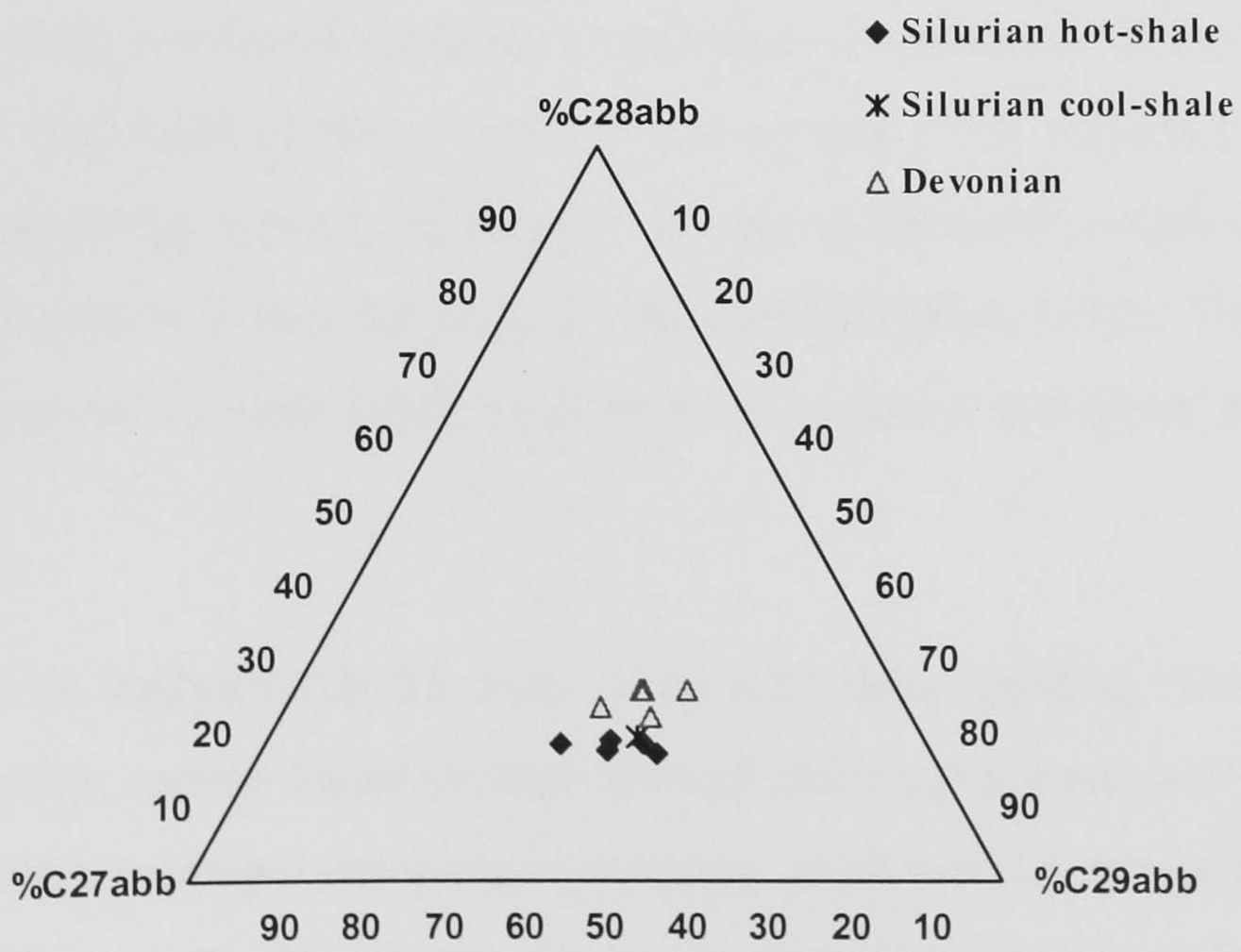

Figure 4.7. Ternary plot of the relative abundance of C_{27}- C_{28}- C_{29} αββ (S+R) steranes in the Silurian and Devonian source rock extracts.

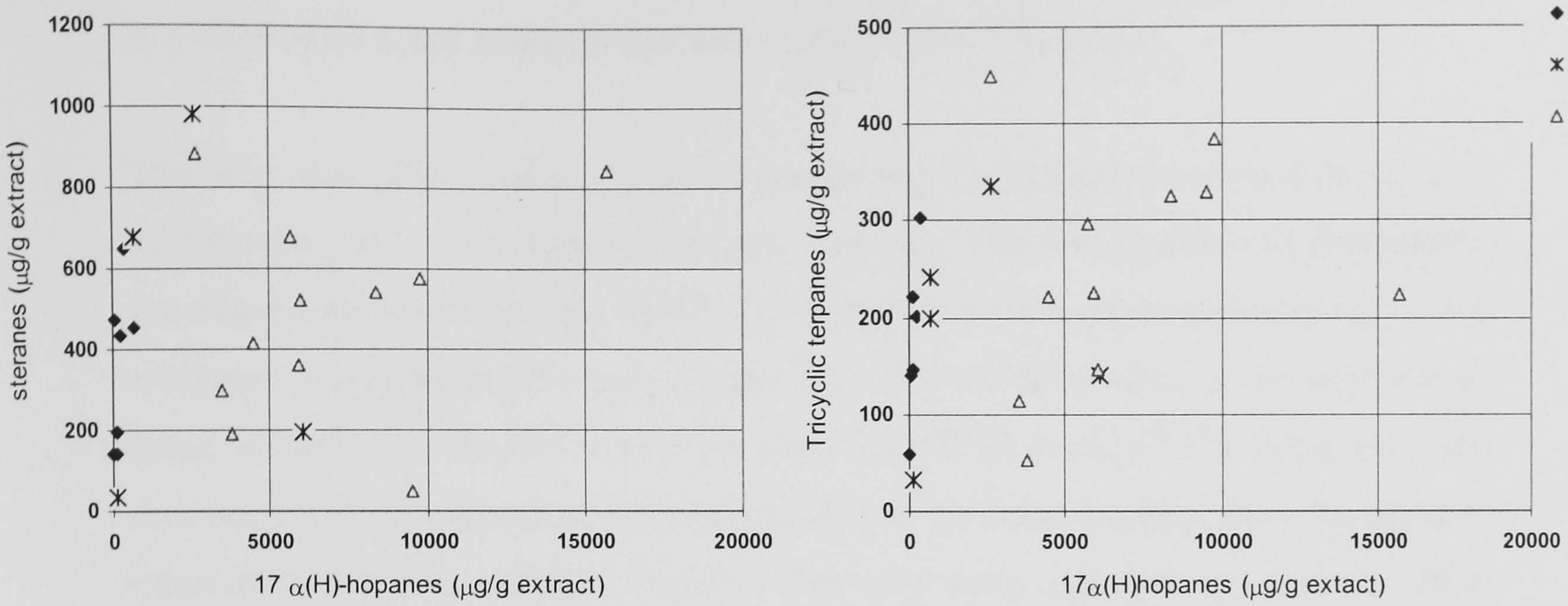

Figure 4.8. The concentrations (µg/g of extract) of total steranes versus total hopanes, and of the total tricyclics versus total hopanes in the Silurian and Devonian samples.

4.2.2 Principal Components Analysis (PCA)

Principal Component Analysis (PCA) is a multivariate statistical method used to recognise the relationships between samples and variables in complex data sets, and summarise the main source of variance as principal components (PCs). The method typically shows that most of the variance is due to just a few principal components, allowing the data to be plotted graphically in two dimensions, while still retaining most of the information within the complex data set (Melglen, 1992). The PCs are, by definition, orthogonal to each other, such that the variance explained by each PC is unique.

This type of analysis can be used as an aid when deciding which molecular biomarker maturity, source facies or depositional environment parameters should be plotted, because the principal component loadings plots tend to extract the biomarker variables related to maturity, source facies or depositional environment controls. Therefore, PCA can be considered as a data reduction technique capable of handling large volumes of data and able to extract the subtle significant differences between the samples. It has been used by a number of authors to analyse geochemical data, e.g.

Kvalheim (1987) for oil-source rock correlation studies, Bigge and Farrimond (1998) and Parfitt and Farrimond (1998) to identify the extent and effects of biodegradation in a suite of oil seeps along the Dorset coast (South of England).

The PCA was performed on a dataset comprising 41 biomarker concentrations from 12 Silurian and 11 Devonian source rock samples, with the objective of establishing the major sources of variance within the steranes, tricyclic terpanes, hopanes, C_{17}-C_{18} *n*-alkanes and pristane (Pr) and phytane (Ph). The variables used in the analysis are listed in Table 5.4. The PCA software used was "SPSS version 8 for Windows". The data were first normalized to eliminate analytical variance resulting from the absolute intensity differences between samples. The first three principal components (PCs) obtained explained 55.95%, 20.85%, and 7.92% of the variance within the scaled data set, respectively. This allows the relationships between the samples to be examined in simple two-dimensional scores plots: PC1 versus PC2 and PC1 versus PC3, which include the effects of all the original biomarker concentrations variables, and display the bulk (84%) of the scaled data variability (Fig. 4.9). Interestingly, these PCA plots demonstrate that the Silurian and Devonian source rock samples can be discriminated into the same groups revealed when using conventional biomarker ratios (cf. Fig. 4.6).

An explanation of the principal components is given by the loading plots shown in Figure 4.10. These diagrams exhibit the loadings of the different variables within the principal components; large loadings, either positive or negative, indicate a significant influence of that variable on that PC. It is usual to regard loading as "high" if the values of the loading are greater than 0.6 (either positive or negative), and "moderately high" if above 0.3 (Kline, 1994). Low loading values (<0.3) may imply that there is no, or almost no, correlation between the variables and the principal component.

The first and second principal components PC1 and PC2 explain 55.95% and 20.85%, respectively, of the total variance of the data set, and the variable loadings indicate that the PC1 is controlled by loadings attributed to the relative concentration of C_{21}-C_{26} tricyclic terpanes, steranes, C_{17}-C_{18} *n*-alkanes, pristane (Pr) and phytane (Ph) versus the hopanes (Fig. 5.10). High positive PC1 loadings are characteristic of the C_{21}-C_{26} tryicyclic terpanes and steranes, while hopanes are characterized by strong

	Tricyclic terpanes and hopanes (m/z = 191)
1	C_{20} Tricyclic terpane
2	C_{21} Tricyclic terpane
3	C_{23} Tricyclic terpane
4	C_{24} Tricyclic terpane
5	C_{25} Tricyclic terpane
6	C_{26} Tricyclic terpane
7	22,29,30-Trisnorneohopane (Ts)
8	22,29,30-Trisnorhopane (Tm)
9	C_{29} 17α(H), 21β(H)-30-norhopane
10	18α(H)-30-norneohopane (C_{29} Ts)
11	C_{30} diahopane
12	C_{29} 17β(H),21α(H) hopanes
13	C_{30} 17α(H),21β(H) hopanes
14	C_{30} 17β(H),21α(H) hopanes
15	C_{31} 17α(H),21β(H) hopanes (22S)
16	C_{31} 17α(H),21β(H) hopanes (22R)
17	C_{32} 17α(H),21β(H) hopanes (22S)
18	C_{32} 17α(H),21β(H) hopanes (22R)
19	C_{33} 17α(H),21β(H) hopanes (22S)
20	C_{33} 17α(H),21β(H) hopanes (22R)
21	C_{34} 17α(H),21β(H) hopanes (22S)
22	C_{34} 17α(H),21β(H) hopanes (22R)
	Steranes (m/z =217)
23	C_{27} 13β(H), 17α(H) diasterane (20S)
24	C_{27} 13β(H), 17α(H) diasterane (20R)
25	C_{29} 13β(H), 17α(H) diasterane (20S)
26	C_{27} 5α(H), 14α(H), 17α(H) sterane (20R)
27	C_{29} 13β(H), 17α(H) diasterane (20R)
28	C_{29} 5α(H), 14α(H), 17α(H) sterane(20S)
29	C_{29} 5α(H), 14β(H), 17β(H) sterane(20R)
30	C_{29} 5α(H), 14β(H), 17β(H) sterane(20S)
31	C_{29} 5α(H), 14α(H), 17α(H) sterane(20R)
	αββ Steranes (m/z = 218)
32	C_{27} 5α(H), 14β(H), 17β(H) sterane (20R)
33	C_{27} 5α(H), 14β(H), 17β(H) sterane (20S)
34	C_{28} 5α(H), 14β(H), 17β(H) sterane (20R)
35	C_{28} 5α(H), 14β(H), 17β(H) sterane (20S)
36	C_{29} 5α(H), 14β(H), 17β(H) sterane (20R)
37	C_{29} 5α(H), 14β(H), 17β(H) sterane (20S)
	n-alkanes and isoprenoids
38	*n*-C_{17}
39	Pr = pristane
40	Ph =phytane
41	*n*-C_{18}

Table 4.4. Biomarker compounds used in the principal components analysis.

negative values. The tricyclic terpanes, hopanes and steranes generally have moderate to high PC2 positive loadings, while C_{17} and C_{18} *n*-alkanes, pristane and phytane have negative PC2 loadings. It could be considered that the source facies has a strong influence on PC1, whilst thermal maturation seems to have an impact on PC2; therefore the distribution of the biomarker concentrations in the Silurian and Devonian rock samples are influenced primarily by source facies and to a lesser extent by maturity.

The third principal component accounts for only 7.92% of the total variance of the data set. Moderately high positive loadings are obtained for ααα steranes and moderately high negative loadings for αββ steranes, suggesting that PC3 may also reflect maturity.

The Silurian source rock samples of Group A are dominated by an abundance of tricyclics from C_{20} to C_{26}, and higher abundance of regular steranes than 17α(H)-hopanes, indicating better preservation of steroidal compounds and tricyclics in a less oxic depositional environment (Moldowan *et al.*, 1985; Connan *et al.*, 1986).

The biomarker distributions of Group B probably differ mainly because of a different lithology and depositional conditions (Chapter 3.0). The differences in the biomarker distribution of Group C probably reflect a more oxic depositional environment leading to poor organic matter preservation.

4.2.3 Maturity

Steranes and Triterpanes

Biomarkers and aromatic compounds have been used extensively to determine the maturity of source rock samples and oils. However, most of the ratios calculated from biomarkers and aromatic compounds are sometimes influenced by organic matter facies and depositional environment. The evaluation of thermal maturity of Silurian and Devonian source rock samples in this study was achieved using the

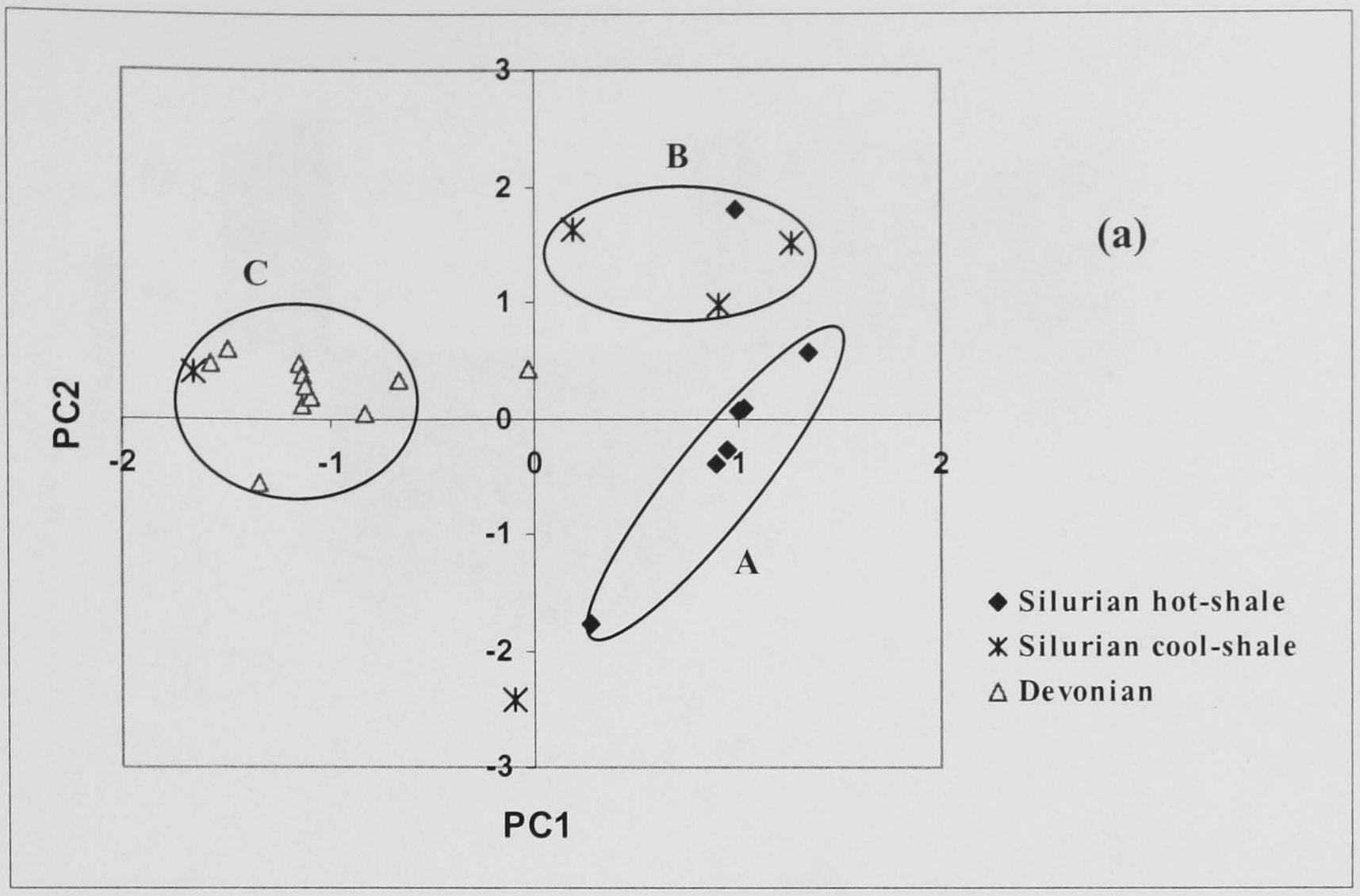

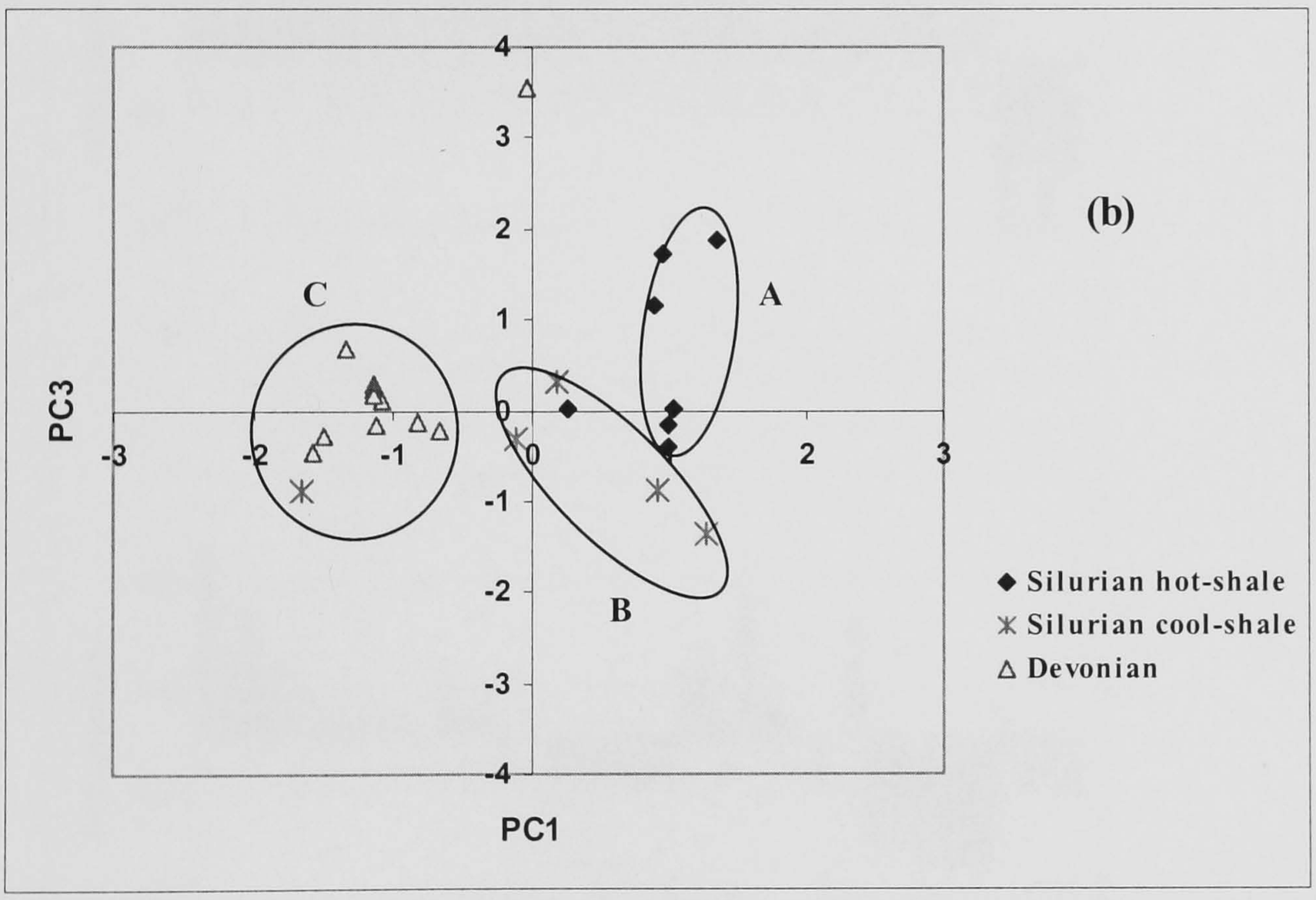

Figure 4.9. Score cross plots of: (a) PC1 versus PC2, and (b) PC1 versus PC3 showing the relationships between Silurian and Devonian source rock samples in terms of the first, second and third principal components; PC1 explains 55.95% of the total variance in the scaled data set, PC2 explains a further 20.85%, and PC3 explains just 7.92%.

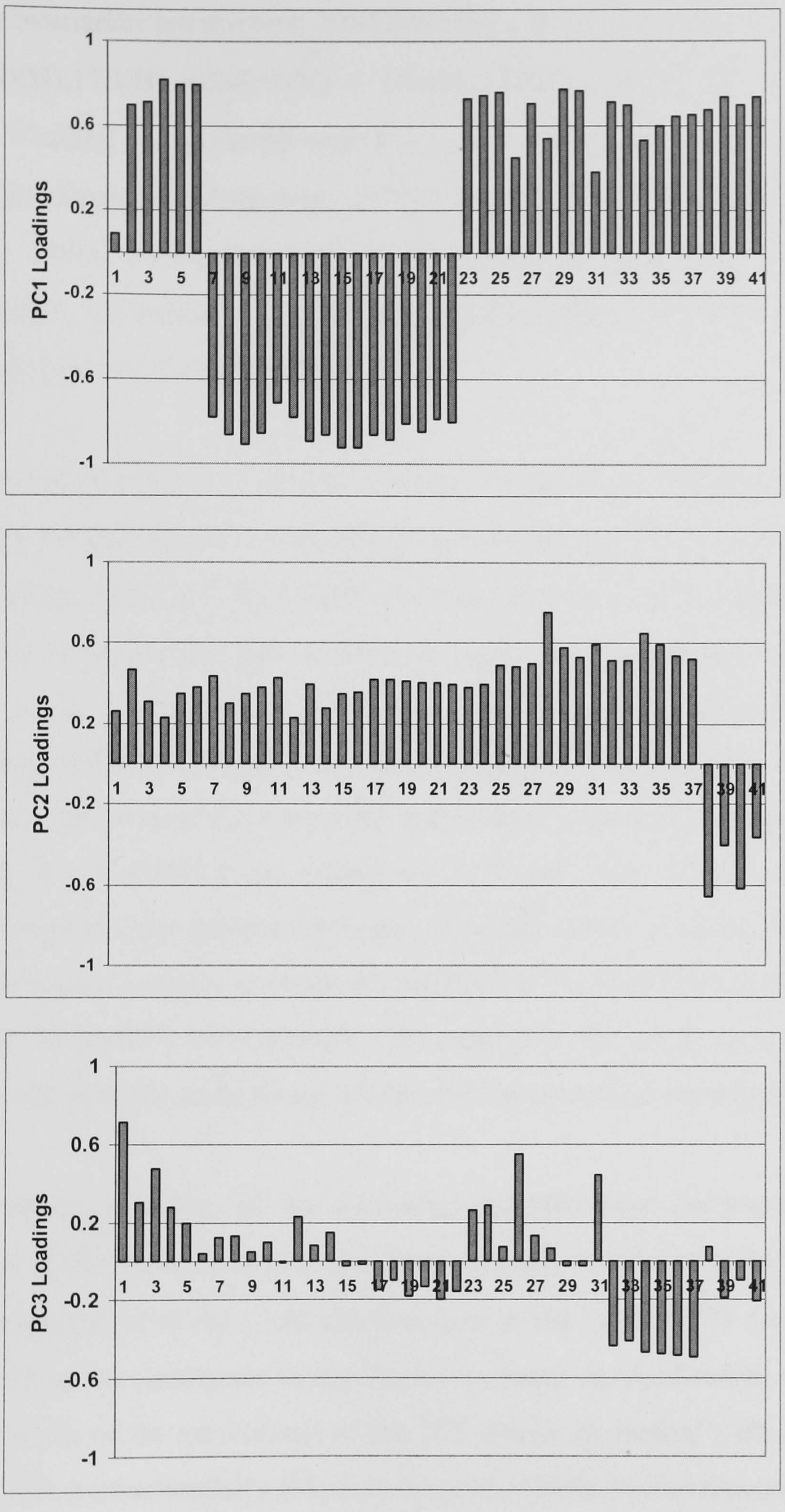

Figure 4.10. Loadings plots showing the contributions of the different biomarkers to the first three principal components.

following biomarker parameters: 20S/(20S+20R)-5α(H),14α(H),17α(H)-C_{29} steranes; 5α(H),14β(H),17β(H) (20S+20R) / [5α(H),14β(H),17β(H) (20S+20R) + 5α(H), 14α(H), 17α(H)] [αββ)/(αββ+ααα)]-C_{29} steranes (Mackenzie *et al.*, 1980); Ts/(Ts+Tm) (Seifert & Moldowan, 1978); C_{29}Ts/(C_{29}Ts+C_{29} αβ hopanes) (Hughes *et al.*, 1985; Sofer, 1988; Cornford *et al.*, 1988; Riediger *et al.*, 1990), and C_{30} diahopane/(C_{30} diahopane + C_{30} αβ hopane) (Conford *et al.*, 1991). The values of these parameters are given in Table 4.3.

The maturity-sensitive sterane stereoisomer ratios of the Devonian and Silurian source rock samples based on percentages of C_{29} 5α(H), 14α(H), 17α(H) 20S steranes and C_{29} 5α(H), 14β(H), 17β(H) (20S+20R) steranes (Fig. 4.11) suggest that not all of the samples have reached their end-point values. The ratios range from 0.22 to 0.63 and 0.25 to 0.63, respectively. Within the Devonian rock samples at well A1-66 (4300') and well F1-66 (3154') the ratios range from 0.22 to 0.34 and 0.25 to 0.34 respectively, and within the Lower Silurian Upper Tanezzuft Formation 'cool shale' from well A1-70 (9049') the values are 0.39 and 0.38. Mackenzie *et al.* (1990) indicate that petroleum generation begins at %20S values of about 40%, so based on this the Devonian samples in wells A1-66(4300'), F1-66 (3154') and Silurian sample at well A1-70 (9049') are immature with respect to the oil window. The rest of the Devonian and Silurian samples are mature and have reached their end-point values.

Interestingly, many of the Devonian samples have proportions of the 20S (relative to 20R) isomers of the C_{29} ααα steranes values of more than 55% (Fig. 4.11). Isomerization at the C-20 chiral centre in the C_{29} 5α (H) 14α (H), 17α (H)-steranes causes the parameter to rise from 0 to reach an equilibrium end-point of 50-55% as a result of the enrichment of the 20S isomer compared with the biologically-inherited 20R stereochemistry (Mackenzie *et al.*, 1980). Partial sterane biodegradation of an oil can result in an increase in ααα 20S/(20S + 20R) sterane ratios to above 55%, presumably by selective removal of the ααα 20R by bacteria (Rullkötter & Wendisch, 1982; McKirdy *et al.*, 1983; Seifert *et al.*, 1984). The unusually high values of the C_{29}ααα 20S/(20S + 20R) sterane ratio in many Devonian rock samples, could be due to factors other than maturity.

The Ts/(Ts+Tm) biomarker maturity ratios (C_{29}Ts/(C_{29}Ts+C_{29} αβ hopane) and C_{30} diahopane/(C_{30} diahopane + C_{30} αβ hopane)), obtained from the m/z 191 mass chromatograms, are both maturity and facies dependent, so these ratios should be used with caution (Moldowan *et al.*, 1986; Rullkotter & Marzi, 1988). However, thay can be useful in distinguishing maturity levels at higher maturities. Figure 4.12 is a cross plot of C_{29}Ts/(C_{29}Ts+C_{29} αβ hopanes) versus Ts/(Ts+Tm) and C_{30} diahopane/(C_{30} diahopane + C_{30} αβ hopane) and shows only a very broad maturity trend between the samples that is unlike that for the sterane maturity parameters, suggesting that these ratios cannot be used to assess the maturity of these samples.

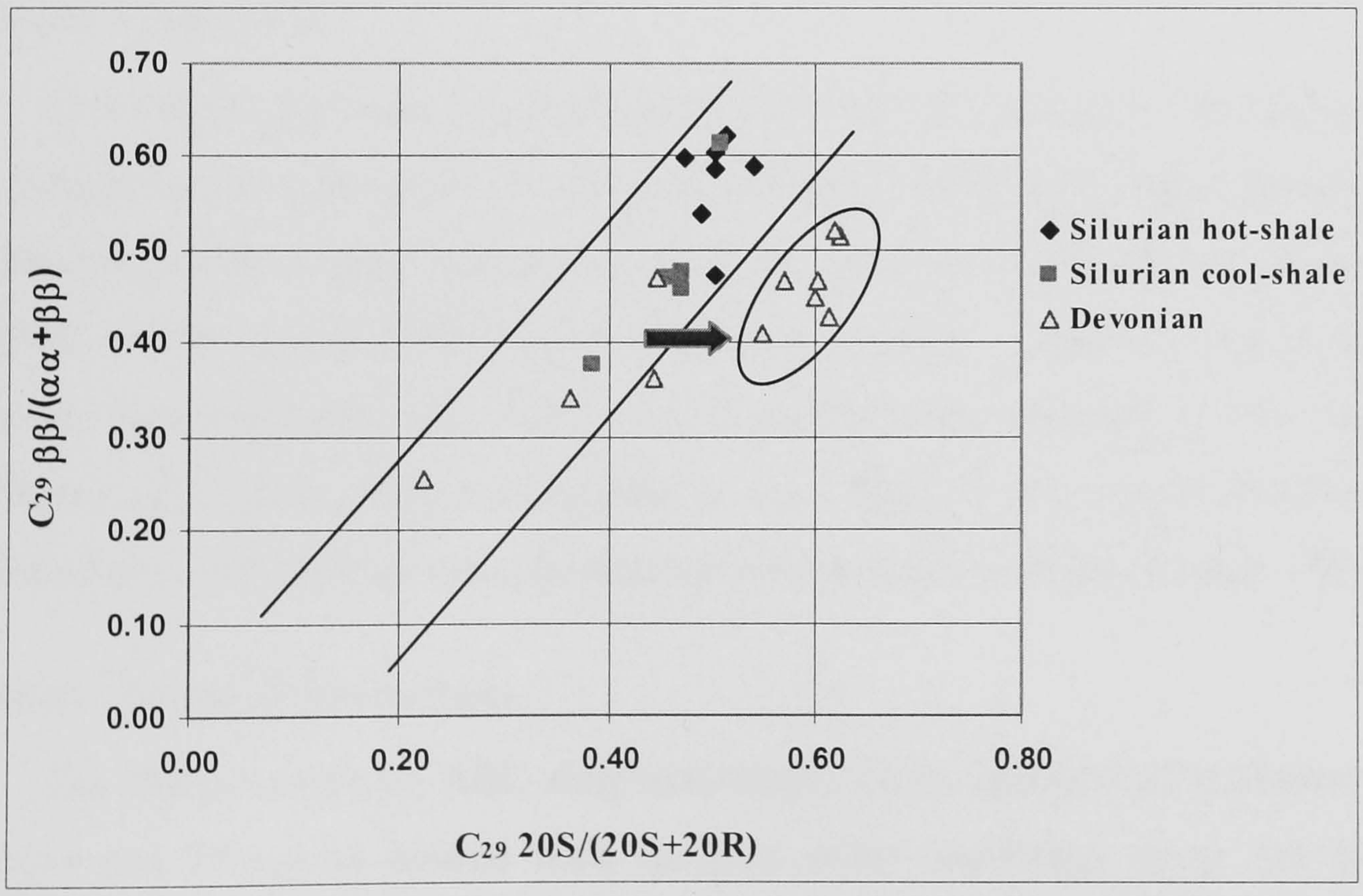

Figure 4.11. Cross plot of the thermal maturity parameter 20S/(20S+20R) versus αββ/(ααα+αββ)-C_{29} steranes for Devonian and Silurian source rock samples (based on the percentages of C_{29} 5α(H), 14α(H), 17α(H) 20S steranes and C29 5α(H), 14β(H), 17β(H) (20S+20R) steranes).

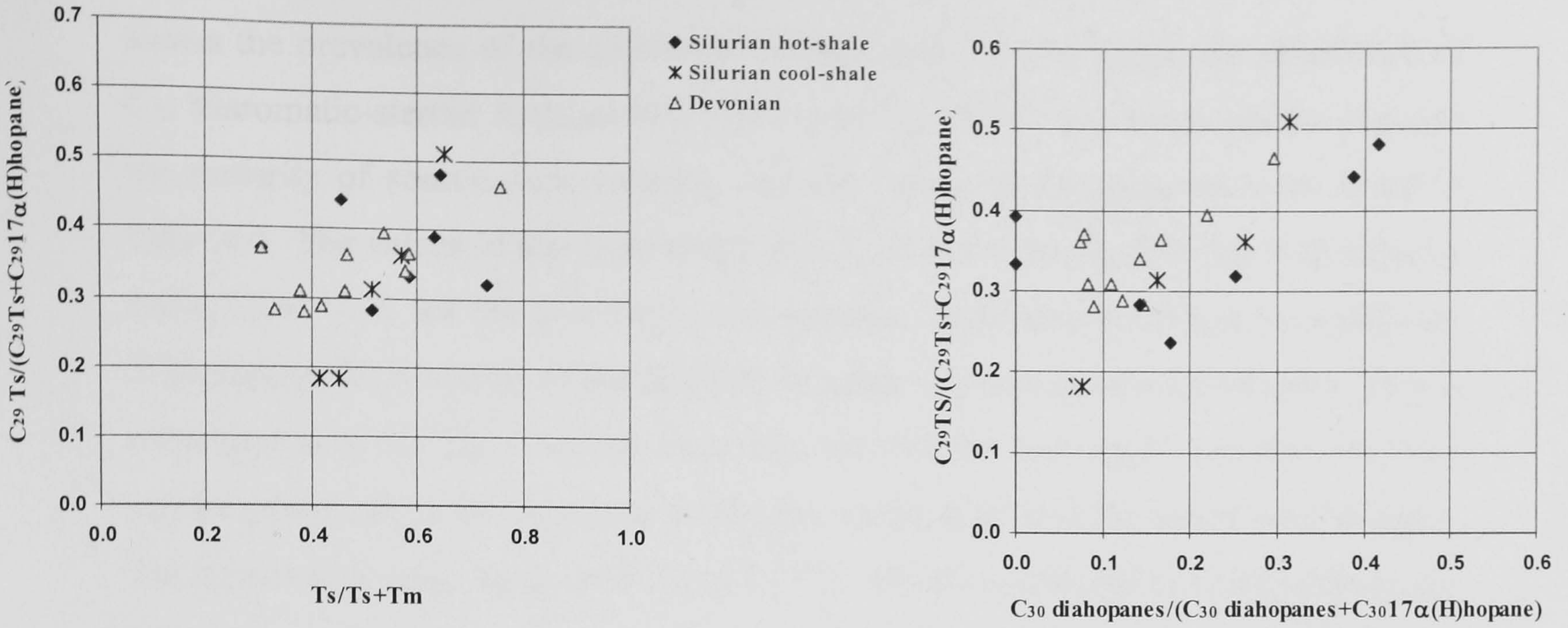

Figure 4.12. Cross plots of the maturity parameters (a) C_{29}Ts/(C_{29}Ts+C_{29}17α(H) hopane) versus Ts/(Ts+Tm), and (b) C_{30} diahopane/(C_{30} diahopane+C_{30}17α(H)-hopane) versus C_{29}Ts/(C_{29}Ts+C_{29}17α(H) hopane) for the Silurian and Devonian source rocks in the Ghadames Basin.

Aromatic Compounds

This section presents the application of a suite of maturity ratios derived from the distribution of triaromatic steroid hydrocarbons and phenanthrenes isolated from the Silurian and Devonian source rock samples. They have been used in an attempt to illustrate further the different levels of thermal maturity. Generally, ratios obtained from the phenanthrenes rely either on an increase with maturity in the degree of alkylation of a given parent compound or on a shift in the isomer distribution of alkylaromatic homologues towards thermally more stable isomers (Radke, 1987).

Aromatic Steroid Hydrocarbons

The distributions of ABC-ring triaromatic (TA) steroid hydrocarbons in the Silurian and Devonian source rock samples were monitored using the m/z 231 fragment ion. Typical mass chromatograms of the distributions of TA-steroid hydrocarbons in the Silurian and Devonian source rock samples are shown in Figure 5.13, and reveal a predominance of the short-chain (C_{20}-C_{21}) compared to long-chain (C_{26}-C_{28}) components. The long-chain C_{26}-C_{28} triaromatic-steroid hydrocarbon homologues are barely present in the Silurian 'hot shale' at well F1-66 (7054'), which

shows the prevalence of the short-chain components. In this work, the abundance of C_{20} triaromatic-steroid hydrocarbon relative to C_{28} (S+R) was employed to evaluate the maturity of source rock samples, and the values of this parameter are listed in Table 4.5. The values of this ratio range from 0.22 to 1.0 for the Silurian rock samples and 0.19 to 0.76 for the Devonian rock samples, indicating that there is significant difference in the maturity of the different Silurian and Devonian rock samples. This is consistent with the Tmax values. Generally the Silurian 'hot shale' samples are more mature compared to the less mature Silurian 'cool shale' and Devonian rock samples. The Silurian samples from wells F1-66 (7053', 7054') and B1-49 (2135m) display the highest maturity values; these wells are located in the southern part of the Ghadames Basin.

Alkylphenanthrenes

The alkylphenanthrene isomers which are substituted at the β-position (Fig. 5.14) have been observed to become increasingly dominant at higher maturity levels compared to related isomers with α-substitution (Radke, 1987). Maturity parameters based on alkylphenanthrenes used in this study and their values are listed in Table 5.5.

The maturity values based on phenathrenes (MPI-1) and the calculated reflectance (VRc%) estimates using the formula proposed by Radke *et al.* (1986) are shown in Table 4.5, indicating that the Silurian rock samples are more mature than the Devonian rock samples. The correlation between microscopy maturity parameters and the (MPI-1 & VRc%) ratios is discussed further in Chapter 5 .

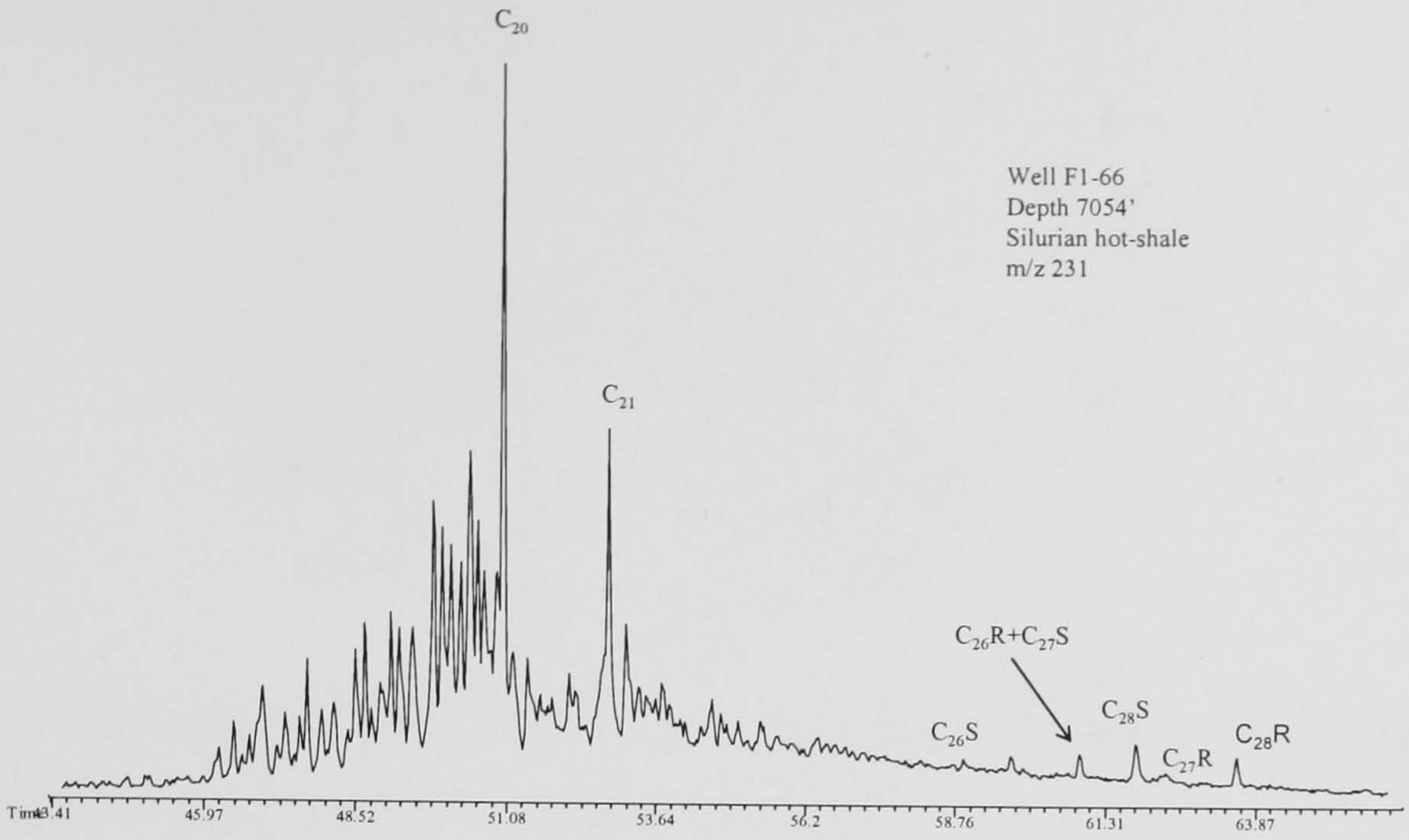

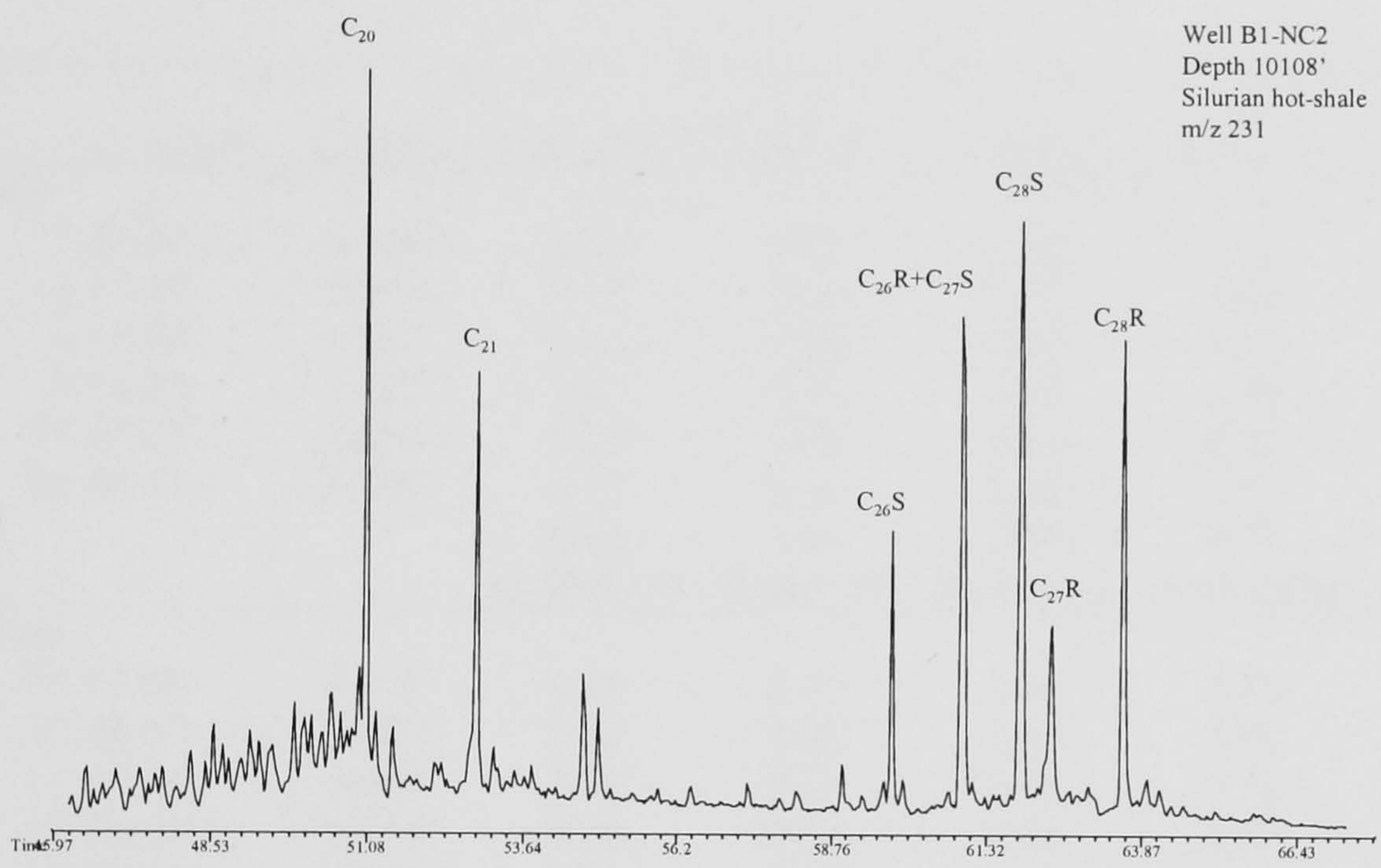

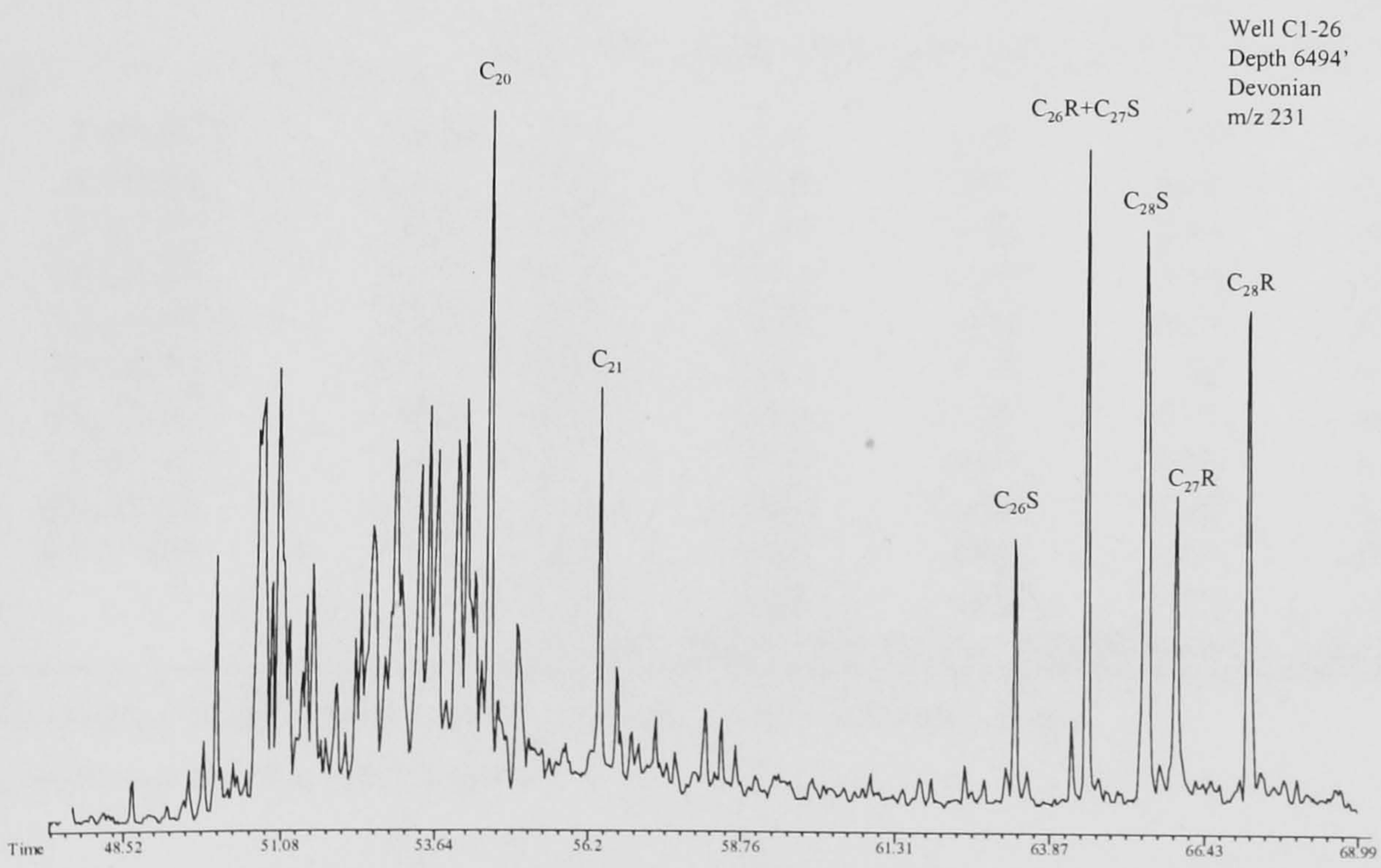

Figure 4.13. Partial m/z 231 mass chromatograms showing the distribution of ABC-ring triaromatic steroid hydrocarbons in a selected Silurian and Devonian samples.

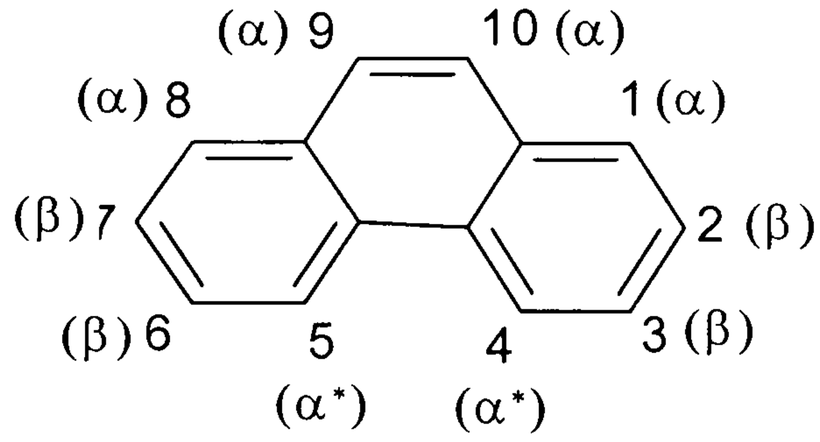

Figure 4.14. Molecular structure and carbon numbering system of phenanthrene. Sterically crowded positions are indicated by asterisks.

Sample	Location	Depth	Triaromatic	MPI-1	MPR	Rc	Tmax °C
Silurian hot-shale							
1	B1-NC2	10108'	0.40	0.60	0.80	0.76	447
2	A1-70	10005'	0.57	0.56	0.76	0.74	443
4	F1-66	7054'	0.91	0.68	0.85	0.81	452
5	F1-66	7053'	0.86	0.71	0.90	0.82	445
21	A1-66	5054'	0.30	0.76	0.92	0.85	435
22	A1-70	10155'	0.70	0.34	0.85	0.61	441
Average			0.61	0.61	0.85	0.71	444
Range			(0.30-0.91)	(0.34-0.76)	(0.76-0.92)	(0.61-0.85)	(435-447)
Silurian cool-shale							
11	F1-66	6473'	0.22	0.70	0.92	0.83	434
15	A1-90	11921'	0.56	0.90	3.81	0.94	364
17	A1-70	9049'	0.32	0.59	0.98	0.75	437
18	Z5-NC5	10124'	0.39	0.70	0.88	0.82	444
19	B1-49	2135(m)	1.00	0.88	0.89	0.93	428
Average			0.46	0.76	1.50	0.83	241
Range			(0.22-1.00)	(0.59-0.90)	(0.88-3.81)	(0.75-0.94)	(364-444)
Devonian shale							
7	A9-NC7	5718	0.76	0.62	0.97	0.79	441
8	C1-26	6488	0.46	0.60	0.92	0.76	440
9	C1-26	6494	0.39	0.60	1.10	0.76	440
10	C1-26	6500	0.40	0.60	0.93	0.76	440
12	M2-NC2	6227	0.33	0.65	0.89	0.79	433
13	M2-NC2	6251	0.47	0.58	1.00	0.75	435
14	A1-90	7569	0.62	0.62	1.12	0.77	442
16	B1-49	1434	0.47	0.63	0.96	0.78	442
20	A1-66	3153	0.19	0.60	0.96	0.76	430
23	F1-66	4300	0.36	0.26	0.96	0.56	422
Average			0.38	0.58	1.00	0.75	437
Range			(0.19-0.76)	(0.26-0.65)	(0.89-1.12)	(0.56-0.79)	(422-442)

MPI-1 = 1.5*(3-MP+2-MP)/(P+9-MP+1-MP) MPR = 2-MP/1-MP %RC = 0.4 +(MPI-1)*0.6

Triaromatic = (C_{20} traromatic)/ (C_{20} +C_{28} S+R) triaromatic

Table 4.5. Aromatic biomarker maturity parameter for Silurian and Devonian rock samples.

4.3 Molecular Composition of the Oils

This section reports the results from seven oil samples that have been analysed by molecular geochemistry. These oil samples collected were from different oil fields distributed throughout the Ghadames Basin: two oil samples from Al-Wafa oil field (NC169) located in the south western part of the basin, three oil samples collected from Al-Hamada field complex located in the south (NC8, NC5) and toward the north two oil samples were also collected from the NC3 oil field (Fig. 2.1).

4.3.1 Source Facies Characterisation

n-Alkanes and Isoprenoid Alkanes

Representative gas chromatograms of the saturated hydrocarbon fraction showing the *n*-alkanes and isoprenoid alkanes distribution (*n*-C_{10}+) within typical oil samples are displayed in Figure 4.15, and values for geochemical parameters obtained from the distributions of *n*-alkanes and isoprenoid alkanes, together with the concentrations of the total *n*-alkanes, are listed in Table 4.6. The *n*-alkane distribution is generally dominated by short-chain (*n*-C_{11} to *n*-C_{18}) over long-chain *n*-alkanes; the *n*-C_{17}/ *n*-C_{27} ratio ranges from 4.00 to 7.45 and the Pr/Ph ratio ranges from 1.2 to 1.4 suggesting that these oils were probably generated from the same or similar source rock.

Steranes and Terpanes

The partial m/z 191 and 217 mass chromatograms of a typical oil sample showing the distributions of triterpanes (tricyclics and hopanes) and steranes are displayed in Figure 4.16. The values of biomarker-based parameters are listed in Table 4.7.

The oil samples can be separated into three groups according to the triterpane and sterane distributions (Fig. 4.17). Group I contains two oil samples collected from the Al-Wafa oil field (A4 & A6- NC169). The oils in this group contain high (C_{20}-C_{26} extended tricyclics)/(C_{20}-C_{26} tricyclics+ C_{29}-C_{30}17α(H) hopanes) and C_{29} (ααα+αββ) S+R regular sterane)/(C_{29} (ααα+αββ) S+R regular steranes + C_{29}-C_{30} 17α(H)-hopanes) ratios. Group II contains three oil samples from Al-Hamada field complex (V6, LL4- NC8 & Z5-NC5) with lower ratios of the tricyclic v. hopane parameter.

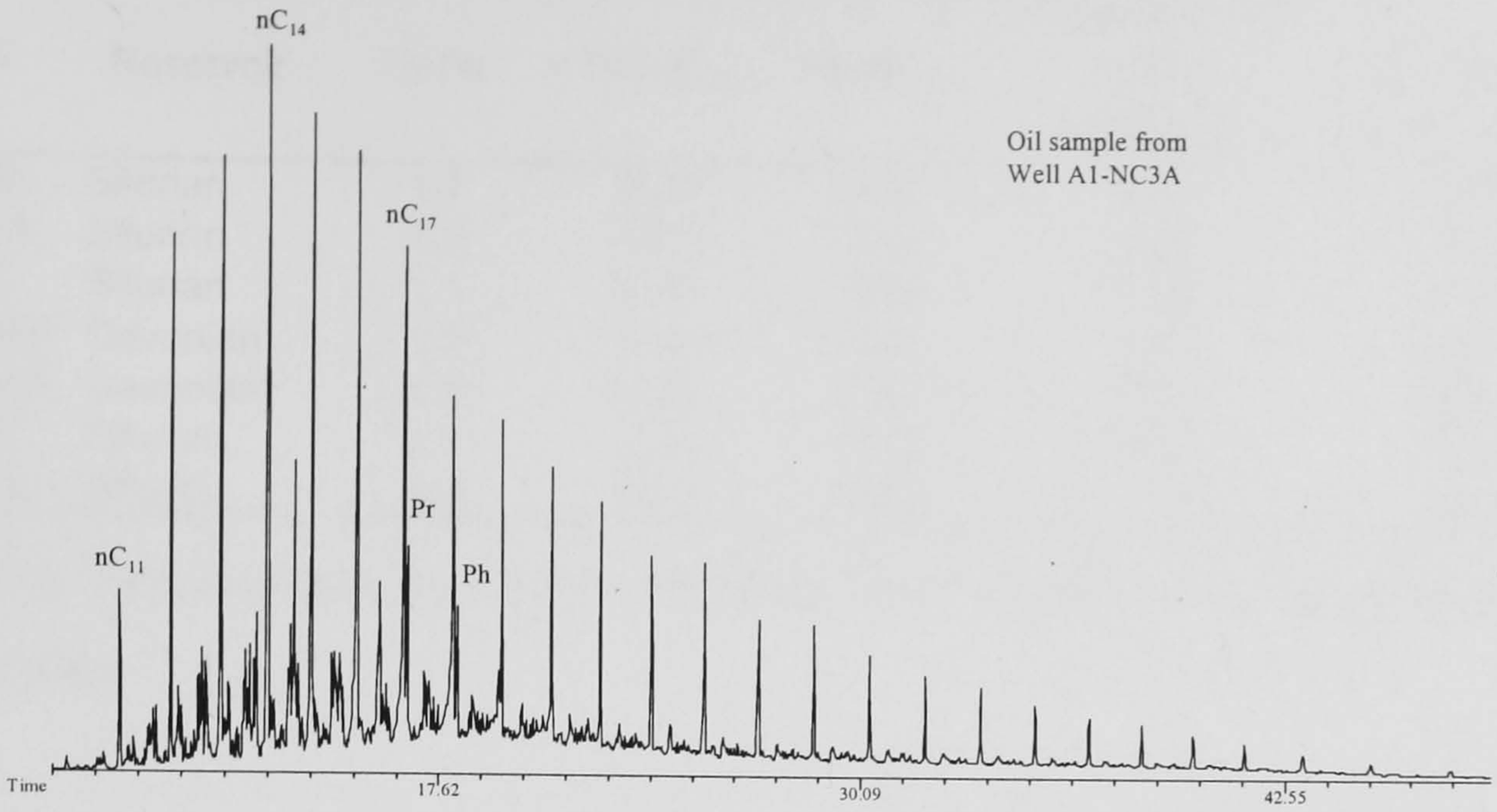

Oil sample from
Well A1-NC3A

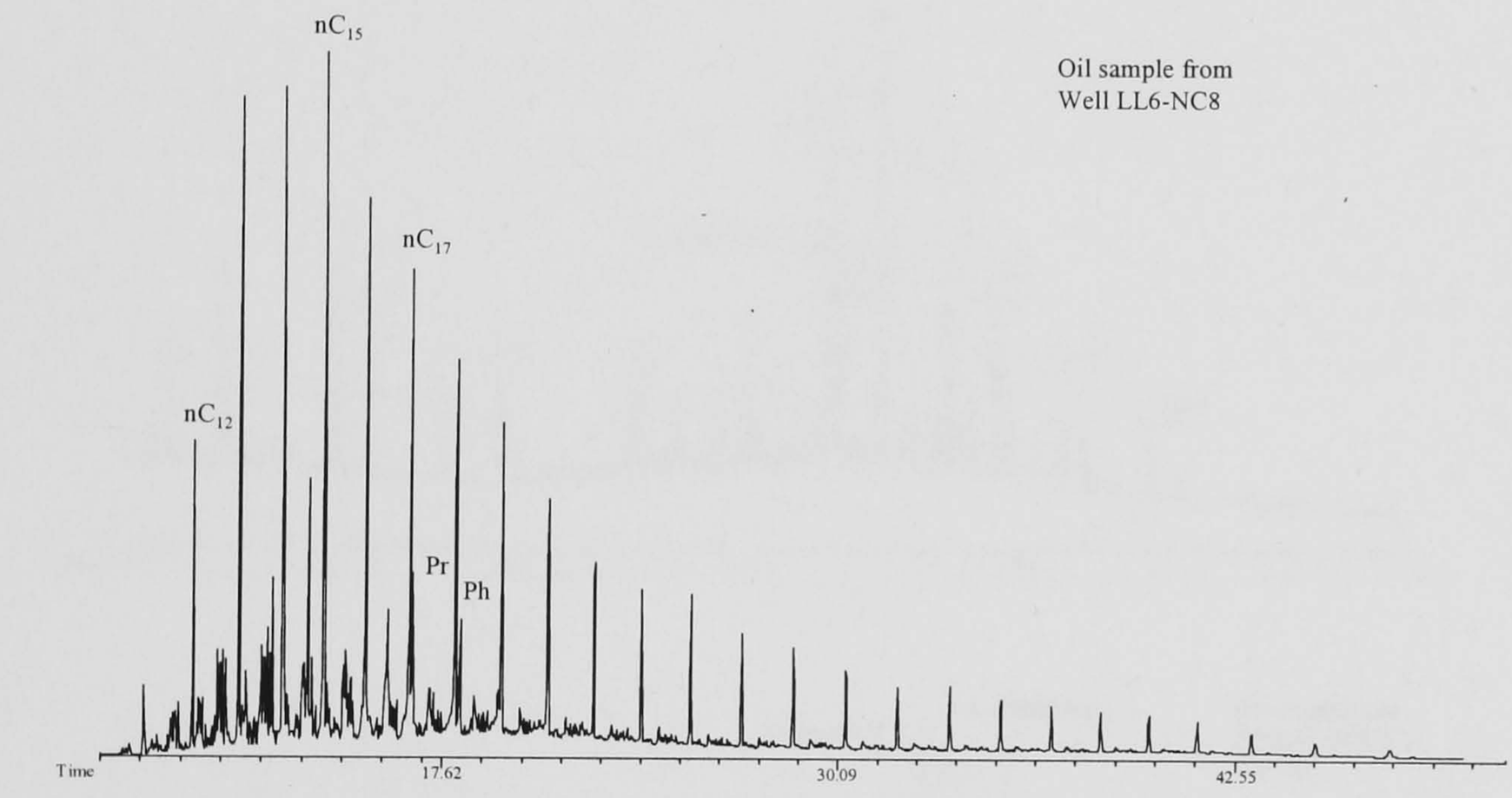

Oil sample from
Well LL6-NC8

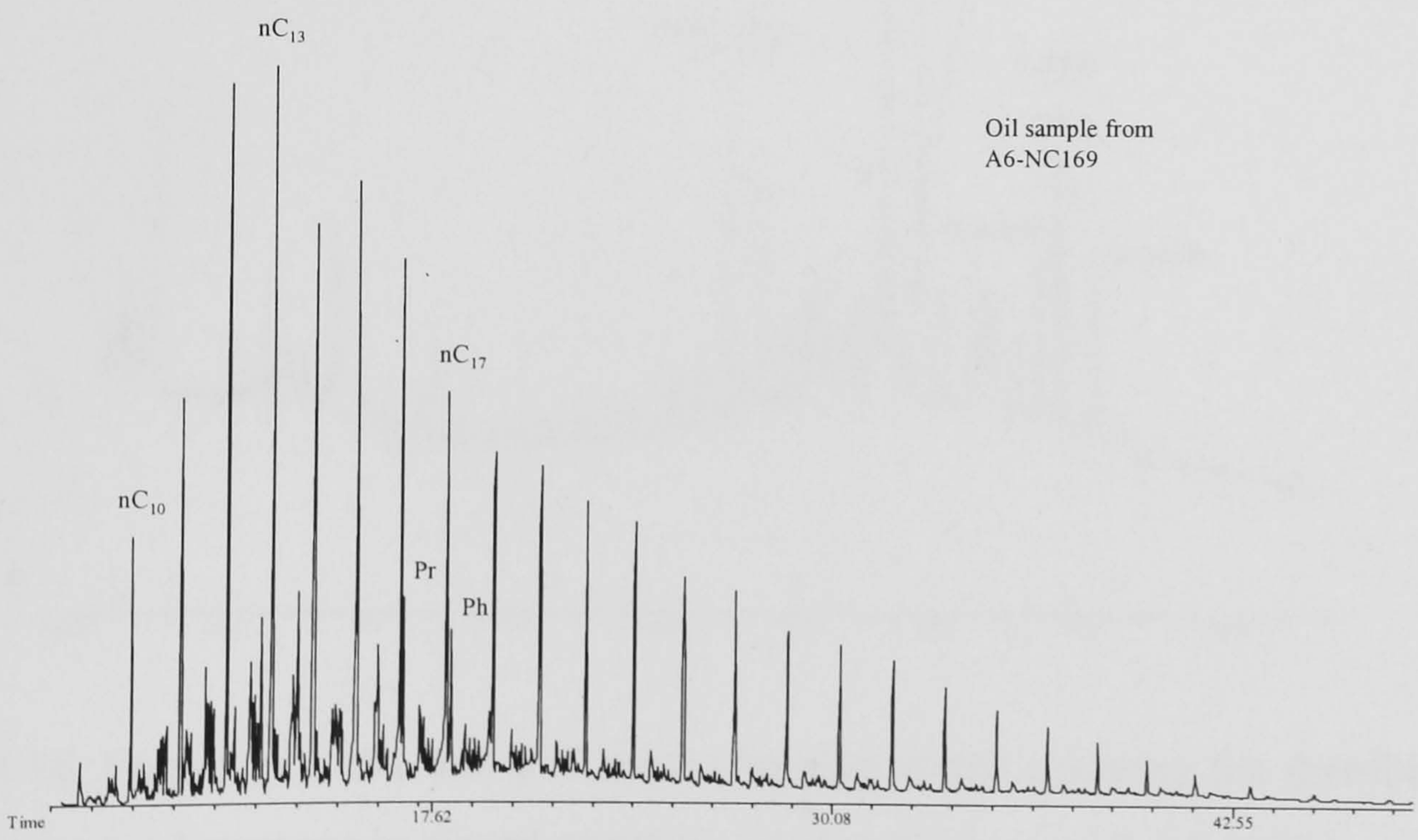

Oil sample from
A6-NC169

Figure 4.15. Gas chromatograms showing *n*-alkane and acyclic isoprenoid alkane distributions of selected oil samples.

Well	Reservoir	Pr/Ph	Pr/n-C_{17}	Ph/n-C_{18}	n-alkane index index n-C_{17}/n-C_{27}	Sum n-alkanes (μg/g extract)
A1-NC3A	Silurian	1.4	0.39	0.39	5.72	62622
A1-NC3A	Silurian	1.3	0.71	0.54	4.02	34055
Z5-NC5	Silurian	1.4	0.45	0.49	6.32	31957
A6-NC169	Devonian	1.2	0.35	0.38	4.03	42274
A4-NC169	Devonian	1.3	0.31	0.42	4.54	52945
V6-NC8	Silurian	1.2	0.44	0.43	5.85	33936
LL4-NC8	Silurian	1.4	0.35	0.32	7.45	54243

Table 4.6. Geochemical parameters obtained from *n*-alkane and isoprenoid alkane distributions.

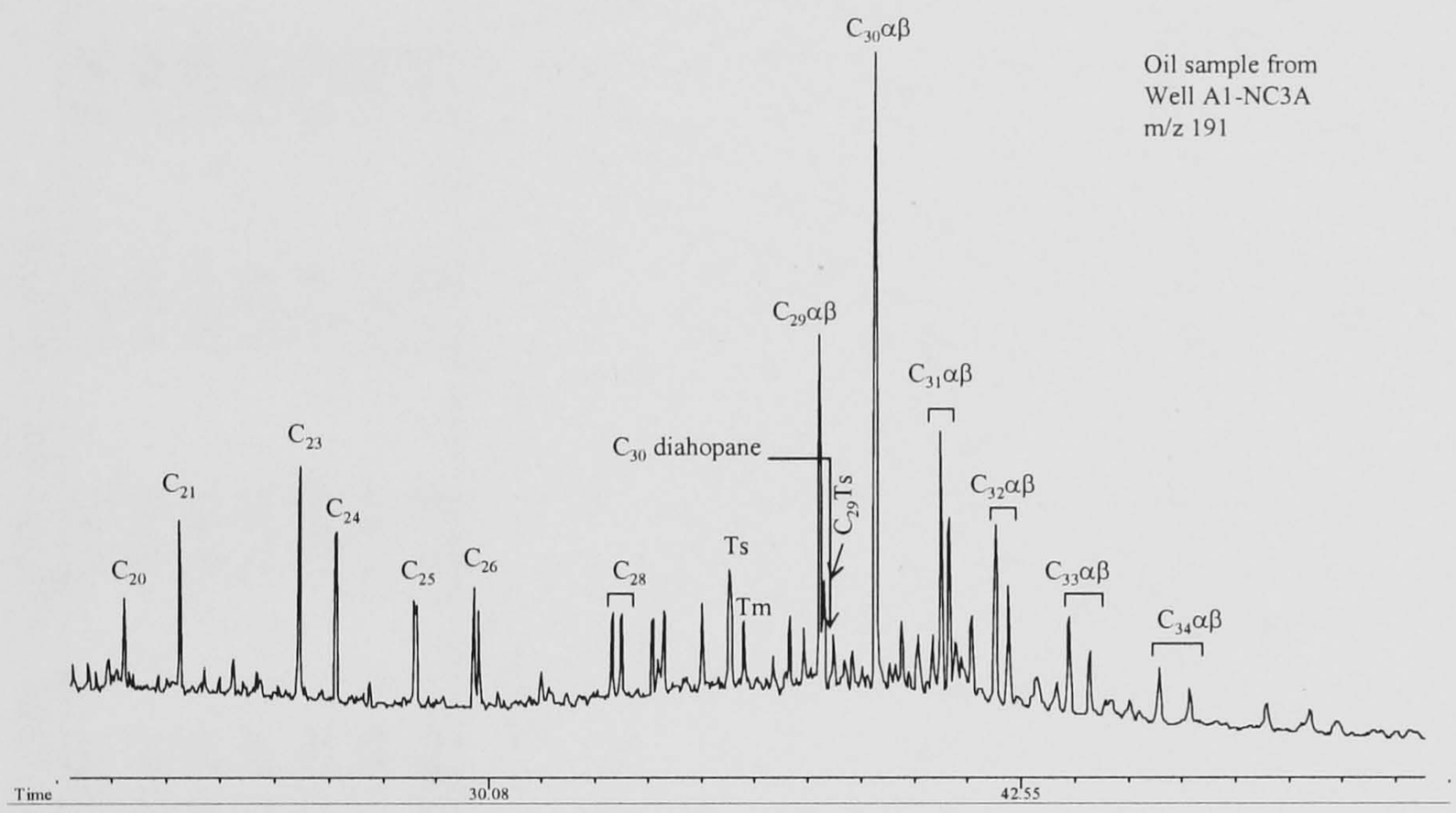

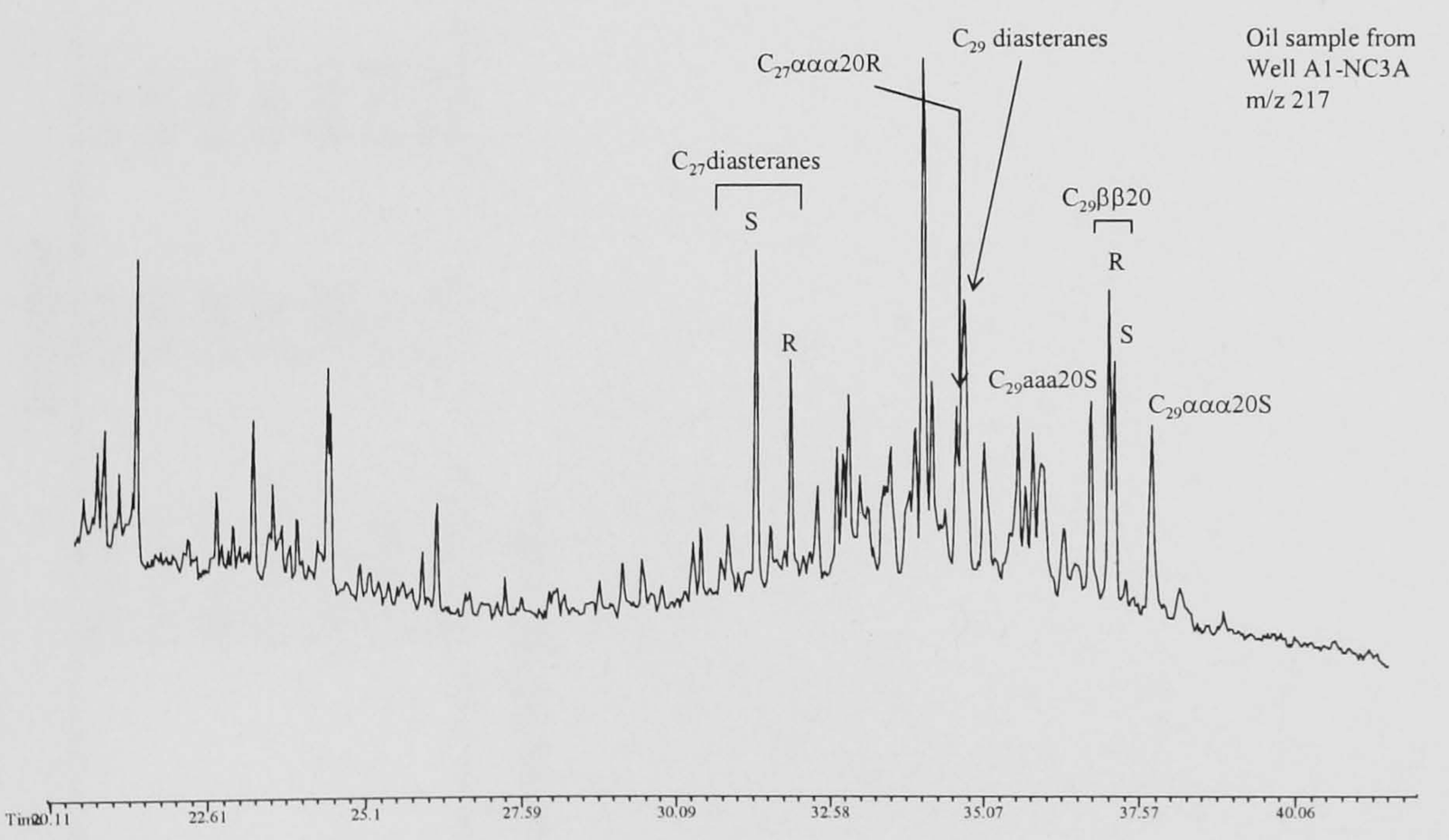

Figure 4.16. Partial m/z 191 and 217 mass chromatograms showing the distributions of triterpanes and steranes in a representative oil sample from well A1-NC3A.

Well	Depth	Reservior	Age	20S/ 20S+20R	ββ/αα+ββ	C_{29}Ts/(C_{29}Ts+C_{29}hop	C_{30}diahop/ (C_{30}hop+ C_{30}diahop)	C_{29}hop /C_{30} hop	Ts/Ts+Tm	C_{20}-C_{26}Tr/ C_{29}+C_{30} hop.	C_{29}ster./ C_{29}+C_{30}hop
A1-NC3A			Silurian	0.51	0.59	0.27	0.19	0.40	0.46	0.43	0.29
A1-NC3A			Silurian	0.49	0.61	0.24	0.08	0.36	0.43	0.35	0.32
Z5-NC5			Silurian	0.52	0.63	0.33	0.15	0.32	0.60	0.50	0.41
A6-NC169			Devonian	0.52	0.60	0.47	0.39	0.36	0.57	0.66	0.38
A4-NC169			Devonian	0.53	0.60	0.52	0.48	0.36	0.55	0.70	0.43
V6-NC8			Silurian	0.52	0.56	0.35	0.14	0.31	0.65	0.41	0.38
LL6-NC8			Silurian	0.53	0.61	0.44	0.21	0.30	0.70	0.49	0.38

Table 4.7. Biomarker ratios of the oils.

Group III contains oil samples collected from NC3 oil field (A1-NC3A). The oils in this group have the lowest (C_{20}-C_{26} extended tricyclics)/(C_{20}-C_{26} tricyclics+ C_{29}-C_{30}17α(H) hopanes) and C_{29} (ααα+αββ) S+R regular steranes/(C_{29} (ααα+αββ) S+R regular steranes + C_{29}-C_{30} 17α(H)-hopanes) ratios.

Oil samples showing higher relative amounts of extended tricyclics terpanes and regular steranes compared to hopanes are believed to be generated from source rocks deposited under anoxic conditions where organic matter from planktonic eukaryotic organisms (mainly marine algae) was well preserved and less microbial activity took place due to the absence of oxygen (Moldowan *et al.*, 1985; Connan *et al.*, 1986). By contrast, oil samples showing higher amounts of hopanes versus steranes suggest that the oils were generated from source rocks with greater organic matter input from prokaryotic organisms versus eukaryotic organisms (Tissot & Welte, 1984).

Seifert and Moldowan (1978) showed that the ratio of regular steranes to regular steranes plus 17α(H)-hopanes is affected by maturity, but in a study of oils from Oman this ratio remained relatively constant for a group of related oils of widely different thermal maturity (Peters & Moldowan, 1993). Moreover, Seifert and Moldowan (1978) showed a systematic increase in the tricyclic/17α (H)-hopanes ratio with increasing thermal maturity. The ratio increases because proportionally more tricyclics than hopanes are released from kerogen at higher levels of maturity (Aquino Neto *et al.*, 1983). In the laboratory, Peters *et al.* (1990) showed an increase in the tricyclics/17α (H)-hopanes ratio during hydropyrolysis of Monterey Formation shale. In the present study both ratios show good correlations with maturity suggesting an increase of both regular steranes and tricyclic terpanes compared to the 17α (H)-hopanes (see Section 4.3.2 below).

Sterane carbon number ternary diagrams are widely used to illustrate relationships between oils and/or source rock bitumens (e.g. Peters *et al.*, 1989). The distribution of C_{27}- C_{28}- C_{29}-αββ steranes allows the differentiation of groups of petroleums from different source rocks or different organic facies of the same source rock. From the C_{27}- C_{28}- C_{29}- 5α(H), 14β(H), 17β(H) (20S + 20R) steranes distribution in Figure 5.18, obtained from the m/z 218 mass chromatograms, it is

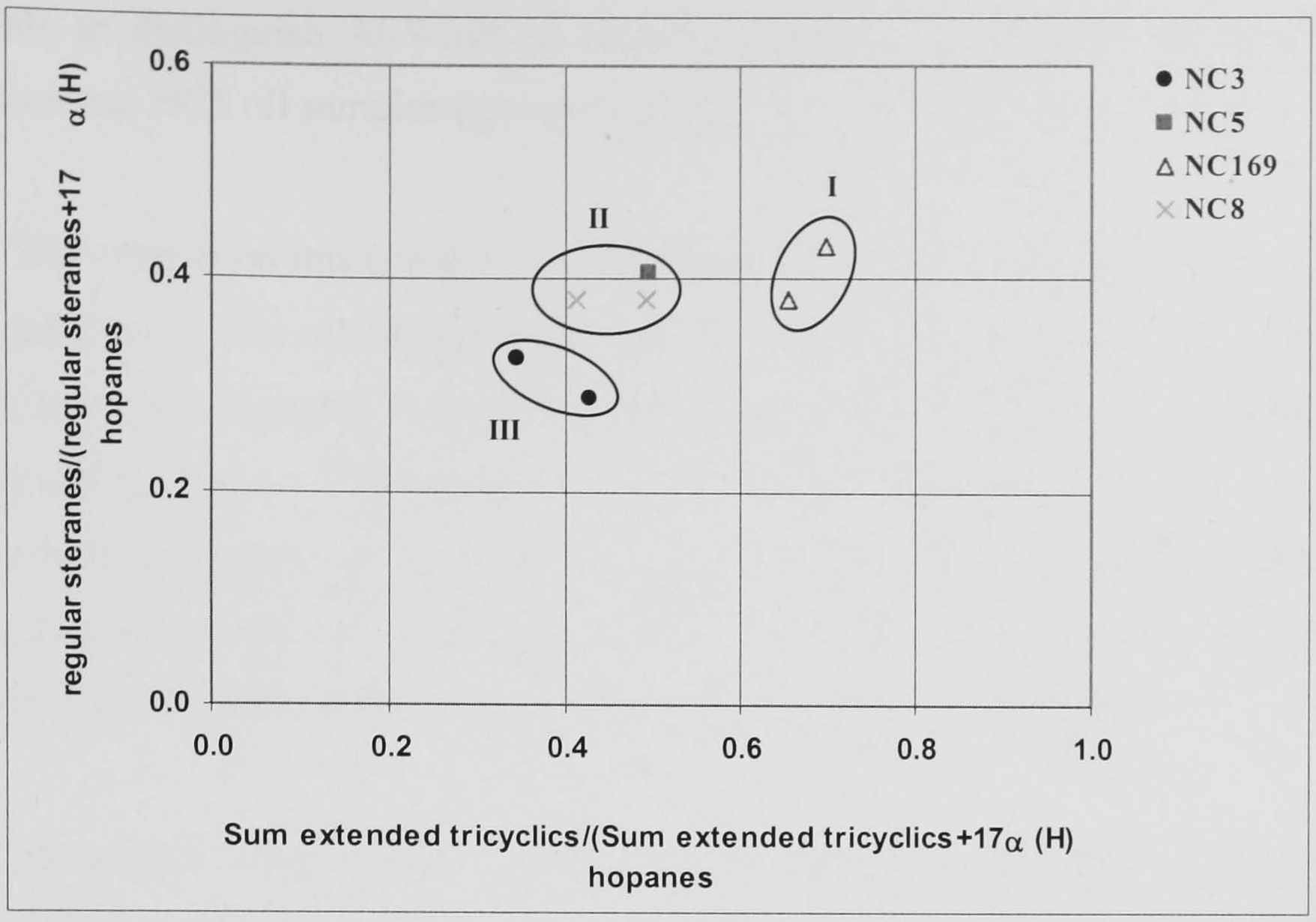

Figure 4.17. Cross plot of the facies parameters of the selected oil samples in the Ghadames Basin.

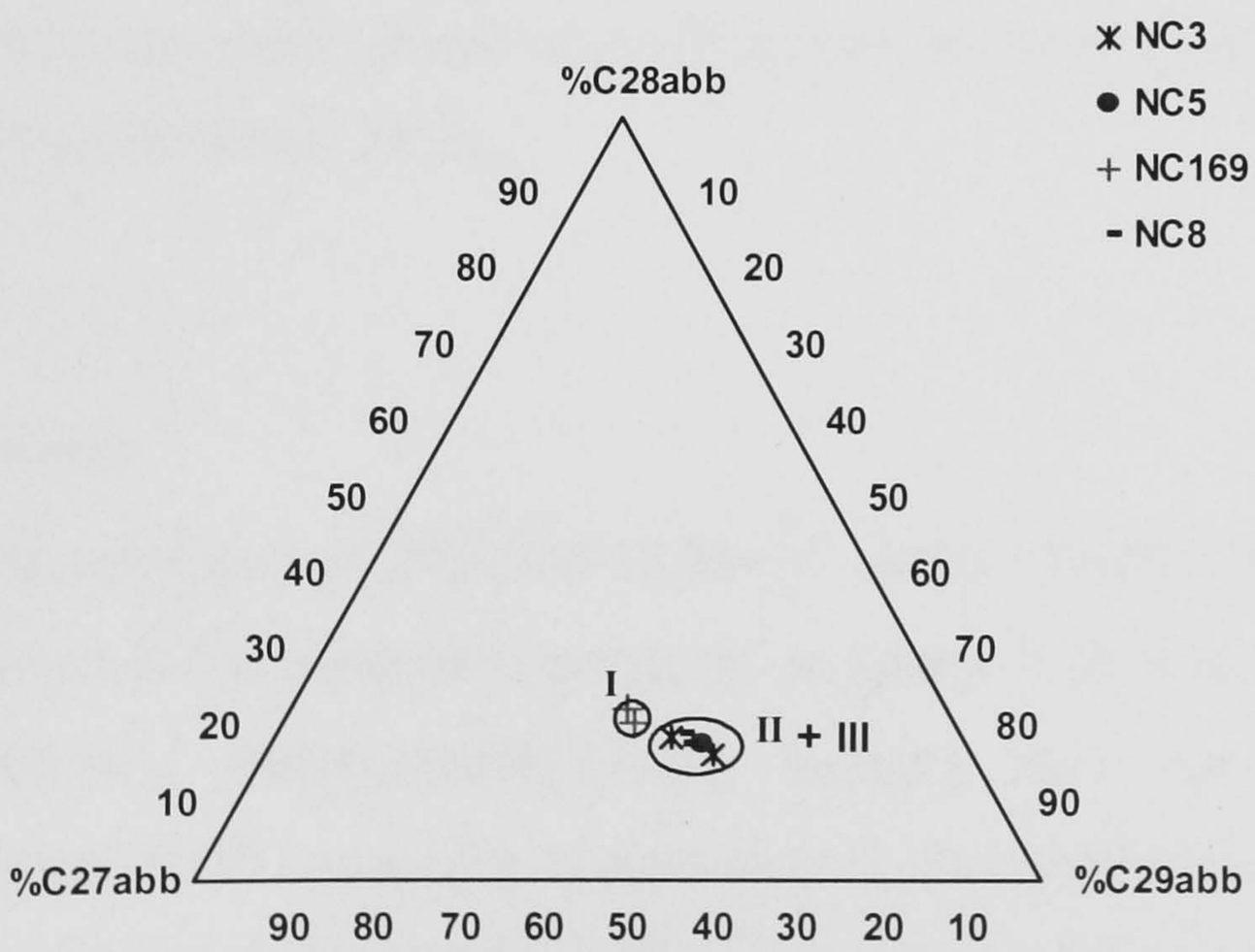

Figure 4.18. Ternary plot of the relative abundance of the C_{27}- C_{28}- C_{29} αββ-steranes for the Ghadames Basin oils.

possible to distinguish Al-Wafa oil samples (Group I) from the Al-Hamada field complex and NC3 oil samples (groups II & III).

The concentrations (μg/g oil) of the biomarkers in the oil samples are displayed in Appendix VI. The oil samples from Groups I and II contain higher concentrations of steranes than hopanes, whereas Group III oils contain higher concentrations of hopanes than steranes. Figures 4.19 and 4.20 reveal that oil samples from NC3 (Group III) contain the highest concentrations of biomarkers (tricyclics terpanes, hopanes and steranes) compared to the oil samples in Groups I and II. Group I, which includes oil samples from NC169, exhibits the lowest concentrations of biomarkers.

In general, high sterane concentrations combined with high $C_{29}\alpha\alpha\alpha+\alpha\beta\beta$ (20S+20R) steranes/($C_{29}\alpha\alpha\alpha+\alpha\beta\beta$ (20S+20R) steranes + C_{29}-C_{30} 17(H)-hopanes) ratio (Figs. 4.17 & 4.18) seem to typify marine organic matter with a major contribution from planktonic and/or benthic algae of the corresponding source rock(s) (Moldowan *et al.*, 1985). Conversely, low sterane concentrations and low $C_{29}\alpha\alpha\alpha+\alpha\beta\beta$ (20S+20R) steranes/($C_{29}\alpha\alpha\alpha+\alpha\beta\beta$ (20S+20R) steranes + C_{29}-C_{30} 17(H)-hopanes) ratios are more indicative of terrigenous and/or microbially reworked organic matter (Tissot & Welte, 1984).

4.3.2 Maturity

Steranes and Terpanes

The maturity cross plot of 20S/(20S+20R)-C_{29} 5α(H),14α(H),17α(H) steranes versus αββ/(αββ+ααα)-C_{29} steranes is presented in Figure 4.21, and indicates that the 20S/(20S+20R)-C_{29} 5α(H),14α(H),17α(H) steranes ratio has reached its maximum value (0.49–0.53) (Appendix 3) equivalent to the equilibrium between 20S and 20R isomers (Seifert & Moldowan, 1986). This ratio is also in agreement with the αββ/(αββ+ααα)-C_{29} steranes. Consequently all the oil samples are mature and cannot be differentiated using these ratios.

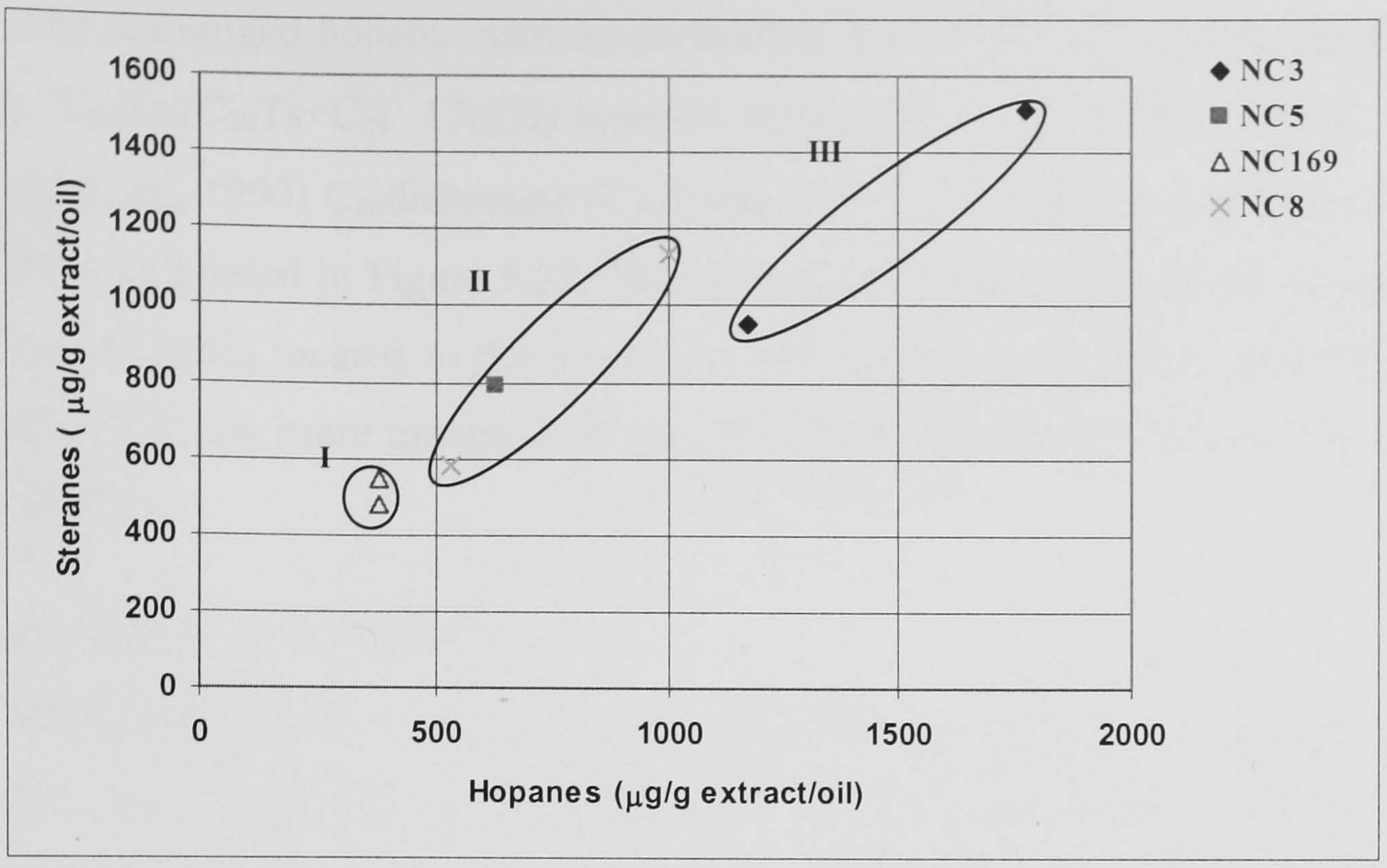

Figure 4.19. Plot of the concentrations of steranes and hopanes for the Ghadames Basin oil samples.

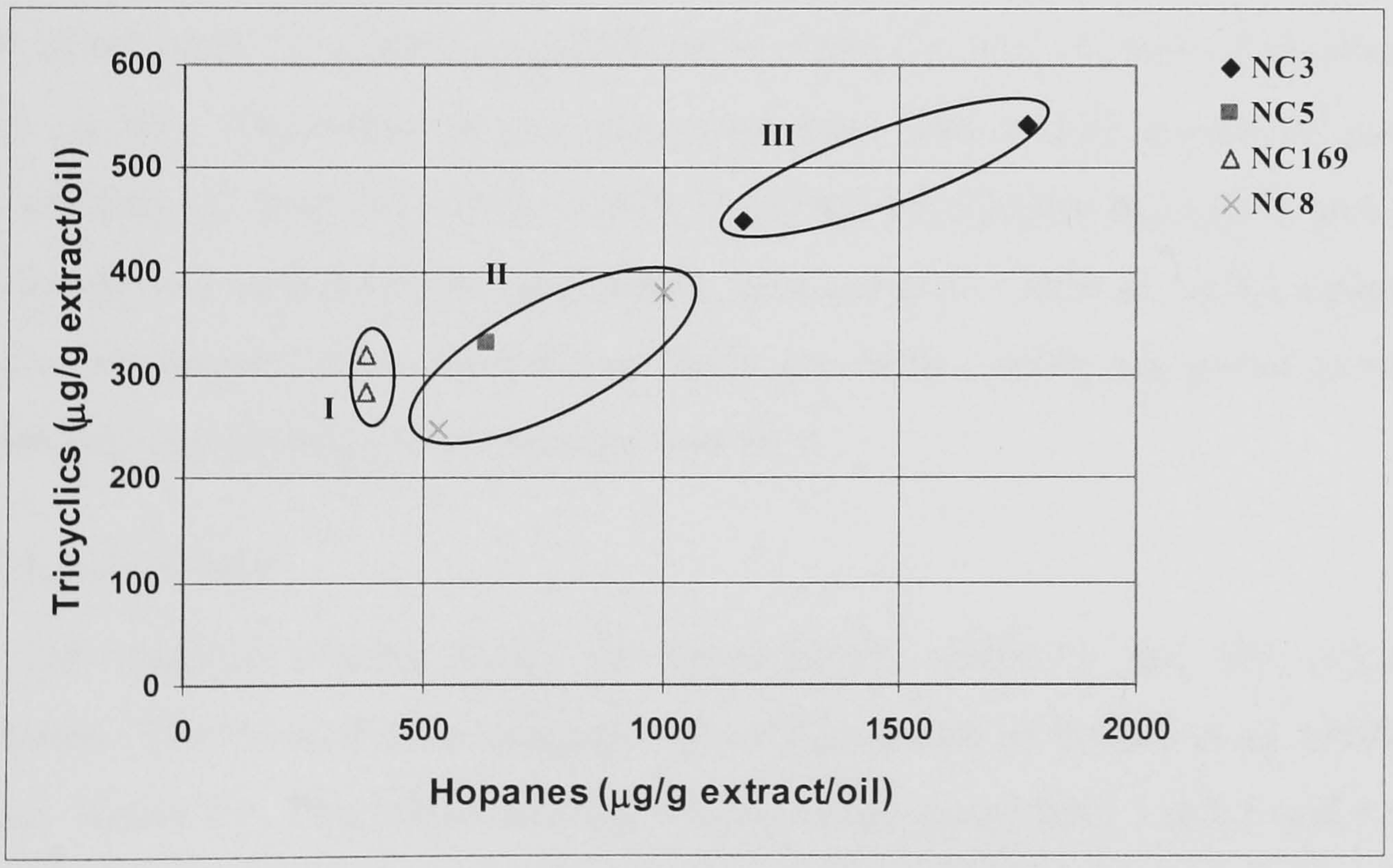

Figure 4.20. Plot of concentrations of tricyclic terpanes and hopanes for the Ghadames Basin oil samples.

The rearranged hopane maturity parameters Ts/(Ts+Tm) (Seifert & Moldowan, 1978), C_{29}Ts/(C_{29}Ts+C_{29} 17α(H)-hopane) (Cornford *et al.*, 1988; Sofer, 1988; Riediger *et al.*, 1990) C_{30}diahopane/(C_{30}diahopane+C_{30}17α(H)-hopanes) (Cornford *et al.*, 1986) are plotted in Figure 5.22. These cross plots indicating that the oil samples from the oil fields located in the South and southwestern part of the basin (NC169, NC8 and NC5) are more mature than the oil samples from the oil field located in the North (NC3).

Aromatic Steroid Hydrocarbons

The distributions of ABC-ring triaromatic (TA) steroid hydrocarbons in the oil samples were monitored using the m/z 231 fragment ion. Typical mass chromatograms of the distributions of TA-steroid hydrocarbons in the oil samples are shown in Figure 4.23. The concentrations of the individual isomers and a maturity parameter calculated from the distributions of the triaromatic steroid hydrocarbons are given in Table 4.8.

In this work, the abundance of C_{20} TA-steroid hydrocarbon relative to the C_{28} 5α(H) (20S+20R) TA-steroid hydrocarbons was employed to evaluate the maturity of the oil samples. The values of this ratio range from 0.88 to 0.90 for the oil samples from Al-Wafa oil field (NC-169), 0.18–0.32 for the oil samples from NC3 and 0.14–0.53) for the oil samples from Al-Hamada field complex (NC8 & NC5), suggesting that the oil samples from Al-Wafa oil field are more mature compared to the oil samples from Al-Hamada field complex and NC3.

Alkylphenanthrenes

The maturity values based on phenathrenes (MPI-1) and the calculated reflectance (VRc%) estimates using the formula proposed by Radke *et al.* (1986) are given in Table 4.6. The MPI-1 and the VRc% values range from 1.0-1.1 and 1.0–1.1 respectively, for the oil samples from Al-Wafa oil field (NC169), from 0.78–0.96 and 0.87–0.98 respectively, for the oil samples from Al-Hamada field complex (NC8 & NC5) and from 0.50–0.65 and 0.70–0.79 respectively, for the oil samples from NC3 oil field. These result indicate that the oil samples from the oil fields located in the South and southwestern part of the basin (NC169, NC8 & NC5) are more mature compared with the oil samples collected from the oil field located in the northern part

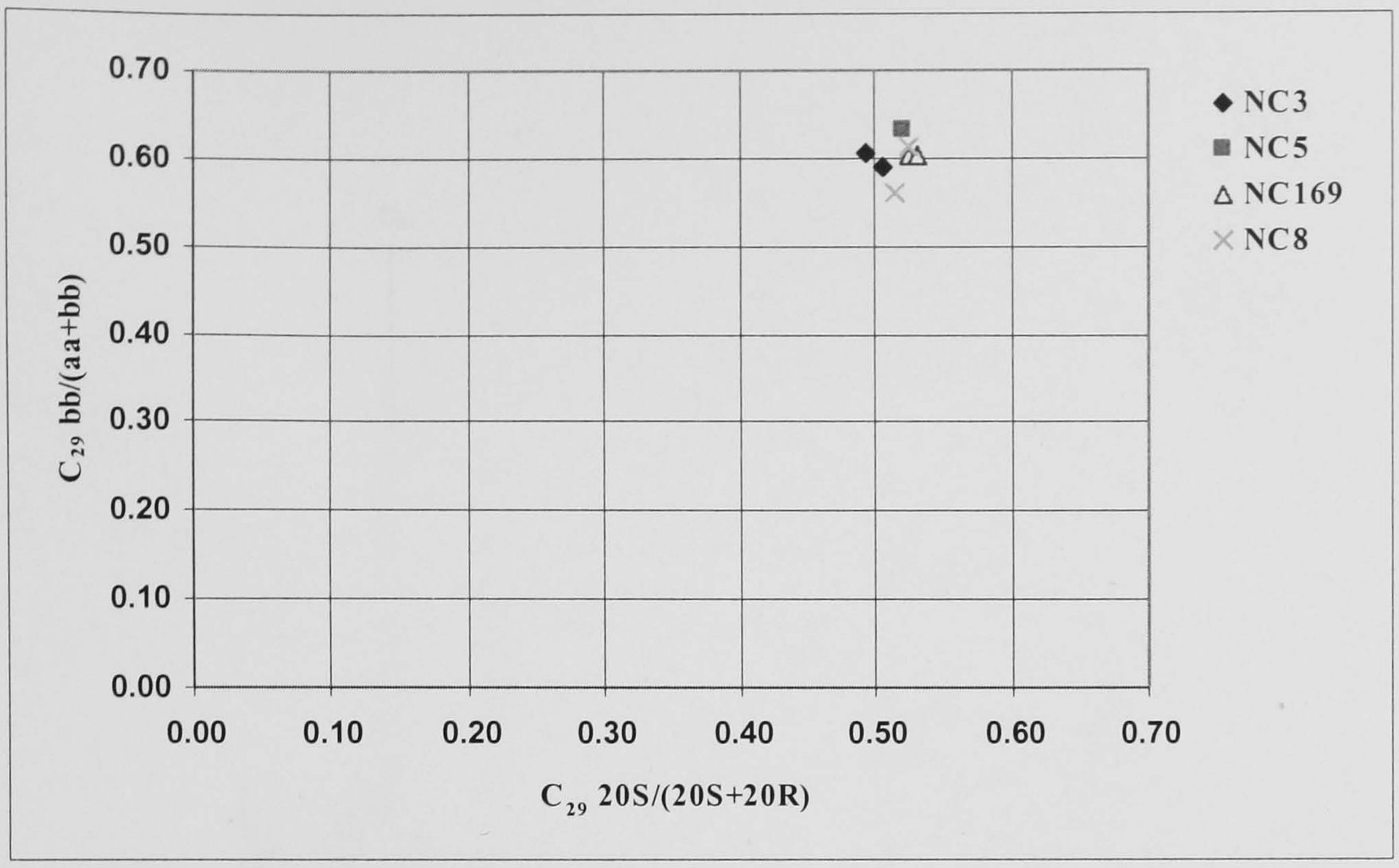

Figure 4.21. Cross plot of the thermal maturity 20S/(20S+20R) and ααα/(ααα+αββ)-C_{29} steranes parameters for Ghadames Basin oil samples.

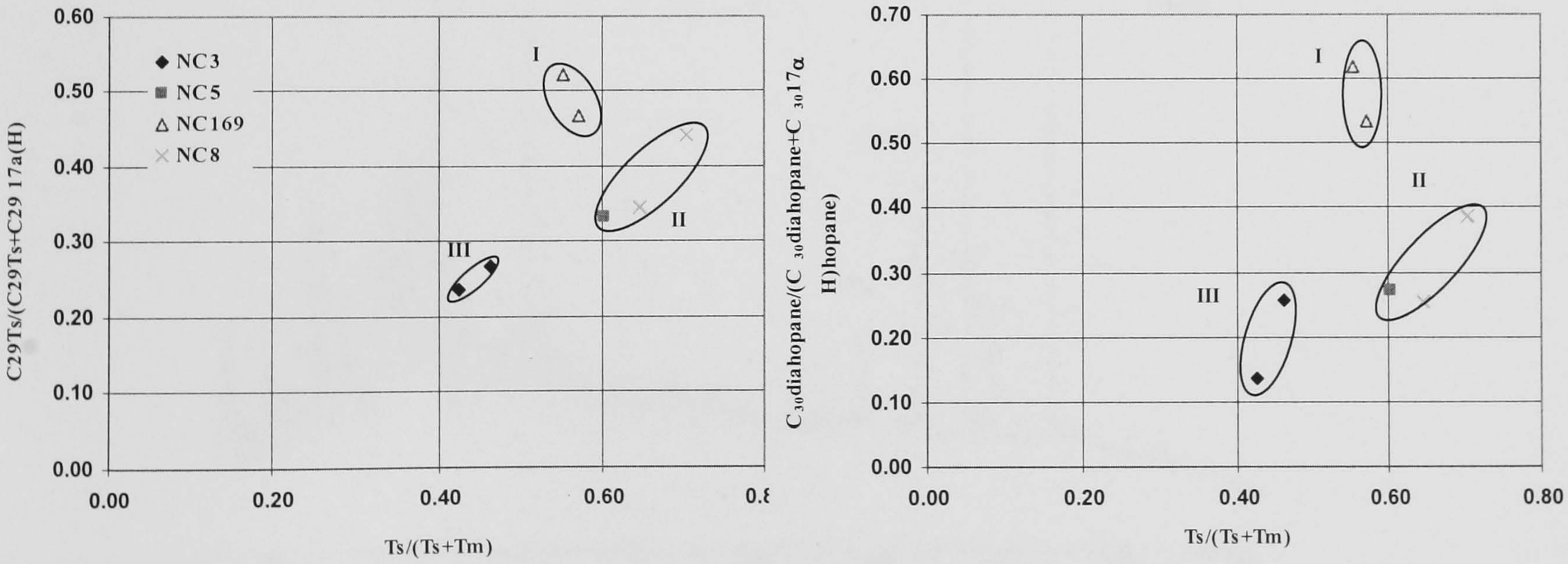

Figure 4.22. Cross plots of the maturity rearranged hopanes-based parameters for the Ghadames Basin oil samples.

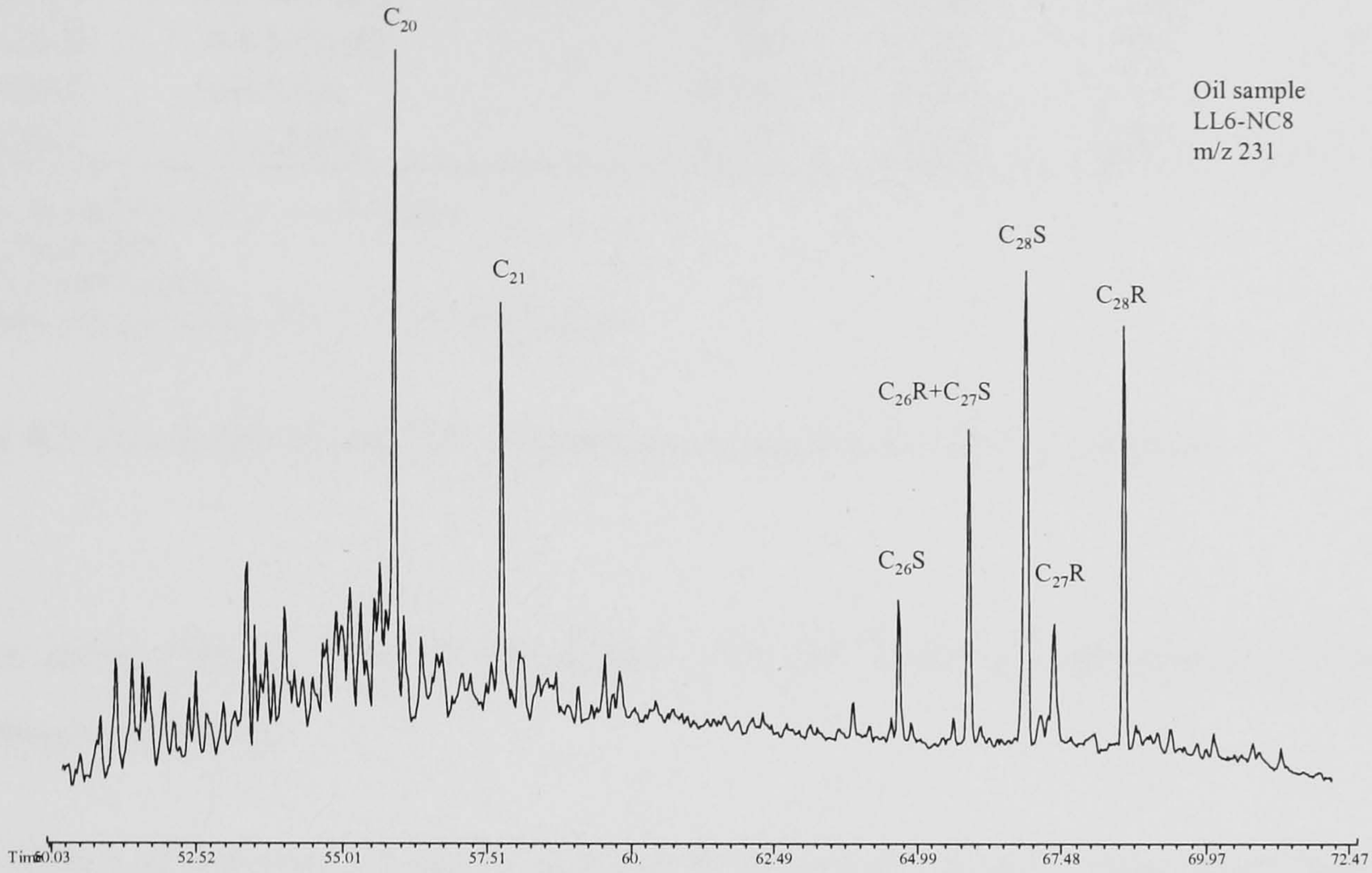

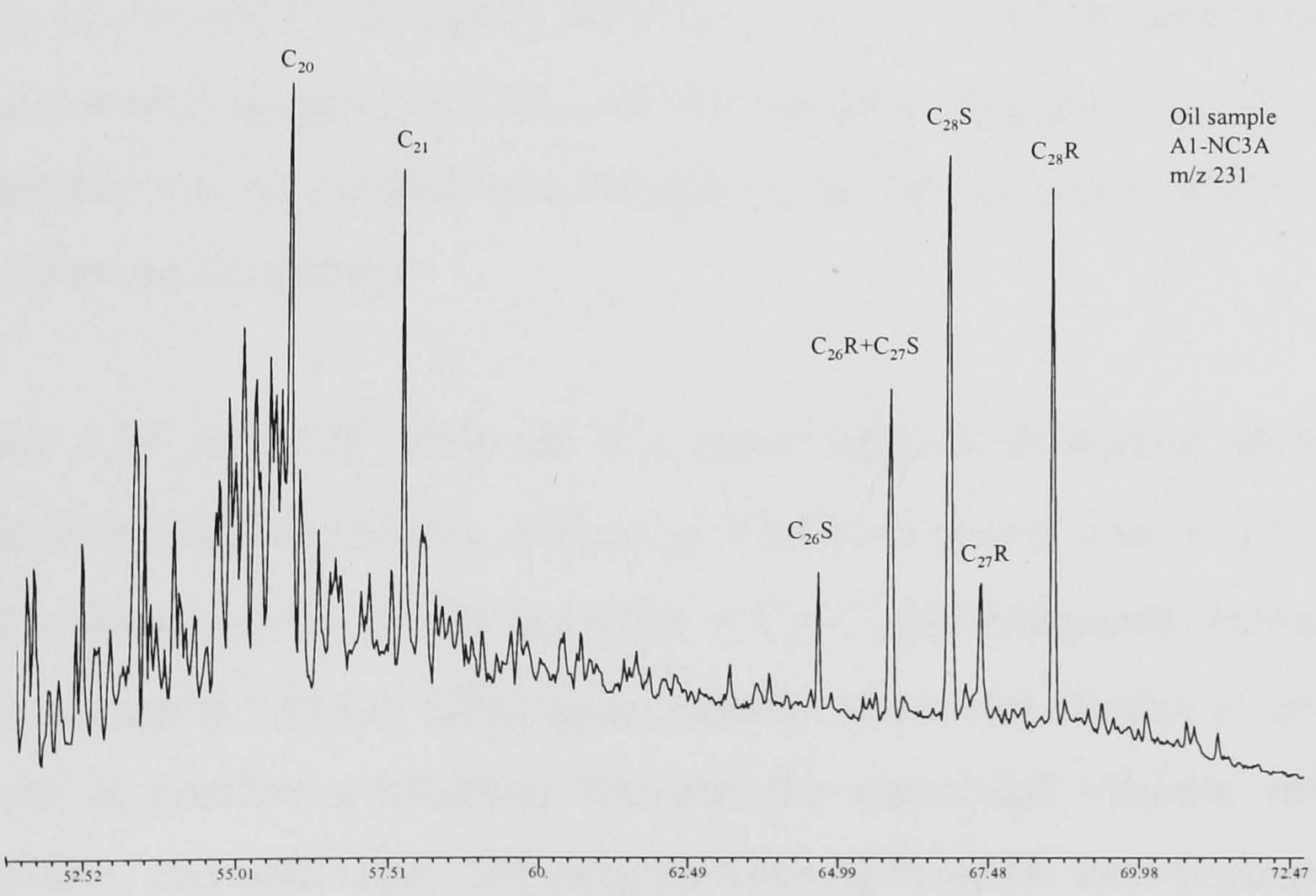

Figure 4.23. Partial m/z 231 mass chromatograms showing the distribution of ABC-ring triaromatic steroid hydrocarbons in selected oil samples from the Ghadames Basin.

Sample	Location	Depth	Triaromatic	MPI-1	MPR	Rc
Oil-1	A1-NC3A		0.35	0.50	1.08	0.70
Oil-2	A1-NC3A		0.22	0.65	0.88	0.79
Oil-3	Z5-NC5		0.61	0.78	0.97	0.87
Oil-4	A6-NC169		0.92	1.09	1.49	1.05
Oil-5	A4-NC169		0.94	1.01	1.43	1.00
Oil-6	V6-NC8		0.20	0.96	1.02	0.98
Oil-7	LL6-NC8		0.43	0.85	0.94	0.91

MP-1=1.5*(3-MP+2-MP)/(P+9-MP+1-MP)
MPR = 2-MP/1-MP
%Rc = 0.4+(MP1-1)*0.6
Triaromatic = (C_{20} traromatic)/ (C_{20} +C_{28} S+R) triaromatic

Table 4.8 Aromatic biomarker maturity parameters for the oil samples.

of the basin (NC3). This is consistent with the maturity parameters based on the rearranged hopanes.

4.3.3 Effect of maturity on facies-dependent biomarker ratios and concentrations

As mentioned in Section 4.3.1, the ratios of C_{29} ($\alpha\alpha\alpha$+$\alpha\beta\beta$) S+R regular steranes/(C_{29} ($\alpha\alpha\alpha$+$\alpha\beta\beta$) S+R regular steranes + C_{29}-C_{30} 17α(H)-hopanes) and (C20-C26 (S+R) extended tricyclics/(C_{20}-C_{26} (S+R) extended tricyclics+ C_{29}-C_{30} 17α(H) hopanes) defined the oil samples into Groups I , II and III, partly due to maturity differences between the groups.

Figures 4.24 and 4.25 show the C_{29} ($\alpha\alpha\alpha$+$\alpha\beta\beta$) S+R regular steranes/(C_{29} ($\alpha\alpha\alpha$+$\alpha\beta\beta$) S+R regular steranes + C_{29}-C_{30} 17α(H)-hopanes) and (C_{20}-C_{26} (S+R) extended tricyclics/(C_{20}-C_{26} (S+R) tricyclics + C_{29}-$C_{30}\alpha$(H)-hopanes) ratios plotted against the calculated vitrinite reflectance maturity parameter (Radke *et al.*, 1986). Indeed, there is positive correlation between the calculated vitrinite reflectance equivalent (%Rc) and both ratios. Oil samples from Al-Wafa oil field (Group I) show higher maturity ratios; oil samples with the lowest maturity from the NC3A oil field exhibit the lowest ratios indicating a strong maturity effect on these ratios.

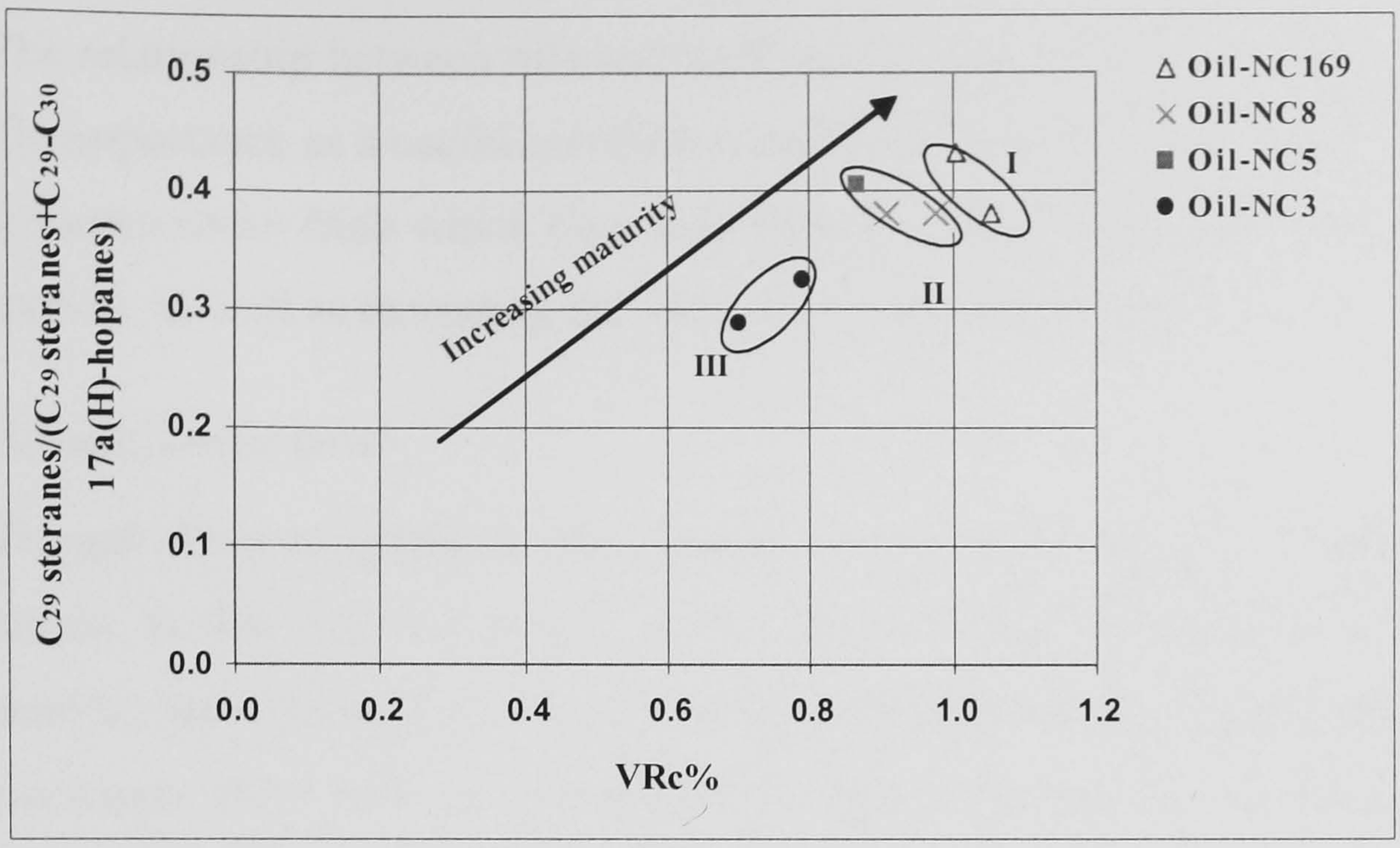

Figure 4.24. Cross plot of C_{29}steranes/(C_{29}sterane +C_{29}-C_{30} 17α(H)-hopanes) versus calculated vitrinite reflectance %Rc for Ghadames Basin oil samples.

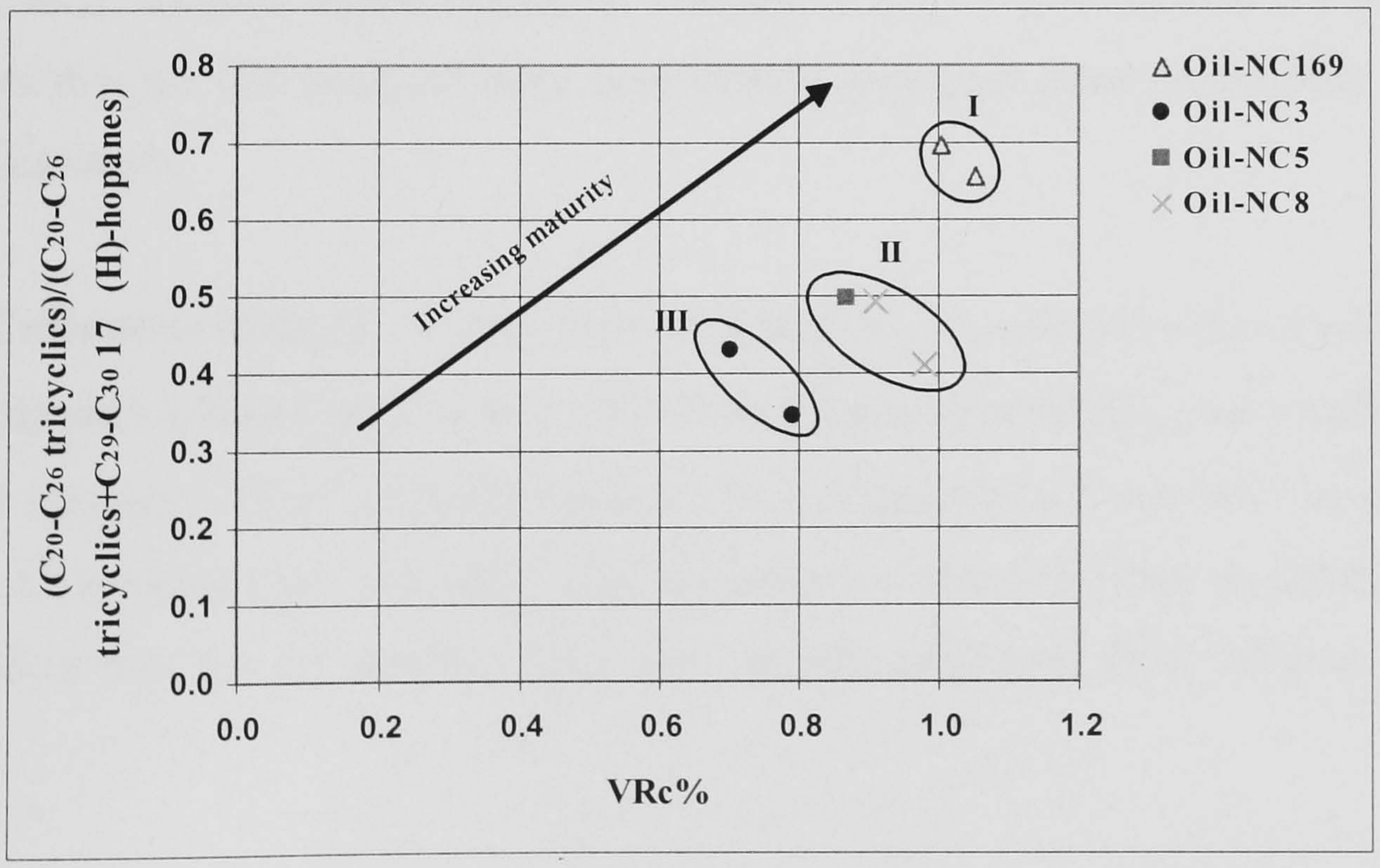

Figure 4.25. Cross plot of (C_{20}-C_{26} tricyclics)/(C_{20}-C_{26}tricyclics+(C_{29}-C_{30}17α(H)-hopanes) versus calculated vitrinite reflectance %Rc for the Ghadames Basin.

4.4 Oil Source Rock Correlations

The relationship between oils and their source rocks are of economic as well as scientific importance as a useful correlation between a discovered oil, seep or oil-stain and the source rocks from which they have been generated might help in discovering new reserves, as well as extending the already discovered reserves.

4.4.1 Facies Comparison

The gas chromatograms of the oils show a very close similarity of the *n*-alkane distributions to the Silurian source rocks. The *n*-alkane distribution is generally dominated by short-chain (*n*-C_{11} to *n*-C_{18}) over long-chain *n*-alkanes, and the *n*-C_{17}/ *n*-C_{27} ratio ranges from 4.00 to 7.45 and Pr/Ph ratio range from 1.2 to 1.4 suggesting that these oils may be generated from the Silurian source rock.

A number of facies-based parameters calculated using sterane and triterpane distributions have been selected in order to perform oil/source rock correlation. The ternary diagram displaying the distribution of C_{27}- C_{28}- C_{29} 5α(H), 14β(H), 17β(H) steranes (Fig. 4.26) clearly shows similarities between all the oils and the Silurian source rock samples which belong to Groups A and B (see Section 3.2.1). This suggests that the oils analysed have been mostly generated from the Silurian source rock succession.

Cross plots of the C_{21}-C_{26} tricyclic terpanes)/(C_{21}-C_{26} tricyclics+C_{29}-C_{30}17α(H)-hopanes) ratio versus the C_{29} (ααα+αββ) S+R regular steranes/(C_{29} (ααα+αββ) S+R regular steranes + C_{29}-C_{30}17α(H)-hopanes) ratio displayed in Figure 4.27 reveal that all the oil samples plot very close to the Silurian samples of Groups A and B, again suggesting that the oil samples have been mostly generated from Silurian source rocks.

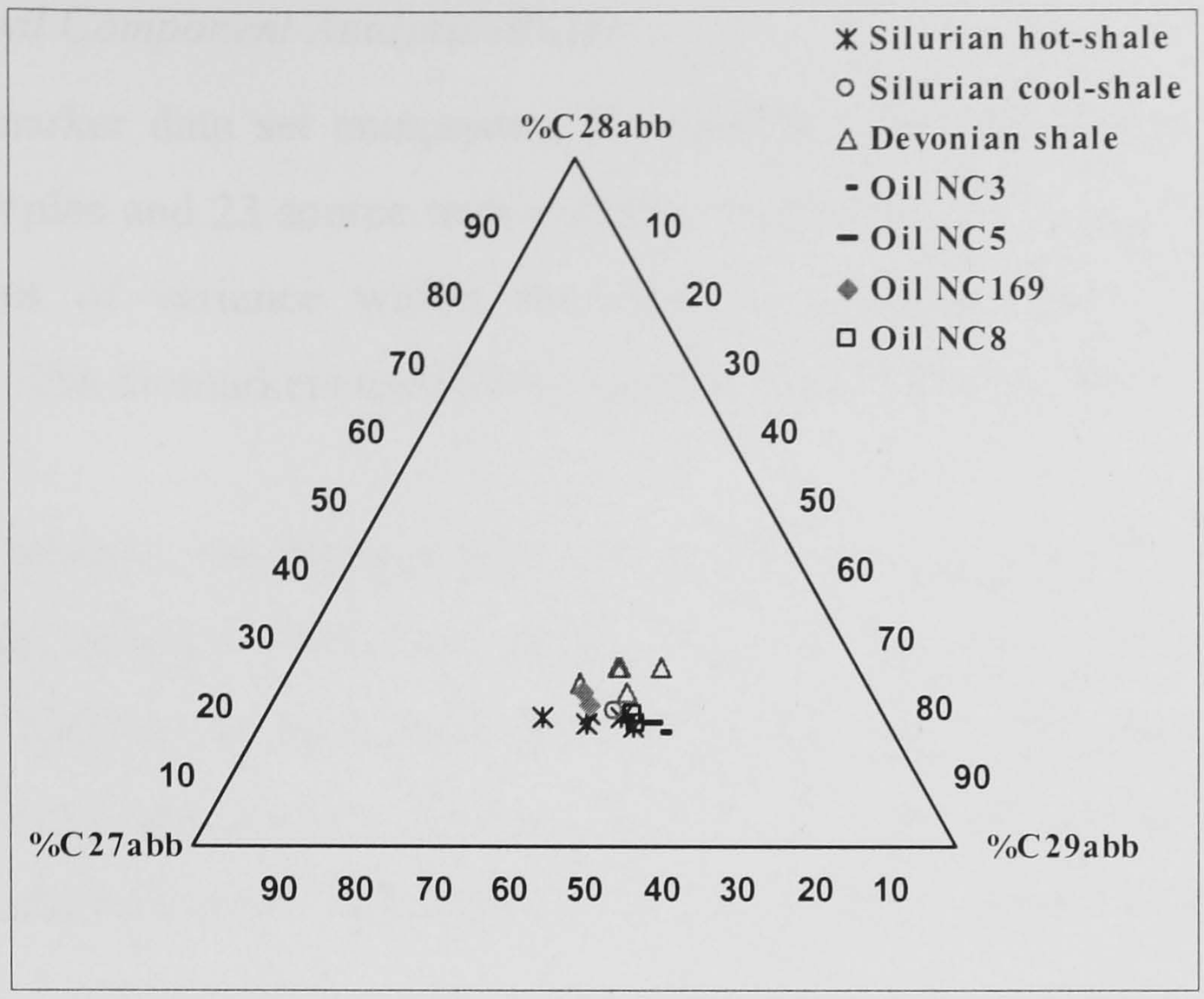

Figure 4.26. Ternary plot of the relative abundance of C27- C28- C29 αββ-steranes for the Silurian and Devonian rock samples and oils from the Ghadames Basin.

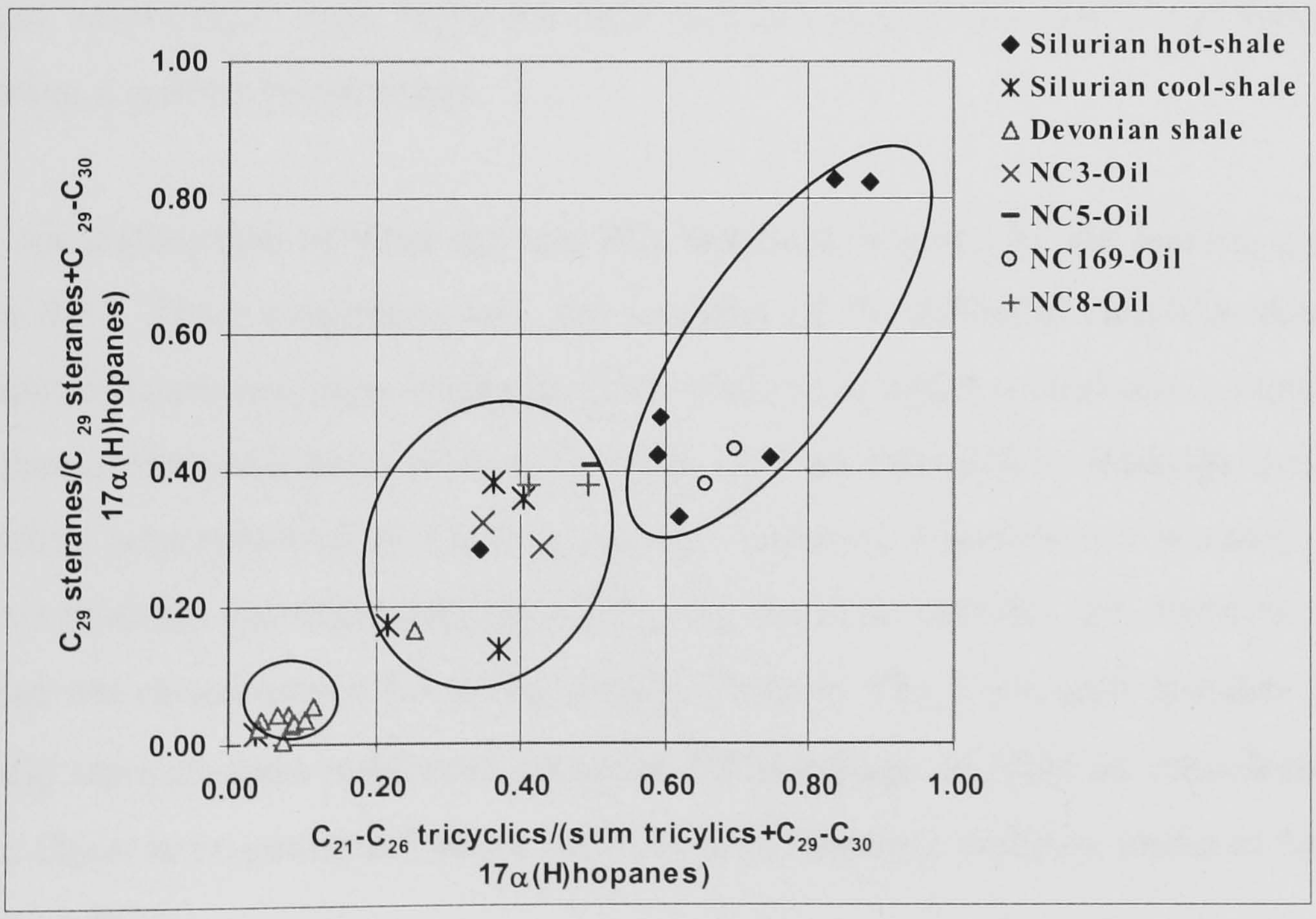

Figure 4.27. Cross plots of the facies parameters tricyclic terpanes C_{21}-C_{26}/(tricyclic terpanes C_{21}-C_{26} + C_{29}-C_{30} 17α(H)-hopanes) for the source rock and oil samples from the Ghadames Basin.

4.4.2 Principal Component Analysis (PCA)

A biomarker data set comprising 37 variables (biomarker concentrations) for seven oil samples and 23 source rock samples, was analysed by PCA to establish the major sources of variance within the steranes, tricyclic terpanes, and hopanes distributions. The biomarkers used in the analysis are listed in Table 4.9.

In this analysis, the first two principal components (PCs) explained 71.29% and 8.33% of the variance within the scaled data set, respectively. This allows the relationships between the samples to be examined in a simple two-dimensional scores plots (PC1 versus PC2) which includes the effects of all the original variables (i.e. biomarker concentrations), and displays 79.62% of the variance in the scaled data (Fig. 4.28).

The scores plot of PC1 versus PC2 reveals that the oil samples from all groups (NC169, NC8, NC5 and NC3) plot closer to the Silurian 'hot-shale' samples from wells A1-70 (10005'), B1-NC2 (10108') and A1-66 (5054') of Group A, and the Silurian 'cool-shale' from wells Z5-NC5 (10124') and F1-66 (6473') of Group B, indicating a genetic relationship.

An explanation of what the two PCs represent is given by the loading plots in Figure 4.29. These diagrams show the loadings of the different variables upon the principal components; large loadings, either positive or negative, indicate a significant influence of the variable on those PCs. Thus, PC1 is controlled by loadings attributed to relative concentration of C_{21}-C_{26} tricyclic terpanes, hopanes and steranes. High positive loadings are characteristics of C_{21}-C_{26} tricyclic terpanes and steranes, while hopanes are characterised by strong negative values. The C_{32}-$C_{34}\alpha\beta$ hopanes (S+R) and $\alpha\beta\beta$ steranes have moderately positive PC2 loadings. It could be considered that source facies have strong influence on PC1, whilst thermal maturity seems to have an impact on PC2.

	Tricyclic terpanes and hopanes (m/z = 191)
1	C_{20} Tricyclic terpane
2	C_{21} Tricyclic terpane
3	C_{23} Tricyclic terpane
4	C_{24} Tricyclic terpane
5	C_{25} Tricyclic terpane
6	C_{26} Tricyclic terpane
7	22,29,30-Trisnorneohopane (Ts)
8	22,29,30-Trisnorhopane (Tm)
9	C_{29} 17α(H), 21β(H)-30-norhopane
10	18α(H)-30-norneohopane (C_{29} Ts)
11	C_{30} diahopane
12	C_{29} 17β(H),21α(H) hopanes
13	C_{30} 17α(H),21β(H) hopanes
14	C_{30} 17β(H),21α(H) hopanes
15	C_{31} 17α(H),21β(H) hopanes (22S)
16	C_{31} 17α(H),21β(H) hopanes (22R)
17	C_{32} 17α(H),21β(H) hopanes (22S)
18	C_{32} 17α(H),21β(H) hopanes (22R)
19	C_{33} 17α(H),21β(H) hopanes (22S)
20	C_{33} 17α(H),21β(H) hopanes (22R)
21	C_{34} 17α(H),21β(H) hopanes (22S)
22	C_{34} 17α(H),21β(H) hopanes (22R
	Steranes (m/z =217)
23	C_{27} 13β(H), 17α(H) diasterane (20S)
24	C_{27} 13β(H), 17α(H) diasterane (20R)
25	C_{29} 13β(H), 17α(H) diasterane (20S)
26	C_{27} 5α(H), 14α(H), 17α(H) sterane (20R)
27	C_{29} 13β(H), 17α(H) diasterane (20R)
28	C_{29} 5α(H), 14α(H), 17α(H) sterane(20S)
29	C_{29} 5α(H), 14β(H), 17β(H) sterane(20R)
30	C_{29} 5α(H), 14β(H), 17β(H) sterane(20S)
31	C_{29} 5α(H), 14α(H), 17α(H) sterane(20R)
	αββ Steranes (m/z = 218)
32	C_{27} 5α(H), 14β(H), 17β(H) sterane (20R)
33	C_{27} 5α(H), 14β(H), 17β(H) sterane (20S)
34	C_{28} 5α(H), 14β(H), 17β(H) sterane (20R)
35	C_{28} 5α(H), 14β(H), 17β(H) sterane (20S)
36	C_{29} 5α(H), 14β(H), 17β(H) sterane (20R)
37	C_{29} 5α(H), 14β(H), 17β(H) sterane (20S)

Table 4.9. Biomarker compounds used in the principal components analysis.

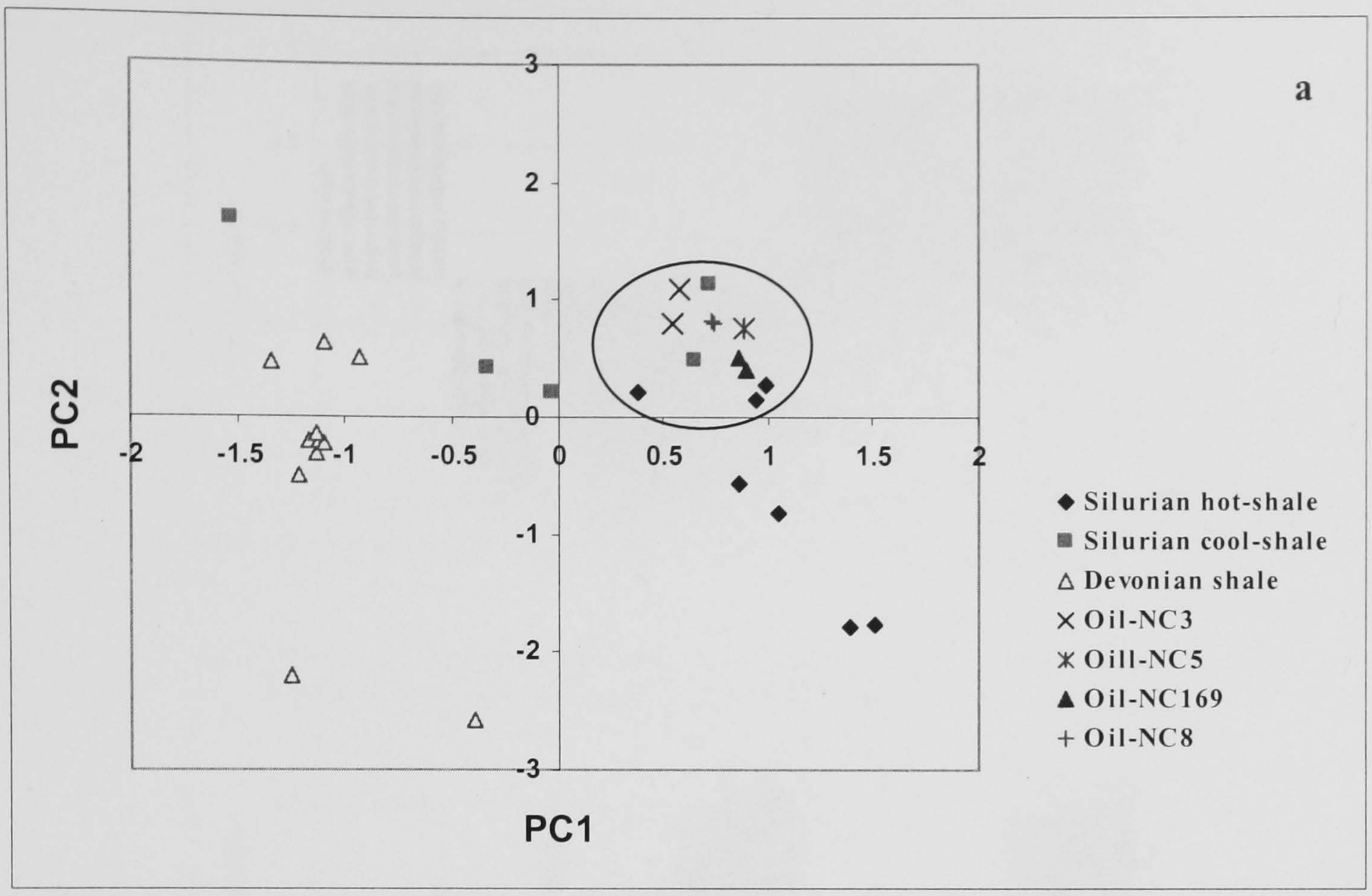

Figure 4.28 Scores plot (PC1 versus PC2) showing the relationship between the source rocks (Silurian and Devonian) and the oils analysed; PC1 explains 71.29% of the total variance in the scaled data set and PC2 explains a further 8.33%.

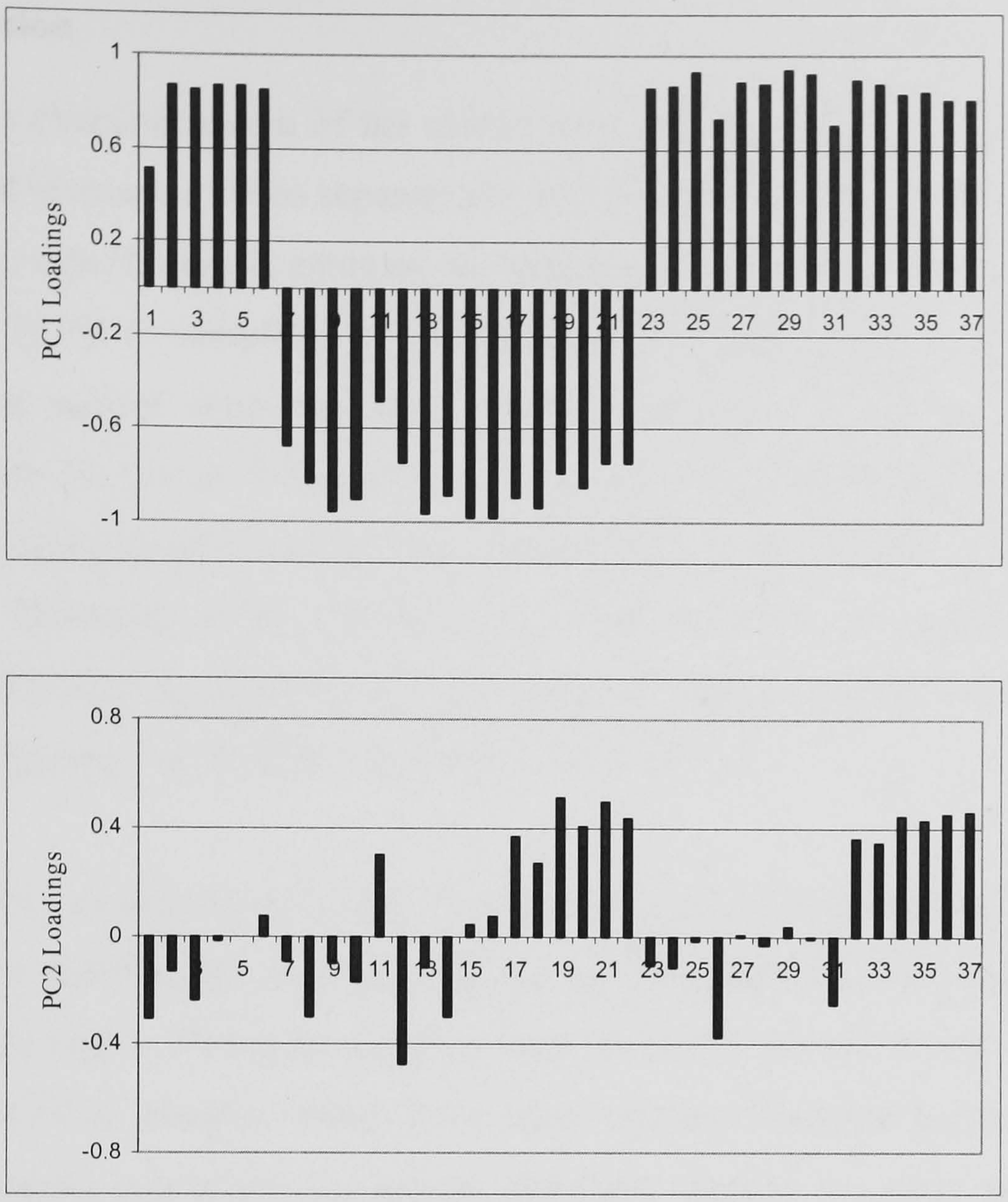

Figure 4.29. Loadings plots showing the contributions of the different biomarkers on the first two principal components.

4.5 Conclusion

Facies characterisation of the source rock samples using principal components analysis and biomarker ratios separate the Silurian and Devonian source rock samples into three groups. Group A contains six samples from the Lower Silurian 'hot shale' from wells F1-66 (3 samples), A1-70 (2 samples) and B1-NC2 (1 sample). Group B contains one sample from the Lower Silurian 'hot shale' from well (A1-66), four samples from the Lower Silurian 'cool shale' from wells (F1-66, A1-70, Z5-NC5 & B1-49) and one Upper Devonian shale sample from well (F1-66). Group C contains ten Upper Devonian shale samples from wells A9-NC7 (2 samples), C1-26 (3 samples), M2-NC2 (2 samples) and three samples from (A1-90, B1-49 & A1-61); and one Lower Silurian 'cool shale' sample from well A1-90.

Maturity evaluation of source rock samples based on biomarker and aromatic hydrocarbon distributions indicates that not all the samples are strongly affected by maturity; the Upper Devonian samples from wells A1-66 and F1-66 are immature, whereas the other samples which have been selected from the Lower Silurian and Upper Devonian succession are mature and have reached the main stage of the oil window. This is consistent with their Tmax values. Moreover, the Lower Silurian source rock strata revealed a trend of increasing maturity towards the South and southwestern Ghadames Basin.

Most of the Upper Devonian source rock samples have unusual proportions of the 20S isomers (relative to 20R isomers) of the C_{29} $\alpha\alpha\alpha$ steranes, with values of more than 55% 20S. Such high values could be due to factors other than maturity.

Most of the facies-based parameters employed in this project using biomarker distributions clearly separate the oil samples into three groups. Group I contains two oil samples from wells within Al-Wafa oil field (A4 &A6-NC169), Group II contains three oil samples collected from Al-Hamada oil field (wells LL4,V6-NC8 & Z5-NC5) and the third group contains two oil samples collected from NC3 oil field (well A1-NC3A).

Maturity evaluation of the oil samples based on the biomarker and aromatic hydrocarbon ratios reveals that the oil samples collected from the oil fields located in the South and southwestern parts of the basin are more mature than the oil samples collected from the northern parts of the basin. This is in consistent with the maturity trends of the source rocks of the Ghadames Basin.

Oil-source correlations revealed that all the oil samples display similar facies features to the Lower Silurian source rock samples from Groups A and B. Therefore there is a high probability that these oils were generated from the Lower Silurian source rocks.

CHAPTER 5.0

THERMAL MATURITY

5.0 THERMAL MATURITY

5.1 Introduction

The importance of determining the thermal maturity of a sedimentary sequence in petroleum exploration has been demonstrated in many published studies. Routine analytical methods include vitrinite reflectance (Tissot & Welte, 1984; Robert, 1988; Durand *et al.*, 1986) which has been calibrated to help define when hydrocarbon generation and expulsion begins and ends in a source rock sequence. Other analyses such as spore colour index (SCI) and pyrolysis Tmax have been used to supplement the vitrinite reflectance maturity measurements (Staplin, 1969; Espitalié, 1977; Peter, 1986; Collins, 1990; Marshall, 1991). All of the above maturity techniques have been used with great success for sedimentary sequences of Devonian or younger age, but there is no standardised objective optical measurement for sequences older than the Devonian because vitrinite and sporomorphs are either absent or rare because higher vascular plants did not begin to evolve until late Silurian time (Richardson, 1969) Recently, graptolite (Goodarzi *et al.*, 1992; Cole, 1994; Gentzis *et al.*, 1996; Suchý *et al.*, 2002), and chitinozoan reflectance (Tricker *et al.*, 1992; Obermajer *et al.*, 1996) have proven useful maturity techniques for Lower Palaeozoic rocks where no alternative maturation data can be gained from other methods.

Several methods were employed: to determine the maturity of the Upper Devonian and Lower Silurian succession in the Ghadames basin, vitrinite and (graptolite fragments or chitinozoans) reflectance, Spore Colour Index (SCI), Acritarch Colour Index (ACI), fluorescence colour, Tmax data and molecular biomarker parameters.

5.2 Bulk Geochemical Maturity Parameters

In this study 110 core and 197 cutting samples from Lower Palaeozoic succession were analyzed by Rock-Eval pyrolysis. These samples were collected from 11 wells distributed throughout the basin. The results are given in Appendices VII and VIII.

The Rock-Eval results (HI and Tmax) for samples from the Lower Palaeozoic succession in different wells throughout the basin, show considerable variation. Figure 5.1A show most of the lower Tanezzuft "hot shale" samples in wells D1-NC2 and A1-70 located in northern part of the basin are within the mature zone: the Tmax ranges from 436 to 445 °C, and current HI values correspond to Type II-III kerogen. Some samples have a relatively high HI considering their maturity. The lower Tanezzuft "hot-shale" samples in well F1-66 located in the south eastern part of the basin are with the late mature stage (Tmax ranges from 444 to 453 °C); they have an HI <250 (Type III kerogen) due to their higher maturity and thus greater reduction in the hydrocarbon potential (S2). These rich samples correspond to intervals with gamma ray values >150 API units. The samples from Lower Tanezzuft Formation are enriched in AOM content and genetically would almost certainly have corresponded to Type II kerogen. In the southwestern part of the basin, the HI of the lower Tanezzuft Formation is reduced to <50 corresponding to IV kerogen (wells B1-49, M2-NC7 and A1-90); this is due to combination of lower preservation under more oxic conditions and maturation. The samples from lower Tanezzuft Formation in this location are associated with low gamma-ray values (<60 API).

The Tmax versus hydrogen index diagram for the upper Tanezzuft "cool-shale" low gamma ray samples site (Fig. 5.1B) shows that most of the samples are located in the immature to early mature zones for petroleum generation (Tmax 430–445 °C), and have HI corresponding to type III kerogen. Microscopic examination of these samples shows that they are dominated by palynomorphs, with low AOM and phytoclasts.

The Tmax obtained from Upper Devonian Tahara and Aouinet Ouenine formation range from 430 to 445°C, indicating they are within the immature to early mature zone. The hydrogen indices versus Tmax (Fig 5.2 C & D) show considerable vertical variation in hydrogen index due to changes in kerogen facies and maturity. Most of the samples have a current HI corresponding to Type III kerogen. The samples of these formations are enriched in phytoclasts, with low poorly preserved AOM.

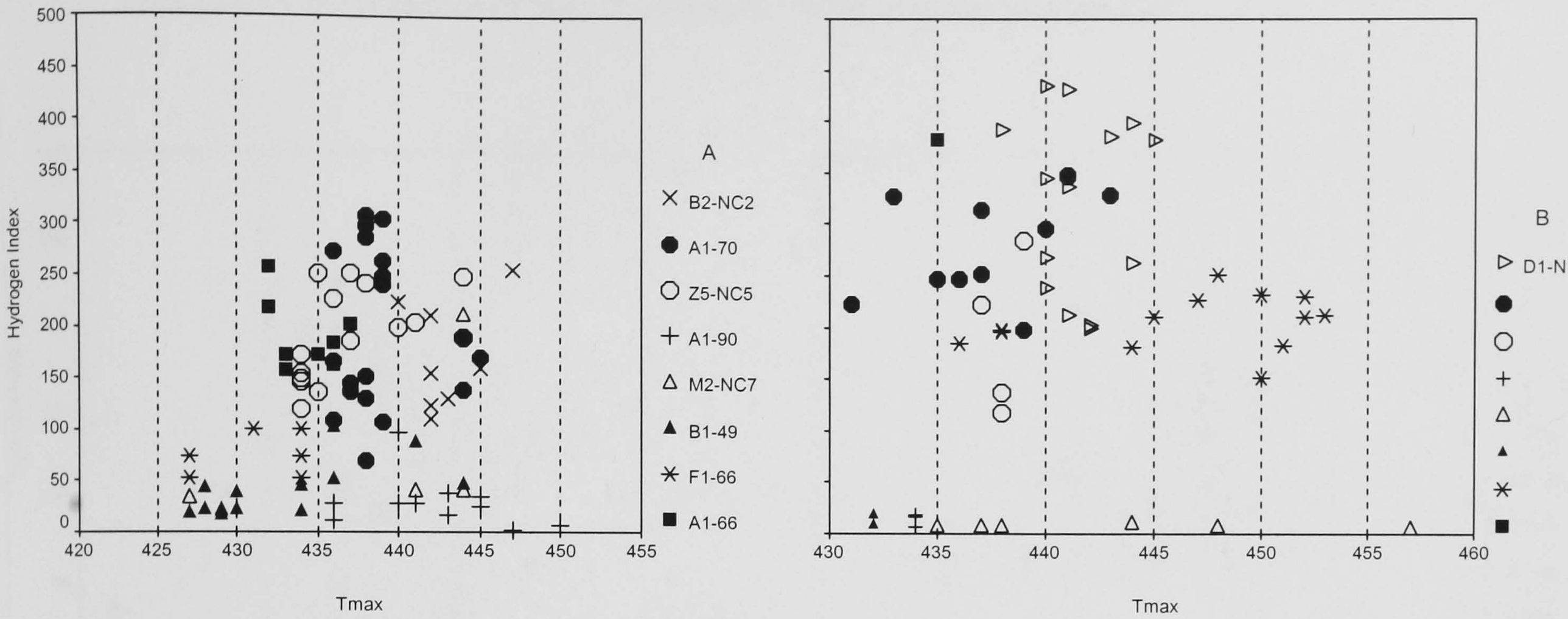

Figure 5.1. Cross plots of Tmax and hydrogen index: (A) samples from upper Tanezzuft, (B) samples from lower Tanezzuft.

5.2.1 Maturation Trends Based on Tmax

Maturation trends based on the interpretation of Tmax data of the cutting samples from the Lower Palaeozoic succession are shown in Figure 5.3 as plots of Tmax versus well depth. In the northern part of the basin (wells D1-NC2 and A1-70) the Upper Devonian Aouinet Ouenine Formation has Tmax values ranges from 415 to 430°C, consistently lower than those from the Tanezzuft Formation (435 to 445°C). In general, the Tmax values begin to increase gradually with increasing depth of burial towards the depocentres of the basin. At wells A1-90 and M2-NC7 the Tmax lies between 435 to 467°C. The Tmax values for the upper and lower Tanezzuft, Aouinet Ouenine (A, B & C) and Tahara sandstone formations are consistently about 15°C higher than in the northern part of the basin, which is attributed to present burial depth. Towards the south and south eastern part of the basin at wells B1-49 and F1-66, the Tmax (Fig. 5.3) is relatively higher than those located in the north (at well B1-49 some samples have unreliable Tmax values due to very low TOC content). In the South and southeastern part of the basin, the sedimentary strata become thinner; this indicates that the maturity levels are not the results of present-day burial. Maybe here

very thick strata were eroded or the geothermal gradient was higher. For some of the palaeo-highs (e.g. Al-Hamra, Nafusa and Al-Qarqaf Arch), low amplitude epeirogenic movements related to Caledonian, Hercynian and Pyrenean (Eocene) phases are indicated by the presence of intra-formational unconformities (Echikh, 1992, p.37)

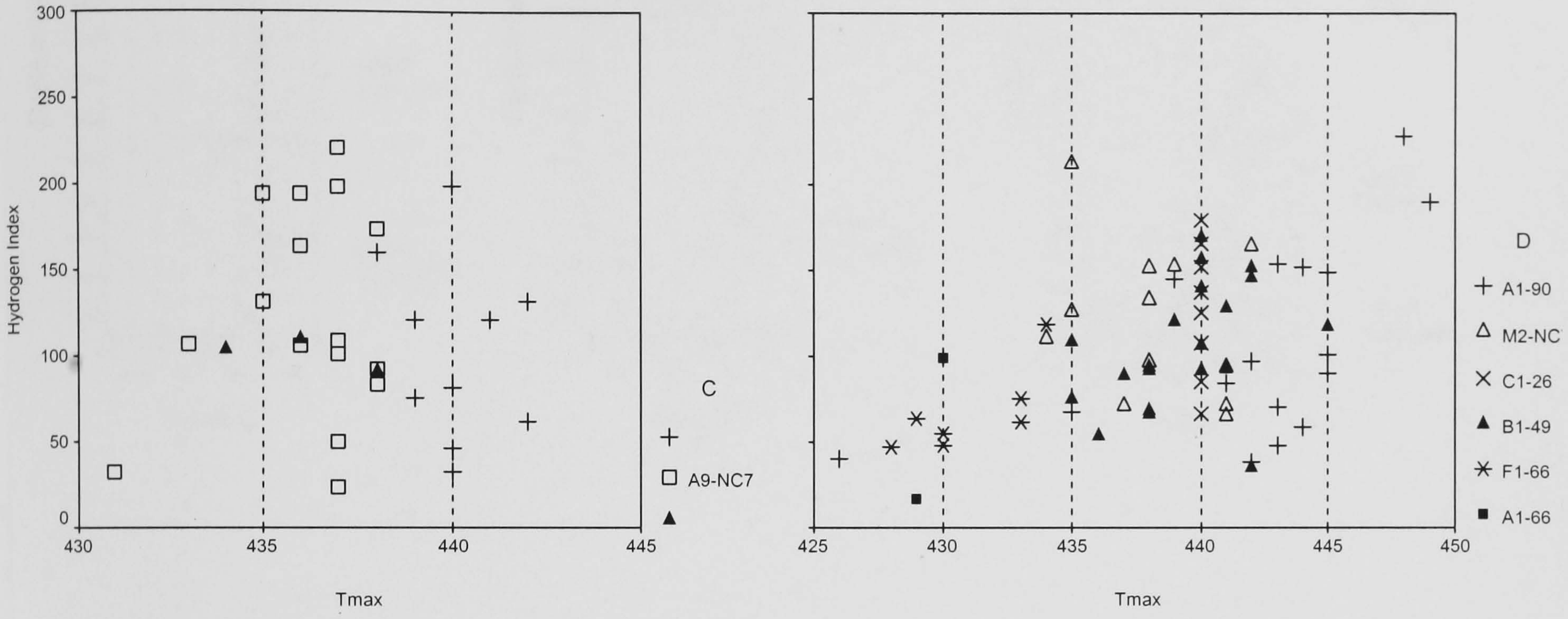

Figure 5.2. Cross plots of Tmax and hydrogen index, (C) samples from upper Tanezzuft, (D) samples from lower Tanezzuft.

5.3 Spore and Acritarchs Colour Indices

The change in spore colour with increasing maturity has been quantified and related systematically to hydrocarbon generation zones (Staplin, 1969). Staplin's Thermal Alteration index (TAI) scale, published in 1969, has provided the basis for one of the most widely used numerical scales. One of these, the ten division Spore Colour Index (SCI) of Fisher *et al*. (1980) has been well calibrated with other maturity indicators including vitrinite reflectance (Collins, 1990). In Lower Palaeozoic sequences, where vitrinite and land plant spores are absent, acritarchs can be used instead of spores. Calibration studies have shown that the major colour change in acritarchs occurs in the late mature zone, i.e. later than for spores and pollen (Collins, 1990).

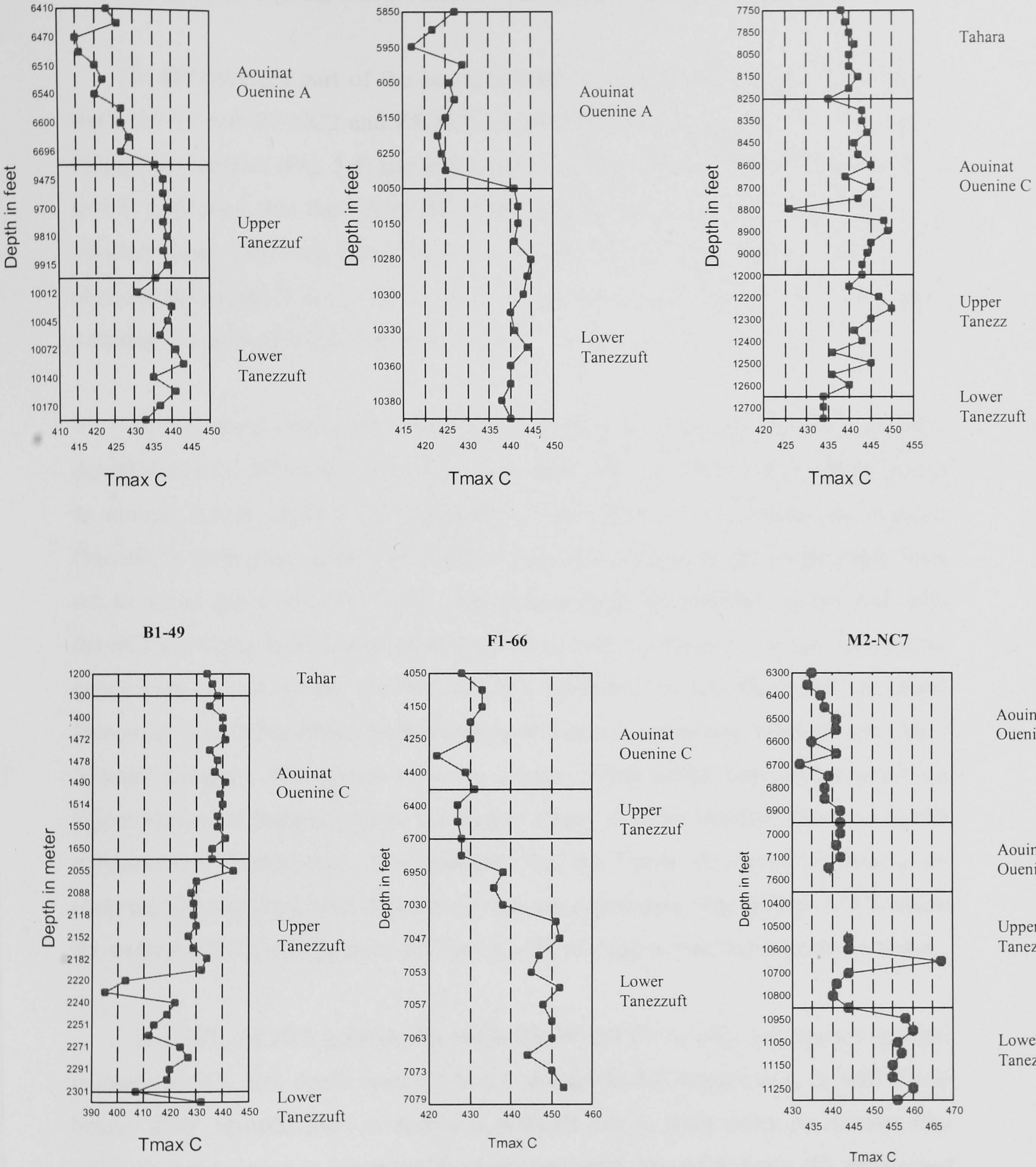

Figure 5.3. Tmax versus depth for investigated wells. Abrupt step-like trends and intervals where Tmax decreases with depth clearly indicate the influence of facies.

In this study 110 core samples from ten wells have been analysed for spore (SCI) and acritarch (ACI) colour indices. The results are given in Appendix VII.

In the northern part of the basin, the SCI and ACI have been determined for wells A1-70 and B1-NC2 and Z5-NC5 (Appendix VII). The results from the Lower Palaeozoic samples (Fig. 5.4) shows a gradual increase of the SCI with depth from 2.0 to 4.5, indicating that the Upper Devonian formations are immature, and the Lower Silurian upper Tanezzuft Formation early mature. The Acritarch Colour Indices were obtained at the same time as the spore colour data. The ACI gradient (Fig. 5.4) shows a modest increase with depth from 1.0 to 2.5.

In the central part of the basin, the SCI for Upper Devonian samples from wells A9-NC7 and C1-26 are 4.5 and 5.0, respectively. The spores exhibit a yellow-orange to orange colour under blue fluorescence. The SCI for the Tahara and Aouinet Ouenine A formations from well M2-NC7, shows a gradual increase with depth from 4.5 to 6.0 at depth of 6227'-7264'. The palynomorph fluorescence agrees well with the SCI and changes with increasing depth from yellow-orange to orange. Toward the depocentre at well A1-90, the SCI and ACI gradient (Fig 5.4) show that the Upper Devonian Tahara Sandstone Formation has SCI of 5.0, increasing to 9.0 for the Upper Silurian samples. The spores show an orange colour under blue fluorescence for Upper Devonian samples, while the deeper Upper Silurian samples show no visible palynomorph fluorescence. This indicates that the Upper Devonian formations are early mature and the Lower Silurian formations postmature. The SCI and ACI values for wells A9-NC7, C1-26, M2-NC7 and A1-90, are higher than those from the North.

The SCI and ACI gradient for wells B1-49 and F1-66 (Fig 5.4) show a gradual increase of SCI with depth from 4.0 to 6.0 and 2.0 to 7.0 respectively. In well F1-66 below 7070' identification of spores is difficult due to their rarity or absence (the palynomorph fraction is dominated by prasinophytes). The ACI shows the same trend as SCI. The palynomorph fluorescence changes from yellow to yellow-orange for Upper Devonian samples to orange-brown for Lower Silurian samples. The maturity of the Lower Palaeozoic succession in the South and southeastern part of the basin are slightly higher than those located in the North. This is not related to present-day

overburden. Maybe southern parts of the basin were tectonically active, and part of the sediment was removed, or the geothermal gradient was higher.

Further to the southeast 40 km from well F1-66, the overall maturity in well A1-66 decreases, associated with thinning of the Palaeozoic. The SCI is 2.5 at a depth of 3153'-4115', then increases gradually to attain 4.0 by a depth of 5054'. Little colour change occurs in the acritarchs (the ACI is 1.5–2.0).

A cross plot of ACI versus SCI for whole dataset (Fig. 5.5) shows a major colour change occurs in acritarchs in the late mature zone, while little colour changes is discernible at lower maturities. This is in good agreement with Collins (1990, p.46).

5.4 Vitrinite, Chitinozoan and Graptolite Reflectance

Measurements of the intensity of reflected light from woody (vitrinite maceral phytoclasts) or 'zooclasts' (graptolites and chitinozoans) are widely used to assess maturity. The application of vitrinite reflectance for estimation of the thermal maturity and burial history of Devonian sediments or younger strata is firmly established as a routine tool for petroleum exploration. Vitrinite reflectivity values characteristically show a progressive but non-linear increase with depth (Robert, 1988; Durand *et al.*, 1986). Vitrinite reflectance is influenced by the effective maximum palaeotemperature and the duration of heating.

The marine deposits of pre-Devonian age often contain little or no vitrinite; however, Silurian shales of the Ghadames Basin contain fragments of graptolites and chitinozoans. Graptolites are the most common type of organic clasts observed in the Lower Silurian lower Tanezzuft 'hot-shale' (Plate II). Graptolites represent colonial zooplankton that occur in Lower Palaeozoic marine sediments (Goodarzi, 1984, 1985). The graptolite skeleton (periderm) is composed of a chitinous substance (Combaz, 1980), or a collagen-like protein (Suchý *et al.*, 2002) and in reflected light has optical properties similar to those of vitrinite (Goodarzi & Norford, 1987; Goodarzi *et al.*, 1992; Cole, 1994). The reflected light colours of graptolite fragments range from medium grey to light grey (Suchý *et al.*, 2002).

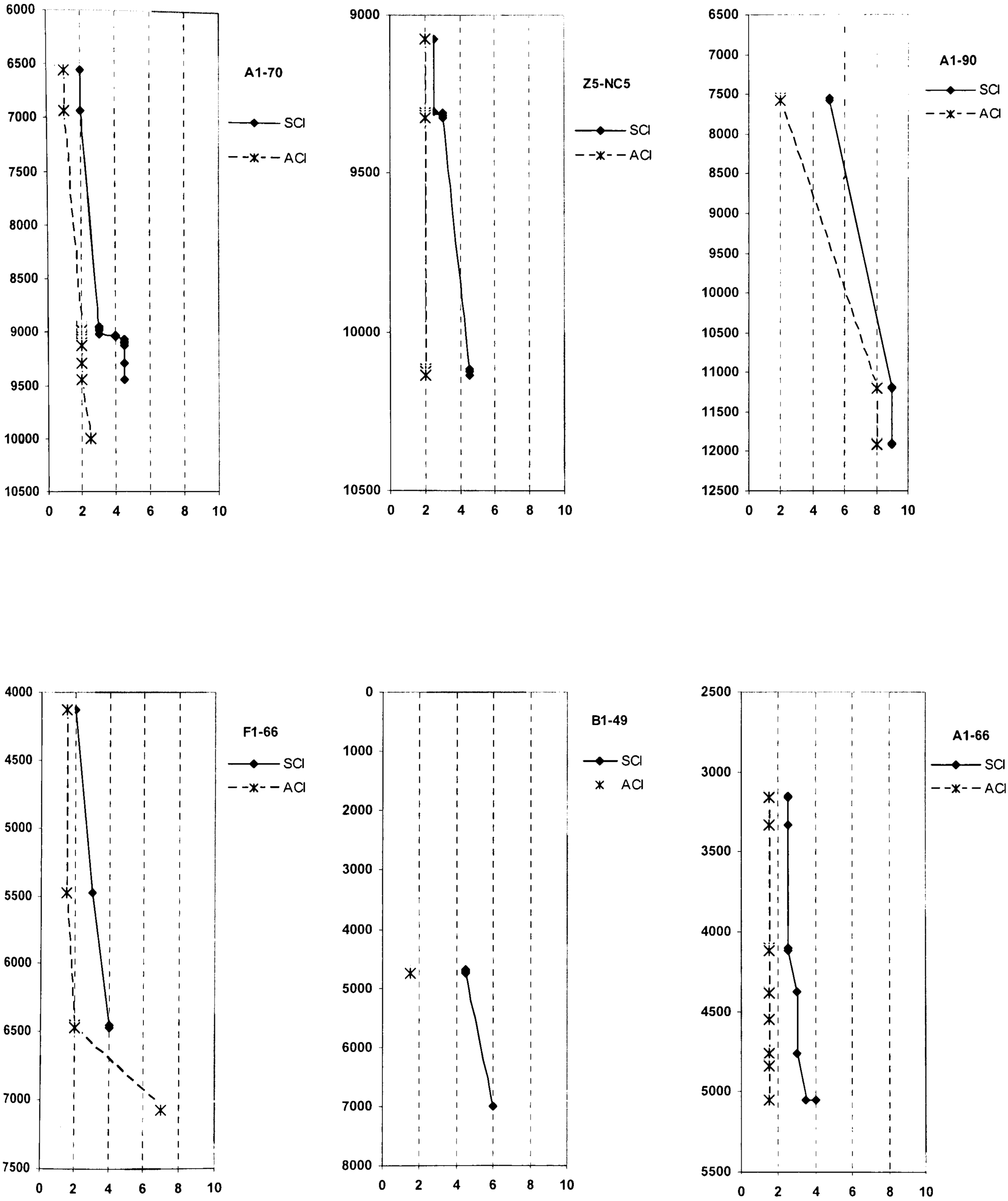

Figure 5.4. Spore Colour and Acritarch Colour Indices versus depth for the investigated wells; (core samples only).

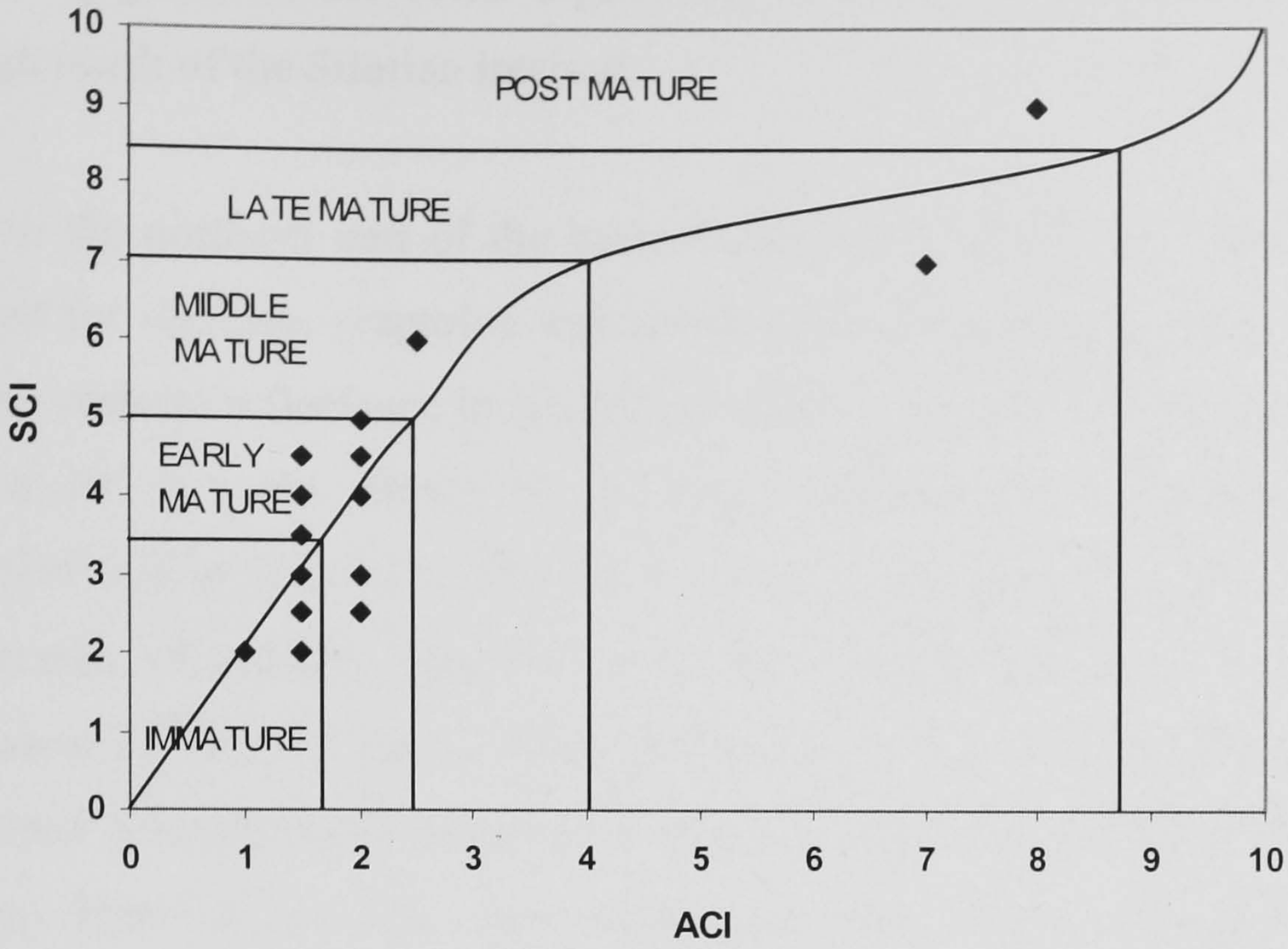

Figure 5.5. Cross plot of Acritarch Colour Index versus Spore Colour Index for the Lower Palaeozoic succession in the Ghadames Basin. The whole data points of ~ 110 samples were superimposed on Collins diagram (1990).

Chitinozoans are also identified in the Silurian shales of the Ghadames Basin (Plate II). Chitinozoa are an extinct group of marine microfossils whose systematic position remains unclear (Jansonius & Jenkins, 1978). They typically have hollow organic-walled tests that are radially symmetrical about a central longitudinal axis and closed at one end, resembling a bottle. The tests of chitinozoans are probably made of polysaccharide-proteinaceous material, similar to that of graptolites (Suchý *et al.*, 2002). The optical reflectance of chitinozoan tests has recently been found to be excellent tool for establishing the thermal maturity of Lower Palaeozoic rocks (Tricker *et al.*, 1992; Marshall, 1995; Obermajer *et al.*, 1996).

The results of the mean reflectance values are given in Table 5.1 and Appendix VII. The graptolites and chitinozoan reflectance values were converted to vitrinite reflectance equivalents (%VR_E) using Cole's (1994) conversion chart (Fig. 5.6) and Tricker's formula [$VR_E = (R_{chit} -0.08)/1.152$] (Tricker *et al.*, 1992) respectively. The results from all wells are shown in Figure 5.7 as plots of VR_E versus well depth in feet. Note these are all the same vertical depth scale to facilitate comparison of

reflectivity gradients and burial depths. The results show clearly a reflectivity gradient through much of the Silurian interval.

In the northern part of the basin wells (A1-70 & B1-NC2 and Z5-NC5) were selected for vitrinite, graptolite and chitinozoan reflectance measurement. The mean random vitrinite reflectance in Aouinet Ouenine Formation of the Devonian age in the well A1-70 is 0.6%. Based on the small percentages of zooclast (chitinozoan), identified within the Upper Silurian Acacus sandstone Formation, the mean random chitinozoan reflectance measured is 0.7% which points to a vitrinite reflectance equivalent (%VR_E) of about 0.54% (Table 5.1 & Fig. 5.7). The underlying strata, of the Lower Silurian lower Tanezzuft 'hot shale' has mean graptolite reflectance values ranging from 0.8 to 0.9%. This reflectance value would correspond to a vitrinite reflectance equivalent (%VR_E) of approximately 0.7–0.8%. These results suggest that the maturity gradients in the wells (A1-70 & B1-NC2 and Z5-NC5) are relatively similar, and that the organic matter within the Middle Devonian Aouinet Ouenine A and Upper Silurian Acacus Sandstone formations is immature. The maturity increases to middle mature within the Lower Silurian 'hot shale'.

Towards the central part of the basin the measured vitrinite reflectance values for the Upper Devonian Tahara and Aouinet Ouenine C in wells A9-NC7 and C1-26 range from 1.0% to 1.3%, suggesting that these formations are within the late mature stage in terms of hydrocarbon generation. However, these results are in disagreement with other maturity parameter such as Tmax and SCI. The high vitrinite reflectance may be due reworked organic matter from older rocks uplifted and eroded during late Silurian time, or measurement of semifusinite instead of vitrinite. Recycled and oxidised phytoclasts are often more abundant within sandy formations.

Depth (ft)	Formation	Age	%R (zooclasts)	n	sd	%Ro	$\%VR_E$
F1-66							
4127	Tahara	U. Devonian		54	0.27	1.0	
6470	upper Tanezzuft	L. Silurian		28	0.16		0.7
7054	lower Tanezzuft	L. Silurian	0.9	41	0.18		0.8
7063	lower Tanezzuft	L. Silurian	0.9	53	0.16		0.8
A1-70							
6561	Aouinet ouenine A	M. Devonian		8	0.1	0.6	
8951	Acacus	U. Silurian	0.7	5	0.03		0.5
10005	upper Tanezzuft	L. Silurian	0.8	37	0.13		0.7
10181	lower Tanezzuft	L. Silurian	0.8	44	0.17		0.7
A9-NC7							
5705	Tahara	U. Devonian		47	0.37	1.0	
5712	Tahara	U. Devonian		53	0.22	0.9	
5733	Tahara	U. Devonian		38	0.23	0.8	
5773	Tahara	U. Devonian		51	0.22	1.0	
5813	Tahara	U. Devonian		40	0.29	1.2	
Z5-NC5							
9074	Acacus	U. Silurian	0.7	6	0.17		0.5
10124	upper Tanezzuft	L. Silurian	1	19	0.18		0.8
10450	lower Tanezzuft	L. Silurian	0.9	28	0.16		0.8
M2-NC7							
6227	Tahara	U. Devonian		8	0.05	0.7	
6247	Tahara	U. Devonian		30	0.32	0.8	
C1-26							
6488	Aouinat ouenine C	U. Devonian		45	0.24	1.3	
6494	Aouinat ouenine C	U. Devonian		55	0.23	1.1	
6500	Aouinat ouenine C	U. Devonian		66	0.3	1.1	
6505	Aouinat ouenine C	U. Devonian		43	0.2	1.3	
A1-90							
7552	Tahara	U. Devonian		43	0.23	1.2	
7569	Tahara	U. Devonian		56	0.26	1.2	
11185	Acacus	U. Silurian	1.4	25	0.16		1.2
12700	lower Tanezzuft	L. Silurian	1.6	15	0.5		1.3
B1-NC2							
10099	upper Tanezzuft	L. Silurian	0.97	5	0.13		0.8
B1-49							
1434	Aouinat ouenine C	U. Devonian		38	0.31	1.2	
1445	Aouinat ouenine C	U. Devonian		35	0.24	1.2	
2132	upper Tanezzuft	L. Silurian	1.2	28	0.18		1.0
2135	upper Tanezzuft	L. Silurian	1.2	49	0.45		1.0
2301	lower Tanezzuft	L. Silurian	1.6	10	0.5		1.3
A1-66							
3153	Aouinat ouenine C	U. Devonian		43	0.2	0.9	
5054	lower Tanezzuft	L. Silurian	0.7	13	0.12		0.6

Table 5.1. Reflectivity data from the Lower Palaeozoic well sections: %Ro mean random vitrinite reflectance, $\%VR_E$ mean equivalent vitrinite reflectance based on graptolites or chitinozoans, n = number of measurements.

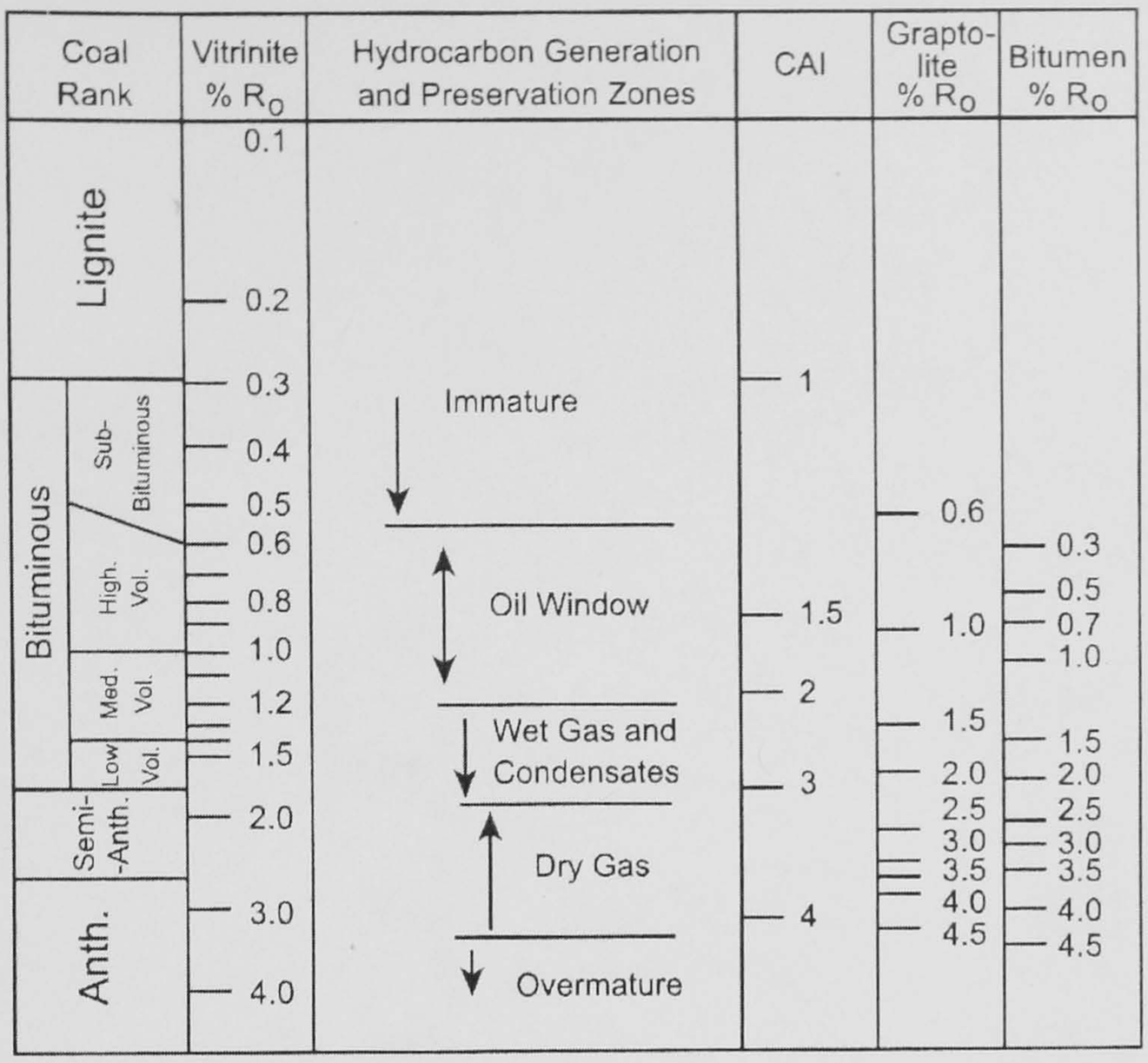

Figure 5.6. Correlation between vitrinite, graptolite reflectance and hydrocarbon generation and preservation zones (from Cole, 1994).

Lower maturity Upper Devonian shales were encountered in the well M2-NC7, about 40 km north of wells A9-NC7 and C1-26. At this site the vitrinite reflectance for core samples from Upper Devonian Tahara Sandstone Formation, was based on large homogenous vitrinite particles (Plate II) and ranged from 0.7% to 0.8%, suggesting that the Upper Devonian section here early to mature.

Chitinozoan and graptolites from Lower Silurian formations in the deepest part of the basin well (A1-90) have VR_E values of 1.15–1.3% (Table 5.1). Some highly reflectance fragments of organic matter of apparently allochthonous nature have been recognized, probably derived from older strata and transported into Silurian shale facies by turbidity currents (e.g. Suchy *et al.*, 2002). These have values higher than those from the northern part of the basin are attributed to present-day burial depth (Fig. 5.7).

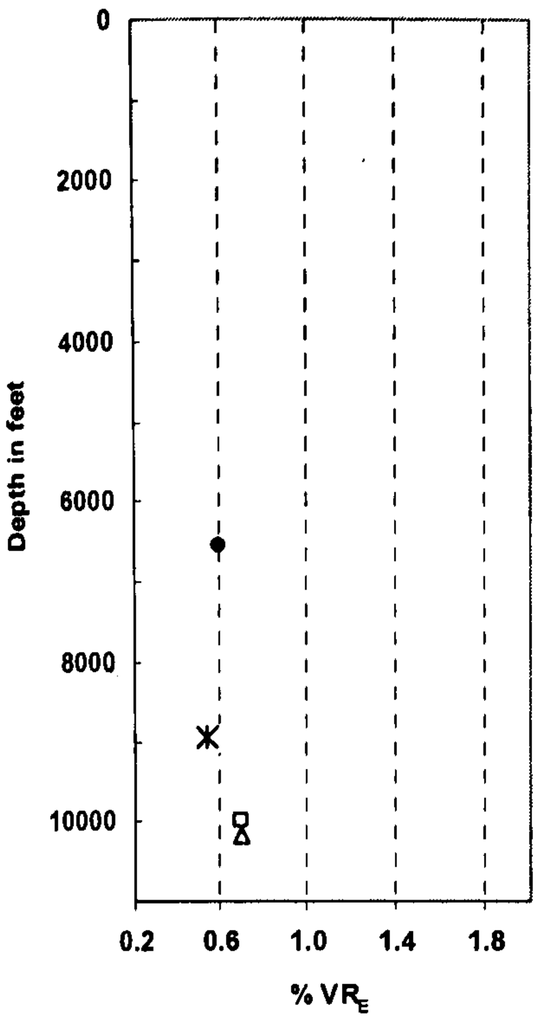
A1-70
● Aouinet Ouenine
✕ Acacus
Depth in feet
0
2000
4000
6000
8000
10000
0.2
0.6
1.0
1.4
1.8
% VR_E

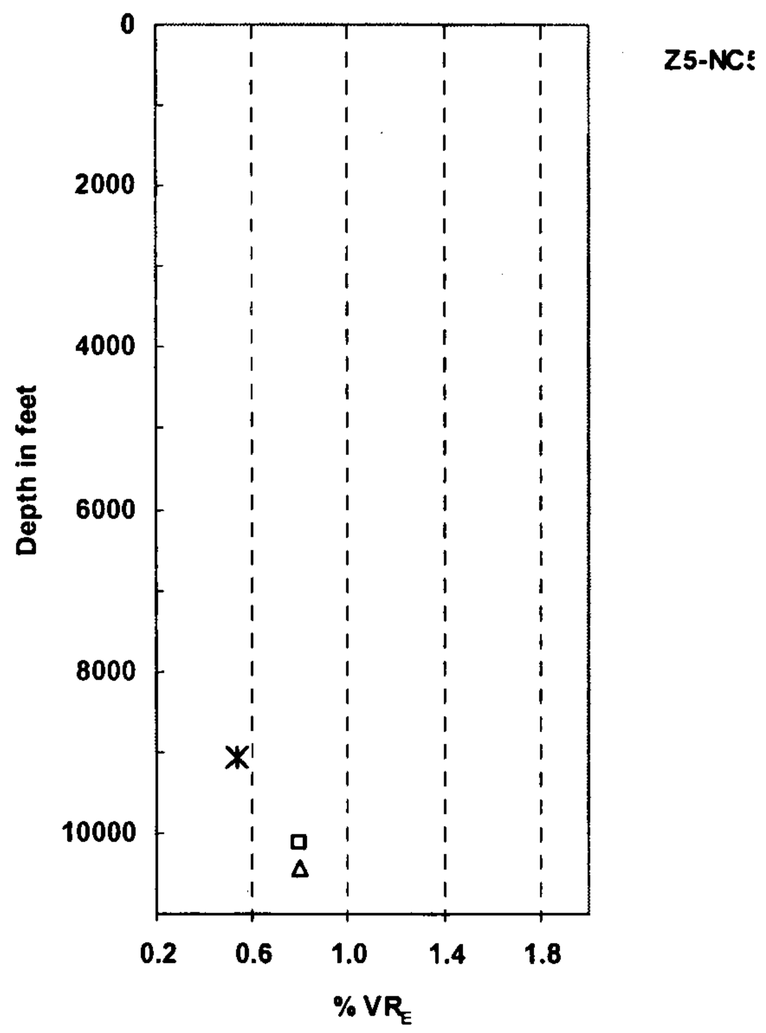
Z5-NC
Depth in feet
0
2000
4000
6000
8000
10000
0.2
0.6
1.0
1.4
1.8
% VR_E

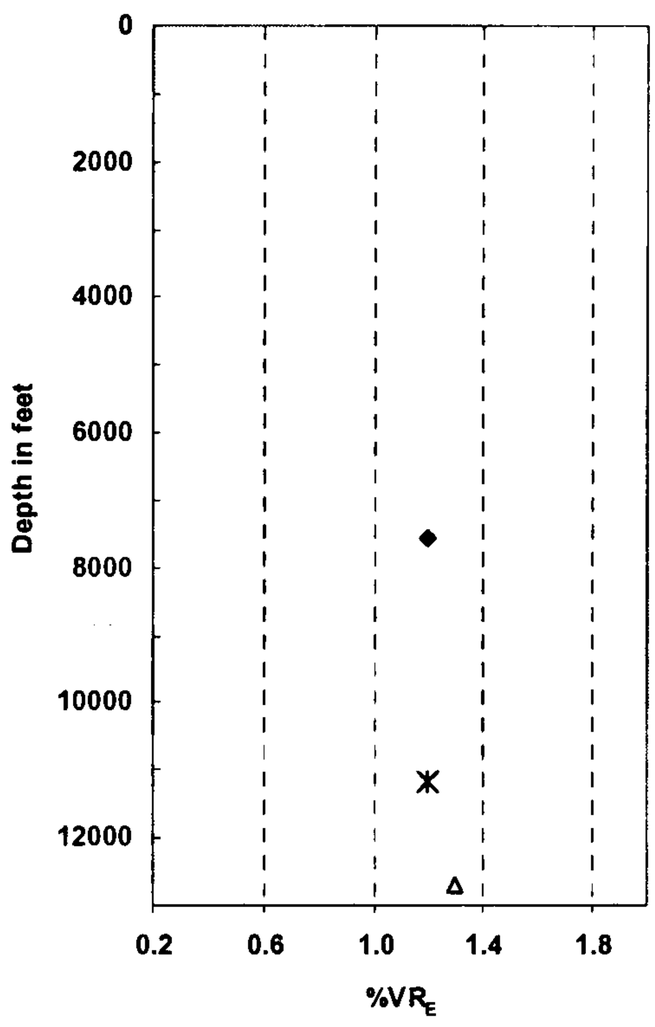
A1-90
Depth in feet
0
2000
4000
6000
8000
10000
12000
0.2
0.6
1.0
1.4
1.8
%VR_E

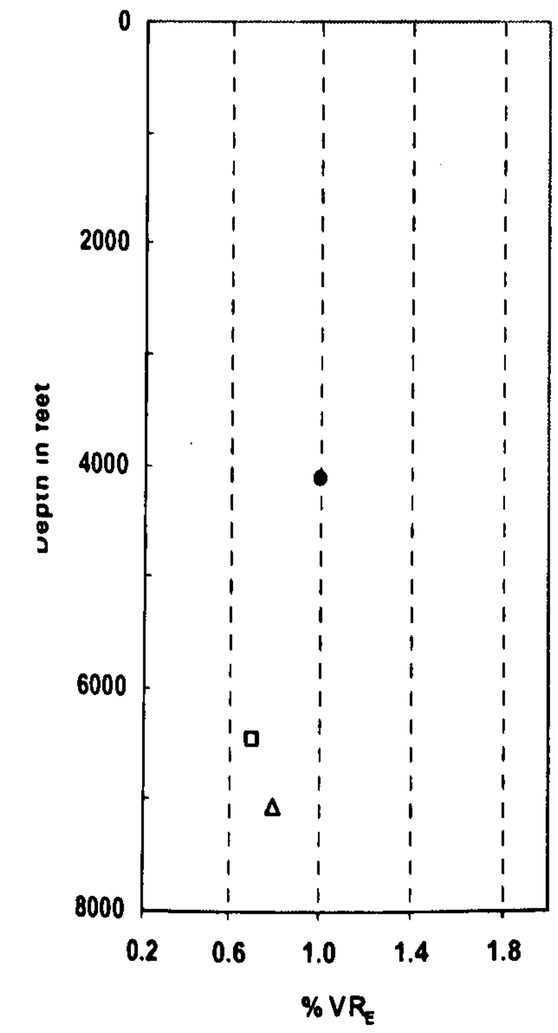
F1- 66
● Tahara
□ upper Tanezzuft 'cool-shale'
△ lower Tanezzuft 'hot-shale'
Depth in feet
0
2000
4000
6000
8000
0.2
0.6
1.0
1.4
1.8
% VR_E

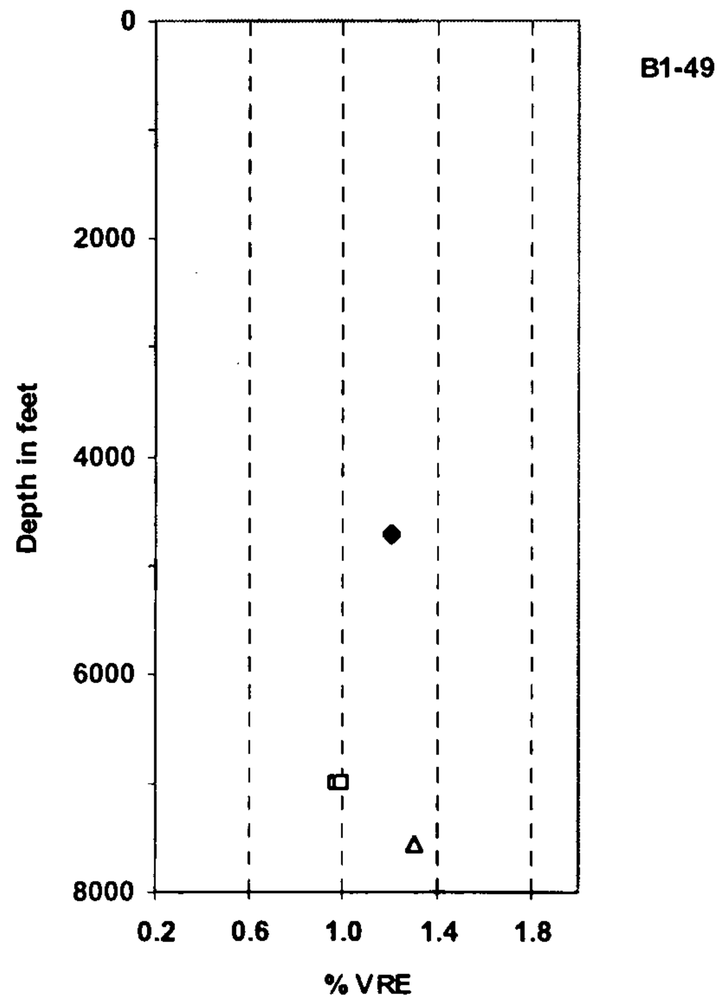
B1-49
Depth in feet
0
2000
4000
6000
8000
0.2
0.6
1.0
1.4
1.8
% VRE

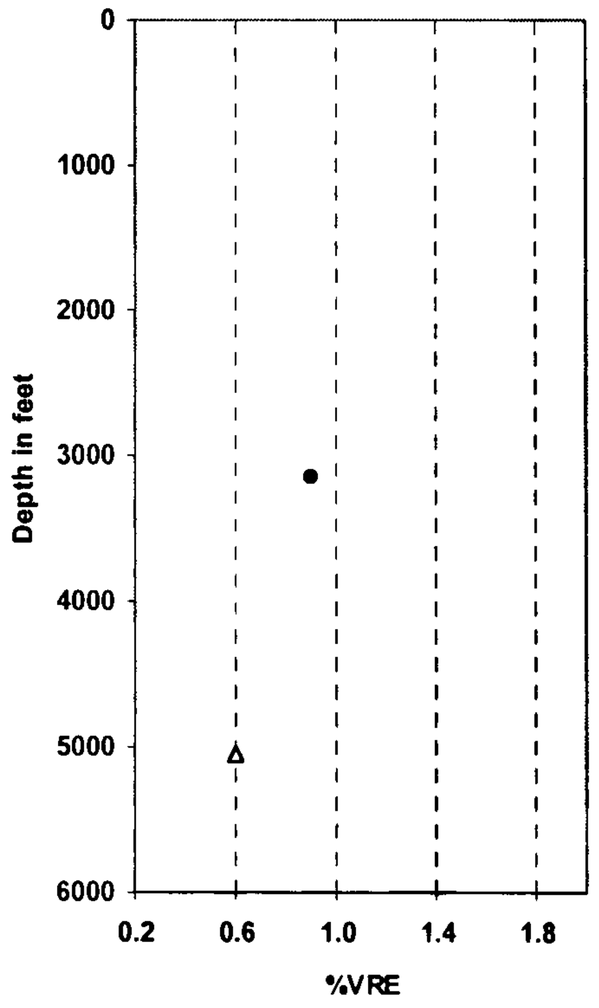
A1-66
Depth in feet
0
1000
2000
3000
4000
5000
6000
0.2
0.6
1.0
1.4
1.8
%VRE

Figure 5.7. Vitrinite and equivalent vitrinite reflectances versus depth for the investigated well sections. Note a significant numbers of Lower Silurian samples were processed, but few of them contain chitinozoan particles.

The measured $\%VR_E$ for Lower Silurian formations in the southeastern part the basin in well F1-66 is comparable to those in the North (Table 5.1& Fig. 5.7). It is noteworthy that there is lack of any relationship between measured reflectance and the present-day burial depth in the in well F1-66 compared to that located in the North. This indicates that the maturity levels are not the result of present-day burial. Further to the South, with thinning of the Palaeozoic strata, the maturity of Lower Silurian Tanezzuft Formation 'hot-shale' decreases at well A1-66. The graptolite reflectance (vitrinite equivalent) measured is reduced to 0.6%.

In the southern part of the basin close to Al-Qarqaf uplift, samples from Tahara and Tanezzuft formations in well B1-49 were selected for vitrinite and zooclast reflectance based on the large percentage of zooclasts (chitinozoan and graptolite fragments) for Silurian formation. The mean VR_E values range from 0.97% to 1.3%, suggesting that the maturity increases with increasing depth of burial, from early mature in the Upper Devonian Aouinet Ouenine C Formation to late mature in the Lower Silurian lower Tanezzuft Formation. The Silurian source rock has a higher maturity than is expected for such shallow depths on the southern flank of Ghadames Basin. There are two possibilities, either:

- These rocks were in the past buried at greater depths and were later uplifted and a thick section removed.
- Or the geothermal gradient was higher in the past.
- Or the deposition took place on a topographic palaeo-high with shallower depth, accompanied by increasing susceptibility of the sediment to erosion and recycling.

5.5 Molecular Maturity Parameters

Biomarker analysis has become a routine tool for the evaluation of maturity (Mackenzie, 1984; Seifert & Moldowan, 1986). The most widely used maturity parameters are steranes and hopanes. These parameters use the relative abundances of two stereoisomers, which change as the more thermally stable (non-biological) isomer

increases relative to the isomer with the original biologically-inherited stereochemistry. Originally, this process was widely assumed to reflect direct isomerisation or epimerisation of the free biomarker in the bitumen (e.g. Seifert & Moldowan, 1980). However, studies providing quantitative data have shown that the mechanisms behind the maturity parameter are more complicated; relative rates of released of kerogen-bound biomarkers (generation), and their thermal stabilities (cracking) are also important (Farrimond, 1998, p.1181). In addition to the saturated hydrocarbons, Radke (1987) reviewed the use aromatic hydrocarbons. He found that the aromatic distributions change in a regular fashion with increasing maturity up to a high level (Ro = 2%), and are thus useful tools in maturity studies.

In this study 23 core samples from lower Palaeozoic succession were selected for molecular geochemistry analysis (Chapter 4.0). In the following section, the maturity parameter results have been compared with the optical maturity data.

5.5.1 Steranes and Triterpanes

The evaluation of thermal maturity of the Silurian and Devonian source rock samples in this study was achieved using the following biomarker parameters: the sterane isomerisation at C-20: 20S/(20S + 20R) (%) and αββ/(αββ + ααα) (%). Ts/(Ts+Tm), C_{29}Ts/(C_{29}Ts+C_{29} αβ hopanes) and C_{30} diahopane/(C_{30} diahopane + C_{30} αβ hopane). The results of these and other bulk and optical parameters are given in Table 5.2.

Well	Depth	Formation	%Ro	SCI		20S/ 20S+20R	ββ/αα+ββ	Ts/Ts+Tm	C_{29}Ts/(C_{29}Ts+C_{29}hop	C_{30}diahop/ (C_{30}hop+ C_{30}diahop)	Triaromatic	MPI-1	Rc
B1-NC2	10108'	lower Tanezzuft	0.8	4.5	447	0.47	0.60	0.64	0.48	0.22	0.40	0.60	0.76
A1-70	10005'	lower Tanezzuft			445	0.52	0.62	0.46	0.44	0.20	0.50	0.56	0.74
A1-70	10155'	lower Tanezzuft	0.7		441	0.49	0.54	0.39	0.24	0.12	0.70	0.34	0.61
F1-66	7053'	lower Tanezzuft	0.9		445	0.50	0.60	0.73	0.32	0.18	0.86	0.71	0.82
F1-66	7054'	lower Tanezzuft	0.9		452	0.50	0.59	0.63	0.39	0.00	0.91	0.68	0.81
F1-66	7065'	lower Tanezzuft	0.9		450	0.54	0.59	0.58	0.33	0.00			
A1-66	5054'	lower Tanezzuft	0.7	4	435	0.50	0.47	0.52	0.28	0.09	0.30	0.76	0.85
F1-66	6473'	upper Tanezzuft	0.6	4	434	0.47	0.46	0.51	0.31	0.11	0.22	0.70	0.83
A1-90	11921'	upper Tanezzuft		9		0.47	0.48	0.42	0.18	0.07	0.56	0.90	0.94
Z5-NC5	10124'	upper Tanezzuft	0.8	4.5	444	0.51	0.61	0.57	0.36	0.15	0.39	0.70	0.82
B1-49	2135 m	upper Tanezzuft	1.0	6		0.46	0.47	0.45	0.18	0.07	1.00	0.88	0.93
A1-70	9049'	upper Tanezzuft	0.5	4	437	0.39	0.38	0.65	0.51	0.18	0.32	0.59	0.75
A9-NC7	5718'	Tahara	0.8	4.5	437	0.45	0.36	0.38	0.31	0.08	0.76	0.62	0.76
A9-NC7	5733'	Tahara	0.8	4.5	438	0.45	0.47	0.47	0.36	0.06			
C1-26	6488'	Tahara	1.3	5	440	0.61	0.43	0.42	0.29	0.10	0.46	0.60	0.76
C1-26	6494'	Tahara	1.1	5	440	0.60	0.47	0.58	0.34	0.11	0.39	0.60	0.76
C1-26	6500'	Tahara	1.1	5	440	0.57	0.47	0.58	0.36	0.10	0.40	0.60	0.76
M2-NC7	6227'	Tahara	0.7	4.5	433	0.60	0.45	0.33	0.28	0.12	0.33	0.65	0.79
M2-NC7	6251'	Tahara		4.5	435	0.55	0.41	0.39	0.28	0.09	0.47	0.58	0.75
A1-90	7569'	Tahara	1.2	5	442	0.63	0.51	0.54	0.39	0.16	0.62	0.62	0.77
F1-66	4300'	Tahara			421	0.22	0.25	0.47	0.31	0.08	0.36	0.26	0.56
B1-49	1434 m	Tahara	1.2	4.5	442	0.62	0.52	0.74	0.47	0.14	0.47	0.63	0.78
A1-66	3153'	Tahara	0.9	2.5	430	0.36	0.34	0.31	0.37	0.05	0.19	0.60	0.76

Table 5.2. Biomarker and microscopy maturity parameter for Silurian and Devonian samples.

Key:

%Rc = 0.4+(MP1-1)*0.6

Triaromatic = (C_{20} traromatic)/ (C_{20} +C_{28} S+R) triaromatic

MPI-1 =1.5*(3-MP+2-MP)/(P+9-MP+1-MP)

Cross plots of 20S/(20S + 20R) and (αββ/(αββ+ααα)) steranes versus measured %Ro (vitrinite equivalent) for Lower Silurian samples (Fig. 5.8) show that the sterane maturity parameters are in agreement with graptolite and chitinozoan reflectances (vitrinite equivalents), with r^2 values of 0.63 and 0.83, respectively.

Based on the percentages of C_{29} 5α(H), 14α(H), 17α(H) 20S steranes and C_{29} 5α(H), 14β(H), 17β(H) (20S+20R) (Fig. 5.8), it is suggested that not all the samples reached their end-point values; the ratios range from 0.39 to 0.52 and 0.38 to 0.62 respectively. The upper Tanezzuft Formation sample from well A1-70 (9049') is early mature as indicated by sterane maturity parameters, vitrinite reflectance, SCI and Tmax (Table 5.2). Mackenzie *et al.* (1980) indicate that the petroleum generation begins at %20S values of about 40%, so based on this statement, the rest of the lower Silurian samples are mature. A slightly higher maturity is recorded within the lower Tanezzuft Formation from well F1-66, located in the southern part of the basin.

The 20S/(20S + 20R) and αββ/(αββ+ααα) steranes ratios of Lower Silurian samples from wells (B1-49 & A1-90) range from 0.46 to 0.47 and 0.47 to 0.48 respectively. Vitrinite reflectance equivalent measured for these samples are more than 1% (Table 5.2), suggesting a disagreement between the sterane maturity parameters and vitrinite reflectance at higher maturity. The main transition in the %20S steranes parameter occurs in the Tmax range of 433–444°C, with higher maturity values of the %20S fluctuating due to the low concentrations of both isomers. There is no firm evidence for inversion of this parameter (Farrimond *et al.*, 1998), sometimes seen under high heating rates (e.g. Lewan *et al.*, 1986; Bishop & Abbott, 1993). The %αββ steranes parameter increases rapidly in the Tmax range of 441–453°C, and behaves erratically at greater maturity (Farrimond *et al.*, 1998).

Cross plots of 20S/(20S + 20R) and (αββ/(αββ+ααα)) steranes versus measured %Ro (Figure 5.9) for the Upper Devonian samples show that the sterane maturity parameters are poorly correlated with vitrinite reflectance; the r^2 values are only 0.36 and 0.22, respectively.

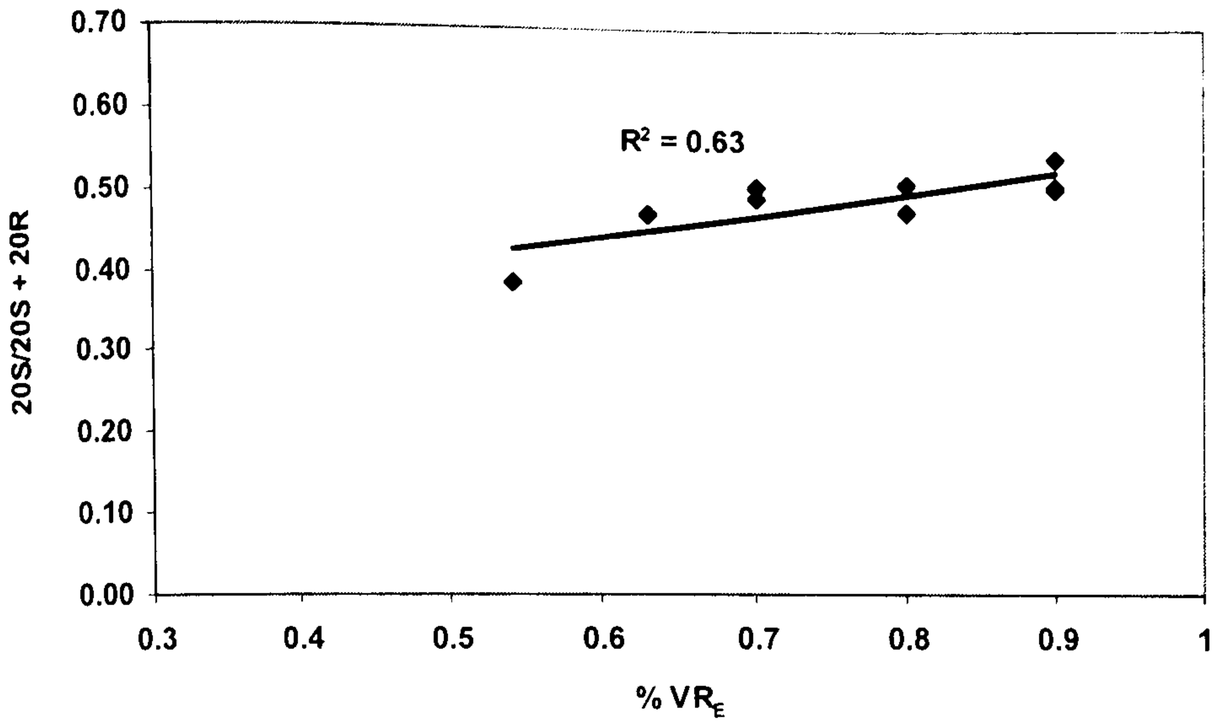

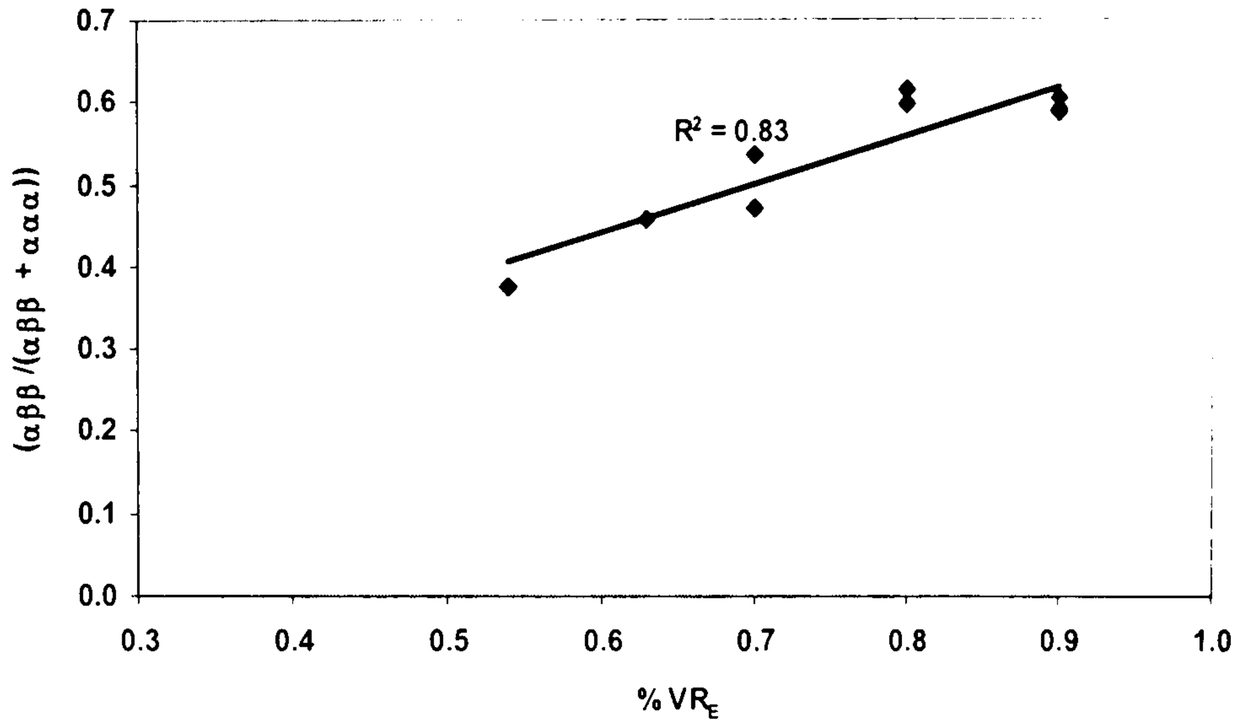

Figure 5.8. Cross plots of 20S/20S+20R and αββ/(αββ+ααα) versus VR_E (graptolite and chitinozoan vitrinite equivalent reflectance) for Lower Silurian samples.

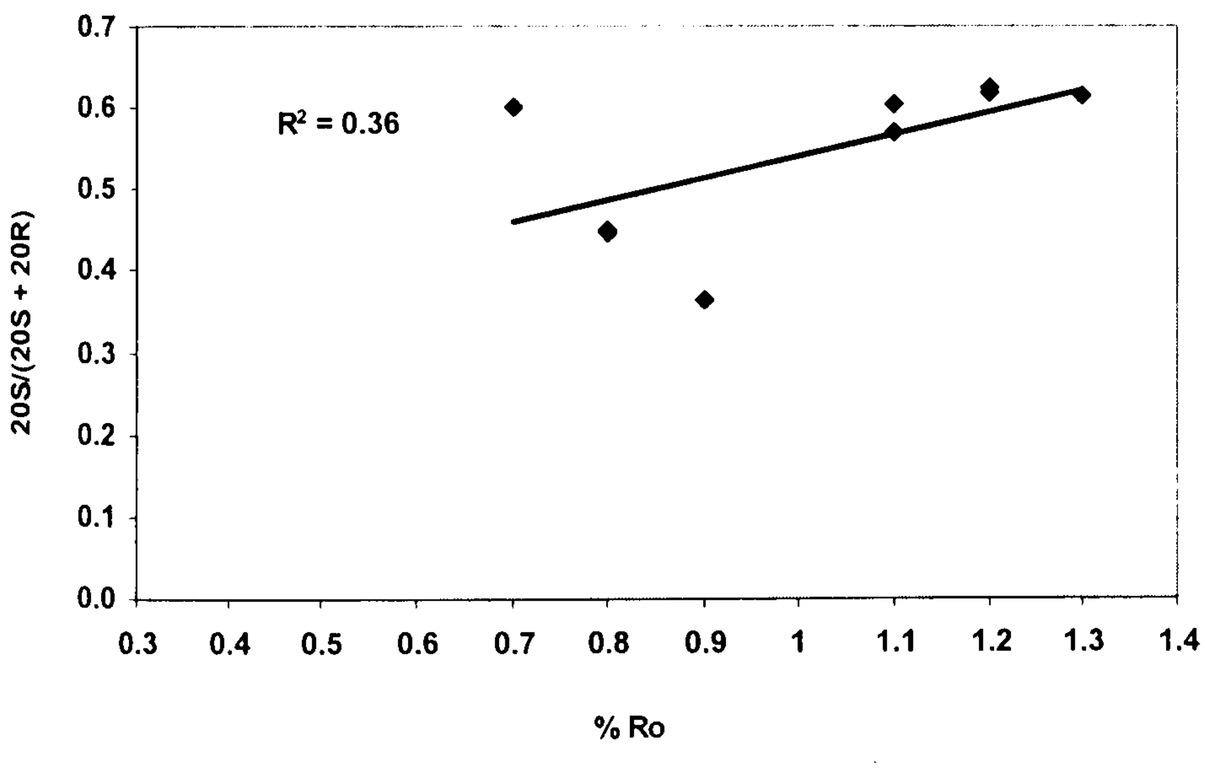

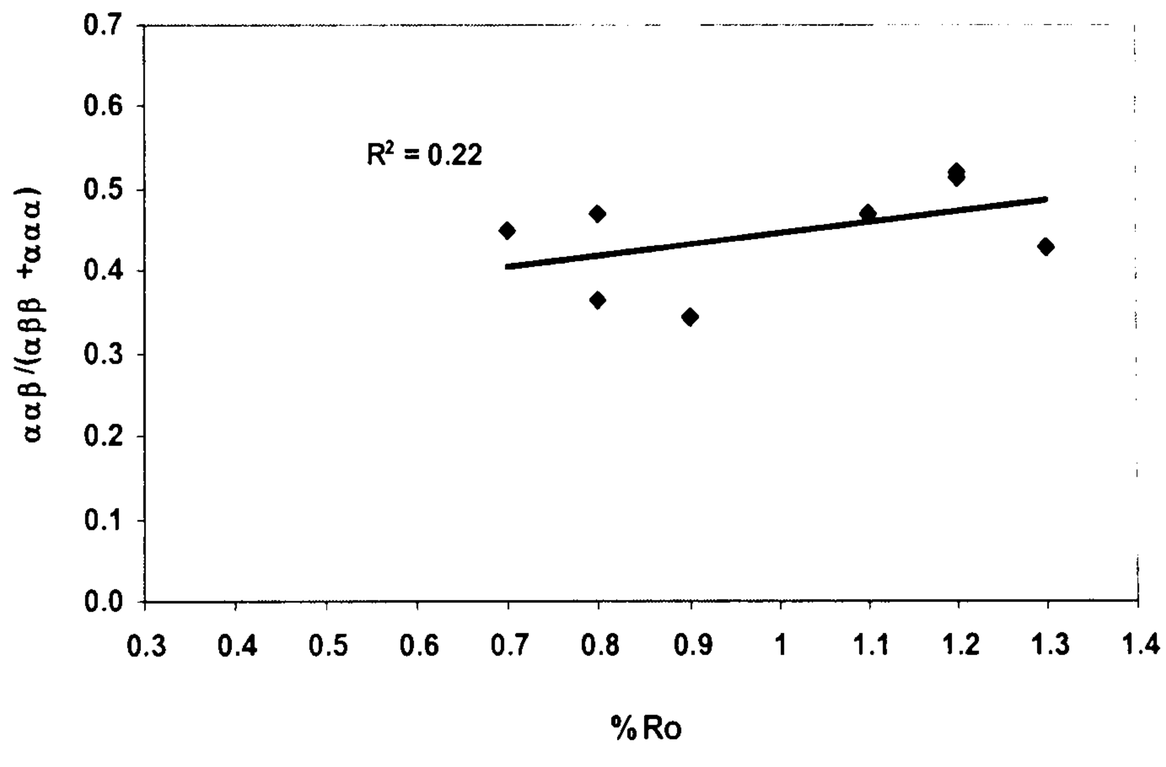

Figure 5.9. Cross plots of 20S/20S +20R and αββ/(αββ +ααα) versus %Ro for Upper Devonian samples.

The relationships between both 20S/(20S + 20R) and αββ/(αββ+ααα) steranes and Tmax for Upper Devonian samples (Fig. 5.10) show strong positive correlations (r^2 values are 0.74 and 0.81, respectively). This suggests that the vitrinite reflectance values for Upper Devonian samples are probably overestimated, due to reworked organic matter from older rocks.

The sterane maturity parameter, SCI and Tmax values (Table 5.2) show that the Upper Devonian samples from wells A1-66 (4300') and F1-66 (3154') are immature. The other Upper Devonian samples from wells A9-NC7, C1-26, M2-NC2, A1-90 and B1-49 are within the mature zone with respect to the hydrocarbon generation window.

The Ts/(Ts + Tm), C_{29}Ts/(C_{29}Ts + C_{29} αβ hopanes) and C_{30} diahopane/(C_{30} diahopane + C_{30} αβ hopane) biomarker maturity ratios, are both maturity and source dependent, these ratios should only be used with caution (Moldowan *et al.*, 1986; Rullkotter & Marzi, 1988). No obvious correlation occurs between most of the hopane maturity parameter ratios and vitrinite reflectance, Tmax or SCI (Table 5.2). Most of the hopane maturity parameters cannot therefore be used to assess the maturity of the Silurian and Devonian source rock samples because they are strongly affected by the facies differences. Except for Upper Devonian samples, cross plots of Ts/(Ts +Tm) and Tmax (Fig. 5.11) for these samples show a positive correlation of (r^2 = 0.71)

5.5.2 Aromatic Compounds

This section presents the application of a suite of maturity ratios derived from the distribution of triaromatic steroid hydrocarbons and phenanthrenes,. The values of these parameters are given in Table 5.2.

The abundance of C_{20} triaromatic-steroid hydrocarbon relative to C_{28} (S+R) was employed to evaluate the maturity of source rock samples. The values of this ratio range from 0.22-1.0 for the Silurian rock samples indicating that there is some variability in the maturity of the different Silurian samples. The triaromatic-steroid ratio is relatively consistent with the equivalent vitrinite reflectance, SCI and Tmax as seen in (Table 5.2).

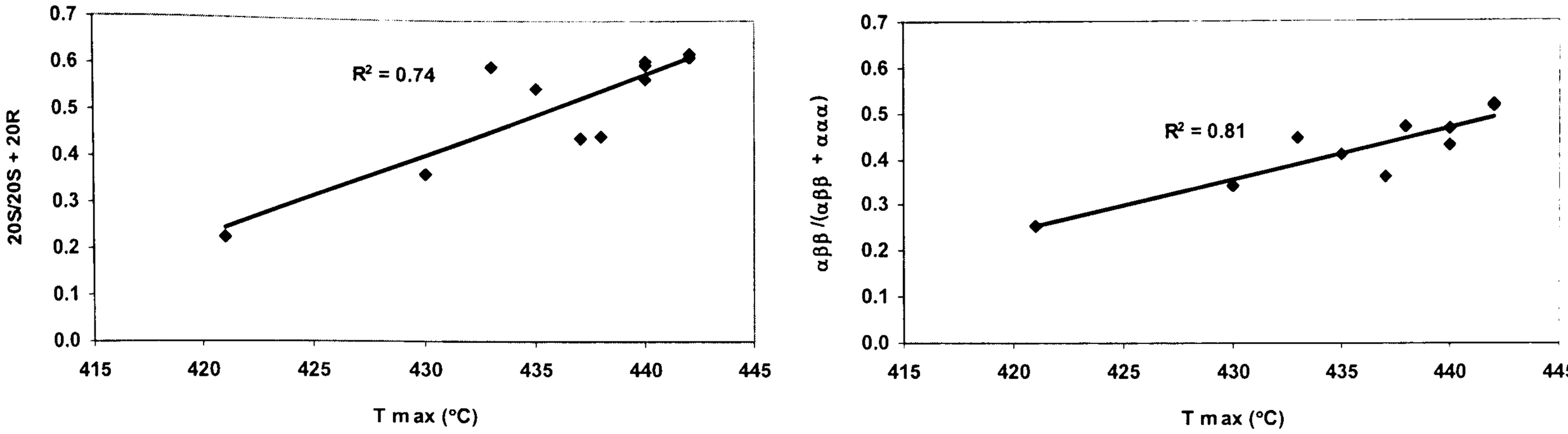

Figure 5.10. Cross plots of 20S/(20S + 20R) and αββ/(αββ+ααα) steranes versus Tmax, for Upper Devonian samples.

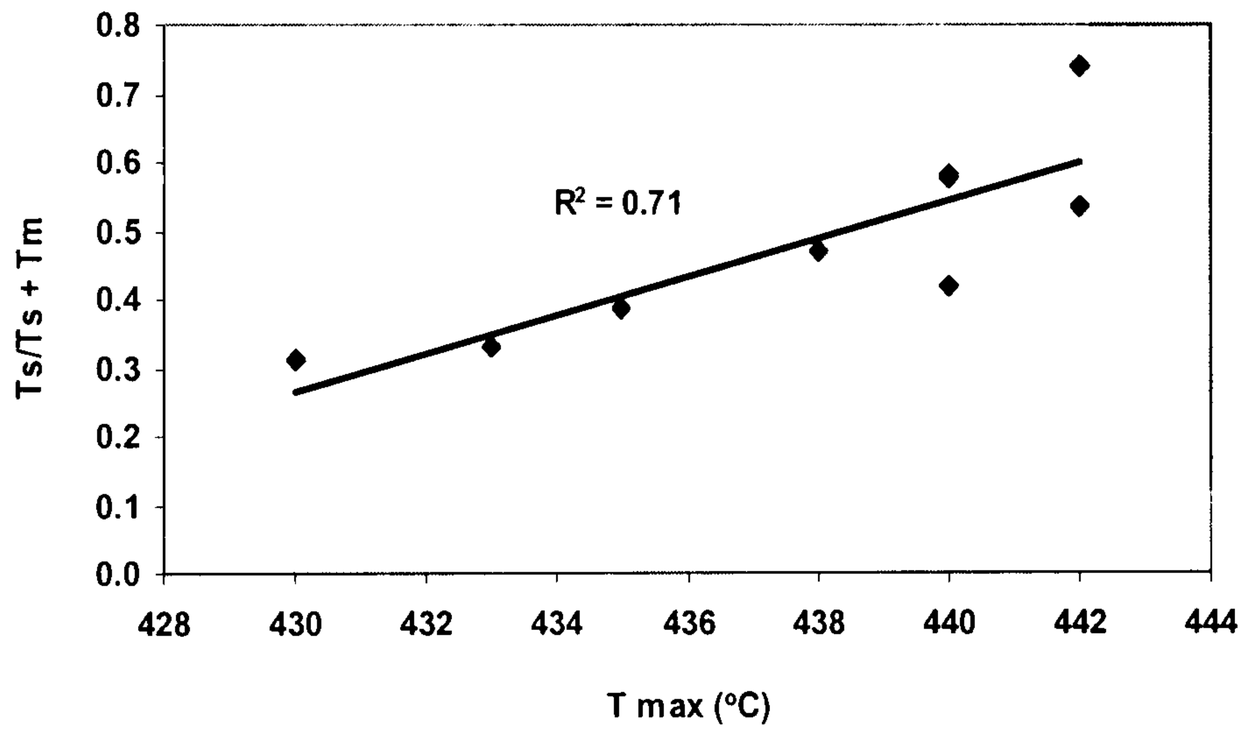

Figure 5.11. Cross plot of Ts/Ts + Tm versus Tmax for Upper Devonian samples.

Cross plots of triaromatic-steroid versus VR_E and Tmax (Fig. 5.12) for Lower Silurian samples show moderate positive correlations (r^2 = 0.66 and 0.53 respectively). The Silurian 'hot shale' samples are more generally mature compared to the Silurian 'cool shale'. The Silurian samples from wells F1-66 (7053', 7054') and B1-49 (2135m) display the highest maturity values; these wells are located in the southern part of the Ghadames Basin.

The triaromatic ratio for Upper Devonian samples ranges from 0.19 to 0.76. These values are inconsistent with measured vitrinite reflectance (Table 5.2), indicating that the vitrinite reflectance has been overestimated, probably due to reworked vitrinite or semifusinite.

The maturity values based on phenanthrenes (MPI-1) and the calculated reflectance (VRc%) estimates using the formula proposed by Radke *et al.* (1986) are shown in Table 1.6. Cross plots of measured chitinozoan and graptolite reflectance vitrinite equivalent versus MPI-1 and %Rc (Fig. 5.13) show that the phenanthrene maturity parameters are in agreement with the measured graptolite and chitinozoan vitrinite equivalent reflectance. These results demonstrate a general linear relationship (r^2 = 0.83) within the vitrinite equivalent (Rm) range of 0.7 to 1.0%. This is in agreement with Radke and Welte (1983) who found a linear relationship between MPI-1 and Rm within the 0.6–1.3% Rm interval, allowing the calculation of mean vitrinite reflectance (Rc), for coals and Type III kerogen-containing rock samples.

The MPI-1, Rc and Rm results (Table 5.2) show no obvious correlation for Upper Devonian samples. This may indicate that the vitrinite reflectance has been overestimated, probably due to reworked vitrinite or semifusinite.

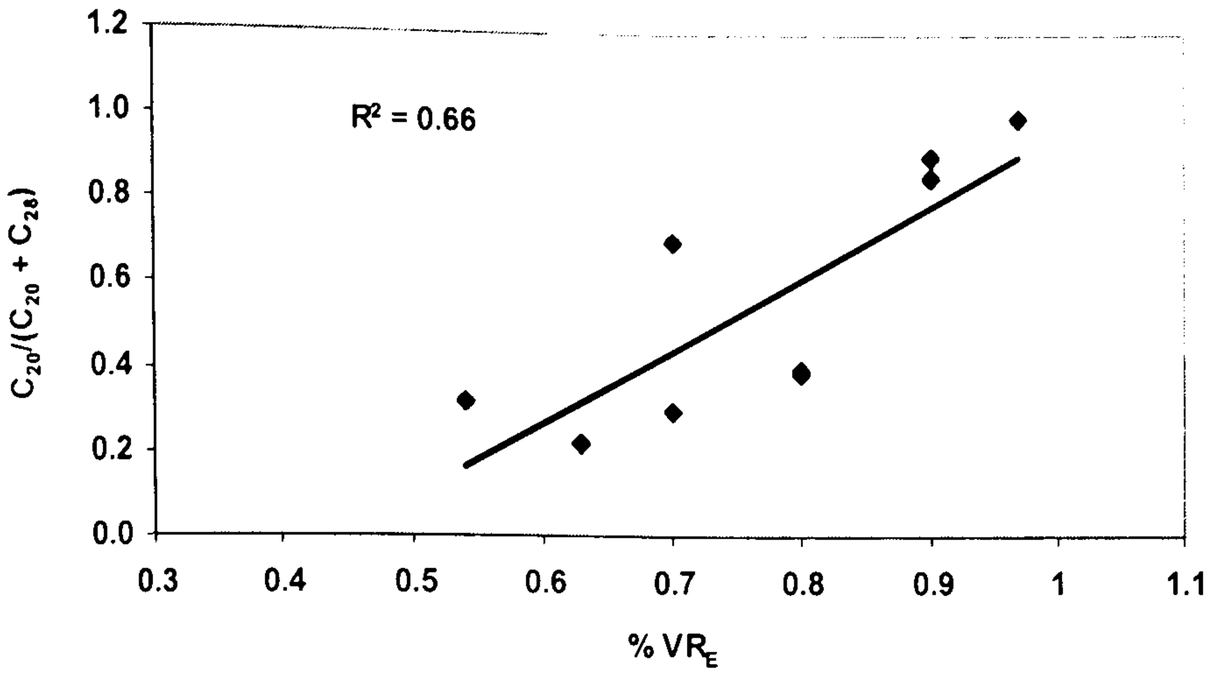

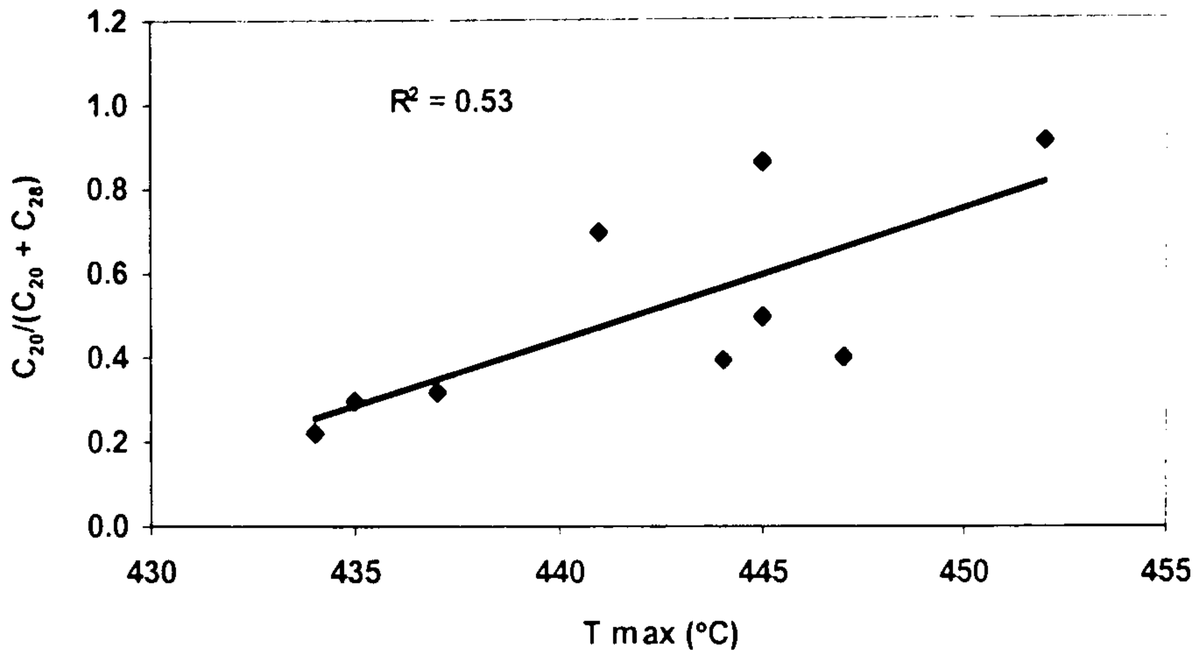

Figure 5.12. Cross plots of C20/C20 +C28 versus $\%VR_E$ (graptolite and chitinozoan vitrinite equivalent reflectance) and Tmax for Lower Silurian samples.

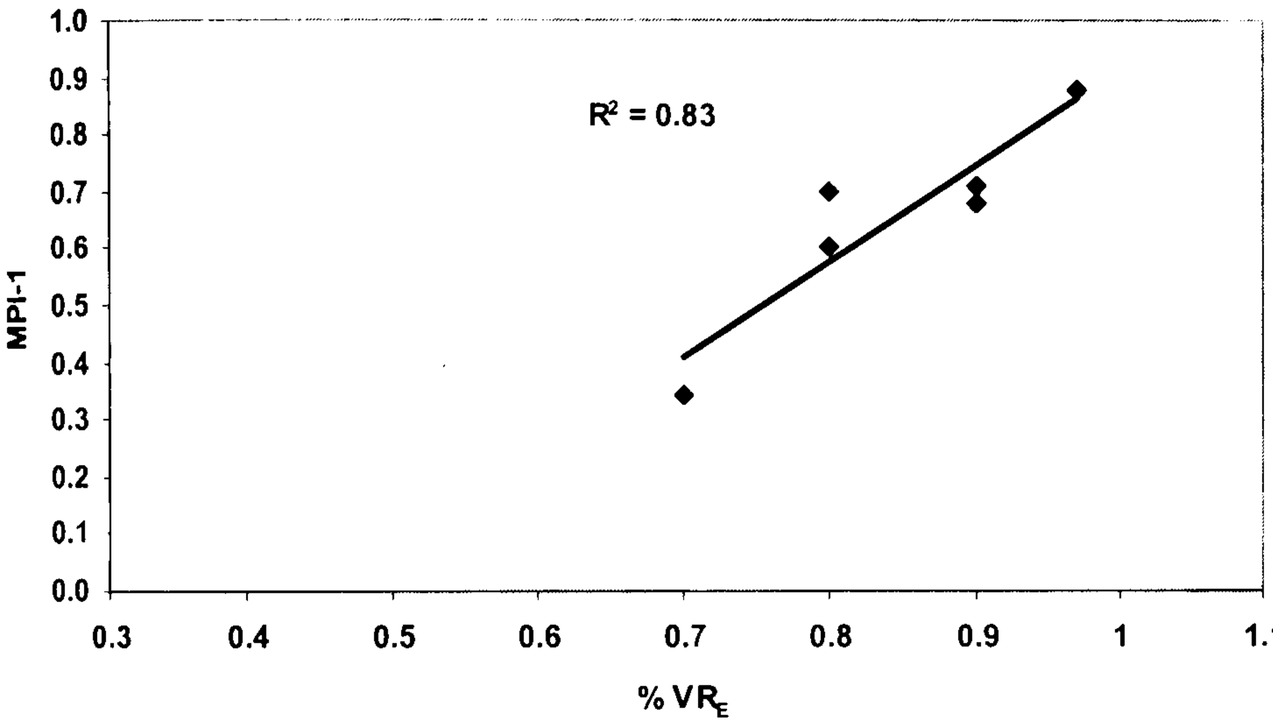

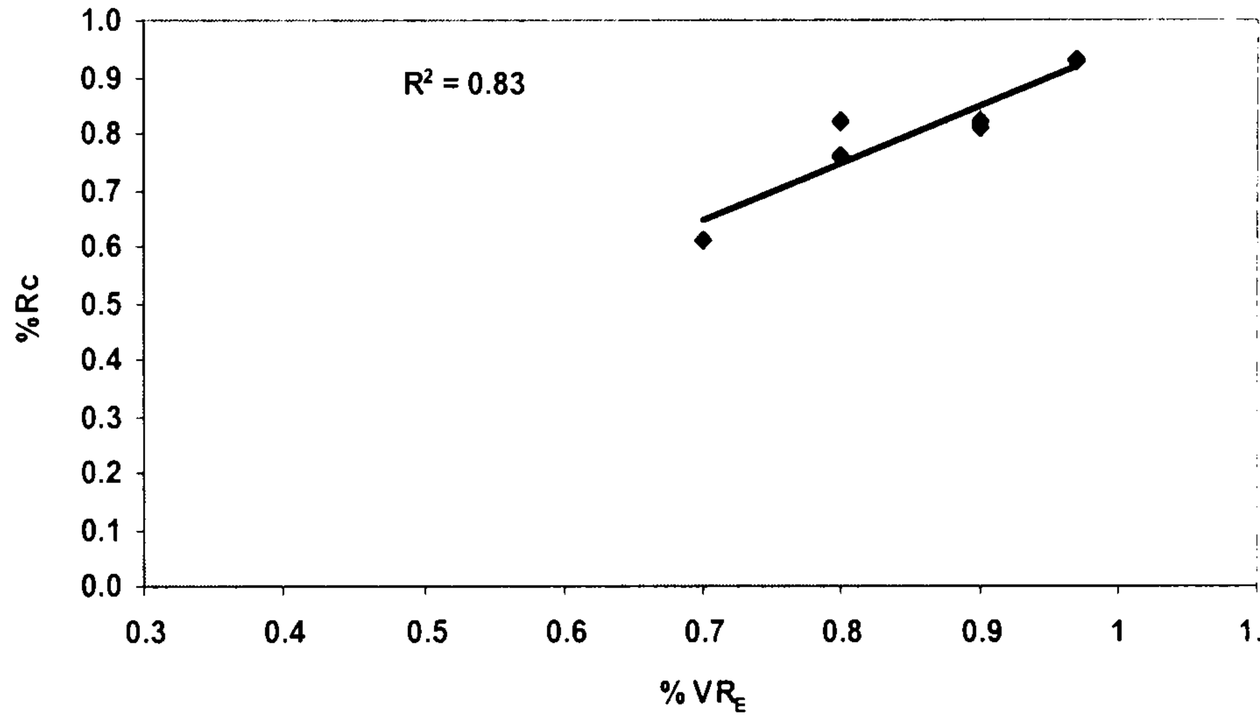

Figure 5.13. Cross plots of MPI-1 and %Rc versus $\%VR_E$ (graptolite and chitinozoan vitrinite equivalent reflectance) for Lower Silurian samples.

5.6. Burial history and Timing of Oil Generation

Burial history reconstruction performed by Dardour (2004) for wells THD-1B and F1-66, located in the central (Algerian part) and southeastern parts of the Ghadames Basin respectively, shows two cycles of subsidence separated by uplift and cooling during Permian-Triassic (Fig. 5.14). The first cycle occurred during the Palaeozoic and is characterized by continuous and rapid burial until late Carboniferous Hercynian inversion and subsequent uplift and erosion, associated with uplift of the Al-Qarqaf Arch to the South. The pre-Hercynian burial and temperature are largely determined by the amount of eroded section. The burial depth reached by the rocks today is result of the second phase of subsidence that occurred after Triassic-Jurassic rifting.

Maturity data and burial history analyses indicate that the Lower Silurian 'hot shale' generated hydrocarbons, but the latter indicates they reached their highest maturity only relatively recently (i.e., during Late Cretaceous-Tertiary). The level of organic maturity reached prior to the Hercynian uplift and erosion is directly proportional to the depth of burial at that time. The early episode of hydrocarbon generation is shown by the position of the modelled hydrocarbon generation window in Figure 5.14.

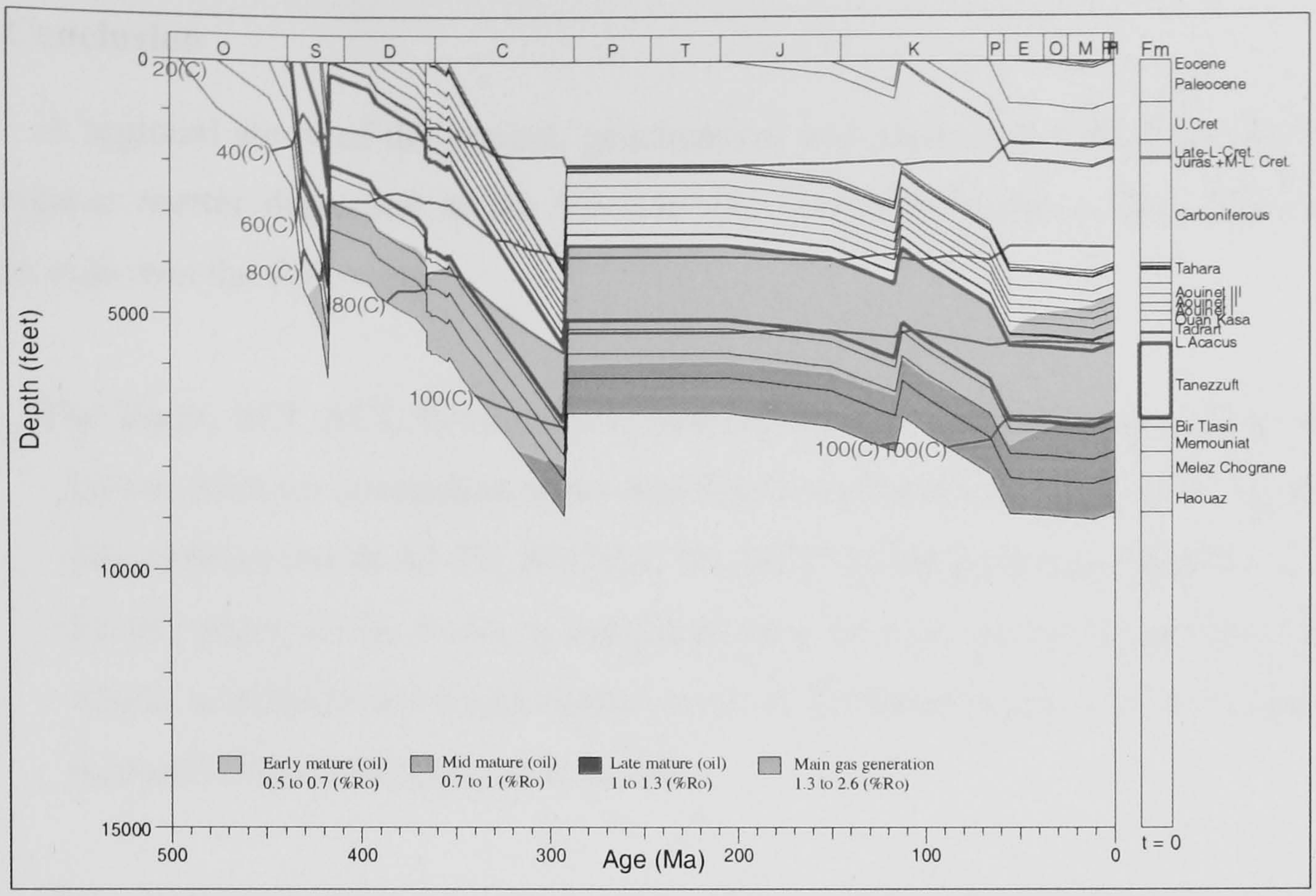

F1-66

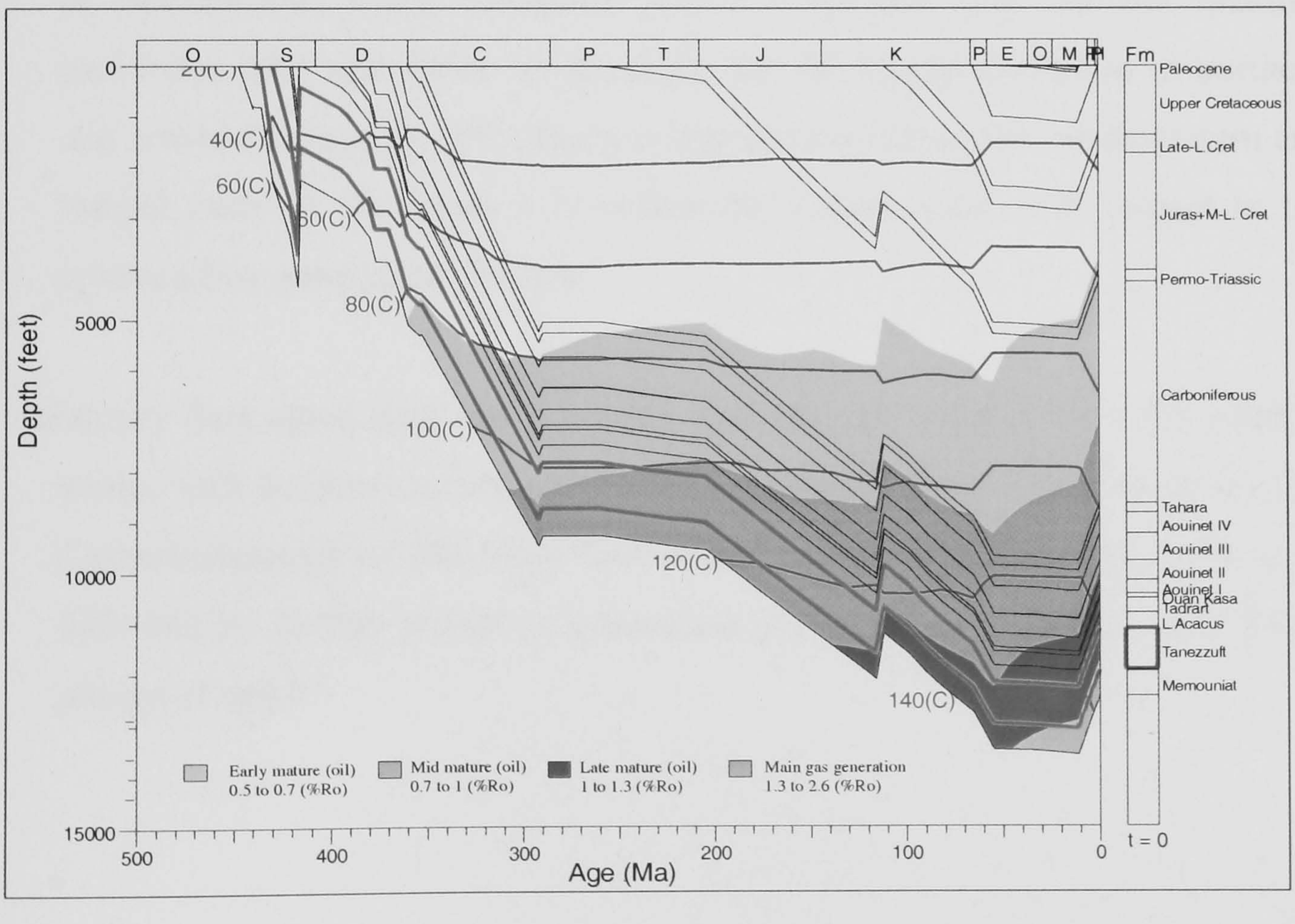

THD.1B

Figure 5.14. Burial history diagrams of wells THD-1B and F1-66 generated by BASINMOD software (from Dardour, 2004).

5.6 Conclusion

A regional study of the optical, geochemical and biomarker maturity properties of organic matter dispersed in the Silurian and Devonian shales of the Ghadames Basin indicates the following:

- The Tmax, SCI, ACI, $\%VR_E$ and biomarker thermal maturity values taken from Lower Silurian succession show that the lower Tanezzuft 'hot shale' facies in the northern (wells A1-70, B1-NC2, D1-NC2, Z5-NC2) and southeastern (well F1-66) parts of the basin is middle mature (within the oil expulsion zone), whilst in deepest and southwestern parts of the basin (wells A1-90 and B1-49 respectively) it is slightly over mature.

- The vitrinite reflectance values for Upper Devonian Tahara and Aouinet Ouenine formation appear to be over estimated due to reworked organic matter or semifusinite being measured (0.8–1.3 %VRo). The sterane maturity parameter, SCI and Tmax values show that the Upper Devonian in northern and southeastern parts of the basin is immature whilst in the southwestern and central parts of the basin it is within the mature zone with respect to the hydrocarbon generation window.

- Maturity data agree with burial history analyses that suggest the basal Silurian source rock became mature and started expelling hydrocarbons during the late Carboniferous (from 345 Ma.). This was terminated by Hercynian uplift, to be followed by further phases of generation preceding the Austrian and Alpine phases of uplift.

CHAPTER 6.0

CONCLUSIONS

6.0 CONCLUSIONS

6.1 General Conclusions

This project involved bulk geochemical, optical and molecular geochemical analyses of the Palaeozoic succession from the Ghadames Basin. The objectives of this study were to characterize the organic matter content, the level of thermal maturity, the organic facies and the source potential of the sediments within the Palaeozoic sequence. Optical observations were used to determine how the bulk geochemical properties are influenced by the combination of maturity, organic matter type, and level of preservation, and to determine the relative importance of each. The correlations between bulk geochemical, optical and molecular maturity parameters, were also appraised, maturity gradients assessed, and oil-source rock correlations attempted.

The bulk geochemical results demonstrate the presence of various organic-rich horizons within lower Palaeozoic succession. The TOC values are generally between 0.5 and 25%. The best TOC values are measured within the dark-coloured non-bioturbated graptolitic "hot shales" of the lower Tanezzuft Formation (average 7%), and Aouinet Ouenine Formation (average 2%); other formations such as Tahara Sandstone Formation contain some thin black shale interbeds that have an average TOC of 4.5%. Hydrogen indices (HI) are mostly below 450, 150–435 in the lower Tanezzuft Formation, and 50–300 in the Aouinet Ouenine Formation

There is a good positive correlation between gamma ray values API units and the TOC contents of the Lower Silurian lower Tanezzuft 'hot shale' source rocks. The isopach map of the Silurian 'hot shale' of >150 API unit indicates a significant spatial variation in the hot shales. The thickest basal Tanezzuft hot shale lies in North and northeastern part of the basin, pinching out toward the South and southwestern part of the basin. The absent of the 'hot shale' in southwestern part of the basin may interpreted as a deposition took place on a topographic palaeo-high with shallower more oxygenated marine conditions.

The palynofacies data from the Lower Palaeozoic succession permit the recognition of different organic facies. The Upper Devonian Tahara and upper

Aouinet Ouenine C samples are commonly associated with oxic conditions and moderate proximity to fluvio-deltaic source(s), with low 'AOM' preservation, abundant spores, and phytoclast assemblages mostly dominated by black wood. The Upper Silurian Acacus Sandstone and upper Tanezzuft formation samples are relatively enriched in palynomorphs, with low AOM and phytoclasts. The marine plankton assemblages are dominated by simple and thin-walled prasinophyte (leiospheres), plus lesser amounts of spores and some tracheid-like fragment of possible land plant origin, suggesting more oxic nearshore shallow marine environments to proximal shelf facies. The samples from lower Tanezzuft Formation are dominated by what was probably originally well preserved AOM, which is typical of laminated black shales with Type II oil-prone kerogen deposited in distal stratified shelf sea basins with dysoxic-anoxic depositional conditions.

Maturity evaluations based on Tmax, SCI, ACI, $\%VR_E$, biomarker and aromatic hydrocarbon distributions for Lower Silurian lower Tanezzuft 'hot shale' source rock facies reveal a trend of increasing maturity from middle mature (expulsion oil zone) in the North and southeast to very mature (gas generation zone) towards the central and southwestern parts of the Ghadames Basin.

The vitrinite reflectance values for Upper Devonian Tahara and Aouinet Ouenine formation appear over estimated (0.8 – 1.3 %VRo) due to reworked organic matter or semifusinite being measured. The other optical, bulk geochemical and molecular maturity parameters show that the Upper Devonian in the northern and southeastern parts of the basin are immature whilst the southwestern and central parts of the basin are within the mature zone with respect to the hydrocarbon generation window.

Oil-source correlations reveal that all the analysed Palaeozoic oils of the Ghadames Basin exhibit similaririties with the Lower Silurian Tanezzuft Formation source rock facies. There is a high probability that these oils were generated from the Lower Silurian 'hot shale' source rocks.

Maturity evaluation of the oil samples based on the biomarker and aromatic hydrocarbon ratios revealed that the oil samples collected from the oil fields located in

the south and southwestern parts of the basin are more mature than the oil samples collected from the northern parts of the basin. This is consistent with the maturity trends of the source rocks of the Ghadames Basin.

Most of the Upper Devonian source rock samples have unusual proportions of the 20S isomers (relative to 20R isomers) of the C_{29} $\alpha\alpha\alpha$ steranes, with values of more than 55% 20S. Such high values could be due to factors other than maturity.

6.2 Suggestions For Future Work

- According to the results obtained in this project, some suggestions for any future research work include:

- More closely space core samples would permit a better assessment of the lateral variation pattern in organic matter assemblages within the Silurian and Devonian formations.

- More Silurian core samples are required for chitinozoan and graptolite reflectance. This may help to clarify the regional thermal maturity gradients.

- More oil samples from other oil fields distributed throughout the basin would be beneficial for correlation studies.

- Most of the Upper Devonian source rock samples have unusual proportions of the 20S isomers (relative to 20R isomers) of the C_{29} $\alpha\alpha\alpha$ steranes, with values of more than 55% 20S. Such high values could be due to factors other than maturity. These results require further molecular investigation.

REFERENCES

References

AL AMERI, T.K., 1980. Palynology, Biostratigraphy and Paleoecology of subsurface Middle Palaeozoic strata from the Ghadames Basin Libya, PhD. Thesis, unpublished, King College, London University, 210pp.

AL-HABA, Y., AL-SAMARRAI, A., AL-JUBORI, F., GEORGIS, N.N. & AHMED, I.M., 1994. Exploration for Paleozoic Prospects in Western Iraq, *Part 1: Exploration of the Paleozoic System in Western Iraq. Proceedings of the Second Seminar on Hydrocarbon Potential of Deep Formations in the Arab Countries (OAPEC), Cairo 10-13 October (in Arabic).*

ALA, M.A. & MOSS, B.J., 1979. Comparative petroleum geology of southeast Turkey and northeast Syria. *Journal of Petroleum Geology,* **1**, 3–27.

ALA, M. A., KINGHORN, R.R.F. & RAHMAN, M., 1980. Organic geochemistry and source rock characteristics of the Zagros Petroleum Province, southwest Iran. *Journal of Petroleum Geology,* **3**, 61–89.

ALSHARHAN, A.S. & NAIRN, A.E.M. 1997. *Sedimentary Basins and Petroleum Geology of the Middle East*, Elsevier, Amsterdam, 843pp.

AOUDEH, S.M. & AL-HAJRI, S.A., 1995. Regional distribution and chronostratigraphy of the Qusaiba Member of the Qalibah Formation in the Nafud Basin, northwestern Saudi Arabia. *In*: HUSSENI, M.I. (ed.) *Middle East Petroleum Geosciences Geo'94*, **1**, Gulf Petrolink, Bahrain, 43–154.

AQRAWI, A.A.M. 1998. Paleozoic stratigraphy and petroleum systems of the western and southwestern desert of Iraq. *GeoArabia,* **3**, 229–248.

AQUINO NETO, F.R., TRENDEL, J.M., RESTLE, A., CONNAN, J. & ALBRECHT, P.A., 1983. Occurrence and formation of tricyclic and tetracyclic terpanes in sediments and petroleum. *In*: BJORØY, M. *et al.* (Eds) *Advances in Organic Geochemistry 1981*, Wiley, Chichester, 659–676.

AQUINO NETO, F. R., TRIGUIS, J., AZEVEDO, D. A., RODRIGUES, R., & SIMONEIT, B. R. T., 1989. Organic geochemistry of geographically unrelated *Tasmanites*. 14th International Meeting on Organic Geochemistry, Paris, September 18-22, 1989. Abstract No. 189.

BANERJEE, S. 1980. Stratigraphic Lexicon of Libya. *Bulletin No. 13, Industrial* Research Center, Tripoli.

BELHAJ, F. 1996. Palaeozoic and Mesozoic stratigraphy of eastern Ghadamis and western Sirt basins. *In*: SALEM, M.J., MOUZUGHI, A.J., & HAMMUDA, O.S. (Eds*) The Geology of the Sirte Basin,* **1**, Elsevier, Amsterdam, pp.57–96.

BELHAJ, F., 2000. Carboniferous and Devonian Stratigraphy-the M'rar and Tadrart Reservoirs, Ghadames Basin, Libya. *In*: SOLA, M. A., & WORSLEY, D. (Eds) *Geological Exploration in Murzuq Basin*. Pp. 117-142.

BELLINI, E. & MASSA, D.1980. A stratigraphic contribution to Palaeozoic of the southern basins of Libya. *In*: SALEM, M.J. & BUSREWIL, M.T. (Eds) *The Geology of Libya,***1**, *Academic Press London, pp.*3–56.

BERRY, W.B., WILDE, P., MARY, S., & HUNT, Q., 1985. The oceanic non-sulfidic oxygen minimum zone: a habitat for graptolites*?. Department of Paleontology, Marine Sciences Group, University of California.*

BEST, J. A., BARANZANGI, M., AL SAAD, D., SAWAF, T. & GEBRAN, A., 1993. Continental margin evolution of the northern Arabian platform in Syria. *American Association of Petroleum Geologists Bulletin,* **77**, 173–193.

BEYDOUN, Z. R., 1988. The Middle East: regional geology and petroleum resources: *Beaconsfield, Bucks, U. K., Scientific Press Ltd.,* 292pp.

BIGGE, M.A. & FARRIMOND, P., 1998. Biodegradation of oils in the Wessex Basin: a complication of correlation. *In*: UNDERHILL, J.R. (Eds) *Development, Evolution and Petroleum Geology of the Wessex Basin. Geological Society of London, Special Publication*, **133**, 373–386.

BISHOP, A. N. & ABBOTT, G. D. 1993. The interrelationship of biological marker maturity parameters and molecular yields during contact metamorphism. *Geochimica et Cosmochimica Acta*, **57**, 3661–3668.

BOOTE, D.R.D., CLARK-LOWES, D.D. & TRAUT, M.W. 1998. Palaeozoic petroleum systems of North Africa. *In:* MACGREGOR, D.S., MOODY, R.T.J. & CLARK-LOWES, D.D. (eds) *Petroleum Geology of North Africa, Geological Society of London, Special Publication*, **132**, 7–68.

BORDENAVE, M.L., ESPITALIÉ, J., LEPLAT, P. OUDIN, J.L. & VANDENBROUKE, M. 1993. Screening techniques for source rock evaluation. *In*: BORDENAVE, M.L. (ed.) *Applied Petroleum Geochemistry*, Editions Technip, Paris, pp.217–279.

BULLMAN, O.M., & STÖRMER, L. 1971. Buoyancy structures in rhabdosomes of *Dictyonema flabelliforme*. *Norsk Geologisk Tids*skrift, **51**, 25-31

COLE, G.A., HALPERN, H.I., & AOUDEH, S.M. 1994. The relationships between iron-sulfur-carbon and gamma ray response, Silurian basal Qusaiba shale, northern Saudi Arabia. *Saudi Arabia Journal of Technology*, Fall/Winter 1994/1995, 9–19.

COLLINS, A., 1990. The 1-10 Spore Colour Index (SCI) scale: a universally applicable colour maturation scale, based on graded, picked palynomorphs *In*: FERMONT, W.J. & WEEGINK, J.W. (eds) *International Symposium on Organic Petrology, mededelingen rijks geologische dienst,* **45**, 40–47.

COLLOMB, G.R. 1962. Etude géologique du jabel Fezzan et de sa bordure

Paleozoique.*Notes et memoires. Compagnie francaise des petroles,* **1**, 7–35, Paris.

COMBAZ, A. 1967. Leiosphaeridaceae Eisenack, 1954, et Protoleiosphaeridae Timofeev, 1959- leurs affinitiés, leur rôle sédimetologique et gélogique. *Review of Palaeobotany and Palynology*, **1**, 309-21.

COMBAZ, A.1986. Les 'Zones Gamma' du Silurien des region Sahariennes; contenu organique et conditions de depot. *Documents du Bureau de Recherches Géologique et Minières*, **110**, 239–58.

COMBAZ, A. 1980. Les kérogènes vus au microscope. *In*: DURAND, B. (ed.) *Kerogen, Insoluble Organic Matter From Sedimentary Rocks*, pp.55–113. Technip, Paris.

CONNAN, J., BOUROULLEC, J., DESSORT, D. & ALBRECHT, P., 1986. The microbial input in carbonate-anhydrite facies of an Abkhaz palaeoenvironment from Guatemala: a molecular approach. *In*: LEYTHAEUSER, D. & RULLKÖTTER, J. (eds) *Advances in Organic Geochemistry 1985*, *Organic Geochemistry* **10**, 29–50.

CORNFORD, C., NEEDHAM, C.E.J. & WALQUE, De L., 1986. Geochemical habitat of North Sea oils and gases. *Habitat of Hydrocarbons on the Norwegian Continental Shelf.* Graham & Trotman, London, 39-54.

CORNFORD, C., CHRISTIE, O., ENDRESEN, U., JENSEN, P., and MYHR, M.B., 1988. Source rock and seep oil maturity in Dorset, Southern England. *In*: MATTAVELLI, L. and NOVELLI, L. (Eds) *Advances in Organic Geochemistry 1985*, *Organic Geochemistry* **13**, 399-409.

DABARD, M.P. & PARIS, F. 1986. Palaeontological and geochemical characteristics of Silurian black shale formations from the Central Brittany domain of the Armorican Massif (NW France). *Chemical Geology*, **55**, 17–29.

DARDOUR, A. 2004. Tectono-stratigraphic evaluation of the Palaeozoic rock and the petroleum systems of the Ghadamis Basin, Libya. PhD. Thesis, unpublished, School of Earth Sciences & Geography, Kingston University.

DASTILLUNG, M. & CORBET, B., 1978. La Géochimie des sédiments marins profonds- I- hydrocarbures saturés et insaturés des sédiments. In: A CANBAZ & R. PELET. (eds.) *Géochimie Organiques des sédiments marins profonds*, Organ II, Atlantique N .E., Brésil, 293-323. CNRS.

DEBYSER, Y., PEIET, R. & DASTILLUNG, M., 1977. Géochimie Organique des sédiments marins récents: Mer Noire, Baltique, Atlantique (Mauritanie). In: R CAMPOS & J GONI. (eds.) *Advances in Organic Geochemistry*, 1975, 289-320. Enadimsa, Madrid.

DEMAISON, G. & MOORE, G.T. 1980. Anoxic environments and oil source bed genesis, *American Association of Petroleum Geologists Bulletin*, **64**, 1179-1209.

DESIO, A. 1963. Stratigraphic studies in the Tripolitanian Jebel (Libya). *Memoria, Rivista Italiana de Paleontologia e Stratigrafia,* 109pp.

DESTOMBES, J., HOLLARD, H. & WILLEFERT, 1988. Lower Palaeozoic rocks of Morocco. *In:* HOLLAND, C.H. (Ed) *Lower Palaeozoic rocks of the world*, **4**, 91-336.

DURAND, B., ALPERN, B., PITTION, J.L. & PRADIER, B., 1986. Reflectance of vitrinite as a control of thermal history of sediments. *In:* BURRUS, J. (eds) *Thermal Modeling in Sedimentary Basins*. 1st IFP Explor. *Res. Conf., Caracans, June 3-7, 1985. Technip, Paris, Coll. Colloq. Semin.*, **44**, pp. 441-474.

ECHIKH, K., 1992. Geology and hydrocarbon occurrences in the Ghadamis Basin . *Internal Report, National Oil Corporation of Libya (NOC), Tripoli.*

EL-ARNAUTI, A. & SHELMANI, M. 1988. A contribution to the northeast Libya subsurface stratigraphy with emphasis on Pre-Mesozoic *In*: EL-ARNAUTI, B. & THUSU, B. (eds) *Subsurface Palynostratigraphy of Northeast Libya. Garyounis University,* pp.1–17

EL-RWEIMI, W. S. 1991. Geology of the Aouinet Ouenine and Tahara Formations. Al Hamadah Al Hamra Area, Ghadames Basin. *In*: *The Geology of Libya*, SALEM, M.J., SBETA, A.M. & BAKBAK, M.R. (eds), **VI,** 2185-2193.

ESPITALIE, J., MADEC, M., TISSOT, B., MENNIG, J.J. & LEPLAT, P. 1977. Source rock characterization method for petroleum exploration. *Proceedings of the 9th Annual Offshore Technology Conference*, Houston 1977, pp.439–444.

FARRIMOND, P., TAYLOR, A. & TELNÆS, N. 1998. Biomarker maturity parameters: the role of generation and thermal degradation. *Organic Geochemistry*, **29**, 1181–1197.

FISHER, M.J., BARNARD, P.C. & COOPER, B.S., 1980. Organic maturation and hydrocarbon generation in the Mesozoic sediments of the Sverdrup Basin, Arctic Canada. *Proc. 4th int. Palynological Conference, Lucknow* (1976–1977), **2**, pp.581–588.

FRANK, M.C. & TYSON, R.V. 1995. Parasequences-scale organic facies variations through an Early Carboniferous Yoredale cyclothem, Middle Limestone Group, Scremerston, Northumberland. *Journal of the Geological Society London*, **152**, 41–50.

GENTZIS, T., FREITAS, T., GOODARZI, F., MECLCHIN, M. & LENZ, A. 1996. Thermal maturity of Lower Palaeozoic sedimentary successions in Arctic Canada. *American Association of Petroleum Geologists Bulletin*, **80**, 1065–1084.

GOODARZI, F. 1984. Organic petrology of graptolite fragments from Turkey. *Marine and Petroleum Geology*, **1**, 202-210.

GOODARZI, F. 1985. Dispersion of optical properties of graptolites with increased maturity in early Palaeozoic organic-rich sediments. *Fuel*, **54**, 1735-1740.

GOODARZI, F. & NOFORD B. S. 1987. Optical properties of graptolite periderm – a review. *Bulletin of the Geological Society Denmark*, **35**, 141–147.

GOODARZI, F., GENTZIS, T., HARRISON, C.H. & THORSTEINSSON, R. 1992. The significance of graptolite reflectance in regional thermal maturity studies, Queen Elizabeth Islands, Arctic Canada. *Organic Geochemistry*, **18**, 347–357.

GRANTHAM, P. J., LIJMBACH, G.W.M., POSTHUMA, J., HUGHES-CLARKE, M.W. & WILLINK, R. J., 1988. Origin of crude oil in Oman: *Journal of Petroleum Geology,* **12**, 81–88.

GRAY, J. & BOUCOT, A.J. 1971. Early Silurian spore tetrads from New York. Earliest New World evidence for vascular plants? *Science,* **173**, 918–921.

HABIB, D. 1982. Sedimentary supply origin of Cretaceous black shales. *In*: SCHLANGER, S.O. & CITA, M.B. (Eds) *Nature and Origin of Cretaceous. Carbon-Rich Facies*, Academic Press, London, pp.113–127.

HALLETT, D. 2002. Petroleum geology of Libya. Elsevier, Amsterdam.

HAMYOUNI, E., AMR, I., RIANI, B., El-GHULL, A. & RAHOMA, S. 1984. Source and Habitat of Oil in Libyan basins. *Internal report, National Oil Corporation of Libya (NOC), Tripoli*

HANGARI, K., ELOUJALI, R., HROUDA, M., ELBADRI, A., ELKELANI, M., GHENIMA, R., SAIDI, M. & INOUBLI, H. 2000. Geochemical characterisation of the source rock potential of Ordovician to Early Carboniferous sediments in eastern Ghadamis Basin. *Geology of Northwest Libya, Abstracts of the Second Symposium, Tripoli, Libya 2000* p.50.

HARTMAN-STROUP, C. 1987. The effect of organic matter type and organic carbon content on Rock-Eval hydrogen index in oil shale and source rock. *Organic Geochemistry*, **11**, 352–369.

HOFFIMEISTER, W.S. 1959. Early Silurian plant spores from Libya, *Micropaleontology*, **5**, 331-334.

HUANG, W-Y. & MEINSCHEIN, W.G., 1979. Sterols as ecological indicators. *Geochimica et Cosmochimica Acta,* **43**, 739–745.

HUGHES, W.B., HOLBA, A.G., MILLER, D.E., & RICHARDSON, J.S., 1985. Geochemistry of greater Ekofisk crude oils. In: B.M THOMAS (eds) *Geochemistry in Exploration of the Norwegian Shelf* Ed.), Graham and Trotman, 75-92.

HUSSEINI, M. I. 1990. The Cambro-Ordovician Arabian and adjoining plates: a glacio-eustatic model. *Journal of Petroleum Geology,* **13**, 267–288.

HUSSEINI, M. I., 1991, Potential petroleum resources of the Paleozoic rock of Saudi Arabia: *13th World Petroleum Congress,* 18 p.

JANSONIUS, J., & JENKINS, W.A.M. 1978. Chitinozoan. *In*: HAQ, B.U. & BOERSMA, A. (eds) *Introduction to Marine Micropalentology*, Elsevier Biomedical, New York, pp.341-357.

JONES, P.J. & STUMP, T.E. 1999. Depositional and tectonic setting of the Lower Silurian hydrocarbon source rock facies, Central Saudi Arabia. *American Association of Petroleum Geologists Bulletin.*, **83**, 314–332.

JONES, R.W. 1987. Organic facies. *In*: BROOKS, J. & WELTE, D. (eds) *Advances in Petroleum Geochemistry*, **2**, 1–90.

KATZ, B.J. 1983. Limitations of 'Rock-Eval' pyrolysis for typing organic matter. *Organic Geochemistry*, **4**, 195–199.

KLINE, 1994. An easy Guide to Factor Analysis. Routeledge, London and New York.

KLITZCH, E. 1968. Die Gotlandium Transgression in der Zentral-Sahara, *Zeitschrift der Deutschen Geologischen Gesellschaft,* **117**, 492–501.

KLITZCH, E. 1969. Stratigraphic section from the type areas of Silurian and Devonian strata at western Murzuq Basin (Libya). *In*: KANES, W.H. (ed.) *Geology, Archaeology, and Prehistory of Southwestern Fassan, Libya. Petroleum Exploration Society of Libya, Tripoli,* pp.83–90.

KLITZCH, E. 1970. Die Strukturgeschichte der Zentralsahara: Neue Erkenntnisse zum Bauund zur Palaogeographic eines Tafellandes, *Geologische Rundschau.*, **59**, 459–527.

KLITZCH, E. 1981. Lower Palaeozoic rocks of Libya, Egypt, and Sudan. *In*: HOLLAND, C.H. (ed.) *Lower Palaeozoic of the Middle East, Eastern and Southern Africa, and Antarctica, Wiley Chichester,* 131–163.

KLITZSCH, E. 1995. Libyen / Libya. *In:* KULKE, H. (ed.) *Regional Petroleum Geology of the World, Part II, Beitrage Regional. Geol. D. Erde, Borntrager, Stuttgart,* **22**, 45–56.

KVALHEIM, O.M. 1987. Oil-source correlation by the combined use of principal component modelling, analysis of variance and coefficient of congruence. *Chemometrics and Intelligent Laboratory Systems*, **2**, 127--136.

LANGFORD, F.F. & BLANC-VALLERON, M-M. 1990. Interpreting Rock-Eval Pyrolysis data using graphs of pyrolizable hydrocarbons vs. total organic carbon. *American Association of Petroleum Geologists Bulletin*, **74**, 799--804.

LELUBRE, M. 1946. Sur la Paleozoique de Fezzan. *Comptes Rendus Academie des Sciences Paris,* 222,(24), 1403–1404.

LEGGETT, J.K., McKRROW, W.S., COCKS, L.R.M. & RICKARDS, R.B. 1981. Periodicity in the early Palaeozoic marine realm, *Journal of the Geological Society*, London, **138**, 167-176.

LEGRAND, P. 1985. Lower Palaeozoic rocks of Algeria. In: HOLLAND, C.H. (ed.) Lower Palaeozoic of North-Western and West Central Africa, Wiley Chichester, pp.5–89.

Le HÉRISSÉ, A. 2002. Paleoecology, biostratigraphy and biogeography of late Silurian to early Devonian acritarchs and prasinophycean phycomata in well A161, Western Libya, North Africa. *Review of Palaebotany and Palynology*, **118**, 359-395.

LEWAN, M. D., BJOROY, M. & DOLCATER, D. L. 1986. Effects of thermal maturation on steroid hydrocarbons as determined by hydrous pyrolysis of Phosphoria Retort Shale. *Geochimica et Cosmochimica Acta* **50**, 1977-1987.

LÜNING, S., CRAIG, J., LOYDELL, D.K., STORCH, P. & FITCHES, B. 2000a. Lower Silurian 'hot shale' in North Africa and Arabia: regional distribution and depositional model, *Earth Science Review,* **49**, 121–200.

LÜNING, S., LOYDELL, D.K., SUTCLIFFE, O., AIT SALEM, A., ZANELLA, E. CRAIG, J. & HAPER, D.A.T. 2000b. Silurian-Lower Devonian black shales in Morocco: where are the organically richest horizons?, *Journal of Petroleum Geology,* **23**, 293–311.

LÜNING, S., & KOLONIC, S., 2003. Uranium spectral gamma-ray response as a proxy for organic richness in black shales: applicability and limitations. *Journal of Petroleum Geology*, **26**, 153-174.

MACKENZIE, A.S., PATIENCE, R. L., MAXWELL, J. R., VANDENBROUCKE, M., DURAND, B. 1980. Molecular parameters of maturation in the Toarcian shales, Paris Basin, France – I. Changes in the configuration of acyclic isoprenoid alkanes, steranes and triterpanes. *Geochimica et Cosmochimica Acta* **44**, 1709–1721.

MACKENZIE, A.S., REN-WEI, L., MAXWELL, J.R., MOLDOWAN, J.M. & SEIFERT, W.K., 1983. Molecular parameters of maturation in the Cretaceous shales. From the Overthrust Bel, Wyoming, USA. In: Bjorøy, M. *et al.* (eds), Advances in *Organic Geochemistry 1981*, J. Wiley and Sons, Chichester, 496-503.

MACKENZIE, A.S. 1984. Application of biological markers in petroleum geochemistry. *In*: BROOKS, J., WELTE, D.H. (eds), *Advances in Petroleum Organic Geochemistry*. Academic Press, London, pp.115-214.

MACKENZIE, A.S. RULLKÖTTER, J., WELTE, D.H. & MANKIEWICZ, P., 1985. Reconstruction of oil formation and accumulation in North Slope, Alaska, using gas chromatography-mass spectrometry. *In*: MAGOON, L.B. & CLAYPOOL, G.E. (eds), Alaska North Slope Oil/Source Rock Correlation Study. *American Association of Petroleum Geologists, Studies in Geology*, **20**, 319–377.

MAHMOUD, M.D., VASLET, D. & HUSSAINI, M.I. 1992. The Lower Silurian Qalibah Formation of Saudi Arabia: an important hydrocarbon source rock. *American Association of Petroleum Geologists Bulletin*, **76**, 1491–1506.

MALLA, M. S., KHATIR, B. & YAHI, N. 1997. Review of the structural evolution and hydrocarbon generation in Ghadames and Illizi basins. *Proceedings of the 15th World Petroleum Congress.*

MAMGAIN, V.D. 1980. The Pre-Mesozoic (Precambrian to Palaeozoic) Stratigraphy of Libya: *A Reappraisal. Industrial Research Centre, Tripoli.*

MARSHALL, J.E.A. 1991. Quantitative spore colour. *Journal of the Geological Society*, London, **148**, 223–233.

MARSHALL, J.E.A. 1995. The Silurian of Saudi Arabia: thermal maturity, burial history and geotectonic environment. *Review of Palaeobotany and Palynology*, **89**, 139-150.

MASSA, D. & COLLOMB, G. 1960. Observations nouvelles sur la region d'Aouinet Ouenine et du Djebel Fazzan (Libye). *21st Int' l Geol. Cong. Proc.* **12,** 65–73.

MASSA, D. & JAEGER, H., 1970: Donnees stratigraphy sur le Silurien de l ouest de la Libye. Colloque Ordovicien-Silurien. *Brest (France), Sept 1970. Memoires du. Bureau de Recherche Geologique et Mineres,* **73**, pp.313–321.

MASSA, D. & MOREAU-BENOIT, A. 1976. Essai de synthese stratigraphique et palynologique du systeme Devonian en Libye occidentale, *Revue de I' Institut Francais du Petrole,* **31**, 287–332.

McGILLIVRAY, J.G. & HUSSEINI, M. I. 1992. The Palaeozoic petroleum geology of Central Arabia. *American Association of Petroleum Geologists Bulletin,* **76**, 1473–1490.

McKIRDY, D.M., ALDRIDGE, A.K. and YPMA, P.J.M., 1983. A geochemical comparison of some crude oils from pre-Ordovician carbonate rocks. *In*: BJOROY, M. *et al.*, (Eds) *Advances in Organic Geochemistry 1981*, Wiley, Chichester, pp.99–107.

MEGLEN, R.R., 1992. Examining large databases, a chemometric approach using principal component analysis. *Marine Chemistry*, **39**, 217–237.

MERGL, M. & MASSA, D. 1992. Devonian and Lower Carboniferous brachiopods and bivalves from Western Libya, *Collection " Biostratigraphie du Paleozoique", 12, Universite Claude Bernared-Lyon, pp,216.*

MOLDOWAN, J.M., SEIFERT, W.K., & GALLEGOS, E.J., 1985. Relationship between petroleum composition and depositional environment of petroleum source rocks. *American Association of Petroleum Geologists Bulletin,* **69**, 1255–1268.

MOLDOWAN, J.M., SUNDARARAMAN, P. & SCHOELL, M. 1986. Sensitivity of biomarker properties to depositional environment and/or source input in the Lower Toarcian of SW. Germany. *Organic Geochemistry,* **10**, 915--926.

MONNIER, F., MOLDOWAN, J.M., SUNDARARAMAN, P. &. TEERMAN, S.C. 1999. Palaeozoic source rocks potential of Saudi Arabia and its contribution to Palaeozoic oils: *Confidential study, Chevron Oil Field Research Company, La Habra, California, no page number given.*

MOORE, G.T. & HAYASHIDA, D.N. 1993. Late Early Silurian (Wenlockian) general circulation model-generated upwelling, graptolitic black shales and organic-rich source rocks - an accident of plate tectonics? *Geology,* **21**, 17–20.

MULLER, J. 1959. Palynology of Recent Orinoco delta and shelf sediments: Reports os the Orinoco Shelf expedition; volume 5. *Micropalaeontology*, **5**, 1–32.

NAGY, J., DYPVIK, H., & BJAERKE, T. 1984. Sedimentological and palaeontological analyses of Jurassic North Sea deposits from deltaic environments. *Journal of Petroleum Geology*, **7**, 169–188.

OBERMAJER, M., FOWLER, M.G., GOODARZI, F. & SNOWDON, L.R., 1996. Assessing thermal maturity of Palaeozoic rocks from reflectance of chitinozoan as constrained by geochemical indicators: an example from southern Ontario, Canada. *Marine and Petroleum Geology,* **13**, 907–919.

ORR, W.L. 1981. Comments on pyrolytic hydrocarbon yields in source-rock evaluation. *In*: BJOROY, M. *et al.* (ed.) *Advances in Organic Geochemistry* 1981, Wiley, London, pp.775–787.

PARFITT, M. & FARRIMOND, P., 1998. The Mupe Bay Oil Seep: a detailed organic geochemical study of a controversial outcrop. *In*: UNDERHILL, J.R. (ed.) Development, Evolution and Petroleum Geology of the Wessex Basin. *Geological Society of London, Special Publication*, **133**, 387–397.

PARIS, F. & ROBADET, M. 1990. Early Palaeozoic palaeobiogeography of the Variscan regions. *Tectonophysics,* **177**, 193–213.

PARRY, C.C., WHITELY, P.K.J. & SIMPSON, R.D.H. 1981. Integration of palynological and sedimentological methods in facies analysis of the Brent Formation. *In*: ILLING, L.V. & HOBSON, G.D.(eds) *Petroleum Geology of the Continental Shelf of North-West Europe*, Heyden, London, pp.205–215.

PETERS, K.E., 1986. Guidelines for evaluating petroleum source rock using programmed pyrolysis. *American Association of Petroleum Geologists Bulletin,* **70,** 318–329.

PETERS, K.E. & MOLDOWAN, J.M., 1993. *The Biomarker Guide. Interpreting Molecular Fossils in Petroleum and Ancient Sediments*. Prentice Hall, New York.

PETERS, K.E., MOLDOWAN, J.M., DRISCOLE, A.R. & DEMAISON, G.J., 1989. Origin of Beatrice oil by co-sourcing from Devonian and Middle Jurassic source rocks, Inner Moray Firth, UK. *American Association of Petroleum Geologists Bulletin*, **73**, 454–471.

PETERS, K.E., MOLDOWAN, J.M. & SUNDARARAMAN, P., 1990. Effects of hydrous pyrolysis on biomarker thermal maturity parameters: Monterey Phosphatic and Siliceous members. *Organic Geochemistry*, **15**, 249–265.

POTTER, P.E., 1982. Appalachian gas bearing Devonian shales: statements and discussions. *Oil & Gas Journal*, **25**, 290-316.

RADKE, M., & WELTE, D.H., 1983. The Methylphenanthrene Index (MPI): a maturity parameter based on aromatic hydrocarbons. *In:* M. BJORØY (eds) *advances in Organic Geochemistry* 1981, 504-512.

RADKE, M., 1987. Organic Geochemistry of aromatic hydrocarbons. *In*: BROOKS, J., WELTE, D. (eds), *Advances in Organic Geochemistry,* **2**. Academic Press, London, pp.141–207.

RADKE, M., WELTE, D.H. & WILLSH, H., 1986. Maturity parameters based on aromatic hydrocarbons: influence of the organic matter type. *In*: LEYTHAEUSER, D. & RULLKÖTTER J. (eds), *Advances in Organic Geochemistry 1985*, *Organic Geochemistry,* **10**, 51–63.

RAHOMA, S., HROUDA, M., DIEP, M. & El KELANI, M. 1994. The hydrocarbon potential of the Palaeozoic rocks of the Ghadames Basin, Libya: *Second Seminar on Hydrocarbon Potential of Deep Formations in the Arab countries, Cairo, Egypt.*

RICHARDSON, J.B. 1969. Devonian spores. *In*: SCHUDY, R.H. & SCOTT, R.A. (eds). *Aspect of Palynology, Wiley International*, pp.191–221.

RICHARDSON, J.B., & IOANNIDES, N. 1973. Silurian palynomorphs from Tanezzuft and Acacus formations, Tripolitania, North Africa, *Micropaleontology*, **19**, 257–307.

RIDER, M. 1996. The geological interpretation of well logs, 2nd eds. Whittles Publishing, London, pp.280.

RIEDIGER, C.L., FOWLER, M.G., BROOKS, P.W. & SNOWDON, L.R., 1990. Triassic oils and potential Mesozoic source rocks, Peace River Arch area, Western Canada Basin. *Organic Geochemistry* **16**, 295–305.

ROBERT, P., 1988. Organic metamorphism and geothermal history. Microscopic study of organic matter and thermal evolution of sedimentary basins. Elf Aquitaine D. Reidel, Dordrecht, 311p.

RULLKÖTTER, J. & MARZI, R., 1988. Natural and artificial maturation of biological markers in Toarcian shale from northern Germany. *Organic Geochemistry* **13**, 639–645.

RULLKÖTTER, J., WENDISCH, D. 1982. Microbial alteration of 17 a (H)-hopane in Madagascar asphalts: Removal of C-10 methyl group and ring opening. *Geochimica et Cosmochimica Acta*, **46**, 1543-1553.

SEIDL, K. & ROHLICH, P. 1984. Geological map of Libya, 1: 250,000. *Sheet Sabha NG 33-2. Industrial Research Centre Tripoli.*

SEIFERT, W. K. & MOLDOWAN, J. M., 1978. Applications of steranes, terpanes and monoaromatics to the maturation, migration and source of crude oils. *Geochimica et Cosmochimica Acta* **42**, 77–95.

SEIFERT, W.K. & MOLDOWAN, J.M., 1980. The effect of thermal stress on source-rock quality as measured by hopanes stereochemistry. *In*: DOUGLAS, A.G. & MAXWELL, J.R. (Eds) *Advances in Organic Geochemistry* 1979, Pergamon Press, Oxford, pp.229–237.

SEIFERT, W.K. & MOLDOWAN, J.M., 1986. Use of biological markers in petroleum exploration. *In*: JONS, R.B. (ed.) *Methods in Geochemistry and Geophysics*, **24**, 261–290.

SELLEY, R.C. 1997b. The basins of Northwest Africa: structural evolution. *In:* SELLEY, R.C. (ed.) African Basins: *Sedimentary Basins of the World 3, Elsevier, Amsterdam,* pp.17-26.

SOFER, Z. 1988 Biomarkers and carbon isotopes of oils in the Jurassic Smackover Trend of the Gulf Coast states, U.S.A. *Organic Geochemistry,* **12**, 421–432.

SPJEDNEAS, N., 1981. Lower Palaeozoic rocks of the Middle East. In: HOLLAND, C.D. (Ed) *Lower Palaeozoic rocks of the world*, **3,** Wiley, New York, 199-256.

STAPLIN, F.L. 1969. Sedimentary organic matter, organic metamorphism, and oil and gas occurrence. *Bulletin of Canadian Petroleum Geology*, **17**, 47–66.

SUBROTO, E.A., ALEXANDER, R. & KAGI, R.I., 1991. 30-Norhopanes: their occurrence in sediments and crude oils. *Chemical Geology*, **93**, 179–192.

SUCHÝ, V., SÝKOROVÁ, I., STEJSKAL, M., ŠAFANDA, J., VLADIMIR, M. & NOVOTNÁ, M. 2002. Dispersed organic matter from Silurian shales of the Barrandian Basin, Czech Republic: optical properties, chemical composition and thermal maturity. *International Journal of Coal Geology*, **53**, 1–25.

SUTCLIFFE, O.E., DOWDESWELL, J.A., WHITTINGTON, R.J., THERON, J.N. & CRAIG, J. 2000. Calibrating the Late Ordovician glaciation and mass extinction by eccentricity cycles of the Earth's orbit, *Geology*, **28**, 967–970.

SUTCLIFFE, O.E., ADAMSON, K. & BEN RAHUMA, M. 2000. The geological evolution of the Palaeozoic rock of Western Libya: *a review and fieldguide*

TRAVERSE, A. 1988. *Palaeopalynology*, Unwin Hyman, Boston, 600pp.

TRAVERSE, A. 1994. Sedimentation of palynomorphs and palynodebris: an introduction. *In*: TRAVERSE, A. (ed.) *Sedimentation of Organic Particles*, Cambridge University Press, Cambridge, 1–8.

TRICKER, P.M., MARSHALL, J.E.A., & BADMAN, T.D. 1992. Chitinozoan reflectance: a Lower Palaeozoic thermal maturity indicator. *Marine and Petroleum Geology*, **9**, 302–307.

TISSOT, B. P. & WELTE, D. H., 1984. Petroleum Formation and Occurrence, 2nd Springer-Verlag, New York.

TUCKER, M.E. 1982. *The Field Description of Sedimentary Rock*, Open University Press, Milton Keynes, 112pp.

TUWENI, A.O. & TYSON, R.V. 1994.Organic facies variations in the Westbury Formation (Rhaetic, Bristol Channel, SW England). *Organic Geochemistry*, **21**, 1001–1014.

TYSON, R.V. 1984. Palynofacies investigation of Callovian (Middle Jurassic) sediments from DSDP Site534, Blake-Bahama, western Central Atlantic. *Marine and Petroleum Geology*, **1**, 3–13.

TYSON, R.V. 1987. The genesis and palynofacies characteristics of marine petroleum source rocks. *In*: BROOKS, J. & FLEET, A.J. (Eds) *Marine Petroleum Source Rocks, Geological Society of London Special Publication*, **26**, 47–67.

TYSON, R.V. 1989. Late Jurassic palynofacies trends, Piper and Kimmeridge Clay Formations, UK onshore and northern North Sea. *In*: BATTEN, D.J. & KEEN, M.C. (Eds) *Northwest European Micropalaeontology and Palynology, British Micropalaeontological Society Series*, Ellis Horwood, Chichester, pp.135–172.

TYSON, R.V. 1993. Palynofacies analysis, *In*: JENKINS, D.G. (ed.) *Applied Micropalaeontology*, Kluwer, Dordrecht, pp.153–191.

TYSON, R.V. 1995. *Sedimentary Organic Matter. Organic Facies and Palynofacies*. Chapman & Hall, London, 625pp.

TYSON, R.V., FOLLOWS, B., 2000. Palynofacies prediction of distance from sediment source: A case study from the Upper Cretaceous of the Pyrenees. *Geology*, **28**, 569-571.

VOLKMAN, J.K., 1986. A review of sterol markers for marine and terrigenous organic matter. *Organic Geochemistry,* **9**, 83–99.

VOLKMAN, J.K., GILLAN, F.T., JOHNS, R.B. & EGLINTON, G., 1981. Sources of neutral lipids in a temperate intertidal sediment. *Geochimica et Cosmochimica Acta*, **45**, 1817–1828.

VOLKMAN, J. K., BANKS, M. R., DENWER, K., & AQUINO NETO, F.R. 1989. Biomarker composition and depositional setting Tasmanite oil shale from northern Tasmania, Australia 14th International Metting on Organic Geochemistry, Paris, September 18-22, 1989, Abstract No. 168.

WHITAKER, M.F., GILES, M.R., & CANNON, S.J.C. 1992. Palynological review of the Brent Group, U.K. sector, North Sea. *In*: MORTON, AC., HAZELDINE, R.S., GILES, M.R., & BROWN, S. (eds) *The Geology of the Brent Group, Geological Society of London Special Publication*, **61**, 169–202.

WIGNALL, P.B. & MEYERS, K.J. 1988. Inerpreting benthic oxygen levels in mudrocks: a new approach. *Geology* **16**, 452-55.

WILSON, M., & GUIRAUD, R. 1998. Late Permian to Recent magmatic activity on the African-Arabian margin of Tethys. *In:* MAcGREGOR, D.S., MOODY, R.T.J. & CLARK-LOWES, D.D. (eds) *Petroleum Geology of North Africa. Geological Society of London, Special Publication,* **132**, 7–68.

WOLFART, R., 1981. Lower Palaeozoic rocks of the Middle East. In: HOLLAND, C.D. (Ed) *Lower Palaeozoic rocks of the world*, **3**, Wiley, New York, 5-130.

YAHI, N., 1999. *Petroleum Generation and Migration in the Berkine (Ghadames) Basin, |Eastern Algeria: An Organic Geochemical and Basin Modelling Study*: Ph.D. thesis, Aachen University of Technology (RWTH Aachen), Germany, 223pp.

YAHI, N., SCHAEFER, R.G., & LITTKE, R. 2001. Petroleum generation and accumulation in the Berkine basin, eastern Algeria. *American Association of Petroleum Geologists Bulletin,* **85**, 1439–1467.

ZIEGLER, A.M., HANSEN, K.S., JOHNSON, M.E., KELLY, M.A., SCOTESE, C.R., & VAN DER VOO, R. 1977. Silurian continental distributions, paleogeography, climatology and biogeography: *Tectonophysics*, **40**, 13-51.

APPENDICES

APPENDIX I

Appendix I: 'Dummy' variables

Key abbreviation used in column headers:

Samno	= sample number
Welln	= well name
Fm	= formation name
Lith	= lithology
Dlith	= dominant lithology
Colour	= shale colour
S.Struct	= sedimentary structure
Bioturb	= bioturbation
Grapto	= graptolite contents
Fossils	= fossil contents
Pyrite	= pyrite contents
Mica	= mica contents

The keys to the number in each of the categories can be found in Table 2.5.

wellname	Samno	Depth	Formation	Age	Lith	Dlith	Colour	S.Struct	Bioturb	Grapto	Fossils	Pyrite	Mica
F1-66	TH1	4127	Tahara	U. Devonian	1	3	7	3	0	0	0	0	1
	TD1	5476	Tadrart	L. Devonian	1	3	7	2	0	0	0	0	1
	UT1	6455	Upper Tanezzuft	L. Silurian	1	3	7	2	0	0	0	0	1
	UT2	6470	Upper Tanezzuft	L. Silurian	1	3	7	2	0	0	0	0	1
	UT3	6473	Upper Tanezzuft	L. Silurian	0	3	7	2	0	0	0	0	1
	LT1	7042	Lower Tanezzuft	L. Silurian	0	0	5	1	0	1	0	0	1
	LT2	7047	Lower Tanezzuft	L. Silurian	0	0	5	1	0	1	0	0	1
	LT3	7051	Lower Tanezzuft	L. Silurian	0	0	4	1	0	2	0	0	1
	LT4	7053	Lower Tanezzuft	L. Silurian	0	0	4	1	0	2	0	1	1
	LT5	7054	Lower Tanezzuft	L. Silurian	0	0	2	1	0	2	0	0	3
	LT6	7057	Lower Tanezzuft	L. Silurian	0	0	5	1	0	1	0	1	1
	LT7	7061	Lower Tanezzuft	L. Silurian	0	0	5	1	0	3	0	1	1
	LT8	7063	Lower Tanezzuft	L. Silurian	1	0	7	0	0	0	0	1	1
	LT9	7065	Lower Tanezzuft	L. Silurian	0	0	3	1	0	0	0	1	2
	LT10	7073	Lower Tanezzuft	L. Silurian	0	0	2	1	0	2	0	0	3
	LT11	7076	Lower Tanezzuft	L. Silurian	0	0	2	1	0	2	0	1	3
A1-70	AOA1	6561	Aouinet ouenine A	M. Devonian	0	0	7	0	0	0	0	0	1
	OK1	6930	Ouan kasa	M. Devonian	0	0	7	0	0	0	0	0	1
	AC1	8951	Acacus	U. Silurian	0	3	7	0	0	0	0	0	1
	AC2	8960	Acacus	U. Silurian	0	3	7	0	0	0	0	0	1
	AC3	8971	Acacus	U. Silurian	0	3	7	0	0	0	0	0	1
	AC4	8980	Acacus	U. Silurian	0	3	7	0	0	0	0	0	1
	UT4	9017	Upper Tanezzuft	L. Silurian	0	0	7	0	0	0	0	0	1
	UT5	9029	Upper Tanezzuft	L. Silurian	0	0	7	0	0	0	0	0	1
	UT6	9049	Upper Tanezzuft	L. Silurian	0	0	7	0	0	0	0	0	1
	UT7	9066	Upper Tanezzuft	L. Silurian	0	0	7	0	0	0	0	0	1
	UT8	9085	Upper Tanezzuft	L. Silurian	0	0	7	0	0	0	0	0	1
	UT9	9103	Upper Tanezzuft	L. Silurian	0	0	7	0	0	0	0	0	1
	UT10	9123	Upper Tanezzuft	L. Silurian	0	0	7	0	0	0	0	0	1
	UT11	9295	Upper Tanezzuft	L. Silurian	0	0	7	0	0	0	0	0	1
	UT12	9447	Upper Tanezzuft	L. Silurian	0	0	6	2	0	0	0	1	2
	UT13	9993	Upper Tanezzuft	L. Silurian	0	0	5	1	0	2	3	0	1
	UT14	9999	Upper Tanezzuft	L. Silurian	0	0	4	1	0	2	0	1	1
	UT15	10005	Upper Tanezzuft	L. Silurian	0	0	5	1	0	1	3	0	1
A9-NC7	TH2	5703	Tahara	U. Devonian	1	3	7	0	1	0	0	0	1
	TH3	5705	Tahara	U. Devonian	1	3	5	0	1	0	0	0	1
	TH4	5708	Tahara	U. Devonian	2	3	5	2	1	0	0	0	1

wellname	Samno	Depth	Formation	Age	Lith	Dlith	Colour	S.Struct	Bioturb	Grapto	Fossils	Pyrite	Mica
A9-NC7	TH5	5712	Tahara	U. Devonian	0	3	5	3	0	0	0	0	1
	TH6	5715	Tahara	U. Devonian	1	3	6	0	1	0	0	0	2
	TH7	5718	Tahara	U. Devonian	0	3	2	1	0	0	0	1	3
	TH8	5721	Tahara	U. Devonian	1	3	7	0	1	0	0	1	1
	TH9	5733	Tahara	U. Devonian	0	3	3	1	0	0	0	0	1
	TH10	5754	Tahara	U. Devonian	1	3	5	3	1	0	0	0	1
	TH11	5762	Tahara	U. Devonian	0	3	4	1	0	0	0	0	1
	TH12	5770	Tahara	U. Devonian	1	3	4	1	1	0	0	0	2
	TH13	5773	Tahara	U. Devonian	0	3	5	1	1	0	0	0	2
	TH14	5783	Tahara	U. Devonian	1	3	5	0	1	0	0	0	1
	TH15	5797	Tahara	U. Devonian	1	3	7	0	1	0	0	0	1
	TH16	5802	Tahara	U. Devonian	0	3	3	1	0	0	0	0	3
	TH17	5813	Tahara	U. Devonian	0	3	4	1	0	0	0	0	2
Z5-NC5	AC5	9074	Acacus	U. Silurian	0	3	7	0	2	0	0	0	1
	UT16	9303	Upper Tanezzuft	L. Silurian	2	0	7	0	2	0	0	0	1
	UT17	9310	Upper Tanezzuft	L. Silurian	1	0	7	0	0	0	0	0	1
	UT18	9317	Upper Tanezzuft	L. Silurian	2	0	7	0	2	0	0	0	1
	UT19	9324	Upper Tanezzuft	L. Silurian	0	0	7	3	1	0	0	1	1
	UT20	10115	Upper Tanezzuft	L. Silurian	0	0	7	3	0	0	5	0	2
	UT21	10124	Upper Tanezzuft	L. Silurian	0	0	7	3	1	0	0	1	1
	UT22	10136	Upper Tanezzuft	L. Silurian	0	0	7	1	0	0	5	1	1
M2-NC7	TH18	6227	Tahara	U. Devonian	0	3	2	1	0	0	0	0	3
	TH19	6247	Tahara	U. Devonian	0	3	2	1	0	0	0	0	3
	TH20	6251	Tahara	U. Devonian	0	0	4	1	0	0	0	1	2
	AOA2	7259	Aouinat ouenine A	U. Devonian	1	0	7	0	0	0	0	1	3
	AOA3	7264	Aouinat ouenine A	U. Devonian	1	0	7	0	0	0	0	1	2
C1-26	AOC1	6485	Aouinat ouenine C	U. Devonian	0	3	5	1	0	0	0	1	3
	AOC2	6488	Aouinat ouenine C	U. Devonian	0	3	5	1	0	0	0	1	3
	AOC3	6491	Aouinat ouenine C	U. Devonian	0	3	5	1	0	0	0	1	3
	AOC4	6494	Aouinat ouenine C	U. Devonian	0	3	5	1	0	0	0	1	3
	AOC5	6497	Aouinat ouenine C	U. Devonian	0	3	5	1	0	0	0	1	3
	AOC6	6500	Aouinat ouenine C	U. Devonian	0	3	5	1	0	0	0	1	3
	AOC7	6503	Aouinat ouenine C	U. Devonian	0	3	5	1	0	0	0	1	3
	AOC8	6505	Aouinat ouenine C	U. Devonian	0	3	5	1	0	0	0	1	3
A1-90	TH21	7552	Tahara	U. Devonian	0	3	4	1	0	0	0	0	2
	TH22	7569	Tahara	U. Devonian	0	3	4	1	0	0	0	0	3

wellIn	Samno	Depth	Formation	Age	Lith	Dlith	Colour	S.Struct	Bioturb	Grapto	Fossils	Pyrite	Mica
A1-90	AC6	11185	Acacus	U. Silurian	2	3	7	0	2	0	0	0	2
	AC7	11195	Acacus	U. Silurian	2	3	7	0	2	0	0	0	2
	UT23	11901	Upper Tanezzuft	L. Silurian	0	0	5	1	0	0	0	1	1
	UT24	11904	Upper Tanezzuft	L. Silurian	0	0	5	1	0	0	0	1	1
	UT25	11905	Upper Tanezzuft	L. Silurian	0	0	5	1	0	0	0	1	1
	UT26	11921	Upper Tanezzuft	L. Silurian	0	0	5	1	0	0	3	1	2
B2-NC2	UT27	10091	Upper Tanezzuft	L. Silurian	1	0	7	3	0	0	0	1	1
	UT28	10093	Upper Tanezzuft	L. Silurian	1	0	7	3	0	0	0	1	1
	UT29	10094	Upper Tanezzuft	L. Silurian	1	0	6	3	0	0	0	1	1
	UT30	10096	Upper Tanezzuft	L. Silurian	1	0	7	3	0	0	0	1	1
	UT31	10099	Upper Tanezzuft	L. Silurian	1	0	7	3	0	0	0	1	1
	UT32	10101	Upper Tanezzuft	L. Silurian	1	0	6	3	0	0	0	1	1
	UT33	10108	Upper Tanezzuft	L. Silurian	0	0	5	2	0	0	4	1	1
	UT34	10105	Upper Tanezzuft	L. Silurian	0	0	5	2	0	0	0	1	3
B1-49	AOC9	1428	Aouinat ouenine C	U. Devonian	1	3	5	2	1	0	0	0	2
	AOC10	1434	Aouinat ouenine C	U. Devonian	0	3	5	1	0	0	0	1	3
	AOC11	1435	Aouinat ouenine C	U. Devonian	0	3	5	1	0	0	0	1	3
	AOC12	1438	Aouinat ouenine C	U. Devonian	0	3	5	1	0	0	0	1	3
	AOC13	1442	Aouinat ouenine C	U. Devonian	0	3	5	1	0	0	0	1	1
	AOC14	1445	Aouinat ouenine C	U. Devonian	0	3	5	1	0	0	0	1	2
	AOC15	1448	Aouinat ouenine C	U. Devonian	0	3	5	1	0	0	0	1	2
	AOC16	1451	Aouinat ouenine C	U. Devonian	0	3	5	1	0	0	0	1	3
	UT35	2132	Upper Tanezzuft	L. Silurian	0	0	5	1	0	0	0	1	3
	UT36	2135	Upper Tanezzuft	L. Silurian	0	0	5	1	0	0	0	1	3
A1-66	AOC17	3153	Aouinat ouenine C	U. Devonian	1	3	5	3	0	0	0	0	2
	AOC18	3156	Aouinat ouenine C	U. Devonian	1	3	5	3	0	0	0	0	2
	AOB1	3330	Aouinat ouenine B	U. Devonian	0	0	7	3	0	0	0	1	1
	OK2	4104	Ouan kasa	M. Devonian	2	0	7	3	0	0	0	1	3
	OK2	4115	Ouan kasa	M. Devonian	0	0	7	2	0	0	0	0	0
	UT35	4379	Upper Tanezzuft	L. Silurian	0	0	7	3	0	0	0	1	1
	UT36	4382	Upper Tanezzuft	L. Silurian	0	0	7	3	0	0	0	1	1
	UT37	4550	Upper Tanezzuft	L. Silurian	0	0	5	3	0	1	0	1	1
	UT38	4553	Upper Tanezzuft	L. Silurian	1	0	5	0	0	0	0	1	1
	UT39	4765	Upper Tanezzuft	L. Silurian	1	0	7	0	0	0	0	1	2
	UT40	4836	Upper Tanezzuft	L. Silurian	0	0	5	2	0	0	0	1	1
	UT41	4842	Upper Tanezzuft	L. Silurian	0	0	5	2	0	0	0	1	1
	UT42	5051	Upper Tanezzuft	L. Silurian	0	0	5	1	0	1	0	1	1
	LT12	5054	Lower Tanezzuft	L. Silurian	0	0	3	1	0	1	0	2	1

APPENDIX II

Appendex II: Simple percentages of the kerogen counts categories

Key to abbreviation used in column headers (parameters all percentages based on 300 counts per sample):

Welln	=	well name
Samno	=	sample number
%Phy.	=	percentage of phytoclasts of total kerogen counts
%AOM	=	percentage of AOM of total kerogen counts
%Paly.	=	percentage of palynomorphs of total kerogen counts
SPORO%	=	sporomorphs
PLANK%	=	marine plankton
UNDIF%	=	undifferentiated palynomorphs
MEM%	=	membranes
CUTIC%	=	cuticle
BLKLAT%	=	lath shaped black wood
BLKEQUI%	=	equant shaped black wood
USPSU%	=	pseudoamorphous non-biostructured brown wood
USCO%	=	corroded non-biostructured brown wood
USUN%	=	Undegraded non-biostructured brown wood
STDEG%	=	total degraded biostructured brown wood
STUND%	=	total Undegraded biostructured brown wood

wellname	Samnos	Depth	%Phy.	%AOM	%Paly.	SPORO%	PLANK%	UNDIF%	MEM%	CUTIC%	BLKLAT%	BLKEQUI%	USPSU%	USCO%	USUN%	STDEG%	STUND%
F1-66	TH1	4127	43	21	36.3	36.2	0.1	0.0	0.0	0.0	10.8	22.2	0	1.1	4.3	3.7	1.1
	TD1	5476	8.6	8.4	83.0	24.6	58.4	0.0	3.8	0.8	0.0	0.0	0	0.7	0.8	2.0	0.5
	UT1	6455	4	70.5	25.5	2.4	22.2	0.9	1.0	0.0	0.0	0.0	0	0.5	0.3	2.0	0.2
	UT2	6470	0	77	23.0	0.0	22.9	0.0	0.0	0.0	0.0	0.0	0	0.0	0.0	0.0	0.0
	UT3	6473	0	78.7	21.3	0.1	20.5	0.7	0.0	0.0	0.0	0.0	0	0.0	0.0	0.0	0.0
	LT1	7042	0	86.6	13.4	0.0	11.3	2.1	0.0	0.0	0.0	0.0	0	0.0	0.0	0.0	0.0
	LT2	7047	0	81	19.0	0.0	17.7	1.3	0.0	0.0	0.0	0.0	0	0.0	0.0	0.0	0.0
	LT3	7051	0	98	2.0	0.0	0.0	2.0	0.0	0.0	0.0	0.0	0	0.0	0.0	0.0	0.0
	LT4	7053	0	98	2.0	0.0	0.0	2.0	0.0	0.0	0.0	0.0	0	0.0	0.0	0.0	0.0
	LT5	7054	0	96	4.0	0.0	0.0	4.0	0.0	0.0	0.0	0.0	0	0.0	0.0	0.0	0.0
	LT6	7057	0	96	3.7	0.0	0.0	3.7	0.0	0.0	0.0	0.0	0	0.0	0.0	0.0	0.0
	LT7	7061	0	78	21.6	0.0	18.6	3.0	0.0	0.0	0.0	0.0	0	0.0	0.0	0.0	0.0
	LT8	7063	0	84	16.0	0.0	12.5	3.5	0.0	0.0	0.0	0.0	0	0.0	0.0	0.0	0.0
	LT9	7065	0	99	1.0	0.0	0.0	1.0	0.0	0.0	0.0	0.0	0	0.0	0.0	0.0	0.0
	LT10	7073	0	97.3	2.7	0.0	0.0	2.7	0.0	0.0	0.0	0.0	0	0.0	0.0	0.0	0.0
	LT11	7076	0	96.3	3.7	0.0	0.0	3.7	0.0	0.0	0.0	0.0	0	0.0	0.0	0.0	0.0
A1-70	AOA1	6561	13.3	15.7	71.0	53.7	17.3	0.0	0.1	0.0	0.6	9.1	0	1.4	1.3	0.8	0.1
	OK1	6930	80	8.4	11.6	11.2	0.4	0.0	73.2	0.0	0.0	6.4	0	0.0	0.4	0.0	0.0
	AC1	8951	21	18.2	61.0	25.7	35.3	0.0	2.7	1.4	0.4	0.2	6.9	1.3	1.3	6.3	0.3
	AC2	8960	8	24.4	67.6	32.4	34.5	0.7	0.3	1.1	0.6	0.2	1.1	0.9	0.5	3.2	0.0
	AC3	8971	13.3	37.4	49.3	7.2	42.1	0.0	1.4	2.3	0.0	0.1	2.7	0.1	0.9	5.2	0.4
	AC4	8980	9.6	27.8	62.6	10.8	51.8	0.0	0.6	0.9	0.0	0.0	2.2	0.3	0.3	5.0	0.3
	UT4	9017	1	21.6	77.4	9.1	68.1	0.2	0.4	0.2	0.0	0.0	0.0	0.0	0.3	0.0	0.1
	UT5	9029	1	53.6	45.4	3.0	41.8	0.6	0.3	0.1	0.0	0.0	0.3	0.1	0.1	0.0	0.1
	UT6	9049	0.3	46	53.7	4.3	49.1	0.3	0.0	0.0	0.0	0.0	0	0.0	0.3	0.0	0.0
	UT7	9066	2	58.4	39.6	7.8	31.8	0.0	0.3	1.0	0.0	0.0	0	0.0	0.7	0.0	0.0
	UT8	9085	4	31.4	64.6	24.5	39.1	0.9	0.8	2.0	0.0	0.0	0	0.0	1.2	0.0	0.0
	UT9	9103	5.4	24.3	70.3	16.5	51.9	2.0	1.4	1.1	0.0	0.0	0	0.2	1.5	1.0	0.1
	UT10	9123	2.5	31.7	65.8	8.4	57.2	0.1	0.7	0.5	0.0	0.0	0	0.1	0.6	0.5	0.1
	UT11	9295	2.6	25.4	72.0	9.8	61.1	1.2	0.6	1.2	0.0	0.0	0	0.0	0.8	0.0	0.0
	UT12	9447	2	79	19.0	0.4	18.6	0.0	0.0	2.0	0.0	0.0	0	0.0	0.0	0.0	0.0
	UT13	9993	0	68	31.7	0.1	31.6	0.0	0.0	0.0	0.0	0.0	0	0.0	0.0	0.0	0.0
	UT14	9999	0	70	31.4	0.0	30.1	0.3	0.0	0.0	0.0	0.0	0	0.0	0.0	0.0	0.0
	UT15	10005	0	66	34.0	0.1	33.5	0.4	0.0	0.0	0.0	0.0	0	0.0	0.0	0.0	0.0
A9-NC7	TH2	5703	25.6	5.6	68.8	67.8	1.0	0.0	0.0	0.5	1.8	12.8	0	2.4	4.5	0.9	2.6
	TH3	5705	40	23	36.6	36.4	0.2	0.0	0.0	1.0	4.0	21.6	0	4.4	4.8	1.6	2.6
	TH4	5708	23.6	2	74.4	73.4	1.0	0.0	0.0	0.0	1.4	11.1	0	0.7	3.5	0.5	6.4
	TH5	5712	29	8.7	62.0	57.4	4.6	0.0	0.8	0.4	3.5	11.2	0	2.8	0.0	1.2	9.4
	TH6	5715	41.6	3	55.4	52.2	3.2	0.0	1.2	0.6	3.7	15.8	0	0.0	3.3	6.0	10.8

welln	Samno	Depth	%Phy.	%AOM	%Paly.	SPORO%	PLANK%	UNDIF%	MEM%	CUTIC%	BLKLAT%	BLKEQUI%	USPSU%	USCO%	USUN%	STDEG%	STUND%
A9-NC7	TH7	5718	48	15	36.6	36.4	0.2	0.0	8.2	0.0	1.9	16.0	0	4.4	9.7	5.3	2.9
	TH8	5721	61	4	35.0	34.7	0.3	0.0	0.0	0.0	5.2	40.2	0	4.6	2.1	4.0	4.9
	TH9	5733	8	76	16.0	16.0	0.0	0.0	0.0	0.0	0.0	1.7	0	0.5	5.4	0.3	0.1
	TH10	5754	26.4	26	47.6	46.6	1.0	0.0	0.0	0.0	1.6	14.0	0	2.0	5.5	0.3	3.0
	TH11	5762	27	6.4	66.6	64.2	2.4	0.0	7.3	0.0	1.2	9.5	0	0.3	5.3	0.0	3.5
	TH12	5770	26	5.8	68.6	67.9	0.7	0.0	0.3	0.0	2.0	16.4	0	0.8	5.1	0.0	1.0
	TH13	5773	28.6	3	68.4	63.7	4.7	0.0	0.4	0.0	2.0	17.3	0	0.3	4.7	0.0	3.9
	TH14	5783	25	14	61.3	60.7	0.6	0.0	0.5	0.4	2.5	19.2	0	0.0	1.4	0.2	0.5
	TH15	5797	19.6	35	45.4	45.3	0.1	0.0	4.6	0.0	0.5	7.8	0	0.4	2.8	0.2	3.3
	TH16	5802	49.6	8.8	41.6	40.4	1.2	0.0	6.4	0.0	5.0	25.8	0	0.0	6.4	0.0	6.0
	TH17	5813	28	5.7	66.3	62.6	3.7	0.0	4.5	0.0	1.4	12.6	0	0.0	4.3	0.0	5.2
Z5-NC5	AC5	9074	12	19.1	69.3	30.7	38.6	0	2.0	4.1	0.0	0.0	0.9	0.1	0.6	3.3	0.6
	UT16	9303	1.3	60.4	38.3	12.5	23.9	1.8	0.3	0.6	0.0	0.0	0.2	0.1	0.1	0.0	0.0
	UT17	9310	4	28	68.0	22.6	45.2	0.2	1.1	0.9	0.0	0.0	0.5	0.2	0.8	0.5	0.1
	UT18	9317	1	41	58.0	8.6	49.2	0.2	0.3	0.3	0.0	0.0	0.1	0.1	0.1	0.0	0.0
	UT19	9324	3	57.7	39.3	4.1	34.6	0.6	0.8	0.3	0.0	0.0	1.4	0.1	0.2	0.1	0.1
	UT20	10115	0	78	21.7	9.9	11.5	0.3	0.0	0.0	0.0	0.0	0.0	0.0	0.0	0.0	0.0
	UT21	10124	2.6	43	54.4	6.2	48.0	0.2	0.9	0.1	0.0	0.0	0.7	0.1	0.4	0.2	0.1
	UT22	10136	0	73	27.0	0.6	26.3	0.1	0.0	0.0	0.0	0.0	0.0	0.0	0.0	0.0	0.0
M2-NC7	TH18	6227	15	49.1	35.6	34	1.6	0	0.0	0.0	0.1	3.8	0	0.2	10.2	0.4	0.6
	TH19	6247	18	38	44.6	44.6	0.0	0.0	0.0	0.0	0.9	4.4	0	0.5	5.5	1.1	5.2
	AOA3	7264	29	12	59.4	49.1	10.3	0.0	0.4	0.9	0.1	0.6	5	17.9	2.1	1.1	0.4
C1-26	AOC1	6485	19	23.1	58.3	55.7	2.6	0.0	0.3	0.1	1.2	7.5	0	2.1	2.2	2.5	2.6
	AOC2	6488	22.6	6.4	71.0	68.3	2.7	0.0	0.2	0.0	1.1	8.9	0	3.1	3.8	1.5	4.0
	AOC3	6491	20.3	4.3	75.4	70.1	5.3	0.0	0.6	0.0	1.1	12.0	0	0.3	3.0	2.3	0.9
	AOC4	6494	33.3	5	61.7	58.9	2.8	0.0	1.5	0.0	1.3	18.3	0	1.0	6.3	1.5	3.3
	AOC5	6497	19.6	30.8	49.6	44.2	5.4	0.0	0.0	0.0	0.9	9.7	0	0.5	4.8	2.0	1.8
	AOC6	6500	26.6	32.6	40.8	38.3	2.5	0.0	0.0	0.0	1.7	12.4	0	1.6	4.9	2.0	4.0
	AOC7	6503	24	26	50.0	48.0	2.0	0.0	0.4	0.0	1.0	8.6	0	1.6	8.0	2.6	1.8
	AOC8	6505	37	1	62.3	60.8	1.5	0.0	3.5	0.0	4.0	16.1	0	2.6	4.4	3.3	2.7
A1-90	TH21	7552	19	6	75.6	73.2	2.4	0.0	0.2	0.0	1.5	8.6	0	2.5	3.7	0.7	1.4
	TH22	7569	23	0	76.7	68.7	8.0	0.0	0.1	0.0	3.0	13.5	0	1.2	4.2	0.8	0.5
B2-NC2	UT27	10091	2	59	39.0	9.6	29.4	0.0	0.1	0.7	0.0	0.0	0.5	0.2	0.4	0.0	0.0
	UT28	10093	1.3	63.7	35.0	7.9	27.1	0.0	0.1	0.1	0.0	0.0	0.4	0.1	0.2	0.3	0.0
	UT29	10094	0	87	13.0	1.7	11.3	0.0	0.0	0.0	0.0	0.0	0	0.0	0.0	0.0	0.0
	UT30	10096	0.6	73.6	25.8	2.2	23.6	0.0	0.1	0.1	0.1	0.0	0	0.0	0.3	0.0	0.0
	UT31	10099	0	53.4	46.6	4.7	41.9	0.0	0.0	0.0	0.0	0.0	0	0.0	0.0	0.0	0.0
	UT32	10101	0	71.4	28.6	1.3	27.3	0.0	0.0	0.0	0.0	0.0	0	0.0	0.0	0.0	0.0
	UT33	10108	0	60	40.0	0.0	40.0	0.0	0.0	0.0	0.0	0.0	0	0.0	0.0	0.0	0.0
	UT34	10105	0	63	37.0	1.6	35.4	0.0	0.0	0.0	0.0	0.0	0	0.0	0.0	0.0	0.0

wellname	Samno	Depth	%Phy.	%AOM	%Paly.	SPORO%	PLANK%	UNDIF%	MEM%	CUTIC%	BLKLAT%	BLKEQUI%	USPSU%	USCO%	USUN%	STDEG%	STUND%
B1-49	AOC9	1428	39.3	7	53.7	53.4	0.3	0.0	0.8	0.4	0.6	11.8	0	0.8	11.2	2.0	11.8
	AOC10	1434	35.6	1.4	63.0	51.8	11.2	0.0	0.0	0.0	3.9	18.5	0	0.7	6.8	0.4	5.3
	AOC11	1435	34	4	62.0	52.1	9.9	0.0	0.0	0.0	3.0	20.0	0	1.0	5.3	0.6	4.1
	AOC12	1438	35	16	49.0	41.9	7.1	0.0	5.8	0.0	1.8	12.3	0	2.5	8.6	1.8	2.5
	AOC13	1442	8	6.8	85.6	75.0	10.6	0.0	0.6	0.0	0.9	3.5	0	0.0	0.9	0.2	1.4
	AOC14	1445	28.3	14.4	57.3	35.3	22.0	0.0	0.6	0.0	1.6	20.4	0	1.0	2.1	0.8	1.8
	AOC15	1448	22	9.4	68.3	64.5	3.8	0.0	2.7	0.1	1.8	9.0	0	1.2	2.1	2.8	2.6
	AOC16	1451	40.3	3.7	56.0	55.3	0.7	0.0	1.8	0.0	1.2	12.9	0	0.4	15.3	1.0	7.7
	UT35	2132	5	44.2	51.0	27.6	22.7	0.5	0	0.0	1.3	0.9	0	1.0	0.2	1.3	0.1
A1-66	AOC17	3153	53.6	7	39.4	39.2	0.2	0.1	1.3	0.0	4.3	30.0	0	4.8	2.7	7.2	3.2
	AOC18	3156	54.6	7	38.4	37.7	0.4	0.3	0.5	0.0	3.3	24.0	0	12.3	5.5	7.1	1.9
	AOB1	3330	2	29.6	68.4	0.0	0.0	0.0	0.1	0.6	0.0	0.0	0	0.0	1.1	0.1	0.1
	OK2	4104	0.3	49	50.7		0.0	0.0	0.0	0.0	0.0	0.0	0	0.0	0.3	0.0	0.0
	OK2	4115					0.0	0.0	0.0	0.0	0.0	0.0	0	0.0	0.0	0.0	0.0
	UT35	4379	0	62.7	37.3	5.4	30.6	1.3	0.0	0.0	0.0	0.0	0	0.0	0.0	0.0	0.0
	UT36	4382	0	70.6	29.4	2.1	26.2	1.1	0.0	0.0	0.0	0.0	0	0.0	0.0	0.0	0.0
	UT37	4550	0	70	30.0	1.1	27.7	1.1	0.0	0.0	0.0	0.0	0	0.0	0.0	0.0	0.0
	UT38	4553	0.3	59	40.7	13.2	26.2	1.3	0.0	0.0	0.0	0.0	0	0.0	0.3	0.0	0.0
	UT39	4765	0	74.4	25.6	1.2	23.9	0.5	0.0	0.0	0.0	0.0	0	0.0	0.0	0.0	0.0
	UT40	4836	0	66.3	33.7	0.8	32.0	0.9	0.0	0.0	0.0	0.0	0	0.0	0.0	0.0	0.0
	UT41	4842	0	66.7	33.3	0.0	32.9	0.4	0.0	0.0	0.0	0.0	0	0.0	0.0	0.0	0.0
	UT42	5051	0	59.4	40.6	2.4	35.7	2.5	0.0	0.0	0.0	0.0	0	0.0	0.0	0.0	0.0
	LT12	5054	0	93	7.0	0.0	7.0	0.0	0.0	0.0	0.0	0.0	0	0.0	0.0	0.0	0.0

APPENDIX III

Appendix III: Simple percentages of the palynomorph count categories

Key to abbreviation used in column headers (parameters all percentages based on 500 counts per sample):

SAMNO	= sample number
%TNWS	= thin-walled
%TKWS	= thick-walled
%AC	= total acritarchs
%TAS	= *Tasmanites*-type prasinophytes
%LEI	= leiospheres
%CH	= chitinozoa
%SCO	= scolecodents
%GRAP	= graptolite siculae
%UNIDN	= unidentified palynomorph
%ACAN	= acanthomorphous acritarchs
%POLY	= polygonomorphous acritarchs
%NETRO	= netromorphous acritarchs
%MIC	= micrhystidium
OTHER	= unidentified palynomorph

WELLN	SAMNO	DEPTH	%TNWS	%TKWS	%AC	%TAS	%LEI	%CH	%SCO	%GRAP	%UNIDN	%ACAN	%POLY	%NETRO	%MIC
F1-66	TH1	4127	0	99.8	0.2	0.0	0.0	0.0	0	0	0	0	0.2	0	0
	TD1	5476	22.6	7	28.0	0.4	41.0	1.0	0	0	0	6.8	18.4	2.2	0.6
	UT1	6455	0	9.5	24.0	0.7	59.1	3.1	0	0	3.6	6.5	5.7	2.8	9.0
	UT2	6470	0.2	0	11.0	0.7	84.9	3.0	0	0	0.2	2.5	1.5	0.5	6.5
	UT3	6473	0.4	0	11.8	2.2	77.7	4.4	0	0	3.5	6.1	2.6	0.8	2.3
	LT1	7042	0	0	23.2	0.0	57.4	1.5	0	2.2	15.7	3.4	16.4	1.9	1.5
	LT2	7047	0	0	27.6	5.3	55.9	4.6	0	0	6.6	12.6	10.0	4.3	0.7
	LT3	7051	0	0	0	0	0	0	0	0	0	0	0	0	0
	LT4	7053	0	0	0	0	0	0	0	0	0	0	0	0	0
	LT5	7054	0	0	0	0	0	0	0	0	0	0	0	0	0
	LT6	7057	0	0	0	0	0	0	0	0	0	0	0	0	0
	LT7	7061	0	0	49.7	1.3	29.8	0.8	0	4.6	13.8	16.9	25.9	5.3	1.6
	LT8	7063	0	0	43.2	0.0	34.3	0.9	0	0	21.6	31.0	11.6	0.6	0.0
	LT9	7065	0	0	0	0	0	0	0	0	0	0	0	0	0
	LT10	7073	0	0	0	0	0	0	0	0	0	0	0	0	0
	LT11	7076	0	0	0	0	0	0	0	0	0	0	0	0	0
A1-70	AOA1	6561	74.4	1.2	23.6	0.6	0	0	0.2	0	0	18.8	2.0	0	2.8
	OK1	6930	90.3	6.5	3.2	0	0	0	0	0	0	3.2	0.0	0	0
	AC1	8951	41	1.2	2.0	1.0	52.6	2.0	0.2	0	0	0.8	1.2	0.0	0
	AC2	8960	47	1	3.2	3.0	42.8	2.0	0	0	1.0	0.3	2.6	0.3	0
	AC3	8971	14	0.6	2.2	0	80.9	2.3	0	0	0	0.6	0.6	1.0	0
	AC4	8980	16.6	0.7	1.0	0	81.4	0.3	0	0	0	0	1.0	0	0
	UT4	9017	11.2	0.6	5.4	1.8	79.0	1.8	0	0	0.2	2.0	2.0	0.2	1.2
	UT5	9029	6.6	0	6.8	2.0	81.6	1.6	0	0	1.4	0.8	2.0	0.2	3.8
	UT6	9049	8	0	9.8	2.4	76.4	2.8	0.6	0	0	2.2	5.0	0.6	2.0
	UT7	9066	19.6	0	11.2	0.3	67.3	1.6	0	0	0	2.3	5.3	1.6	2.0
	UT8	9085	27.8	10.2	8.4	2.0	45.8	4.0	0.4	0	1.4	2.8	1.8	1.2	2.6
	UT9	9103	21.96	1.44	15.0	3.0	52.6	3.2	0	0	2.8	4.1	6.2	1.2	3.5
	UT10	9123	9.4	3.4	21.0	1	64.6	1.4	0	0	0.2	4.2	11.4	2.0	3.4
	UT11	9295	12	1.6	10.4	1.6	70.2	2.6	0	0	1.6	2.6	6.0	1.0	0.8
	UT12	9447	2.3	0	11.2	24.0	59.0	3.5	0	0	0.0	4.0	0.6	0.6	6.0
	UT13	9993	0.3	0	14.5	8.9	75.3	0.0	0	0	0.0	6.6	6.6	0.3	2.0
	UT14	9999	0	0	12.4	15.5	67.9	0.8	0	2.4	1.0	0.9	8.5	1.0	2.0
	UT15	10005	0.2	0	11.6	12.6	72.2	1.2	0	1	1.2	5.4	6.2	0	0
A9-NC7	TH2	5703	77	21.6	1.4	0	0	0	0	0	0	0	1.4	0	0
	TH3	5705	70	29.4	0	0.6	0	0	0	0	0	0	0	0	0
	TH4	5708	72.4	26.2	1.4	0	0	0	0	0	0	0.8	0.6	0	0

WELLN	SAMNO	DEPTH	%TNWS	%TKWS	%AC	%TAS	%LEI	%CH	%SCO	%GRAP	%UNIDN	%ACAN	%POLY	%NETRO	%MIC
A9-NC7	TH5	5712	0	92.6	3.6	3.8	0	0	0	0	0	2.8	0.8	0	0
	TH6	5715	75.2	19	5.4	0	0	0	0.4	0	0	4.4	1.0	0	0
	TH7	5718	17.6	81.6	0	0.8	0	0	0.0	0	0	0	0	0	0
	TH8	5721	30	69.2	0	0.6	0	0	0.2	0	0	0	0	0	0
	TH9	5733	30.7	69	0	0	0	0	0	0	0	0	0	0	0
	TH10	5754	53	44.8	2.2	0	0	0	0	0	0	0	2.2	0	0
	TH11	5762	58.2	38.2	3.6	0	0	0	0	0	0	0	3.6	0	0
	TH12	5770	29	70	1.0	0	0	0	0	0	0	0	1.0	0	0
	TH13	5773	61.8	31.4	6.8	0	0	0	0	0	0	1.6	5.2	0	0
	TH14	5783	31	69	0	0	0	0	0	0	0	0	0.0	0	0
	TH15	5797	28.2	71.6	0.2	0	0	0	0	0	0	0.2	0.0	0	0
	TH16	5802	0	97	0.0	3.0	0	0	0	0	0	0.0	0.0	0	0
	TH17	5813	38.4	56	5.6	0.0	0	0	0	0	0	0.0	5.6	0	0
Z5-NC5	AC5	9074	44.3	0	15.9	4.3	35.5	0	0	0	0	4.3	5.3	4.3	2.0
	UT16	9303	32.7	0	4.7	1.0	54.8	2.0	0	0	4.8	1.3	3.1	0.3	0
	UT17	9310	33.3	0	7.6	0.3	57.2	1.3	0	0	0.3	1.6	5.0	1.0	0
	UT18	9317	14.8	0	8.8	2.5	71.5	2.0	0	0	0.4	3.2	4.2	1.0	0.4
	UT19	9324	0	10.4	8.4	3.0	64.0	12.4	0.2	0	1.6	0.8	0.8	6.4	0.4
	UT20	10115	0	45.4	4.0	15.6	34.0	0.4	0	0	0.6	1.2	1.4	1.0	0.4
	UT21	10124	11.4	0	4.6	2.8	78.0	2.8	0	0	0.4	1.4	2.0	1.2	0
	UT22	10136	2.2	0	15.6	9.4	68.0	4.4	0	0	0.4	9.4	4.8	1.0	0.4
M2-NC7	TH18	6227	0	95.6	0	4.4	0	0	0	0	0	0	0	0	0
	TH19	6247	0	100.0	0	0	0	0	0	0	0	0	0	0	0
	TH20	6251	0	0	18.0	14.0	65.8	0.8	0	1.4	0	9.4	8.6	0	0
	AOA2	7259													
	AOA3	7264	13.4	69.0	12.6	3.0	0	1.2	0.8	0	0	5.0	7.6	0	0
C1-26	AOC1	6485	4.6	91	4.4	0	0	0	0	0	0	0	4.4	0	0
	AOC2	6488	44.4	51.8	3.8	0	0	0	0	0	0	1.0	2.8	0	0
	AOC3	6491	24	69	7.0	0	0	0	0	0	0	0	7.0	0	0
	AOC4	6494	37.4	58	4.6	0	0	0	0	0	0	0.2	4.4	0	0
	AOC5	6497	34.6	54.6	10.8	0	0	0	0	0	0	0	10.8	0	0
	AOC6	6500	40	53.6	6.2	0.2	0	0	0	0	0	0	6.2	0	0
	AOC7	6503	37	59	4.0	0	0	0	0	0	0	0	4.0	0	0
	AOC8	6505	0	97.6	2.4	0	0	0	0	0	0	0	2.4	0	0
A1-90	TH21	7552	0	97	3.2	0	0	0	0	0	0	0.7	2.5	0	0
	TH22	7569	10.6	79	10.4	0	0	0	0	0	0	1.6	8.8	0	0

WELLN	SAMNO	DEPTH	%TNWS	%TKWS	%AC	%TAS	%LEI	%CH	%SCO	%GRAP	%UNIDN	%ACAN	%POLY	%NETRO	%MIC
A1-90	AC6	11185													
	AC7	11195													
	UT23	11901													
	UT24	11904													
	UT25	11905													
	UT26	11921													
B2-NC2	UT27	10091	23.5	1	3.6	0.0	71.8	0.1	0	0	0	0.4	1.4	1.8	0
	UT28	10093	22	0.6	1.6	0.3	71.9	3.6	0	0	0	0.3	1.0	0.3	0
	UT29	10094	12.7	0.7	7.7	4.4	65.6	8.9	0	0	0	0.7	2.1	4.9	0
	UT30	10096	8.4	0	8.6	4.2	76.4	2.4	0	0	0	1.2	4.6	2.8	0
	UT31	10099	10	0	7.0	5.6	76.2	1.2	0	0	0	1.4	3.2	2.4	0
	UT32	10101	4.4	0	6.8	8.4	78.4	2.0	0	0	0	1.4	4.0	0.6	0.8
	UT33	10108	0	0	6.2	19.4	72.0	2.4	0	0	0	1.0	1.0	0.6	3.6
	UT34	10105	4.2	0	6.8	9.4	71.6	8.0	0	0	0	1.6	1.2	1.0	3.0
B1-49	AOC9	1428	45.2	54.2	0.6	0	0	0	0	0	0	0	0.6	0	0
	AOC10	1434	64.8	17.4	17.8	0	0	0	0	0	0	6.8	11.0	0	0
	AOC11	1435	0	84	16.0	0	0	0	0	0	0	5.0	11.0	0	0
	AOC12	1438	53.8	31.8	14.2	0	0	0.2	0	0	0	1.6	12.4	0.2	0
	AOC13	1442	0	87.6	12.2	0.2	0	0	0	0	0	5.2	7.0	0	0
	AOC14	1445	25	36.6	38.4	0	0	0	0	0	0	5.0	33.4	0	0
	AOC15	1448	0	94.4	4.8	0.6	0	0.2	0	0	0	2.0	2.8	0	0
	AOC16	1451	24	74.8	1.2	0	0	0	0	0	0	0.0	1.2	0	0
	UT35	2132	50.8	3.4	11.8	0	31.0	2.0	0	0	1.0	7.4	2.8	1.6	0
	UT36	2135													
A1-66	AOC17	3153	63.6	35.8	0.2	0.2	0	0	0	0	0.2	0.2	0.0	0	0
	AOC18	3156	62.8	35.4	0.8	0.2	0	0	0	0	0.8	0.4	0.4	0	0
	AOB1	3330	35	0	9.4	2.8	52.6	0.6	0	0	0.0	2.6	6.8	0	0
	OK2	4104	4.2	0	11.4	0.2	78.6	0.8	0	0	4.8	3.8	3.6	0.8	3.2
	OK2	4115	65.9	0	4.6	0.6	26.7	1.6	0	0	0.6	1.7	1.7	0.2	1.0
	UT35	4379	14.6	0	15.6	0.2	64.6	1.6	0	0	3.4	4.6	6.0	1.6	3.4
	UT36	4382	7.2	0	15.2	0.6	71.4	1.8	0	0	3.8	4.7	5.4	0.8	4.3
	UT37	4550	3.8	0	21.6	1.4	67.6	1.8	0	0	3.8	6.0	8.2	0.6	6.8
	UT38	4553	2.6	0	14.6	0.6	79.0	0	0	0	3.2	6.0	6.2	0.6	1.8
	UT39	4765	4.8	0	7.0	4.6	80.4	1.4	0	0	1.8	2.0	3.6	0.0	1.4
	UT40	4836	2.4	0	29.8	2.4	61.6	1.2	0	0	2.6	6.8	12.0	2.0	9.0
	UT41	4842	0	0	22.4	0.4	74.6	1.4	0	0	1.2	10.2	7.8	1.4	3.0
	UT42	5051	5.8	0	44.8	0.0	43.2	0.0	0	0	6.2	19.2	21.4	4.2	0
	LT12	5054	0	0	0	0	0	0	0	0	0	0	0	0	0

APPENDIX IV

Appendix IV: Parameters derived from kerogen counts (also includes the results of the geochemical analyses).

Key to abbreviation used in column headers (parameter expressed as a percentage unless otherwise stated):

tnws/sp	= thin-walled of spores
Log 10 (tnws/sp)	= Log 10 ratio thin-walled:total spores
tkws/sp	= thick-walled of spores
Log 10 (tkws/sp)	= Log 10 ratio thick-walled:total spores
ac/mp	= acritarchs of marine plankton
Log 10 (ac/mp)	= Log 10 ratio acritarchs:marinplankton
tas/mp	= *Tasmanites* type prasinophyte of marine plankton
Log 10 (tas/mp)	= Log 10 ratio *Tasmanites*:marine plankton
lei/mp	= leiospheres of marine plankton
Log 10 (lei/mp)	= Log 10 ratio leiospheres:marine plankton
mp/sp	= ratio of total marine plankton:total sporomorph
Log 10 (mp/sp)	= Log 10 ratio marine plankton:total sporomorph
tprasino	= *Tasmanites* + leiospheres
ac/tprasino	= ratio of acritarchs:total prasinophyte
Log 10 (ac/tprasino)	= Log 10 ratio acritarchs:total prasinophyte
acan/poly	= ratio of acantomorphous:polygonomorphous acritaechs
Log 10 (acan/poly)	= Log 10 ratio acantomorphous:polygonomorphous
acan/mic	= ratio of acantomorphous:micrhystidium achritarchs
Log 10 (acan/mic)	= Log 10 ratio acantomorphous:micrhystidium
acan/netro	= ratio of acantomorphous:netromorphous
Log 10 (acan/netro)	= Log 10 ratio acantomorphous:netromorphous
tblk/tbr	= ratio of total black wood:total brown wood
Log 10 (tblk/tbr)	= Log 10 ratio total black wood:total brown wood
blklat/blkeque	= ratio of black lath:black equant wood
Log 10 (blklat/blkeque)	=Log 10 ratio black lath:black equant
phyTOC	= 'phyTOC' parameter (not percentage)
AmOC	= 'AmOC' parameter (not percentge)

WELLN	SAMNO	DEPTH	tnws/sp	Log10(Tnws/sp)	tkws/sp	Log10(Tkws/sp)	ac/mp	Log10(ac/mp)	tas/mp	Log10(tas/mp)	lei/mp	Log10(lei/mp)	mp/sp	Log10(mp/sp)
F1-66	TH1	4127	0.0	#NUM!	1.0	0.0	1.0	0.0	0.0	#NUM!	0.0	#NUM!	0.0	-2.7
	TD1	5476	0.8	-0.1	0.2	-0.6	0.4	-0.4	0.0	-2.2	0.6	-0.2	2.3	0.4
	UT1	6455	0.0	#NUM!	1.0	0.0	0.3	-0.5	0.0	-2.1	0.7	-0.2	8.8	0.9
	UT2	6470	1.0	0.0	0.0	#NUM!	0.1	-0.9	0.0	-2.1	0.9	-0.1	483.0	2.7
	UT3	6473	1.0	0.0	0.0	#NUM!	0.1	-0.9	0.0	-1.6	0.8	-0.1	229.3	2.4
	LT1	7042	#DIV/0!	#DIV/0!	#DIV/0!	#DIV/0!	0.3	-0.5	0.0	#NUM!	0.7	-0.1	#DIV/0!	#DIV/0!
	LT2	7047	#DIV/0!	#DIV/0!	#DIV/0!	#DIV/0!	0.3	-0.5	0.1	-1.2	0.6	-0.2	#DIV/0!	#DIV/0!
	LT3	7051	#DIV/0!	#DIV/0!	#DIV/0!	#DIV/0!	#DIV/0!	#DIV/0!	#DIV/0!	#DIV/0!	#DIV/0!	#DIV/0!	#DIV/0!	#DIV/0!
	LT4	7053	#DIV/0!	#DIV/0!	#DIV/0!	#DIV/0!	#DIV/0!	#DIV/0!	#DIV/0!	#DIV/0!	#DIV/0!	#DIV/0!	#DIV/0!	#DIV/0!
	LT5	7054	#DIV/0!	#DIV/0!	#DIV/0!	#DIV/0!	#DIV/0!	#DIV/0!	#DIV/0!	#DIV/0!	#DIV/0!	#DIV/0!	#DIV/0!	#DIV/0!
	LT6	7057	#DIV/0!	#DIV/0!	#DIV/0!	#DIV/0!	#DIV/0!	#DIV/0!	#DIV/0!	#DIV/0!	#DIV/0!	#DIV/0!	#DIV/0!	#DIV/0!
	LT7	7061	#DIV/0!	#DIV/0!	#DIV/0!	#DIV/0!	0.6	-0.2	0.0	-1.8	0.4	-0.4	#DIV/0!	#DIV/0!
	LT8	7063	#DIV/0!	#DIV/0!	#DIV/0!	#DIV/0!	0.6	-0.3	0.0	#NUM!	0.4	-0.4	#DIV/0!	#DIV/0!
	LT9	7065	#DIV/0!	#DIV/0!	#DIV/0!	#DIV/0!	#DIV/0!	#DIV/0!	#DIV/0!	#DIV/0!	#DIV/0!	#DIV/0!	#DIV/0!	#DIV/0!
	LT10	7073	#DIV/0!	#DIV/0!	#DIV/0!	#DIV/0!	#DIV/0!	#DIV/0!	#DIV/0!	#DIV/0!	#DIV/0!	#DIV/0!	#DIV/0!	#DIV/0!
	LT11	7076	#DIV/0!	#DIV/0!	#DIV/0!	#DIV/0!	#DIV/0!	#DIV/0!	#DIV/0!	#DIV/0!	#DIV/0!	#DIV/0!	#DIV/0!	#DIV/0!
A1-70	AOA1	6561	1.0	0.0	0.0	-1.8	1.0	0.0	0.0	-1.6	0.0	#NUM!	0.3	-0.5
	OK1	6930	0.9	0.0	0.1	-1.2	1.0	0.0	0.0	#NUM!	0.0	#NUM!	0.0	-1.5
	AC1	8951	1.0	0.0	0.0	-1.5	0.0	-1.4	0.0	-1.7	0.9	0.0	1.3	0.1
	AC2	8960	1.0	0.0	0.0	-1.7	0.1	-1.2	0.1	-1.2	0.9	-0.1	1.0	0.0
	AC3	8971	1.0	0.0	0.0	-1.4	0.0	-1.6	0.0	#NUM!	1.0	0.0	5.7	0.8
	AC4	8980	1.0	0.0	0.0	-1.4	0.0	-1.9	0.0	#NUM!	1.0	0.0	4.8	0.7
	UT4	9017	0.9	0.0	0.1	-1.3	0.1	-1.2	0.0	-1.7	0.9	0.0	7.3	0.9
	UT5	9029	1.0	0.0	0.0	#NUM!	0.1	-1.1	0.0	-1.7	0.9	0.0	13.7	1.1
	UT6	9049	1.0	0.0	0.0	#NUM!	0.1	-1.0	0.0	-1.6	0.9	-0.1	11.1	1.0
	UT7	9066	1.0	0.0	0.0	#NUM!	0.1	-0.8	0.0	-2.4	0.9	-0.1	4.0	0.6
	UT8	9085	0.7	-0.1	0.3	-0.6	0.1	-0.8	0.0	-1.4	0.8	-0.1	1.5	0.2
	UT9	9103	0.9	0.0	0.1	-1.2	0.2	-0.7	0.0	-1.4	0.7	-0.1	3.0	0.5
	UT10	9123	0.7	-0.1	0.3	-0.6	0.2	-0.6	0.0	-1.9	0.7	-0.1	6.8	0.8
	UT11	9295	0.9	-0.1	0.1	-0.9	0.1	-0.9	0.0	-1.7	0.9	-0.1	6.0	0.8
	UT12	9447	1.0	0.0	0.0	#NUM!	0.1	-0.9	0.3	-0.6	0.6	-0.2	41.0	1.6
	UT13	9993	1.0	0.0	0.0	#NUM!	0.1	-0.8	0.1	-1.0	0.8	-0.1	332.3	2.5
	UT14	9999	#DIV/0!	#DIV/0!	#DIV/0!	#DIV/0!	0.1	-0.9	0.2	-0.8	0.7	-0.1	#DIV/0!	#DIV/0!
	UT15	10005	1.0	0.0	0.0	#NUM!	0.1	-0.9	0.1	-0.9	0.7	-0.1	482.0	2.7
A9-NC7	TH2	5703	0.8	-0.1	0.2	-0.7	1.0	0.0	0.0	#NUM!	0.0	#NUM!	0.0	-1.8
	TH3	5705	0.7	-0.2	0.3	-0.5	0.0	#NUM!	1.0	0.0	0.0	#NUM!	0.0	-2.2
	TH4	5708	0.7	-0.1	0.3	-0.6	1.0	0.0	0.0	#NUM!	0.0	#NUM!	0.0	-1.8

WELLN	SAMNO	DEPTH	tnws/sp	Log10(Tnws/sp)	tkws/sp	Log10(Tkws/sp)	ac/mp	Log10(ac/mp)	tas/mp	Log10(tas/mp)	lei/mp	Log10(lei/mp)	mp/sp	Log10(mp/sp)
A9-NC7	TH5	5712	0.0	#NUM!	1.0	0.0	0.5	-0.3	0.5	-0.3	0.0	#NUM!	0.1	-1.1
	TH6	5715	0.8	-0.1	0.2	-0.7	1.0	0.0	0.0	#NUM!	0.0	#NUM!	0.1	-1.2
	TH7	5718	0.2	-0.8	0.8	-0.1	0.0	#NUM!	1.0	0.0	0.0	#NUM!	0.0	-2.1
	TH8	5721	0.3	-0.5	0.7	-0.2	0.0	#NUM!	1.0	0.0	0.0	#NUM!	0.0	-2.2
	TH9	5733	0.3	-0.5	0.7	-0.2	#DIV/0!	#DIV/0!	#DIV/0!	#DIV/0!	#DIV/0!	#DIV/0!	0.0	#NUM!
	TH10	5754	0.5	-0.3	0.5	-0.3	1.0	0.0	0.0	#NUM!	0.0	#NUM!	0.0	-1.6
	TH11	5762	0.6	-0.2	0.4	-0.4	1.0	0.0	0.0	#NUM!	0.0	#NUM!	0.0	-1.4
	TH12	5770	0.3	-0.5	0.7	-0.2	1.0	0.0	0.0	#NUM!	0.0	#NUM!	0.0	-2.0
	TH13	5773	0.7	-0.2	0.3	-0.5	1.0	0.0	0.0	#NUM!	0.0	#NUM!	0.1	-1.1
	TH14	5783	0.3	-0.5	0.7	-0.2	#DIV/0!	#DIV/0!	#DIV/0!	#DIV/0!	#DIV/0!	#DIV/0!	0.0	#NUM!
	TH15	5797	0.3	-0.5	0.7	-0.1	1.0	0.0	0.0	#NUM!	0.0	#NUM!	0.0	-2.7
	TH16	5802	0.0	#NUM!	1.0	0.0	0.0	#NUM!	1.0	0.0	0.0	#NUM!	0.0	-1.5
	TH17	5813	0.4	-0.4	0.6	-0.2	1.0	0.0	0.0	#NUM!	0.0	#NUM!	0.1	-1.2
Z5-NC5	AC5	9074	1.0	0.0	0.0	#NUM!	0.3	-0.5	0.1	-1.1	0.6	-0.2	1.3	0.1
	UT16	9303	1.0	0.0	0.0	#NUM!	0.1	-1.1	0.0	-1.8	0.9	0.0	1.9	0.3
	UT17	9310	1.0	0.0	0.0	#NUM!	0.1	-0.9	0.0	-2.3	0.9	-0.1	2.0	0.3
	UT18	9317	1.0	0.0	0.0	#NUM!	0.1	-1.0	0.0	-1.5	0.9	-0.1	5.6	0.7
	UT19	9324	0.0	#NUM!	1.0	0.0	0.1	-1.0	0.0	-1.4	0.8	-0.1	7.3	0.9
	UT20	10115	0.0	#NUM!	1.0	0.0	0.1	-1.1	0.3	-0.5	0.6	-0.2	1.2	0.1
	UT21	10124	1.0	0.0	0.0	#NUM!	0.1	-1.3	0.0	-1.5	0.9	0.0	7.5	0.9
	UT22	10136	1.0	0.0	0.0	#NUM!	0.2	-0.8	0.1	-1.0	0.7	-0.1	42.3	1.6
M2-NC2	TH18	6227	0.0	#NUM!	1.0	0.0	0.0	#NUM!	1.0	0.0	0.0	#NUM!	0.0	-1.3
	TH19	6247	0.0	#NUM!	1.0	0.0	#DIV/0!	#DIV/0!	#DIV/0!	#DIV/0!	#DIV/0!	#DIV/0!	0.0	#NUM!
	TH20	6251	#DIV/0!	#DIV/0!	#DIV/0!	#DIV/0!	0.2	-0.7	0.1	-0.8	0.7	-0.2	#DIV/0!	#DIV/0!
	AOA2	7259	#DIV/0!	#DIV/0!	#DIV/0!	#DIV/0!	#DIV/0!	#DIV/0!	#DIV/0!	#DIV/0!	#DIV/0!	#DIV/0!	#DIV/0!	#DIV/0!
	AOA3	7264	0.2	-0.8	0.8	-0.1	0.8	-0.1	0.2	-0.7	0.0	#NUM!	0.2	-0.7
C1-26	AOC1	6485	0.0	-1.3	1.0	0.0	1.0	0.0	0.0	#NUM!	0.0	#NUM!	0.0	-1.3
	AOC2	6488	0.5	-0.3	0.5	-0.3	1.0	0.0	0.0	#NUM!	0.0	#NUM!	0.0	-1.4
	AOC3	6491	0.3	-0.6	0.7	-0.1	1.0	0.0	0.0	#NUM!	0.0	#NUM!	0.1	-1.1
	AOC4	6494	0.4	-0.4	0.6	-0.2	1.0	0.0	0.0	#NUM!	0.0	#NUM!	0.0	-1.3
	AOC5	6497	0.4	-0.4	0.6	-0.2	1.0	0.0	0.0	#NUM!	0.0	#NUM!	0.1	-0.9
	AOC6	6500	0.4	-0.4	0.6	-0.2	1.0	0.0	0.0	-1.5	0.0	#NUM!	0.1	-1.2
	AOC7	6503	0.4	-0.4	0.6	-0.2	1.0	0.0	0.0	#NUM!	0.0	#NUM!	0.0	-1.4
	AOC8	6505	0.0	#NUM!	1.0	0.0	1.0	0.0	0.0	#NUM!	0.0	#NUM!	0.0	-1.6
A1-90	TH21	7552	0.0	#NUM!	1.0	0.0	1.0	0.0	0.0	#NUM!	0.0	#NUM!	0.0	-1.5
	TH22	7569	0.1	-0.9	0.9	-0.1	1.0	0.0	0.0	#NUM!	0.0	#NUM!	0.1	-0.9

WELLN	SAMNO	DEPTH	tnws/sp	Log10(Tnws/sp)	tkws/sp	Log10(Tkws/sp)	ac/mp	Log10(ac/mp)	tas/mp	Log10(tas/mp)	lei/mp	Log10(lei/mp)	mp/sp	Log10(mp/sp)
A1-90	AC6	11185	#DIV/0!	#DIV/0!	#DIV/0!	#DIV/0!	#DIV/0!	#DIV/0!	#DIV/0!	#DIV/0!	#DIV/0!	#DIV/0!	#DIV/0!	#DIV/0!
	AC7	11195	#DIV/0!	#DIV/0!	#DIV/0!	#DIV/0!	#DIV/0!	#DIV/0!	#DIV/0!	#DIV/0!	#DIV/0!	#DIV/0!	#DIV/0!	#DIV/0!
	UT23	11901	#DIV/0!	#DIV/0!	#DIV/0!	#DIV/0!	#DIV/0!	#DIV/0!	#DIV/0!	#DIV/0!	#DIV/0!	#DIV/0!	#DIV/0!	#DIV/0!
	UT24	11904	#DIV/0!	#DIV/0!	#DIV/0!	#DIV/0!	#DIV/0!	#DIV/0!	#DIV/0!	#DIV/0!	#DIV/0!	#DIV/0!	#DIV/0!	#DIV/0!
	UT25	11905	#DIV/0!	#DIV/0!	#DIV/0!	#DIV/0!	#DIV/0!	#DIV/0!	#DIV/0!	#DIV/0!	#DIV/0!	#DIV/0!	#DIV/0!	#DIV/0!
	UT26	11921	#DIV/0!	#DIV/0!	#DIV/0!	#DIV/0!	#DIV/0!	#DIV/0!	#DIV/0!	#DIV/0!	#DIV/0!	#DIV/0!	#DIV/0!	#DIV/0!
B2-NC2	UT27	10091	1.0	0.0	0.0	-1.4	0.0	-1.3	0.0	#NUM!	1.0	0.0	3.1	0.5
	UT28	10093	1.0	0.0	0.0	-1.6	0.0	-1.7	0.0	-2.4	1.0	0.0	3.3	0.5
	UT29	10094	0.9	0.0	0.1	-1.3	0.1	-1.0	0.1	-1.2	0.8	-0.1	5.8	0.8
	UT30	10096	1.0	0.0	0.0	#NUM!	0.1	-1.0	0.0	-1.3	0.9	-0.1	10.6	1.0
	UT31	10099	1.0	0.0	0.0	#NUM!	0.1	-1.1	0.1	-1.2	0.9	-0.1	8.9	0.9
	UT32	10101	1.0	0.0	0.0	#NUM!	0.1	-1.1	0.1	-1.0	0.8	-0.1	21.3	1.3
	UT33	10108	#DIV/0!	#DIV/0!	#DIV/0!	#DIV/0!	0.1	-1.2	0.2	-0.7	0.7	-0.1	#DIV/0!	#DIV/0!
	UT34	10105	1.0	0.0	0.0	#NUM!	0.1	-1.1	0.1	-1.0	0.8	-0.1	20.9	1.3
B1-49	AOC9	1428	0.5	-0.3	0.5	-0.3	1.0	0.0	0.0	#NUM!	0.0	#NUM!	0.0	-2.2
	AOC10	1434	0.8	-0.1	0.2	-0.7	1.0	0.0	0.0	#NUM!	0.0	#NUM!	0.2	-0.7
	AOC11	1435	0.0	#NUM!	1.0	0.0	1.0	0.0	0.0	#NUM!	0.0	#NUM!	0.2	-0.7
	AOC12	1438	0.6	-0.2	0.4	-0.4	1.0	0.0	0.0	#NUM!	0.0	#NUM!	0.2	-0.8
	AOC13	1442	0.0	#NUM!	1.0	0.0	1.0	0.0	0.0	-1.8	0.0	#NUM!	0.1	-0.8
	AOC14	1445	0.4	-0.4	0.6	-0.2	1.0	0.0	0.0	#NUM!	0.0	#NUM!	0.6	-0.2
	AOC15	1448	0.0	#NUM!	1.0	0.0	0.9	-0.1	0.1	-1.0	0.0	#NUM!	0.1	-1.2
	AOC16	1451	0.2	-0.6	0.8	-0.1	1.0	0.0	0.0	#NUM!	0.0	#NUM!	0.0	-1.9
	UT35	2132	0.9	0.0	0.1	-1.2	0.3	-0.6	0.0	#NUM!	0.7	-0.1	0.8	-0.1
	UT36	2135	#DIV/0!	#DIV/0!	#DIV/0!	#DIV/0!	#DIV/0!	#DIV/0!	#DIV/0!	#DIV/0!	#DIV/0!	#DIV/0!	#DIV/0!	#DIV/0!
A1-66	AOC17	3153	0.6	-0.2	0.4	-0.4	0.5	-0.3	0.5	-0.3	0.0	#NUM!	0.0	-2.4
	AOC18	3156	0.6	-0.2	0.4	-0.4	0.8	-0.1	0.2	-0.7	0.0	#NUM!	0.0	-2.0
	AOB1	3330	1.0	0.0	0.0	#NUM!	0.1	-0.8	0.0	-1.4	0.8	-0.1	1.9	0.3
	OK2	4104	1.0	0.0	0.0	#NUM!	0.1	-0.9	0.0	-2.7	0.9	-0.1	21.5	1.3
	OK2	4115	1.0	0.0	0.0	#NUM!	0.1	-0.8	0.0	-1.7	0.8	-0.1	0.5	-0.3
	UT35	4379	1.0	0.0	0.0	#NUM!	0.2	-0.7	0.0	-2.6	0.8	-0.1	5.5	0.7
	UT36	4382	1.0	0.0	0.0	#NUM!	0.2	-0.8	0.0	-2.2	0.8	-0.1	12.1	1.1
	UT37	4550	1.0	0.0	0.0	#NUM!	0.2	-0.6	0.0	-1.8	0.7	-0.1	23.8	1.4
	UT38	4553	1.0	0.0	0.0	#NUM!	0.2	-0.8	0.0	-2.2	0.8	-0.1	36.2	1.6
	UT39	4765	1.0	0.0	0.0	#NUM!	0.1	-1.1	0.1	-1.3	0.9	-0.1	19.2	1.3
	UT40	4836	1.0	0.0	0.0	#NUM!	0.3	-0.5	0.0	-1.6	0.7	-0.2	39.1	1.6
	UT41	4842	#DIV/0!	#DIV/0!	#DIV/0!	#DIV/0!	0.2	-0.6	0.0	-2.4	0.8	-0.1	#DIV/0!	#DIV/0!
	UT42	5051	1.0	0.0	0.0	#NUM!	0.5	-0.3	0.0	#NUM!	0.5	-0.3	15.2	1.2
	LT12	5054	#DIV/0!	#DIV/0!	#DIV/0!	#DIV/0!	#DIV/0!	#DIV/0!	#DIV/0!	#DIV/0!	#DIV/0!	#DIV/0!	#DIV/0!	#DIV/0!

WELLN	SAMNO	DEPTH	tnws/tkws	Log10(tnws/tkws)	tprasino	ac/Tprasion	Log10(ac/Tprasio)	acan/poly	Log10(acan/poly)	acan/mic	Log10(acan/mic)	acan/netro	Log10(acan/netro)
F1-66	TH1	4127	0.0	#NUM!	0.0	#DIV/0!	#DIV/0!	0.0	#NUM!	#DIV/0!	#DIV/0!	#DIV/0!	#DIV/0!
	TD1	5476	3.2	0.5	41.4	0.3	-0.6	0.4	-0.4	11.3	1.1	3.1	0.5
	UT1	6455	0.0	#NUM!	59.8	0.2	-0.7	1.1	0.1	0.7	-0.1	2.3	0.4
	UT2	6470	#DIV/0!	#DIV/0!	85.6	0.3	-0.6	1.7	0.2	0.4	-0.4	5.0	0.7
	UT3	6473	#DIV/0!	#DIV/0!	79.9	0.3	-0.5	2.3	0.4	2.7	0.4	7.6	0.9
	LT1	7042	#DIV/0!	#DIV/0!	57.4	0.0	#NUM!	0.2	-0.7	2.3	0.4	1.8	0.3
	LT2	7047	#DIV/0!	#DIV/0!	61.2	0.0	#NUM!	1.3	0.1	18.0	1.3	2.9	0.5
	LT3	7051	#DIV/0!	#DIV/0!	0.0	#DIV/0!	#DIV/0!	#DIV/0!	#DIV/0!	#DIV/0!	#DIV/0!	#DIV/0!	#DIV/0!
	LT4	7053	#DIV/0!	#DIV/0!	0.0	#DIV/0!	#DIV/0!	#DIV/0!	#DIV/0!	#DIV/0!	#DIV/0!	#DIV/0!	#DIV/0!
	LT5	7054	#DIV/0!	#DIV/0!	0.0	#DIV/0!	#DIV/0!	#DIV/0!	#DIV/0!	#DIV/0!	#DIV/0!	#DIV/0!	#DIV/0!
	LT6	7057	#DIV/0!	#DIV/0!	0.0	#DIV/0!	#DIV/0!	#DIV/0!	#DIV/0!	#DIV/0!	#DIV/0!	#DIV/0!	#DIV/0!
	LT7	7061	#DIV/0!	#DIV/0!	31.1	0.0	#NUM!	0.7	-0.2	10.6	1.0	3.2	0.5
	LT8	7063	#DIV/0!	#DIV/0!	34.3	0.0	#NUM!	2.7	0.4	#DIV/0!	#DIV/0!	51.7	1.7
	LT9	7065	#DIV/0!	#DIV/0!	0.0	#DIV/0!	#DIV/0!	#DIV/0!	#DIV/0!	#DIV/0!	#DIV/0!	#DIV/0!	#DIV/0!
	LT10	7073	#DIV/0!	#DIV/0!	0.0	#DIV/0!	#DIV/0!	#DIV/0!	#DIV/0!	#DIV/0!	#DIV/0!	#DIV/0!	#DIV/0!
	LT11	7076	#DIV/0!	#DIV/0!	0.0	#DIV/0!	#DIV/0!	#DIV/0!	#DIV/0!	#DIV/0!	#DIV/0!	#DIV/0!	#DIV/0!
A1-70	AOA1	6561	62.0	1.8	0.6	3.3	0.5	9.4	1.0	6.7	0.8	#DIV/0!	#DIV/0!
	OK1	6930	13.9	1.1	0.0	#DIV/0!	#DIV/0!	#DIV/0!	#DIV/0!	#DIV/0!	#DIV/0!	#DIV/0!	#DIV/0!
	AC1	8951	34.2	1.5	53.6	0.0	-1.4	0.7	-0.2	#DIV/0!	#DIV/0!	#DIV/0!	#DIV/0!
	AC2	8960	47.0	1.7	45.8	0.0	-1.7	0.1	-0.9	#DIV/0!	#DIV/0!	1.0	0.0
	AC3	8971	23.3	1.4	80.9	0.1	-1.2	1.0	0.0	#DIV/0!	#DIV/0!	0.6	-0.2
	AC4	8980	23.7	1.4	81.4	0.1	-1.1	0.0	#NUM!	#DIV/0!	#DIV/0!	#DIV/0!	#DIV/0!
	UT4	9017	18.7	1.3	80.8	0.1	-0.9	1.0	0.0	1.7	0.2	10.0	1.0
	UT5	9029	#DIV/0!	#DIV/0!	83.6	0.1	-0.9	0.4	-0.4	0.2	-0.7	4.0	0.6
	UT6	9049	#DIV/0!	#DIV/0!	78.8	0.1	-1.0	0.4	-0.4	1.1	0.0	3.7	0.6
	UT7	9066	#DIV/0!	#DIV/0!	67.6	0.2	-0.7	0.4	-0.4	1.2	0.1	1.4	0.2
	UT8	9085	2.7	0.4	47.8	0.4	-0.4	1.6	0.2	1.1	0.0	2.3	0.4
	UT9	9103	15.3	1.2	55.6	0.2	-0.7	0.7	-0.2	1.2	0.1	3.4	0.5
	UT10	9123	2.8	0.4	65.6	0.2	-0.8	0.4	-0.4	1.2	0.1	2.1	0.3
	UT11	9295	7.5	0.9	71.8	0.2	-0.7	0.4	-0.4	3.3	0.5	2.6	0.4
	UT12	9447	#DIV/0!	#DIV/0!	83.0	0.1	-0.8	6.7	0.8	0.7	-0.2	6.7	0.8
	UT13	9993	#DIV/0!	#DIV/0!	84.2	0.1	-0.9	1.0	0.0	3.3	0.5	22.0	1.3
	UT14	9999	#DIV/0!	#DIV/0!	83.4	0.0	-1.8	0.1	-1.0	0.5	-0.3	0.9	0.0
	UT15	10005	#DIV/0!	#DIV/0!	84.8	0.0	#NUM!	0.9	-0.1	#DIV/0!	#DIV/0!	#DIV/0!	#DIV/0!
A9-NC7	TH2	5703	3.6	0.6	0.0	#DIV/0!	#DIV/0!	0.0	#NUM!	#DIV/0!	#DIV/0!	#DIV/0!	#DIV/0!
	TH3	5705	2.4	0.4	0.6	6.0	0.8	#DIV/0!	#DIV/0!	#DIV/0!	#DIV/0!	#DIV/0!	#DIV/0!
	TH4	5708	2.8	0.4	0.0	#DIV/0!	#DIV/0!	1.3	0.1	#DIV/0!	#DIV/0!	#DIV/0!	#DIV/0!

WELLN	SAMNO	DEPTH	tnws/tkws	Log10(tnws/tkws)	tprasino	ac/Tprasion	Log10(ac/Tprasio)	acan/poly	Log10(acan/poly)	acan/mic	Log10(acan/mic)	acan/netro	Log10(acan/netro)
A9-NC7	TH5	5712	0.0	#NUM!	3.8	0.0	#NUM!	3.5	0.5	#DIV/0!	#DIV/0!	#DIV/0!	#DIV/0!
	TH6	5715	4.0	0.6	0.0	#DIV/0!	#DIV/0!	4.4	0.6	#DIV/0!	#DIV/0!	#DIV/0!	#DIV/0!
	TH7	5718	0.2	-0.7	0.8	0.0	#NUM!	#DIV/0!	#DIV/0!	#DIV/0!	#DIV/0!	#DIV/0!	#DIV/0!
	TH8	5721	0.4	-0.4	0.6	3.7	0.6	#DIV/0!	#DIV/0!	#DIV/0!	#DIV/0!	#DIV/0!	#DIV/0!
	TH9	5733	0.4	-0.4	0.0	#DIV/0!	#DIV/0!	#DIV/0!	#DIV/0!	#DIV/0!	#DIV/0!	#DIV/0!	#DIV/0!
	TH10	5754	1.2	0.1	0.0	#DIV/0!	#DIV/0!	0.0	#NUM!	#DIV/0!	#DIV/0!	#DIV/0!	#DIV/0!
	TH11	5762	1.5	0.2	0.0	#DIV/0!	#DIV/0!	0.0	#NUM!	#DIV/0!	#DIV/0!	#DIV/0!	#DIV/0!
	TH12	5770	0.4	-0.4	0.0	#DIV/0!	#DIV/0!	0.0	#NUM!	#DIV/0!	#DIV/0!	#DIV/0!	#DIV/0!
	TH13	5773	2.0	0.3	0.0	#DIV/0!	#DIV/0!	0.3	-0.5	#DIV/0!	#DIV/0!	#DIV/0!	#DIV/0!
	TH14	5783	0.4	-0.3	0.0	#DIV/0!	#DIV/0!	#DIV/0!	#DIV/0!	#DIV/0!	#DIV/0!	#DIV/0!	#DIV/0!
	TH15	5797	0.4	-0.4	0.0	#DIV/0!	#DIV/0!	#DIV/0!	#DIV/0!	#DIV/0!	#DIV/0!	#DIV/0!	#DIV/0!
	TH16	5802	0.0	#NUM!	3.0	5.3	0.7	#DIV/0!	#DIV/0!	#DIV/0!	#DIV/0!	#DIV/0!	#DIV/0!
	TH17	5813	0.7	-0.2	0.0	#DIV/0!	#DIV/0!	0.0	#NUM!	#DIV/0!	#DIV/0!	#DIV/0!	#DIV/0!
Z5-NC5	AC5	9074	#DIV/0!	#DIV/0!	39.8	0.2	-0.7	0.8	-0.1	2.2	0.3	1.0	0.0
	UT16	9303	#DIV/0!	#DIV/0!	55.8	0.2	-0.8	0.4	-0.4	#DIV/0!	#DIV/0!	4.3	0.6
	UT17	9310	#DIV/0!	#DIV/0!	57.5	0.1	-0.8	0.3	-0.5	#DIV/0!	#DIV/0!	1.6	0.2
	UT18	9317	#DIV/0!	#DIV/0!	74.0	0.1	-1.3	0.8	-0.1	8.0	0.9	3.2	0.5
	UT19	9324	0.0	#NUM!	67.0	0.1	-1.2	1.0	0.0	2.0	0.3	0.1	-0.9
	UT20	10115	0.0	#NUM!	49.6	0.3	-0.5	0.9	-0.1	3.0	0.5	1.2	0.1
	UT21	10124	#DIV/0!	#DIV/0!	80.8	0.0	#NUM!	0.7	-0.2	#DIV/0!	#DIV/0!	1.2	0.1
	UT22	10136	#DIV/0!	#DIV/0!	77.4	0.0	#NUM!	2.0	0.3	23.5	1.4	9.4	1.0
M2-NC2	TH18	6227	0.0	#NUM!	4.4	4.1	0.6	#DIV/0!	#DIV/0!	#DIV/0!	#DIV/0!	#DIV/0!	#DIV/0!
	TH19	6247	0.0	#NUM!	0.0	#DIV/0!	#DIV/0!	#DIV/0!	#DIV/0!	#DIV/0!	#DIV/0!	#DIV/0!	#DIV/0!
	TH20	6251	#DIV/0!	#DIV/0!	79.8	0.2	-0.8	1.1	0.0	#DIV/0!	#DIV/0!	#DIV/0!	#DIV/0!
	AOA2	7259	#DIV/0!	#DIV/0!	0.0	#DIV/0!	#DIV/0!	#DIV/0!	#DIV/0!	#DIV/0!	#DIV/0!	#DIV/0!	#DIV/0!
	AOA3	7264	0.2	-0.7	3.0	1.3	0.1	0.7	-0.2	#DIV/0!	#DIV/0!	#DIV/0!	#DIV/0!
C1-26	AOC1	6485	0.1	-1.3	0.0	#DIV/0!	#DIV/0!	0.0	#NUM!	#DIV/0!	#DIV/0!	#DIV/0!	#DIV/0!
	AOC2	6488	0.9	-0.1	0.0	#DIV/0!	#DIV/0!	0.4	-0.4	#DIV/0!	#DIV/0!	#DIV/0!	#DIV/0!
	AOC3	6491	0.3	-0.5	0.0	#DIV/0!	#DIV/0!	0.0	#NUM!	#DIV/0!	#DIV/0!	#DIV/0!	#DIV/0!
	AOC4	6494	0.6	-0.2	0.0	#DIV/0!	#DIV/0!	0.0	-1.3	#DIV/0!	#DIV/0!	#DIV/0!	#DIV/0!
	AOC5	6497	0.6	-0.2	0.0	#DIV/0!	#DIV/0!	0.0	#NUM!	#DIV/0!	#DIV/0!	#DIV/0!	#DIV/0!
	AOC6	6500	0.7	-0.1	0.2	12.0	1.1	0.0	#NUM!	#DIV/0!	#DIV/0!	#DIV/0!	#DIV/0!
	AOC7	6503	0.6	-0.2	0.0	#DIV/0!	#DIV/0!	0.0	#NUM!	#DIV/0!	#DIV/0!	#DIV/0!	#DIV/0!
	AOC8	6505	0.0	#NUM!	0.0	#DIV/0!	#DIV/0!	0.0	#NUM!	#DIV/0!	#DIV/0!	#DIV/0!	#DIV/0!
A1-90	TH21	7552	0.0	#NUM!	0.0	#DIV/0!	#DIV/0!	0.3	-0.6	#DIV/0!	#DIV/0!	#DIV/0!	#DIV/0!
	TH22	7569	0.1	-0.9	0.0	#DIV/0!	#DIV/0!	0.2	-0.7	#DIV/0!	#DIV/0!	#DIV/0!	#DIV/0!

WELLN	SAMNO	DEPTH	tnws/tkws	Log10(tnws/tkws)	tprasino	ac/Tprasion	Log10(ac/Tprasio)	acan/poly	Log10(acan/poly)	acan/mic	Log10(acan/mic)	acan/netro	Log10(acan/netro)
A1-90	AC6	11185	#DIV/0!	#DIV/0!	0.0	#DIV/0!	#DIV/0!	#DIV/0!	#DIV/0!	#DIV/0!	#DIV/0!	#DIV/0!	#DIV/0!
	AC7	11195	#DIV/0!	#DIV/0!	0.0	#DIV/0!	#DIV/0!	#DIV/0!	#DIV/0!	#DIV/0!	#DIV/0!	#DIV/0!	#DIV/0!
	UT23	11901	#DIV/0!	#DIV/0!	0.0	#DIV/0!	#DIV/0!	#DIV/0!	#DIV/0!	#DIV/0!	#DIV/0!	#DIV/0!	#DIV/0!
	UT24	11904	#DIV/0!	#DIV/0!	0.0	#DIV/0!	#DIV/0!	#DIV/0!	#DIV/0!	#DIV/0!	#DIV/0!	#DIV/0!	#DIV/0!
	UT25	11905	#DIV/0!	#DIV/0!	0.0	#DIV/0!	#DIV/0!	#DIV/0!	#DIV/0!	#DIV/0!	#DIV/0!	#DIV/0!	#DIV/0!
	UT26	11921	#DIV/0!	#DIV/0!	0.0	#DIV/0!	#DIV/0!	#DIV/0!	#DIV/0!	#DIV/0!	#DIV/0!	#DIV/0!	#DIV/0!
B2-NC2	UT27	10091	23.5	1.4	71.8	0.1	-1.0	0.3	-0.5	#DIV/0!	#DIV/0!	0.2	-0.7
	UT28	10093	36.7	1.6	72.2	0.1	-0.9	0.3	-0.5	#DIV/0!	#DIV/0!	1.0	0.0
	UT29	10094	18.1	1.3	70.0	0.1	-1.0	0.3	-0.5	#DIV/0!	#DIV/0!	0.1	-0.8
	UT30	10096	#DIV/0!	#DIV/0!	80.6	0.1	-1.1	0.3	-0.6	#DIV/0!	#DIV/0!	0.4	-0.4
	UT31	10099	#DIV/0!	#DIV/0!	81.8	0.1	-1.1	0.4	-0.4	#DIV/0!	#DIV/0!	0.6	-0.2
	UT32	10101	#DIV/0!	#DIV/0!	86.8	0.1	-1.1	0.4	-0.5	1.8	0.2	2.3	0.4
	UT33	10108	#DIV/0!	#DIV/0!	91.4	0.0	-2.2	1.0	0.0	0.3	-0.6	1.7	0.2
	UT34	10105	#DIV/0!	#DIV/0!	81.0	0.2	-0.7	1.3	0.1	0.5	-0.3	1.6	0.2
B1-49	AOC9	1428	0.8	-0.1	0.0	#DIV/0!	#DIV/0!	0.0	#NUM!	#DIV/0!	#DIV/0!	#DIV/0!	#DIV/0!
	AOC10	1434	3.7	0.6	0.0	#DIV/0!	#DIV/0!	0.6	-0.2	#DIV/0!	#DIV/0!	#DIV/0!	#DIV/0!
	AOC11	1435	0.0	#NUM!	0.0	#DIV/0!	#DIV/0!	0.5	-0.3	#DIV/0!	#DIV/0!	#DIV/0!	#DIV/0!
	AOC12	1438	1.7	0.2	0.0	#DIV/0!	#DIV/0!	0.1	-0.9	#DIV/0!	#DIV/0!	8.0	0.9
	AOC13	1442	0.0	#NUM!	0.2	24.0	1.4	0.7	-0.1	#DIV/0!	#DIV/0!	#DIV/0!	#DIV/0!
	AOC14	1445	0.7	-0.2	0.0	#DIV/0!	#DIV/0!	0.1	-0.8	#DIV/0!	#DIV/0!	#DIV/0!	#DIV/0!
	AOC15	1448	0.0	#NUM!	0.6	19.7	1.3	0.7	-0.1	#DIV/0!	#DIV/0!	#DIV/0!	#DIV/0!
	AOC16	1451	0.3	-0.5	0.0	#DIV/0!	#DIV/0!	0.0	#NUM!	#DIV/0!	#DIV/0!	#DIV/0!	#DIV/0!
	UT35	2132	14.9	1.2	31.0	0.0	-2.2	2.6	0.4	#DIV/0!	#DIV/0!	4.6	0.7
	UT36	2135	#DIV/0!	#DIV/0!	0.0	#DIV/0!	#DIV/0!	#DIV/0!	#DIV/0!	#DIV/0!	#DIV/0!	#DIV/0!	#DIV/0!
A1-66	AOC17	3153	1.8	0.2	0.2	47.0	1.7	#DIV/0!	#DIV/0!	#DIV/0!	#DIV/0!	#DIV/0!	#DIV/0!
	AOC18	3156	1.8	0.2	0.2	57.0	1.8	1.0	0.0	#DIV/0!	#DIV/0!	#DIV/0!	#DIV/0!
	AOB1	3330	#DIV/0!	#DIV/0!	55.4	0.1	-1.1	0.4	-0.4	#DIV/0!	#DIV/0!	#DIV/0!	#DIV/0!
	OK2	4104	#DIV/0!	#DIV/0!	78.8	0.2	-0.7	1.1	0.0	1.2	0.1	4.8	0.7
	OK2	4115	#DIV/0!	#DIV/0!	27.3	0.6	-0.3	1.0	0.0	1.7	0.2	8.5	0.9
	UT35	4379	#DIV/0!	#DIV/0!	64.8	0.3	-0.5	0.8	-0.1	1.4	0.1	2.9	0.5
	UT36	4382	#DIV/0!	#DIV/0!	72.0	0.2	-0.7	0.9	-0.1	1.1	0.0	5.9	0.8
	UT37	4550	#DIV/0!	#DIV/0!	69.0	0.1	-1.0	0.7	-0.1	0.9	-0.1	10.0	1.0
	UT38	4553	#DIV/0!	#DIV/0!	79.6	0.4	-0.4	1.0	0.0	3.3	0.5	10.0	1.0
	UT39	4765	#DIV/0!	#DIV/0!	85.0	0.3	-0.6	0.6	-0.3	1.4	0.2	#DIV/0!	#DIV/0!
	UT40	4836	#DIV/0!	#DIV/0!	64.0	0.7	-0.2	0.6	-0.2	0.8	-0.1	3.4	0.5
	UT41	4842	#DIV/0!	#DIV/0!	75.0	0.0	#NUM!	1.3	0.1	3.4	0.5	7.3	0.9
	UT42	5051	#DIV/0!	#DIV/0!	43.2	0.0	#NUM!	0.9	0.0	#DIV/0!	#DIV/0!	4.6	0.7
	LT12	5054	#DIV/0!	#DIV/0!	0.0	#DIV/0!	#DIV/0!	#DIV/0!	#DIV/0!	#DIV/0!	#DIV/0!	#DIV/0!	#DIV/0!

WELLN	SAMNO	DEPTH	tblk/tbr	Log10(tblk/tbr)	blkEque/blklath	TOC%	Log10(BlkEqu/BlkLath)	PhyTOC	AmOC	HI	S2	Tmax
F1-66	TH1	4127	3.3	0.5	2.1	1.4	0.3	0.9	0.4	119	1.6	434
	TD1	5476	0.0	#NUM!	#DIV/0!	0.4	#DIV/0!	0.2	0.2	50	0.2	434
	UT1	6455	0.0	#NUM!	#DIV/0!	0.8	#DIV/0!	0.0	0.8	53	0.4	434
	UT2	6470	#DIV/0!	#DIV/0!	#DIV/0!	1.0	#DIV/0!	0.0	1.0	73	0.7	434
	UT3	6473	#DIV/0!	#DIV/0!	#DIV/0!	1.0	#DIV/0!	0.0	1.0	100	1.0	434
	LT1	7042	#DIV/0!	#DIV/0!	#DIV/0!	4.4	#DIV/0!	0.0	4.4	183	8.0	432
	LT2	7047	#DIV/0!	#DIV/0!	#DIV/0!	4.4	#DIV/0!	0.0	4.4	210	9.2	434
	LT3	7051	#DIV/0!	#DIV/0!	#DIV/0!	5.7	#DIV/0!	0.0	5.7	227	13.0	435
	LT4	7053	#DIV/0!	#DIV/0!	#DIV/0!	5.3	#DIV/0!	0.0	5.3	210	11.1	435
	LT5	7054	#DIV/0!	#DIV/0!	#DIV/0!	11.6	#DIV/0!	0.0	11.6	230	26.7	438
	LT6	7057	#DIV/0!	#DIV/0!	#DIV/0!	4.9	#DIV/0!	0.0	4.9	252	12.3	434
	LT7	7061	#DIV/0!	#DIV/0!	#DIV/0!	2.9	#DIV/0!	0.0	2.9	232	6.8	436
	LT8	7063	#DIV/0!	#DIV/0!	#DIV/0!	1.7	#DIV/0!	0.0	1.7	181	3.1	440
	LT9	7065	#DIV/0!	#DIV/0!	#DIV/0!	20.3	#DIV/0!	0.0	20.3	152	30.8	427
	LT10	7073	#DIV/0!	#DIV/0!	#DIV/0!	11.8	#DIV/0!	0.0	11.8	213	25.1	431
	LT11	7076	#DIV/0!	#DIV/0!	#DIV/0!	5.8	#DIV/0!	0.0	5.8	192	11.2	433
A1-70	AOA1	6561	2.8	0.4	15.2	0.3	1.2	0.2	0.2	80	0.3	431
	OK1	6930	16.0	1.2	#DIV/0!	0.4	#DIV/0!	0.3	0.0	32	0.1	431
	AC1	8951	0.0	-1.4	0.5	0.2	-0.3	0.1	0.1	123	0.2	436
	AC2	8960	0.1	-0.9	0.4	0.1	-0.4	0.0	0.1	117	0.2	435
	AC3	8971	0.0	-1.9	#DIV/0!	0.2	#DIV/0!	0.0	0.1	100	0.2	436
	AC4	8980	0.0	#NUM!	#DIV/0!	0.2	#DIV/0!	0.0	0.1	63	0.1	435
	UT4	9017	0.0	#NUM!	#DIV/0!	0.2	#DIV/0!	0.0	0.2	108	0.3	436
	UT5	9029	0.0	#NUM!	#DIV/0!	0.3	#DIV/0!	0.0	0.3	165	0.4	436
	UT6	9049	0.0	#NUM!	#DIV/0!	0.4	#DIV/0!	0.0	0.4	136	0.6	437
	UT7	9066	0.0	#NUM!	#DIV/0!	0.4	#DIV/0!	0.0	0.4	107	0.5	439
	UT8	9085	0.0	#NUM!	#DIV/0!	0.4	#DIV/0!	0.0	0.4	151	0.6	438
	UT9	9103	0.0	#NUM!	#DIV/0!	0.3	#DIV/0!	0.1	0.2	129	0.4	438
	UT10	9123	0.0	#NUM!	#DIV/0!	0.3	#DIV/0!	0.0	0.3	68	0.2	438
	UT11	9295	0.0	#NUM!	#DIV/0!	0.3	#DIV/0!	0.0	0.3	143	0.4	437
	UT12	9447	#DIV/0!	#DIV/0!	#DIV/0!	0.8	#DIV/0!	0.0	0.8	247	2.0	439
	UT13	9993	#DIV/0!	#DIV/0!	#DIV/0!	1.8	#DIV/0!	0.0	1.8	188	3.4	444
	UT14	9999	#DIV/0!	#DIV/0!	#DIV/0!	1.2	#DIV/0!	0.0	1.2	185	2.3	444
	UT15	10005	#DIV/0!	#DIV/0!	#DIV/0!	1.7	#DIV/0!	0.0	1.7	169	2.9	445
A9-NC7	TH2	5703	1.4	0.1	7.1	0.5	0.9	0.4	0.1	107	0.6	433
	TH3	5705	1.9	0.3	5.4	0.9	0.7	0.6	0.3	50	0.4	437
	TH4	5708	1.1	0.1	7.8	1.7	0.9	1.5	0.1	101	1.7	437

WELLN	SAMNO	DEPTH	tblk/tbr	Log10(tblk/tbr)	blkEque/blklath	TOC%	Log10(BlkEqu/BlkLath)	PhyTOC	AmOC	HI	S2	Tmax
A9-NC7	TH5	5712	1.1	0.0	3.2	1.2	0.5	0.9	0.3	83	1.0	438
	TH6	5715	1.0	0.0	4.2	0.8	0.6	0.7	0.1	24	0.2	
	TH7	5718	0.8	-0.1	8.3	9.9	0.9	7.5	2.3	194	19.1	
	TH8	5721	2.9	0.5	7.7	0.5	0.9	0.4	0.0	32	0.2	431
	TH9	5733	0.3	-0.5	43.0	6.3	1.6	0.6	5.7	221	13.9	
	TH10	5754	1.4	0.2	8.7	2.2	0.9	1.1	1.1	92	2.0	
	TH11	5762	1.2	0.1	7.8	5.0	0.9	4.0	0.9	194	9.6	
	TH12	5770	2.7	0.4	8.0	4.3	0.9	3.5	0.8	131	5.6	435
	TH13	5773	2.2	0.3	8.7	3.0	0.9	2.7	0.3	109	3.3	
	TH14	5783	10.4	1.0	7.8	3.3	0.9	2.1	1.2	106	3.5	
	TH15	5797	1.2	0.1	16.0	1.0	1.2	0.3	0.6	174	1.7	
	TH16	5802	2.5	0.4	5.2	6.9	0.7	5.9	1.0	198	13.7	437
	TH17	5813	1.5	0.2	9.0	3.6	1.0	3.0	0.6	164	6.0	
Z5-NC5	AC5	9074	0.0	#NUM!	#DIV/0!	0.1	#DIV/0!	0.1	0.1	90	0.1	433
	UT16	9303	0.0	#NUM!	#DIV/0!	0.2	#DIV/0!	0.0	0.2	145	0.3	434
	UT17	9310	0.0	#NUM!	#DIV/0!	0.2	#DIV/0!	0.0	0.2	113	0.3	434
	UT18	9317	0.0	#NUM!	#DIV/0!	0.3	#DIV/0!	0.0	0.3	136	0.4	435
	UT19	9324	0.0	#NUM!	#DIV/0!	0.5	#DIV/0!	0.0	0.5	153	0.8	434
	UT20	10115	#DIV/0!	#DIV/0!	#DIV/0!	0.4	#DIV/0!	0.0	0.4	246	0.9	444
	UT21	10124	0.0	#NUM!	#DIV/0!	0.8	#DIV/0!	0.0	0.8	45	0.4	444
	UT22	10136	#DIV/0!	#DIV/0!	#DIV/0!	0.8	#DIV/0!	0.0	0.8	202	1.5	441
M2-NC2	TH18	6227	0.3	-0.5	50.0	38.6	1.7	9.2	29.4	269	104.0	433
	TH19	6247	0.4	-0.4	5.0	7.5	0.7	2.4	5.1	139	10.4	436
	TH20	6251	#DIV/0!	#DIV/0!	#DIV/0!	3.8	#DIV/0!	0.0	3.8	81	3.1	437
	AOA2	7259	#DIV/0!	#DIV/0!	#DIV/0!	0.4	#DIV/0!	#DIV/0!	#DIV/0!	63	0.2	438
	AOA3	7264	0.0	-1.6	4.0	0.4	0.6	0.3	0.1	64	0.2	438
C1-26	AOC1	6485	0.9	0.0	6.2	3.3	0.8	1.5	1.8	179	5.9	440
	AOC2	6488	0.8	-0.1	7.9	3.5	0.9	2.7	0.8	166	5.7	440
	AOC3	6491	2.0	0.3	10.7	3.2	1.0	2.6	0.6	125	4.0	440
	AOC4	6494	1.6	0.2	13.8	2.9	1.1	2.5	0.4	85	2.4	440
	AOC5	6497	1.2	0.1	11.0	3.7	1.0	1.4	2.3	67	2.5	440
	AOC6	6500	1.1	0.1	7.2	4.3	0.9	1.9	2.4	108	4.7	440
	AOC7	6503	0.7	-0.2	9.0	5.1	1.0	2.4	2.6	137	6.9	440
	AOC8	6505	1.5	0.2	4.0	3.9	0.6	3.8	0.1	152	5.9	440
A1-90	TH21	7552	1.2	0.1	5.8	3.0	0.8	2.3	0.7	75	2.2	439
	TH22	7569	2.5	0.4	4.5	2.4	0.6	2.4	0.0	131	3.1	442

WELLN	SAMNO	DEPTH	tblk/tbr	Log10(tblk/tbr)	blkEque/blklath	TOC%	Log10(BlkEqu/BlkLath)	PhyTOC	AmOC	HI	S2	Tmax
A1-90	AC6	11185	#DIV/0!	#DIV/0!	#DIV/0!	0.2	#DIV/0!	0.1	0.1	107	0.2	512
	AC7	11195	#DIV/0!	#DIV/0!	#DIV/0!	0.2	#DIV/0!	0.0	0.2	24	0.1	
	UT23	11901	#DIV/0!	#DIV/0!	#DIV/0!	0.8	#DIV/0!	0.0	0.8	26	0.2	406
	UT24	11904	#DIV/0!	#DIV/0!	#DIV/0!	0.5	#DIV/0!	#DIV/0!	#DIV/0!	38	0.2	390
	UT25	11905	#DIV/0!	#DIV/0!	#DIV/0!	0.8	#DIV/0!	0.1	0.7	33	0.3	383
	UT26	11921	#DIV/0!	#DIV/0!	#DIV/0!	1.2	#DIV/0!	0.0	1.2	17	0.2	364
B2-NC2	UT27	10091	0.0	#NUM!	#DIV/0!	0.3	#DIV/0!	0.0	0.3	123	0.4	
	UT28	10093	0.0	#NUM!	#DIV/0!	0.4	#DIV/0!	0.0	0.3	109	0.4	442
	UT29	10094	#DIV/0!	#DIV/0!	#DIV/0!	0.7	#DIV/0!	0.0	0.7	153	1.1	442
	UT30	10096	0.3	-0.5	0.0	0.4	#NUM!	0.0	0.4	129	0.5	443
	UT31	10099	#DIV/0!	#DIV/0!	#DIV/0!	0.6	#DIV/0!	0.0	0.6	159	1.0	445
	UT32	10101	#DIV/0!	#DIV/0!	#DIV/0!	1.0	#DIV/0!	0.0	1.0	223	2.2	440
	UT33	10108	#DIV/0!	#DIV/0!	#DIV/0!	2.3	#DIV/0!	0.0	2.3	254	5.8	447
	UT34	10105	#DIV/0!	#DIV/0!	#DIV/0!	1.4	#DIV/0!	0.0	1.4	209	2.9	442
B1-49	AOC9	1428	0.5	-0.3	20.0	2.2	1.3	1.9	0.3	157	3.5	440
	AOC10	1434	1.7	0.2	4.7	2.9	0.7	2.8	0.1	146	4.2	442
	AOC11	1435	2.1	0.3	6.7	2.8	0.8	2.5	0.3	170	4.8	440
	AOC12	1438	0.9	0.0	7.0	2.3	0.8	1.6	0.7	54	1.3	436
	AOC13	1442	1.7	0.2	3.8	1.9	0.6	1.0	0.9	118	2.2	445
	AOC14	1445	3.8	0.6	13.1	1.4	1.1	0.9	0.5	35	0.5	442
	AOC15	1448	1.2	0.1	5.1	2.9	0.7	2.0	0.8	92	2.6	438
	AOC16	1451	0.6	-0.2	10.7	2.7	1.0	2.5	0.2	152	4.1	442
	UT35	2132	0.8	-0.1	0.7	0.8	-0.2	0.1	0.7	44	0.3	434
	UT36	2135	#DIV/0!	#DIV/0!	#DIV/0!	0.9	#DIV/0!	#DIV/0!	#DIV/0!	42	0.4	428
A1-66	AOC17	3153	1.9	0.3	7.0	2.6	0.8	2.3	0.3	99	2.6	430
	AOC18	3156	1.0	0.0	7.3	2.1	0.9	1.8	0.2	17	0.4	429
	AOB1	3330	0.0	#NUM!	#DIV/0!	0.5	#DIV/0!	0.0	0.5	58	0.3	425
	OK2	4104	0.0	#NUM!	#DIV/0!	0.5	#DIV/0!	0.0	0.5	81	0.4	429
	OK2	4115	#DIV/0!	#DIV/0!	#DIV/0!	0.1	#DIV/0!	#DIV/0!	#DIV/0!	221	0.2	427
	UT35	4379	#DIV/0!	#DIV/0!	#DIV/0!	0.7	#DIV/0!	0.0	0.7	172	1.3	433
	UT36	4382	#DIV/0!	#DIV/0!	#DIV/0!	0.9	#DIV/0!	0.0	0.9	157	1.5	433
	UT37	4550	#DIV/0!	#DIV/0!	#DIV/0!	1.4	#DIV/0!	0.0	1.4	217	3.0	432
	UT38	4553	0.0	#NUM!	#DIV/0!	1.7	#DIV/0!	0.0	1.7	156	2.6	432
	UT39	4765	#DIV/0!	#DIV/0!	#DIV/0!	0.6	#DIV/0!	0.0	0.6	208	1.2	435
	UT40	4836	#DIV/0!	#DIV/0!	#DIV/0!	1.0	#DIV/0!	0.0	1.0	161	1.7	436
	UT41	4842	#DIV/0!	#DIV/0!	#DIV/0!	1.6	#DIV/0!	0.0	1.6	183	3.0	436
	UT42	5051	#DIV/0!	#DIV/0!	#DIV/0!	1.1	#DIV/0!	0.0	1.1	165	1.8	437
	LT12	5054	#DIV/0!	#DIV/0!	#DIV/0!	10.6	#DIV/0!	0.0	10.6	383	40.6	435

APPENDIX V

Appendix V: Biomarker concentrations of the Silurian and Devonian source rock samples (μg/g extract)

Well	Depth	Formation	Age	$C_{20}T$	$C_{21}T$	$C_{23}T$	$C_{24}T$	$C_{25}T$	$C_{26}T$	Ts	Tm	C29αβ	$C_{29}Ts$	C_{30}dia	C_{29}ba	$C_{30}αβ$
B1-NC2	10108	L.Tanezzuft	L. Silurian	29.0	86.7	111.1	50.7	24.8	49.5	36.9	20.4	34.3	31.8	24.5	7.1	88.6
A1-70	10005	L.Tanezzuft	L. Silurian	22.7	58.2	67.1	35.5	17.0	28.6	19.5	23.1	22.9	18.1	14.5	3.3	57.1
A1-70	10155	L.Tanezzuft	L. Silurian	40.5	42.9	35.2	18.2	8.8	18.2	7.1	11.3	23.9	7.3	5.1	2.9	37.7
F1-66	7053	L.Tanezzuft	L. Silurian	27.2	46.7	88.6	39.3	19.2	41.0	23.3	8.7	23.7	11.1	7.9	4.8	35.7
F1-66	7054	L.Tanezzuft	L. Silurian	14.1	31.9	56.2	24.4	14.5	25.8	10.8	6.3	12.6	8.1	0.0	0.0	19.9
F1-66	7065	L.Tanezzuft	L. Silurian	10.6	13.7	22.6	8.7	4.3	7.2	5.3	3.8	4.0	2.0	0.0	0.0	4.8
A1-66	5054	L.Tanezzuft	L. Silurian	29.3	56.8	61.8	30.0	17.7	60.2	56.6	53.2	108.7	43.0	17.9	15.3	176.6
F1-66	6473	U.Tanezzuft	L. Silurian	28.3	73.4	56.3	26.4	14.2	56.0	43.1	40.9	95.4	43.5	18.5	15.3	153.7
A1-90	11921	U.Tanezzuft	L. Silurian	15.3	22.2	58.1	29.1	14.6	37.8	230.3	321.0	1069.9	237.8	80.2	120.4	1144.2
Z5-NC5	10124	U.Tanezzuft	L. Silurian	22.3	54.9	83.1	52.5	29.7	74.0	44.9	33.9	81.2	46.1	29.1	7.3	160.6
B1-49	2135	U.Tanezzuft	L. Silurian	9.2	5.4	8.2	5.5	3.9	8.5	5.1	6.2	18.0	4.0	1.5	1.8	18.6
A1-70	9049	U.Tanezzuft	L. Silurian	35.6	132.7	101.7	43.1	22.1	117.7	175.3	94.9	292.1	304.9	133.3	62.1	595.2
A9-NC7	5718	Tahara	U.Devonian	39.3	27.8	19.9	13.8	12.1	99.3	134.8	220.9	671.7	300.0	60.4	126.1	743.0
A9-NC7	5733	Tahara	U.Devonian	53.3	48.2	54.6	36.1	32.1	288.2	724.6	820.7	2882.5	1631.4	230.2	674.6	3483.0
C1-26	6488	Tahara	U.Devonian	77.8	64.2	48.6	24.3	11.2	166.9	312.2	434.2	1064.0	430.3	148.7	133.0	1337.9
C1-26	6494	Tahara	U.Devonian	92.3	89.6	84.4	39.3	19.7	261.8	547.7	402.4	1358.1	698.6	225.8	173.3	1900.3
C1-26	6500	Tahara	U.Devonian	125.3	94.1	92.8	49.5	22.4	274.1	668.8	478.5	1411.8	809.9	282.4	185.8	2541.3
M2-NC7	6227	Tahara	U.Devonian	14.3	11.1	11.9	5.0	9.8	59.4	109.2	220.4	663.5	262.0	114.1	102.8	856.9
M2-NC7	6251	Tahara	U.Devonian	37.9	35.1	46.2	16.9	9.2	159.0	219.1	349.9	1212.4	472.2	120.2	187.3	1219.4
A1-90	7569	Tahara	U.Devonian	58.6	57.0	59.2	25.6	20.2	145.7	216.2	187.4	654.2	426.9	183.0	82.1	948.1
F1-66	4300	Tahara	U.Devonian	90.6	92.7	153.6	77.5	35.0	134.4	165.3	190.1	466.9	209.1	57.8	144.6	712.7
B1-49	1434	Tahara	U.Devonian	70.9	75.9	83.6	42.9	22.4	197.8	487.1	156.2	611.1	533.0	257.3	73.5	1525.5
A1-66	3153	Tahara	U.Devonian	114.2	87.9	87.1	29.6	11.0	143.2	376.1	852.9	1396.8	819.3	120.9	617.8	2337.0

Appendix V: Biomarker concentrations of the Silurian and Devonian source rock samples (µg/g extract)

Well	Depth	Formation	Age	C30βα	C31αβ S	C31αβ R	C32αβ S	C32αβ R	C33αβ S	C33αβ R	C34αβ S	C34αβ R	C35αβ S	C35αβ R	Sum hopanes	Sum tricys
B1-NC2	10108	L.Tanezzuft	L. Silurian	10.0	29.3	23.1	28.6	16.9	15.5	7.7	6.7	5.1	4.3	3.1	394	302
A1-70	10005	L.Tanezzuft	L. Silurian	5.6	20.3	14.6	15.9	10.6	9.5	5.6	5.0	3.2	0.0	0.0	249	200
A1-70	10155	L.Tanezzuft	L. Silurian	4.0	11.4	8.7	7.7	5.1	3.4	2.3	2.0	1.1	1.0	0.9	143	146
F1-66	7053	L.Tanezzuft	L. Silurian	3.2	8.7	6.0	5.2	4.0	3.3	3.1	0.0	0.0	0.0	0.0	149	221
F1-66	7054	L.Tanezzuft	L. Silurian	0.0	0.0	0.0	0.0	0.0	0.0	0.0	0.0	0.0	0.0	0.0	58	141
F1-66	7065	L.Tanezzuft	L. Silurian	0.0	0.0	0.0	0.0	0.0	0.0	0.0	0.0	0.0	0.0	0.0	20	60
A1-66	5054	L.Tanezzuft	L. Silurian	20.9	61.1	47.8	37.6	26.6	17.0	11.1	9.6	6.8	4.8	4.5	719	196
F1-66	6473	U.Tanezzuft	L. Silurian	25.3	64.0	42.5	39.5	26.4	18.5	12.5	12.5	7.6	6.0	4.4	670	199
A1-90	11921	U.Tanezzuft	L. Silurian	163.5	620.4	549.8	364.1	260.1	260.1	167.2	163.5	110.7	137.5	89.2	6090	139
Z5-NC5	10124	U.Tanezzuft	L. Silurian	15.2	64.3	43.6	46.1	30.3	25.5	15.6	13.3	8.5	7.3	4.8	678	242
B1-49	2135	U.Tanezzuft	L. Silurian	2.7	11.6	8.1	4.5	3.5	2.9	2.4	2.2	1.9	0.0	0.0	95	32
A1-70	9049	U.Tanezzuft	L. Silurian	94.9	220.9	171.6	126.0	91.3	87.6	54.8	58.4	38.3	23.7	18.3	2644	335
A9-NC7	5718	Tahara	U.Devonian	147.8	343.4	223.0	160.0	115.2	94.3	56.5	55.6	30.4	17.4	13.0	3514	113
A9-NC7	5733	Tahara	U.Devonian	580.5	1541.3	960.8	670.6	480.4	300.3	230.2	220.2	140.1	60.1	50.0	15682	224
C1-26	6488	Tahara	U.Devonian	195.6	618.1	409.2	291.8	217.5	148.7	93.9	68.9	46.9	0.0	0.0	5951	226
C1-26	6494	Tahara	U.Devonian	301.8	974.7	626.0	458.3	278.3	178.8	134.1	83.8	55.9	0.0	0.0	8398	325
C1-26	6500	Tahara	U.Devonian	356.7	1047.7	676.2	438.4	282.4	208.1	147.1	102.5	72.8	41.6	29.7	9782	384
M2-NC7	6227	Tahara	U.Devonian	166.5	369.7	284.0	186.1	122.4	106.8	71.0	75.9	49.0	26.9	14.7	3802	52
M2-NC7	6251	Tahara	U.Devonian	240.3	629.2	417.1	296.9	197.9	148.5	90.5	91.9	56.6	60.1	22.6	6032	145
A1-90	7569	Tahara	U.Devonian	144.2	482.4	346.5	266.1	183.0	133.1	82.1	74.8	47.1	27.7	19.4	4504	221
F1-66	4300	Tahara	U.Devonian	137.2	185.9	171.5	59.9	61.1	27.7	28.1	16.5	16.5	8.3	9.1	2668	449
B1-49	1434	Tahara	U.Devonian	188.4	556.0	381.4	303.3	211.4	156.2	96.5	82.7	48.7	27.6	19.3	5715	296
A1-66	3153	Tahara	U.Devonian	678.3	987.2	683.6	216.2	214.9	69.8	80.6	40.3	44.3	0	0	9536	330

Appendix V: Biomarker concentrations of the Silurian and Devonian source rock samples (μg/g extract)

Well	Depth	Formation	Age	C_{27}diabaS	C_{27}diabaR	$C_{27}\alpha\alpha\alpha$	C_{29}diabαS	$C_{27}\beta\beta$S	$C_{27}\alpha\alpha$R	C_{29}diaR	$C_{28}\alpha\alpha$R	$C_{29}\alpha\alpha$S	$C_{29}\beta\beta$R
B1-NC2	10108	L.Tanezzuft	L. Silurian	95.7	58.8	33.3	119.8	49.4	35.5	65.1	12.9	33.9	61.4
A1-70	10005	L.Tanezzuft	L. Silurian	58.7	33.7	21.5	80.3	30.0	19.2	41.3	7.9	28.0	48.1
A1-70	10155	L.Tanezzuft	L. Silurian	8.3	5.6	9.9	18.5	17.9	21.2	5.4	4.4	11.2	14.7
F1-66	7053	L.Tanezzuft	L. Silurian	24.5	13.8	11.6	34.4	14.3	9.9	18.7	3.6	12.9	21.4
F1-66	7054	L.Tanezzuft	L. Silurian	60.2	32.9	25.2	76.0	37.8	31.2	39.9	12.8	32.2	48.5
F1-66	7065	L.Tanezzuft	L. Silurian	18.7	13.0	8.8	23.7	12.2	10.3	10.7	3.8	9.0	11.6
A1-66	5054	L.Tanezzuft	L. Silurian	30.3	19.6	38.6	54.0	36.8	40.0	24.3	17.6	52.0	51.8
F1-66	6473	U.Tanezzuft	L. Silurian	49.0	31.4	59.7	77.2	50.2	64.3	36.9	29.4	71.8	72.2
A1-90	11921	U.Tanezzuft	L. Silurian	16.0	9.4	14.1	26.5	15.8	23.3	9.9	11.1	17.6	18.9
Z5-NC5	10124	U.Tanezzuft	L. Silurian	64.5	41.4	34.8	114.2	53.0	38.1	55.9	17.4	51.3	90.9
B1-49	2135	U.Tanezzuft	L. Silurian	2.4	1.9	2.4	5.8	1.9	3.2	1.6	1.8	2.7	2.8
A1-70	9049	U.Tanezzuft	L. Silurian	103.9	62.6	55.0	124.3	47.6	96.1	83.1	57.2	84.0	76.9
A9-NC7	5733	Tahara	U.Devonian	53.2	35.6	34.4	127.7	31.9	45.0	68.4	50.8	94.2	83.9
C1-26	6488	Tahara	U.Devonian	46.3	29.0	18.0	69.8	22.3	19.4	34.5	12.2	38.8	25.2
C1-26	6494	Tahara	U.Devonian	54.6	34.3	28.3	84.9	32.3	36.4	46.5	22.2	65.1	53.5
C1-26	6500	Tahara	U.Devonian	54.6	33.7	30.2	86.9	37.3	35.5	46.1	23.4	69.2	62.1
M2-NC7	6227	Tahara	U.Devonian	12.6	8.3	7.7	44.9	7.1	6.2	26.3	7.3	22.9	16.1
M2-NC7	6251	Tahara	U.Devonian	59.4	35.3	30.1	82.5	25.0	32.3	48.3	23.6	59.8	36.6
A1-90	7569	Tahara	U.Devonian	66.9	32.9	19.9	77.2	27.1	17.6	43.4	10.3	36.3	34.7
F1-66	4300	Tahara	U.Devonian	57.4	45.3	50.9	62.7	25.4	172.7	43.2	81.6	56.8	56.2
B1-49	1434	Tahara	U.Devonian	83.5	58.7	37.1	108.0	43.5	37.6	58.2	19.0	68.4	67.9
A1-66	3153	Tahara	U.Devonian	3.3	2.5	2.2	4.8	1.4	6.3	3.5	1.4	5.5	4.3

Appendix V: Biomarker concentration of the Silurian and Devonian source rock samples (µg/g extract)

Well	Depth	Formation	Age	$C_{29}\beta\beta S$	$C_{29}\alpha\alpha R$	$C_{27}\beta\beta R$	$C_{27}\beta\beta S$	$C_{28}\beta\beta R$	$C_{28}\beta\beta S$	$C_{29}\beta\beta R$	$C_{29}\beta\beta S$	Sum steranes
B1-NC2	10108	L.Tanezzuft	L. Silurian	44.7	37.6	84.5	56.0	30.3	31.7	82.3	66.7	648.2
A1-70	10005	L.Tanezzuft	L. Silurian	40.8	26.3	50.6	37.0	20.1	24.7	66.0	59.6	435.9
A1-70	10155	L.Tanezzuft	L. Silurian	11.9	11.7	23.4	21.3	8.8	12.8	23.9	20.3	140.7
F1-66	7053	L.Tanezzuft	L. Silurian	17.8	12.7	23.5	17.6	8.4	13.4	29.6	25.2	195.7
F1-66	7054	L.Tanezzuft	L. Silurian	42.4	31.7	18.7	14.3	6.5	9.8	18.6	17.1	470.8
F1-66	7065	L.Tanezzuft	L. Silurian	12.2	7.6	8.0	5.2	2.7	2.7	5.2	5.4	141.6
A1-66	5054	L.Tanezzuft	L. Silurian	40.0	50.9	61.9	58.3	29.4	38.6	81.0	69.9	455.9
F1-66	6473	U.Tanezzuft	L. Silurian	57.1	80.7	88.4	78.1	42.6	51.2	111.5	104.4	679.8
A1-90	11921	U.Tanezzuft	L. Silurian	15.2	19.8	28.0	23.7	17.1	20.5	31.1	26.4	197.5
Z5-NC5	10124	U.Tanezzuft	L. Silurian	69.5	49.3	104.8	77.8	44.1	60.6	147.1	128.1	680.2
B1-49	2135	U.Tanezzuft	L. Silurian	2.4	3.2	5.8	3.5	2.4	2.7	3.9	3.7	32.3
A1-70	9049	U.Tanezzuft	L. Silurian	54.1	133.7	84.7	60.1	53.3	56.7	104.1	92.1	978.4
A9-NC7	5718	Tahara	U.Devonian	18.9	38.7	25.9	10.6	12.9	17.1	24.7	24.0	299.8
A9-NC7	5733	Tahara	U.Devonian	101.5	115.9	82.2	45.1	61.1	65.8	125.0	110.4	842.6
C1-26	6488	Tahara	U.Devonian	22.3	24.5	44.9	25.0	19.9	24.3	36.8	35.3	362.3
C1-26	6494	Tahara	U.Devonian	41.4	42.8	61.3	40.2	29.0	42.1	74.8	68.7	542.3
C1-26	6500	Tahara	U.Devonian	44.4	52.0	73.9	47.5	46.1	55.4	89.4	76.5	575.4
M2-NC7	6227	Tahara	U.Devonian	14.9	15.2	18.3	6.1	11.0	10.4	21.5	20.3	189.4
M2-NC7	6251	Tahara	U.Devonian	38.5	48.9	45.8	27.9	28.2	28.5	47.2	42.4	520.4
A1-90	7569	Tahara	U.Devonian	26.5	21.7	49.0	34.1	27.0	28.8	51.9	44.8	414.4
F1-66	4300	Tahara	U.Devonian	30.7	198.7	6.8	4.1	3.6	3.3	8.2	6.0	881.4
B1-49	1434	Tahara	U.Devonian	51.9	42.2	83.5	56.1	50.0	53.6	106.5	92.8	676.0
A1-66	3153	Tahara	U.Devonian	3.6	9.7	29.2	14.9	24.2	18.2	36.3	26.4	48.5

APPENDIX VI

Appendix 4 Biomarker concentrations of the oils (μg/g oil)

Well	Depth	Formation	Age	$C_{20}T$	$C_{21}T$	$C_{23}T$	$C_{24}T$	$C_{25}T$	$C_{26}T$	Ts	Tm	C29αβ	$C_{29}Ts$	C_{30}dia	$C_{29}\beta\alpha$	$C_{30}\alpha\beta$
A1-NC3A				53	82	135	116	63	138	65	75	160	58	55	24	239
A1-NC3A				66	122	163	114	75	157	65	88	247	77	38	26	443
Z5-NC5				32	78	105	80	35	86	48	32	75	38	28	10	159
A6-NC169				29	60	88	72	35	79	47	35	32	28	36	11	57
A4-NC169				33	71	99	80	37	80	51	41	26	28	41	10	46
V6-NC8				39	105	122	77	37	99	75	41	115	61	39	14	251
LL6-NC8				31	80	67	48	22	67	55	23	48	38	30	11	112

Continued

Well	Depth	Formation	Age	C30βα	C31αβ S	C31αβ R	C32αβ S	C32αβ R	C33αβ S	C33αβ R	C34αβ S	C34αβ R	C35αβ S	C35αβ R	Sum hopanes	Sum tricys
A1-NC3A				36.2	110.2	75.8	72.9	46.1	46.1	30.7	28.5	17.6	16.5	16.5	1172.7	448.4
A1-NC3A				48.3	184.8	125.1	125.1	83.9	68.2	46.1	38.4	26.4	20.5	19.9	1770.7	541.0
Z5-NC5				18.5	52.3	43.4	37.1	24.7	19.8	12.8	11.8	8.9	7.7	6.4	633.0	329.8
A6-NC169				12.4	28.8	22.0	16.2	9.9	14.2	11.4	9.9	6.4	0.0	0.0	377.0	284.6
A4-NC169				11.7	33.7	19.1	13.8	10.2	16.8	9.0	11.3	7.7	0.0	0.0	376.3	320.4
V6-NC8				32.3	89.0	68.9	62.8	43.6	34.9	20.9	20.9	14.0	11.9	8.7	1004.1	380.2
LL6-NC8				17.2	41.0	36.4	33.1	23.8	17.1	12.1	11.1	7.3	6.6	6.1	530.3	248.6

Appendix 4 Biomarker concentrations of the oils (μg/g oil)

Well	Depth	Formation	Age	C_{27}diabaS	C_{27}diabaR	$C_{27}\alpha\alpha\alpha$	C_{29}diabαS	$C_{27}\beta\beta$S	$C_{27}\alpha\alpha$R	C_{29}diaR	$C_{28}\alpha\alpha$R	$C_{29}\alpha\alpha$S	$C_{29}\beta\beta$R
A1-NC3A				112	74	49	169	64	56	91	22	66	105
A1-NC3A				130	82	72	251	109	74	122	34	124	216
Z5-NC5				81	52	35	143	53	40	80	16	56	98
A6-NC169				76	47	21	96	33	23	58	9	24	39
A4-NC169				89	55	23	108	37	26	64	10	28	43
V6-NC8				112	74	61	184	77	72	100	31	95	127
LL6-NC8				69	39	30	102	41	28	57	13	41	64

Continued

Well	Depth	Formation	Age	$C_{29}\beta\beta$S	$C_{29}\alpha\alpha$R	$C_{27}\beta\beta$R	$C_{27}\beta\beta$S	$C_{28}\beta\beta$R	$C_{28}\beta\beta$S	$C_{29}\beta\beta$R	$C_{29}\beta\beta$S	Sum steranes
A1-NC3A				82	64	133	93	53	69	164	143	952
A1-NC3A				169	127	204	167	86	114	342	304	1510
Z5-NC5				85	51	111	75	43	64	156	151	791
A6-NC169				32	22	73	44	27	37	66	63	479
A4-NC169				36	25	73	46	29	42	63	62	543
V6-NC8				110	90	161	110	65	80	201	196	1133
LL6-NC8				58	37	82	58	35	47	101	101	579

APPENDIX VII

Appendix VII: Bulk and microscopy maturity parameters for core samples. (%VR_E) converted graptolite and chitinozoan reflectance to vitrinite reflectance equivelent.

Well name	Depth	Formation	Age	Tmax	HI	PI	SCI	ACI	Flourscence Colours		%Ro	%VR_E
									Spores	Acritarchs		
F1-66	4127	Tahara	U. Devonian	434	119	0.1	2	1.5	yellow		1.0	
	5476	Tadrart	L. Devonian	434	50	0.2	3	1.5	yellow-orange			
	6455	upper Tanezzuft	L. Silurian	434	53	0.5	4	2	yellow-orange			
	6470	upper Tanezzuft	L. Silurian	434	73	0.4	4	2	yellow-orange			
	6473	upper Tanezzuft	L. Silurian	434	100	0.3	4	2	yellow-orange		0.7	
	7042	lower Tanezzuft	L. Silurian	451	183	0.1		7		orange-brown		
	7047	lower Tanezzuft	L. Silurian	452	210	0.2						
	7051	lower Tanezzuft	L. Silurian	447	227	0.1		7		orange-brown		
	7053	lower Tanezzuft	L. Silurian	445	210	0.1						
	7054	lower Tanezzuft	L. Silurian	452	230	0.1		7		orange-brown		0.8
	7057	lower Tanezzuft	L. Silurian	448	252	0.1						
	7061	lower Tanezzuft	L. Silurian	450	232	0.2						
	7063	lower Tanezzuft	L. Silurian	450	181	0.2	7	7	orange-brown	orange-brown		0.8
	7065	lower Tanezzuft	L. Silurian	444	152	0.1	7	7	orange-brown	orange-brown		
	7073	lower Tanezzuft	L. Silurian	450	213	0.1		7		orange-brown		
	7076	lower Tanezzuft	L. Silurian	453	192	0.1		7		orange-brown		
A1-70	6561	Aouinet ouenine A	M. Devonian	431	80	0.2	2	1	yellow	yellow	0.6	
	6930	Ouan kasa	M. Devonian	431	32	0.3	2	1	yellow	yellow		
	8951	Acacus	U. Silurian	436	123	0.2	3	2	yellow-orange	yellow		0.5
	8960	Acacus	U. Silurian	435	117	0.2	3	2	yellow-orange	yellow		
	8971	Acacus	U. Silurian	436	100	0.4	3	2	yellow-orange	yellow		
	8980	Acacus	U. Silurian	435	63	0.3	3	2	yellow-orange	yellow		
	9017	upper Tanezzuft	L. Silurian	436	108	0.2	3	2	yellow-orange	yellow		
	9029	upper Tanezzuft	L. Silurian	436	165	0.2	4	2	orange-brown	yellow		
	9049	upper Tanezzuft	L. Silurian	437	136	0.1	4	2	orange-brown	yellow		
	9066	upper Tanezzuft	L. Silurian	439	107	0.2	4.5	2	orange-brown	yellow		
	9085	upper Tanezzuft	L. Silurian	438	151	0.1	4.5	2	orange-brown	yellow		
	9103	upper Tanezzuft	L. Silurian	438	129	0.2	4.5	2	orange-brown	yellow		
	9123	upper Tanezzuft	L. Silurian	438	68	0.3	4.5	2	orange-brown	yellow		
	9295	upper Tanezzuft	L. Silurian	437	143	0.5	4.5	2	orange-brown	yellow		
	9447	upper Tanezzuft	L. Silurian	439	247	0.2	4.5	2	orange-brown	yellow		
	9993	upper Tanezzuft	L. Silurian	444	188	0.2		2.5		yellow-orange		
	9999	upper Tanezzuft	L. Silurian	444	137	0.2		2.5		yellow-orange		
	10005	upper Tanezzuft	L. Silurian	445	169	0.2		2.5		yellow-orange		0.7

Well name	Depth	Formation	Age	Tmax	HI	PI	SCI	ACI	Flourscence Colours		%Ro	$\%VR_E$
									Spores	Acritarchs		
A9-NC7	5703	Tahara	U. Devonian	433	107	0.5	4.5	2	yellow-orange	yellow		
	5705	Tahara	U. Devonian	437	50	0.3	4.5	2	yellow-orange	yellow	1.0	
	5708	Tahara	U. Devonian	437	101	0.1	4.5	2	yellow-orange	yellow		
	5712	Tahara	U. Devonian	438	83	0.1	4.5	2	yellow-orange	yellow	0.9	
	5715	Tahara	U. Devonian		24	0.3	4.5	2	yellow-orange	yellow		
	5718	Tahara	U. Devonian		194	0.1	4.5	2	yellow-orange	yellow		
	5721	Tahara	U. Devonian	431	32	0.3	4.5	2	yellow-orange	yellow		
	5733	Tahara	U. Devonian		221	0.1	4.5	2	yellow-orange	yellow	0.8	
	5754	Tahara	U. Devonian		92	0.1	4.5	2	orange	yellow		
	5762	Tahara	U. Devonian		194	0.1	4.5	2	orange	yellow		
	5770	Tahara	U. Devonian	435	131	0.2	4.5	2	orange	yellow		
	5773	Tahara	U. Devonian		109	0.1	4.5	2	orange	yellow	1.0	
	5783	Tahara	U. Devonian		106	0.1	4.5	2	orange	yellow		
	5797	Tahara	U. Devonian		174	0.2	4.5	2	orange	yellow		
	5802	Tahara	U. Devonian	437	198	0.1	4.5	2	orange	yellow		
	5813	Tahara	U. Devonian		164	0.1	4.5	2	orange	yellow	1.2	
Z5-NC5	9074	Acacus	U. Silurian	433	90	0.2	2.5	2	yellow-orange	yellow-green		0.5
	9303	upper Tanezzuft	L. Silurian	434	145	0.2	2.5	2	yellow-orange	yellow-green		
	9310	upper Tanezzuft	L. Silurian	434	154	0.2	3	2	yellow-orange	yellow		
	9317	upper Tanezzuft	L. Silurian	435	136	0.3	3	2	yellow-orange	yellow		
	9324	upper Tanezzuft	L. Silurian	434	120	0.2	3	2	yellow-orange	yellow		
	10115	upper Tanezzuft	L. Silurian	444	246	0.3	4.5	2	orange	yellow		
	10124	upper Tanezzuft	L. Silurian	444	45	0.5	4.5	2	orange	yellow	0.8	0.8
	10136	upper Tanezzuft	L. Silurian	441	202	0.3	4.5	2	orange	yellow		
M2-NC7	6227	Tahara	U. Devonian	433	269	0.1	4.5	2	yellow-orange		0.7	
	6247	Tahara	U. Devonian	436	139	0.1	4.5	2	orange		0.8	
	6251	Tahara	U. Devonian	437	81	0.1	4.5	2				
	7259	Aouinat ouenine A	U. Devonian	438	63	0.3	6	2.5				
	7264	Aouinat ouenine A	U. Devonian	438	64	0.6	6	2.5	orange			
C1-26	6485	Aouinat ouenine C	U. Devonian	440	179	0.1	5	2	orange	yellow-green		
	6488	Aouinat ouenine C	U. Devonian	440	166	0.1	5	2	orange	yellow-green	1.3	
	6491	Aouinat ouenine C	U. Devonian	440	125	0.1	5	2	orange	yellow-green		
	6494	Aouinat ouenine C	U. Devonian	440	85	0.2	5	2	orange	yellow-green	1.1	
	6497	Aouinat ouenine C	U. Devonian	440	67	0.2	5	2	orange	yellow-green		
	6500	Aouinat ouenine C	U. Devonian	440	108	0.2	5	2	orange	yellow-green	1.1	
	6503	Aouinat ouenine C	U. Devonian	440	137	0.2	5	2	orange	yellow-green		
	6505	Aouinat ouenine C	U. Devonian	440	152	0.2	5	2	orange	yellow-green	1.3	

Well name	Depth	Formation	Age	Tmax	HI	PI	SCI	ACI	Flourscence Colours		%Ro	
									Spores	Acritarchs		
A1-90	7552	Tahara	U. Devonian	439	75	0.3	5	2	orange		1.2	
	7569	Tahara	U. Devonian	442	131	0.1	5	2	orange		1.2	
	11185	Acacus	U. Silurian	512	107	0.5	9	8			1.2	
	11195	Acacus	U. Silurian		24	0.5	9	8				
	11901	upper Tanezzuft	L. Silurian	406	26	0.5	9	8	none	none		
	11904	upper Tanezzuft	L. Silurian	390	38	0.3	9	8	none	none		
	11905	upper Tanezzuft	L. Silurian	383	33	0.5	9	8	none	none		
	11921	upper Tanezzuft	L. Silurian	364	17	0.4	9	8	none	none		
B1-NC2	10091	upper Tanezzuft	L. Silurian		123	0.3	4.5	2	orange	yellow		
	10093	upper Tanezzuft	L. Silurian	442	109	0.3	4.5	2	orange	yellow		
	10094	upper Tanezzuft	L. Silurian	442	153	0.2	4.5	2	orange	yellow		
	10096	upper Tanezzuft	L. Silurian	443	129	0.3	4.5	2	orange	yellow		
	10099	upper Tanezzuft	L. Silurian	445	159	0.3	4.5	2	orange	yellow		0.8
	10101	upper Tanezzuft	L. Silurian	440	223	0.2	4.5	2	orange	yellow		
	10105	upper Tanezzuft	L. Silurian	442	209	0.2	4.5	2	orange	yellow		
	10108	upper Tanezzuft	L. Silurian	447	254	0.1	4.5	2	orange	yellow		
B1-49	1428	Aouinat ouenine C	U. Devonian	440	157	0.1	4.5	1.5	orange-brown			
	1434	Aouinat ouenine C	U. Devonian	442	146	0.1	4.5	1.5	orange-brown	orange	1.2	
	1435	Aouinat ouenine C	U. Devonian	440	170	0.2	4.5	1.5	orange-brown	orange		
	1438	Aouinat ouenine C	U. Devonian	436	54	0.3	4.5	1.5	orange-brown	orange		
	1442	Aouinat ouenine C	U. Devonian	445	118	0.2	4.5	1.5	orange-brown	orange		
	1445	Aouinat ouenine C	U. Devonian	442	35	0.3	4.5	1.5	orange-brown	orange	1.2	
	1448	Aouinat ouenine C	U. Devonian	438	92	0.3	4.5	1.5	orange-brown	orange		
	1451	Aouinat ouenine C	U. Devonian	442	152	0.2	4.5	1.5	orange-brown	orange		
	2132	upper Tanezzuft	L. Silurian	434	44	0.6	6		orange-brown	none		1.0
	2135	upper Tanezzuft	L. Silurian	428	42	0.6	6		orange-brown	none		1.0
A1-66	3153	Aouinat ouenine C	U. Devonian	430	99	0.1	2.5	1.5	orange	yellow-green	0.9	
	3156	Aouinat ouenine C	U. Devonian	429	17	0.2	2.5	1.5	orange			
	3330	Aouinat ouenine B	U. Devonian	425	58	0.4	2.5	1.5	orange	yellow-green		
	4104	Ouan kasa	M. Devonian	429	81	0.6	2.5	1.5	orange	yellow-green		
	4115	Ouan kasa	M. Devonian	427	221	0.4	2.5	1.5	orange	yellow-green		
	4379	upper Tanezzuft	L. Silurian	433	172	0.2	3	1.5	orange	yellow-green		
	4382	upper Tanezzuft	L. Silurian	433	157	0.2		1.5	orange	yellow-green		
	4550	upper Tanezzuft	L. Silurian	432	217	0.2		1.5	orange	yellow		
	4553	upper Tanezzuft	L. Silurian	432	257	0.2		1.5	orange	yellow		
	4765	upper Tanezzuft	L. Silurian	435	171	0.2	3	1.5	orange	yellow		
	4836	upper Tanezzuft	L. Silurian	436	161	0.3		1.5		yellow-green		
	4842	upper Tanezzuft	L. Silurian	436	183	0.3		1.5		yellow-green		
	5051	upper Tanezzuft	L. Silurian	437	201	0.3	3.5	1.5	yellow-orange	yellow-green		
	5054	lower Tanezzuft	L. Silurian	435	383	0.1	4	1.5		yellow-green		0.6

APPENDIX VIII

Appendix VIII: Bulk geochemical parameters for cutting samples.

Well name	Depth	Formation	Age	TOC	%S	S1	S2	Tmax	HI	PI
A1-90	7750	Tahara	U. Devonian	2.5	0.3	1.0	4.0	438	160	0.2
	7800	Tahara	U. Devonian	1.8	1.1	0.7	2.2	439	121	0.2
	7850	Tahara	U. Devonian	1.5	0.7	0.7	2.9	440	198	0.2
	7900	Tahara	U. Devonian	1.6	1.0	0.4	2.0	441	121	0.2
	8050	Tahara	U. Devonian	1.4	1.1	0.5	1.2	440	81	0.3
	8100	Tahara	U. Devonian	2.5	1.3	0.4	0.8	440	32	0.3
	8150	Tahara	U. Devonian	2.1	3.0	0.5	1.3	442	62	0.3
	8200	Tahara	U. Devonian	1.9	3.0	0.3	0.9	440	46	0.3
	8250	Aouinat ouenine C	U. Devonian	4.3	2.3	1.1	2.9	435	68	0.3
	8300	Aouinat ouenine C	U. Devonian	2.0	2.5	0.5	1.4	443	71	0.3
	8350	Aouinat ouenine C	U. Devonian	1.9	3.2	0.4	0.9	443	48	0.3
	8400	Aouinat ouenine C	U. Devonian	1.9	3.0	0.4	1.1	444	59	0.3
	8450	Aouinat ouenine C	U. Devonian	2.7	3.3	0.7	2.3	441	84	0.2
	8550	Aouinat ouenine C	U. Devonian	2.0	2.5	0.7	2.0	442	97	0.3
	8600	Aouinat ouenine C	U. Devonian	2.7	2.8	0.9	2.8	445	101	0.2
	8650	Aouinat ouenine C	U. Devonian	2.2	2.6	0.8	3.2	439	145	0.2
	8700	Aouinat ouenine C	U. Devonian	2.1	3.1	0.6	1.9	445	90	0.2
	8750	Aouinat ouenine C	U. Devonian	2.8	1.5	0.5	1.1	442	38	0.3
	8800	Aouinat ouenine C	U. Devonian	1.7	1.6	0.4	0.7	426	40	0.4
	8850	Aouinat ouenine C	U. Devonian	0.3	0.1	0.4	0.7	448	228	0.3
	8900	Aouinat ouenine C	U. Devonian	0.3	0.1	0.3	0.6	449	190	0.3
	8950	Aouinat ouenine C	U. Devonian	1.8	1.7	1.0	2.7	445	149	0.3
	9000	Aouinat ouenine C	U. Devonian	2.0	1.9	1.1	3.0	444	152	0.3
	9050	Aouinat ouenine C	U. Devonian	1.8	1.8	1.1	2.8	443	154	0.3
	12000	upper Tanezzuft	L. Silurian	1.0	2.0	0.3	0.4	443	37	0.4
	12090	upper Tanezzuft	L. Silurian	0.6	2.4	0.3	0.6	440	97	0.4
	12200	upper Tanezzuft	L. Silurian	0.5	2.7	0.1	0.0	447	2	0.9
	12250	upper Tanezzuft	L. Silurian	0.6	2.5	0.2	0.0	450	7	0.8
	12300	upper Tanezzuft	L. Silurian	0.7	2.6	0.1	0.2	445	24	0.3
	12350	upper Tanezzuft	L. Silurian	0.5	2.7	0.1	0.1	441	27	0.3
	12400	upper Tanezzuft	L. Silurian	0.7	2.9	0.1	0.1	443	17	0.5
	12450	upper Tanezzuft	L. Silurian	0.7	3.1	0.2	0.2	436	28	0.5
	12500	upper Tanezzuft	L. Silurian	0.6	3.0	0.1	0.2	445	34	0.3
	12550	upper Tanezzuft	L. Silurian	0.9	3.0	0.1	0.1	436	12	0.4
	12600	upper Tanezzuft	L. Silurian	0.9	3.1	0.1	0.3	440	28	0.3
	12650	upper Tanezzuft	L. Silurian	1.1	3.5	0.3	0.2	434	18	0.6
	12700	upper Tanezzuft	L. Silurian	1.8	3.4	0.1	0.3	434	17	0.3
	12750	upper Tanezzuft	L. Silurian	2.2	3.2	0.1	0.2	434	7	0.4
F1-66	4050	Aouinat ouenine C	U. Devonian	0.8	0.4	0.1	0.4	428	47	0.2
	4100	Aouinat ouenine C	U. Devonian	1.0	0.4	0.2	0.7	433	75	0.2
	4150	Aouinat ouenine C	U. Devonian	1.1	0.6	0.2	0.7	433	62	0.2
	4200	Aouinat ouenine C	U. Devonian	2.4	2.0	0.2	1.2	430	48	0.2
	4250	Aouinat ouenine C	U. Devonian	1.8	1.8	0.3	1.0	430	55	0.3
	4300	Aouinat ouenine C	U. Devonian	3.4	3.1	0.2	4.8	422	142	0.0
	4400	Aouinat ouenine C	U. Devonian	1.8	1.7	0.2	1.1	429	64	0.1
	6300	upper Tanezzuft	L. Silurian	0.4	1.2	0.2	0.4	431	100	0.3
	6400	upper Tanezzuft	L. Silurian	0.5	1.1	0.1	0.3	427	52	0.2
	6500	upper Tanezzuft	L. Silurian	0.6	1.5	0.1	0.4	427	74	0.2
	6700	upper Tanezzuft	L. Silurian	1.2	1.8	0.3	0.8	428	69	0.3
	6900	upper Tanezzuft	L. Silurian	0.8	2.0	0.2	0.4	428	47	0.3
	6950	upper Tanezzuft	L. Silurian	6.1	2.8	1.0	12.0	438	196	0.1
	7000	upper Tanezzuft	L. Silurian	7.5	4.8	2.7	13.7	436	184	0.2
	7030	upper Tanezzuft	L. Silurian	6.6	4.0	2.8	13.0	438	197	0.2
M2-NC7	6300	Aouinat ouenine C	U. Devonian	2.2	0.9	0.6	2.7	435	126	0.2
	6350	Aouinat ouenine C	U. Devonian	2.7	1.7	0.5	3.0	434	111	0.2
	6400	Aouinat ouenine C	U. Devonian	2.0	1.7	0.3	1.4	437	72	0.2
	6450	Aouinat ouenine C	U. Devonian	1.7	1.0	0.5	1.7	438	97	0.2
	6500	Aouinat ouenine C	U. Devonian	1.1	0.9	0.2	0.8	441	72	0.2
	6550	Aouinat ouenine C	U. Devonian	1.4	1.4	0.3	1.3	441	94	0.2
	6600	Aouinat ouenine C	U. Devonian	2.5	1.9	0.7	5.3	435	213	0.1
	6650	Aouinat ouenine C	U. Devonian	1.2	1.2	0.5	0.8	441	66	0.4
	6700	Aouinat ouenine C	U. Devonian	5.3	2.9	2.2	17.3	432	325	0.1
	6750	Aouinat ouenine C	U. Devonian	2.1	1.6	0.8	3.3	439	153	0.2

Well name	Depth	Formation	Age	TOC	%S	S1	S2	Tmax	HI	PI
M2-NC7	6800	Aouinat ouenine C	U. Devonian	1.4	1.4	0.6	1.8	438	133	0.3
	6850	Aouinat ouenine C	U. Devonian	1.4	1.2	1.0	2.1	438	152	0.3
	6900	Aouinat ouenine C	U. Devonian	1.2	1.2	0.9	2.0	442	165	0.3
	6950	Aouinat ouenine B	M. Devonian	0.9	1.3	0.8	1.3	442	151	0.4
	7000	Aouinat ouenine B	M. Devonian	0.4	0.3	0.6	1.0	442	242	0.4
	7050	Aouinat ouenine B	M. Devonian	0.5	0.5	0.4	0.8	441	171	0.3
	7100	Aouinat ouenine B	M. Devonian	0.7	0.5	0.5	0.8	442	120	0.4
	7550	Aouinat ouenine B	M. Devonian	0.3	0.6	0.7	0.9	439	298	0.4
	7600	Aouinat ouenine B	M. Devonian	0.2	0.1	0.3	0.4	354	213	0.4
	10350	upper Tanezzuft	L. Silurian	0.3	0.3	0.4	0.4	362	153	0.5
	10400	upper Tanezzuft	L. Silurian	0.3	0.7	0.3	0.5	374	166	0.4
	10450	upper Tanezzuft	L. Silurian	0.3	0.7	0.3	0.4	396	139	0.4
	10500	upper Tanezzuft	L. Silurian	0.3	0.7	0.3	0.5	383	175	0.4
	10550	upper Tanezzuft	L. Silurian	0.3	1.3	0.4	0.7	444	209	0.4
	10600	upper Tanezzuft	L. Silurian	0.4	1.4	0.4	0.6	416	152	0.4
	10650	upper Tanezzuft	L. Silurian	0.4	2.3	0.1	0.1	467	34	0.4
	10700	upper Tanezzuft	L. Silurian	0.4	2.4	0.2	0.2	444	39	0.5
	10750	upper Tanezzuft	L. Silurian	0.4	2.9	0.1	0.2	441	40	0.3
	10800	upper Tanezzuft	L. Silurian	0.4	2.9	0.1	0.1	427	32	0.3
	10900	upper Tanezzuft	L. Silurian	2.0	4.1	0.3	0.2	444	9	0.6
	10950	upper Tanezzuft	L. Silurian	1.6	2.6	0.2	0.1	492	8	0.6
	11000	upper Tanezzuft	L. Silurian	2.7	3.8	0.4	0.1	511	5	0.7
	11050	upper Tanezzuft	L. Silurian	6.2	4.2	0.5	0.3	594	5	0.6
	11100	upper Tanezzuft	L. Silurian	2.5	5.7	0.4	0.1	457	5	0.8
	11150	upper Tanezzuft	L. Silurian	1.7	3.8	0.2	0.1	435	6	0.7
	11200	upper Tanezzuft	L. Silurian	2.8	4.6	0.5	0.2	455	6	0.8
	11250	upper Tanezzuft	L. Silurian	2.0	4.1	0.3	0.1	460	7	0.7
	11300	upper Tanezzuft	L. Silurian	2.7	3.4	0.5	0.2	456	6	0.8
D1-NC2	5850	Aouinat ouenine A	M. Devonian	0.1	0.2	0.3	0.2	427	170	0.7
	5900	Aouinat ouenine A	M. Devonian	0.2	0.3	0.2	0.2	422	108	0.5
	5950	Aouinat ouenine A	M. Devonian	0.2	0.5	0.2	0.2	417	96	0.4
	6000	Aouinat ouenine A	M. Devonian	0.2	0.3	0.4	0.2	429	72	0.7
	6050	Aouinat ouenine A	M. Devonian	0.2	0.1	0.1	0.2	426	98	0.4
	6100	Aouinat ouenine A	M. Devonian	0.1	0.3	0.1	0.2	427	102	0.3
	6150	Aouinat ouenine A	M. Devonian	0.1	0.3	0.1	0.1	425	104	0.3
	6200	Aouinat ouenine A	M. Devonian	0.2	0.2	0.1	0.2	423	73	0.5
	6250	Aouinat ouenine A	M. Devonian	0.3	0.2	0.2	0.2	424	80	0.5
	6300	Aouinat ouenine A	M. Devonian	0.3	0.1	0.1	0.2	425	54	0.3
	10050	lower Tanezzuft	L. Silurian	3.0	3.2	1.2	10.0	441	337	0.1
	10100	lower Tanezzuft	L. Silurian	0.9	2.1	0.3	1.8	442	202	0.1
	10150	lower Tanezzuft	L. Silurian	0.9	3.1	0.2	1.7	442	200	0.1
	10200	lower Tanezzuft	L. Silurian	0.8	2.0	0.2	1.6	441	212	0.1
	10280	lower Tanezzuft	L. Silurian	5.1	2.8	2.7	19.6	445	383	0.1
	10290	lower Tanezzuft	L. Silurian	5.1	2.6	3.2	20.3	444	398	0.1
	10300	lower Tanezzuft	L. Silurian	4.8	3.0	2.6	18.5	443	386	0.1
	10310	lower Tanezzuft	L. Silurian	4.5	3.0	2.8	19.6	440	435	0.1
	10330	lower Tanezzuft	L. Silurian	6.4	3.0	3.4	27.7	441	432	0.1
	10350	lower Tanezzuft	L. Silurian	17.2	6.1	4.6	45.2	444	263	0.1
	10360	lower Tanezzuft	L. Silurian	23.1	6.2	6.1	55.1	440	238	0.1
	10370	lower Tanezzuft	L. Silurian	15.7	4.6	7.3	42.0	440	268	0.1
	10380	lower Tanezzuft	L. Silurian	7.7	6.0	5.4	30.0	438	392	0.2
	10390	lower Tanezzuft	L. Silurian	10.0	4.3	2.9	34.4	440	344	0.1
A1-70	6410	Aouinat ouenine A	M. Devonian	0.2	0.3	0.3	0.4	423	166	0.4
	6430	Aouinat ouenine A	M. Devonian	0.3	0.3	0.5	0.5	426	161	0.5
	6470	Aouinat ouenine A	M. Devonian	0.3	0.3	0.5	0.3	415	109	0.6
	6490	Aouinat ouenine A	M. Devonian	0.2	0.3	0.4	0.4	416	155	0.5
	6510	Aouinat ouenine A	M. Devonian	0.2	0.2	0.3	0.3	420	134	0.5
	6520	Aouinat ouenine A	M. Devonian	0.3	0.3	0.7	0.5	422	190	0.6
	6540	Aouinat ouenine A	M. Devonian	0.2	0.2	0.5	0.4	420	175	0.6
	6560	Aouinat ouenine A	M. Devonian	0.3	0.2	0.3	0.3	427	95	0.5
	6600	Aouinat ouenine A	M. Devonian	0.3	0.3	0.3	0.3	427	112	0.5
	6620	Aouinat ouenine A	M. Devonian	0.4	0.3	0.4	0.5	429	138	0.5
	6696	Aouinat ouenine A	M. Devonian	0.4	0.4	0.6	0.5	427	128	0.5
	9413	upper Tanezzuft	L. Silurian	1.1	2.2	0.8	2.9	436	272	0.2
	9475	upper Tanezzuft	L. Silurian	0.7	1.9	1.0	2.0	438	295	0.3
	9655	upper Tanezzuft	L. Silurian	0.9	1.9	0.8	2.6	438	285	0.2
	9700	upper Tanezzuft	L. Silurian	0.7	1.6	0.5	1.7	439	239	0.2

Well name	Depth	Formation	Age	TOC	%S	S1	S2	Tmax	HI	PI
A1-70	9765	upper Tanezzuft	L. Silurian	0.7	1.6	0.5	2.2	438	305	0.2
	9810	upper Tanezzuft	L. Silurian	0.9	1.8	0.7	2.3	439	261	0.2
	9870	upper Tanezzuft	L. Silurian	0.8	1.6	0.5	2.3	438	284	0.2
	9915	upper Tanezzuft	L. Silurian	1.0	1.8	0.8	2.9	439	302	0.2
	10009	lower Tanezzuft	L. Silurian	6.4	2.3	3.4	15.7	436	246	0.2
	10012	lower Tanezzuft	L. Silurian	9.4	1.4	4.8	20.8	431	222	0.2
	10030	lower Tanezzuft	L. Silurian	2.4	1.7	1.5	7.1	440	295	0.2
	10045	lower Tanezzuft	L. Silurian	1.4	1.9	0.8	2.9	439	198	0.2
	10065	lower Tanezzuft	L. Silurian	2.1	2.0	1.3	5.2	437	251	0.2
	10072	lower Tanezzuft	L. Silurian	6.2	4.3	3.9	21.6	441	346	0.2
	10105	lower Tanezzuft	L. Silurian	7.8	3.9	4.5	25.8	443	329	0.1
	10140	lower Tanezzuft	L. Silurian	10.7	2.1	5.1	26.3	435	246	0.2
	10155	lower Tanezzuft	L. Silurian	17.3	5.1	10.0	60.3	441	348	0.1
	10170	lower Tanezzuft	L. Silurian	25.1	3.2	12.3	78.6	437	313	0.1
	10181	lower Tanezzuft	L. Silurian	11.8	2.0	5.1	38.6	433	327	0.1
Z5-NC5	9500	upper Tanezzuft	L. Silurian	0.5	1.0	1.2	1.1	436	225	0.5
	9700	upper Tanezzuft	L. Silurian	0.7	0.9	1.4	1.7	435	250	0.5
	9800	upper Tanezzuft	L. Silurian	0.5	1.7	0.7	1.2	437	250	0.4
	9890	upper Tanezzuft	L. Silurian	0.5	1.9	0.6	1.1	438	241	0.3
	10000	upper Tanezzuft	L. Silurian	0.5	1.5	0.7	0.8	434	171	0.4
	10090	upper Tanezzuft	L. Silurian	0.5	1.3	0.5	1.0	440	197	0 3
	10200	upper Tanezzuft	L. Silurian	0.5	1.2	0.7	0.9	437	185	0.4
	10240	upper Tanezzuft	L. Silurian	0.9	1.7	1.3	1.3	434	148	0.5
	10300	lower Tanezzuft	L. Silurian	2.4	3.0	1.6	3.3	438	138	0.3
	10410	lower Tanezzuft	L. Silurian	1.1	3.0	0.5	1.3	438	118	0.3
	10490	lower Tanezzuft	L. Silurian	22.8	5.0	7.3	50.7	437	222	0.1
	10510	lower Tanezzuft	L. Silurian	12.1	2.4	5.8	34.5	439	285	0.1
B1-49	1200	Tahara	U. Devonian	1.1	0.3	0.7	1.2	434	104	0.4
	1250	Tahara	U. Devonian	1.0	0.5	0.7	1.1	436	110	0.4
	1300	Tahara	U. Devonian	0.9	0.4	0.4	0.8	438	91	0.3
	1350	Aouinat ouenine C	U. Devonian	0.7	0.9	0.3	0.5	435	75	0.4
	1400	Aouinat ouenine C	U. Devonian	0.9	0.7	0.4	1.0	440	107	0.3
	1450	Aouinat ouenine C	U. Devonian	1.0	0.7	0.2	0.9	440	92	0.2
	1472	Aouinat ouenine C	U. Devonian	1.2	1.2	0.3	1.1	441	93	0.2
	1475	Aouinat ouenine C	U. Devonian	1.4	2.1	0.5	1.5	435	109	0.3
	1478	Aouinat ouenine C	U. Devonian	0.7	0.8	0.2	0.5	438	69	0.3
	1487	Aouinat ouenine C	U. Devonian	0.9	1.3	0.4	0.8	437	89	0.3
	1490	Aouinat ouenine C	U. Devonian	1.5	3.0	0.4	1.9	441	128	0.2
	1502	Aouinat ouenine C	U. Devonian	1.1	2.3	0.3	1.4	439	121	0.2
	1514	Aouinat ouenine C	U. Devonian	1.5	3.2	0.3	2.1	440	140	0.1
	1523	Aouinat ouenine C	U. Devonian	0.9	1.0	0.3	0.9	438	94	0.2
	1550	Aouinat ouenine C	U. Devonian	0.8	0.9	0.2	0.6	438	67	0.2
	1600	Aouinat ouenine C	U. Devonian	0.9	0.9	0.3	0.8	441	86	0.3
	1650	Aouinat ouenine C	U. Devonian	0.7	0.8	0.3	0.7	436	102	0.3
	2053	upper Tanezzuft	L. Silurian	0.4	1.1	0.2	0.2	436	50	0.5
	2055	upper Tanezzuft	L. Silurian	0.3	0.8	0.1	0.2	444	46	0.5
	2070	upper Tanezzuft	L. Silurian	0.5	2.8	0.3	0.2	430	38	0.6
	2088	upper Tanezzuft	L. Silurian	0.7	3.3	0.3	0.2	428	22	0.7
	2103	upper Tanezzuft	L. Silurian	0.7	4.2	0.2	0.2	429	21	0.6
	2118	upper Tanezzuft	L. Silurian	1.0	5.7	0.3	0.2	429	17	0.7
	2134	upper Tanezzuft	L. Silurian	0.8	4.4	0.2	0.2	430	21	0.5
	2152	upper Tanezzuft	L. Silurian	0.9	5.4	0.2	0.2	427	18	0.6
	2167	upper Tanezzuft	L. Silurian	0.7	5.1	0.2	0.1	429	19	0.5
	2182	upper Tanezzuft	L. Silurian	0.6	3.5	0.2	0.1	434	20	0 6
	2197	upper Tanezzuft	L. Silurian	0.6	2.5	0.1	0.1	432	18	0.5
	2220	upper Tanezzuft	L. Silurian	0.4	1.2	0.2	0.1	403	21	0.7
	2226	lower Tanezzuft	L. Silurian	0.5	2.6	0.3	0.1	395	22	0.7
	2240	lower Tanezzuft	L. Silurian	0.7	2.8	0.3	0.1	422	13	0.8
	2243	lower Tanezzuft	L. Silurian	1.0	4.1	0.4	0.2	419	17	0.7
	2251	lower Tanezzuft	L. Silurian	0.8	3.2	0.2	0.1	414	9	0.7
	2261	lower Tanezzuft	L. Silurian	0.7	2.4	0.4	0.1	412	16	0.8
	2271	lower Tanezzuft	L. Silurian	0.7	2.8	0.2	0.1	424	13	0.7
	2281	lower Tanezzuft	L. Silurian	0.8	3.3	0.2	0.1	427	11	0.7
	2291	lower Tanezzuft	L. Silurian	0.7	2.8	0.2	0.1	420	12	0.7
	2297	lower Tanezzuft	L. Silurian	0.8	1.8	0.1	0.1	419	9	0.7
	2301	lower Tanezzuft	L. Silurian	1.4	2.0	0.2	0.1	407	7	0.7
	2304	lower Tanezzuft	L. Silurian	1.3	2.8	0.2	0.1	432	8	0.6

PLATES

PLATE I

1- Black equant wood, angular (x 20), Tahara Sandstone Formation. Well A9-NC7, 5705'.
2- Black lath-shaped phytoclast (x-20), upper Aouinet Ouenine C Formation. Well C1-26, 6488'.
3- Corroded opaque lath-shaped phytoclast (x-20), Tahara Sandstone Formation. Well A9-NC7, 5721'.
4- Undegraded biostructured brown wood phytoclast (x-20), upper Aouinet Ouenine C Formation. Well C1-26, 6485'.
5- Opaque biostructured phytoclast (x-20), Tahara Sandstone Formation. Well M2-NC7, 6247'.
6- Degraded biostructured phytoclast (x-20), Tahara Sandstone Formation. Well F1-66, 4127'.
7- Brown corroded phytoclast (x-20), Tahara Sandstone Formation. Well A9-NC7, 5705'.
8- Cuticle showing visible cell structure (x-20), upper Aouinet Ouenine C Formation. Well B1-49, 1428m.
9- Thick-walled spore showing characteristic trilete mark (x 20), Aouinet Ouenine Formation. Well C1-26, 6488'.
10- Prasinophytes (*Tasmanite*-type) (x-20), upper Tanezzuft Formation. Well A1-70, 9993'.
11- Prasinophytes (*Tasmanite*-type) (x-20), upper Tanezzuft Formation. Well Z5-NC5, 10163'.
12- Polyognomorph acritarchs (Veryhachium) (x-20), upper Tanezzuft Formation. Well A1-70, 9123'.
13- Acanthomorph acritarchs (x-20), upper Tanezzuft Formation. Well Z5-NC5, 10136'.
14- Netromorphous acritarchs (x-20), upper Tanezzuft Formation. Well Z5-NC5, 10124'.
15- Chitinozoa (x-20), upper Tanezzuft Formation. Well A1-70, 9295'.
16- Chitinozoa (x-20), upper Tanezzuft Formation. Well A1-70, 9123'.
17- Graptolite (x-20), upper Tanezzuft Formation. Well A1-70, 10005'

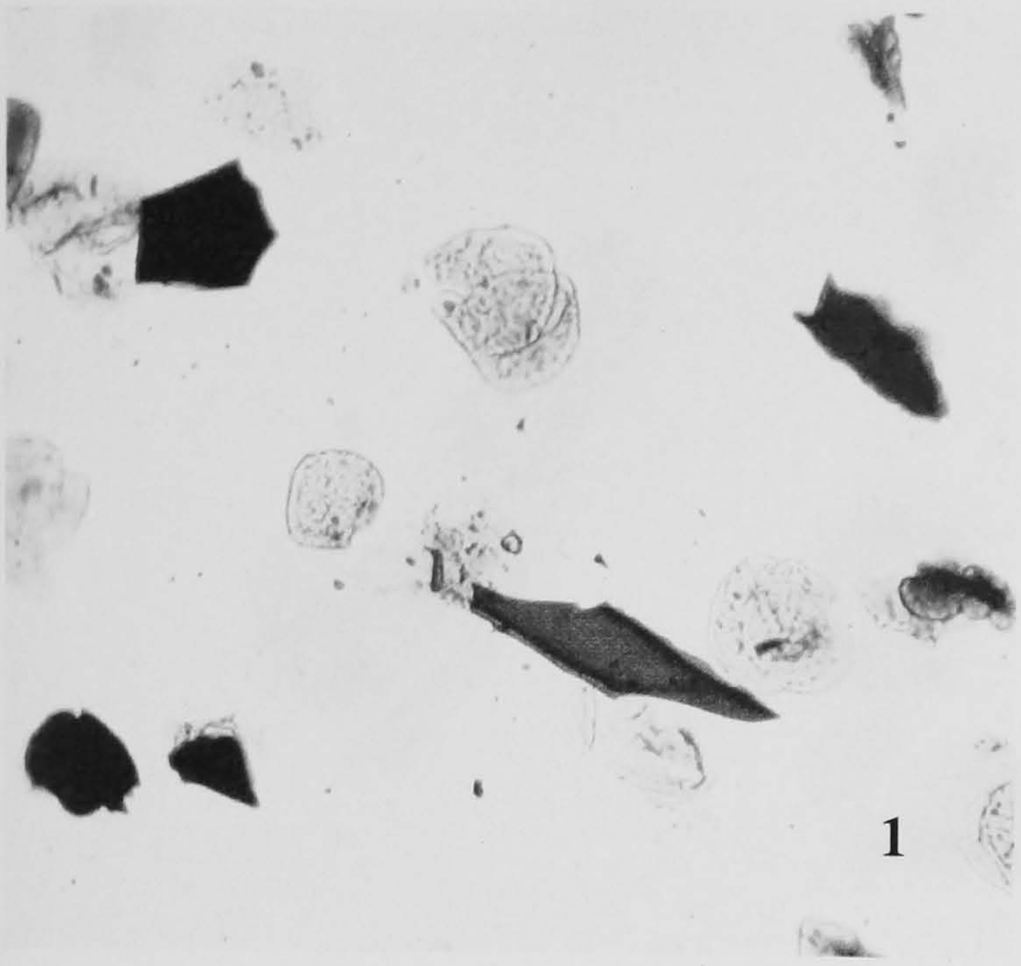

1

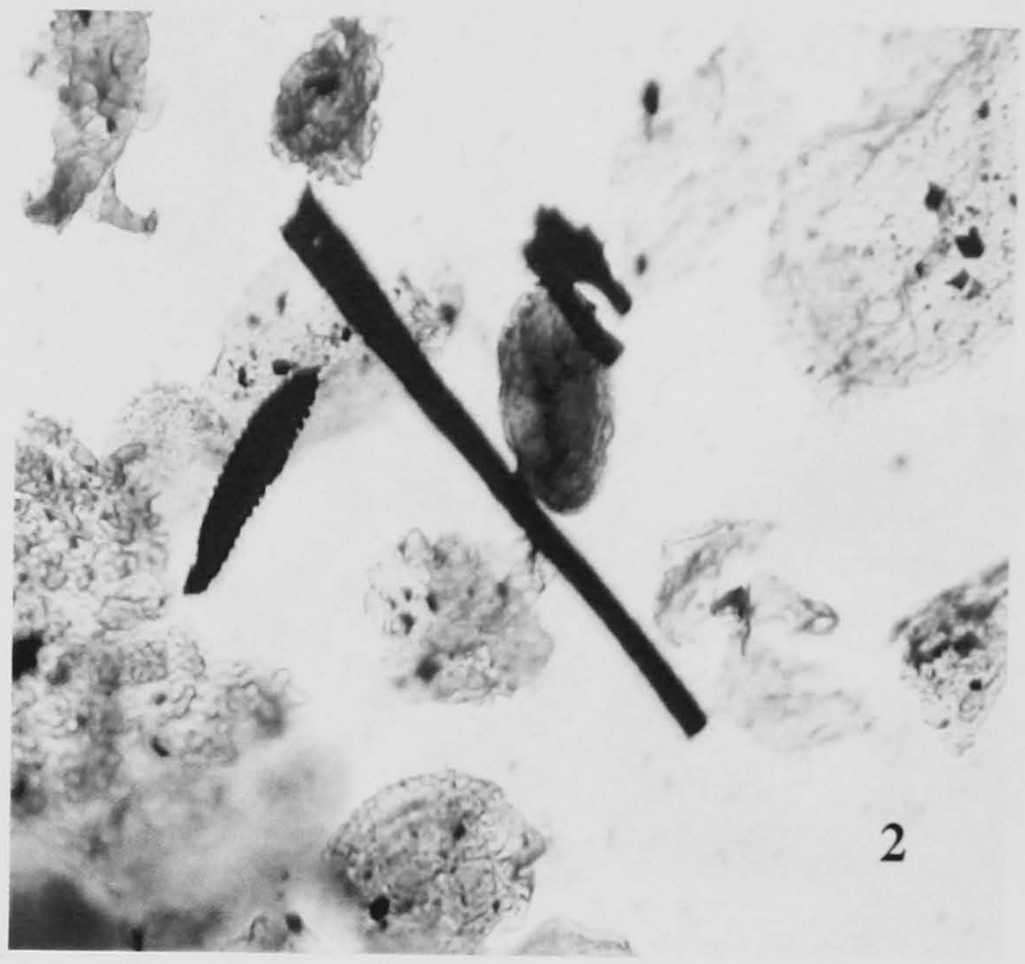

2

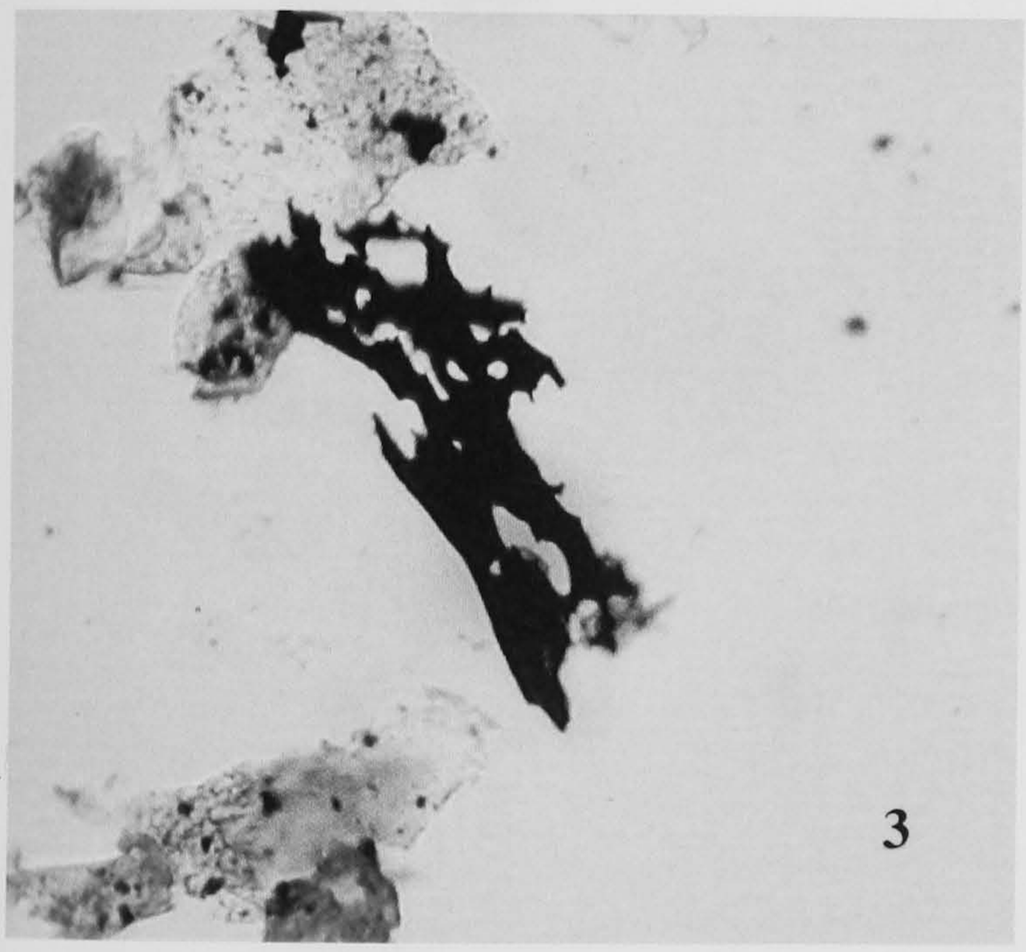

3

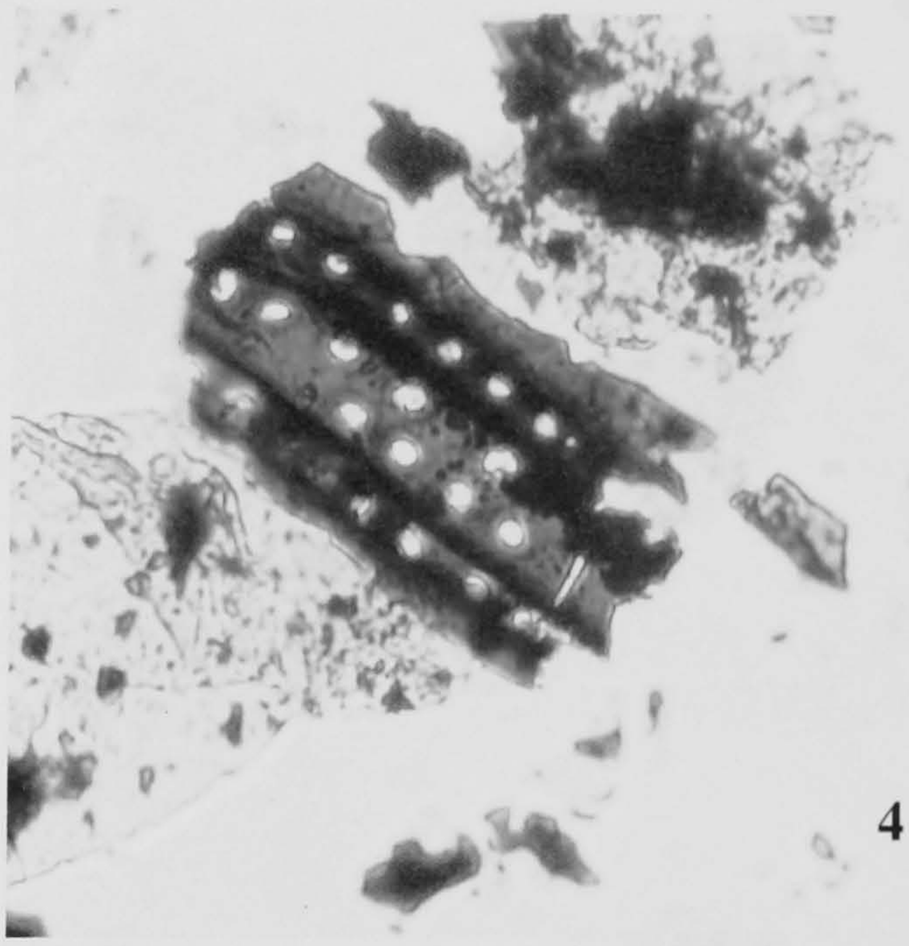

4

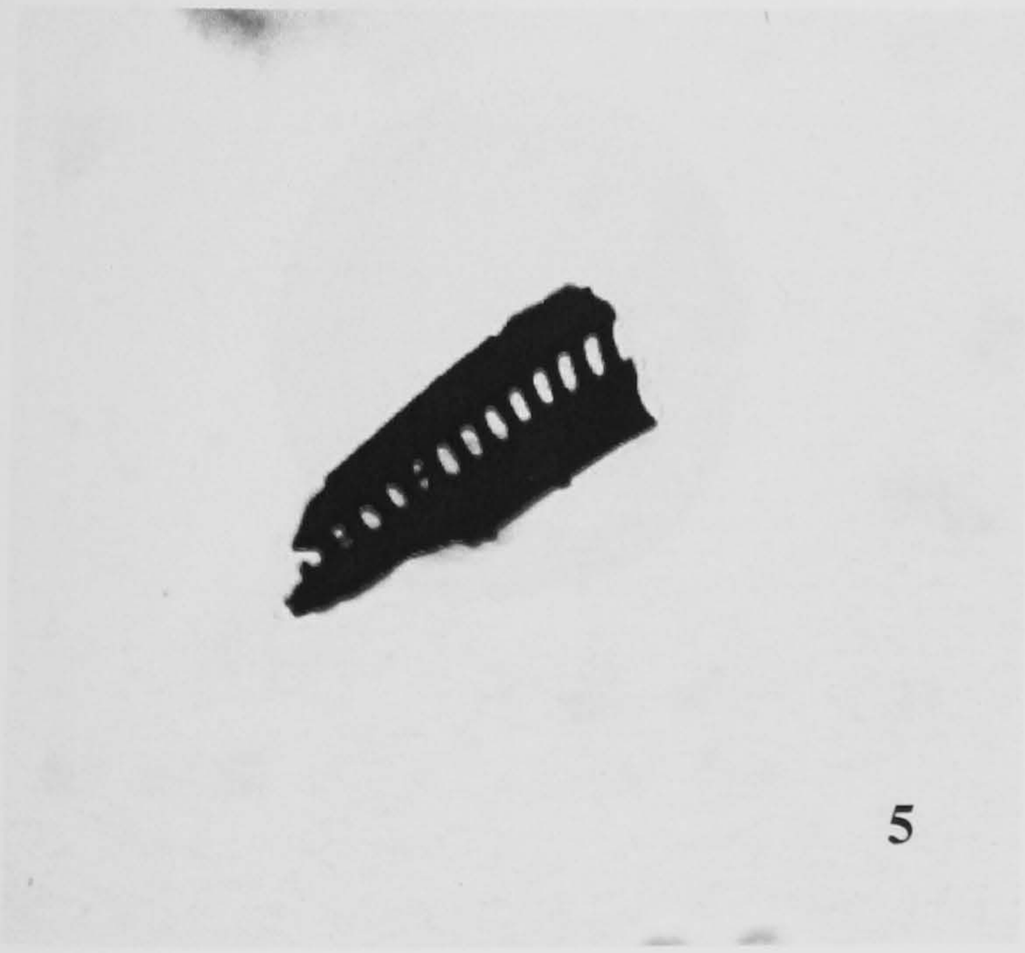

5

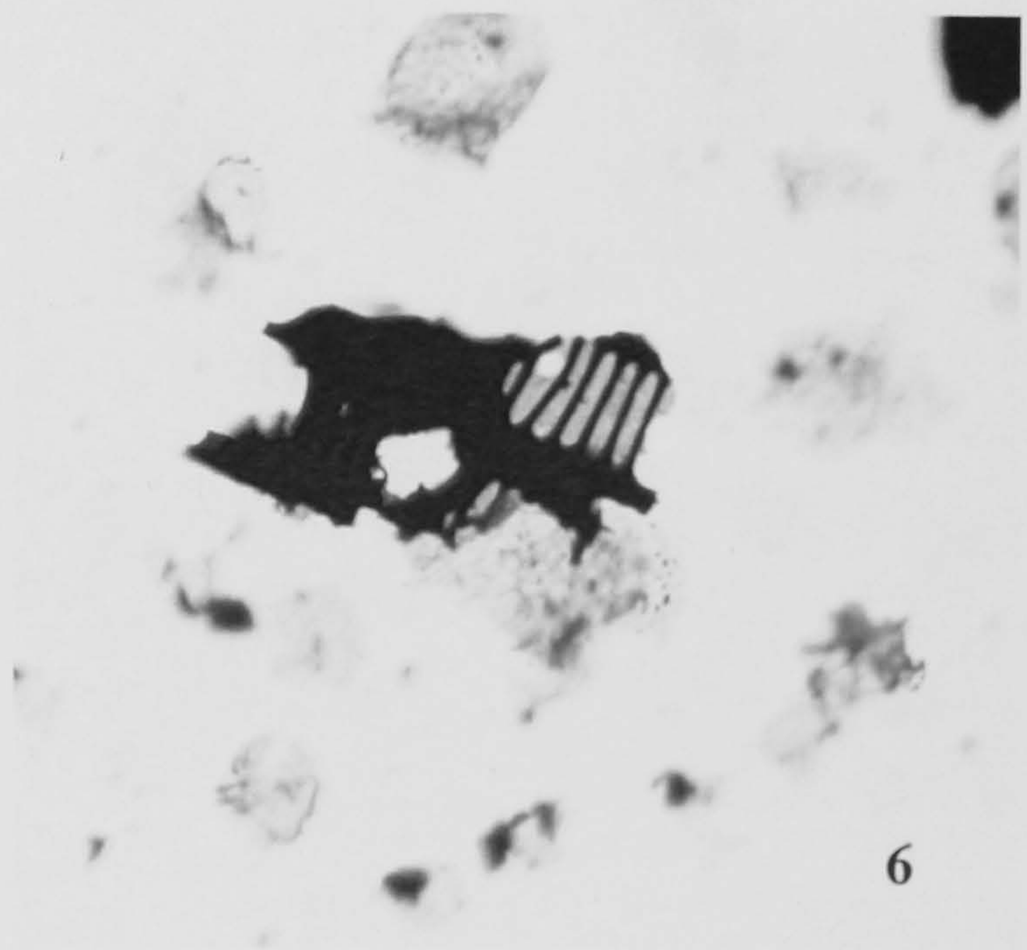

6

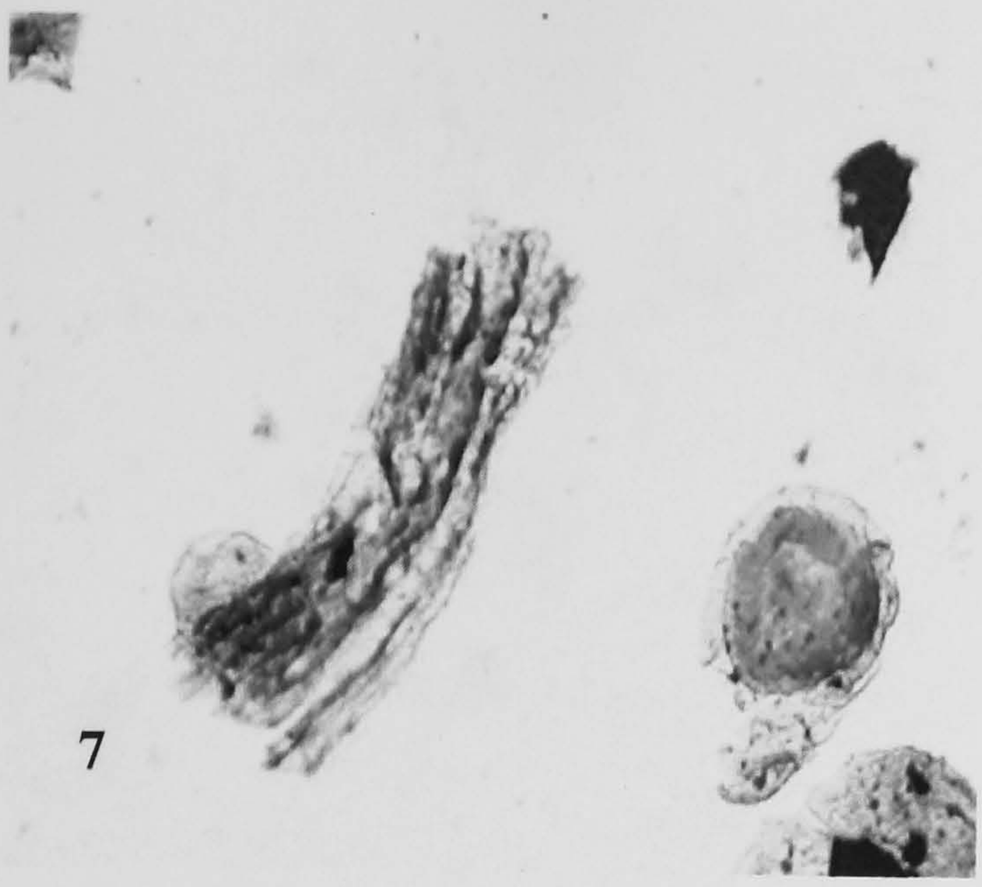

7

8

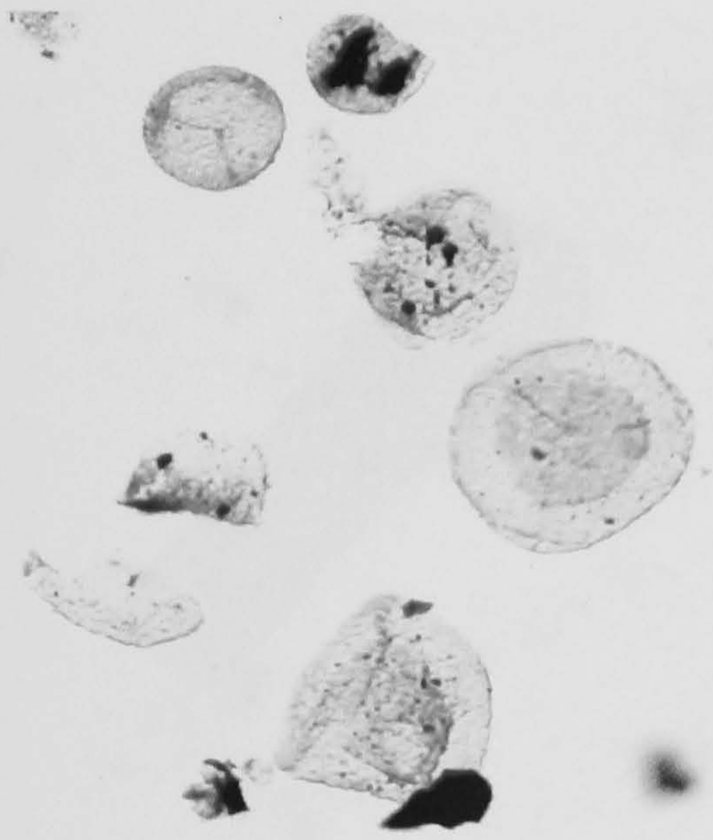

9

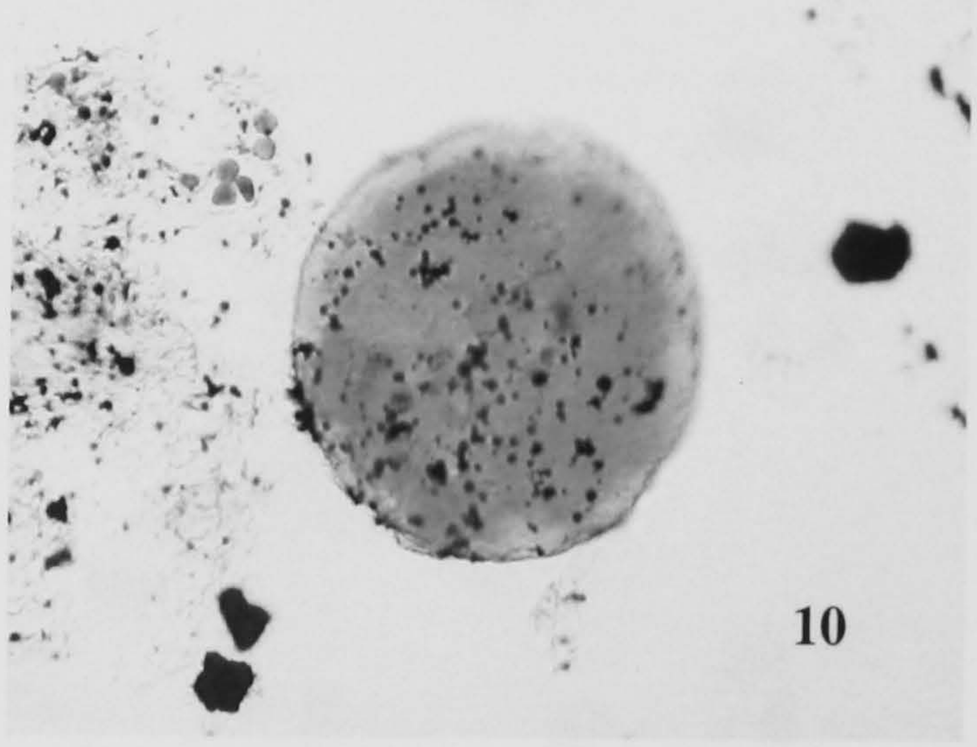

10

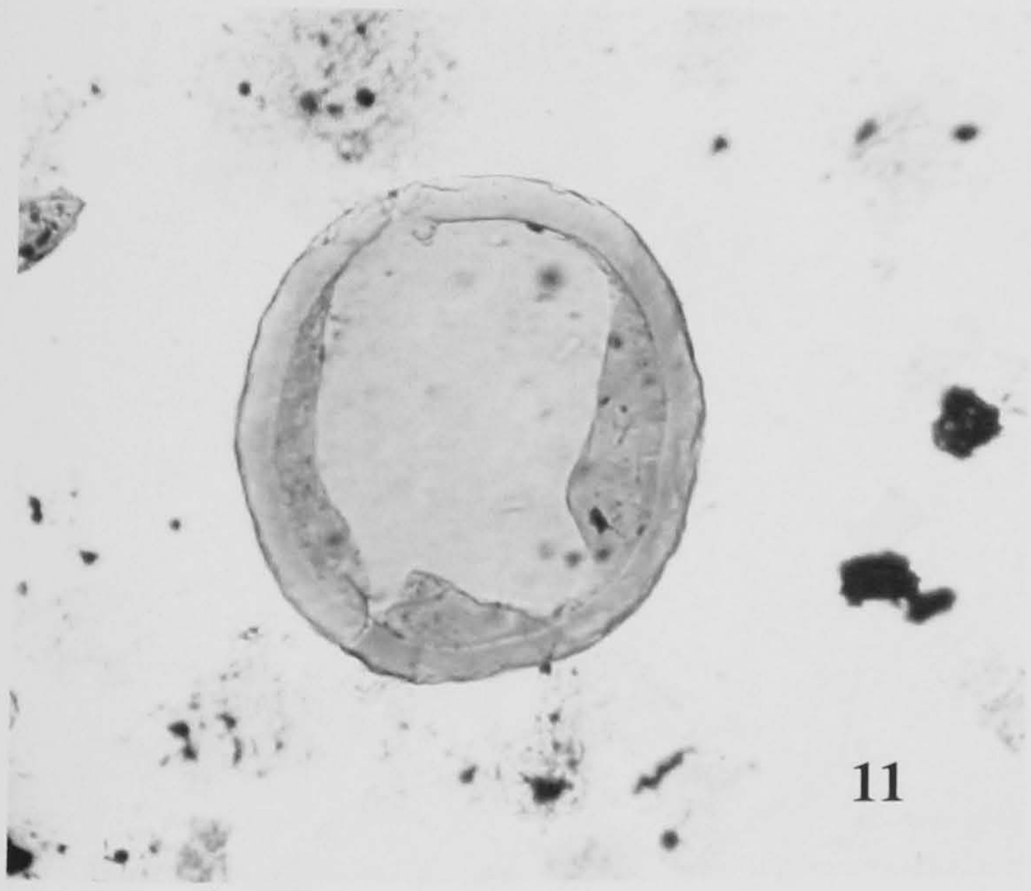

11

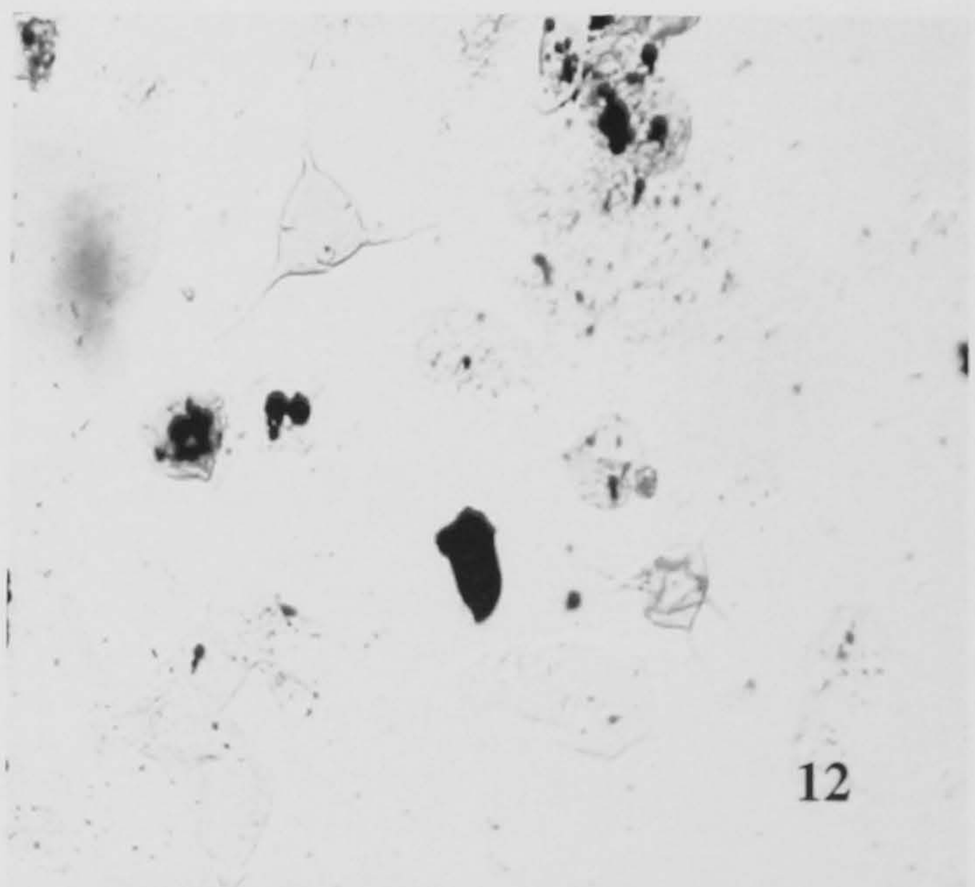

12

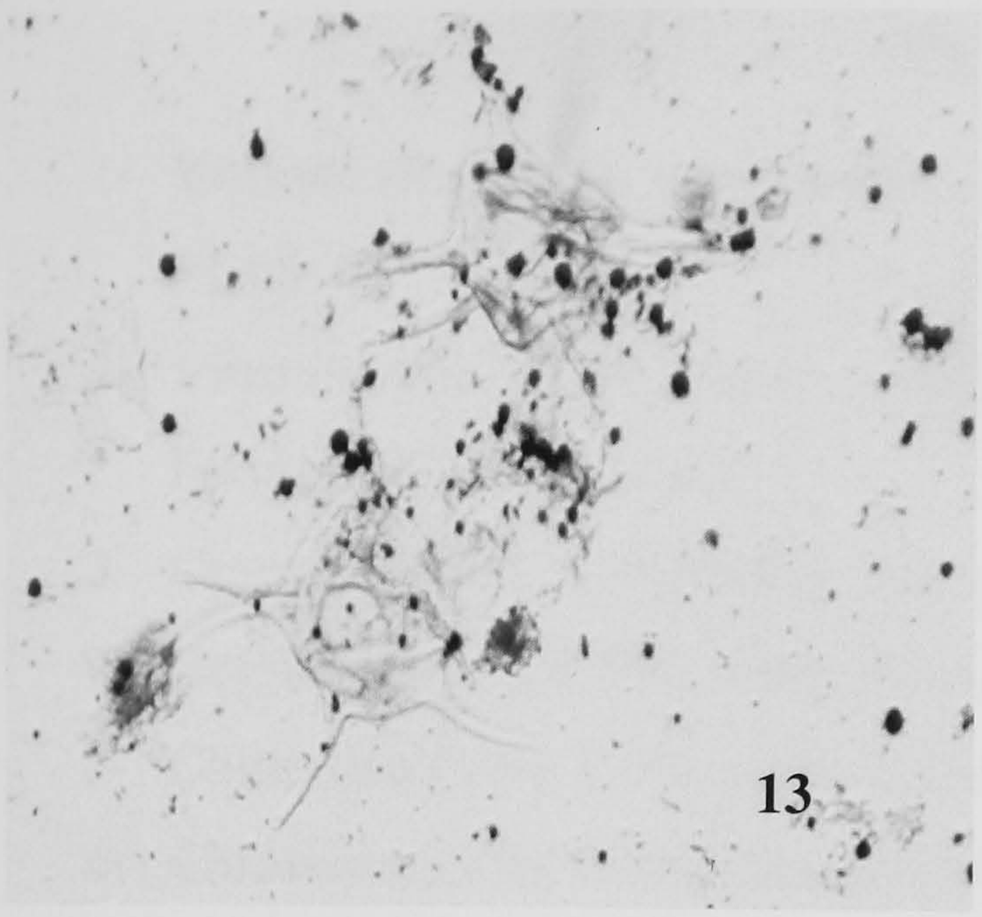

13

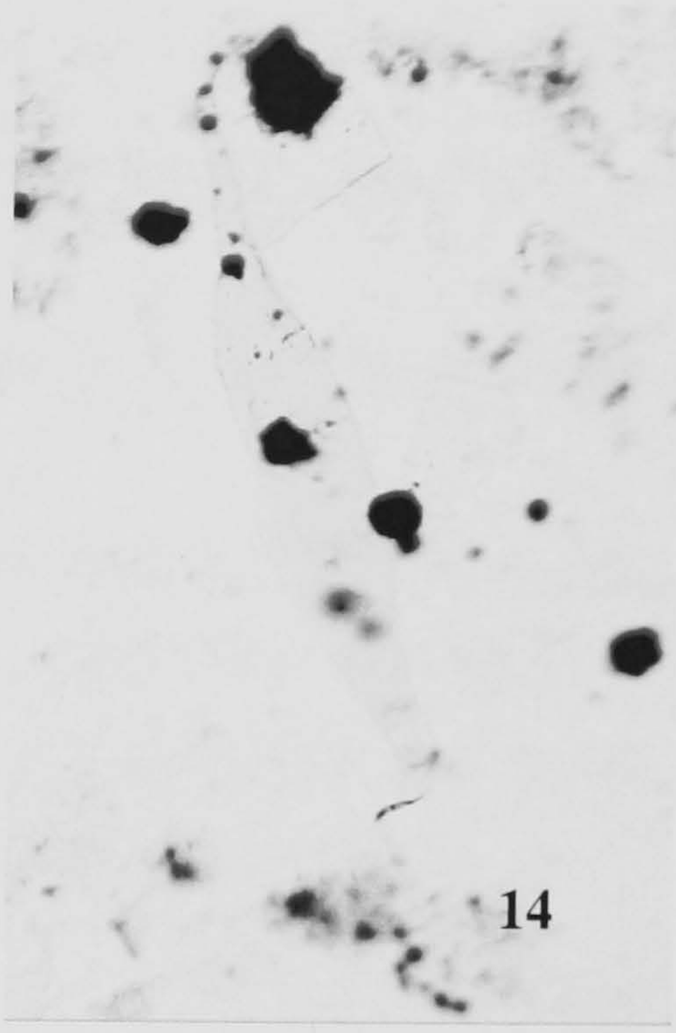

14

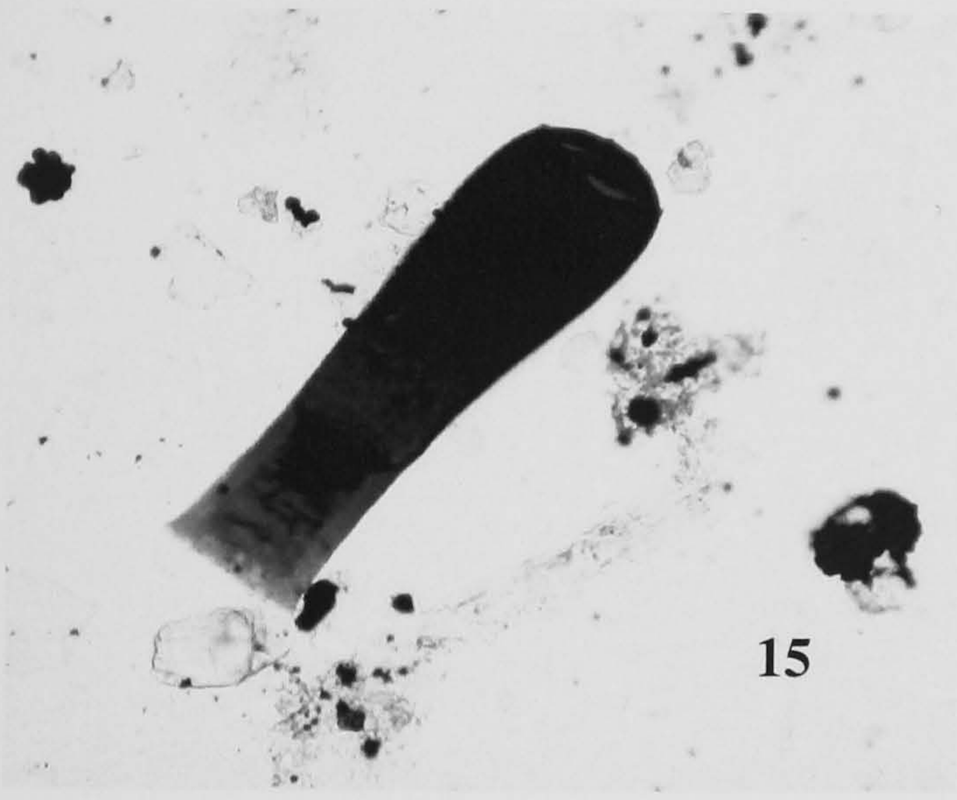

15

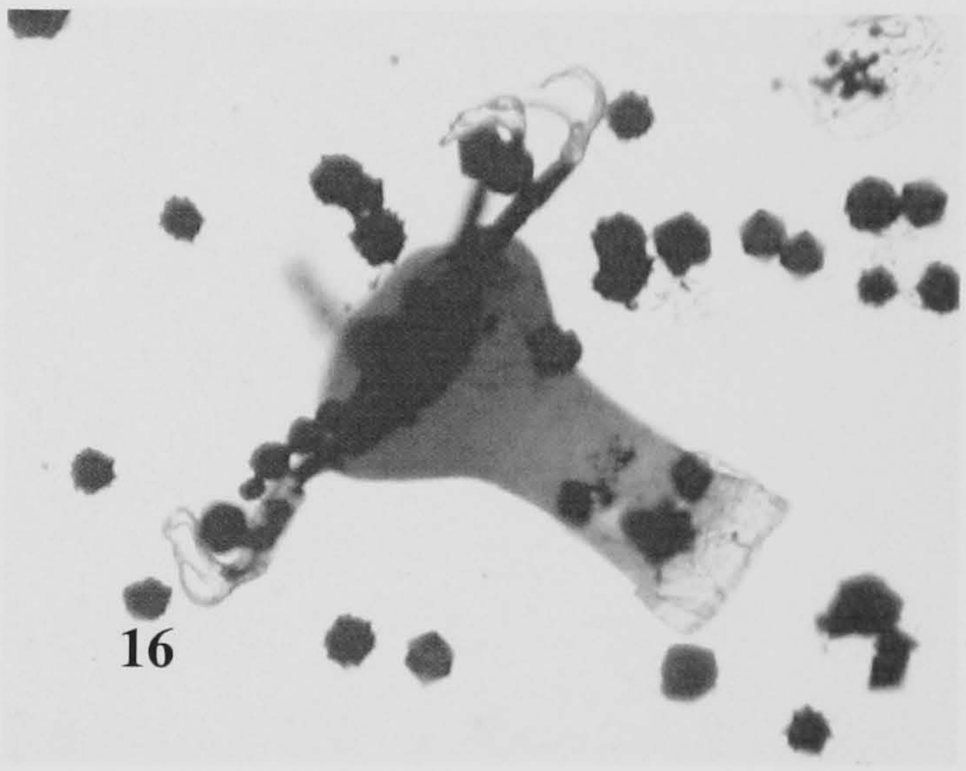

16

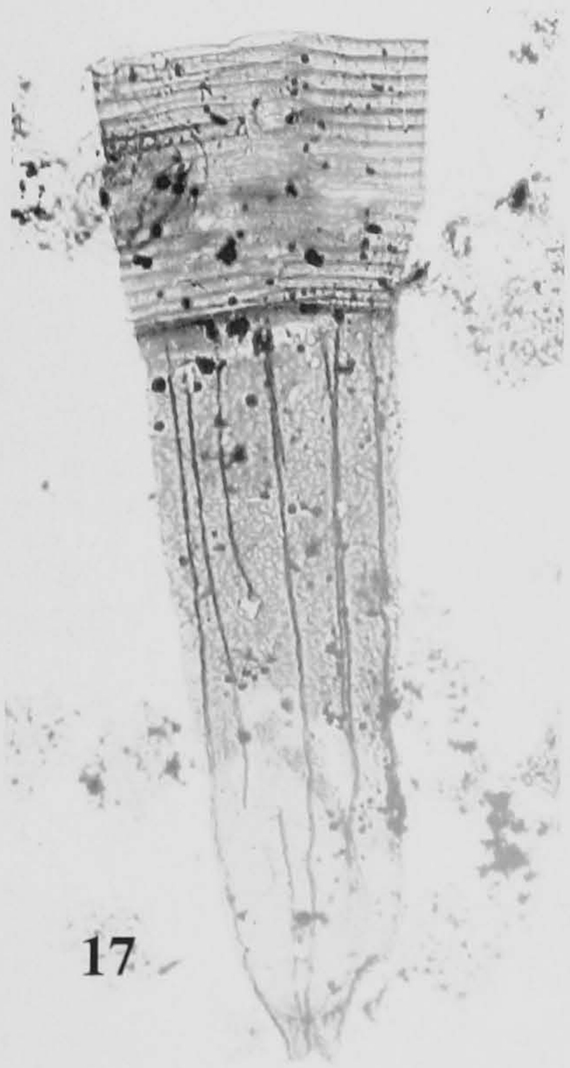

17

PLATE II

1- Vitrinite (Ro 1.0%), semifusinite, Tahara Sandstone Formation, depth 4127`, well F1-66.

2- Vitrinite (Ro 0.7%), large homogenous vitrinite particles, Tahara Sandstone Formation, well M2-NC7.

3- Graptolite (VR_E 0.7%) lower Tanezzuft Formation, depth 10181', well A1-70.

4- Graptolite (VR_E 0.8%) lower Tanezzuft Formation, depth 7054', well F1-66.

5- Chitinozoa (VR_E 1.0%) upper Tanezzuft Formation, depth 2135m, well B1-49.

6- Chitinozoa (VR_E 0.5%) Acacus Sandstone Formation, depth 8915', A1-70.

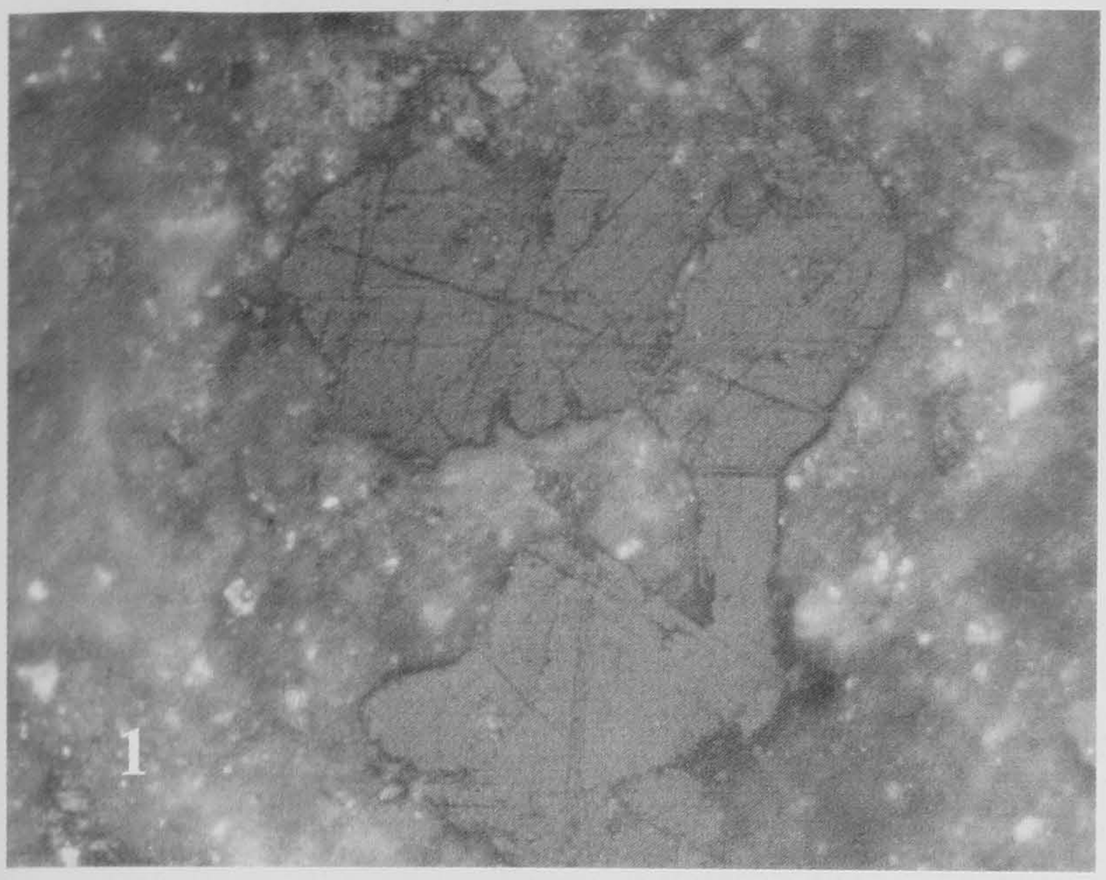
1

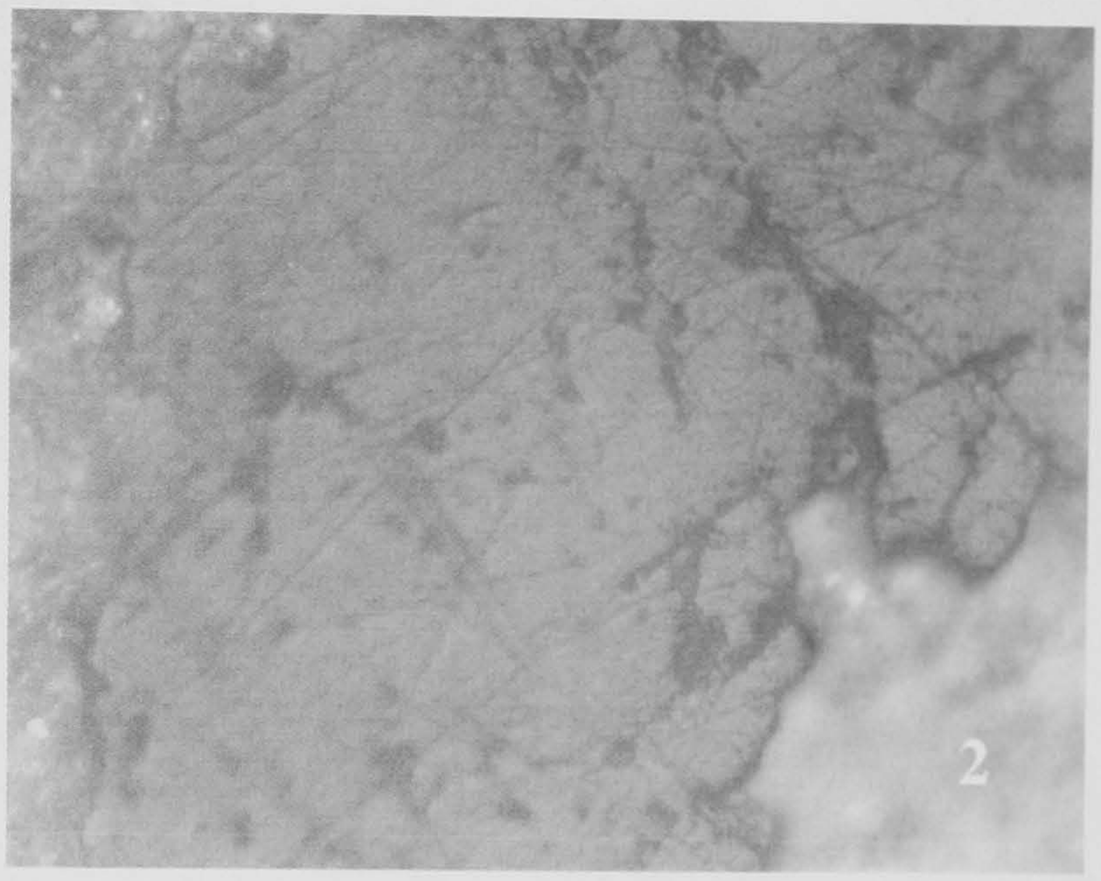
2

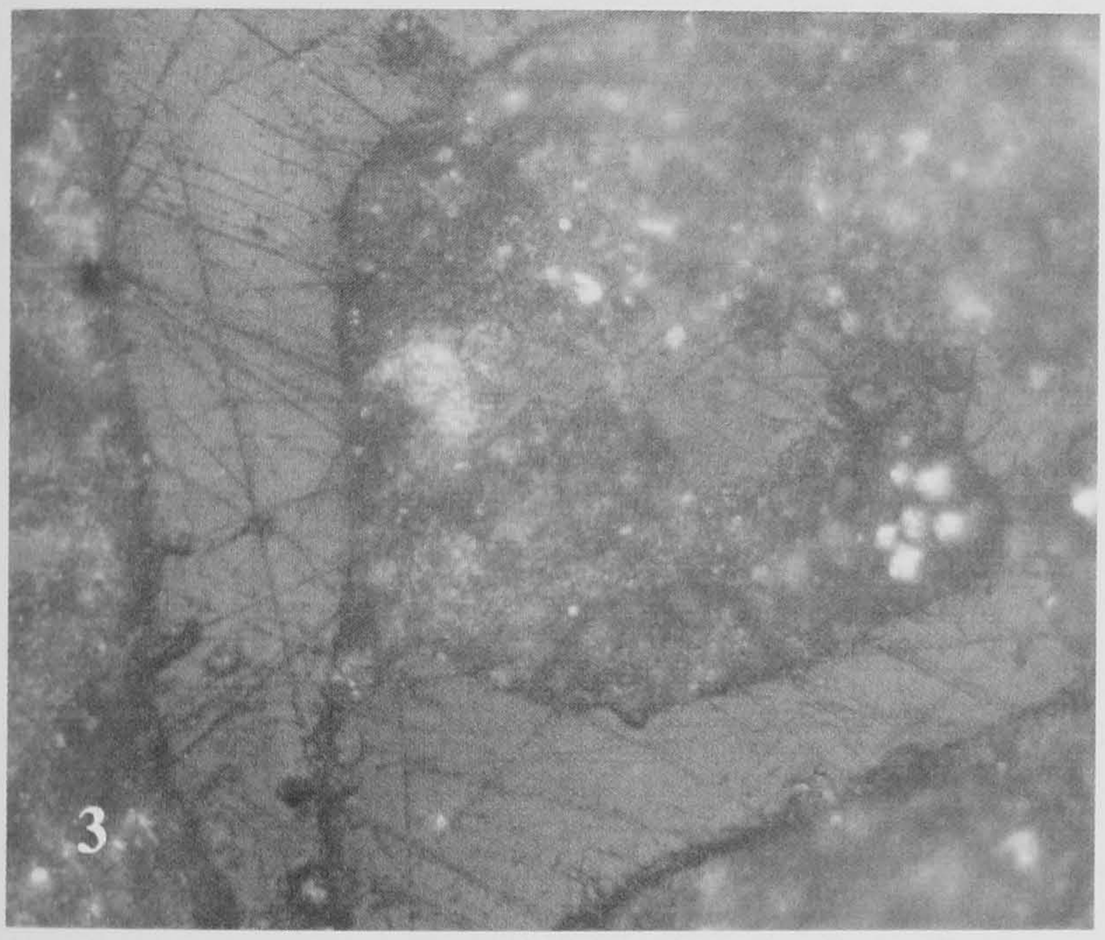
3

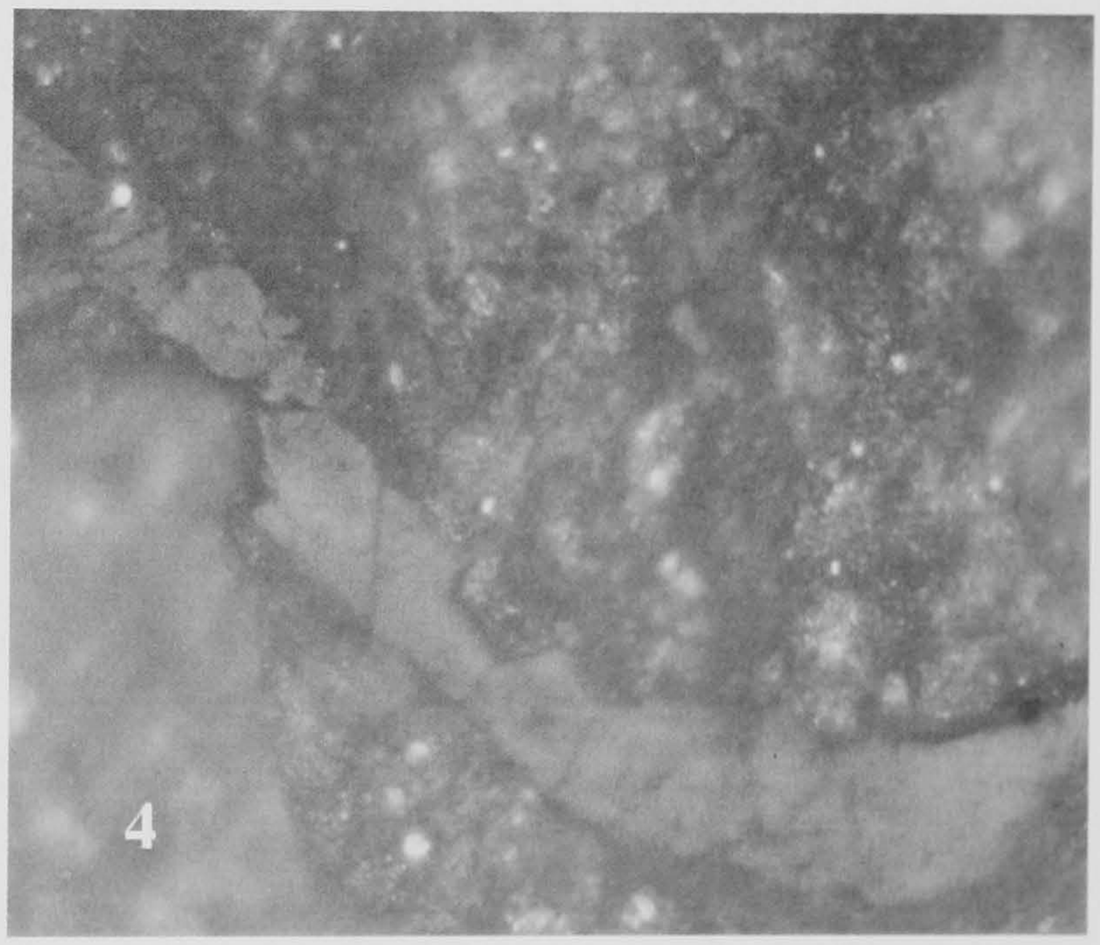
4


5

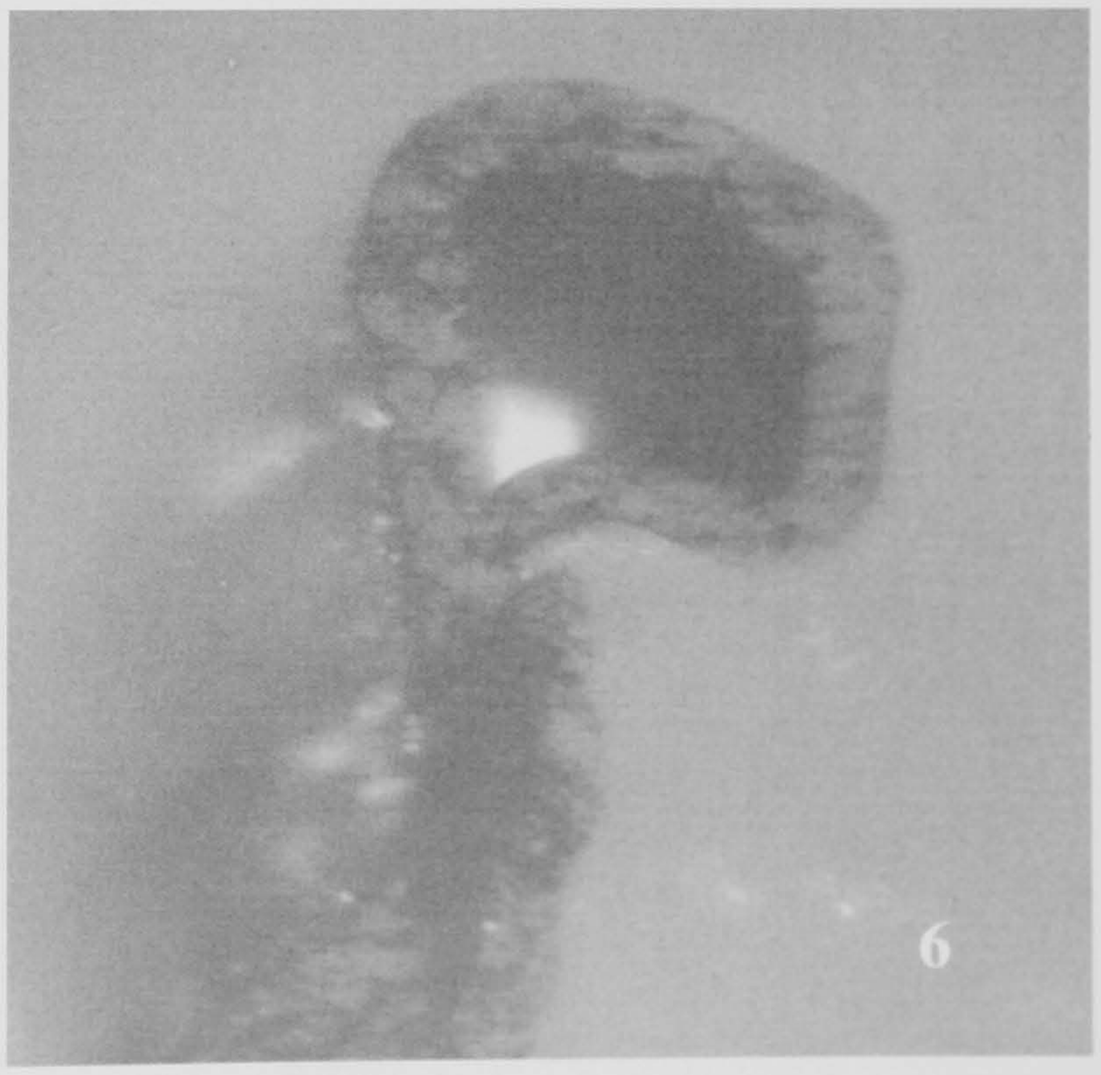
6